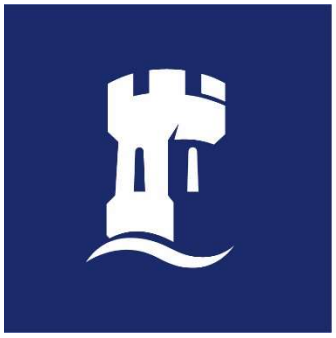

University of Nottingham
UK | CHINA | MALAYSIA

Techno-economic analysis and method development applied to an aerobic gas fermentation and supercritical water gasification process

By

Sarah Rodgers

Thesis submitted to the University of Nottingham for the degree of Doctor of Philosophy

March 2024

Abstract

The chemical and fuels industry's reliance on fossil-based feedstocks necessitates a shift to low-emission renewables like agricultural residues, municipal solid wastes, and industrial off-gases. Gas fermentation employs microbes to convert gaseous carbon-rich streams into renewable chemicals. The current state of commercial gas fermentation relies on anaerobic bacteria. However, aerobic bacteria offer the potential to target a broader range of products. Despite this, an inherent disadvantage of aerobic gas fermentation is its poor thermodynamic efficiency. Integrating aerobic gas fermentation with Supercritical Water Gasification (SCWG) addresses this challenge, creating a promising biochemical production platform. The integration utilises the low-temperature fermentation heat to pre-heat biomass for SCWG and reclaims the energy from depressurising the SCWG effluent using a turbo-expander. In addition, a key benefit of SCWG is its ability to exploit wet, low-value wastes. Such feedstocks are abundantly available and have limited resource competition as they are uneconomical to exploit via conventional gasification. Despite these benefits, the economic feasibility needs verifying which includes the selection of optimal feedstocks, feasible production capacities, and geographic considerations to identify promising biorefinery scenarios.

Essential for assessing emerging technologies, Techno-Economic Analyses (TEAs) were conducted to rigorously model and assess two case studies for the proposed integrated technology. The first considered commodity chemicals as direct products from fermentation (co-produced isopropanol and acetone), achieving a cumulative Net Present Value (NPV) of $42 million. Results compared favourably to anaerobic fermentation, with a minimum fuel selling price of $2.87/GGE. The second case study considered hybrid processing, integrating bio- and chemo-catalytic upgrading to produce 1,3-butadiene. This process showed profitability, achieving an MSP of $1367/tn, a $2.8M NPV, and a 19% probability of positive NPV. Part of the success of these two case studies was due the use of low-cost black liquor as the feedstock. SCWG allows for the successful exploitation of this wet feedstock. As such, a final study was undertaken to identify promising biorefinery scenarios for hydrogen production via SCWG, considering different feedstock-capacity-location combinations. The Levelised Cost of Hydrogen (LCOH) ranged from 3.81 to 18.72 $/kg$H_2$ across the considered scenarios. At capacities >50 m3/h, the LCOH's (2.76–4.21 $/kg$H_2$ for China, 3.41–5.07 $/kg$H_2$ for Brazil, 4.31–6.62 $/kg$H_2$ for the UK) were competitive with MW-scale electrolysis costs (3.10–6.70 $/kg$H_2$ for China, 3.70–5.90 $/kg$H_2$ for Brazil, and 4.81–6.31 $/kg$H_2$ for the UK). The range of results highlights the significance of feedstock-capacity-location considerations during technology evaluation.

In evaluating the economic feasibility of bio-derived chemicals and fuels, it's crucial to conduct Life Cycle Assessment (LCA) to quantify environmental impact. This facilitates a comparison of the trade-offs between a process' economic and environmental performance. For both commodity chemical case studies net negative emissions were achieved due to biogenic carbon sequestration. Isopropanol and acetone exhibited GHG emissions of -2.10 and -2.21 kgCO_2eq/kg compared to conventional production of 2.07 and 2.43 kgCO_2eq/kg. For 1,3-butadiene production emissions were -3.23 kgCO_2eq/kg, contrasting with the conventional 1.2 kgCO_2eq/kg. Hydrogen production from the final case study also demonstrated low process emissions, averaging 0.46 kgCO_2eq/GJH2 (China and Brazil), and 0.37 kgCO_2eq/GJH_2 (UK), compared to 8 kgCO_2eq/GJH_2 for steam methane reforming with carbon capture and storage (excluding natural gas leakage). These favourable emissions across all studies highlight the benefits of exploiting low-value, low-emission feedstocks.

As part of a TEA product prices for 20-25 years into the future are required to assess potential profitability. A Machine Learning (ML) method for projecting future commodity prices was

developed to allow for unbiased price selection procedures to input into TEAs. Initially, a Radial Basis Function Neural Network (RBFNN) was trained using 10 historic prices, optimising weights and centre points. The model was run recursively, with predicted prices becoming inputs. Stochastic uncertainty was incorporated using a ±30/20% uniform distribution from the projected price. The method was later refined using 100 LSTM models, leveraging historic commodity data (2009-2021) and Energy Information Administration's (EIA) Brent crude oil price projection. Training and validation sets were based on a 30% historic data and 70% projection horizon ratio, ensuring optimal hyperparameter selection. Probabilistic projections provided nominal, range, and probability distributions to input into the economic, sensitivity, and uncertainty analysis. The resulting price distributions showed variability between commodities, emphasising the need for tailored TEA uncertainty considerations instead of relying on arbitrary percentages. Compared to the initial RBFNN method, the refined approach was found to alter the NPV distributions' 70% window from $35-$95M to $45-$80M (isopropanol and acetone) and from -$45M-$65M to -$35M-$80M (1,3-butadiene), highlighting the importance of price selection procedures on TEA outcomes.

Conducting TEAs is time consuming and requires expert knowledge, hindering widespread application. To facilitate quick biorefinery scenario evaluations a ML method was developed. This was created for the TEA of hydrogen production via SCWG. An ML surrogate model was developed to predict the LCOH based on different feedstock-capacity-location combinations. The training data included 40 biomass compositions, five processing capacities (ranging from 10 to 200 m^3/hr), and three geographical locations (China, Brazil, UK). Three ML algorithms were compared for the ML surrogate model: Random Forests, Support Vector Regression, and an ensemble of Artificial Neural Networks (ANNs). The ANN ensemble was the most accurate during cross-validation and achieved an accuracy of Mean Absolute Percentage Error: <4.6%, Route Mean Squared Error: <0.39, and R^2: >0.99 on the test set. The final model was published for users to evaluate their own feedstocks. Overall, the model enables the identification of promising biorefinery scenarios for valorisation to maximise the economic potential of the technology.

There are two key contributing areas of this thesis, firstly, the rigorous techno-economic and environmental assessment of the technology and secondly, the development of TEA methods using ML to aid these evaluations. The techno-economic and environmental assessment demonstrates the economic and environmental viability of the proposed technology platform compared to both conventional and alternative renewable production routes. The development of TEA methods used ML to create an unbiased methodology to select product price and price distributions in TEAs and to produce a TEA surrogate model for early-stage screening of feedstock scenarios for SCWG. The methods developed demonstrate the potential of ML to enhance TEA practices.

Acknowledgements

Firstly, I would like to thank my (large) academic supervision team. Professor Alex Conradie, for first teaching me how to undertake a Techno-Economic Analysis during the naivety of Master's year. Also, for his support, teaching experiences, and numerous creative, challenging, and fruitful discussions on methodological developments. Professor Jon McKechnie, for his guidance through all things Life Cycle Assessment, additional research opportunities, his time and willingness to listen to my worries, and all the laughter shared in his office. Dr Fanran Meng for his quick response to all my questions, no matter how small, and for his continued companionship throughout my academic journey. And lastly, Professor Ed Lester, for joining us for the final lap. It has been a pleasure to work with you all.

I would also like to acknowledge the Engineering and Physical Sciences Research Council (EPSRC) and Johnson Matthey for their funding of my CASE studentship. I'd like to thank my industrial supervisor, Stephen Poulston, for his time and support throughout my PhD. In addition, thank you to Martin Hayes for the impromptu presentation opportunities and interest in my research. A special thank you goes to Laura Wells, for taking the time to introduce me to people at Johnson Matthey, discussions around the future, but mostly for the surprising but welcome friendship we formed through working together.

My PhD journey would not have been the same without the supportive, friendly, and utterly fabulous LCA research group, both past and present. Thank you for the laughter filled office lunches, critical and rewarding presentation feedback, concerned looks when the torrential rain pours outside the ITRC, and friendship along this journey.

Finally, I would like to thank my partner, Alex. This would not have been possible without you. Thank you for putting up with me complaining, sharing in my successes, and helping me to find my path. You are amazing.

Publications

First author publications (included in this thesis):

- Reconciling the Sustainable Manufacturing of Commodity Chemicals with Feasible Technoeconomic Outcomes: Assessing the investment case for heat integrated aerobic gas fermentation. *Johnson Matthey Technology Review Journal* (July 2021).
- Renewable butadiene: A case for hybrid processing via bio- and chemo-catalysis. *Journal of Cleaner Production* (June 2022).
- Probabilistic commodity price projections for unbiased techno-economic analyses. *Engineering Applications of Artificial Intelligence* (June 2023).
- A surrogate model for the economic evaluation of renewable hydrogen production from biomass feedstocks via supercritical water gasification. *International Journal of Hydrogen Energy* (January 2024).

Co-authored publications (excluded from this thesis):

- BEIS GGR Innovation Phase 1 Project. Bio-waste to Biochar (B to B) via Hydrothermal Carbonisation and Post-Carbonisation Final Report.
- Biowaste to Biochar: A techno-economic and life cycle assessment of biochar production from food-waste digestate and its agricultural field application. *Currently under review in Waste Management.*
- Bayesian and ultrasonic sensor aided multi-objective optimisation for sustainable clean-in-place processes. *Food and Bioproducts Processing* (September 2023).
- Development of an Open-Source Carbon Footprint Calculator of the UK Craft Brewing Value Chain Presentations. *Journal of Cleaner Production.* (January 2024).

Presentations

- 22/03/21 Johnson Matthey Academic Conference. Flash presentation.
  - *"Techno-Economics of Renewable Butadiene Production"*
- 22/09/21 High Value Biorenewables Network Conference. Presentation.
  - *"Why techno-economic analysis should be the first question"*
- 14/10/21 Biomass Biorefinery Network Conference. Flash and poster presentation.
  - *"Techno-Economics and Life Cycle Analysis of Renewable 1,3-Butadiene from a Pulp Mill Biorefinery"*
- 22/03/22 Environmental Sustainability – an SMEs approach. Presentation.
  - *"Techno-economic analyses and life cycle assessment of biorenewable chemical production"*
- 05/04/22 Johnson Matthey Academic Conference. Poster presentation.
  - *"The Power, Challenges and Future of Techno-Economic Analyses"*
- 23/05/22 SCI Engineering Biology. Presentation.
  - *"Reconciling the Sustainable Manufacturing of Commodity Chemicals with Feasible Technoeconomic Outcomes"*
- 19/07/22 The Carbon Recycling Network Policy Roundtable. Presentation on evidence gathered.
- 08/02/23 AI and Engineering University of Nottingham Internal Conference. Poster presentation (best poster award).
  - *"Applications of Machine Learning in Techno-Economic Analyses"*
- 22/03/23 Biomass Biorefinery Network Conference. Poster presentation.
  - *"Feedstock evaluation tool for renewable hydrogen production via low temperature supercritical water gasification"*

Table of Contents

List of Tables

List of Figures

Abbreviations

AACE	Association for the Advancement of Cost Engineering
ACCE	Aspen Capital Cost Estimator
ANN	Artificial Neural Network
ATP	Adenosine triphosphate
BEIS	Business, Energy and Industrial Strategy
CAPEX	Capital Expenditure
CCS	Carbon Capture and Storage
COD	Chemical Oxygen Demand
EIA	Energy Information Administration
FCI	Fixed Capital Investment
F-T	Fischer Tropsch
GGE	Gallon Gasoline Equivalent
GHG	Greenhouse Gas
HHV	Higher Heating Value
HTL	Hydrothermal Liquefaction
HTS	High Temperature Shift
IEA	International Energy Agency
IHS	Information Handling Services
IRR	Internal Rate of Return
ISBL	Inside Battery Limit
LCA	Life Cycle Assessment
LCOH	Levelised Cost of Hydrogen
LSTM	Long-Short Term Memory
LTS	Low Temperature Shift
MAPE	Mean Absolute Percentage Error
MFSP	Minimum Fuel Selling Price
ML	Machine Learning
MSE	Mean Squared Error
MSP	Minimum Selling Price
MTP	Methanol-to-Propene
NPV	Net Present Value
NREL	National Renewable Energy Laboratory
OPEX	Operating Expenditure
OSBL	Outside Battery Limit
PHA	Polyhydroxyalkanoate
PHB	Polyhydroxybutyrate
RBFNN	Radial Basis Function Neural Network
RF	Random Forests
ROM	Reduced Order Model
RMO	Ratio of Moles of Oxygen
RMSE	Route Mean Squared Error
SCWG	Supercritical Water Gasification
SHAP	SHapley Additive explanation
SMR	Steam Methane Reforming
SVR	Support Vector Regression
TAC	Total Annualised Cost
TEA	Techno-Economic Analysis
TS	Tower and Sinnott
TRL	Technical Readiness Level

1. Introduction

1.1 Background and motivation

Transitioning from fossil-based resources to renewable resources such as agricultural residues, municipal solid wastes, and industrial off-gases is essential for the development of a sustainable chemical and fuels industry (Fackler et al., 2021). Gas fermentation, which utilises microbes for chemical production, shows promise in upgrading recalcitrant feedstocks to chemicals. Unlike cellulosic fermentation which cannot utilise the lignin fraction in feedstocks, gas fermentation is able to exploit the entire biomass compound (Liew et al., 2016). In addition, in contrast to thermochemical technologies, gas fermentation operates at low temperatures and pressures, handles chaotic inputs, and tolerates contaminants in the gas stream (Fackler et al., 2021).

Currently, the only operational commercial gas fermentation technology is LanzaTech's anaerobic gas fermentation process in Beijing, which uses steel mill off-gas (Fackler et al., 2021). However, anaerobic fermentations are limited in their ability to produce Adenosine triphosphate (ATP)-intensive products due to their energetically limited CO_2 fixation pathway (Dürre, 2017). In contrast, aerobic gas fermentation can target a broader product spectrum than anaerobic but suffers from poor thermodynamic efficiency due to the loss of H_2 as water during respiration (Emerson & Stephanopoulos, 2019). Bommareddy et al. (2020) proposed a solution to this inefficiency by utilising the low-temperature heat produced during fermentation to pre-heat the biomass feed for Supercritical Water Gasification (SCWG). The benefit of SCWG is its ability to exploit wet, low-value wastes. Such feedstocks are abundantly available, typically low-cost, and have limited resource competition as they uneconomical to exploit via conventional gasification technologies (Lee et al., 2021). In addition, as per Bommareddy et al. (2020), the high pressure required for SCWG (>22.1 MPa) can be recovered as renewable electricity upon letting down the product syngas. This recovered energy comfortably meets the air compression requirement for the aerobic bioreactor. This process engineering synergy between the two technologies claims to overcome some of the limitations of aerobic gas fermentation and create an economically viable platform (Bommareddy et al., 2020). However, the economic feasibility of this platform, along with promising feedstock, location, and capacity considerations requires verification.

To assess the economic feasibility of emerging technologies, a Techno-Economic Analysis (TEA) is required. TEAs play a critical role in identifying cost bottlenecks, evaluating research options, and guiding future research directions (Scown et al., 2021). These analyses involve full system design, virtual scale-up, and economic evaluation based on empirical data. Typically, TEAs begin at a Technical Readiness Level (TRL) of 3 (technical proof of concept) and are modified and updated up to TRL 7 (integrated pilot continuous operation) (Figure 1.1). Highlighting their importance, TEAs are undertaken across the ‘valley-of-death’ stages of technology development, which is often the hurdle to commercialisation (Köpke & Simpson, 2020). Furthermore, bio-derived chemicals and fuels can offer a significant environmental advantage compared to their fossil fuel counterparts. However, this benefit needs to be quantified through Life Cycle Assessment (LCA). Therefore, simultaneous TEAs and LCAs need to be conducted to understand the trade-off between a process's economic and environmental performance (Mahmud et al., 2021).

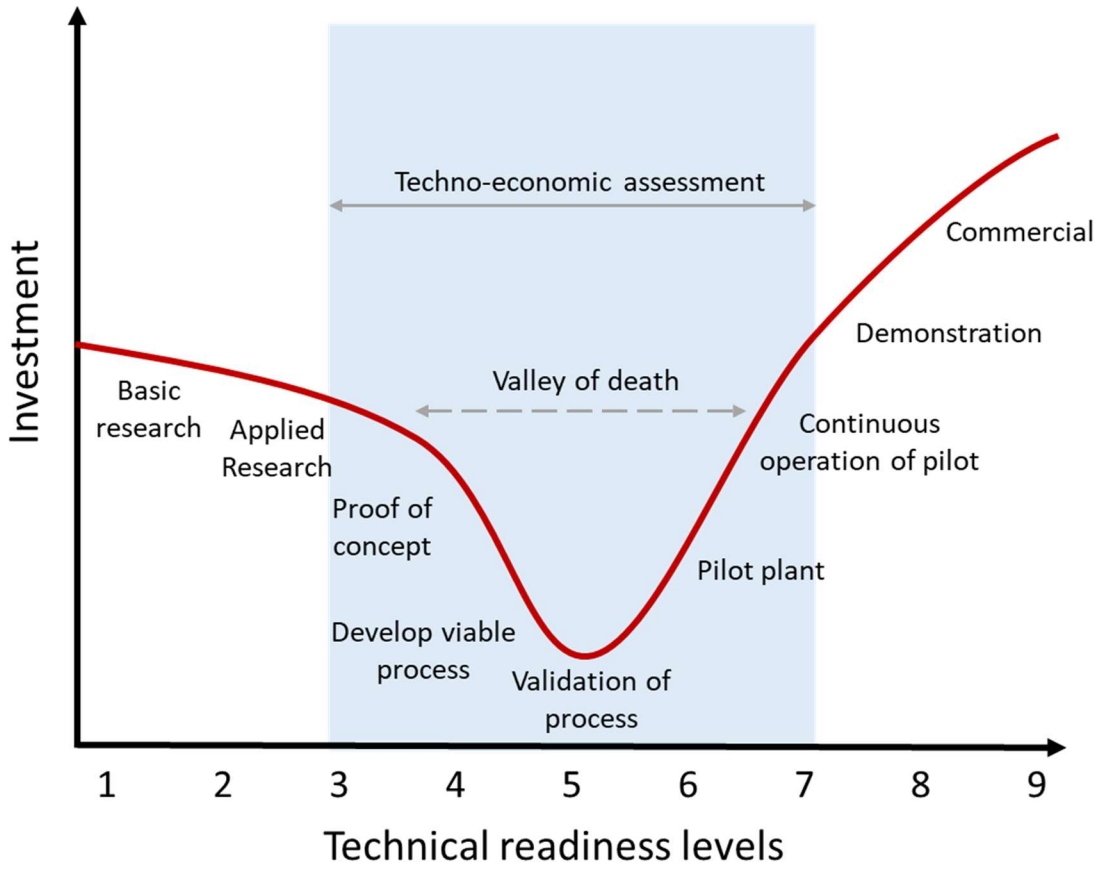

Figure 1.1: Valley-of-death of emerging technologies. Technical readiness level definitions relate to the expanded levels developed for the bioeconomy (Humbird, 2018).

TEAs are widely employed to evaluate bio-derived chemical and fuel production processes, with the National Renewable Energy Laboratory (NREL) studies serving as a benchmark (Scown et al., 2021). NREL's analyses extensively report the costing models, assumptions, mass and energy balances, and publish the Aspen models used as the analysis basis (NREL, 2023). This transparency allows for updates to be made to techno-economic models based on new data and facilitates comparisons between different studies and models. However, in the wider TEA literature there is currently no consensus on a TEA framework (Faber et al., 2021), making comparisons between studies difficult.

Current TEA methods face challenges such as assuming stability in product prices (Scown et al., 2021) and providing single-point estimates despite the high variability in TEA inputs and assumptions (Fu et al., 2022). Additionally, conducting these analyses demands significant time, engineering expertise, and specialized software (Huntington et al., 2023). Machine Learning (ML) is emerging as a valuable tool to tackle some of these challenges. For instance, ML is widely applied in price forecasting fields to predict future commodity and energy prices (Wu et al., 2019). ML surrogate models can also be used to effectively represent complex unit operations within process simulations, enabling robust uncertainty analyses that consider both economic and technical parameters (Scown et al., 2021). Surrogate models can also be applied to full economic analyses, providing a lightweight tool to compare different scenarios (Huntington et al., 2023).

The **aim** of this thesis is to develop and apply techno-economic analysis tools to evaluate the integrated aerobic gas fermentation and supercritical water gasification process.

Objectives:

1. **Develop process simulations for the aerobic gas fermentation and supercritical water gasification process, incorporating heat integration and downstream processing.** Two simulations were created for the case studies examined in this thesis, forming the foundation for economic and environmental assessments. An additional simulation, considering only SCWG was created for feedstock evaluation purposes.
2. **Determine an appropriate techno-economic framework and perform a comprehensive techno-economic analysis of the simulated process.** Selecting a cost model framework ensures comparability across studies. The economic analysis provides metrics to assess the competitiveness of the technology with market prices.
3. **Quantify the greenhouse gas emissions associated with chemical and fuel production from the process and compare them with conventional production methods.** This assessment allows for the evaluation of the environmental benefits or drawbacks of the renewable chemical platform compared to conventional approaches.
4. **Compare the economic and environmental competitiveness of the process with alternative renewable production methods.** This analysis contextualises the technology's economic potential relative to other technologies.
5. **Develop a methodology to project future prices, considering future price variability, for use in techno-economic, sensitivity, and uncertainty analyses.** This approach eliminates practitioner bias in price selection and places the economic results in the context of projected prices, ensuring the economic competitiveness is easily interpreted.
6. **Create a machine learning surrogate model of a techno-economic analysis to rapidly evaluate the economic potential of feedstock-capacity-location combinations for supercritical water gasification.** This model represents an advancement in techno-economic analysis methods, creating an ML surrogate representing an entire TEA. This enables the quick evaluation of biorefinery scenarios by non-experts and the identification of promising opportunities for their valorisation.

1.2 Contributions and novelty

There are two key contributing areas of this thesis. Firstly, it rigorously evaluates the technological, economic, and environmental aspects of the aerobic gas fermentation and SCWG process. Secondly, it develops TEA methodologies to facilitate these evaluations.

This technology evaluations were undertaken through rigorously modelling and conducting economic and environmental assessments for two case studies:

1) The assessment of commodity chemicals as direct products of fermentation (co-production of isopropanol and acetone).
2) The evaluation of hybrid processing by integrating fermentation and catalytic upgrading to produce a commodity chemical with a projected future shortage by fossil fuel-based production (1,3-butadiene).

Methodological advancements were achieved through the application of ML and comprised:

1) The development of a method to project future commodity chemical prices and price variability, which is then integrated into TEA procedures, removing user bias in price selection processes.

2) The creation of a method for predicting TEA outcomes based on various feedstock-capacity-location combinations. This aids in the identification of promising biorefinery scenarios.

The overall contributions of this thesis can be summarised as follows:

Chapter 4:

- Rigorous TEA of the proposed heat integrated aerobic gas fermentation platform. Existing gas fermentation TEAs are largely based on anaerobic gas fermentation. Existing studies investigating aerobic gas fermentation have focused on identifying process parameters (productivity and yield) to define future research targets (Khan et al., 2014), general assessments for renewable chemical production including higher value co-products Choi et al. (2010), and the potential to reduce energy consumption through using thermophilic bacteria (Levett et al., 2016). In contrast, the analysis in this thesis aimed to evaluate the economic potential by applying process engineering solutions to some inherent disadvantages of aerobic gas fermentation.
- Comparison of different techno-economic costing models to evaluate the economic feasibility of the platform. Existing comparisons in capital costing methods exist. However, the comparisons are limited to equipment cost and capital cost estimation, excluding fixed operating cost considerations (e.g. van Amsterdam, 2018; Brown, 2015). Furthermore, these comparisons were not undertaken within a TEA study.
- Techno-economic and environmental comparison between aerobic and anaerobic gas fermentation. Existing technology comparisons have focused on comparisons between gas fermentation and hydrolysis-based fermentation (Piccolo & Bezzo, 2009; Choi et al., 2010; Christodoulou & Velasquez-Orta, 2016) or thermochemical conversion (Haro et al., 2013; Tan et al., 2016; Okoro & Faloye, 2020).

Chapter 5:

- Rigorous assessment of combining gas fermentation with catalytic upgrading (hybrid processing) for chemical production. Previous hybrid processing has been undertaken by Haro et al. (2013) for ethylene production and Tan et al. (2016) for distillate range fuels. In the study by Haro et al. (2013), only the catalytic upgrading was modelled, and cost estimates for different ethanol sources were taken from the literature, meaning results were reliant on the quality of ethanol price estimates. In this thesis the comparative routes were rigorously modelled. Tan et al. (2016) modelled the routes in their comparative study. However, the study investigated the production of distillate range fuels rather than commodity chemicals.
- Comparing hybrid bio- and chemo-catalytic production with purely chemo-catalytic production of 1,3-butadiene. Existing studies for 1,3-butadiene production have investigated hybrid bio-catalytic and chemo-catalytic production by upgrading fermentation derived ethanol e.g. Moncada et al. (2018), or chemo-catalytic production via a renewable olefin intermediate e.g. Hanaoka et al. (2021).

Chapter 6:

- Using machine learning to produce commodity price projections for techno-economic analyses. Previous TEAs have employed stochastic modelling (e.g. Manca et al., 2011), correlating prices to an existing projection for a different commodity (e.g. Brown and Wright, 2015), or employed traditional econometric tools (e.g. Nguyen and Tyner, 2021).
- Producing a probabilistic price projection methodology which exploits the underlying stochastic and/or deterministic trends within a commodity's historic time series. The probabilistic projection provides the range and distribution for the sensitivity and

uncertainty analyses. Previous approaches have relied on historic variability (e.g. Diniz et al., 2018) or applying an arbitrary percentage (e.g. Moncada et al., 2018).

Chapter 7:

- Development of a published surrogate model of a TEA to evaluate the economic potential of different feedstock-capacity-location combinations for SCWG. This facilitates experimentalists and industrialists in identifying promising biorefinery scenarios for valorisation to inform targeted research and investment. To the best of the author's knowledge, the only other study to produce a surrogate model for a full TEA was Huntington et al. (2023), who used hydrolysis-based ethanol production as a case study.
- Creation of a reliability measure for the developed surrogate model to determine the confidence in the model's predictions for unseen user inputs, preventing model misuse. The validity of predictions made by the surrogate model on unseen data was not discussed in the work by Huntington et al. (2023). The method developed in this thesis takes principles from anomaly detection using autoencoders where an anomaly threshold is set by the reconstruction error (Ndubuaku et al., 2019). However, in this thesis the threshold is set based on the error between the predictions by the ensemble of Artificial Neural Networks on a validation set.

1.3 Thesis overview

This thesis is constructed of journal publications. **Chapter 2** consists of a literature review that complements these publications by providing contextual information about their position and contribution within the broader literature. The articles in this thesis all contribute towards the *evaluation* of the technology. However, the articles included in this thesis can be divided into two sections. The first section focuses on the *Techno-economic analysis* of the aerobic gas fermentation and SCWG platform undertaken through two case studies. The second section concentrates on *Method development* for TEAs where a method to project future commodity prices for inclusion in techno-economic and uncertainty analyses, and a surrogate model for feedstock evaluation are developed. The interactions between these sections and the transfer of methods and data from each chapter is depicted in Figure 1.2.

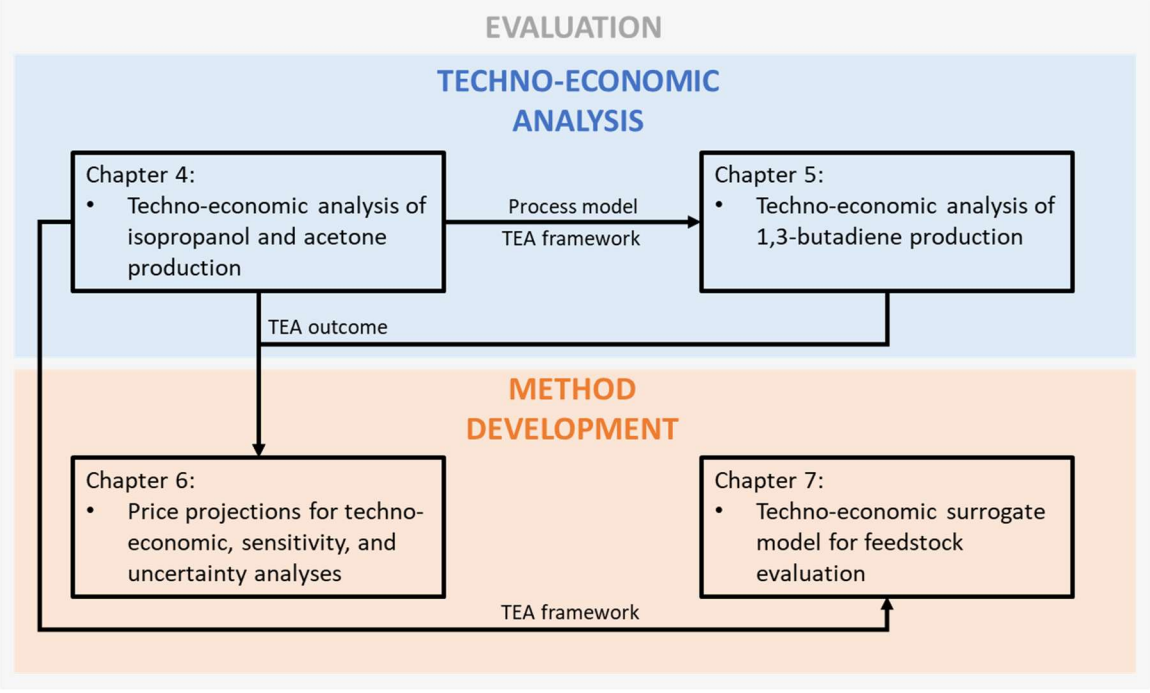

Figure 1.2: Schematic of the articles included in this thesis and their interactions

Chapter 3 provides a detailed description and critical analysis of the methodology employed in this thesis, covering process modelling, techno-economic cost models, sensitivity analysis methodology, and methodological advancements.

Chapter 4 presents a research article titled: "*Reconciling the Sustainable Manufacturing of Commodity Chemicals with Feasible Technoeconomic Outcomes: Assessing the investment case for heat integrated aerobic gas fermentation"*. The article was published in the *Johnson Matthey Technology Review Journal* in July 2021. This article focuses on the techno-economic and life cycle assessment of the novel aerobic gas fermentation platform, which integrates SCWG with aerobic gas fermentation to achieve positive economic outcomes. Furthermore, three different methods for calculating capital and fixed operating costs are compared. The main conclusion from this work was the cost competitive production of isopropanol and acetone using the platform and the achievement of net negative greenhouse gas emissions owing to the sequestration of biogenic carbon. In addition, the economic and environmental results were found to be comparable to a anaerobic gas fermentation process.

Chapter 5 comprises a research article titled: *"Renewable butadiene: A case for hybrid processing via bio- and chemo-catalysis".* The article was published in the *Journal of Cleaner Production* in June 2022. The novelty of this work is the evaluation of the same aerobic gas fermentation and SCWG platform presented in Chapter 4, but for 1,3-butadiene production, a chemical with projected future shortages via conventional fossil fuel-based production. The study explores hybrid processing, coupling of bio- and thermo-chemical technologies, to upgrade the fermentation product to produce a reduced commodity chemical. The aerobic gas fermentation platform is compared to two purely chemo-catalytic renewable technologies, all originating from biomass gasification. The main conclusion from this work was that the aerobic gas fermentation platform outperformed the two alternative chemo-catalytic l pathways to 1,3-butadiene from both an economic and environmental perspective.

Chapter 6 features a research article titled: *"Probabilistic commodity price projections for unbiased techno-economic analyses".* The article was published in *Engineering Applications of Artificial Intelligence* in June 2023. This work introduces the use of machine learning to generate 20-25-year probabilistic commodity price projections for techno-economic, sensitivity, and uncertainty analyses. An ensemble of 100 LSTMs was utilised to leverage the determinism and/or stochastic variability within the commodity's historical time series. These price projections were then used in the techno-economic and uncertainty analyses from Chapters 4 and 5, highlighting the importance of price selection procedures in techno-economic outcomes. The main conclusion from this work was the importance of commodity prices and price distributions during technology assessment, demonstrating the need for an unbiased selection method.

Chapter 7 contains a research article titled: *"A surrogate model for the economic evaluation of biomass feedstocks for renewable hydrogen production via supercritical water gasification".* The article was published in *International Journal of Hydrogen Energy, currently in press*. The novelty of this work lies in the creation of a publicly available ML surrogate model for the TEA of SCWG to predict the Levelised Cost of Hydrogen from various feedstock-capacity-location combinations. The surrogate model is developed based on the simulation and economic evaluation of 40 different biomass feedstock compositions across three geographic locations and five processing capacities (10 – 200 m^3/hr). The main conclusion from this work was the impact of different feedstock-capacity-location combinations on the LCOH, evidencing the significance of biorefinery scenario selection during technology evaluation. This highlights the need for early-stage screening tools to inform targeted research and development into promising resource valorisation opportunities.

Chapter 8 presents the major conclusions and limitations of the work undertaken in this thesis and discusses potential directions for future research.

1.4 References

Bommareddy, R.R; Wang, Y; Pearcy, N; Hayes, M; Lester, E; Minton, N.P; Conradie, A.V., 2020. A Sustainable Chemicals Manufacturing Paradigm Using CO_2 and Renewable H_2. *iScience*, 23(6), 101218.

Brown, T. R., 2015. A critical analysis of thermochemical cellulosic biorefinery capital cost estimates. *Biofuels, Bioproducts and Biorefining*.

Brown T.R., Wright M.M. 2015. A framework for defining the economic feasibility of cellulosic biofuel pathways. *Biofuels*, 579-590

Choi, D., Chipman, D. C., Bents, S. C. & Brown, R. C., 2010. A Techno-economic Analysis of Polyhydroxyalkanoate and Hydrogen Production from Syngas Fermentation of Gasified Biomass. *Applied Biochemistry and Biotechnology*, 160, 1032-1046.

Christodoulou, X. & Velasquez-Orta, S. B., 2016. Microbial Electrosynthesis and Anaerobic Fermentation: An Economic Evaluation for Acetic Acid Production from CO2 and CO. *Environmental Science & Technology*, 50(20), pp. 11234-11242.

Diniz A.P.M.M., Sargeant R., Millar G.J., 2018. Stochastic techno-economic analysis of the production of aviation biofuel from oilseeds. *Biotechnology for Biofuels and Bioproducts*, 11, 1-15

Dürre, P., 2017. Gas fermentation – a biotechnological solution for today's challenges. *Microbial biotechnology*, 10(1), 14-16.

Emerson, D.F & Stephanopoulos, G., 2019. Limitations in converting waste gases to fuels and chemicals. *Current Opinion in Biotechnology*. 59, 39-45.

Faber, G; Mangin, C; Sick, V., 2021. Life Cycle and Techno-Economic Assessment Templates for Emerging Carbon Management Technologies. *Frontiers in Sustainability*, 2.

Fackler, N; Heijstra, B.D; Rasor, B.J; Brown, H; Martin, J; Ni, Z; Shebek, K.M; Rosin, R.R; Simpson, S.D; Tyo, K.E; Giannone, R.J; Hettich, R.L; Tschaplinski, T.J; Leang, C; Brown, S.D; Jewett, M.C; Köpke, M., 2021. Stepping on the Gas to a Circular Economy: Accelerating Development of Carbon-Negative Chemical Production from Gas Fermentation. Annual *Review of Chemical and Biomolecular Engineering*, 12:1, 439-470.

Fu, R; Kang, L; Zhang, C; Fei, Q., 2022. Application and progress of techno-economic analysis and life cycle assessment in biomanufacturing of fuels and chemicals. *Green Chemical Engineering, Article in press.*

Hanaoka, T., Fujimoto, S., Kihara, H., 2021. Evaluation of n-butene synthesis from dimethyl ether in the production of 1,3-butadiene from lignin: a techno-economic analysis. *Renewable Energy*, 163, 964-973

Haro, P., Ollero, P. & Trippe, F., 2013. Technoeconomic assessment of potential processes for bio-ethylene production. *Fuel Processing Technology*, 114, 35-48.

Humbird, D., 2018. *Expanded Technology Readiness Level (TRL) Definitions for the Bioeconomy*. Accessed [17/05/2023] URL: https://www.biofuelsdigest.com/bdigest/2018/10/01/expanded-technology-readiness-level-trl-definitions-for-the-bioeconomy/

Huntington, T., Baral, N.R., Yang, M., Sundstrom, E., Scown, C.D., 2023. Machine learning for surrogate process models of bioproduction pathways. *Bioresource Technology*, 370, 128528.

Khan, N. E., Myers, J. A., Tuerk, A. L. & Curtis, W. R., 2014. A process economic assessment of hydrocarbon biofuels production using chemoautotrophic organisms. *Bioresource Technology*, 172, 201-211.

Köpke, M. & Simpson, S.D., 2020. Pollution to products: recycling of 'above ground' carbon by gas fermentation. *Current Opinion in Biotechnology*, 65, 180-189.

Lee, C. S., Conradie, A. V. & Lester, E., 2021. Review of supercritical water gasification with lignocellulosic real biomass as the feedstocks: Process parameters, biomass composition, catalyst development, reactor design and its challenges. *Chemical Engineering Journal*, 145, 128837.

Liew, F., Martin, M.E., Tappel, R.C., Heijstra, B.J., Mihalcea, C., Köpke, M., 2016. Gas Fermentation—A Flexible Platform for Commercial Scale Production of Low-Carbon-Fuels and Chemicals from Waste and Renewable Feedstocks. *Frontiers in Microbiology*, 7.

Mahmud, R., Moni, S,M., High, H., Carbajales-Dale, M., 2021. Integration of techno-economic analysis and life cycle assessment for sustainable process design – A review. *Journal of Cleaner Production*, 317, 128247.

Manca D., Fini A., Oliosi M., 2011. Dynamic conceptual design under market uncertainty and price volatility *Computer Aided Chemical Engineering*, 336-340.

Moncada, J., Gursel, I.V., Worrell, E., Ramírez A., 2018. Production of 1,3-butadiene and ε-caprolactam from C6 sugars: Techno-economic analysis. *Biofuels, Bioproducts and Biorefining*, 12(4)

Ndubuaku, M. U., Anjum, A., Liotta., A., 2019. Unsupervised Anomaly Thresholding from Reconstruction Errors, in: Montella, R., Ciaramella, A., Fortino, G., Guerrieri, A., Liotta, A. (Eds.), *Internet and Distributed Computing Systems*. IDCS 2019. *Lecture Notes in Computer Science*. Springer, Cham. 123–129.

Nguyen N., Tyner W.E., 2021. Assessment of the feasibility of the production of alternative jet fuel and diesel using catalytic hydrothermolysis technology: a stochastic techno-economic analysis. *Biofuels, Bioproducst and Biorefining*, 16 (1), 91-104

NREL., 2023 *Biochemical Conversion Techno-Economic Analysis*. Accessed [17/05/2023] URL: https://www.nrel.gov/bioenergy/biochemical-conversion-techno-economic-analysis.html

Okoro, O. & Faloye, F., 2020. Comparative Assessment of Thermo-Syngas Fermentative and Liquefaction Technologies as Waste Plastics Repurposing Strategies. *AgriEngineering,* 2, 378-392.

Piccolo, C. & Bezzo, F., 2009. A techno-economic comparison between two technologies for bioethanol production from lignocellulose. *Biomass & Bioenergy*, 33(3), 478-491.

Queneau, Y. & Han, B., 2022. Biomass: Renewable carbon resource for chemical and energy industry. *The Innovation,* 3, 100184.

Scown, C.D; Baral, N.R; Yang, M; Vora, N; Huntington, T., 2021 Technoeconomic analysis for biofuels and bioproducts. *Current Opinion in Biotechnology*, 67, 58-64

Tan, E.C.D., Snowden-Swan, L.J., Talmadge, M., Dutta, A., Jones, S., Ramasamy, K.K., Gray, M., Dagle, R., Padmaperuma, A., Gerber, M., Sahir, A.H., Tao, L., Zhang, Y., 2016. Comparative techno-economic analysis and process design for indirect liquefaction pathways to distillate-range fuels via biomass-derived oxygenated intermediates upgrading. *Biofuels, Bioproducts & Biorefining.*

van Amsterdam, M., 2018. Factorial Techniques applied in Chemical Plant Cost Estimation: A Comparative Study based on Literature and Cases. Delft: s.n.

Wu Y.X., Wu Q.B., Zhu J.Q., 2019. Improved EEMD-based crude oil price forecasting using LSTM networks. *Physica A*, 516, 114-124

2 Literature Review

The chemical industry's current reliance on fossil fuel feedstocks and linear value chain has adverse environmental impacts (Meng et al., 2023). Furthermore, growing pressures on fossil fuel reserves require the exploitation of alternative chemical feedstocks. As a renewable carbon source, biomass plays a key role in the transition away from fossil fuel use and towards the development of a renewable chemical industry (Queneau & Han., 2022). The use of biomass harnesses the CO_2 captured from the air through photosynthesis during growth as a chemical feedstock, which is eventually released upon the end-of-life of the chemical product, resulting in net zero emissions (Gabrielli et al., 2023). Consequently, chemicals produced using biomass resources often have low associated emissions.

Despite the proposed environmental benefit of biomass feedstocks, their higher water content and lower energy density make them less favourable compared to fossil fuel resources (Gabrielli et al., 2023). In addition, the abundance of cheap fossil fuels has historically led the chemical industry to favour the use of fossil fuels (Lopez et al., 2023). Therefore, processes utilising biomass are both more challenging and less established than petrochemical processes. Despite this, first-generation biomass is commercialised for bioethanol and biodiesel production. However, its use of edible biomass (i.e., starch and sugar) as a feedstock increases production costs, competes with food security, and requires significant amounts of land, water, and fertiliser for production (Alalwan et al., 2019). Second-generation technologies exploit inedible lignocellulosic biomass, representing more sustainable renewable feedstocks (Alalwan et al., 2019). Three second generation technologies capable of upgrading lignocellulosic biomasses exist: biochemical processing (lignocellulosic fermentation), thermochemical processing (chemo-catalytic technologies), and hybrid processing (gasification followed by gas fermentation). Table 2.1 summarises these three technologies, including their advantages and disadvantages.

Table 2.1: Comparison of lignocellulosic biomass utilisation technologies. Details taken from (Daniell et al., 2012; De Buck et al., 2020).

	Biochemical *(lignocellulosic fermentation)*	**Thermochemical** *(catalytic technologies)*	**Hybrid** *(gas fermentation)*
Process description	1. Biomass is delignified by a pre-treatment step 2. Hydrolysis of hemicellulose and cellulose to sugars 3. Fermentation 4. Product recovery	1. Biomass drying and size reduction 2. Gasification to produce syngas 3. Syngas upgrading: • Particulate removal • Water gas shift 4. Syngas upgrading over a metal catalyst 5. Product separation	1. Biomass drying and size reduction 2. Gasification to produce syngas 3. Gas is treated to remove impurities 4. Gas fermentation 5. Product separation
Advantages	• High selectivity • Mild operating conditions	• Established technologies exist for fossil feedstocks • All carbon content converted to syngas	• All carbon content converted to syngas • Mild operating conditions • High selectivity • Flexible CO:H_2 ratios
Disadvantages	• Pre-treatment step is costly and complex • Hydrolysis inhibit enzyme activity • Cannot use lignin fraction for chemical production	• Low selectivity • Low tolerance for inhibitors, complex (expensive) gas clean-up required • Higher temperatures and pressures	• Hydrogen cyanide inhibits microbes • Mass transfer limitations between gas and liquid

		• Requires specific CO:H_2 ratios	

Biochemical processing (lignocellulosic fermentation) has been extensively researched. However, expensive and complicated pre-treatment methods currently hinder commercialisation (Preethi et al., 2021). A further disadvantage of this technology is its inability to exploit the lignin fraction of a feedstock (Liew et al., 2016). Contrastingly, both thermochemical and hybrid technologies originate from biomass gasification, enabling the full exploitation of the feedstock. In addition, both these technologies can exploit waste gas streams as well as lignocellulosic feedstocks (Daniell et al., 2012). Whilst thermochemical technologies have the advantage of being established for fossil fuel feedstocks, the technology's harsh operating conditions, low tolerance to inhibitors, and specific CO:H_2 requirements are inherent disadvantages (Daniell et al., 2012). Hybrid processing (gas fermentation) operates at low temperatures and pressures, can handle chaotic inputs, and tolerates contaminating products in the gas stream (Fackler et al., 2021). However, gas-liquid mass transfer limitations, low productivity, and high production costs remain current challenges.

Successful process scale-up of microbial processes is highly dependent on the development of a conceptual process and Techno-Economic Analysis (TEA) prior to undertaking laboratory experiments (Crater & Lievense, 2018). These analyses provide technology targets to guide research and development efforts. The need for these analyses is emphasised in both the UK Chemical Sector's Decarbonisation Roadmap (BEIS, 2017) and E4Tech's evaluation of the UK's Top Bio-based Chemical Opportunities (E4tech, 2017). Importantly, TEAs are often iterative processes whereby process changes are made upon determining the economic outcome and primary cost drivers, depicted in the flow diagram in Figure 2.1. However, there is no methodological standard for TEAs. Whilst most academic TEAs follow practices outlined in engineering textbooks, there is still room for choices and assumptions to be made (Zimmermann et al., 2020). Furthermore, the range of applications of TEAs means the assumptions, scenarios considered, and scope of analyses differ between studies.

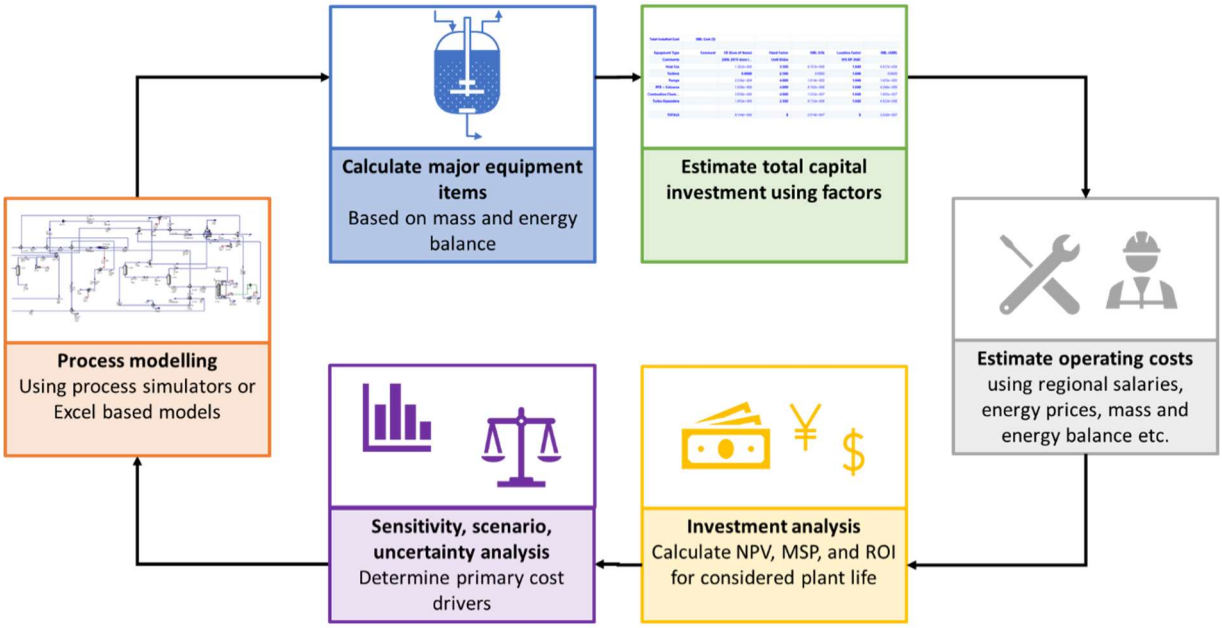

Figure 2.1: Flow diagram of overall TEA methodology

The first section of this review covers TEA methods and recent advancements in this field. Since gas fermentation is the central technology evaluated in this thesis, a comprehensive

review of TEAs related to gas fermentation is provided. This detailed review offers insights into the diverse objectives of differing TEA studies, the various tools employed in these studies, and the differing outcomes that can be achieved. Lastly, the review includes an overview of TEAs applied to Supercritical Water Gasification (SCWG), providing information on the current status of the technology and assessments in this area.

2.1 Techno-economic analyses methods and advancements

This section reviews the literature on TEA methods, trends, and advancements to these methods within bioconversion processes. The review scope is depicted in Figure 2.2 and covers process modelling, cost models, product price considerations, performance metrics, sensitivity, scenario, and uncertainty analyses, and lightweight assessment tools.

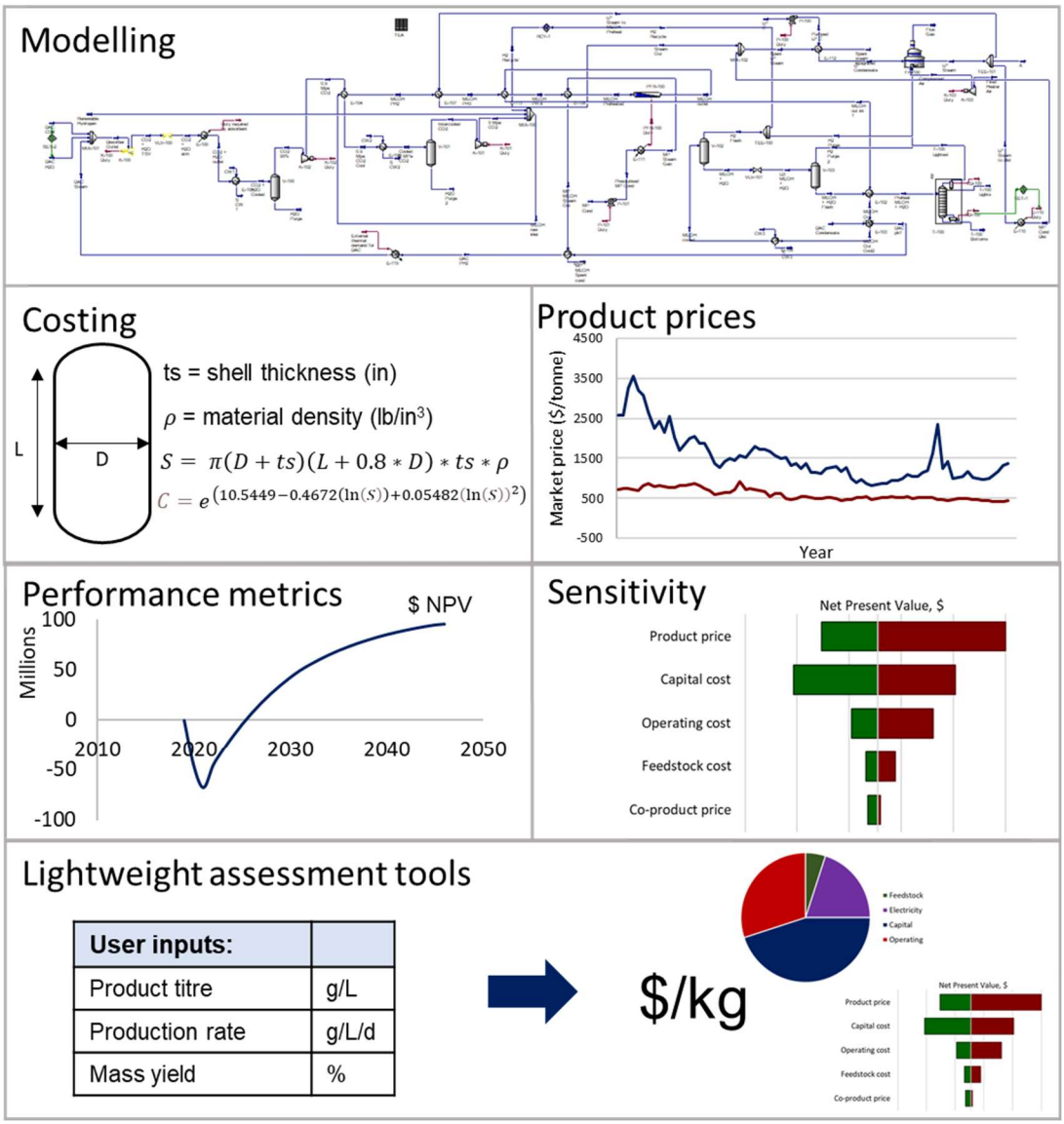

Figure 2.2: Scope of techno-economic analysis literature covered.

2.1.1 Process modelling

Techno-economic analyses conventionally originate from process design and simulation. These simulations typically use commercial software such as Aspen Plus or SuperPro Designer (Scown et al., 2021). Commercial simulators are used to develop rigorous process

models incorporating energy integration, recycle considerations, and complex separation sequences.

Conventional process synthesis methods are time-consuming and require a certain level of expertise to develop realistic and representative process models. To overcome this challenge, there is an emerging trend in developing automated process synthesis methods using Machine Learning (ML). Investigated methods include evolutionary programming (Neveux, 2018), reinforcement learning (Khan & Lapkin, 2022), and transformer-based language models (Vogel et al., 2023a). These methods aim to create, complete, and optimise process flowsheets. With autonomous process design as the ultimate goal, there are ongoing research efforts into creating databases of chemical process flowsheets under standard notation e.g. SFILES 2.0 (Simplified Flowsheet Input-Line Entry-System) (Vogel et al., 2023b), and the use of ontological representations of process (Seidenberg et al., 2023). A standard representation of flowsheets would allow ML algorithms to leverage existing fundamental process knowledge. These approaches require minimal user inputs but allow for the synthesis of detailed, optimised process flowsheets. While this research direction is still developing and has not yet been applied to TEAs, its evolution offers the opportunity for emerging technologies to be quickly and rigorously evaluated by non-experts.

Surrogate modelling is also being adopted as a process modelling tool. Surrogate models are approximate models that map the input-output relationship of more complex models (Mcbride & Sundmacher, 2019). They can be used to model complex unit operations in process flowsheets. Replacing rigorous models with surrogates reduces the computational burden of optimisation problems and sensitivity analyses by providing predictions based on different technical parameter inputs without needing to converge a rigorous process simulation. Jiang et al. (2023) recently demonstrated the use of a surrogate model to represent packed bubble column contactors in the optimisation of their CO_2 capture process (Jiang et al., 2023). The surrogate model was developed by firstly creating a physics-based mechanistic model using governing kinetic and mass transport equations. After model validation, the physics-based model was used generate data used to train the surrogate model, which comprised of an ensemble of polynomial response surface, Kriging, radial basis function, support vector regression (SVR), and moving least squares. The surrogate model was then used for the process optimisation, where various contactor design variables including the particle size diameter, bed height, and superficial gas velocity, were optimised. The optimal trade-off solution between CO_2 capture and energy consumption was then used to conduct a TEA. In addition to optimisation, surrogate models are also useful in representing complex reactor units, removing the need to model detailed kinetics or equations. For example, Olafasakin et al. (2021) developed a Kriging-based Reduced Order Model (ROM) to represent the pyrolysis reactor in their economic and emission assessment of gasoline and diesel production from biomass (Olafasakin et al., 2021). The surrogate model was trained to predict the pyrolysis yields based on the biomass composition. The predicted yields were then fed into a process model in Aspen Plus to complete the TEA and Life Cycle Assessment (LCA). Similarly, Fózer et al. (2021) investigated methanol production considering microalgae as a feedstock. An Artificial Neural Network (ANN) was used to represent the SCWG reactor to account for biomass variations. Experimental yields from 55 experimetnal results were used to create the model and the predicted ANN yields were modelled in Aspen Plus using a yield reactor and the resulting simulation was used in the TEA (Fózer et al., 2021).

2.1.2 Cost models

Cost estimation methods vary based on the maturity of the project and available data (van Amsterdam, 2018). The Association for the Advancement of Cost Engineering (AACE) classify estimates from Class 5 to 1, with the purpose of Class 5 being to screen different options and

assess the initial feasibility, and Class 1 being used to check bidding and tender quotes (AACE International, 2020). Class 5 estimates can be undertaken using exponential relationships between plants of different capacities, i.e., the sixth-tenths rule (Sinnott & Towler, 2013). Contrastingly, estimates for Classes 1-3 are based on individually costed equipment from detailed mass and energy balances (AACE International, 2020). For emerging bioproduction pathways, individual equipment costs are common in TEAs, as exemplified by the National Renewable Energy Laboratory (NREL) reports (Scown et al., 2021). However, models for equipment costs and their translation to the Total Capital Investment (TCI) vary (Brown, 2015), leading to different outcomes for similar pathways. Several studies exist comparing different equipment cost and TCI estimation methods.

Feng & Rangaiah (2011) compared five capital cost estimation programs: CapCost, EconExpert, AspenTech Process Economic Analyzer, Detailed Factorial Program, and Capital Cost Estimation Program (Feng & Rangaiah, 2011). They found variations of up to 200% in individual equipment costs and around 100% in TCI for seven case studies. Symister (2016) also compared equipment cost methods including Aspen Capital Cost Estimator (ACCE), module costing (Turton et al., 2013), and factorial costing (Sinnott & Towler, 2013). Note that the ACCE software is an advancement of AspenTech Process Economic Analyzer, analysed by Feng & Rangaiah (2011). The ACCE estimates were used as the benchmark for the comparison. However, on average, the ACCE method was found to produce the lowest equipment cost estimates of the three results. The ACCE database claims not to rely on capacity factor curves and uses a comprehensive design-based installation model (AspenTech, 2012). However, it's black-box nature means the underlying calculation methods are unknown by the user. This is unlike cost correlations where the driving force (size factor) for the equipment is known, facilitating an understanding between design decisions and cost during process development.

Common methods to translate collective equipment costs to the TCI include the Lang factor based, detailed factorial based, or module costing methods (Feng & Rangaiah 2011). The Lang factor and detailed factorial methods are both factorial-based methods. Lang factor methods, first introduced by Lang (Lang, 1947), apply a universal factor to the equipment cost to achieve the TCI. Detailed factorial methods were first developed by Hand (1958) and apply individual factors specific to the equipment type to determine the TCI. However, as these methods have evolved different factors have been proposed and adopted. A detailed review of the evolution from these original methods is provided in (van Amsterdam, 2018). Contrastingly to the latter two methods, module costing, introduced by Gurthie (Guthrie, 1969), uses costing data from vendor quotes and literature. Costs are then scaled using factors specific to the material of construction, operating pressure, and temperature (Symister, 2016). Brown (2015) compared TCI computation methods using different Lang factors for six biofuel production facilities and observed differences up to $320 million. van Amsterdam (2018) compared six different equipment cost and TCI models for twelve case studies. In all cases significant differences were observed between the estimation methods. Similarly to Feng & Rangaiah (2011), greater variability was observed between individual equipment types than between overall plant estimates. When comparing the results to the actual plant costs the average of the six estimation methods had a lower absolute error compared with the individual method's absolute errors. van Amsterdam (2018) suggested that an analysis considering multiple factorial based methods to derive a range of total estimates would improve overall estimation accuracy. Using this approach, if estimates were found to vary significantly the practitioner is made aware that greater uncertainty exists around the estimated cost for the investigated project.

After computing the TCI, another cost factor impacting the investment analysis of a technology are fixed operating costs. Models to compute these costs are functions of both the TCI and estimated operating labour. Similarly to equipment costs and TCI, there are numerous reported factors to compute these costs. However, there is a lack of comparative studies evaluating these costs and their impact on techno-economic outcomes.

Cost engineering's progress is currently hampered by limited industry cost data (van Amsterdam, 2018). Costing correlations are largely based on historic data, for example the cost correlations by Seider et al. (2017) are based on the data in 13 publications between 1949 and 2003 (Seider et al., 2017). In contrast, costing software programs can periodically update methods based on new data and vendor quotes. However, the data and methods behind these programs are proprietary, resulting in limited information available on the estimation models' underlying methods. Increased transparency in capital costs from commercial processes would improve costing methods specific to bioprocesses. The process block method for costing early-stage biorefineries developed by Tsagkari et al. (2020) is an example of exploiting recent costing data. The approach uses module costing where different unit operations or processing sections i.e. saccharification, anaerobic fermentation, distillation, and dehydration are costed based on a reference capacity price and updated using an appropriate exponent. To determine the reference costs and exponents, data was collected from two databases consisting of plant costs from press releases for 331 commercial scale biorefineries and 39 Information Handling Services (IHS) Markit reports. The data from the IHS reports was used as the reference capacities and costs for the analysis and the exponents were determined by minimising the error between the summed total cost of the process blocks and the reported total capital investment from the 331 collected commercial plant costs. The method was evaluated on a biodiesel plant and demonstrated on a pioneering Polyhydroxybuturate (PHB) plant (Tsagkari et al., 2020). However, a limitation of this method is that costs reported in press-releases may be unrepresentative of the final plant cost and/or different companies may include different cost representations in their publicly released costs. Another recent costing development for bioprocesses was study undertaken by Humbird et al. (2017), the study aimed to reduce uncertainty surrounding bioreactor capital cost estimates in TEAs (Humbird et al., 2017). An in-depth analysis of aeration costs in aerobic stirred-tank and bubble column bioreactors was undertaken in Aspen Plus. Simulations were developed based on oxygen mass transfer correlations as a function of aeration rate and power input and their cost estimates developed in ACCE were validated against vendor quotations.

Equipment cost and cost model methods exhibit considerable variability, whilst some work has been undertaken to compare methods and develop correlations specifically for bioprocesses there is a lacking consensus on preferred models for project evaluation. This highlights the importance of detailing methods, assumptions, and factors in TEAs to enable comparisons. NREL's benchmark studies adopt this approach, and their transparency is partially responsible for the success of their analyses (Scown et al., 2021). The reviewed literature comparing costing models consists of two master's theses (van Amsterdam, 2018; Symister, 2016), one magazine article from The Chemical Engineer (Feng & Rangaiah, 2011), and one journal article on TEAs (Brown, 2015). This suggests that despite the observed variability in cost models, the impact of model selection and assumptions is seldom discussed or investigated in TEA literature.

2.1.3 Product Prices

The price used for the product being considered in a TEA significantly influences the economic outcome. Given that analyses are usually considered over a 20-25 year project life to calculate the project's Net Present Value (NPV), product prices are subject to fluctuations, leading to considerable uncertainty. Long-term prices to input into these analyses are selected by the

TEA practitioner. Unfortunately, finding references to representative prices can be challenging, and there is often uncertainty regarding the reliability of the source, geographic location, and time frame for which the price is representative (Hubbard, 2018). Moreover, while the Minimum Selling Price (MSP) calculation avoids inputting prices into TEAs, contextualising the obtained MSP necessitates representative market prices. Various approaches used to select prices in existing TEAs include averaging prices from Alibaba (Moncada et al., 2018), using individual market values (Bastos et al., 2022), averaging prices across the previous year (Okoro et al., 2020), and referencing industry reports (de Medeiros et al., 2017).

Although the non-stationary nature and uncertainty surrounding commodity prices is not commonly applied in TEA literature, several studies have considered it. For instance, Manca et al. (2011) proposed forecasting the price of a reference component (crude oil) and correlating the future costs of other commodities to this using an Autoregressive Distributed Lag model (Manca et al., 2011). They used a stochastic Markovian process to produce a price projection for the reference component and employed Monte Carlo methods to generate a distribution of prices (Manca, 2012). This was developed into a systematic framework to inform optimal plant designs under market uncertainty and has been applied to case studies such as styrene monomer manufacturing (Barzaghi et al., 2016), the cumene process (Sepiacci et al., 2017), and a CO_2 separation process (Gutierrez et al., 2019). However, a drawback of stochastic modelling is the inability to exploit deterministic trends within the historic time series.

Another approach is the use of traditional stochastic/econometric modelling. In assessing bioethanol production, prices for feedstock, bioethanol, soya oilcake, electricity, and petroleum were stochastically modelled using a multi-variate empirical distribution based on 1999-2008 historical fluctuations (Amigun et al., 2011). Yao et al. (2017) conducted statistical tests for each commodity, determining the best method to represent historical price trends and incorporated these models into their stochastic TEAs (Yao et al., 2017). Geometric Brownian motion and a PERT distribution were used to represent jet fuel price growth (McGarvey & Tyner, 2018). Ioannou et al. (2018) compared different econometric models to project electricity prices in an economic assessment of offshore wind energy production (Ioannou et al., 2018). Nguyen and Tyner (2021) employed @Risk software to project jet fuel and carinata oil prices. The two series were found to be non-stationary and follow random walk. However, a trend was observed between historic soybean oil and jet fuel. As such, the projected distribution was produced to ensure that each commodity's historic probability distribution function and the trend between the commodities was maintained. Puig-Gamero et al. (2021) considered damped trend, local linear trend, and local linear trend with cycle. A gaussian distribution of the projected pricing errors based on the historic data was produced and used in the Monte Carlo simulation. These studies all utilise different approaches, indicating that no single econometric method is applicable to all commodities, necessitating statistical tests to prepare and analyse the data. Additionally, these methods often assume near-linear time series and may not capture complex long-running features.

Some studies have made use of the Energy Information Administration's (EIA) price projections to account for future prices. Zhang et al. (2013) used the EIA's petroleum prediction and correlated other commodity prices to it in their TEA (Zhang et al., 2013). The disadvantage of this approach is the EIA's projections are point forecasts, neglecting probabilistic uncertainty (Kaack et al., 2017) required for use in an uncertainty analysis. However, Brown and Wright (2015) used the EIA's projections to aid their simulated future commodity prices (Brown & Wright, 2015). The prices were projected using a random walk with drift. The random changes were based on the probability density function of historic prices and the drift ensured the mean of monthly price distributions matched the EIAs 2013-2032 projections.

Notably, whilst future price considerations are not commonplace in TEA literature, those studies that have considered it have all adopted different approaches. A standard method to account for price and distribution variability across a plant's life would facilitate its widespread consideration in future TEA studies. However, of the outlined methods only purely stochastic processes are applicable to any time series. A major disadvantage of this is its inability to exploit any underlying trends within the commodity's price data. Despite not being currently adopted in TEAs ML methods are widely applied in price forecasting fields to predict future commodity and energy prices (Wu et al., 2019). These methods are able to accommodate non-linear, non-stationary, and complex sequences, making them applicable to any time series. In addition, contrastingly to stochastic methods, ML can exploit the underlying trends within a time series. ML therefore offers the opportunity to standardise price selection procedures in TEAs.

2.1.4 Technical performance metrics

Technical performance metrics are a key comparative indicator between technologies. Common metrics include energy and carbon efficiency. Energy efficiency is a measure of the amount of energy in the feedstock that ends up in the final product and is often reported in biofuel TEAs (Dimitriou et al., 2018). Similarly, carbon efficiency is the measure of carbon in the initial feedstock that is retained in the final product (Pandey et al. 2022). Reporting these metrics provides key process information that relates to resource usage and enables technology comparisons that aren't solely based on economic metrics.

2.1.5 Economic metrics

Various economic metrics can be employed to quantify a process' profitability. The payback period (equation 2.1) and return on investment (equation 2.2) are more commonly computed in industrial settings where private companies are evaluating potential investments (Scown et al., 2021).

MSP, the most commonly reported metric in TEAs, is calculated based on the price required to obtain an NPV (equation 2.4) of zero at the end of plant life, using a specified discount rate. For biorefinery processes, the discount rate is often set as 10% to remain consistent with the Biofuels Techno-Economic Analyses database (Kinchin, 2020). However, for certain technologies governing bodies publish specific discount rates, for example anaerobic digestion (8.3%) and renewable electricity from biomass (7.9%) (BEIS, 2020). MSP has been argued to be a more interpretable metric than NPV, particularly when the NPV is negative, as is often the case with emerging technologies (Zhao et al., 2016). For example, NREL's TEAs present MSP results along with a breakdown of the corresponding cost contributors. However, MSP is highly sensitive to co-product prices and yields, which can lead to potentially misleading results (Pereira et al., 2017). Moreover, assessing the profitability of the process according to the reader's personal views on future fossil fuel prices introduces subjective judgment, impacting the perceived market competitiveness (Zhao et al., 2016).

Similar to MSP, levelised costs are a metric representing the average production cost of a product over the lifetime of the plant. A predefined discount rate is used to discount both the annual costs and production volume (equation 2.1). Levelised costs are commonly reported in the context of energy projects e.g., hydrogen production and renewable electricity production.

$$Levelised\ cost = \frac{\frac{annaul\ cost\ (\$)}{(1+discount\ rate)^{years}}}{\frac{annual\ production\ (kg\ or\ kw)}{(1+discount\ rate)^{years}}} \quad (2.1)$$

$$Payback\ period\ (yr) = \frac{Tocal\ capuial\ investment\ (\$)}{Annual\ average\ net\ cash\ flow\ (\$/yr)} \quad (2.2)$$

$$Return\ on\ investment\ (\%) = \frac{Annual\ net\ profit\ (\$)}{Total\ capial\ investment\ (\$)} \quad (2.3)$$

$$Net\ present\ value = \frac{net\ cash\ flow\ (\$)}{(1+discount\ rate)^{years}} \quad (2.4)$$

NPV rigorously assesses process profitability by considering the time value of money and requires a selling price to be input for all products, thereby eliminating co-product bias or subjective interpretation of the economic viability. One disadvantage of this approach is that it is heavily influenced by the scale of the initial investment. Therefore, when comparing technologies with different capital requirements, the NPV can vary significantly.

Evidently, the computation of a single metric when analysing a process can be misleading. Calculating multiple metrics is recommended for a comprehensive analysis. The study into polybutylene succinate from food waste by Naveenkumar & Jeehoon (2023) is an example of the utility of computing multiple metrics. Naveenkumar & Jeehoon (2023) reported the MSP: $ 3.5/kg, NPV: $ 58.9 Million, return on investment: 15.79 %, payback period: 6.33 years, and Internal Rate of Return (IRR): 16.48 % (Naveenkumar & Jeehoon, 2023). Presenting these metrics together offers greater insight into the process's economic feasibility than individual metrics. For instance, a standalone MSP of $3.5/kg lacks interpretational context without market price information. However, combining this with an NPV of $58.9 million, evidences the profit-generating potential. Additionally, a payback period of 6.33 years indicates early profitability in the plant's lifespan. Furthermore, an internal rate of return of 16.48% demonstrates that the process exceeds the commonly adopted 10% discount rate, suggesting that it generates sufficient income to attract investment.

2.1.6 Sensitivity, scenario, and uncertainty analyses

The number of assumptions required to generate a process model, cost the proposed plant, and undertake an investment analysis leads to inherent uncertainty around TEA outcomes. To account for this, single-point sensitivity, scenario, and global uncertainty analyses are generally undertaken. These analyses highlight the most influential variables and frame the TEA within a band of uncertainty based on initial assumptions and calculations. Figure 2.3 illustrates the differences between these analyses considering NPV as the objective function. During a sensitivity analysis, parameters are independently varied between two bounds to show the individual impact of each variable on the objective function. Scenario analysis involves the use of a combination of variables at once. These scenarios often represent either a pessimistic, base, and optimistic cases for a technology, or the current state of technology and different outlooks into the future. Uncertainty analyses (or Monte Carlo simulations) vary the chosen parameters simultaneously within a defined probability distribution. Uncertainty analyses are more extensive, providing a probabilistic distribution of the chosen objective function (Scown et al., 2021), commonly NPV or MSP.

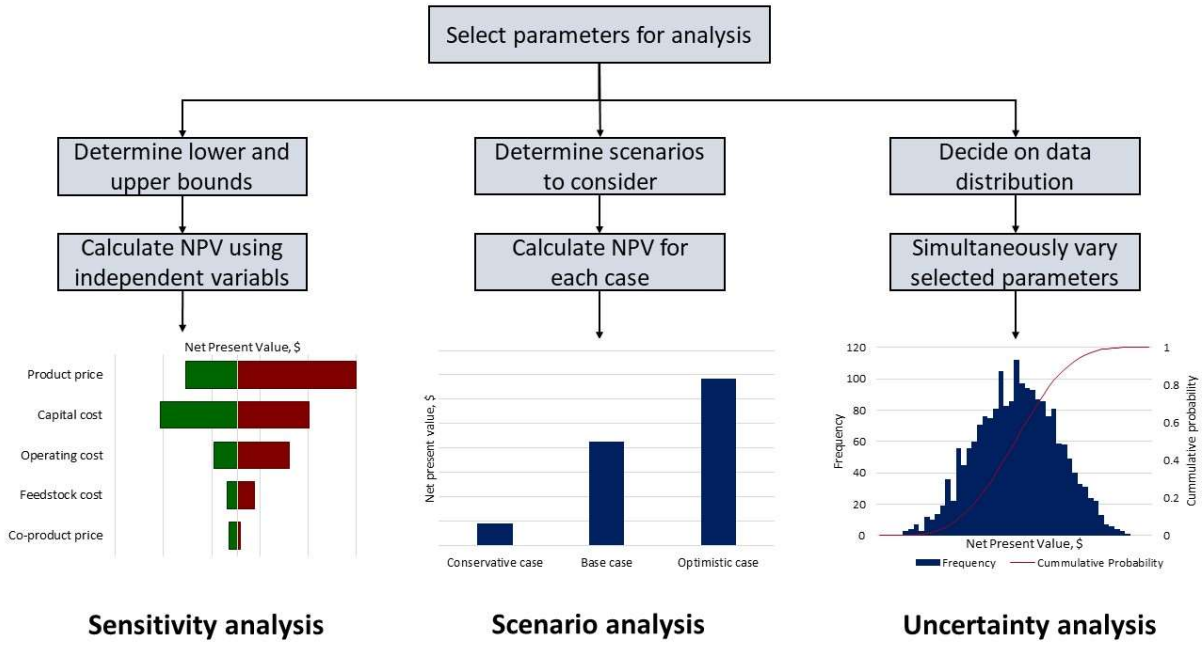

Figure 2.3: Difference between sensitivity, scenario, and uncertainty analyses. NPV is used as the objective function for illustrative purposes.

Single point sensitivity analyses are typically employed in NREL reports. In the Humbird et al. (2011) report for lignocellulosic ethanol, technical parameters and capital costs were varied within defined ranges to determine their impact on the MSP. Parameter ranges were based on anticipated deviations from pilot-scale demonstration runs, with 2012 performance targets as baselines. In TEA literature ranges for sensitivity analyses are often uniformly applied to parameters. For example, in the study into 1,3-butadiene and ε-caprolactam production from C6 sugars an arbitrary ±50% variation was used for the feedstock, utility, product prices and capital investment cost (Moncada et al., 2018). The base values for each parameter were taken from academic literature, textbooks, and price indices. A similar approach was taken in the TEA for combined oil and power production from biomass (Khan et al., 2023). The majority of cost and pricing parameters were varied ±30% with the exception of operating hours and capital costs which were varied ±10% and ±50%, respectively. Nonetheless, the uniform application of parameter ranges might yield unrepresentative results, especially when positive and negative deviations are not equally realistic, as demonstrated by capital cost overruns (Brown, 2015).

A scenario analysis is similar to a sensitivity analysis in that it is deterministic. However, unlike a sensitivity analysis a set of parameters are changed simultaneously to represent a defined case. This analysis can be used to demonstrate the future potential of a technology based on achieving certain targets. For example, Fei et al. (2020) included a scenario analysis in their TEA for lactic acid production from natural gas (Fei et al., 2020). They considered four cases, ranging from the current technology state to long-term scenarios with ideal targets. The MSP ranged from $24.39 to 2.17/kg, showing both potential and necessary technological advancements for commercial viability.

Uncertainty analyses (or Monte Carlo simulations) stochastically vary all considered parameters within defined ranges and distributions, resulting in a probability distribution of the objective function (commonly MSP or NPV). These analyses allow the uncertainty surrounding the TEA outcome to be quantified. For example, in the TEA by Campbell et al., (2018) into biofuel and biochar production from forest biomass the case presenting the highest likelihood

of profitability achieved a mean NPV of $45.1 million with 90% of outcomes between −$34 million and $139 million (Campbell et al., 2018). The case demonstrated a 20% likelihood of achieving a negative NPV. By framing the mean NPV with the 90% probability band the uncertainty and risk surrounding the nominal result is quantified. A challenge with these analyses is obtaining probability distributions for input parameters. Commonly, triangular and normal distributions are used in TEAs (Barahmand & Eikeland, 2022), requiring median, lower, and upper bounds. As discussed in Section 2.1.3 Product prices, some studies have undertaken statistical tests to obtain a probability distribution that represents the deviations observed in historic commodity pricing data (Amigun et al., 2011; McGarvey & Tyner, 2018; Yao et al., 2017). However, in the absence of estimated and actual cost data for commercial projects this cannot be quantified for other parameters such as fixed capital and operating costs.

Combined sensitivity and uncertainty analyses are also often undertaken in TEAs, examples of these are both the assessment of different biomass to liquid routes by Dimitriou et al. (2018) and the cyanobacteria biorefinery assessment by Beattie et al. (2021). A sensitivity and uncertainty analysis was undertaken by Dimitriou et al. (2018). However, when comparing the analysis outcomes, it was found that the deterministic base case result was lower than the median value determined by the sensitivity analysis (Dimitriou et al., 2018). Beattie et al. (2021) firstly undertook a sensitivity analysis to determine the most influential parameters for use in the Monte Carlo uncertainty analysis (Beattie et al., 2021). Similarly to Dimitriou et al. (2018), they found a large discrepancy between the lower, median, and upper Monte Carlo results compared with the conservative, base, and optimistic scenario (determined from the sensitivity analysis). This suggests that deterministic scenario and sensitivity analysis can often lead to over- and under-estimation of the range of TEA outcomes. An alternative to undertaking these analyses separately is to extract the relative importance of each variable from the uncertainty analysis results. This has been undertaken in several studies (McGarvey & Tyner, 2018; Campbell et al., 2018) and removes the unrepresentative range potentially presented by a single-point sensitivity analysis.

Some studies have considered technical parameters in addition to economic parameters in sensitivity and uncertainty analyses (Humbird et al., 2011; Beattie et al., 2021). However, flexible process models are required to compute the uncertainty associated with technical parameters such as feedstock variability, reactor performance, and process conditions. Several stochastic TEAs have been developed using rigorous simulation software. For example, Salman et al. (2020) undertook a TEA on a waste to biofuel facility which considered various feedstock compositions, pressure and temperature deviations, and economic parameters (Salman et al. 2020). The process model was created in Aspen Plus and deviations in feedstock composition and processing conditions were updated using the Aspen Simulation Workbook in Excel. The mass and energy balance results were then passed from the Aspen Simulation Workbook to MATLAB where the economic and uncertainty outcomes were computed. Similarly, Baral et al. (2019) undertook a stochastic TEA for bio-jet fuel production using SuperPro Designer (Baral et al. 2019). Feedstock, technical, and economic parameters were varied by connecting the simulation to Excel. The TEA was undertaken in Excel and the outcomes from the 5,000 simulations using different parameter combinations were used to generate the Monte Carlo distribution of the MSP. However, as Monte Carlo simulations require thousands of simulations to run these analyses are computationally expensive. ML surrogate models or ROMs representing rigorous simulations can be used to reduce the computational expense. Li et al. (2021) developed a general framework for techno-economic uncertainty analysis based on the creation of a ROM in Excel to represent the rigorous process model in Aspen Plus. The framework was demonstrated for a Hydrothermal Liquefaction (HTL) facility producing biocrude (Li et al., 2021). The analysis considered the

impact of uncertainties in feedstock composition, HTL yield, aqueous-phase product treatment, utility consumption, and equipment sizing and costing on MSP. Use of the ROM to represent the process simulation reduced the computational time for the uncertainty analysis by 2,000 times, emphasising the potential benefits of implementing reduced models.

2.1.7 Lightweight assessment tools

Early-stage technology analyses promote economically driven research and development. However, undertaking TEAs is time consuming and requires engineering knowledge and economic modelling expertise (Huntington et al., 2023). This hinders technology assessment by non-experts i.e. experimentalists and industrialists. As such, there is a trend in developing simplified methods and tools to assess bioprocesses.

Specifically for bioreactors, Dheskali et al. (2020) developed an equation-based model to estimate the capital cost and utility usage and costs of a typical biotransformation technology (Dheskali et al., 2020). Response surface methodology was used to determine the relationship between utility consumption and fixed capital investment. Experimentally obtained data for the fermentation time, final broth concentration, and the aeration rate were used to build the models. The proposed model consists of three equations requiring fermentation time, final broth concentration, and the aeration rate as inputs, outputting the estimated capital and utility costs. The model's ease of use allows for the simple comparison of technologies and to quantify cost reductions attainable through process improvements facilitating targeted research and development.

With regards to publicly available models, Viswanathan et al. (2020) developed ESTEA2 (Early State Technoeconomic Analysis, version 2) which is a spreadsheet-based platform that computes a process's MSP based on minimal user inputs. The model includes both fermentation and catalytic processes, as well as downstream processing. During tool development the model was validated against literature estimates, SuperPro Designer, and other third-party process models for ethanol and sorbic acid production (Viswanathan et al., 2020). BioSTEAM is a python-based platform developed for early-stage technology comparison (Cortes-Peña et al., 2020). The tool incorporates uncertainty to demonstrate the relative importance of different parameters based on their impact on the process's MSP. The tool was validated against SuperPro Designer results for biodiesel and ethanol production from lipid cane. Further work is being undertaken to add an LCA component to the platform and create a web-based interface to allow wider adoption of the tool. The Bioprocess TEA calculator is an online calculator for early-stage TEAs specifically tailored to aerobic bioprocesses, with plans to expand its application (Lynch, 2021). In contrast to other tools its primary purpose is to translate financial outcomes to technology targets. The tool identifies the most important variables limiting commercial success of a technology and proposes targets for these. The tools utility is demonstrated by reviewing the commercial targets for aerobic production of diethyl malonate.

While lightweight TEA models offer quick estimations, comparisons, and suggest research targets, their usability may compromise accuracy (Scown et al., 2021). Furthermore, they lack flexibility to implement heat and mass integration, which could improve process economics. One approach to overcome this reduced accuracy is the use of ML methods. By mapping inputs to outputs ML can be used to represent rigorous process simulations. Huntington et al. (2023) demonstrated this with a surrogate model representing a TEA for lignocellulosic bioethanol production. Their model, based on SuperPro simulations, was developed using 10,000 simulations with different operating and cost parameters. The operating parameters allowed adjustments to plant throughput, feedstock composition, conversion efficiencies, and cost considerations. Their method used the Tree-Based Pipeline Optimisation Tool

considering four ensemble regression models, Random Forests (RF), Stacking, Extra Trees, and Gradient Boosting. The surrogate model was trained to predict the MSP and mass and energy balance outputs. While this approach maintains rigorous economic assessment, it lacks the flexibility to be used to evaluate other processes. Furthermore, a significant number of simulations are required to produce a surrogate model that can predict over the desired parameter ranges.

2.2 Gas fermentation techno-economic analyses and commercial status

The following section provides a comprehensive review of the literature on existing TEAs of gas fermentation technologies for biofuel and biochemical production considering gaseous mixtures of CO, CO_2, and H_2 as a feedstock. Note that TEA studies solely investigating microbial electrosynthesis and photosynthetic bacteria considering the use of photobioreactors or open ponds for cultivation are excluded from this review. Table 2.2 presents the gas fermentation TEA studies included. Greater detail on these studies, their purpose, key findings and TEA tools employed is discussed in the following sections. A brief summary of the current commercial status of gas fermentation is also included. A generic block flow diagram illustrating the major steps involved in gas fermentation is presented in Figure 2.4.

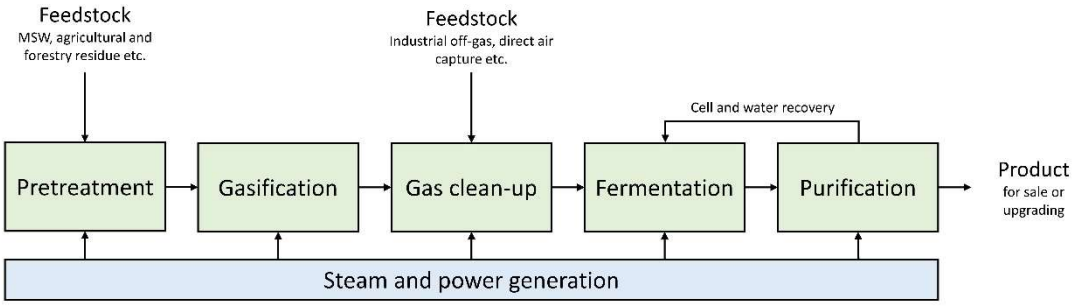

Figure 2.4: Gas fermentation block flow diagram.

To summarise the overall findings, out of the 24 studies analysed, 16 consider ethanol as the fermentation product. However, higher value products are likely to have a more favourable economic outlook. As suggested by Regis et al. (2023) biofuels can be used as starting points for higher-value chemicals, listing butanol and 1,3-butadiene as examples (Regis et al., 2023). Notably, two previous studies have explored the catalytic upgrading of ethanol to higher value products, one to ethylene (Haro et al., 2013), and the other to distillate range fuels (Tan et al., 2016). In the studies evaluated, the most commonly computed performance metric is MSP. However, the reported MSP's for the same products vary appreciably between studies (e.g. \$0.31-\$2.52/L for ethanol). This is likely due to variations in cost models, technology assumptions, feedstock, and location considerations between studies.

While only five previous studies consider an LCA in conjunction with the TEA, eight studies comment on the technology's CO_2 reduction potential. The United States is the most commonly reported plant location, however several studies left this undisclosed. In addition, woody biomass and agricultural residues form the majority of the investigated feedstocks, with a few studies considering off-gas streams. Aspen Plus was the most commonly adopted modelling software. Considering sensitivity analyses, single point analyses was the most commonly employed. Most studies have considered solely financial parameters as part of the sensitivity analysis with only four studies including technical parameters, likely attributed to the complexity in modelling changes associated with technical parameters.

Table 2.2: Summary of existing techno-economic analyses of gas fermentation

Study	Modelling	Bacteria	Feedstock	Product	Capacity	Location	Performance metrics	Sensitivity analysis	LCA
(Piccolo & Bezzo, 2009)	Aspen plus	*Clostridium ljungdahlii*	Woody biomass	Ethanol	700,000 t/yr of dry biomass	-	NPV: -€48.9 M IRR: 7.7% ROI: 20.2 % Using €0.68/L ethanol price	• Scenario analysis • Single point	×
(Choi et al., 2010)	Aspen plus	*Rhodospirillum rubrum*	Switchgrass	PHA	12 t/d PHA production	US	MSP: $1.65/kg	• Single point	×
(Haro et al., 2013)	Aspen Plus	Not specified	Not specified	Ethylene	300 to 1000 ML/year	-	Production cost: € 0.535-0.563/kg	• Plant capacity	×
(Khan et al., 2014)	Aspen Plus	*Cupriavidus necator* *Rhodobacter Capsulatus*	CO_2 from a power plant	Botryococcene	5000 bbl/day	-	Production cost: $127/bbl-fuel Assuming electricity cost <2¢/kWh	• None	×
(Roy et al., 2015)	Aspen Plus	*Clostridium ljungdahlii*	Miscanthus	Ethanol	158–171 t/day dry biomass	Canada	Production cost: $ 0.78- 0.9 /L	• Single point	✓
(Levett et al., 2016)	Aspen plus	Methanotroph	Methane	PHB	100,000 t/a PHB	US	MSP: $4.1–$6.8/kg	• Single point	×
(Christodoulou & Velasquez-Orta, 2016)	-	Clostridium	CO and H_2O	Acetic Acid	100 t/yr acetic acid	UK	Production cost: £ 4.14/kg	• None	×
(Tan et al., 2016)	Aspen plus	*Clostridia*	Wood chips	gasoline, jet and diesel blendstocks	2000 t/d dry biomasss	US	MFSP: 3.40-5.04 $/GGE	• Co-product pricing	✓
(Benalcázar et al., 2017) Note: production costs are approximated from graphical data	Aspen plus	Acetogenic bacteria	Pine	Ethanol, 2,3-Butanediol, Hexanoic acid	Equivalent syngas capacity to produce 240000 m^3 y^{-1} of ethanol	Netherlands	Production costs: Ethanol: $ 1.15/kg, 2,3-Butanediol: $ 1.4/kg Hexanoic acid: $ 1.6/kg	• Single point • Technical parameters	✓
			Corn stover				Production costs: Ethanol: $ 1.3/kg 2,3-Butanediol: $ 1.5/kg Hexanoic acid: $ 1.8/kg		
			Sugarcane bagasse				Production costs: Ethanol: $ 1.25/kg 2,3-Butanediol: $ 1.5/kg Hexanoic acid: $ 1.7/kg		
			Eucalyptus				Production costs: Ethanol: $ 1.25/kg 2,3-Butanediol: $ 1.45/kg Hexanoic acid: $ 1.7/kg		
			Sugarcane bagasse			Brazil	Production costs: Ethanol: $ 1.05/kg		

Study	Modelling	Bacteria	Feedstock	Product	Capacity	Location	Performance metrics	Sensitivity analysis	LCA
							2,3-Butanediol: $ 1.25/kg Hexanoic acid: $ 1.4/kg		
			Eucalyptus				Production costs: Ethanol: $ 1.1/kg 2,3-Butanediol: $ 1.25/kg Hexanoic acid: $ 1.45/kg		
			Pine			US	Production costs: Ethanol: $ 0.9/kg 2,3-Butanediol: $ 1.1/kg Hexanoic acid: $ 1.3/kg		
			Corn Stover				Production costs: Ethanol: $ 1.05/kg 2,3-Butanediol: $ 1.2/kg Hexanoic acid: $ 1.35/kg		
(de Medeiros et al., 2017)	Aspen plus	*Clostridium ljungdahlii*	Bagasse	Ethanol	624 t/d dry biomass	Brazil	MSP: $ 0.706 /L	• Monte Carlo simulation	×
(Redl et al., 2017)	Aspen plus and SuperPro Designer	*Moorella thermoacetica*	basic oxygen furnace gas	Acetone	30 kt/yr	US	Production cost: $ 389 /t	• None	×
			Natural gas				Production cost: $ 1724 /t		
			Corn stover				Production cost: $ 2878 /t		
(Michailos et al., 2019a)	Aspen plus	Acetogenic bacteria	Bagasse	Ethanol	100 t/hr dry biomass	-	NPV: $ 8.5 M ROI: 14.5 % MSP: $ 0.69 /L	• Single point • Monte Carlo Simulation	✓
(Michailos et al., 2019b)	Aspen Plus	Acetogenic bacteria	Woody biomass	Methane	6.25 t/hr dry biomass	UK	MSP: 92.14£/MWh	• Single point • Monte Carlo Simulation • Plant capacity	✓
(Ro et al., 2019)	Gasification - Proe Power Systems'	Acetogenic bacteria	wood	Ethanol	50 million gallons per year (MGY) ethanol 1–2 million gallons per year (MGY) ethanol	US	MSP (50 MGY): $ 2.24-2.36 /gal MSP (1-2 MGY): $ 5.61-5.68 /gal	• None	×
			wheat straw				MSP (50 MGY): $ 2.84-2.96 /gal MSP (1-2 MGY): $ 7.03-7.09 /gal		
			wheat straw and manure				MSP (50 MGY): $ 2.79-2.84 /gal MSP (1-2 MGY): $ 7.31-7.39 /gal		
			Oilseed rape meal				MSP (50 MGY): $ 5-5.13 /gal MSP (1-2 MGY): $ 9.49-9.54 /gal		
			corn stover				MSP (50 MGY): $ 2.54-2.63 /gal		

Study	Modelling	Bacteria	Feedstock	Product	Capacity	Location	Performance metrics	Sensitivity analysis	LCA
							MSP (1-2 MGY): $ 6.68-6.79 /gal		
(Okoro & Faloye 2020)	Aspen plus	Acetogenic bacteria	Waste plastic	Ethanol	1000 kg/h	US	IRR: 22.2 % MSP: $ 0.42 /kg	• Single point	×
(de Medeiros et al., 2020)	Aspen plus	Acetogenic bacteria	Syngas	Ethanol	-	Brazil	MSP: $ 1.0–1.3 /L	• Single point • Technical parameters (as part of optimisation)	×
(Huang et al., 2020)	Aspen plus	Acetogenic bacteria	CO_2 from corn mill ethanol	Ethanol	40 M gal/yr corn ethanol	US	MSP: $ 2.84 /gal	• Single point • Technical parameters	×
(Huang et al., 2021)	-	Acetogenic bacteria	CO_2	Acetic acid	200 Million gal/yr bioethanol	US	Current: $ 0.95/kg Future: $ 0.34 /kg Theoretical: $ 0.21/kg	• Single point • Technical parameters	×
				Methane			Current: $ 2.22/kg Future: $ 1.04/kg Theoretical: $ 0.64/kg		
				Ethanol			Current: $ 1.27/kg Future: $ 0.64/kg Theoretical: $ 0.39/kg		
				PHB			Current: $ 1.36/kg Future: $0.64/kg Theoretical: $ 0.37/kg		
(Okolie et al., 2021a)	Aspen plus	Acetogenic bacteria	Glycerol	Ethanol	50,000 t/yr glycerol	Canada	MSP: $ 1.40 /L MSP (inc. CO_2 capture): $ 1.31/L MSP (inc. CO_2 capture and methane upgrading): $0.31/L	• Single point	×
(Petersen et al., 2021)	Aspen plus	Acetogenic bacteria	Invasive alien plant species	Ethanol	37.5 t/hr	South Africa	MSP: $ 0.91/L	• Single point	×
			ferroalloy off-gas		36,131 Nm^3/hr		MSP: $ 0.61/L		
(Ma et al., 2022)	Aspen plus	*Clostridium ljungdahlii*	Woody biomass	Ethanol	200,000 ton/yr	-	Production cost: €430/t	• Technical parameters (as part of optimisation)	×
(Regis et al., 2023)	Aspen plus	*Clostridium ljungdahlii*	Switchgrass	Ethanol	750,000 t/yr dry bimoass	US	MSP (current): $ 1.07/L MSP (2050 H_2) $ 0.71 /L	• Plant scale	×
(Giwa et al., 2023)	Aspen plus	*Clostridium ljundhalii*	Spruce woodchips	Ethanol	2000 t/day dry biomass	Canada	IRR (ethanol from biochar and syngas): 11.93% IRR (ethanol from biochar, hydrogen from syngas): 13.01%	• Single point • Monte Carlo • Simulation Scale	×

2.2.1 Comparative studies

Comparative TEA studies are incredibly important in determining technology advantages, disadvantages, and benchmarking research targets for economic processes. It is difficult to make comparisons across different studies undertaken by different research groups as data assumptions, modelling procedures, and costing models are open to interpretation (Piccolo & Bezzo, 2009). Studies comparing gas fermentation to different biochemical and thermochemical routes are discussed in the following section.

2.2.1.1 Biochemical

The first TEA of gas fermentation compared the production of ethanol from lignocellulosic biomass using both enzymatic hydrolysis followed by fermentation, and gasification followed by gas fermentation (Piccolo & Bezzo, 2009). The analysis revealed that under the considered conditions, neither process was profitable using market prices for ethanol. However, a less negative NPV was achieved for the more mature hydrolysis process (-$22.1 million), compared to the gas fermentation process (-$48.9 million). High capital costs and energy costs to recover the fermentation product were identified as key cost drivers. The authors emphasised the need from improvement in mass transfer limitations and strain resistance to ethanol, as well as the importance of process systems engineering to enhance technologies beyond lab-scale, including modelling, design, and process optimisation.

Choi et al. (2010) conducted the first TEA investigating Polyhydroxyalkanoate (PHA) production via gas fermentation. PHA has similar properties to propylene and can be used as a biodegradable plastic (Choi et al., 2010). In their study, the authors compared the gas fermentation process to their previous sugar-based fermentation TEA. Hydrogen was produced as a co-product from the gas fermentation process and, using a hydrogen selling price of $2/kg, the process achieved an MSP of $1.65/kg, much lower than the authors previously reported $4 - $6/kg for sugar-based fermentation. However, the low MSP was heavily influenced by the hydrogen sales which were produced at a rate of approximately four times that of PHA.

Christodoulou & Velasquez-Orta (2016) compared the production of acetic acid via microbial electrosynthesis and anaerobic fermentation. Their study found neither process to be cost competitive, yielding production costs of £1.44/kg and £4.14/kg for microbial electrosynthesis and anaerobic fermentation, respectively (Christodoulou & Velasquez-Orta, 2016). The higher cost of anaerobic fermentation was attributed to the higher costs of the CO feedstock, £ 18.95 /t (used by anaerobic fermentation) compared with £ 0/t for CO_2 (used by microbial electrosynthesis). The authors then explored an integrated approach where the CO_2 off-gas from anaerobic gas fermentation was utilised as a feedstock for microbial electrosynthesis, doubling the acetic acid production capacity. This configuration led to a cost-competitive process with a production cost of £0.24/kg, compared to the £0.48/kg market price of acetic acid. Notably, when scaling the integrated process up from 2 kt/yr to 200 kt/yr capacity the authors reported a >7 times increase in production cost. This led to the conclusion that the industrialisation of bioprocesses is better suited to small scale high-value chemicals.

2.2.1.2 Thermochemical

In addition to comparing alternative biochemical pathways, several studies have compared thermochemical pathways, including hybrid bio-chemical pathways where the gas fermentation product is upgraded using catalytic technologies.

Haro et al. (2013) investigated the production of ethylene from various bioethanol sources. The bioethanol sources considered were commercial 1st generation ethanol, 2nd generation enzymatic hydrolysis ethanol, 2nd generation syngas fermentation ethanol, and 2nd generation thermochemically derived ethanol (Haro et al., 2013). Ethanol costs, which accounted for 85%

of production costs, were obtained from literature sources, and downstream catalytic upgrading was modelled. The study used a significantly lower price for syngas-derived ethanol ($1/gal, referenced from Coskata) compared to higher values for other technologies (e.g., commercial 1st generation Brazilian ethanol priced at $1.93-$2.35/gal). Whilst the results for combining syngas fermentation with catalytic upgrading to ethylene looked promising, the heavy reliance on the ethanol prices and much higher costs for other ethanol production technologies suggest the ethanol price estimate for gas fermentation from Coskata may be unrealistic. This study therefore highlights the importance of obtaining accurate feedstock and chemical costs when undertaking TEAs.

A comprehensive TEA comparing routes from syngas to distillate-range fuels was undertaken by Tan et al. (2016). Four pathways were compared, including two syngas fermentation pathways and two catalytic syngas technologies, with Fischer Tropsch (F-T) technology used as a benchmark (Tan et al., 2016). The syngas fermentation was based on an anaerobic *Clostridia* organism. Each pathway was modelled and costed in Aspen Plus considering a 2,000 dry tn/day biorefinery. One of the syngas fermentation technologies demonstrated economic competitiveness with the F-T benchmark, achieving ±5% the Minimum Fuel Selling Price (MFSP). The other syngas fermentation technology performed less favourably with a 41% higher MFSP, attributed to the inefficiency of the different catalytic technologies used for upgrading the fermentation product rather than the fermentation itself. Importantly, the capital expenditure for the syngas fermentation route ($478.9 MM) was significantly lower than the alternative high-pressure mixed alcohol synthesis technology ($735.8 MM), highlighting the lower capital of syngas fermentation attributed to the use of lower pressure and temperature conditions. Finally, the study highlighted syngas fermentation's ability to co-produce higher value chemicals as a key advantage of the technology. For example, the co-production of 2,3-butanediol demonstrated a ~37% reduction in the MFSP for both considered syngas fermentation routes.

Okoro & Faloye (2020) compared HTL to gas fermentation from waste plastic. Their analysis found the HTL route to be economically favourable, producing an IRR of 51.3 % and production cost of $ 0.38/kg, compared to 22.2 % and $ 0.42/kg for syngas fermentation (Okoro & Faloye, 2020). The higher cost for fermentation was attributed to the higher capital cost due to its larger number of unit operations (gasifier, fermenter, and separation sequence) compared to HTL (HTL reactor and decanter).

2.2.2 Feedstock comparison studies

In addition to technology comparisons, studies comparing feedstock sceanarios are also commonplace. Feedstock costs are a dominating economic factor in bioproduction pathways. A key benefit of producing chemicals via gas fermentation is the ability to use low cost feedstocks. Despite this, feedstock costs are still a primary contributor to operating costs, and the choice of feedstocks vastly impacts the economics. Examples of gas fermentation studies comparing feedstocks are discussed below.

Redl et al. (2017) conducted a TEA study into acetone production, revealing that using basic oxygen furnace process gas resulted in the lowest variable costs ($389/t), compared to natural gas ($1724/t) and corn stover ($2878/t) (Redl et al., 2017). Similarly, Ro et al. (2019) demonstrated that low-value agricultural residues (wheat straw, corn stover, and manure) could achieve ethanol MSP's of $2.24–$2.96/gal, comparable to gasoline prices. Contrastingly, higher value feedstocks such as oilseed rape meal led to costs of $5-5.12/gal (Ro et al., 2019). In the comparative study for ethanol production in South Africa, Petersen et al. (2021) found the use of ferroalloy off-gas ($0.61/L) to be cheaper than the gasification of invasive alien plants ($0.91/L).

Considering supply chain configurations, Benalcázar et al. (2017) undertook an analysis into different options for the production of ethanol, 2,3-butanediol, and hexanoic acid via syngas fermentation. The different configurations considered were, Brazil (sugarcane bagasse and eucalyptus wood), the USA (forestry residues and corn stover), and the Netherlands (imported feedstocks) (Benalcázar et al., 2017). In the Netherlands, where biomass was imported, biomass production and supply costs represented the highest contribution to the cost of syngas production. Overall, using locally sourced biomass presented better economics than relying on imported biomass. These findings highlight the significance of transportation on the cost of feedstocks and the economic benefit of processing point source residues.

2.2.3 Co-product considerations

As demonstrated by Choi et al. (2010) and Tan et al. (2016), the inclusion of co-products has a significant impact on biorefinery economics. This has been further explored in the studies by Okolie et al. (2021a) and Giwa et al. (2023). Okolie et al. (2021) used crude glycerol as a feedstock for bioethanol production via Supercritical Water Gasification (SCWG). The study explored the capture and utilisation of the bioreactor off-gas for methane production, with a water electrolysis unit providing hydrogen to the methanation unit. Through the sale of methane and oxygen (produced during water electrolysis) the MSP of ethanol was reduced from $1.32/L to $0.31/L (Okolie et al., 2021a). Giwa et al. (2023) explored the production of bio-oil, ethanol, and hydrogen from woodchips, finding the highest IRR (13.01%) by selling bio-oil, combusting biochar to produce ethanol, and using syngas to produce hydrogen. In contrast, using biochar and syngas to produce ethanol achieved an IRR of 11.93 %, whilst the sale of bio-oil alone achieved 7%.

Whilst the inclusion of high value co-products demonstrates potential to vastly improve biorefinery economics, their inclusion also presents challenges. Firstly, the inclusion of co-product pricing in the MSP calcaultion makes the final product price highly sensitive to these prices and yields, potentially misleading investors when comapred to fossil fuel-based products (Pereira et al., 2017). Secondly, high value co-products often have limited market sizes, and their co-production risks market saturation, making them unsustainable as co-products for commodity chemical and fuel scale facilities (Wiatrowski et al., 2022). When including high value co-products, these factors need to be considered in addition to the economic viability of a process.

2.2.4 Hydrogen

A key benefit of gas fermentation is its ability to utilise low cost feedstocks. However, when using industrial off-gas as a feedstock the use of CO, CO_2, and H_2 containing gases are economically favourable to purely CO_2 streams due to the inherent energy content of CO and H_2. The economic viability of utilising CO_2 rich streams is therefore heavily dependent on the cost of electricity used to activate the inert CO_2 (Takors et al., 2018). For example, in the TEA by Khan et al. (2014) the aerobic production of botryococcene via both *Cupriavidus necator* and *Rhodobacter Capsulatus* was investigated. However, the platforms reliance on hydrogen via water electrolysis resulted in electricity costs contributing >90% of the fuel costs. An electricity price of <$0.02/kwh was required for economic feasibility. An approach to reducing electricity costs is the use of curtailed renewable electricity, but it poses challenges associated with electricity storage to maximise capital utilisation of the biochemical production facility (Prévoteau et al., 2020).

The TEA study by Huang et al. (2020) considered the use of intermittent electricity to upgrade the CO_2-rich bioreactor off-gas from a corn mill ethanol facility (Huang et al., 2020). A CO_2 electrolyser and water electrolyser for hydrogen generation were required to produce syngas for the gas fermenter. Upgrading the off-gas led to an increase in carbon efficiency from 46%

to 68%. However, the additional capital (84-91% increase) and operating costs (330% increase in electricity use) led to an increase in MSP from $1.78/gal to $2.84/gal. Notably, the use of intermittent electricity (40% capacity at $0.02/kwh) reduced the MSP by $0.36/gal. However, this was still higher than the base case without CO_2 upgrading.

The study by Regis et al. (2023) also demonstrated sensitivity to hydrogen pricing. They investigated supplementing the syngas produced from switchgrass gasification with hydrogen for ethanol production, leading to a 23% increase in carbon yield (Regis et al., 2023). A $1.07/L minimum selling price was achieved using a green hydrogen price of $6/kg. However, using the projected hydrogen price for 2050 ($1.50/kg) reduced the MSP to $0.77/L, demonstrating a 30% decrease and highlighting the strong influence of hydrogen pricing and the importance in including pricing ranges when uncertainty exists around future prices.

2.2.5 Energy considerations

Efficient energy use significantly impacts the economics and emissions of a process. Benalcázar et al. (2017) found that recovering the heat generated during gasification for internal steam generation reduced both the syngas production costs by 22 to 29% and the environmental impact by 19-31 % Global Warming Potential (Benalcázar et al., 2017). The choice of fuel sources is also an important consideration. In the different product scenarios considered by Giwa et al. (2023) the use of both biomass and natural gas were explored as an energy source. In all scenarios a lower operating cost was found for the use of natural gas owing to its lower price and higher heating value than biomass. However, the absence of an LCA in the analysis prevented any discussion around emissions trade-offs by using different energy sources.

The importance of energy efficiency and integration has resulted in a few TEA studies making it a major consideration in their work. In the study by de Medeiros et al. (2017) an energetically self-sufficient plant was investigated for the production of hydrous ethanol from the gasification and subsequent gas fermentation of switchgrass. The study diverted syngas to energy and electricity generation and employed multiple-effect distillation to reduce the overall energy requirement. A 30% carbon conversion efficiency and MSP of $2.66/gal was achieved. The benefit of an energetically self-sufficient platform is the absence of additional fuel imports as either biomass or natural gas. However, this may not be the most cost-effective configuration, as it necessitates the diversion of syngas from chemical production. Petersen et al. (2021) addressed this trade-off in their comparative study for ethanol production. They considered two energetic scenarios: 1) energetic self-sufficiency, where the feedstock was used to satisfy the thermal and electrical demand of the plant, and 2) a maximum ethanol case, where the feedstock was diverted solely to ethanol production and additional renewable electricity was purchased (Petersen et al., 2021). The authors found that importing electricity led to the lowest MSPs. This was attributed to the 42% average reduction in ethanol yield when diverting syngas to electricity generation which resulted in a 42% and 73% increase in MSP for the off-gas fermentation and syngas fermentation cases, respectively. While this comparison highlights the compromise in achieving an energetically self-sufficient platform, the lack of accompanying LCA neglected a discussion on the trade-off between economics and emissions.

2.2.6 Optimisation

Three studies have incorporated optimisation in their TEA of gas fermentation (Michailos et al., 2019a; de Medeiros et al., 2020; Ma et al., 2022). These studies all considered multi-objective optimisation of both economics and energy, demonstrating the trade-offs between both parameters.

The multi-objective optimisation problem investigated by Michailos et al. (2019a) considered two decision variables, CO and H_2 conversion to ethanol. The multi-objective function aimed to reduce the Total Annualised Cost (TAC) whilst increasing exergy efficiency (ratio of energy input into the process compared to the final ethanol product) (Michailos et al., 2019a). Using a genetic algorithm in MATLAB and Component Object Model technology to update the Aspen process model, a linear relationship was observed between exergy efficiency and TAC. However, a maximum exergy efficiency of 44-46% was reached, at which point the TAC increased but exergy plateaued. Two optimal solutions were determined, the first achieved an efficiency of 44.95 %, NPV of $44.37 M, and emissions of 14.1 gCO_2MJ^{-1}, and the second achieved an efficiency of 45.70 %, NPV of $44.94 M, and emissions of 14.9 gCO_2MJ^{-1}. The difference in these two solutions demonstrates a 1.3% reduction in NPV and a 5.4% reduction in emissions. This highlights the importance of multiple considerations during process optimisation and the balance between economics and emissions. However, as the emissions were not included in the multi-objective optimisation function, the optimisation procedure led to an increase in process emissions compared to the base case which achieved emissions of 11.5 gCO_2MJ^{-1}.

In the work by de Medeiros et al. (2020) for the optimisation of anhydrous ethanol production ANN surrogate models were developed for both the bubble column bioreactor and distillation columns. The kinetic bioreactor model and distillation sequence in Aspen Plus are both computationally expensive to optimise (de Medeiros et al., 2020). As such, reducing these models to ANN surrogates allows for the optimisation of decision variables that directly impact the mass and energy balance. Two multi-objective optimisation problems were defined, firstly the bioreactor was optimised for maximum ethanol production and minimum capital cost and secondly, the whole process was optimised by minimising capital cost and MSP while maximising thermodynamic efficiency. The analysis demonstrated smaller optimum decision variable ranges when optimising the whole process compared to the bioreactor in isolation. This suggests that the bioreactor productivity is not necessarily tied to the economic and thermodynamic efficiency of the overall process. This emphasises the importance in considering entire processes during technology assessment and determining performance targets for continued research and development efforts.

Lastly, Ma et al. (2022) optimised the production of ethanol from wood chips using a gasification-solid oxide fuel cell system. The solid oxide fuel cell was used to generate steam and power for the process, increasing energy efficiency (Ma et al., 2022). Parametric analysis was first undertaken to determine the operating conditions of the gasifier and distillation sequence. The multi-objective optimisation was used to determine the optimum amount of syngas entering the solid oxide fuel cell system considering the energy efficiency, TAC, and total product price as the objective function. However, as demonstrated by de Medeiros et al. (2020), the inclusion of the entire process in the optimisation function has the potential to yield different optimal economic results.

Notably, none of these existing studies included the process emissions as part of the objective function. In addition, only Michailos et al. (2019a) computed the associated emissions and discussed the trade-off in economic, energy, and emissions. This demonstrates a key limitation of the currently undertaken multi-objective optimisation studies for gas fermentation.

2.2.7 Policy

Two of the existing gas fermentation TEAs have incorporated policy implications into their analyses. Michailos et al. (2019b) undertook a rigorous TEA on methane production via syngas fermentation using Aspen Plus. Two cases were considered, one including Carbon Capture and Storage (CCS) and one without (Michailos et al., 2019b). The analysis included

the UK's Renewable Heat Incentive policy scheme, considering a subsidy of £62/MWh. Including this policy, the case without CCS was able to achieve a positive economic return, producing a methane price lower than fossil natural gas. However, despite not being economically feasible the case considering CCS demonstrated a sequestration potential of 2.88 tCO_2/h. To break even, a carbon credit of £98-142/tCO_2 was required. The authors highlighted a hurdle in current CCS policy as the absence of a price for biomass-based CO_2 storage. The inclusion of policy in this TEA therefore evidenced pitfalls in currently available policy frameworks, helping to inform future decisions by policymakers.

In the economic study converting CO_2 to fuels via various pathways, Huang et al. (2021) also included an analysis to help inform policy. The study considered direct (low-temperature electrolysis, high-temperature electrolysis, and microbial electrosynthesis) and indirect (electrolytic hydrogen through biological conversion and thermochemical conversion) pathways to chemicals with regard to their current, near term, and theoretical potential (Huang et al., 2021). Only gas fermentation for PHB production was found to meet market prices under the current state of technology. As an additional analysis, the impact of CO_2 pricing was included to calculate CO_2 credits necessary to achieve market prices for the other considered products. For the gas fermentation routes (biochemical conversion), CO_2 credits of $470/t, $190/t, and $735/t were required for ethanol, acetic acid, and methane, respectively. These costs provide policymakers with benchmarking information on the cost-competitiveness of current technologies and their potential for carbon sequestration.

2.2.8 Life cycle assessment

The simultaneous conduction of TEAs and LCAs aids in understanding the trade-off between a process's economic and environmental performance (Mahmud et al., 2021). In addition, a rigorous TEA requires a mass and energy balance which provides the process information required for an LCA to be undertaken. Despite this, the simultaneous conduction of these studies is not ubiquitous. Furthermore, studies often comment on the evaluated technology's potential for CO_2 reduction yet don't conduct an LCA to quantify this, e.g, Haro et al. (2013); Christodoulou et al. (2016); de Medeiros et al. (2020); Huang et al. (2020); Okolie et al. (2021a); Huang et al. (2021); Petersen et al. (2021); Regis et al. (2023). The studies that included an LCA as part of their TEA are discussed below.

In the study into ethanol production from miscanthus, Roy et al. (2015) found an economic and emission benefit in using untreated feedstock. However, the use of chemical looping gasification demonstrated a reduction in emissions, but the increased cost of gasification led to higher production costs. This simultaneous computation of both metrics allowed for the identification of mutually beneficial process decisions and identification and quantification of the compromise between these decisions.

Tan et al. (2016) used sustainability metrics as an additional performance parameter in their comparative technology study to distillate range fuels. Importantly, one of the most promising routes (non-gas fermentation) from an economic perspective demonstrated higher Greenhouse Gas (GHG) emissions than the F-T benchmark used for comparison. This was attributed to the import of natural gas within the process, absent in the comparative technologies.

Benalcázar et al. (2017) included GHG emissions in their supply chain configuration study. Among the considered feedstocks, corn stover demonstrated the highest emissions for syngas production, and the Netherlands had the highest emissions among the evaluated locations. (Benalcázar et al., 2017). This was attributed to the international transport of biomass required for the Netherlands location. Comparing their results with other studies, they found that using lignocellulosic materials such as wood and maize straw could achieve up to a 45% reduction

in emissions compared to first-generation materials like wheat and sugarcane. This potential reduction demonstrates the benefit of gas fermentation over other biochemical production pathways that cannot efficiently utilise lignocellulosic biomass sources.

In both Michailos et al. (2019a & b) an LCA was conducted in conjunction with the TEA. In the multi-objective optimisation study, a trade-off between emissions and economics was found between the two pareto optimal parameters, demonstrating that a 1.3% reduction in NPV led to a 5.4% reduction in emissions, discussed in section 2.2.6 Optimisation (Michailos et al., 2019a). In their second study, investigating the production of bio-methane with and without CCS, an LCA was used to demonstrate the environmental benefit of CCS in contrast to the economic disbenefit (Michailos et al., 2019b). However, as discussed in section 2.2.7 Policy, this study demonstrates an additional benefit of calculating GHG emissions by also quantifying the impact of carbon pricing initiatives on the economic outcome.

2.2.9 Bacteria

Micro-organisms can grow either anaerobically or aerobically. Anaerobic bacteria grow in the absence of oxygen. Anaerobic acetogenic bacteria are the most commonly studied bacteria for gas fermentation and their use is industrialised for ethanol production (Fackler et al., 2021). Contrastingly to anaerobic gas fermentation, aerobic gas fermentation is still in its infancy. This is partially attributed to aerobic bacteria being less well characterised and having limited molecular toolboxes (Takors et al., 2018). Also, from a processing perspective, the handling of hydrogen in the presence of oxygen requires extensive safety precautions (Takors et al., 2018). An additional challenge is the significant amount of heat produced owing to the loss of H_2 as water during respiration (Emerson & Stephanopoulos, 2019). This requires sufficient cooling capacity to be installed to control the heat released, coming at a capital and operating expense. However, aerobic bacteria, e.g. *Cupriavidus* have higher Adenosine triphosphate (ATP) availability than anaerobes meaning they can target more ATP-intensive products (e.g. butanol and PHB) in comparison to simpler products such as ethanol (Köpke & Simpson, 2020). More ATP-intensive products typically command higher market prices, potentially leading to economically favourable processes.

The majority of the reviewed gas fermentation TEAs consider anaerobic acetogens as the microbial cell factory. Only three of the reviewed studies considered aerobic bacteria. Firstly, Choi et al. (2010) considered the use of *Rhodospirillum rubrum*. However, anaerobic conditions were considered within the study. Khan et al. (2014) compared *Cupriavidus necator* and *Rhodobacter Capsulatus* for botryococcene production, discussed section 2.2.24 Hydrogen. Finally, Levett et al. (2016) considered a mixed methanotrophic culture for PHB production. Importantly, whilst *Rhodobacter Capsulatus* and *Rhodospirillum rubrum* are both photosynthetic, neither study employed a photobioreactor or open pond cultivation for the fermenter and were therefore included in this review. The thermodynamic inefficiency of aerobic gas fermentation was demonstrated in the TEA by Levett et al. (2016), where the heat removal costs contributed 28% of the operating costs.

2.2.10 Commercial status

LanzaTech is currently leading the way in commercialised gas fermentation with its operational 46,000 t/yr ethanol facility using steel mill off-gas in China (Köpke & Simpson, 2020). LanzaTech also have a commercial facility processing steel mill off-gas in Ghent (LanzaTech, 2023), a demonstration facility in Japan processing municipal solid waste (LanzaTech, 2022), and plans for a 10 million US gallon/year ethanol facility in Georgia (LanzaJet, 2022). The company's technology is based on their proprietary acetogen, *Clostridium autoethanogenum*. Which, in addition to ethanol, has demonstrated its capability to produce acetone and isopropanol, 2,3-butanediol (Liew et al., 2022), and n-octanol (Sapp, 2021).

Evonik and Siemens are actively researching the commercialisation of gas fermentation and partnered on project Rheticus in 2018. The project aims to synthesise 1-butanol and 1-hexanol by electrolysing CO_2 and H_2O to syngas for fermentation using artificial photosynthesis (Haas et al., 2018). A pilot plant in Marl, Germany, was brought online in 2020 (Evonik, 2020).

Other companies to previously operate or conduct research into gas fermentation include Synata Bio (formerly Coskata) who previously owned the Abengoa Kansas site which produced cellulosic ethanol. The site was adapted the plant for syngas fermentation but was sold in 2021 (Pacheco et al., 2023). INEOS bio previously operated the demonstration scale Vero Beach plant in Florida. The plant produced ethanol from municipal solid waste-derived syngas (Pacheco et al., 2023). However, the plant was closed in 2015 due to issues with hydrogen cyanide contamination (Lane, 2014). The facility was later acquired by Jupeng bio, but is not currently operational (Jupeng Bio, 2017).

Evidently, commercial gas fermentation has only been achieved and maintained by LanzaTech to date. While other companies such as Evonik and Siemens are still actively researching the field, others have faced challenges in remaining operational. As highlighted by Fackler et al. (2021), the development and commercialisation of gas fermentation technologies are arduous and lengthy processes, and many companies fail to cross the 'valley-of-death' stages of development, which span from Technical Readiness Level (TRL) 3 (proof of concept) to 7 (continuous operation of a pilot plant) (Fackler et al., 2021). Notably, TEAs are undertaken across these stages of technology development, making them of critical importance in identifying cost bottlenecks, performance targets, and prioritising resource allocation.

2.3 Supercritical water gasification techno-economic analyses

Gas fermentation can utilise a broad range of feedstocks, including various waste gases from industrial sources or syngas derived from municipal solid wastes, agricultural residues, or organic industrial wastes (Köpke & Simpson, 2020). Originating from biomass gasification offers the opportunity to exploit a range of abundant, low-cost wastes for chemical synthesis. Different mediums can be used as gasyfing agents and ultimately affect the product gas composition and energy balance of the system. Air, oxygen, steam, and supercritical water can all be used as gasifying agents. Table 2.3 presents the benefits and limitations of each of these mediums.

Table 2.3: Comparison between gasifying agents, details taken from (Mishra & Upadhyay, 2021; Moghaddam et al., 2021; Saxena et al., 2008)

Gasifying Agent	Benefits	Limitations
Air	• Low cost • Easily available	• High tar production • Lower heating value due to presence of N_2
Oxygen	• High quality syngas production	• Creating pure O_2 is costly and energy intensive • Safety concerns around pure O_2
Steam	• Higher H_2/CO ratio achieved	• Corrosion and poisoning of catalysts • Tar formation
Supercritical Water	• Can be used for high moisture content feedstocks • Increased H_2 formation	• High energy requirement for the endothermic reactions • Plugging and fouling due to salts

Notably, a key benefit of using supercritical water is its ability to utilise high moisture content biomass. For biomass with moisture contents >30%, SCWG has a lower energy requirement than drying (Yoshida et al., 2003). As such, feedstocks suitable for SCWG have limited resource competition as they are uneconomical for conventional gasification. This makes SCWG a promising technology for low-cost, wet feedstock valorisation. Existing TEAs investigating SCWG have been undertaken into the production of syngas, hydrogen, methanol, and other fuels. An overview of existing TEAs for SCWG is provided in this section.

Kumar et al. (2019) compared the production of hydrogen via thermal gasification and SCWG from microalgae. Due to the drying required for thermal gasification, the SCWG process demonstrated lower hydrogen product costs of $4.59/kg compared to $5.66/kg for thermal gasification (Kumar et al., 2019). Similar was found by Sanaye et al. (2022), who compared the valorisation of digested sewage sludge by gasification via conventional gasification and SCWG to produce syngas. Their economic assessment demonstrated SCWG had an 8% higher energetic efficiency and 19% lower syngas production cost ($82.5/GJ) than conventional gasification ($102/GJ) (Sanaye et al., 2022). Shi et al. (2023) considered SCWG for waste sludge treatment in comparison to both conventional incineration with chemical looping combustion and steam gasification with chemical looping combustion. While steam gasification with chemical looping combustion performed best from an economic perspective, SCWG had the highest energy efficiency (Shi et al., 2023). The higher cost of SCWG was primarily attributed to the capital cost of the high-pressure SCWG reactor. In addition, the steam gasification with chemical looping technology received additional income from CO_2 capture. In contrast to these studies, Ma et al. (2022) found steam gasification to be more energetically efficient and economically favourable in comparison to SCWG when considering poultry litter as a feedstock. Importantly, the SCWG process required large inputs of external thermal energy to heat the dilution water added to the poultry litter, whereas steam gasification used steam generated internally as the gasification medium (Ma et al., 2022). Whilst the first three studies demonstrated the energetic benefit of SCWG for wet feedstock processing (Kumar et al., 2019; Sanaye et al., 2022; Shi et al., 2023), the contrasting results by Ma et al. (2022), who used a dryer feedstock, illustrate the importance of matching feedstocks to the most suitable technology.

Despite being more energetically efficient than drying, SCWG still requires a significant amount of energy to heat dilute feedstocks to supercritical conditions. Consequently, several studies have incorporated heat integration into their analyses to better utilise the process energy. For example, Okolie et al. (2021b) used heat integration to create an energetically self-sufficient platform for hydrogen production from soybean straw. Resultantly utility costs were minimal, resulting in a hydrogen production cost of $1.94/kg, comparing favourably to alternative hydrogen production processes, namely, gasification, steam reforming, solar thermochemical cycle, and water electrolysis (Okolie et al., 2021b). Considering black liquor as a feedstock, both Liang et al. (2023) and Özdenkçi et al. (2019) employed heat integration to recover the energy from the SCWG outlet. Revenue from hydrogen production, electricity generation, and captured CO_2 were considered in the study by Liang et al. (2023), achieving a positive annual revenue for all temperatures investigated for SCWG. A positive economic outcome was also achieved by Özdenkçi et al. (2019) considering both combined heat and power and hydrogen production.

Whilst heat integration can better utilise the process energy, external energy is still often required by SCWG. The source of this energy has a vast impact on the overall process economics. Solar assisted SCWG has been considered as an approach to prevent the import of external fossil-fuel sources and remain renewable. For example, Onigbajumo et al. (2021) compared the use of solar tower, solar parabolic trough, natural gas and electricity in a SCWG

plant producing syngas from microalgae. The study found that natural gas or solar parabolic trough with supplementary natural gas was the most economical, however, the MSP was still 3-7 times higher than market prices (Onigbajumo et al., 2021). Later, the authors conducted a study considering solely solar-driven SCWG, three different heat exchanger configurations were compared (Onigbajumo et al., 2022). The most efficient process configuration, considering solar parabolic trough and two heat exchangers, led to greater utilisable energy which increased the exergy flow in the microalgae inlet stream compared to the alternative configurations. This processing route achieved an MSP of $34/GJ, compared to $50/GJ and $37/GJ from the alternative heat integration configurations. Rahbari et al. (2019, 2021a, 2021b) also considered solar assisted SCWG using an algae feedstock. Both F-T fuels (Rahbari et al., 2019, 2021a) and methanol (Rahbari et al., 2021b) were considered as products. Whilst the solar-assisted production provides energy to the gasifier and reforming unit, the on-stream capacity and storage requirements increase the capital intensity of the process. Ultimately, the authors found methanol to be a better choice of downstream fuel synthesis owing to its faster ramping and increased output compared with F-T fuels (Rahbari et al., 2021b).

Also considering fuel synthesis, Umenweke et al. (2023) investigated the production of sustainable aviation fuel from tall oil fatty acid. Two production routes were compared using catalytic deoxygenation, firstly a route using commercial hydrogen and secondly, a route using hydrogen produced via SCWG of crude glycerol from the biodiesel industry (Umenweke et al., 2023). Both routes were found to be economical compared to petroleum derived jet fuel. However, the use of green hydrogen via SCWG led to a lower MSP of $0.39/L compared to $0.62/L using commercial hydrogen.

As discussed in Section 2.1.1 Process Modelling, the TEA of methanol production from microalgae via SCWG by Fózer et al. (2021) employed an ANN to represent the SCWG in their process model. Water electrolysis was added to supplement the hydrogen feed into the process. Production costs ranged from $3.16/kg to $3.39/kg, in line with other biomass-to-methanol studies.

Overall, existing TEAs illustrate that SCWG is a promising technology to valorise low-value wet feedstocks. However, it is not the optimal gasification technology for all feedstocks. Therefore, these studies emphasise the importance in matching feedstocks to suitable technologies. The thermal requirements of SCWG are significant, meaning heat integration strategies are important in realising the potential of the technology. Solar assisted SCWG offers the potential to utilise renewable energy to support SCWG, however, on-stream capacity and the capital associated with solar cells can pose economic challenges. As such, investigations into alternative, low-cost, renewable thermal energy inputs would be beneficial to SCWG. Some studies have considered upgrading the gasifier product to fuels. However, there are limited assessments of SCWG for higher value products. Finally, to the best of the author's knowledge, only Okolie et al. (2021a) considered SCWG as a gasification technology for gas fermentation (discussed in Section 2.2.3 Co-product considerations).

2.4 Conclusions and research gaps

The conclusions of the main findings from this literature review, identified gaps, and gaps addressed as part of this thesis are outlined in the following section.

2.4.1 Techno-economic methods

While most TEAs stem from comprehensive process models, the complexity of creating representative models can hinder early-stage assessments. Autonomous process synthesis is emerging as a trend and has promise to overcome this challenge. Furthermore, surrogate

modelling is being adopted as a tool to both represent complex unit operations and reduce the computational burden during process optimisation.

There remains no consensus on the cost models that are best suited for biochemical processes. Additionally, whilst existing comparisons in capital costing methods exist, the comparisons are limited to equipment cost and capital cost estimation, excluding fixed operating cost considerations. Furthermore, these comparisons are not undertaken within TEA studies, but as standalone pieces of work. A comparison of TEA capital and fixed operating cost models within a TEA study is therefore a current gap in the literature. Progress in developing cost estimation methods are currently limited by the lack of transparency surrounding estimation and actual costs for commercialised bioprocesses.

The computation of multiple performance metrics aids in TEA interpretability and provides sufficient information to determine the economic feasibility of the process by a broad range of audiences. This requires the product price to be input into the analysis and used to compare against the MSP. Currently, product prices are often selected as spot prices or averages from literature. Methods which consider non-stationary prices and the uncertainty around future prices exist. However, the only method applicable to all time series is stochastic modelling, which doesn't account for trends in the data. While ML methods remain unused in price and variability projections for TEAs, these methods offer the opportunity to exploit existing trends and patters within the data without any prerequisites for the time series.

The inclusion of sensitivity, scenario, and/or uncertainty analyses within TEAs is important to determine the most influential parameters and frame the economic outcome within a band of uncertainty. Most studies consider purely cost based parameters in these analyses owing to the complexity and computational burden associated with varying technical parameters. However, ML-based ROMs of process simulations or complex equipment have demonstrated their ability to reduce this computational burden.

There is a trend in developing simplified TEA models and tools, aimed at enabling non-experts such as experimentalists and industrialists to undertake technology evaluations. These lightweight tools require minimal user inputs, providing preliminary techno-economic insights for various technical parameters and scenario considerations. Enabling non-experts to conduct these initial assessments facilitates focused research and development into areas with potential, whilst preventing the allocation of resources to less promising technologies or scenarios. However, the usability of these models comes at the expense of accuracy and mass and energy integration opportunities. There is an opportunity for ML to be used to represent rigorous process models and/or equipment providing for more accurate predictions. However, the flexibility of surrogate models depends on what they were trained to do. I.e. representing an entire process would limit its applicability to that technology, whereas representing individual unit operations would allow for building up process models. Whilst surrogate models of unit operations are being used for process modelling, there is limited application of creating surrogate models to predict economic outcomes based on different technical or scenario inputs.

2.4.2 Gas fermentation techno-economic analyses

Gas fermentation is a promising technology for renewable chemical production from recalcitrant feedstocks. A number of TEAs have assessed gas fermentation, demonstrating varying economic outcomes. In some cases, gas fermentation performs favourably whereas in others it has proved to be more capital intensive than alternative technologies. The difference in techno-economic outcomes highlights the need to evaluate feedstock-technology-chemical combinations individually. Furthermore, for meaningful technology comparisons, it's essential to perform these evaluations within a single study, accounting for

varying scenarios, assumptions, and methodologies. Most current gas fermentation TEAs explore the production of ethanol, however the commercial viability of chemicals with higher market value remains underexplored. Notably, evaluating the cost-effectiveness of catalytic upgrading for commodity chemical production lacks rigorous investigation.

Co-product pricing significantly influences overall economics, often enhancing outcomes in gas fermentation studies. However, integrating co-product pricing requires careful handling to prevent bias in the economic results. Energy considerations emerge as a crucial aspect affecting process economics, leading to various studies conducting multi-objective optimisations that factor in both economic and energetic objectives. However, an integrated LCA and TEA is necessary to fully quantify the trade-offs of processing choices involving heat integration and fossil fuel inputs. The inclusion of an LCA also allows for the incorporation of policy influences such as CO_2 pricing, evidencing required initiatives for economically sustainable processes and identifying gaps in policy frameworks. Despite this potential, the combination of TEA and LCA studies for gas fermentation is lacking.

In the reviewed TEA literature, the analysis of aerobic gas fermentation technologies remains limited. As such, the viability of aerobic gas fermentation for commodity chemical production remains unexplored. Moreover, while technology comparisons between gas fermentation and biochemical and thermochemical processes exist, there is currently no comparison between aerobic and anaerobic gas fermentation.

2.4.3 Supercritical water gasification techno-economic analyses

SCWG demonstrates a promising technology for low-value wet feedstock valorisation. However, it is not universally superior to alternative gasification technologies, i.e. when processing dry wastes alternative gasification technologies are more suited. The high thermal energy demand of SCWG highlights the importance of heat integration and the thermal energy sources used to achieve economically feasible processes. However, to the best of the author's knowledge, no studies have investigated the use of low-grade process heat as a thermal source for SCWG. Furthermore, to the best of the author's knowledge, only Okolie et al. (2021a) have used SCWG as a gasification technology for gas fermentation. The low-grade heat produced via aerobic gas fermentation represents an abundantly available thermal energy source that is conventionally removed at a cost to the process. The integration of these two technologies represents a promising opportunity that is yet to be explored.

Additionally, there is a gap in evaluating a wide range of feedstocks suitable for SCWG. Existing studies have primarily focused on single biorefinery scenarios, examining specific biomass streams without considering different capacities and locations. Consequently, there remains a gap in the development of a feedstock-agnostic TEA suitable for evaluating various feedstocks using SCWG.

2.4.4 Research gaps addressed in this thesis

The research gaps addressed in this thesis and the chapter in which these are addressed are summarised in Table 2.4.

Table 2.4: Research gaps and the thesis section and chapter within which these gaps are addressed.

Research gap	Thesis section	Chapter
The evaluation of aerobic gas fermentation integrated with supercritical water gasification from a techno-economic and life cycle perspective.	Evaluation	Chapters 4 and 5
The comparison of aerobic gas fermentation to anaerobic gas fermentation.		Chapter 4
The economic evaluation of aerobic gas fermentation coupled with catalytic upgrading for chemical production.		Chapter 5
The comparison of capital and fixed operating cost methods within a techno-economic analysis.		Chapter 4
The use of machine learning to project commodity prices for techno-economic analyses.	Method development	Chapter 6
The creation of a probabilistic price projection to incorporate price variability into sensitivity and uncertainty analyses.		Chapter 6
The creation of a surrogate model representing a full techno-economic analysis allowing for the quick economic evaluation of different feedstocks.		Chapter 7

2.5 References

AACE International, 2020. Cost Estimate Classification System, s.l.: s.n.

Alalwan, H.A., Alminshid, A.H., Alijaafari, H.A.S., 2019. Promising evolution of biofuel generations: Subject review. *Renewable Energy Focus,* 28, 127-139.

Amigun, B., Petrie, D., Görgens, J., 2011. Economic risk assessment of advanced process technologies for bioethanol production in South Africa: Monte Carlo analysis. *Renewable Energy*, 36(11).

AspenTech, 2012. Aspen Economic Evaluation Family. [Online] Available at: http://www.zy-aoto.com/file/Aspen%20Economic%20Evaluation%20Family%20Brochure.pdf [Accessed 24 May 2023].

Barahmand, Z. & Eikeland, M. S., 2022. Techno-Economic and Life Cycle Cost Analysis through the Lens of Uncertainty: A Scoping Review. *Sustainability*, 14(19).

Baral, N., Kavvada, O., Mendez-Perez, D., Mukhopadhyay, A., Lee, T.S., Simmons, B.A., Scown, C.D., 2019. Techno-economic analysis and life-cycle greenhouse gas mitigation cost of five routes to bio-jet fuel blendstocks. *Energy & Environmental Science*.

Barzaghi, R., Conte, A., Sepiacci, P., Manca, D., 2016. Optimal design of a styrene monomer plant under market volatility. *Computer Aided Chemical Engineering*, 38, 1653-1658.

Bastos, J. B. V., Maia, J.G.S.S., Borschiver, S., Szklo, A., Secchi, A.R. 2022. Addressing scale and seasonality in the design of sugarcane to ethylene guiacol biorefineries. *Journal of Cleaner Production,* 337.

Beattie, A., Vermass, W., Darzins, A., Holland, S.C., Li, S., McGowen, J., Nielsen, D., Quinn, J.C., 2021. A probabilistic economic and environmental impact assessment of a cyanobacteria-based biorefinery. *Algal Research*, 59, 102454.

BEIS, 2017. Industrial Decarbonisation and Energy Efficiency Roadmap Action Plan , s.l.: s.n.

BEIS, 2020. BEIS Electricity Generation Costs (2020). [Online] Available at: https://www.gov.uk/government/publications/beis-electricity-generation-costs-2020 [Accessed 01 February 01].

Benalcázar, E. A., Deynoot, B.G., Noorman, H., Osseweijer, P., Posada, J.A., 2017. Production of bulk chemicals from lignocellulosic biomass via thermochemical conversion and syngas fermentation: a comparative techno-economic and environmental assessment of different site-specific supply chain configurations. *Biofuels, Bioproducts and Biorefining*, 11(5), 861-886.

Brown, T. R., 2015. A critical analysis of thermochemical cellulosic biorefinery capital cost estimates. *Biofuels Bioproducts & Biorefining*.

Brown, T. R. & Wright, M. M., 2015. A Framework for Defining the Economic Feasibility of Cellulosic Biofuel Pathways. *Biofuels*, 579-590.

Campbell, R., Anderson, N., Daugaard, D., Naughton, H., 2018. Financial viability of biofuel and biochar production from forest biomass in the face of market price volatility and uncertainty. *Applied Energy*, 230, 330-343.

Choi, D., Chipman, D. C., Bents, S. C., Brown, R. C., 2010. A Techno-economic Analysis of Polyhydroxyalkanoate and Hydrogen Production from Syngas Fermentation of Gasified Biomass. *Applied Biochemistry and Biotechnology*, 160, 1032-1046.

Christodoulou, X. & Velasquez-Orta, S. B., 2016. Microbial Electrosynthesis and Anaerobic Fermentation: An Economic Evaluation for Acetic Acid Production from CO2 and CO. *Environmental Science & Technology*, 50(20), 11234-11242.

Cortes-Peña, Y., Kumar, D., Singh, V., Guest, J. S., 2020. BioSTEAM: A Fast and Flexible Platform for the Design, Simulation, and Techno-Economic Analysis of Biorefineries under Uncertainty. *ACS Sustainable Chemistry and Engineering*, 3302-3310.

Crater, J. & Lievense, J., 2018. Scale-up of industrial microbial processes. *Microbiology Letters*, 365(13).

Daniell, J., Köpke, M., Simpson, S., 2012. Commercial Biomass Syngas Fermentation. *Energies*, 5(12), 5372-5417.

De Buck, V., Polanska, M. & Van Impe, J., 2020. Modeling Biowaste Biorefineries: A Review. *Frontiers in Sustainable Food Systems*, 4.

Dürre, P. (2017) Gas fermentation – a biotechnological solution for today's challenges. *Microbial biotechnology*, 10:1, 14-16.

de Medeiros, E. M., Noorman, H., Maciel Filho, R. & Posada, J. A., 2020. Production of ethanol fuel via syngas fermentation: Optimization of economic performance and energy efficiency. *Chemical Engineering Science: X*, 5, 100056.

de Medeiros, E. M. et al., 2017. Hydrous bioethanol production from sugarcane bagasse via energy self-sufficient gasification-fermentation hybrid route: Simulation and financial analysis. *Journal of Cleaner Production*, 168, 1625-1635.

Dheskali, E., Koutinas, A. A. & Kookos, I. K., 2020. A simple and efficient model for calculating fixed capital investment and utilities consumption of large-scale biotransformation processes. *Biochemical Engineering Journal*, 154.

Dimitriou, I., Goldingay, H., Bridgwater, A. V., 2018. Techno-economic and uncertainty analysis of Biomass to Liquid (BTL) systems for transport fuel production. *Renewable and Sustainable Energy Reviews*, 160-175.

E4tech, 2017. UK Top Bio-based Chemicals Opportunities, London: s.n.

Emerson, D.F & Stephanopoulos, G., 2019 Limitations in converting waste gases to fuels and chemicals. *Current Opinion in Biotechnology*, 59, 39-45.

Evonik, 2020. For a climate-friendly industry: Using carbon dioxide and hydrogen as raw materials for sustainable chemicals. [Online] Available at: https://corporate.evonik.com/en/media/press-releases/corporate/for-a-climate-friendly-industry-using-carbon-dioxide-and-hydrogen-as-raw-materials-for-sustainable-c-143559.html [Accessed 13 July 2023].

Fackler, N., Heijstra, B.D., Rasor, B.J; Brown, H., Martin, J., Ni, Z., Shebek, K.M., Rosin, R.R., Simpson, S.D., Tyo, K.E., Giannone, R.J., Hettich, R.L., Tschaplinski, T.J., Leang, C., Brown, S.D., Jewett, M.C., Köpke, M., 2021 Stepping on the Gas to a Circular Economy: Accelerating Development of Carbon-Negative Chemical Production from Gas Fermentation. *Annual Review of Chemical and Biomolecular Engineering*, 12(1), 439-470.

Fei, Q., Liang, B., Tao, L., Tan, E.C.D., Gonzalez, R., Henard, C.A., Guarnieri, M.T., 2020. Biological valorization of natural gas for the production of lactic acid: Techno-economic analysis and life cycle assessment. *Biochemical Engineering Journal*, 158, 107500.

Feng, Y. & Rangaiah, G., 2011. Evaluating Capital Cost Estimation Programs. *Chemical Engineering Journal*, 22-29.

Fózer, D., Tóth, A. J., Varbanov, P. S., Klemeš, J. J., & Mizsey, P., 2021. Sustainability assessment of biomethanol production via hydrothermal gasification supported by artificial neural network. *Journal of Cleaner Production*, 318, 128606.

Furlan, F.F., Costa, C.B.B., Secchi, A.R., Woodley, J.M., Giordano, R.C., 2016. Retro-Techno-Economic Analysis: Using (Bio)Process Systems Engineering Tools To Attain Process Target Values. *Industrial & Engineering Chemistry Research*, 55(37), 9865-9872.

Gabrielli, P., Rosa, L., Gazzani, M., Meys, R., Bardown, A., Mazzotti, M., Sansavini, G., 2023. Net-zero emissions chemical industry in a world of limited resources. O*ne Earth*, 6(6), 682-704.

Giwa, T., Akbari, M., Kumar, A., 2023. Techno-economic assessment of an integrated biorefinery producing bio-oil, ethanol, and hydrogen. *Fuel*, 332, 126022.

Guthrie, K., 1969. Capital Cost Estimating. *Chemical Engineering*, 76(6), 114-142.

Gutierrez, J. P., Erdmann, E. & Manca, D., 2019. Optimal Design of a Carbon Dioxide Separation Process with Market Uncertainty and Waste Reduction. *Processes*, 7(6).

Haas, T., Krause, R., Weber, R., Demler, M., Schmid, G., 2018. Technical photosynthesis involving CO2 electrolysis and fermentation. *Nature Catalysis*, 1, 32-39.

Hand, W., 1958. From Flow Sheet to Cost Estimate. *Petroleuym Refinery*, 37, 331-334.

Haro, P., Ollero, P., Trippe, F., 2013. Technoeconomic assessment of potential processes for bio-ethylene production. *Fuel Processing Technology*, 114, 35-48.

Huang, Z., Grim, G., Schaidle, J., Tao, L., 2020. Using waste CO2 to increase ethanol production from corn ethanol biorefineries: Techno-economic analysis. *Applied Energy*, 280.

Huang, Z., Grim, R. G., Schaidle, J. A.,Tao, L., 2021. The economic outlook for converting CO2 and electrons to molecules. *Energy & Environmental Science*, 7.

Hubbard, D.E., 2018. Chemical pricing information for student design projects and cost engineering: Challenges and opportunities, in: ASEE Annual Conference and Exposition. Salt Lake City, Utah.

Humbird, D., Davis, R., Tao, L., Kinchin, C., Hsu, D., Aden, A., Schoen, P., Lukas, J., Olthof, B., Worley, M., Sexton, D., Dudgeon, D., 2011. Process Design and Economics for Biochemical Conversion of Lignocellulosic Biomass to Ethanol: Dilute-Acid Pretreatment and Enzymatic Hydrolysis of Corn Stover, s.l.: s.n.

Humbird, D., Davis, R., McMillan, J. D., 2017. Aeration costs in stirred-tank and bubble column bioreactors. *Biochemical Engineering Journal*, 127, 161-166.

Huntington, T., Baral, N.R., Yang, M., Sundstrom, E., Scown, C.D., 2023. Machine learning for surrogate process models of bioproduction pathways. *Bioresource Technology*, 370, 128528.

Ioannou, A., Angus, A., Brennan, F., 2018. Effect of electricity market price uncertainty modelling on the profitability assessment of offshore wind energy through an integrated lifecycle techno-economic model. *Journal of Physics: Conference Series*.

Jiang, H., Wang, S., Xing, L., Pinfield, V.J., Xuan, J., 2023. Machine learning based techno-economic process optimisation for CO2 capture via enhanced weathering. *Energy and AI*, 12, 100234.

Jupeng Bio, 2017. History. [Online] Available at: http://www.jupengbio.com/history [Accessed 13 July 2023].

Kaack, L. H., Apt, J., Morgan, M. G., McSharry, P., 2017. Empirical prediction intervals improve energy forecasting. *Proceedings of the National Academy of Sciences*, 144(33), 8752-8757.

Khan, A. & Lapkin, A., 2022. Designing the process designer: Hierarchical reinforcement learning for optimisation-based process design. *Chemical Engineering and Processing - Process Intensification*, 180, 108885.

Khan, N. E., Myers, J. A., Tuerk, A. L. & Curtis, W. R., 2014. A process economic assessment of hydrocarbon biofuels production using chemoautotrophic organisms. *Bioresource Technology*, 172, 201-211.

Khan, R., Zeeshan, M., Fatima, S., Ciolkosz, D., Dimitriou, I., Jin, H., 2023. A comparative techno-economic analysis of combined oil and power production from pyrolysis and co-pyrolysis plants utilizing rice straw and scrap rubber tires. *Fuel*, 348, 128639.

Kinchin, C., 2020. BETO Biofuels TEA Database. [Online] Available at: https://bioenergykdf.net/content/beto-biofuels-tea-database [Accessed 29 July 2022].

Köpke, M. & Simpson, S. D., 2020. Pollution to products: recycling of 'above ground' carbon by gas fermentation. *Current Opinion in Biotechnology*, 65, 180-189.

Kumar, M., Oyedun, A.O., Kumar, A., 2019. A comparative analysis of hydrogen production from the thermochemical conversion of algal biomass. *International Journal of Hydrogen Energy*, 44 (21), 10384-10397.

Lane, J., 2014. On the Mend: Why INEOS Bio isn't producing ethanol in Florida. [Online] Available at: https://www.biofuelsdigest.com/bdigest/2014/09/05/on-the-mend-why-ineos-bio-isnt-reporting-much-ethanol-production/ [Accessed 13 July 2023].

Lang, H., 1947. Engineering Approach to Preliminary Cost Estimates. *Chemical Engineering*, 54, 130-133.

LanzaJet, 2022. LanzaJet Marks Major Milestone on its Freedom Pines Fuels Construction. [Online] Available at: https://www.lanzajet.com/lanzajet-marks-major-milestone-on-its-freedom-pines-fuels-construction/ [Accessed 13 July 2023].

LanzaTech, 2022. New Waste-to-Ethanol Facility in Japan Turns Municipal Solid Waste into Products. [Online] Available at: https://lanzatech.com/new-waste-to-ethanol-facility-in-japan-turns-municipal-solid-waste-into-products/ [Accessed 07 July 2023].

LanzaTech, 2023. World's leading steel company, ArcelorMittal and LanzaTech announce first ethanol samples from commercial flagship carbon capture and utilisation facility in Ghent, Belgium. [Online] Available at: https://lanzatech.com/worlds-leading-steel-company-arcelormittal-and-lanzatech-announce-first-ethanol-samples-from-commercial-flagship-carbon-capture-and-utilisation-facility-in-ghent-belgium/ [Accessed 6 July 2023].

Levett, I., Birkett, G., Davies, N., Bell, A., Langford, A., Laycock, B., Lant, P., Pratt, S., 2016. Techno-economic assessment of poly-3-hydroxybutyrate (PHB) production from methane—The case for thermophilic bioprocessing. *Journal of Environmental Chemical Engineering*, 4(4), 3724-3733.

Liang, J., Liu, Y., Chen, J., E, J., Leng, E., Zhang, F., Liao, G., 2023. Performance comparison of black liquor gasification and oxidation in supercritical water from thermodynamic, environmental, and techno-economic perspectives. *Fuel,* 334, 126787.

Liew, F., Martin, M.E., Tappel, R.C., Heijstra, B.J., Mihalcea, C., Köpke, M., 2016. Gas Fermentation—A Flexible Platform for Commercial Scale Production of Low-Carbon-Fuels and Chemicals from Waste and Renewable Feedstocks. *Frontiers in Microbiology,* 7.

Liew, F.E., Nogle, R., Abdalla, T., Rasor, B.J., Canter, C., Jensen, R.O. Wang, L., Strutz, J., Chirania, P., Tissera, S.D., Mueller, A.P., Ruan, Z., Gao, A., Tran, L., Engle, N.L., Bromley, J.C., Daniell, J., Conrado, R., Tschaplinski, T.J., GIannone, R.J., Hettich, R.L., Karim, A.S., Simpson, S.D., Brown, S.D., Leang, C., Jewett, M.C., Köpke, M., 2022. Carbon-negative production of acetone and isopropanol by gas fermentation at industrial pilot scale. *Nature Biotechnology*, 40, 335-344.

Li, S., Jiang, Y., Snowden-Swan, L.J., Askander, J.A., Schmidt, A.J., Billing, J.M., 2021. Techno-economic uncertainty analysis of wet waste-to-biocrude via hydrothermal liquefaction. *Applied Energy*, 283.

Lopez, G., Keiner, D., Fashi, M., Koiranen, T., Breyer, C., 2023. From fossil to green chemicals: sustainable pathways and new carbon feedstocks for the global chemical industry. *Energy and Environmental Science*, 16, 2879-2909.

Lynch, M. D., 2021. The bioprocess TEA calculator: An online technoeconomic analysis tool to evaluate the commercial competitiveness of potential bioprocesses. *Metabolic Engineering*, 65, 42-51.

Manca, D., 2012. A methodology to forecast the price of commodities. *Computer Aided Chemical Engineering*, 1306-1310.

Manca, D., Fini, A., Oliosi, M., 2011. Dynamic Conceptual Design under Market Uncertainty and Price Volatility. *Computer Aided Chemical Engineering*, 336-340.

Mahmud, R., Moni, S,M., High, H., Carbajales-Dale, M., 2021. Integration of techno-economic analysis and life cycle assessment for sustainable process design – A review. *Journal of Cleaner Production*, 317, 128247.

Ma, K., Shi, T., Hu, Y., Yang, S., Shen, W., He, C., Liu, Y., Liu, Z., R, J., 2022. Poultry litter utilization for waste-to-wealth: Valorization process simulation and comparative analysis based on thermodynamic and techno-economic assessment. *Energy Conversion and Management,* 269, 116135.

Ma, S., Dong, C., Hu, X., Xue, J., Zhao, Y., Wang, X., 2022. Techno-economic evaluation of a combined biomass gasification-solid oxide fuel cell system for ethanol production via syngas fermentation. *Fuel*, 324, 124395.

Mcbride, K. & Sundmacher, K., 2019. Overview of Surrogate Modeling in Chemical Process Engineering. *Chemie Ingenieur Technik*, 91(3), 228-239.

McGarvey, E. & Tyner, W. E., 2018. A stochastic techno-economic analysis of the catalytic hydrothermolysis aviation biofuel technology. *Biofuels, Bioproducts and Biorefining*, 12(3), 474-484.

Meng, F., Wagner, A., Kremer, A.B., Kanazawa, D., Leung, J.J., Goult, P., Guan, M., Herrmann, S., Speelman, E., Sauter, P., Lingeswaran, S., Stuchtey, M.M., Hansen, K., Masanet, E., Serrenho, A.C., Ishii, N., Kikuchi, Y., Cullen, J.M., 2023. Planet-compatible pathways for transitioning the chemical industry. *Proceedings of the National Academy of Sciences*, 120(8).

Michailos, S., Parker, D., Webb, C., 2019a. Design, Sustainability Analysis and Multiobjective Optimisation of Ethanol Production via Syngas Fermentation. *Waste Biomass Valorisation*, 10, 865-876.

Michailos, S., Emeike, O., Ingham., D Hghes, K.J., Pourkashanian, M., 2019b. Methane production via syngas fermentation within the bio-CCS concept: A techno-economic assessment. *Biochemical Engineering Journal*, 150(15), 107-290.

Mishra & Upadhyay, 2021. Review on biomass gasification: Gasifiers, gasifying mediums, and operational parameters. *Materials Science for Energy Technologies,* 4, 329-340.

Moghaddam, E. M., Goel, A., Siedlecki, M., Michalska, K., Yakaboylu, O., de Jong, W., 2021. Supercritical water gasification of wet biomass residues from farming and food production practices: lab-scale experiments and comparison of different modelling approaches. *Sustainable Energy Fuels.* 5, 1521-1537.

Moncada, J., Gursel, I., Worrell, E., 2018. Production of 1,3-butadiene and ε-caprolactam from C6 sugars: Techno-economic analysis. Biofuels, *Bioproducts & Biorefining*, 12, 600-623.

Naveenkumar, R. & Jeehoon, H., 2023. Techno-economic analysis and life cycle assessment of poly (butylene succinate) production using food waste. *Waste Management*, 156, 168-176.

Neveux, T., 2018. Ab-initio process synthesis using evolutionary programming. *Chemical Engineering Science*, 209-221.

Nguyen, N. & Tyner, W. E., 2021. Assessment of the feasibility of the production of alternative jet fuel and diesel using catalytic hydrothermolysis technology: a stochastic techno-economic analysis. *Biofuels, Bioproducts and Biorefining*, 16(1), 91-104.

Okolie, J.A., Tabat, M.E., Gunes, B., Epelle, E.I., Mukherjee, A., Nanda, S., Dalai, A.K., 2021a. A techno-economic assessment of biomethane and bioethanol production from crude glycerol through integrated hydrothermal gasification, syngas fermentation and biomethanation. *Energy Conversion and Management: X*, 12.

Okolie, J. A., Nanda, S., Dalai, A. K., Kozinski, J. A., 2021b. Techno-economic evaluation and sensitivity analysis of a conceptual design for supercritical water gasification of soybean straw to produce hydrogen. *Bioresource Technology.* 331, 125005.

Okoro, O. & Faloye, F., 2020. Comparative Assessment of Thermo-Syngas Fermentative and Liquefaction Technologies as Waste Plastics Repurposing Strategies. *AgriEngineering*, 2, 378-392.

Olafasakin, O., Chang, Y., Passalacqua, A., Subramaniam, S., Brown, R.C., Wright, M.M. 2021. Machine Learning Reduced Order Model for Cost and Emission Assessment of a Pyrolysis System. *Energy and Fuels*, 35, 9950-9960.

Onigbajumo, A., Taghipour, A., Ramirez, J., Will, G., Ong, T-C., Couperthwaite, S., Steinberd, T., Rainey, T., 2021. Techno-economic assessment of solar thermal and alternative energy integration in supercritical water gasification of microalgae. *Energy Conversion and Management,* 230, 113807.

Onigbajumo, A., Taghipour, A., Will, G., Van, T. C., Couperthwaite, S., Steinberd, T., Rainey, T., 2022. Effects of process-thermal configuration on energy, exergy, and thermo-economic performance of solar driven supercritical water gasification. *Energy Conversion and Management,* 251, 115002.

Özdenkçi, K., De Blasio, C., Sarwar, G., Melin, K., Koskinen, J., Alopaeus, V., 2019. Techno-economic feasibility of supercritical water gasification of black liquor. *Fuel.* 189, 116284.

Pacheco, M., Moura, P., Silva, C., 2023. A Systematic Review of Syngas Bioconversion to Value-Added Products from 2012 to 2022. *Energies*, 16(1), 3241.

Pandey, U., Putta, K. R., Rout, K., Rytter, E., Blekkan, E. A., Hillestad, M., 2022. Conceptual design and techno-economic analysis of biomass to liquid processes. *Frontiers in Energy Research.* 10.

Pereira, L. G., MacLean, H. L., Saville, B. A., 2017. Financial analyses of potential biojet fuel production technologies. *Biofuels, Bioproducts and Biorefining*, 11(4), 665-681.

Petersen, A.M., Okoro, O.V., Chireshe, F., Moonsamy, T., Görgens, J.F., 2021. Systematic cost evaluations of biological and thermochemical processes for ethanol production from biomass residues and industrial off-gases. *Energy Conversion and Management*, 243, 114398.

Piccolo, C. & Bezzo, F., 2009. A techno-economic comparison between two technologies for bioethanol production from lignocellulose. *Biomass & Bioenergy*, 33(3), 478-491.

Preethi, M, G., Kumar, G., Karthikeyan, O.P., Varjani, S., J, R.B., 2021. Lignocellulosic biomass as an optimistic feedstock for the production of biofuels as valuable energy source: Techno-economic analysis, Environmental Impact Analysis, Breakthrough and Perspectives. *Environmental Technology & Innovation*, 24, 102080.

Prévoteau, A., MCarvajal-Arroyo, J., Ganigué, R., Rabaey, K., 2020. Microbial electrosynthesis from CO2: forever a promise?. *Current Opinion in Biotechnology*, 62, 48-57.

Puig-Gamero, M., Trapero, J.R., Pedregal, D.J., Sanchex, P., Sánchez-Silva, L., 2021. Impact of the forecast price on economic results for methanol production from olive waste. *Fuel*, 295.

Queneau, Y. & Han, B., 2022 Biomass: Renewable carbon resource for chemical and energy industry. *The Innovation*, 3, 100184.

Rahbari, A., Shirazi, A., Venkataraman, M. B., Pye, J., 2019. A solar fuel plant via supercritical water gasification integrated with Fischer–Tropsch synthesis: Steady-state modelling and techno-economic assessment. *Energy Conversion and Management,* 184, 636-648.

Rahbari, A., Shirazi, A., Venkataraman, M. B., Pye, J., 2021a. Solar fuels from supercritical water gasification of algae: Impacts of low-cost hydrogen on reformer configurations. *Applied Energy.* 288, 116620.

Rahbari, A., Shirazi, A., Pye, J., 2021b. Methanol fuel production from solar-assisted supercritical water gasification of algae: a techno-economic annual optimisation. *Sustainable Energy & Fuels.* 5, 4913-4931.

Redl, S., Sukumara, S., Ploeger, T., Wu, L., Jensen. T. Ø., Nielsen, A.T., Noorman, H., 2017. Thermodynamics and economic feasibility of acetone production from syngas using the thermophilic production host Moorella thermoacetica. *Biotechnology for Biofuels and Bioproducts*, 10.

Regis, F., Hugo, A., Monteverde, A., Fino, D., 2023. A techno-economic assessment of bioethanol production from switchgrass through biomass gasification and syngas fermentation. *Energy*, 274, 127318.

Ro, K., Dietenberger, M.A., Libra, J.A., Proeschel, R., Atiyeh, H.K., Sahoo, K., Park, W.J., 2019. Production of Ethanol from Livestock, Agricultural, and Forest Residuals: An Economic Feasibility Study, *Environments*, 6(8).

Roy, P., Dutta, A., Deen., 2015. Greenhouse gas emissions and production cost of ethanol produced from biosyngas fermentation process. *Bioresource Technology*, 192, 185-191.

Salman, C., Thorin, E., Yan, J., 2020. Uncertainty and influence of input parameters and assumptions on the design and analysis of thermochemical waste conversion processes: A stochastic approach. *Energy Conservation and Management*, 214, 112867.

Sanaye, S., Alizadeh, P., Yazdani, M., 2022. Thermo-economic analysis of syngas production from wet digested sewage sludge by gasification process. *Renewable Energy.* 190, 524-539.

Sapp, M., 2021. LanzaTech and BASF achieve first n-octanol milestone. [Online] Available at: https://www.biofuelsdigest.com/bdigest/2021/05/11/lanzatech-and-basf-achieve-first-n-octanol-milestone/ [Accessed 13 July 2023].

Saxena, R. C., Seal, D., Kumar, S., Goyal, H. B., 2008. Thermo-chemical routes for hydrogen rich gas from biomass: A review. *Renewable and Sustainable Energy Reviews.* 12 (7), 1909-1927.

Scown, C.D; Baral, N.R; Yang, M; Vora, N; Huntington, T., 2021. Technoeconomic analysis for biofuels and bioproducts. *Current Opinion in Biotechnology*, 67, 58-64.

Seidenberg, J., Khan, A., Lapkin, A., 2023. Boosting autonomous process design and intensification with formalized domain knowledge. *Computers & Chemical Engineering*, 169, 108097.

Seider, W.D; Lewin, D.R; Seader, J.D; Widago, S; Gani, R; Ming Ng, K. 2017. '*Cost Accounting and Capital Cost Estimation',* in *'Prododuct and Process Design Principles. Synthesis Analysis and Evaluation'*, Fourth Edition, John Wiley & Sons Inc., 2017, New York.

Sepiacci, P., Depetri, V. & Manca, D., 2017. A systematic approach to the optimal design of chemical plants with waste reduction and market uncertainty. *Computers & Chemical Engineering*, 102, 96-109.

Sinnott, R. & Towler, G., 2013. Chemical Engineering Design - Principles, Practice and Economics of Plant and Process Design. 2nd ed. s.l.:Elsevier.

Shi, T., Moktadir, M. A., Ren, J., Shen, W., 2023. Comparative economic, environmental and exergy analysis of power generation technologies from the waste sludge treatment. *Energy Conversion and Management,* 286, 117074.

Symister, O., 2016. An Analysis of Capital Cost Estimation Techniques for Chemical Processing. Melbourne, Florida: s.n.

Takors, R., Kopf, M., Mampel, J., Bluemke, W., Blombach, B., Eikmanns, B., Bengelsdorf, F.R., Weuster-Botz, D., Dürre, P., 2018. Using gas mixtures of CO, CO2 and H2 as microbial substrates: the do's and don'ts of successful technology transfer from laboratory to production scale. *Microbial Biotechnology*, 11(4), 606-625.

Tan, E.C.D., Snowden-Swan, L.J., Talmadge, M., Dutta, A., Jones, S., Ramasamy, K.K., Gray, M., Dagle, R., Padmaperuma, A., Gerber, M., Sahir, A.H., Tao, L., Zhang, Y., 2016. Comparative techno-economic analysis and process design for indirect liquefaction pathways to distillate-range fuels via biomass-derived oxygenated intermediates upgrading. *Biofuels, Bioproducts & Biorefining.*

Temitayo, G., Akbari, M., Kumar, A., 2023. Techno-economic assessment of an integrated biorefinery producing bio-oil, ethanol, and hydrogen. *Fuel,* 332, 126022.

Tsagkari, M., Kokossis, A., Dubois, J.-L., 2020. A method for quick capital cost estimation of biorefineries beyond the state of the art. *Biofuels, Bioproducts and Biorefining*, 14(5), 1061-1088.

Turton, R., Bailie, R.C., Whiting, W.B., Shaeiwitz, J.A., Bhattacharyya, D. 2013. Analysis, Synthesis, and Design of Chemical Processes. 4th Edition ed. s.l.:Prentice Hall.

Umenweke, G. C., Pace, R. B. Santillan-Jimenez, E., Okolie, J. A., 2023. Techno-economic and life-cycle analyses of sustainable aviation fuel production via integrated catalytic deoxygenation and hydrothermal gasification. *Chemical Engineering Journal,* 452, 139215.

van Amsterdam, M., 2018. Factorial Techniques applied in Chemical Plant Cost Estimation: A Comparative Study based on Literature and Cases. Delft: s.n.

Viswanathan, M. B., Raman, D. R., Rosentrater, K. A., Shanks, B. H., 2020. A Technoeconomic Platform for Early-Stage Process Design and Cost Estimation of Joint Fermentative–Catalytic Bioprocessing. *Processes*, 8(2), 229.

Vogel, G., Balhorn, L., Schweidtmann, A., 2023a. Learning from flowsheets: A generative transformer model for autocompletion of flowsheets. *Computers & Chemical Engineering*, 171, 108162.

Vogel, G., Hirtreiter, E., Balhorn, L., Schweidtmann, A., 2023b. SFILES 2.0: an extended text-based flowsheet representation. *Optimization and Engineering*, 565.

Wiatrowski, M., Klein, B.C., Davis, R.W., Quiroz-Artia, C., Tan, E.C.D., Hunt, R.W., David, R.E., 2022. Techno-economic assessment for the production of algal fuels and value-added products: opportunities for high-protein microalgae conversion. *Biotechnology for Biofuels and Bioproducts*, 15.

Wu Y.X., Wu Q.B., Zhu J.Q., 2019. Improved EEMD-based crude oil price forecasting using LSTM networks. *Physica A*, 516, 114-124

Wunderlich, J., Armstrong, K., Buchner, G.A., Styring, P., Schomäcker, R., 2021. Integration of techno-economic and life cycle assessment: Defining and applying integration types for chemical technology development. *Journal of Cleaner Production*, 287.

Yao, G., Staples, M. D., Malina, R., Tyner, W. E., 2017. Stochastic techno-economic analysis of alcohol-to-jet fuel production. *Biotechnology for Biofuels and Bioproducts*, 10.

Yoshida, Y., Daraki, K., Matsumura, Y., Matsuhashi, R., Li, D., Ishitani, H., Komiyama, H., 2003. Comprehensive comparison of efficiency and CO_2 emissions between biomass energy conversion technologies—position of supercritical water gasification in biomass technologies. *Biomass and Bioenergy*, 25 (3) 257-272.

Zhang, Y., Brown, T. R., Hu, G., Brown, R. C., 2013. Techno-economic analysis of two bio-oil upgrading pathways. *Chemical Engineering Journal*, 895-904.

Zhao, X., Yao, G., Tyner, W. E., 2016. Quantifying breakeven price distributions in stochastic techno-economic analysis. *Applied Energy*, 318-326.

Zimmermann, A., Wunderlich, J., Müller, L., Buchner, G.A., Marxen, A., Michailos, S., Armstrong, K., Naims, H., McCord, S., Strying, P., Sick, V., Schomäcker, R., 2020. Techno-Economic Assessment Guidelines for CO2 Utilization. *Frontiers in Energy Research*, 8.

3 Methodology

The following section outlines and critically evaluates the overall methodology developed and used throughout this thesis, which can be broadly categorised into the following areas: process modelling, techno-economic analysis, sensitivity analysis, life cycle assessment, commodity price projections, and surrogate modelling. The methodology employed in each of these categories is discussed in the respective subsections. Figure 3.1 illustrates the chapters in which each of these methods are implemented, and Table 3.1 summarises the contribution of each chapter.

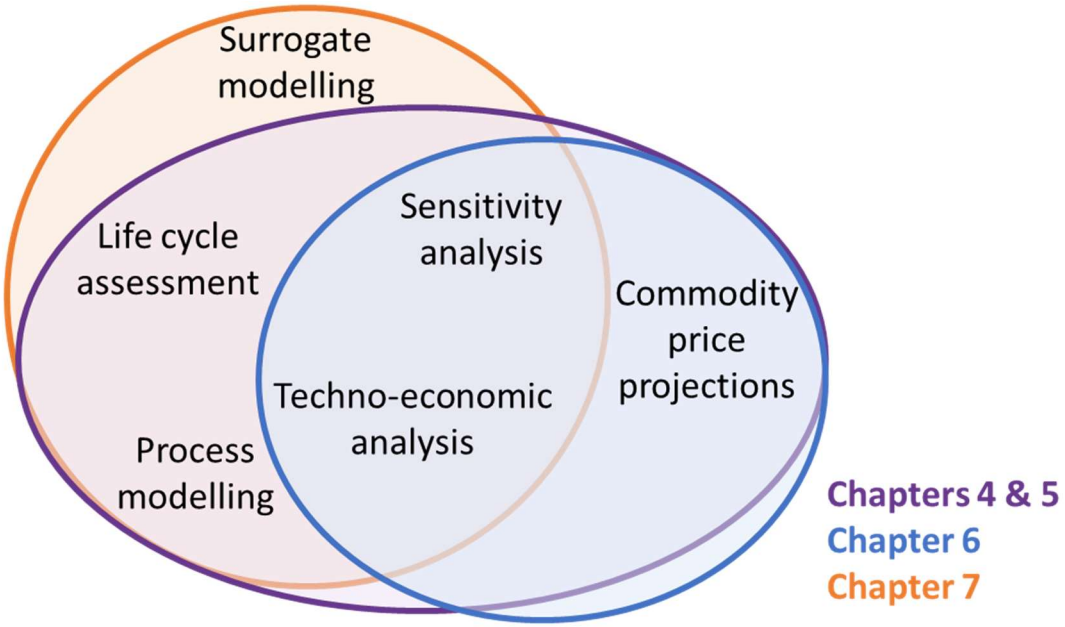

Figure 3.1: Summary of overall thesis methodology and chapter implementation.

Table 3.1: Summary of chapter contributions.

Chapter	Article Title	Novelty	Case Study
4: Initial techno-economic analysis of the integrated platform	Reconciling the Sustainable Manufacturing of Commodity Chemicals with Feasible Technoeconomic Outcomes: Assessing the investment case for heat integrated aerobic gas fermentation	First TEA and LCA of the proposed aerobic gas fermentation and SCWG platform. The novel platform consisted of SCWG heat integrated with aerobic gas fermentation. Three different methods of calculating the capital and fixed operating costs are assessed.	Isopropanol and acetone production
5: Comparative techno-economic analysis of the integrated platform	Renewable butadiene: A case for hybrid processing via bio- and chemo-catalysis	Comparative TEA and LCA for the production of 1,3-butadiene. The aerobic gas fermentation and SCWG platform was followed by catalytic upgrading to produce the reduced 1,3-butadiene product. Two alternative purely chemo-catalytic routes to 1,3-butadiene were modelled and compared to the aerobic gas fermentation route.	1,3-butadiene production
6: Creating a robust, unbiased, price selection procedure for techno-economic analyses	Probabilistic commodity price projections for unbiased techno-economic analyses	ML was used to produce 20-25 year probabilistic commodity price projections for techno-economic, sensitivity, and uncertainty analyses. An ensemble of 100 LSTMs was used to exploit the underlying determinism and/or stochastic variability within the commodity's historic time series.	Isopropanol and acetone production 1,3-butadiene production
7: Creation of a surrogate model for the economic evaluation of feedstocks	A surrogate model for the economic evaluation of renewable hydrogen production from biomass feedstocks via supercritical water gasification	An ML surrogate model of the TEA for hydrogen production via low temperature SCWG was created. The model predicts the LCOH based on user input feedstock-capacity-location combinations and is made publicly available.	Renewable hydrogen production

3.1 Overview of the heat integrated platform

This thesis examines the heat integrated SCWG and aerobic gas fermentation platform as presented by Bommareddy et al. (2020). Figure 3.2 depicts the thermal cycle between the two integrated technologies considering guaiacol as a renewable carbon source, reprinted from Bommareddy et al., (2020). The purple cycle highlights the cumulative energy recovery within the heat pump cycle. The blue arc represents the renewable carbon feedstock flow prior to fermentation. The pink arc illustrates the energy flow from the fermentation product.

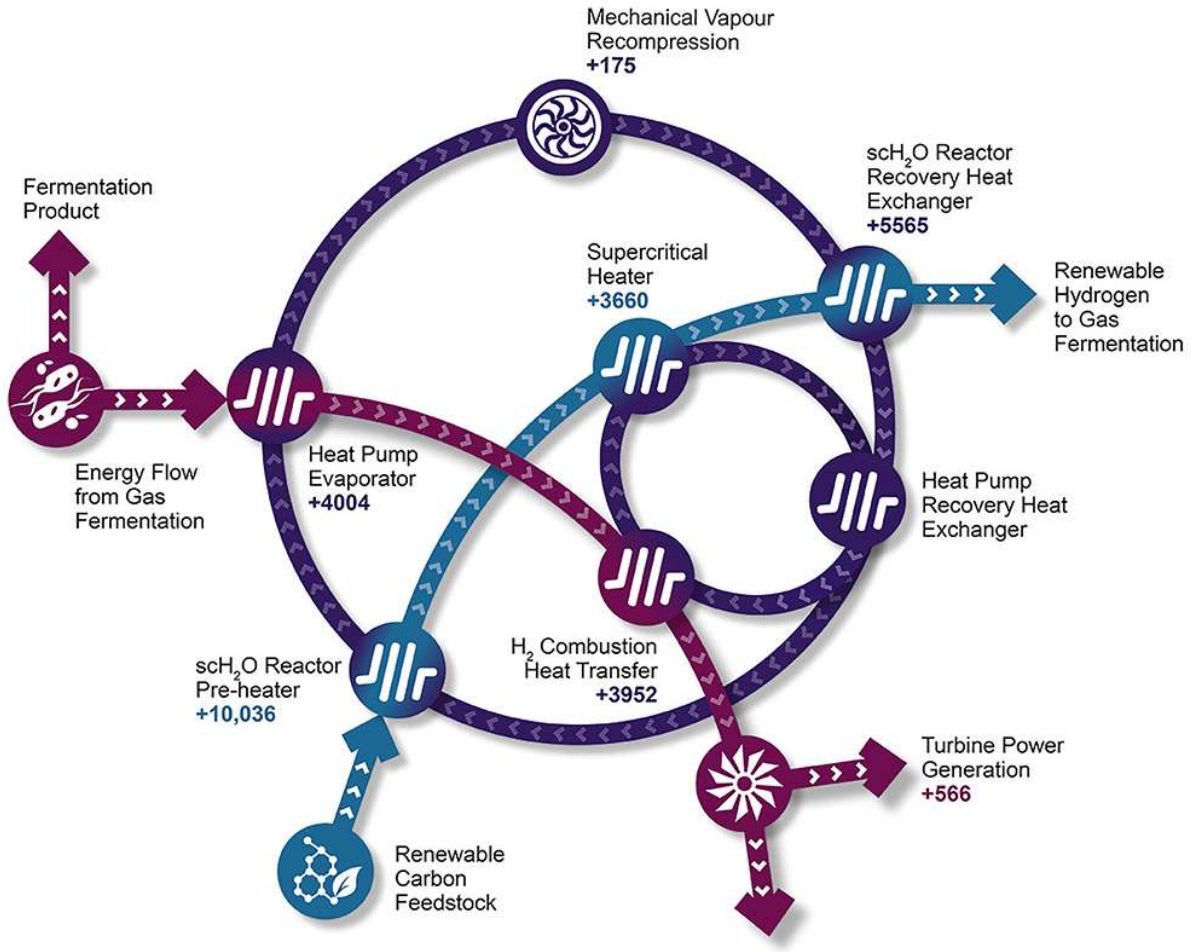

Figure 3.2: Schematic of the heat integrated SCWG and aerobic gas fermentation process, taken from Bommareddy et al., (2020).

The thermal cycle commences with the utilisation of heat generated from aerobic fermentation to vaporise the thermal fluid used in the process (4,004 kW/ton of guaiacol). Isopentane was chosen as the thermal fluid owing to its vaporisation temperature (~28°C) allowing it to utilise the low temperature heat produced from fermentation (~37°C). The vaporised isopentane then undergoes compression, further increasing the enthalpy of the stream by 175 kW/ton of guaiacol. To optimise energy recovery, a sequence of heat exchangers is employed, reclaiming heat from the SCWG effluent (5,565 kW/ton guaiacol) and within the isopentane loop after heating the renewable carbon feedstock. Additional heat contribution comes from the combustion chamber (3,952 kW/ton of guaiacol) which operates on a portion of the syngas produced from SCWG. This integration elevates the temperature of isopentane to a level suitable to convert the sub-critical renewable carbon feedstock to supercritical conditions prior to the SCWG reactor (3,660 kW/ton of guaiacol). The cycle concludes with the condensation of the isopentane vapor upon preheating the renewable carbon feedstock. This is followed by expansion of the isopentane to its starting pressure, preparing it for the next cycle. Notably, in addition to the heat integration, upon expanding the SCWG effluent using a turbo-expander 566 kW/ton guaiacol of renewable electricity is generated (Turbine Power Generation). The technology integration links low-temperature, exothermic, gas fermentation with high temperature, endothermic, SCWG.

3.2 Process modelling

Process models built in Aspen HYSYS formed the basis for the TEAs undertaken in this thesis. The accuracy and comprehensiveness of these process simulations greatly influences the evaluation of the technologies and the resulting conclusions. As emphasised by Scown et al. (2021) rigorous process models are required to capture process complexities, model utility and energy integration, incorporate co-generation of heat and power, and exploit recycling opportunities. Therefore, to thoroughly assess the techno-economic potential of the proposed heat integrated aerobic gas fermentation and SCWG platform, detailed process models were developed. A process simulation was created for Chapters 4, 5, and 7, based on the production of isopropanol and acetone, 1,3-butadiene, and hydrogen, respectively.

The five stages of process synthesis and design, as outlined by Seider et al. (2017) were followed to develop each simulated process. These following steps, along with heuristics followed during each step, are:

1. Eliminate differences in molecular types (Chemical reactions)
    - Identifying reactions pathways to target chemicals
2. Distribute Chemicals (Mixing and recycles)
    - Purging inert species or inhibitory compounds
    - Recycling reactants to increase product yields
3. Eliminate composition differences (Separation sequences)
    - Utilising flash drums to separate vapour-liquid mix streams before distillation or adsorption
    - Performing marginal vapour rate analysis to optimise distillation sequences
4. Eliminate temperature pressure and phase differences (Energy adjustments)
    - Adjusting temperatures and pressures for reaction and separation sequences
    - Prioritising pumping liquids over compressing gases
5. Task integration (Connecting unit operations, utility integration)
    - Minimising external material and energy use

Where available, kinetic models from literature were prioritised to facilitate the development of these detailed models. Kinetic models allowed for the optimisation of reaction conditions, incorporation of recycling schemes, and served as the basis for reactor sizing. In cases where kinetic models were not available, conversion data from experimental literature, industrial patents, and internal experimental results were utilised. Table 3.2 provides an overview of the data sources used as the foundation for modelling each reaction. Additionally, when replicating industrialised processes, the reactor configurations, recycling schemes, and separation methods were also obtained from relevant literature.

Table 3.2: Data sources for process modelling

Process section	Data source	Chapter
Aerobic gas fermentation	Conditions and yields from internal experimental results	Chapter 4 and 5
Acetaldehyde hydrogenation to Ethanol	Conditions and conversion data from industrial patents for butanal hydrogenation (Europe Patent No. 0073129, 1982) (Europe Patent No. 0008767A1, 1979)	Chapter 5
Ethanol to Butadiene	Conditions and conversion data from experimental study (Dai et al., 2017)	
Mixed alcohol synthesis	Yields from 2011 NREL report (Dutta et al., 2011)	
Biomass gasification	Conditions and conversion data (Dutta et al., 2011) (Tan et al., 2015)	
Syngas to methanol	Conditions and kinetics for the commercial $Cu/ZnO/Al_2O_3$ catalyst (Vanden Bussche & Froment, 1996)	
Methanol dehydration to DME	Conditions and kinetics for the commercial γAl_2O_3 catalyst (Ng et al., 1999) (Diep & Wainwright, 1987)	
Methanol to Propene	Conditions and kinetics for the commercial H-ZSM-5 zeolite catalyst (Huang et al., 2016)	
Oxo-alcohols process Propene to Butanol	Conditions and conversion data from Johnson Matthey patents Hydroformylation: US patent 4,593,127 (Patent No. 4593127, 1986) Hydrogenation: European Patent 0,008,767 (Europe Patent No. 0008767A1, 1979)	
Dehydration (Butanol to Butene)	Process conditions and conversion data from industrial patents for a silane-modified γAl_2O_3 catalyst (United States Patent No. 0238788 A1, 2012)	
Oxidative dehydrogenation (Butene to Butadiene)	Conditions and conversion data for a multi-component bismuth molybdate ($Co_9Fe_3Bi_1Mo_{12}O_{51}$) catalyst (Jung et al., 2008)	
Steam methane reforming	Conditions and kinetics for the commercial Ni/α-Al2O3 catalyst (Hou & Hughes, 2001)	Chapter 7
High temperature shift	Conditions and kinetics for a commercial iron-based catalyst (Hla et al., 2009)	
Low temperature shift	Conditions and kinetics for the Sud-Chemie Cu/ZnO/Al2O3 catalyst (Choi & Stenger, 2003)	

3.3 Techno-economic analysis

The mass and energy balance obtained from the process simulations served as the basis for determining the major equipment cost, which, in turn, was used to calculate the total capital investment and fixed operating costs. The variable operating costs were directly derived from the mass and energy balance. These capital, fixed operating, and variable operating costs were subsequently employed in the investment analysis to evaluate the economic viability. Figure 3.3 provides a simplified flow diagram illustrating this methodology, further detail on each of these steps is provided in the subsequent sections.

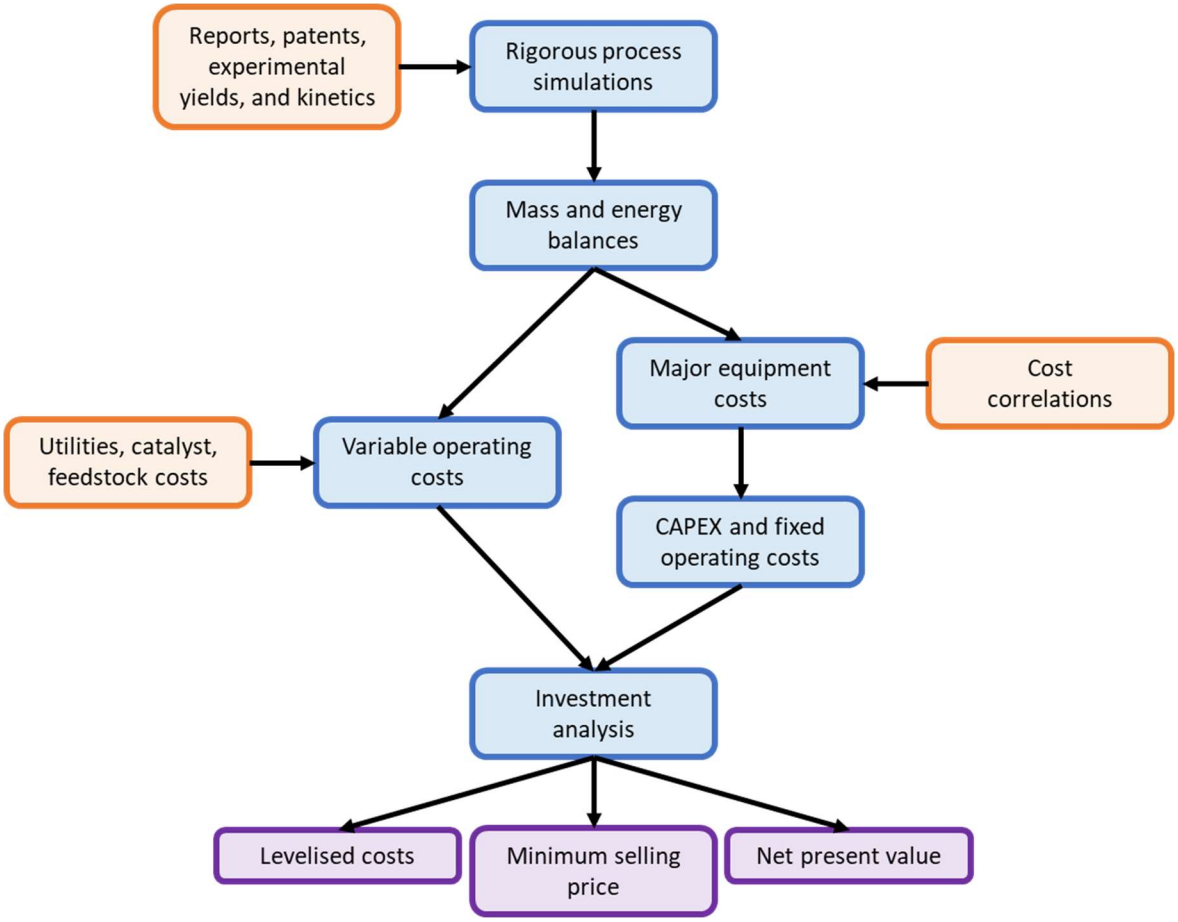

Figure 3.3: Simplified flow diagram of the techno-economic analysis methodology employed

3.3.1 Major equipment costs

The estimation of major equipment costs was carried out using costing models from Seider et al. (2017) and adjusted to reflect the prices of 2019-2021 based on the Chemical Engineering Plant Cost Index (Chemengonline). While other methods such as those found in Chemical Engineering Design (Sinnott & Towler, 2013), Aspen Capital Cost Estimator software, or vendor quotes with scaling factors can be used for equipment cost correlations, the equipment cost models from Seider et al. (2017) were chosen due to their wide coverage of equipment types, detailed calculation methods for sizing factors, and consideration of pressure, material, and temperature factors. Furthermore, using equations rather than software estimates allows practitioners to comprehend the key factors influencing equipment costs, such as reactor residence times and heat transfer areas. Table 3.3 presents the bare module equipment cost correlations employed in the TEAs conducted in this thesis. It should be noted that material factors, pressure factors, and type factors are not presented as they vary depending on the

equipment type. Type factors may include the drive type for compressors, tube lengths for heat exchangers, or the number of stages in a pump. Further detail on these factors can be found in Seider et al. (2017), Chapter 16.

Table 3.3: Equipment cost correlations.

Equipment type	Size factor (S)	Cost correlation (Cb, bare module cost)
Centrifugal pump (excluding motor)	$S = Q * H^{0.5}$ Q = flowrate (gpm) H = Head of fluid (ft)	$Cb = e^{(12.1656 - 1.1448(\ln(S)) + 0.0862(\ln(S))^2)}$
Compressor	S = Horsepower (Hp)	$Cb = e^{(9.1552 + 0.63(\ln(S)))}$
Distillation column, absorber, stripper (tower)	S = weight of tower (lb) $S = \pi(D + ts)(L + 0.8 * D) * ts * \rho$ D = diameter (in) L = tan-tan length (in) Ts = shell thickness (in) P = material density (lb/in^3)	$Cb = Cv + Cpl + VPCPK + CDR$ $Cv = e^{(10.5449 - 0.4672(\ln(S)) + 0.05482(\ln(S))^2)}$ $Cpl = 341 * D^{0.63316} * L^{0.80161}$ $VPCPK = VP * 2825$ $CDR = 140 * CSA$ VP = volume of packing (ft^3) CSA = cross sectional area of tower (ft^2)
Electric motor (for pumps)	S = Pump horsepower (Hp)	$Cb = e^{(5.9332 + 0.16829(\ln(S)) + 0.0110056(\ln(S))^2 + 0.071413(\ln(s))^3 - 0.0063788(\ln(s))^4)}$
Fired heaters	S = duty (Btu/hr)	$Cb = 0.416 * S^{0.77}$ (steam boiler) $Cb = 0.974 * S^{0.81}$ (reformer)
Flash drums, fermenters (vertical pressure vessel)	S = weight of pressure vessel (lb) $S = \pi(D + ts)(L + 0.8 * D) * ts * \rho$ D = diameter (in) L = tan-tan length (in) Ts = shell thickness (in) P = material density (lb/in^3)	$Cb = Cv + Cpl$ $Cv = e^{(7.139 + 0.18255(\ln(S)) + 0.02297(\ln(S))^2)}$ $Cpl = 410 * D^{0.73960} * L^{0.70684}$
Heat exchanger	S = Heat transfer area (m^2)	$Cb = e^{(11.4185 - 0.9228(\ln(S)) + 0.09861(\ln(S))^2)}$
High pressure gear pump (excluding motor)	S = flowrate through pump (gpm)	$Cb = e^{(7.6964 + 0.1986(\ln(S)) + 0.091(\ln(S))^2)}$
Reactors (horizontal pressure vessel)	S = weight of pressure vessel (lb) $S = \pi(D + ts)(L + 0.8 * D) * ts * \rho$ D = diameter (in) L = tan-tan length (in) Ts = shell thickness (in) P = material density (lb/in^3)	$Cb = Cv + Cpl$ $Cv = e^{(5.6336 + 0.4599(\ln(S)) + 0.00582(\ln(S))^2)}$ $Cpl = 2275 * D^{0.2094}$
Turbine	S = Horsepower (Hp)	$Cb = 10660 * S^{0.41}$ (steam, non-condensing) $Cb = 28350 * S^{0.405}$ (steam, condensing) $Cb = 2835 * S^{0.76}$ (gas)
Turbo-expander[1]	S = power (kW)	$Cb = 126.9 * S + 661111$

[1]Turbo-expander correlation obtained from Rangaiah, (2009)

3.3.2 Fixed cost models

The estimation of Fixed Capital Investment (FCI) and fixed operating costs was based on the major equipment costs. Three different methods were compared for computing FCI, taking into account the various approaches found in TEA literature, as discussed in Chapter 2. The three methods used for FCI calculation were the: National Renewable Energy Laboratory (NREL) method outlined in the 2011 NREL report (Humbird et al., 2011), Towler and Sinnott (TS) method from Chemical Engineering Design (Sinnott & Towler, 2013) by Towler and Sinnott, and Hand method presented in Sustainable Design Through Process Integration (El-Halwagi, 2017). The NREL method was selected owing to the 2011 report being seen as a the 'gold-standard' for TEA studies (Scown et al., 2021). The TS method uses universally applied Lang factors to translate equipment costs to installed costs whereas the Hand method is a detailed factorial method which individually applies factors depending on the equipment type. These three methods are summarised in Table 3.4. Similarly, the three fixed operating cost models used are presented in Table 3.5, named the NREL method (Humbird et al., 2011), the TS method (Sinnott & Towler, 2013), and the Coulson & Richardson method from Coulson & Richardson Volume 6 (Sinnott, 2005). As the Hand method used for FCI does not provide a corresponding fixed operating cost calculation, the third fixed operating cost method was taken from Coulson & Richardson Volume 6 and referred to as 'Coulson & Richardson'. Labour costs were included in the fixed operating costs, and regional-specific salary estimates were obtained from SalaryExpert.com (Salary Expert, 2023), rather than relying on outdated estimates from engineering textbooks.

In Chapter 4, the three costing models were compared, and the method yielding the median result was selected for the detailed analysis and used as the costing method in the subsequent TEAs (Chapters 5 and 7). Whilst the median result is not necessarily the most accurate, it is impossible to determine method accuracy without the costs of a commercialised facility for comparison. Noting that vendor quotes may be inaccurate compared with the built facility cost. Moreover, as discussed in Chapter 2, there is no consensus on the optimal method for economic evaluations. The commercialisation and commissioning of biorefinery projects and processes offers an opportunity to reach a consensus. However, this is reliant on greater transparency in primary cost estimations, final project costs, and cost breakdowns from commercialised projects. In the absence of this, maintaining the same cost models throughout this thesis ensures comparability of the assessments. Additionally, the cost models, factors, assumptions, and variable costs are extensively documented in the published papers and corresponding supplementary information, following a similar approach to the widely cited NREL reports.

Table 3.4: Fixed capital cost models

	NREL	TS	Hand
Year basis (Chemical Engineering Plant Cost Index)	2019 (607.5) 2020 (596) 2021 (739)		
Operating hours	8400 hours		
Installation Factor (Multiplied by equipment cost) – Inside Battery Limit (ISBL)	NREL factor, specific to equipment type	Universal installation factor, 3.3	Hand factors, specific to equipment type
Outside Battery Limit (OSBL)	See Chapter 4 for details	30% of ISBL	25% of ISBL
Contingency		10% of ISBL	
Commissioning Cost	5% of ISBL		5% of ISBL
Design and Engineering Cost		10% of ISBL	
Fixed Capital Investment (FCI)	ISBL + OSBL + Commissioning	ISBL + OSBL + Contingency + Design and Engineering	ISBL + OSBL + Commissioning
Working Capital	10% of FCI		
Total Capital Investment (TCI)	FCI + Working Capital		

Table 3.5: Fixed operating cost models

Parameters	NREL	TS	Coulson & Richardson
Operating Labour *(Salary estimates obtained from salaryexpert.com)*	Process operator, engineering and maintenance	3 process operators per shift 4 shift teams	Process operator, engineering and maintenance
Supervisory Labour		25% of Operating Labour	
Direct Salary Overhead	90% of Operating and Supervisory Labour	50% of Operating and Supervisory Labour	
Maintenance	3% of ISBL	3% of ISBL	5% of ISBL + OSBL (conventionally 5% FCI)
Property Taxes and Insurance	0.7% of FCI	1% of ISBL	2% of ISBL +OSBL (conventionally 2-3% FCI)
Rent of Land		1% of FCI	
General Plant Overhead		65% of Total Labour and Maintenance	50% of Operating Labour
Allocated Environmental Charges		1% of FCI	

3.3.3 Variable operating costs

Variable operating costs were estimated using the material and energy usage calculated from the process simulations. The costs for utilities were taken from Seider et al. (2017). Whilst these costs may vary between countries they constitute a relatively minor proportion of the overall operating costs. However, it is recognised that obtaining costs representative of the considered geographic location would have improved the analysis. Specialist chemical costs were taken as spot prices or from literature, catalyst costs were taken from data available in existing TEA studies or, in the absence of cost data, calculated based on the material composition. Where necessary prices were updated from their base year using the Chemicals and Allied Products Producer Price Index (FRED, 2023a). All variable operating costs were subjected to an annual inflation of 2% throughout the life of the project.

3.3.4 Feedstock costs

The feedstock cost for each case study was undertaken based on data availability and previous literature estimates. The approach undertaken for the feedstocks considered throughout the thesis is outlined below.

3.3.4.1 Black liquor

Black liquor was considered as a feedstock in both Chapters 4 and 5. As black liquor is used for energy recovery within the Kraft pulping process it has no economic value as a product. However, a cost is associated with its diversion from energy recovery. In both Chapters the cost was calculated based on its conventional use for renewable electricity generation, requiring capital investment in increased steam turbine capacity. The foregone NPV from this conventional use represents the feedstock's utility value and is subtracted from the evaluated process' NPV.

3.3.4.2 Virgin pulpwood and residues

In Chapter 5 pulpwood and wood residues in China were used as a feedstock. Pulpwood costs were estimated based on prices prepared in a report on the development of industrial wood demand in the district by the Guangxi Forestry Bureau (Cossalter & Barr, 2005). The average cost from three competitive production profiles and locations was calculated and updated to a 2020 basis using the Lumber and Wood Products Producer Price Index (FRED, 2023b). The resulting cost ($102.62 tn^{-1}) was similar to US pulpwood chip costs, $109.64 tn^{-1}, as analysed by Idaho National Laboratory (Jacobson et al., 2014). Residue costs were estimated based on the ratio between the China and Idaho National Laboratory, resulting in a cost of $ 69.67 tn^{-1}. The obtained price was in line with the range reported by (Anttila et al., 2015), for forestry residues for energy production in northern China, and to the prices reported in Gosens database for Chinese biomass power projects (Gosens, 2015). Accordingly, using a blend of 20% pulpwood and 80% forestry residues the delivered biomass cost was $76.26 tn^{-1}.

3.3.4.3 Biomass residues

In Chapter 7 a feedstock agnostic process simulation and economic analysis for low value biomass wastes was created. As such, no specific feedstock cost was derived. Instead, a universal method based on the Higher Heating Value (HHV) of the biomass relative to natural gas was created. This cost therefore represents the feedstock's utility value. The HHV of the biomass was calculated using a correlation based on the ultimate analysis of the compound, created specifically for biomass (Huang & Lo, 2020). An efficiency factor of 70% was applied to the HHV based on anaerobic digestion as a next best alternative waste utilisation method. Anaerobic digestion can only exploit the Biological Oxygen Demand of a feedstock, whereas Supercritical Water Gasification (SCWG) exploits the Chemical Oxygen Demand (COD). The 70% efficiency factor reflects a high Biological Oxygen Demand to COD ratio (Kumar et al. 2010). The feedstock's price was then computed based on the adjusted HHV relative to the HHV of natural gas using the Energy Information Administration's (EIA's) natural gas prices (EIA, 2022).

3.3.4.4 Transportation costs

In Chapter 7 feedstocks were assumed to be processed at their point of origin, meaning no transportation costs were included. However, as the impact of capacity on processing costs was assessed, an investigation into of the impact of transporting localised waste streams to larger facilities was also included. The cost of transporting the feedstocks was taken as £ 0.25 t/km based on costs for digestate transportation (WRAP, 2016) and updated using the ratio of UK diesel prices in 2022 to 2016. A nominal 30 km transport distance was selected.

3.3.5 Investment analysis

The investment analysis for each process was calculated using the aforementioned cost models (section 3.2.2. Fixed cost models). Different evaluation metrics can be computed for a TEA. Common metrics are the MSP and the cumulative NPV for a process. The cumulative NPV is a metric representing the final value of the investment at the end of the considered plant life, it is discounted across its plant life based on a selected discount rate and presented in millions of dollars. The MSP is the minimum selling price the product(s) can be sold at to achieve an NPV of zero at the end of the considered plant life, presented as dollars per unit of product. Zhao et al. (2016) argue that NPV is a less interpretable profitability indicator than MSP, particularly when the NPV is negative, as is often the case with emerging technologies (Zhao et al., 2016). However, caution is required when a process has multiple products, as the MSP is highly sensitive to co-product prices and yields, creating potentially misleading results (Pereira et al., 2017). Furthermore, as computing the MSP bypasses the need to utilise product prices within the analysis studies often either neglect to comment on the MSP in relation to market prices or select an arbitrary historic price for comparison. This leaves interpretation of future market competitiveness open to subjective judgement. In Chapter 4 the cumulative NPV was computed. However, to overcome the shortcomings of these methods individually, both the cumulative NPV and MSP were computed in Chapter 5.

The discount rate used in the investment analysis was selected based on the perceived risk associated with a technology or process, i.e. the riskier a project the higher the required rate of return. In Chapters 4 and 5 a 10% discount rate was selected, to adhere to the discount rates used studies in the BETO Biofuels TEA Database (Kinchin, 2020). In Chapter 7 an 8% discount rate was used based on Europe's hurdle rates for electricity generation costs from biomass sources (BEIS, 2020).

Contrastingly to Chapters 4 and 5, in Chapter 7 the economic metric computed was the Levelised Cost. This metric represents the production costs of a technology, i.e. how much it costs to produce 1 kWh or kg of a product. The levelised cost is a commonly reported metric for energy production, it represents the lifetime cost of a production method and allows for fair comparison of technologies with different life spans, capacities, capital intensity, and risk (DOE, 2015). The investment analysis parameters used for Chapters 4, 5, and 7 are presented in Table 3.6.

Table 3.6: Investment analysis parameters

Parameters	**Value**	**Comments**
Discounted Rate of Return	10% [1] 8% [2]	[1] In line with studies in the BETO Biofuels TEA Database (Kinchin, 2020). (Chapters 4 and 5) [2] In line with Europe's hurdle rates for electricity generation costs from biomass (BEIS, 2020) (Chapter 7)
Corporation Tax	25%	Corporation tax in China. Not used in LCOH calculation (Chapter 7).
Annual Inflation	2%	
Plant Life	25 years	
Depreciation	10 years	Straight line.

Plant Salvage Value	No value	
Construction Period	2 years	

3.4 Commodity price projections

Price projections were undertaken for the products produced in each TEA. To exploit any existing underlying pricing dynamics that may be present within the historic prices Machine Learning (ML) methods were used. These methods offer benefits over traditional statistical methods such as Autoregressive Integrated Moving Average models and Generalised Autoregressive Conditional Heteroscedasticity models, as they are able to exploit complex, non-stationary, and non-linear trends (Lago et al., 2018).

3.4.1 Radial Basis Function Neural Networks

In Chapters 4 and 5 a Radial Basis Function Neural Network (RBFNN) containing eight neurons was used as the machine learning model. This approach ensured the TEA inputs and sensitivity analysis were unbiased, opposed to selecting a subjective time period to obtain an average price. The weights and centre points of the network were determined during model training whereby the network behaved as a one step ahead predictor by minimising the Mean Squared Error (MSE) of the difference between the actual and predicted prices. Once trained the network was initialised with ten real historic prices and then run recursively meaning the successive predictions became inputs to the model. The number of model inputs remained at ten. Therefore, after ten successive predictions, the model was predicting based solely on predicted prices as inputs. The projection procedure is presented in Figure 3.4. The confidence limits corresponding to the trained RBFNN were calculated as a reliability measure of the prediction (Leonard et al., 1992). To account for price variability in the uncertainty analysis a uniform distribution of ±30 % and ±20 % was applied to the predicted future prices for Chapters 4 and 5, respectively.

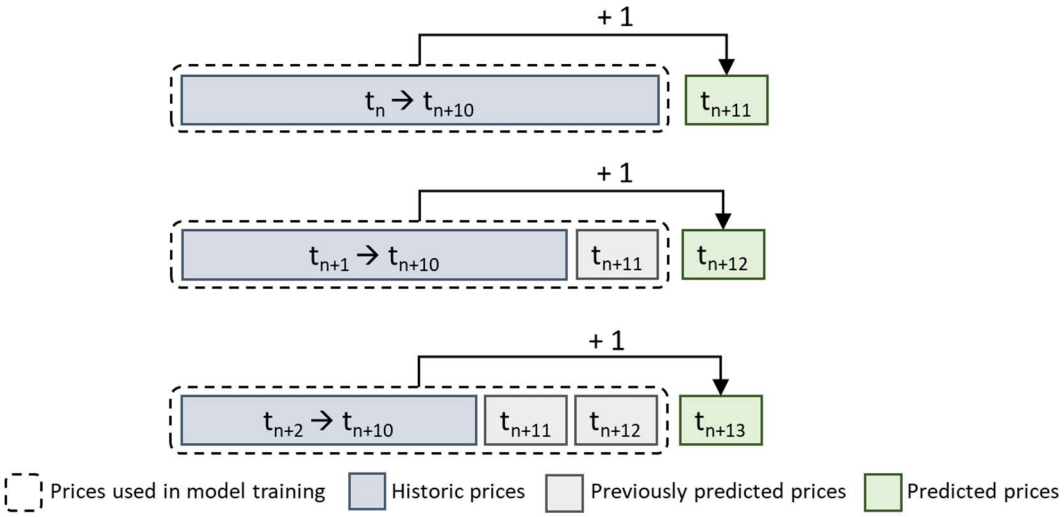

Figure 3.4: The RBFNN price projection procedure. The model was trained to predict the next monthly price based on ten previous prices. The model was initiated using ten historic prices. After initialisation the model was recursive, whereby model predictions became inputs and were used in the prediction of the next monthly price.

3.4.1.1 Method limitations

The outlined method had a number of limitations. The use of an RBFNN as the algorithm, using eight neurons, and using ten historic time-steps as the model input was arbitrarily

selected, making it biased and unlikely to be optimal. Furthermore, when the model was trained the entire historic time series was used to minimise the MSE. This may have led to network overfitting and lead to limited predictive capability beyond the training data. Model initiation relied on ten real historic prices, excluding recent data from the price projection. Finally, price variability, required for a sensitivity and uncertainty analysis, was accounted for using a subjective percentage rather than accounting for observed price variability within the historic time series.

3.4.2 Long-Short Term Memory Neural Networks

Owing to the outlined limitations of the previously adopted approach, in Chapter 6 an advancement to the price projection methodology was created. In the advanced method a grid search was undertaken to determine the optimal hyperparameters for each commodity time series. The entire time series was used as a model input, facilitating the exploitation of long-running underlying trends that may exist within the time series. Finally, a validation set was used to assess the methods ability to predict beyond the training set.

A Long-Short Term Memory (LSTM) neural network was used as the basis for the new price projection methodology, the parameters used, and their rationale are summarised in Table 3.7, further clarity on the model criteria and methodology is provided in the following sections.

Table 3.7: Summary of the model criteria selection for the advanced price projection method

Parameter	Selection	Rationale
ML algorithm	LSTM	Suited to learning temporal patterns in time series data Allows the entire time series to be used as a model input.
Number of models	Ensemble of 100	To produce a distribution of future prices used to calculate the 5th, 25th, 50th, 75th and 95th price percentiles.
Model inputs	Historic commodity prices time series	Allows the model to exploit any deterministic trends and/or stochastic variability specific to the commodity.
	EIA crude oil prices and long-term projection	Provides information on trends in world energy markets.
Size of model inputs	Entire data series up to the point of projection	Allows the model the opportunity to learn long-running trends within the data.
Strategy	Direct, recursive, joint	Better-reported performance than single output methods (Taieb et al., 2012, 2010; Taieb and Atiya, 2016).
Projection horizon	12 time-steps into the future	Represents annual projections, the required frequency to input into a TEA.
Data set split	30 % training and 70 % validation	To obtain representative hyperparameters for the final task. Based on the relationship between historic data availability (12 years, 30%) and the required projection horizon (26 years, 70%). A test set was excluded due to dataset size limitations.
Hyperparameters optimised	LSTM units	Determines the model's capability to capture patterns in the data.
	Epochs	Prevents overfitting or/underfitting of the models.

	Learning rate	Important in ensuring the model converges effectively.

An ensemble of 100 ML models was trained on the commodity's historic dataset (2009-2021), producing a probabilistic projection of future prices based on deterministic trend and/or stochastic variability within the historic price data. The produced distribution was then used to calculate the 5th, 25th, 50th, 75th and 95th price percentiles for use in the techno-economic, sensitivity, and uncertainty analyses. The EIA's historic prices and reference case projection of future Brent crude oil prices was used as an additional model input, providing information on future trends in world energy markets.

LSTM neural networks were employed for the machine learning task. LSTMs are a type of recurrent neural network which use gate units to update their internal network state (Hochreiter & Schmidhuber, 1997). These gate units reduce the likelihood of exploding and vanishing gradients by enabling the LSTM cells to regulate the inward and outward flow of information. Ultimately, these units prevent the network from remembering information from only recent time-steps allowing the learning of temporal patterns.

3.4.2.1 Projection strategy

A hybrid direct, recursive, and joint strategy was employed for the price projection problem. The model was trained using the entire data set prior to the point being projected to predict monthly prices 12 time-steps into the future (joint). After model training the previously predicted 12 time-steps were added to the historic data (recursive) and a new model was trained (direct). As such, the input sequence to the LSTM increased by 12 time-steps after each model training. In addition to being the required frequency appropriate to input into a TEA, 12 time-steps were used as a compromise between accuracy and compounding errors. Longer horizons require projections further into the future, reducing accuracy. Whereas shorter horizons require more models to project the required horizon. This increases error propagation as more predicted data points are used in the model training. Whilst the optimal number of time-steps could be investigated as part of the validation procedure, this was not undertaken in this work.

In contrast to the previous RBFNN method, model outputs were only used as inputs when historic prices were no longer available to leverage all the information in the commodity's historic time series. Furthermore, the entire historic dataset was used as a model input, rather than the previous ten prices as in the RBFNN procedure. This allows the potential for the exploitation of long-running trends that span the entire time series to be used within the price projection. The projection strategy is presented in Figure 3.5.

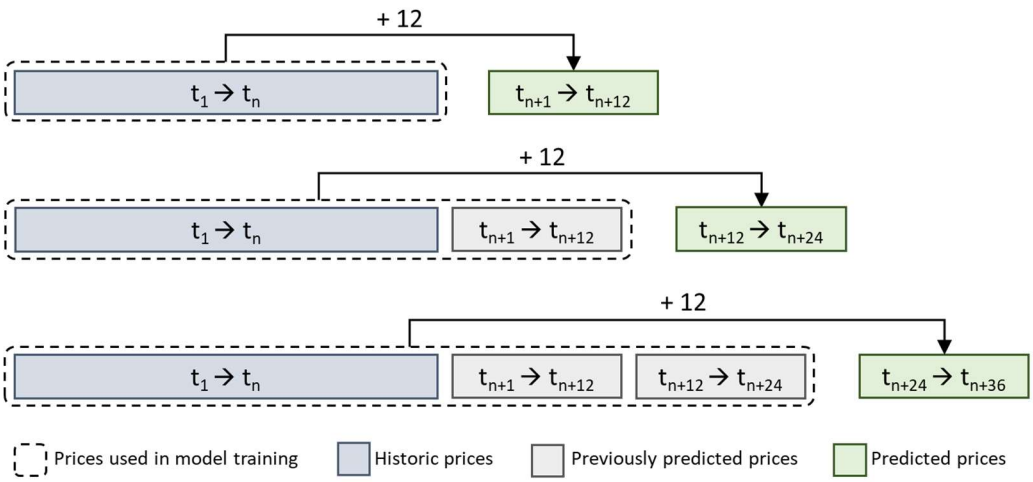

Figure 3.5: The ensemble LSTM price projection procedure. Each of the 100 models was trained to reconstruct the historic time series and predict 12 time-steps into the future. The predicted time-steps were added to the historic dataset and used as inputs to train the next model. Therefore, the dataset increases by 12 time-steps after each model training.

3.4.2.2 Machine Learning

The commodity's historic dataset (2009-2021) was split into a training and validation set based on the ratio between the historic data (12 years, 30%) and projection horizon (26 years, 70%) required for a TEA. Only 12 years of historic data were available for each commodity, translating to 30% of the final projection horizon. As such, a training and validation split of 30% and 70% was necessary to obtain representative hyperparameters for the final task. A test set was not employed due to the limitations in dataset size. As the true prices for the projection horizon (2021 to 2046) are unknown, the optimal model was selected based on its performance on the validation set. This is also how the method would be adopted when using it within in a TEA.

The network architecture is presented in Figure 3.6 and consists of a fully connected layer and a LSTM layer. The fully connected layer contains two neurons, creating new feature combinations of the model inputs to feed into the LSTM layer. This layer facilitates the use of any interdependencies present between the crude oil and commodity price being projected by the network. The size of the LSTM layer was determined through the validation procedure and is specific to each commodity.

During each model training, the networks were trained using the entire historic dataset. For the validation procedure the size of the input sequence ranged from 2 x 36 to 2 x 132 time-steps, owing to the addition of 12 time-steps after each model training. Similarly, the final model's input size ranged from 2 x 144 to 2 x 432 time-steps. To reduce concerns with exploding and vanishing gradients, the models were trained to produce an output at each time-step and a gradient threshold of 1 was implemented (Brownlee, 2017). An ensemble of 100 ML models was trained using a randomly assigned number of hidden units below a maximum selected during the grid search procedure. This LSTM ensemble of models, each trained to reproduce the entire historic time series, facilitates the exploitation of different underlying trends embedded within the historic time series, producing a distribution of potential futures.

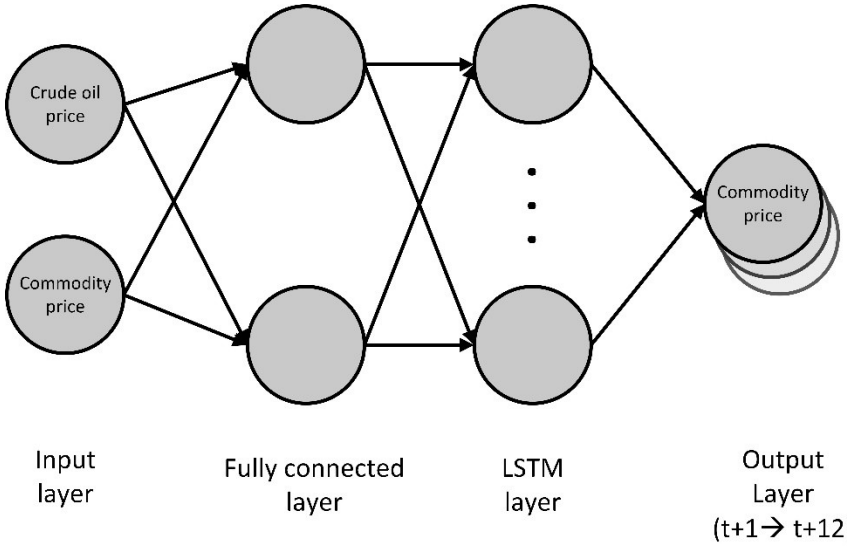

Figure 3.6: Model structure for commodity price projections. The EIA's historic and projected Brent Crude oil prices and the historic pricing data for the commodity being projected are used as model inputs. The prices are fed into a fully connected layer containing two neurons, followed by an LSTM layer. The number of LSTM hidden units was optimised as part of the validation procedure. The output layer consists of the price predictions for 12 time-steps into the future.

Each of the models were trained to reduce the MSE between the training data and the model predictions using the Adam optimisation algorithm (Mathworks, 2018). A grid search of optimal hyperparameter combinations was undertaken to evaluate the model performance over the validation set. The learning rate, number of epochs, and maximum number of hidden units in the LSTM layer were optimised during the grid search. The Continuous Rank Probability Score (CRPS) (equation 3.1) was used to evaluate the model performance where: F is the forecast, y is the prediction, and x is the actual value (observation).

$$CRPS(F,x) = \int_{-\infty}^{\infty}\left(F(y) - 1(y-x)\right)^2 dy \qquad (3.1)$$

CRPS is a generalisation of the mean absolute error within probabilistic forecasting, encompassing both sharpness and calibration (Gneiting & Katzfuss, 2014). Sharpness refers to the forecast variance, i.e. the sharper the forecast the narrower the projected distribution. Calibration is the accuracy of the prediction, it reflects the consistency between the predictions and observations.

3.4.2.3 Method limitations

The LSTM ensemble method is an improvement on the previously applied RBFNN approach however, there are a number of remaining limitations. For example, whilst the number of LSTM units, epochs, and learning rate were optimised during training the number of layers, number of neurons in the fully connected layer, use of a fully connected layer, number of time-steps being predicted etc. were all arbitrarily selected. In future work further investigation into these parameters could be undertaken. However, the computational expense increases the more hyperparameter combinations are investigated. As the purpose of the method is to produce an unbiased probabilistic 25-year price projection where the true prices are unknown the computational expense vs. perceived accuracy is up to the discretion of the practitioner.

Cross-validation was not considered as part of the validation procedure. Given that the input data is a time series, the conventional cross-validation method, which randomly assigns data

points to k-folds, cannot be applied. However, a suitable approach involves leveraging different time-series lengths for validation. For instance, in a 4-fold cross-validation procedure applied to a time series comprising 144 data points, the model's performance can be evaluated using varying time-series lengths e.g., 36, 72, 108, and 144 data points, while maintaining a consistent 30% training and 70% validation split. The optimal hyperparameters would then be determined based on the overall performance across all validation sets. This allows for an assessment of the model's performance across different stages of the time series.

An additional limitation of the method lies in how historical commodity prices and EIA pricing projections were integrated into the model. To enhance prediction accuracy, a more effective approach would have involved staggering the inputs, whereby future crude oil price projections from the EIA served as inputs for the corresponding commodity price predictions. For instance, inputting ethanol prices from January 2009 to December 2020 alongside the EIA's crude oil prices for January 2010 to December 2021 would provide the model with insights into future price dynamics, rather than solely on the current time-step data. As such, the model would be trained to learn the relationship between future crude oil prices and the respective commodity price, potentially increasing prediction accuracy.

3.5 Sensitivity analysis

A Monte Carlo simulation sensitivity analyses were undertaken in Chapters 4, 5, 6, and 7 whereby the defined cost parameters were varied within the predefined bounds to produce a probability distribution of the performance metric. The performance metric used for this analysis in Chapters 4, 5, and 6 was NPV and LCOH in Chapter 7. The cost parameters and ranges varied for each case study are presented in Table 3.8. The parameters varied were based on recommendations from Sinnott and Towler (2013). As the black liquor feedstock in Chapter 4 and 5 was costed based on the forgone NPV from conventional renewable electricity generation the parameters listed in Table 3.8 were also varied for the investment analysis undertaken for this alternate use. The resulting NPV distribution fed directly into the aerobic gas fermentation investment analysis. Conversely, the wood residue feedstock had an associated cost, and was therefore varied as part of the uncertainty analysis. In Chapter 4 the upper limit for each variable was the same, with the exception of renewable electricity, which was set to 1, assuming current subsidy rates were the maximum. This was based on the decreasing trend in biomass subsidies (Reuters, 2019). Contrastingly, in Chapter 5 the ranges were updated to follow the recommendations in Sinnott and Towler (2013). This led to higher upper bounds for the ISBL capital, OSBL capital, and Labour cost compared with ranges used in Chapter 4. Furthermore, the lower range of the generated electricity price was reduced in Chapter 5. The lower bound was selected to include scenarios where grid parity prices were met.

With the exception of the commodity price, the same ranges presented in Table 3.8 were used in Chapter 6 to produce the comparative Monte Carlo simulations to assess the impact of the different commodity price projection methods. The recently observed volatility in electricity prices (European Commission, 2022), meant the previously applied cap to renewable electricity prices was not maintained in the simulation for Chapter 7. In Chapter 7 the generated electricity price was varied based on the recommended range for the ‘fuel cost’ parameter presented in Sinnott and Towler (2013). Furthermore, the parameters varied in the Monte Carlo simulation differ to the preceding Chapters. The parameters were changed to simplify the Monte Carlo simulation procedure as the case study in Chapter 7 contained 600 TEA models. Each of the TEA models represented a different feedstock-capacity-location combination. The TEA and variables required for the Monte Carlo simulation were contained within each of the 600 Aspen HYSYS simulations. Therefore, it was less computationally expensive to export the LCOH breakdown and vary the parameters within the breakdown than

to stochastically vary the parameters within each of the simulations. The parameters varied were selected to closely resemble the parameters varied within Chapters 4 and 5. With hindsight the variables used in Chapters 4 and 5 could have been made easily exploitable during the creating of the Aspen HYSYS simulations.

For each study the Monte Carlo simulation was run 2,000 times, generating a stochastic parameter set for each scenario using a uniform distribution within the defined lower and upper limits for the parameters. Different probability distributions can be used for sensitivity parameters. For example, Dimitriou et al. (2018) used a normal distribution for all parameters in their TEA for biofuel production, with ranges obtained from literature and industry experts. This was justified as more data supported the base assumptions/estimations than the ranges (Dimitriou et al., 2018). However, there are a limited number of commercialised biorefineries, meaning probability distributions are often arbitrarily selected rather than based on observed data. Furthermore, it has been noted that cost overruns are more frequent and of a greater magnitude than underruns, suggesting that asymmetrical distributions would better fit capital cost estimation data (Brown, 2015). Asymmetrical distributions have been employed in uncertainty analyses e.g., Zhao et al. (2016). Despite this, symmetrical distributions such as triangular and normal are commonly applied in TEAs (Barahmand & Eikeland, 2022). In the absence of distribution data surrounding cost predictions vs. observations for second generation biochemical production, uniform distributions were used in this work. Uniform distributions are thought to provide the most information about a parameter when only the upper and lower bound are known (Mishra & Datta-Gupta, 2018). Using a uniform distribution means any value between the lower and upper limit has an equal probability occurring. This approach negates the need for an additional distribution assumption. The use of a uniform distribution gives rise to the broadest range for the cumulative NPV (within the defined parameter ranges), whilst the wider upper range applied (Table 3.8) skews the capital cost contribution to the upper end.

The exception to the application of a uniform distribution is commodity prices. In Chapter 6, a methodology to determine the probability distribution for future prices was developed and incorporated into the Monte Carlo analysis.

Table 3.8: Monte Carlo simulation parameters. The values presented are multiplied by the nominal value. All variables were assigned a uniform distribution between the ranges outlined.

Monte Carlo Input parameter	**Chapter 4**		**Chapter 5**		**Chapter 7**	
	Chapter 6					
	Lower	**Upper**	**Lower**	**Upper**	**Lower**	**Upper**
Product price	0.7	1.3	0.8	1.2		
Generated electricity price	0.7	1	0.48	1	0.8	2
Feedstock cost			0.7	1.3	0.9	1.3
ISBL capital	0.8	1.3	0.8	1.5		
OSBL capital	0.8	1.3	0.8	1.5		
Labour cost	0.8	1.3	0.8	1.5		
Variable operating					0.8	2
Fixed capital					0.8	1.5

In Chapter 5 a single point sensitivity analysis using a tornado chart was conducted in conjunction with the Monte Carlo analysis. Here, each parameter was varied independently within the range presented in Table 3.8 to determine the relative importance of the different variables with respect to the product's MSP.

3.6 Life cycle assessment

In Chapters 4, 5, and 7 a cradle-to-gate LCA was undertaken following ISO Standards 14040 (International Organization for Standardization, 2006a) and 14044 (International Organization for Standardization, 2006b). Greenhouse gas (GHG) emissions were calculated based on the most recent Integrated Pollution Prevention and Control 100-year Global Warming Potential factors, thereby quantifying GHG emissions in terms of CO_2 equivalents (CO_2eq) (Stocker et al. (2014).

The functional units were defined as 1 kg or 1 kWh depending on the product, outlined in Table 3.9. In Chapter 4, emissions were allocated between the products using both energy and economic allocation. However, the results were largely the same, indicating that the $/KJ value of the products was similar. In Chapters 5 and 7 energy allocation was utilised to allocate emissions between products.

Table 3.9: Functional units used to quantify the cradle-to-gate life cycle emissions

Product	Functional Unit	Chapter
Isopropanol	1 kg	Chapter 4
Acetone	1 kg	
1,3-Butadiene	1 kg	Chapter 5
Renewable Electricity	1 kWh	
Higher alcohols	1 kg	
Butane-rich product	1 kg	
Hydrogen	1 kg	Chapter 7

No emissions were assigned to the black liquor feedstock, which is considered a by-product from pulp production. Consequently, the upstream forestry management and transportation of virgin pulp wood to the pulp mill are attributed to the pulp product and not to black liquor. In Chapter 5, emissions were assigned for the collection, chipping, loading, and transportation of wood residues and virgin wood. Similarly, in Chapter 7, waste biogenic feedstocks such as vinasse and distillery wastewater were considered by-products and were not assigned emissions. As no emissions were attributed to the carbon content of these biogenic feedstocks, any CO_2 released during their combustion in processing was not accounted for. Additionally, owing to the cradle-to-gate framework used, negative emissions were assigned to products sequestering biogenic carbon.

For wood residues, collection, chipping and loading emissions were taken from (McKechnie et al., 2011). Pulpwood emissions were taken from (Bernstad et al., 2017) (excluding land use change). Transport emissions for both feedstocks were updated to EURO 6 freight lorries using data from ecoinvent 3.7 and the transportation distance modified to reflect the Chinese production profiles used during the wood chip cost calculation (Cossalter & Barr, 2005). Raw material and utility emission factors were largely obtained from the ecoinvent 3.7 inventory database (Wernet et al., 2016). However, where materials were not available factors listed in existing TEA and LCA studies were used. For example, in Chapter 5 emission factors for catalysts were largely obtained from (Wang et al., 2022). Electricity grid emission factors were obtained for the country where the assessment was conducted.

In all chapters, the calculated emissions of the products were compared to emissions from conventional production methods. While the framework considered in all chapters was cradle-to-gate, the downstream use of the product would be the same regardless of its origin.

Therefore, the comparative emissions are valid beyond the cradle-to-gate framework considered.

3.7 Surrogate modelling

In Chapter 7 a feedstock agnostic process simulation was created for hydrogen production from low temperature SCWG (430°C) considering a feedstock concentration corresponding to a COD of 75 g/L_{COD}. The SCWG temperature was selected owing to the economic benefit of low-temperature SCWG which reduces the energetic burden required to preheat the feedstock (Lee et al., 2021). Furthermore, the concentration was selected as low solids concentrations lead to increased hydrogen production through enhancing steam methane reforming and water gas shift reactions (Lee et al., 2021). The simulation was conducted for 40 biomass feedstocks at five different processing capacities (10 to 200 m^3/hr). The biomass compositions were collected from experimental literature investigating low-temperature SCWG (380 to 500°C). The selected processing capacities allow for comparison to other low-carbon hydrogen technologies and represent realistic point source waste stream availability. From the resulting simulations a TEA was undertaken considering three geographic locations (China, Brazil, and the UK) for each feedstock-capacity combination, giving rise to 600 TEAs. The geographic locations were selected as case studies with abundant wet wastes suitable for SCWG, i.e., black liquor in China, vinasse in Brazil, and distillery wastewater in the UK and provide global coverage.

A machine learning surrogate model of the 600 economic analyses was then created whereby the nominal LCOH and 70% probability band could be computed based on six user input variables, namely; the weight percentage of C, H, O, and N, processing capacity (in m^3/hr), and geographic location. Three ML algorithms were investigated for the surrogate model, Random Forests (RF), Support Vector Regression (SVR), and Artificial Neural Networks (ANNs) as they have been previously considered for surrogate model representation of the SCWG gasifier to predict hydrogen production (Li et al., 2021a; Zhao et al., 2022).

The 600 TEA combinations were split into a training set of 360, validation set of 120, and test set of 120 parameter combinations. As the purpose of the surrogate model was to predict a feedstock's economic potential for hydrogen production via SCWG the biomass samples were distributed among these sets. Therefore, if a biomass composition was in the test set, the entire set of parameter combinations (facility size and location) for that feedstock was also included in the test set. Through splitting the biomass samples in this way, the model trained to generalise across the biomass composition. Distributing the biomass feedstocks among the sets resulted in 24 biomass samples in the training set, 8 in the validation set, and 8 in the test set.

A grid search was undertaken using a 4-fold cross-validation procedure using GridSearchCV from scikit-learn was used to determine the best-performing hyperparameters on the validation set (Pedregosa et al., 2011). The Root Mean Squared Error (RMSE) was used as the performance metric for each algorithm and as the loss function in the ANN during the cross-validation procedure. The hyperparameters that were optimised for each algorithm are presented in Table 3.10 along with the considered ranges.

Table 3.10: Hyperparameters and ranges considered for each algorithm during the cross-validation grid search procedure

Random forests	**Support vector regression**	**Artificial neural network**
Number of trees (10 – 500)	L2 Regularisation penalty	Number of layers (1 – 3)

	(0.1 – 1000)	
Maximum number of features for split (1 - 6)	Kernel type (linear, polynomial, radial basis function, sigmoidal)	Neurons in each layer (2-256)
Maximum depth of the tree (10 - 500)	Kernel coefficient (0.01 – 100)	L2 Regularisation penalty (0.00001 – 0.1)
Minimum number of samples before split (1 – 10)	Degree (for polynomial kernel function only) (1 – 3)	Learning rate (0.00001 – 0.1)
Minimum data in a leaf (1 - 10)	Epsilon (0.001 – 10)	Epochs (1000 – 10,000)
Bootstrap sampling (with or without replacement)		Batch size (2 – 256)

The RF algorithm produces an ensemble of predictions, with the final output being the average of each decision tree's prediction. Ensemble methods typically have higher prediction accuracy because they reduce dispersion error and bias by averaging model predictions. Consequently, an ensemble approach was also applied to ANNs, which randomly initialise starting weights and biases. The average prediction from ten ANN models using the optimised hyperparameters was used to evaluate the algorithm performance. Unlike ANNs, SVR does not contain random elements during model training, so an ensemble of SVR using optimised hyperparameters was not implemented.

After determining the optimal hyperparameters for each algorithm, it was evaluated on the test set to provide an indicative performance measure of the model's generalisability to unseen samples. Three performance metrics were used to assess the model's prediction accuracy: Root Mean Squared Error (RMSE), Mean Absolute Percentage Error (MAPE), and the determination coefficient (R^2). Each metric has its own advantages: RMSE measures the standard deviation of the prediction errors, penalising large errors and making it more sensitive to outliers; MAPE measures the absolute error between the true and predicted values and presents them as a percentage, being less sensitive to larger errors than RMSE; and R^2 represents the fitness of the model to the true values and provides an intuitive result, with a value of 1 representing a perfect fit. Equations 3.2-3.4 present these metrics, where N is the number of datums, y_j is the true value, $\hat{y}_t$ is the predicted value, and y_M is the mean value. The surrogate model presented to the research community was trained on the entire dataset using the algorithm and hyperparameter set that produced the most accurate predictions during the cross-validation procedure.

$$RMSE = \sqrt{\frac{1}{N}\sum_{t=1}^{N}\left(y_j - \hat{y}_t\right)^2} \quad (3.2)$$

$$MAPE = \frac{1}{N}\sum_{t=1}^{N}\frac{y_j - \hat{y}_t}{y_j} \quad (3.3)$$

$$R^2 = \frac{\sum_{t=1}^{N}\left(y_j - y_M\right)^2}{\sum_{t=1}^{N}(\hat{y}_t - y_M)^2} \quad (3.4)$$

3.7.1 Feature importance

The internal workings of ML models are not easily interpretable, resulting in a lack of understanding regarding the reasons behind the model's predictions. To address this interpretability challenge, feature importance methods are employed. One such method is SHapley Additive exPlanation (SHAP) Values which is based on cooperative game theory. SHAP values assign a contribution score to each feature, indicating its importance and impact on the model's output. By utilising SHAP values, users can gain a better understanding of the relationships between input features and model outputs (Sison et al., 2023). In this work, SHAP values are used to highlight the relative importance of the input features. The SHAP Values were obtained for the best-performing ML model using the SHAP library in Python.

3.8 References

Anttila, P., Vaario, L., Pulkkinen, P., Asikainen, A., Duan, J., 2015. Availability, supply technology and costs of residual forest biomass for energy - a case study in northern China. *Biomass and Bioenergy*, 224-232.

Barahmand, Z. & Eikeland, M. S., 2022. Techno-Economic and Life Cycle Cost Analysis through the Lens of Uncertainty: A Scoping Review. *Sustainability*, 14(19).

BEIS, 2020. BEIS Electricity Generation Costs, 2020. [Online] Available at: https://www.gov.uk/government/publications/beis-electricity-generation-costs-2020 [Accessed 01 February 2023].

Bernstad Saraiva, A., Valle, R., Bosquê, A., Berglin, N., & Schenck, A. v., 2017. Provision of pulpwood and short rotation eucalyptus in Bahia, Brazil – environmental impacts based on lifecycle assessment methodology. *Biomass and Bioenergy*, 41-50.

Bradley, M.W., Hiles, A.G., Kippax, J.W., 1982. Hydrogenation Process. 0073129.

Brown, T. R., 2015. A critical analysis of thermochemical cellulosic biorefinery capital cost estimates. *Biofuels, Bioproducts and Biorefining*.

Brownlee J., 2017. Techniques to Handle Very Long Sequences with LSTMs [Online] Available at: https://machinelearningmastery.com/handle-long-sequences-long-short-term-memory-recurrent-neural-networks/ [Accessed 14 January 2022].

Bunning, D.L., Blessing, M.A., 1986. HYDROFORMYLATON PROCESS. 4593127.

Chemengonline, n.d. The Chemical Engineering Plant Cost Index. [Online] Available at: https://www.chemengonline.com/pci-home [Accessed 31 March 2023].

Choi, Y. & Stenger, H., 2003. Water gas shift reaction kinetics and reactor modeling for fuel cell grade hydrogen. *Journal of Power Sources*, 124(2), 432-439

Cossalter, C. & Barr, C., 2005. Fast growing plantation development and industrial wood demand in China's Guangxi Zhuang autonomous region, s.l.: Center for International Forestry Research.

Dai, W., Zhang, S., Yu, Z., Yan, T., Wu, G., Guan, N., Li, L., 2017. Zeolite Structural Confinement Effects Enhance One-Pot Catalytic Conversion of Ethanol to Butadiene. *ACS Catalysis*, 7, 3703–3706.

Diep, B.T., Wainwright, M.S., 1987. Thermodynamic Equilibrium Constants for the Methanol-Dimethyl Ether-Water System. *Journal of Chemical Engineering Data*. 32, 330–333.

Dimitriou, I., Goldingay, H. & Bridgwater, A. V., 2018. Techno-economic and uncertainty analysis of Biomass to Liquid (BTL) systems for transport fuel production. *Renewable and Sustainable Energy Reviews*, 160-175.

DOE, 2015. Levelized Cost of Energy (LCOE). [Online] Available at: https://www.energy.gov/sites/prod/files/2015/08/f25/LCOE.pdf [Accessed 4 April 2023].

Dutta, A., Talmadge, M., Hensley, J., Worley, M., Dudgeon, D., Barton, D., Groenendijk, P., Ferrari, D., Stears, B., Searcy, E.M., Wright, C.T., Hess, J., 2011. Process Design and Economics for Conversion of Lignocellulosic Biomass to Ethanol Thermochemical Pathway by Indirect Gasification and Mixed Alcohol Synthesis, NREL technical report NREL/TP-5100-51400.

EIA, 2022. ANNUAL ENERGY OUTLOOK 2022, Washington DC: s.n.

El-Halwagi, M. M., 2017. Sustainable Design Through Process Integration: Fundamentals and Applications to Industrial Pollution Prevention, Resource Conservation, and Profitability Enhancement'. s.l.:Elsevier.

European Commission, 2022. High volatility and geopolitical tensions impact electricity and gas market developments in Q1 2022. [Online] Available at: https://commission.europa.eu/news/high-volatility-and-geopolitical-tensions-impact-electricity-and-gas-market-developments-q1-2022-2022-07-08_en [Accessed 25 January 2023].

FRED, 2023a. Producer Price Index by Commodity: Chemicals and Allied Products (WPU06). [Online] Available at: https://fred.stlouisfed.org/series/WPU06 [Accessed 1 March 2023].

FRED, 2023b. Producer Price Index by Commodity: Lumber and Wood Products: Logs, Bolts, Timber, Pulpwood and Wood Chips. [Online] Available at: https://fred.stlouisfed.org/series/WPU0851 [Accessed 4 April 2023].

Gosens, J., 2015. Biopower from direct firing of crop and forestry residues in China: a review of developments and investment outlook. *Biomass and Bioenergy*, 110-123.

Gneinting, T. & Katzfuss, M., 2014. Probabilistic Forecasting. *Annual Review of Statistics and Its Application*, 1, 125-151.

Hochreiter, S. & Schmidhuber, J., 1997. Long short-term memory. *Neural Computation*. 1735-1780.

Hou, K. & Hughes, R., 2001. The kinetics of methane steam reforming over a Ni/α-Al2O catalyst. *Chemical Engineering Journal*, 82, 311-328.

Hla, S., Park, D., Duffy, G., Edwards, J., Roberts, D., Ilyushechkin, A., Morpeth, L., Nguyen, T., 2009. Kinetics of high-temperature water-gas shift reaction over two iron-based commercial catalysts using simulated coal-derived syngases. *Chemical Engineering Journal,* 146 (1), 148-154.

Huang, Y. & Lo, S.-L., 2020. Predicting heating value of lignocellulosic biomass based on elemental analysis. *Energy*, 191, 116501.

Huang, X., Li, Hu, Li, Hui, Xiao, W.-D., 2016. Modeling and analysis of the Lurgi-type methanol to propylene process: Optimization of olefin recycle. *AIChE Journal*. 63, 306–313.

Humbird, D., Davis, R., Tao, L., Kinchin, C., Hsu, D., Aden, A., Schoen, P., Lukas, J., Olthof, B., Worley, M., Sexton, D., Dudgeon, D., 2011. Process Design and Economics for

Biochemical Conversion of Lignocellulosic Biomass to Ethanol: Dilute-Acid Pretreatment and Enzymatic Hydrolysis of Corn Stover, s.l.: s.n.

International Organization for Standardization, 2006a International Organization for Standardization ISO 14040:2006: Environmental Management - Life Cycle Assessment - Principles and Framework (2006) London

International Organization for Standardization, 2006b International Organization for Standardization ISO 14044:2006 Environmental Management — Life Cycle Assessment — Requirements and Guidelines (2006) London

Jacobson, J., Roni, M., Cafferty, K., Kenney, K., Searcy, E., & Hansen, J. 2014. Biomass Feedstock and Conversion Supply System Design and Analysis, Idaho Falls, ID (United States): Idaho National Lab. (INL).

Jung, J., Lee, H., Kim, H., Chung, Y.M., Kim, T., Lee, J.S., Oh, S., Kim, Y.S., Song, I.K., 2008. Effect of Oxygen Capacity and Oxygen Mobility of Pure Bismuth Molybdate and Multicomponent Bismuth Molybdate on their Catalytic Performance in the Oxidative Dehydrogenation of n Butene to 1,3Butadiene. *Catalysis Letters*, 262-267.

Kinchin, C., 2020. BETO Biofuels Techno-Economic Analyses (TEA) Database. [Online] Available at: https://bioenergykdf.net/content/beto-biofuels-tea-database [Accessed 1 February 2021].

Kumar, A., Dhall, P., Kumar, R., 2010. Redefining BOD:COD ratio of pulp mill industrial wastewaters in BOD analysis by formulating a specific microbial seed. *International Biodeterioration & Biodegradation*, 64, 197-202.

Lago, J., De Ridder, F., De Schutter, B., 2018. Forecasting spot electricity prices: Deep learning approaches and empirical comparison of traditional algorithms. *Applied Energy*, 221, 386-405.

Lee, C. S., Conradie, A. V. & Lester, E., 2021. Review of supercritical water gasification with lignocellulosic real biomass as the feedstocks: Process parameters, biomass composition, catalyst development, reactor design and its challenges. *Chemical Engineering Journal*, 145, 128837.

Leonard, J., Kramer, M. & Ungar, I., 1992. A neural network architecture that computes its own reliability. *Computers & Chemical Engineering*, 819-835.

Li, J., Pan, L., Survarna, M. & Wang, X., 2021. Machine learning aided supercritical water gasification for H2-rich syngas production with process optimization and catalyst screening. *Chemical Engineering Journal,* 426, 131285.

McKechnie, J., Colombo, S., Chen, J., Mabee, W., MacLean, H. 2011. Forest bioenergy or forest carbon? Assessing trade-offs in greenhouse gas mitigation with wood-based fuels. *Environmental Science Technology*, 789-795.

Mathworks, 2018. Training Options ADAM [WWW Document]. URL https://uk.mathworks.com/help/deeplearning/ref/nnet.cnn.trainingoptionsadam.html (accessed 10.10.21).

Mishra, S. & Datta-Gupta, A., 2018. Uncertainty quantification. In: Applied Statistical Modeling and Data Analytics: A Practical Guide for the Petroleum Geosciences. s.l.:Elsevier.

Ng, K.L., Chadwick, D., Toseland, B.A., 1999. Kinetics and modelling of dimethyl ether synthesis from synthesis gas. *Chemical Engineering Science*, 54, 3587–3592.

Pai, C.C., 1979. A heterogeneous vapor phase process for the catalytic hydrogenation of aldehydes to alcohols. 0008767A1.

Pedregosa, F., Varoquaux, G., Gramfort, A., Michel, V., Thirion, B., Grisel, O., Blondel, M., Müller, A., Nothman, J., Louppe, G., Prettenhofer, P., Weiss, R., Dubourg, V., Vanderplas, J., Passos, A., Cournapeau, A., Brucher, M., Perrot, M., Duchesnay, E., 2011. Scikit-learn: Machine Learning in Python. *Journal of Machine Learning Research*, 12, 2825-2830.

Pereira, L. G., MacLean, H. L. & Saville, B. A., 2017. Financial analyses of potential biojet fuel production technologies. *Biofuels, Bioproducts and Biorefining*.

Rangaiah, G.P., 2009. Multi-Objective Optimization: Techniques and Applications in Chemical Engineering. *World Scientific*.

Reuters, 2019. China to cut subsidies for renewable power by 30 per cent to US$807 million in 2020. South China Morning Post. [Online] Available at: https://www.scmp.com/news/china/society/article/3038591/china-cut-subsidies-renewable-power-30-cent-us807-million-2020 [Accessed 2021 January 01].

Salary Expert, 2023. Salary Calculator. [Online] Available at: https://www.salaryexpert.com/ [Accessed 13 04 2023].

Scown, C.D. Baral, N.R., Yang, M., Vora, N., Huntington, T., 2021 Technoeconomic analysis for biofuels and bioproducts. *Current Opinion in Biotechnology*, 67, 58-64.

Seider, W.D; Lewin, D.R; Seader, J.D; Widago, S; Gani, R; Ming Ng, K. 2017. '*Cost Accounting and Capital Cost Estimation',* in *'Product and Process Design Principles. Synthesis Analysis and Evaluation'*, Fourth Edition, John Wiley & Sons Inc., 2017, New York.

Sinnot, R., 2005. Coulson and Richardson's Chemical Engineering Volume 6 - Chemical Engineering Design. s.l.:Elsevier.

Sinnott, R. & Towler, G., 2013. Chemical Engineering Design - Principles, Practice and Economics of Plant and Process Design. 2nd ed. s.l.:Elsevier.

Sison, A. E., Etchieson, S. A., Güleç, ,. F., Epelle, E. I., Okolie, J., 2023. Process modelling integrated with interpretable machine learning for predicting hydrogen and char yield during chemical looping gasification. *Journal of Cleaner Production*, 414, 137579.

Stocker, T.F., D. Qin, G.-K. Plattner, M. Tignor, S.K. Allen, J. Boschung, A. Nauels, Y. Xia, V. Bex and P.M. Midgley. 2014. IPCC Working Group I Climate Change 2013 – The Physical Science Basis: Working Group I Contribution to the Fifth Assessment Report of the Intergovernmental Panel on Climate Change Intergovernmental Panel on Climate Change, Cambridge University Press (2014)

Tan, E.C., Talmadge, M., Dutta, A., Hensley, J., Schaidle, J., Biddy, M., Humbird, D., Snowden-Swan, L.J., Ross, J., Sexton, D., Yap, R., Lukas, J., 2015. Process Design and Economics for the Conversion of Lignocellulosic Biomass to Hydrocarbons via Indirect Liquefaction.

Vanden Bussche, K.M. & Froment, G.F., 1996. A steady-state kinetic model for methanol synthesis and the water gas shift reaction on a commercial Cu/ZnO/Al2O3 catalyst. *Journal of Catalysis*, 161, 1–10.

Wang, M., Elgowainy, A., Lu, Z., Baek, K. H., Bafana, A., Benavides, P. T., Burnham, A., Cai, H., Cappello, V., Chen, P., Gan, Y., Gracida-Alvarez, U.R., Hawkins, T.R., Iyer, R. K., Kelly,

J.C., Kim, T., Kumar, S., Kwon, H., Lee, K., Liu, X., Lu, Z., Masum, F.H., Ng, C., Ou, L., Reddi, K., Siddique, N., Sun, P., Vyawahare, P., Xu, H., Zaimes, G.G., 2022. Greenhouse gases, Regulated Emissions, and Energy use in Technologies Model ®, s.l.: USDOE Office of Energy Efficiency and Renewable Energy (EERE).

Wernet, G., Bauer, C., Steubing, B., Reinhard, J., Moreno-Ruiz, E., & Weidema, B., 2016. The ecoinvent database version 3 (part I): overview and methodology. *International Journal of Life* Cycle Assessment, 21, 1218-1230.

WRAP, 2016. Digestate and compost use in agriculture, Banbury: s.n.

Wright, M.E., 2012. Process for the Dehydration of Aqueous Bio-Derived Terminal Alcohols to Terminal Alkenes. US 2012 0238788 A1.

Zhao, X., Yao, G. & Tyner, W. E., 2016. Quantifying breakeven price distributions in stochastic techno-economic analysis. *Applied Energy*, 318-326.

Zhao, S., Jian, L., Chen, C., Yan, B., Tao, J., & Chen, G., 2022 Interpretable machine learning for predicting and evaluating hydrogen production via supercritical water gasification of biomass. *Journal of Cleaner Production*, 316, 128244.

4 Initial techno-economic analysis of the integrated platform

4.1 Preface

This chapter contributes to the overall thesis aim of developing and applying Techno-Economic Analysis (TEA) methods to evaluate the proposed aerobic gas fermentation and Supercritical Water Gasification (SCWG) process by developing the detailed process model for the novel aerobic gas fermentation platform, comparing and selecting the cost model to use in this and future case studies, producing the investment analysis for the initial case study, and undertaking the environmental assessment. It therefore contributes to the following thesis objectives:

1. Develop process simulations for the aerobic gas fermentation and supercritical water gasification process, incorporating heat integration and downstream processing.
2. Determine an appropriate techno-economic framework and perform a comprehensive techno-economic analysis of the simulated process.
3. Quantify the greenhouse gas emissions associated with chemical and fuel production from the process and compare them with conventional production methods.
4. Compare the economic and environmental competitiveness of the process with alternative renewable production methods.

This initial piece of work served as the primary analysis of the technical and economic feasibility of the heat integrated aerobic gas fermentation platform. The proposed platform was previously suggested in the experimental paper by Bommareddy et al. (2020). This experimental paper first introduced the concept of heat integrating exothermic aerobic gas fermentation with endothermic SCWG to overcome the energetic inefficiency of the aerobic gas fermentation. The focus of the experimental paper was on the fermentation results and initial conceptual design of the heat integrated platform. However, without a thorough TEA the economic potential of the platform was unknown.

To determine the techno-economic feasibility, a rigorous process model of the platform was built in Aspen HYSYS for the production of isopropanol and acetone. These were selected as the first case study as they represent commodity chemicals that are direct products from fermentation. A heat pump using isopentane as the working fluid was incorporated to utilise the abundant low temperature heat from the fermentation to support the SCWG reaction. Furthermore, the energy from the high pressure SCWG effluent was recovered using a turbo-expander and used to supply air to the fermentation. The developed platform was energetically self-sufficient, including downstream processing. Owing to the high energy recovery from the turbo-expander additional renewable electricity was exported to the grid for sale, generating additional revenue. Importantly, the initial process simulation for this case study was undertaken by Alex Conradie. However, the TEA, Life Cycle Assessment (LCA), and journal writing were undertaken by the author of this thesis.

The TEA was undertaken in the context of a China based paper and pulp mill, with black liquor used as the renewable carbon source. As a wet lignin-rich feedstock black liquor is particularly suited as a feedstock for SCWG. The study was conducted for a China location owing to it being the second largest virgin pulp manufacturer, representing an abundance of black liquor feedstock, and having lower capital and operating costs than other geographic locations. It was assumed that 25% of the mill's black liquor production could be diverted from conventional energy recovery towards chemical production. This assumption was based on research into improved heat integration Kraft mills suggesting a 40% reduction in energy can be achieved

(Ahmetović & Grossmann, 2020), and that the Tomlinson Boiler (used for conventional energy recovery) is often the bottleneck of increased mill capacity (Berntsson et al., 2008).

The mass and energy balances from the process model were used to undertake the TEA. Three capital expenditure and operating expenditure methods were used to evaluate the process, the method yielding the median results in both cases was used in the formal analysis of the platform. This provided a methodology basis to use in the subsequent TEAs undertaken in this thesis. Whilst the median result is not necessarily the most accurate, it is impossible to determine method accuracy without a commercialised facility.

In addition, as black liquor has no economic value, this work developed a method to cost the waste black liquor feedstock. The feedstock was costed based on its utility value, calculated as foregone renewable electricity generation. A process model for conventional renewable electricity generation was created and costed. The Net Present Value (NPV) leveraged from this alternate use was subtracted from the aerobic gas fermentation's initial NPV to obtain the final NPV delivered through the aerobic gas fermentation platform for chemical production.

To remove bias from the product price selection procedure price projections for both isopropanol and acetone were produced using a Radial Basis Function Neural Network (RBFNN). The RBFNN was trained as one step ahead predictor based on 10 historic prices. The weights and centre points were optimised during training. Once optimised the RBFNN was initiated with 10 real data points and ran recursively where predicted prices were used as inputs to the model. Stochastic uncertainty was accounted for by employing a uniform distribution of ±30% from the forecast centre point.

As highlighted in Chapter 2 the intrinsic uncertainty within early-stage feasibility studies necessitates an uncertainty analyses to band the results within a range of potential outcomes. This work incorporates this through conducting a Monte Carlo uncertainty analysis. The rigorous process modelling enabled the expansion of the economic analysis to include a cradle-to-gate LCA to quantify the process' Greenhouse Gas (GHG) emissions. This was compared with conventional production methods and facilitated a thorough technology evaluation based on both economic and environmental results.

To determine the potential of a technology it is important to compare it to feasible alternative production methods. As such, the TEA and LCA results were compared to a benchmark anaerobic gas fermentation process. As commercial gas fermentation is largely dominated by anaerobic bacteria this was used as the benchmark alternative. In addition to commercialising ethanol production via gas fermentation, LanzaTech have also investigated the production of acetone, a precursor to isopropanol. As such, LanzaTech's investigation undertaken for the Department of Energy, in collaboration with Oak Ridge National Laboratory, was used as the anaerobic process for comparison (Simpson et al., 2019).

The novelty of this work was the TEA of the proposed heat integrated aerobic gas fermentation and SCWG platform. Limited TEA studies have been conducted into aerobic gas fermentation. Existing studies have focused on identifying process parameters (productivity and yield) to define future research targets (Khan et al., 2014), general assessments for renewable chemical production including higher value co-products Choi et al. (2010), and the potential to reduce energy consumption through using thermophilic bacteria (Levett et al., 2016). In contrast, the analysis in this thesis aimed to evaluate the economic potential by applying process engineering solutions to some inherent disadvantages of aerobic gas fermentation. In addition, this study compares different techno-economic costing models to evaluate the economic feasibility of the platform. Existing comparisons in capital costing methods for TEAs exist; however, the comparisons are limited to equipment cost and capital cost estimation,

excluding fixed operating cost considerations (Brown, 2015; Symister, 2016; van Amsterdam, 2018; Feng & Rangaiah, 2011). Furthermore, these studies did not undertake the comparison within a TEA. Finally, this study compares both the TEA and LCA results of the proposed aerobic gas fermentation and SCWG platform and a benchmark anaerobic gas fermentation process. Existing gas fermentation technology comparisons have focused on comparisons between gas fermentation and hydrolysis-based fermentation (Piccolo & Bezzo, 2009; Choi et al., 2010; Christodoulou & Velasquez-Orta, 2016) or thermochemical conversion pathways (Haro et al., 2013; Tan et al., 2016; Okoro & Faloye, 2020), detailed in Chapter 2.

This study demonstrated the proposed technology achieved a cumulative NPV of $42 million using the nominal TEA inputs. The uncertainty analysis demonstrated a 70% NPV probability band of between $35 and $85 million with no negative outcomes. Therefore, under the considered scenario, the platform demonstrates it is able to cost-competitively produce the commodity chemicals isopropanol and acetone. Using a cradle-to-gate framework, net negative emissions were obtained owing to the sequestration of biogenic carbon (Isopropanol: -2.10 $kgCO_{2eq}$/kg, Acetone: -2.21 $kgCO_{2eq}$/kg). This is in comparison to 2.07 $kgCO_{2eq}$/kg and 2.43 $kgCO_{2eq}$/kg via conventional production. When compared to the benchmark anaerobic process a comparable techno-economic outcome was achieved. LanzaTech's anaerobic study claimed that by selling acetone at market prices ethanol could be sold at or below the US Department of Energy's 2022 target of $ 3/Gasoline Gallon Equivalent (GGE). By marketing isopropanol and acetone produced from the aerobic platform as a biofuel mixture a sales price of $2.87/GGE was achieved, meeting the $3/ GGE target. Furthermore, the LCA results were also comparable with the anaerobic process. Achieving emissions of -2.04 $kgCO_{2eq}$/kg for the combined isopropanol and acetone product compared to -1.9 $kgCO_{2eq}$/kg for a combined ethanol and acetone product in LanzaTech's anaerobic gas fermentation study. This suggests that the intrinsic energetic efficiency of anaerobic gas fermentation can be attained by aerobic gas fermentation through process engineering. It also demonstrates the potential of heat integrated aerobic gas fermentation with SCWG as a renewable biochemical technology platform.

A limitation of this study was neglecting to compare different equipment cost models. This has been previously investigated and is detailed in Chapter 2: Literature Review (Symister, 2016; van Amsterdam, 2018; Feng & Rangaiah, 2011) However, there is currently no consensus on the most accurate or appropriate cost model. As such, the potential to produce representative cost models based on recent commercialised projects is proposed as an area of further investigation, discussed further in Chapter 8. Furthermore, a single point sensitivity analysis was not undertaken in this study. This prevents the identification of the relative importance of each variable to the process' economic outcome. To rectify this, a single point sensitivity analysis was conducted in Chapter 5. In addition, the upper limit used for the sensitivity analysis parameters were uniformly set in this analysis. However, the ranges recommended in Sinnott & Towler (2013) have higher upper bounds for the inside battery limit capital, outside battery limit capital, and labour cost. This is attributed to the fact that cost overruns are more common and acute than cost underruns (Brown, 2015). To rectify this, the recommended bounds from Sinnott and Towler (2013) were adopted in Chapters 5 and 7. To account for product price variability and uncertainty in the projected prices an arbitrary ±30% was used. Therefore, the product price uncertainty band used in the Monte Carlo simulation had no bearing on the actual variability within the historic commodity price data. This price projection method is modified in Chapter 6 and the Monte Carlo simulations are rerun and compared to evidence the importance of price distributions consideration to TEA outcomes. Another limitation was representing the SCWG of black liquor using kinetics for the gasification of guiacol. Whilst guiacol is commonly used as a model compound for lignin (Hu et al., 2020), it does not represent the actual composition of black liquor. This simplified approach is modified

in Chapter 7 to allow for the input of actual biomass compositions to the gasifier model. Finally, a remaining limitation of this study is the failure to model anaerobic gas fermentation for comparison, whilst a benchmark study was used for the analysis, the differences in the considered scenarios and TEA methodologies make accurate comparisons between studies difficult. As such, in the subsequent TEA in Chapter 5 the technologies compared are all rigorously modelled.

This work was published in the *Johnson Matthey Technology Review Journal* in July 2021 entitled "Reconciling the Sustainable Manufacturing of Commodity Chemicals with Feasible Technoeconomic Outcomes: Assessing the investment case for heat integrated aerobic gas fermentation" and is presented in this thesis as Chapter 4. The corresponding supplementary information as published alongside the manuscript is reprinted in Appendix A.1.

Article Title: Reconciling the Sustainable Manufacturing of Commodity Chemicals with Feasible Technoeconomic Outcomes: Assessing the investment case for heat integrated aerobic gas fermentation

Journal: Johnson Matthey Technology Review Journal

Date: July 2021

DOI: 10.1595/205651321X16137377305390

Authors: Sarah Rodgers, Alex Conradie, Rebekah King, Stephen Poulston, Martin Hayes, Rajesh Reddy Bommareddy, Fanran Meng, Jon McKechnie

Author Contributions: Sarah Rodgers: Methodology, Software, Formal analysis, Investigation, Writing - Original Draft, writing – Review & Editing, Visualisation. Alex Conradie: Conceptualisation, Methodology, Software, Formal analysis, Investigation, Writing - Original Draft, Writing – Review & Editing, Visualisation, Supervision, Funding Acquisition. Rebekah King: Methodology, Software, Formal Analysis, Investigation, Writing – Review & Editing. Stephen Poulston: Writing – Review & Editing. Martin Hayes: Writing – Review & Editing. Rajesh Reddy Bommareddy: Conceptualisation, Writing – Review & Editing. Fanran Meng: Methodology, Software, Formal Analysis, Investigation, Writing – Review & Editing, Visualisation. Jon McKechnie: Methodology, Software, Formal Analysis, Investigation, Writing – Review & Editing, Supervision, Funding Acquisition.

4.2 References

Ahmetovi, E., and Grossmann, I. E., 2020. 'A Review of Recent Developments of Water and Energy Optimisation Methods Applied to Kraft Pulp and Paper Mills', in '4th South East Eur. Conf. Sustain. Dev. Energy, Water and Environment Systems (4th SEE SDEWES)',

Berntsson, T., Axegard, P., Backlund, B., Samuelsson, A., Berglin N., and Lindgren, K., 2008.

Swedish Pulp Mill Biorefineries', https://www.osti.gov/etdeweb/servlets/purl/951488

Bommareddy, R.R; Wang, Y; Pearcy, N; Hayes, M; Lester, E; Minton, N.P; Conradie, A.V., 2020. A Sustainable Chemicals Manufacturing Paradigm Using CO_2 and Renewable H_2. *iScience,* 23(6), 101218.

Brown, T. R., 2015. A critical analysis of thermochemical cellulosic biorefinery capital cost estimates. *Biofuels, Bioproducts and Biorefining*.

Choi, D., Chipman, D. C., Bents, S. C. & Brown, R. C., 2010. A Techno-economic Analysis of Polyhydroxyalkanoate and Hydrogen Production from Syngas Fermentation of Gasified Biomass. *Applied Biochemistry and Biotechnology*, 160, 1032-1046.

Christodoulou, X. & Velasquez-Orta, S. B., 2016. Microbial Electrosynthesis and Anaerobic Fermentation: An Economic Evaluation for Acetic Acid Production from CO2 and CO. *Environmental Science & Technology*, 50(20), 11234-11242.

Feng, Y. & Rangaiah, G., 2011. Evaluating Capital Cost Estimation Programs. *Chemical Engineering Journal*, 22-29.

Haro, P., Ollero, P. & Trippe, F., 2013. Technoeconomic assessment of potential processes for bio-ethylene production. *Fuel Processing Technology*, 114, 35-48.

Hu, Y., Gong, M., Xing, X., Wang, H., Zeng, Y., Xu, C.C., 2020. Supercritical water gasification of biomass model compounds: A review. *Renewable and Sustainable Energy Reviews*, 118, 109529.

Khan, N. E., Myers, J. A., Tuerk, A. L. & Curtis, W. R., 2014. A process economic assessment of hydrocarbon biofuels production using chemoautotrophic organisms. *Bioresource Technology*, 172, 201-211.

Levett, I., Birkett, G., Davies, N., Bell, A., Langford, A., Laycock, B., Lant, P., Pratt, S., 2016. Techno-economic assessment of poly-3-hydroxybutyrate (PHB) production from methane—The case for thermophilic bioprocessing. *Journal of Environmental Chemical Engineering*, 4(4), 3724-3733.

Okoro, O. & Faloye, F., 2020. Comparative Assessment of Thermo-Syngas Fermentative and Liquefaction Technologies as Waste Plastics Repurposing Strategies. *AgriEngineering*, 2, 378-392.

Piccolo, C. & Bezzo, F., 2009. A techno-economic comparison between two technologies for bioethanol production from lignocellulose. *Biomass & Bioenergy*, 33(3), 478-491.

Simpson, S D., Abdalla, T., Brown, S D., Canter, C., Conrado, R., Daniell, J., Dassanayake, A., Gao, A., Jensen, R. O., Köpke, M., Leang, C., Liew, FungMin E., Nagaraju, S., Nogle, R., Tappel, R. C., Tran, L., Charania, P., Engle, N., Giannone, R., Hettich, R., Klingeman, D., Poudel, S., Tschaplinski, T., & Yang, Z., 2019. Development of a Sustainable Green Chemistry Platform for Production of Acetone and Downstream Drop-in Fuel and Commodity Products directly from Biomass Syngas via a Novel Energy Conserving Route in Engineered Acetogenic Bacteria. United States.

Sinnott, R. & Towler, G., 2013. Chemical Engineering Design - Principles, Practice and Economics of Plant and Process Design. 2nd ed. s.l.:Elsevier.

Symister, O., 2016. An Analysis of Capital Cost Estimation Techniques for Chemical Processing. Melbourne, Florida: s.n.

van Amsterdam, M., 2018. Factorial Techniques applied in Chemical Plant Cost Estimation: A Comparative Study based on Literature and Cases. Delft: s.n.

Tan, E.C.D, Snowden-Swan, L.J., Talmadge, M., Dutta, A., Jones, S., Ramasamy, K.K., Gray, M., Dagle, R., Padmaperuma, A., Gerber, M., Sahir, A.H., Tao, L., Zhang, Y., 2016. Comparative techno-economic analysis and process design for indirect liquefaction pathways to distillate-range fuels via biomass-derived oxygenated intermediates upgrading. *Biofuels, Bioproducts & Biorefining.*

This page has been left intentionally blank

https://doi.org/10.1595/205651321X16137377305390 *Johnson Matthey Technol. Rev.*, 2021, **65**, (3), 375–394

JOHNSON MATTHEY
TECHNOLOGY REVIEW
www.technology.matthey.com

Reconciling the Sustainable Manufacturing of Commodity Chemicals with Feasible Technoeconomic Outcomes

Assessing the investment case for heat integrated aerobic gas fermentation

Sarah Rodgers*, Alex Conradie*, Rebekah King
Sustainable Process Technologies Research Group, Faculty of Engineering, University of Nottingham, Nottingham, NG7 2RD, UK

Stephen Poulston
Johnson Matthey, Blounts Court Road, Sonning Common, Reading, RG4 9NH, UK

Martin Hayes
Johnson Matthey, 28 Cambridge Science Park, Milton Road, Cambridge, CB4 0FP, UK

Rajesh Reddy Bommareddy
Hub for Biotechnology in the Built Environment, Department of Applied Sciences, Faculty of Health and Life Sciences, Northumbria University, Ellison Building, Newcastle upon Tyne, NE1 8ST, UK

Fanran Meng
Department of Engineering, University of Cambridge, Trumpington Street, Cambridge, CB2 1PZ, UK

Jon McKechnie**
Sustainable Process Technologies Research Group, Faculty of Engineering, University of Nottingham, Nottingham, NG7 2RD, UK

***Joint first authors**
****Email:** jon.mckechnie@nottingham.ac.uk

The manufacturing industry must diverge from a 'take, make and waste' linear production paradigm towards more circular economies. Truly sustainable, circular economies are intrinsically tied to renewable resource flows, where vast quantities need to be available at a central point of consumption. Abundant, renewable carbon feedstocks are often structurally complex and recalcitrant, requiring costly pretreatment to harness their potential fully. As such, the heat integration of supercritical water gasification (SCWG) and aerobic gas fermentation unlocks the promise of renewable feedstocks such as lignin. This study models the technoeconomics and life cycle assessment (LCA) for the sustainable production of the commodity chemicals, isopropanol and acetone, from gasified Kraft black liquor. The investment case is underpinned by rigorous process modelling informed by published continuous gas fermentation experimental data. Time series analyses support the price forecasts for the solvent products. Furthermore, a Monte Carlo simulation frames an uncertain boundary for the technoeconomic model. The technoeconomic assessment (TEA) demonstrates that production of commodity chemicals priced at ~US$1000 per tonne is within reach of aerobic gas fermentation. In addition, owing to the sequestration of biogenic carbon into the solvent products, negative greenhouse gas (GHG) emissions are achieved within a cradle-to-gate LCA framework. As such, the heat integrated aerobic gas fermentation platform has promise as a best-in-class technology for the production of a broad spectrum of renewable commodity chemicals.

1. Introduction

The development of a sustainable chemical industry requires a transition from the use of finite fossil reserves to renewable carbon feedstocks. Second generation biochemical

technologies utilise carbon feedstocks outside the food value chain. Such technologies allow agricultural, industrial and organic municipal solid wastes to be used for chemical production (1). These carbon sources are inexpensive, abundant and renewable, contributing towards the development of a sustainable, circular economy (2). Lignocellulosic biomass typically consists of cellulose, hemicellulose and lignin. However, owing to its recalcitrance, lignin cannot be utilised by conventional fermentation, which accounts for up to 40% of lignocellulosic biomass (3).

Black liquor is a coproduct from Kraft paper and pulp mills, consisting of the residual lignin after recovery of the cellulosic pulp product. In Kraft mills approximately 10 tonnes of weak black liquor is produced per air dried tonne of pulp (4). The combustion of this lignin-rich coproduct in Tomlinson boilers makes modern Kraft mills self-sufficient in steam and electrical energy (4, 5). However, research into Kraft mill heat integration over the last two decades has highlighted the potential to reduce mill energy consumption by up to 40% (6, 7). Such projects would free up a portion of weak black liquor for alternative income generation. Additionally, in mills where the Tomlinson boiler is the bottleneck for the process, diverting a portion of black liquor away from the recovery boiler could allow mills to increase their capacity by 25% (8). Whilst the traditional use for the black liquor coproduct is renewable electricity generation, gasification of this carbon-rich feedstock creates opportunities for biochemical production, expanding the product range of a Kraft mill.

SCWG has emerged as a hydrothermal technology suited to the gasification of wet biomass feedstocks to produce synthesis gas (syngas). SCWG is particularly advantageous for processing feedstocks with moisture contents >30%, where it energetically outcompetes the inherent drying required by conventional gasification (9). It is therefore capable of utilising streams such as black liquor, food waste, sewage sludge and manure which are typically uneconomical as feedstocks for traditional gasification technologies (10). Furthermore, the dissolution of the carbon feedstock in water leads to low tar and coke production in comparison with conventional gasification (11), simplifying purification technologies. Upgrading syngas to fuels and chemicals using metal-based catalysts is an established technology for coal feedstocks. As such, these technologies have been applied to syngas derived from renewable feedstocks, where Johnson Matthey and bp recently licenced their Fischer-Tropsch technology to Fulcrum Bioenergy (12). However, such technologies experience high capital and operating costs due to the utilisation of high operating temperatures and pressures, the prerequisite for specific carbon monoxide to hydrogen ratios and potential catalyst poisoning from gas impurities (13). Moreover, low chemocatalytic selectivity remains a challenge for converting syngas to commodity chemicals. Gas fermentation, on the other hand, circumvents these intrinsic challenges, notably through high selectivity biocatalysis, and has emerged as an alternative technology for syngas upgrading (13). Gas fermentation exploits microbial cell factories able to utilise carbon dioxide and hydrogen as a sole carbon and energy source to produce target chemicals through metabolic engineering (14).

The commercialisation of gas fermentation technology is dominated by anaerobic fermentation, where LanzaTech leads the way in the utilisation of carbon monoxide-rich steel mill off-gas to produce ethanol (15). Their Jintang plant has a 46,000 tonne year^{-1} operating capacity and uses their proprietary anaerobic acetogen, *Clostridium autoethanogenum*, as a microbial cell factory. This microorganism employs the Wood-Ljungdahl pathway, which is a thermodynamically efficient carbon dioxide fixation pathway compared to other biological C1 fixation pathways (16). However, such anaerobic carbon dioxide fixation presents energetic limitations which limit the product scope (17). Also, low value byproducts are common, negatively impacting on the carbon efficiency of the desired product whilst complicating downstream processing (18).

Aerobic cell factories on the other hand, are energetically advantaged compared to anaerobic cell factories (19). Therefore, the use of aerobic bacteria allows for the production of more complex chemicals *via* energy-intensive biochemical pathways (18), broadening the renewable chemical spectrum. However, a disadvantage of aerobic gas fermentation is its reliance on the Calvin-Benson-Bassham cycle. Whilst this cycle achieves favourable kinetics by investing appreciable energy into C1 fixation (20), it is consequently thermodynamically inefficient compared to the Wood-Ljungdahl pathway. Due to the greater heat generation, aerobic bioreactors require the installation of substantial cooling capacity, translating to both capital and operating cost burden (19). In addition, compressors are required to satisfy the oxygen demand and the presence of oxygen necessitates

the use of more expensive stainless steel reactors. Historically, aerobic fermentation has been used for high value, low volume products (21). However, for the production of higher volume commodity products, where utility costs dominate (22), aerobic fermentation has been hindered by process economics. This is a result of the aforementioned cooling requirements, associated air compression and reduced economies of scale compared with anaerobic fermentation (23).

The difference between aerobic and anaerobic fermentation's process economics is highlighted in recent work by Dheskali *et al*. who developed an estimation tool for the fixed capital investment (FCI) and utility consumption for large-scale biotransformation processes (24). Their model presented a ~20% increase in unitary FCI and a >1.5 times increase in energy requirement for aerobic fermentation over anaerobic, for a modest aeration rate. This was attributed to the capital and operating costs associated with the air compressors required for aerobic fermentation (24). Gunukula *et al*. also presented an almost 30% increase in the minimum selling price for commodity chemicals produced *via* aerobic compared to anaerobic fermentation (25). Similarly, in a series of technoeconomic studies for cellulosic ethanol production by the National Renewable Energy Laboratory (NREL), the fermentation area was found to be the primary cost for aerobic fermentation, with the fermentation compressors having the greatest power requirement (26). On the other hand, for anaerobic fermentation, the pretreatment section was found to be the largest cost driver with a less pronounced compressor duty (27).

The potential of aerobic fermentation can only be effectively realised by reducing these costs, notably through improved engineering design. This work evaluates the integration of aerobic gas fermentation with SCWG as a solution to economically feasible commodity chemical production as proposed by Bommareddy *et al*. (28). The integration of gas fermentation with SCWG *via* a heat pump allows for the low temperature heat released by gas fermentation to be utilised by the high temperature, endothermic SCWG process. This both removes the cooling water burden required by the bioreactors and reduces the fraction of hydrogen that needs to be combusted to support the endothermic gasification process. Furthermore, the duty released by expanding the high-pressure gas product from SCWG is recovered using a turbo expander and subsequently used to power the air compression, negating the need for external power provision. This integration has the potential to overcome the barriers to cost effective, commercial scale, aerobic gas fermentation for commodity chemical production.

Cupriavidus necator (formerly, *Alcaligenes eutrophus* and *Ralstonia eutropha*) is employed as the microbial cell factory in this work. *Cupriavidus necator* is a chemolithoautotrophic bacterium capable of aerobic, autotrophic growth using carbon dioxide as the sole carbon source, hydrogen as electron donor and oxygen as the electron acceptor (29). This cell factory benefits from the kinetic advantage of the Calvin-Benson-Bassham cycle and is strictly respiratory, which compared to anaerobic cell factories results in negligible synthesis of low value, fermentative byproducts. Bommareddy *et al*. (28) detail the continuous production of isopropanol and acetone using aerobic gas fermentation. This first generation *Cupriavidus necator* cell factory produces acetone as an overflow coproduct from the engineered biochemical pathway to isopropanol, which is subject to future optimisation of this carbon flux bottleneck. Further relevant to the process design, this cell factory has not been adapted to be tolerant to concentrations of isopropanol >15 g l^{-1}, necessitating a dilution strategy through an engineering solution. Relying on the sustainable manufacturing paradigm in Bommareddy *et al*. (28), this work presents the TEA and LCA for a solvent plant, that exploits this first generation cell factory, producing isopropanol and acetone *via* aerobic gas fermentation and purifying the solvents *via* a heat and mass integrated separation train network.

2. Materials and Methods

2.1 Conceptual Process

The proposed solvent plant is co-located with a Kraft paper and pulp mill in China with throughput as defined in **Table I**. **Figure 1** outlines the Kraft process, which conventionally directs weak black liquor to multi-effect evaporators, producing strong black liquor which is combusted in a Tomlinson boiler to produce steam (4). This steam makes the mill self-sufficient in steam and electrical energy. Importantly, the cooking chemicals (NaOH and Na_2S) are recovered and recycled to the pulping process.

As previously mentioned, investments in heat integration have freed up a portion of the weak

Table I Kraft Mill Plant Capacity

Parameter	Value	Unit	Reference
Pulp mill capacity	130	Air dried tonne h^{-1}	–
Total weak black liquor production	1300	tonne h^{-1}	(4)
Black liquor solids content	17.5	% (w/w)	(4)
Lignin content in solids	41.5	% (w/w)	(30)
Lignin content in black liquor	7.3	% (w/w)	–

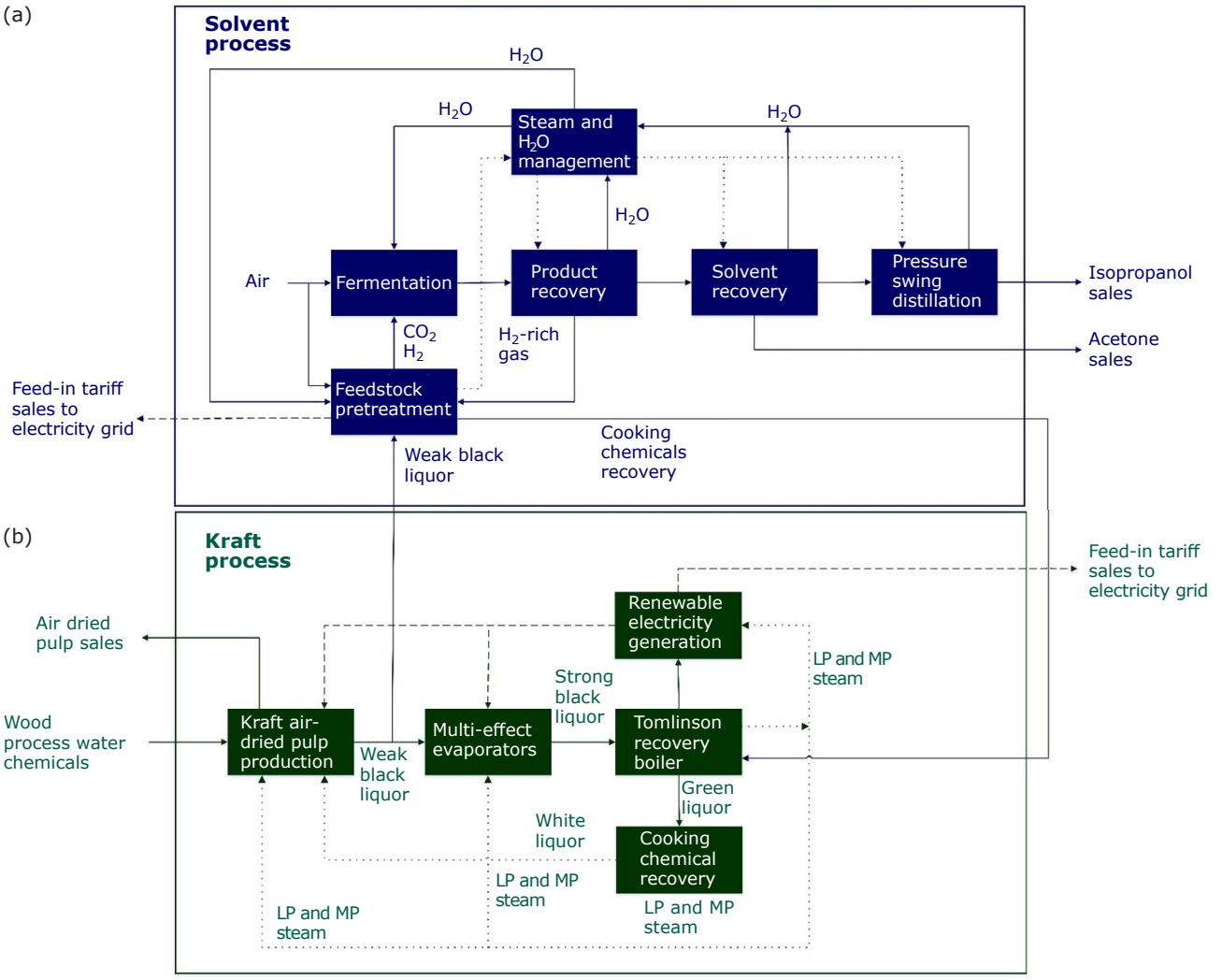

Fig. 1. Conceptual solvent process integration with Kraft process, outlining materials (solid lines), power (dashed lines) and steam (dotted lines) flows. Excess weak black liquor is fed to the solvent process from the Kraft process and cooking chemicals are returned to the Tomlinson recovery boiler. LP = low pressure; MP = medium pressure

black liquor coproduct for alternative uses. This study explores the opportunity of utilising this excess coproduct, taken as 25% of total production, for isopropanol and acetone production through aerobic fermentation in an integrated solvent plant as outlined in **Figure 1**.

Given black liquor has no economic value as a product, it is costed at its utility value. This is calculated based on its conventional use for renewable electricity generation, requiring capital investment in increased steam turbine capacity. The foregone net present value (NPV) associated with this conventional use is used as the utility value for the black liquor feedstock.

In the proposed solvent plant (**Figure 1**), weak liquor undergoes SCWG to carbon dioxide and

hydrogen. A challenge, however, is the efficient recovery of the cooking chemicals from the SCWG reactor and their recycle to the pulp mill digestor. Loss of these salts would result in a significant cost to the pulp mill. Under supercritical conditions, the properties of water change from polar to apolar, where the solubility of inorganic salts is very low (31). Cao *et al*. described the precipitation of alkali sodium salts in SCWG, reporting a neutral pH for the reactor effluent, suggesting that under supercritical conditions the salts largely precipitate from the solution (32). However, this precipitation can cause issues with plugging and fouling within the reactor (33). In this study the salts are removed prior to entering the SCWG reactor, in a manner similar to supercritical water desalination (34, 35) and modelled for SCWG of black liquor (33).

2.2 Process Intensification, Heat and Mass Integration

The solvent plant's mass and energy balance was informed by experimental data from continuous gas fermentation (28), and rigorous process simulation using Aspen HYSYS v11. The lignin content in black liquor was modelled as guaiacol, a model compound for lignin (36), as principal feed to the solvent plant. The weak black liquor is further diluted prior to entering the SCWG reactor, as lower biomass concentrations promote superior thermal cracking and yields greater hydrogen and carbon dioxide owed to the increased water concentration favouring the forward water-gas shift reaction (37).

The simplified flow diagram (**Figure 1**) outlines the six plant sections of the solvent plant, whilst **Figure 2** presents a detailed process flow diagram and operating conditions for upstream and downstream processing. The unit operations included in each of the six plant sections are summarised in **Table II**. **Table III** summarises the scale-up of the experimental gas fermentation data for the process simulation, which recognises the oxygen mass transfer limitations associated with the safety requirement to maintain non-flammable operating conditions. The heat integration between the low temperature exothermic gas fermentation and the high temperature endothermic SCWG is facilitated using a heat pump with isopentane as the working fluid (28).

Isopropanol and acetone are produced in both the aqueous and vapour phase of the bioreactors. The solvents in the vapour phase are recovered *via* gas absorption through mass integration using internal process streams, i.e. the isopropanol product was utilised to recover acetone, and water to recover isopropanol. For the isopropanol in the aqueous phase, azeotropic distillation is required due to the homogeneous minimum boiling point azeotrope formed between isopropanol and water (38). Conventionally, this azeotrope is broken using an entrainer, historically benzene (39). However, owed to its carcinogenic properties, alternative entrainers such as cyclohexane have been adopted (40). An alternative azeotropic separation technique is pressure swing distillation, taking advantage of the composition differences in the azeotrope at different pressures (41). In this work, pressure swing distillation was employed with the coproduct acetone acting as an unconventional entrainer. Further detail of the separation train is presented in **Figure 2**.

A U-loop bioreactor, similar to the one used by Peterson *et al*., is used in this work (42). The benefit of a U-loop bioreactor is that high mass transfer coefficients can be achieved without the need for mechanical agitation, leading to greater oxygen transfer rate and a reduced power requirement compared to conventional stirred tank reactors (42). The oxygen mass transfer coefficient calculation associated with the solvent plant's mass balance is presented in Table S1 in the Supplementary Information (available with the online version of this article), falling at the lower end of the range of mass transfer coefficients reported by Peterson *et al*. (42). Details of the experimental gas fermentation data is presented in **Table III**; a more detailed explanation of the experimental procedure can be found in Bommareddy *et al*. (28).

Significant heat integration makes the solvent plant self-sufficient in electricity and both low and medium pressure steam. Furthermore, process water recovered from distillation and the steam condensate is recycled to reduce the water make-up burden.

The process flow diagram for conventional renewable electricity generation, used to value the black liquor, is presented in Figure 3. An additional steam turbine is required to produce the renewable electricity for sale, relying upon the existing multi-effect evaporators, air compression and Tomlinson boiler. Superheated steam at 9000 KPa and 480ºC is used in the steam turbine (44). The medium pressure steam exiting the turbine is used in the multi-effect evaporators to concentrate the excess black liquor to 75% and to preheat the auxiliary air supplied to the Tomlinson boiler. Similarly, the associated electricity demand for the air

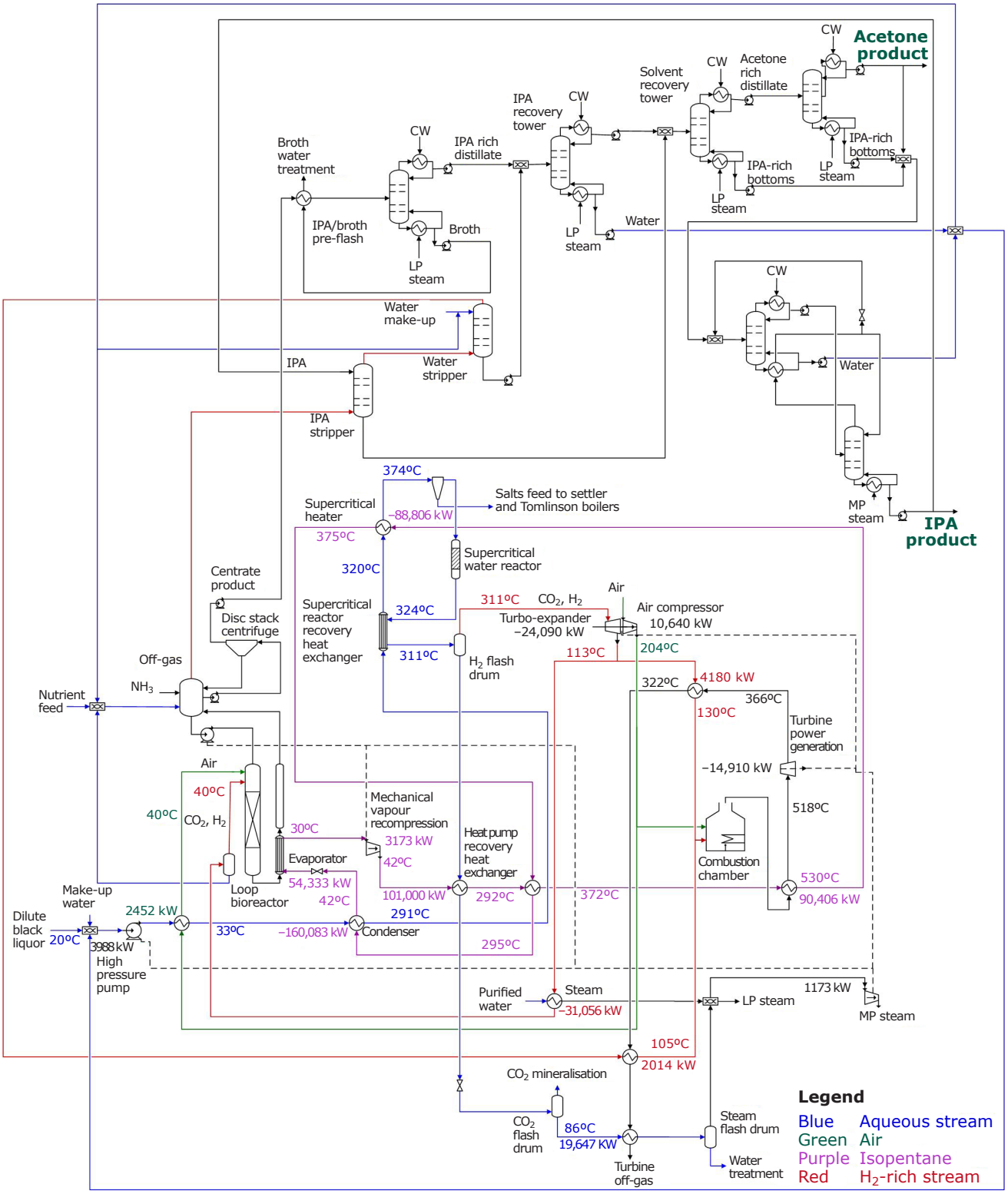

Fig. 2. Solvent plant process flow diagram, detailing the heat integration between gas fermentation and SCWG *via* a heat pump. The heat and mass integrated separation train constitutes the downstream processing, including gas absorption and heat integrated distillation. IPA = isopropanol; LP = low pressure; MP = medium pressure; CW = cooling water

Table II Solvent Plant Section Unit Operations

Plant Section	Unit Operations	Thermodynamic model
Feedstock pre-treatment	SCWG reactor, combustion chamber, combustion turbine, isopentane heat pump cycle	Lee Kesler Plocker
Fermentation	Seed and production bioreactors, pumps, centrifuge	Lee Kesler Plocker
Product recovery	Acetone stripper, water stripper, water removal columns	UNIQUAC
Solvent recovery	Acetone separation and purification columns	UNIQUAC
Isopropanol pressure swing distillation	Low- and high-pressure distillation columns	PSRV
Steam and water management	Mechanical vapour compressor, water and steam heat exchangers	Lee Kesler Plocker

Table III Summary of Scale-Up of Experimental Gas Fermentation Data for ASPEN HYSYS Process Simulation

Sources and sinks	Unit	Carbon dioxide and hydrogen as sole energy and carbon source
Bioreactors		
Oxygen transfer coefficient	$1\ h^{-1}$	415
Oxygen concentration in off-gas[a]	% (mol/mol)	3.35
Vessel volume	m^3	500
Number of bioreactor trains	–	4
Gas uptake rates		
Oxygen	mmol $l^{-1}\ h^{-1}$	230
Carbon dioxide	mmol $l^{-1}\ h^{-1}$	125
Hydrogen	mmol $l^{-1}\ h^{-1}$	1006
Isopropanol		
Specific productivity	kg $m^{-3}\ h^{-1}$	1.46
Broth concentration[b]	g l^{-1}	12.4
Acetone		
Specific productivity	kg $m^{-3}\ h^{-1}$	0.38
Broth concentration	g l^{-1}	1.7
Biomass		
Growth rate	h^{-1}	0.025
Dry cell weight with cell retention	g l^{-1}	21.5

[a] Maintained to ensure oxygen concentration is below hydrogen's limiting oxygen concentration of 4.6% (mol/mol) (43)
[b] Controlled *via* disc stack centrifugation, adding to the capital burden

compressor and pump is provided by the electricity generated. Resultantly, through conventional renewable electricity generation, the excess black liquor produces 138 GWh $year^{-1}$ for sale to the grid.

2.3 Costing Models

The mass and energy balance associated with the rigorous process simulation informs the capital cost, fixed operating cost and variable operating cost estimation. For the capital cost estimation, major equipment purchase costs were estimated using the models from Seider *et al*. (45), with the exception of the turbo-expander (46). Three different methods are used to calculate the FCI, owed to differences in the estimation methods. These three methods are designated as: the NREL method outlined in the 2011 NREL report (27), the Towler and Sinnott (TS) method taken from Chemical Engineering

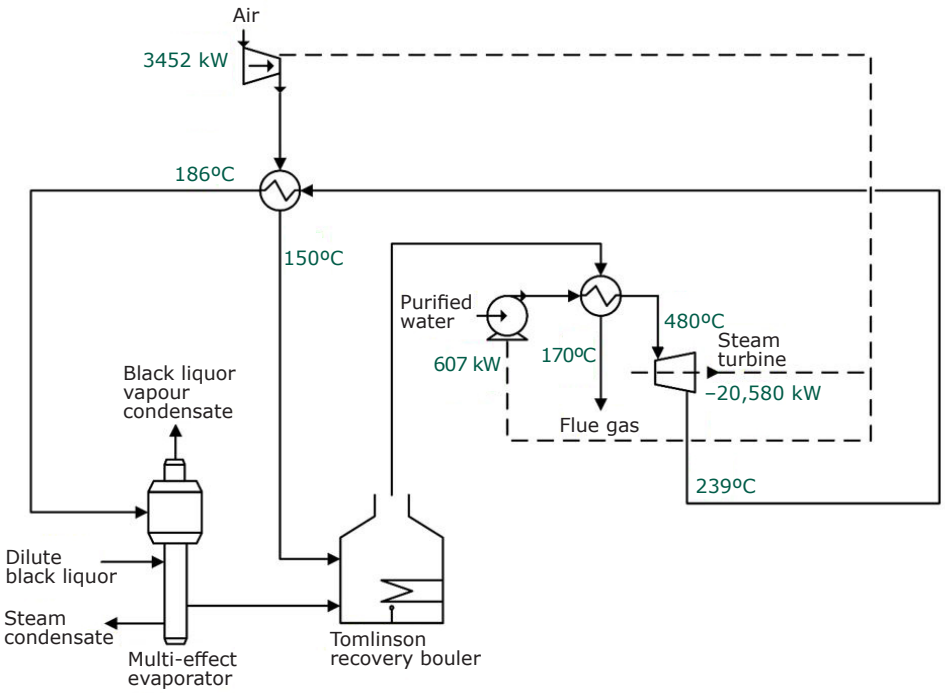

Fig. 3. Process flow diagram for black liquor's conventional use, renewable electricity generation

Table IV Fixed Capital Cost Models

	NREL	TS	Hand
Year basis	2019		
Production year	8110 h[a]		
Installation factor (multiplied by equipment cost) – inside battery limit (ISBL)	Table S2	Table S4	Table S5
Outside battery limit (OSBL)	Table S3	30% of ISBL	25% of ISBL
Contingency	–	10% of ISBL	–
Commissioning cost	5% of ISBL	–	5% of ISBL
Design and engineering cost	–	10% of ISBL	–
Fixed capital investment (FCI)	ISBL + OSBL + commissioning	ISBL + OSBL + contingency + design and engineering	ISBL + OSBL + commissioning
Working capital	10% of FCI		
Total capital investment (TCI)	FCI + working capital		

[a] Based on bioreactor cycle time

Design (47) and the Hand method detailed in Sustainable Design Through Process Integration (48). The calculation basis of the three methods is presented in **Table IV**.

For all three methods, the calculated equipment purchase costs are multiplied by an installation factor to obtain the inside battery limit (ISBL) installed costs. Both the NREL and Hand methods use installation factors dependant on the equipment type, whereas the TS method uses a universal multiplier. All installed equipment costs were adjusted to 2019 costs using the Chemical Engineering Plant Cost Index of 607.5 (49). A location factor of 0.51 was used for China (using indigenous materials), based on the 2003 location factor of 0.61 (47), updated to 2019 *via* the Chinese Yuan to US dollar exchange rate.

Three methods were used to calculate the fixed operating costs as summarised in **Table V**. As before, the NREL method (27) and the TS method (47) were employed. However, as the Hand method is solely for FCI, the third was the taken from Coulson and Richardson Volume 6 (50). Variable operating costs were estimated based on the costs detailed in **Table VI**, subject to annual inflation as outlined in **Table VII**.

Table V Fixed Operating Cost Models

Parameters	NREL	TS	Coulson and Richardson
Operating labour	Salary estimates in China obtained from salaryexpert.com (process operator, engineering and maintenance)[a]	Salary estimates in China obtained from salaryexpert.com 3 process operators per shift 4 shift teams	Salary estimates in China obtained from salaryexpert.com (process operator, engineering and maintenance)
Supervisory labour		25% of operating labour	
Direct salary overhead	90% of operating and supervisory labour	50% of operating and supervisory labour	–
Maintenance	3% of ISBL	3% of ISBL	5% of ISBL + OSBL (conventionally 5% FCI)
Property taxes and insurance	0.7% of FCI	1% of ISBL	2% of ISBL +OSBL (conventionally 2–3% FCI)
Rent of land	–	1% of FCI	–
Royalties	–	–	0% of FCI (conventionally 1% FCI)
General plant overhead	–	65% of total labour and maintenance	50% of operating labour
Allocated environmental charges	–	1% of FCI	–

[a] For a detailed breakdown of operating and supervisory labour for the NREL method see Supplementary Information (Table S6)

Table VI Variable Operating Cost

Raw material	Cost	Unit	Reference	Comments
Ammonia	250	US$ tonne^{-1}	(51)	Average price for 2019
Cooling water	0.753	US$ m^{-3}	(52)	–
Electricity	0.06	US$ kWh^{-1}	(52)	–
Nutrients	0.75	US$ m^{-3} media water	–	Mineral salt media, containing no complex media or vitamins
Process water	0.53	US$ m^{-3}	(47)	–

Table VII Investment Analysis Parameters

Parameters	Value	Comments
Discounted rate of return	10%	In line with studies in the BETO Biofuels TEA Database (57)
Corporation tax	25%	Corporation tax in China
Annual inflation	2%	–
Plant life	25 years	–
Depreciation	10 years	Straight line
Plant salvage value	No value	–
Construction period	2 years	–

2.4 Product Price Forecasting

Time series analysis was used to forecast the long-term average price of isopropanol and acetone. Takens' theorem was used as the basis for this analysis (53). Takens' theorem states that for a deterministic system, the underlying state variables that created the time series are embedded within the data. Using this theorem a deterministic, dynamic system can be reconstructed based on the observed time series. Forecast models constructed using the embedded state variables assume that

the market drivers underpinning the trajectory of the state variables in phase space remain largely unchanged. An embedding dimension of 10 was used to reconstruct the isopropanol and acetone price models from monthly average price data obtained from the Intratec database (54). In this work, a radial basis function neural network (RBFNN) containing eight neurons was used as a model to predict the future commodity prices. The network was trained as a one step ahead predictor by minimising the mean square error of the difference between the actual and predicted prices. Once trained, the network was evaluated (tested) in free run mode, where successive predicted prices (outputs) become inputs to the RBFNN. The confidence limits corresponding to the trained RBFNN were calculated as a reliability measure of the prediction as per the work undertaken by Leonard, Kramer and Ungar (55). The benefit of using an RBFNN is that the resultant forecast price is an impartial product of the dataset's underlying state variables.

The long-term average price for renewable electricity sales was taken as US$0.109 kWh^{-1} as per the biomass subsidy in China (56). This is used to inform the renewable electricity project to value the black liquor and for the excess electricity generated by the solvent plant.

2.5 Investment Analyses

The cost models from Section 2.3 and the product price forecast models from Section 2.4 inform the investment analyses. The black liquor is costed at its utility value, calculated as the foregone NPV from generating renewable electricity. Resultantly, the NPV for the solvent plant is calculated by subtracting the NPV of renewable electricity generation. The investment analysis parameters used are detailed in **Table VII**.

2.6 Sensitivity Analysis

A sensitivity analysis was conducted using a Monte Carlo simulation based on the cost parameters in **Table VIII**, creating an uncertainty framework. The cost parameters were taken from (47), with the exception of renewable electricity sale price where the upper limit for the long-term average price was capped at the current biomass subsidy in China, US$0.109 kWh^{-1}. This limit was applied due to the decreasing trend in renewable electricity subsidies (58). In contrast, the long-term average prices for isopropanol and acetone were varied ±30% from the forecast price. This provides a stochastic counter to the assumption used to determine the forecast prices: that the deterministic market drivers underpinning the trajectory of the state variables remain largely unchanged. However, given that market drivers are subject to change, the long-term average price may be banded with an equal likelihood of being higher or lower than the forecast price.

A uniform distribution for these parameters was used and varied for the solvent plant and conventional renewable electricity generation (used to value the black liquor). All the cost parameters in **Table VIII**, other than labour and electricity, were varied independently. 2000 simulations were run, stochastically varying the parameters within the defined lower and upper limits to produce a probability distribution of the solvent plant's NPV.

2.7 Life Cycle Assessment

A cradle-to-gate LCA model was developed using the ecoinvent 3.6 inventory database, following ISO Standards 14040 (59) and 14044 (60). GHG emissions were calculated based on the most recent Integrated Pollution Prevention and Control 100-year global warming potential (GWP) factors

Table VIII Uncertainty Framework for Monte Carlo Simulation Sensitivity Analysis

Monte Carlo input parameter	Lower limit	Upper limit
Product long term average pricing		
Isopropanol price	0.7	1.3
Acetone price	0.7	1.3
Renewable electricity price	0.7	1
Costing uncertainty factor		
ISBL capital cost	0.8	1.3
OSBL capital cost	0.8	1.3
Labour costs	0.8	1.3

to quantify GHG emissions in terms of carbon dioxide equivalents (CO_{2eq}) (61). Functional units were defined as 1 kg isopropanol, 1 kg acetone and 1 kWh of electricity. In line with the investment analysis, the LCA model considers the net electricity output of solvent plant by subtracting the foregone electricity from combustion of black liquor at the pulp mill. Life cycle environmental impacts are allocated between these three products using both economic and energy allocation. The GHG emission rate for the external process inputs: cooling water, process water and ammonia were taken from the ecoinvent 3.6 inventory database using the allocation at the point of substitution system model (62), whereas electricity was taken as the 2018 China electricity mix (63). The bio-based solvents isopropanol and acetone sequester biogenic carbon dioxide and hence are credited with a negative GHG emission based on their carbon content. Downstream activities, including the use and end-of-life of isopropanol and acetone products are not considered. These activities are assumed to be identical to those of conventional isopropanol and acetone, given that they are chemically and functionally identical, and therefore have no influence on the relative GHG emissions of renewable and conventional solvent products.

3. Results and Discussion

The major equipment items were sized using the mass and energy balance from the rigorous HYSYS simulation. The capital cost estimation for the solvent plant using the three methods outlined in **Table IV** is summarised in **Figure 4**. The underlying capital cost estimation data is detailed in Tables S2–S5 in the Supplementary Information. Due to the close agreement of the NREL and Hand methods, US$64 million and US$65 million respectively (**Figure 4**), and the greater simplicity of the Hand method, this method was used as the capital cost estimation basis. Table S10 details the capital cost estimation for the conventional generation of renewable electricity.

Similarly, the three fixed operating cost methods (**Table V**) are summarised in **Figure 5**, where the underlying fixed operating cost data is detailed in Tables S6–S8. Though sharing the same author, the TS and Coulson and Richardson methods have a dissimilar calculation method. However, the results of these two methods are in close agreement, US$4.62 million and US$5.01 million respectively (**Figure 5**). The substantially lower estimate by the NREL method (US$2.48 million) was therefore set aside, and the TS method employed as the fixed operating cost basis. The fixed operating costs for the conventional generation of renewable electricity are detailed in Table S11.

Figure 6 compares the capital estimation, fixed and variable operating cost models for the solvent plant and conventional renewable electricity generation. The large difference between the capital

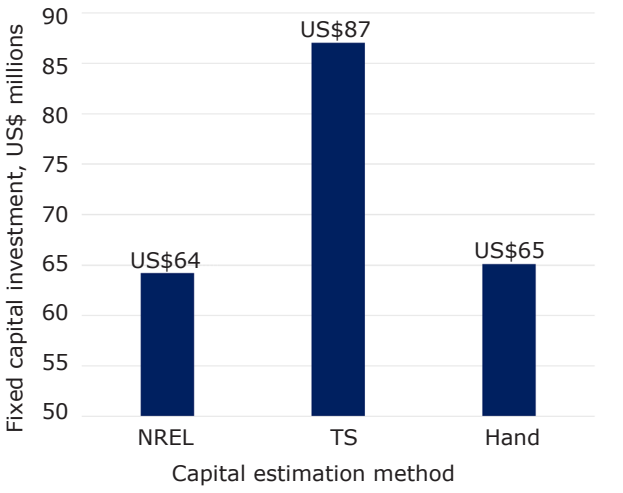

Fig. 4. Comparison of three fixed capital investment estimates using the NREL, TS and Hand methods for the solvent plant. The NREL and Hand methods are in close agreement. The Hand method estimate was taken forward into the investment analyses

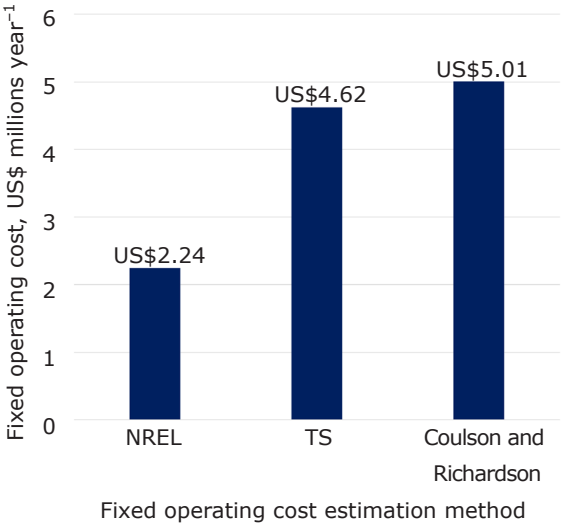

Fig. 5. Comparison of three fixed operating cost estimates using the NREL, TS and Coulson and Richardson methods for the solvent plant. Though related, the TS and Coulson and Richardson methods are in close agreement. The TS method estimate was taken forward into the investment analysis

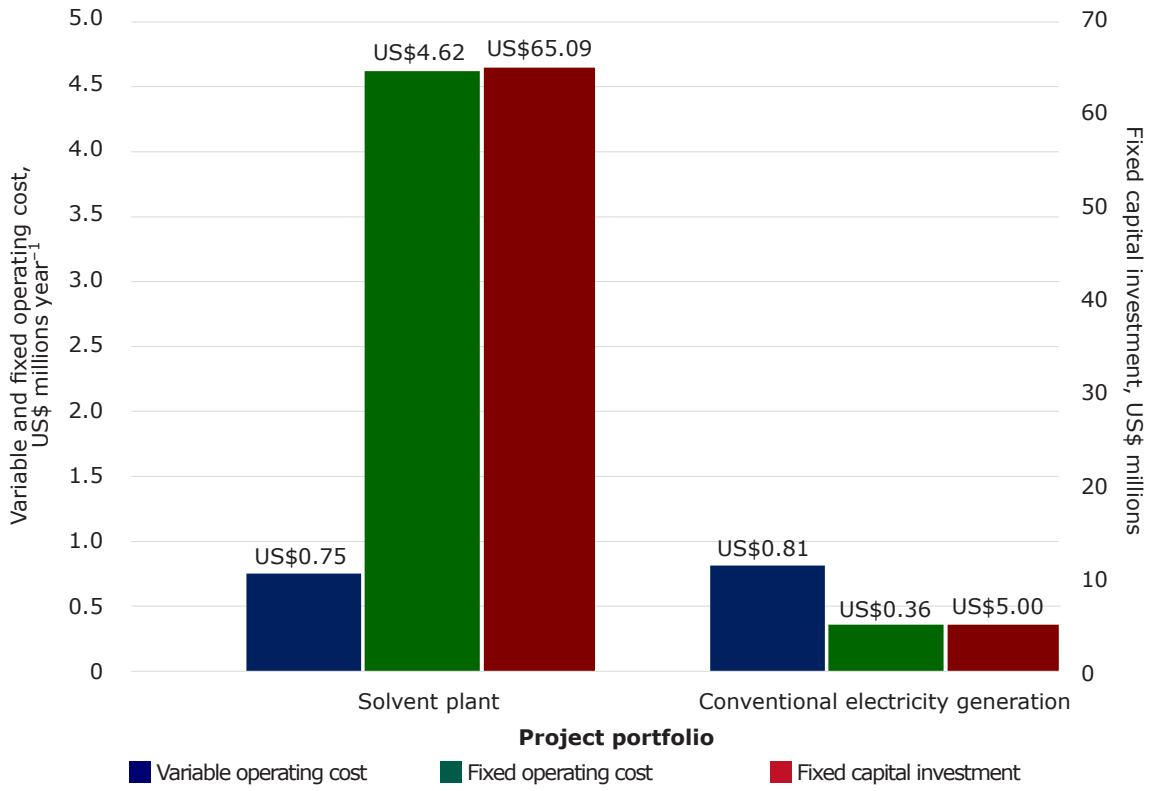

Fig. 6. Comparison between production costs and fixed capital investment for the solvent plant and conventional renewable electricity generation

investment highlights the greater complexity of the proposed solvent plant as an alternate opportunity to conventional renewable electricity generation.

The free-run forecasts for both isopropanol (**Figure 7**) and acetone (**Figure 8**) are shown to track the historical data within the confidence limits of the RBFNN, before settling on a forecast for the long-term average price. For comparative purposes the moving average for the previous ten prices is also plotted in Figures 7 and 8. The difference in the moving average and predicted forecast suggests that the RBFNN has identified pricing dynamics other than the time weighted average, i.e. the underlying state variables within the time series. As such, using this forecast price to inform the investment analysis ensures the nominal TEA inputs and sensitivity analysis are unbiased and centred upon market dynamics, opposed to an artefact of average pricing.

3.1 Investment Analysis

The solvent plant (**Figure 2**) produces three products, summarised in **Table IX**. The contribution of each product to the plant's income is also presented. Whilst isopropanol contributes to almost half the solvent plant income the renewable electricity fraction is the second highest contributor, highlighting the significant amount of renewable electricity generated by the solvent plant.

The investment analyses for the solvent plant and conventional renewable electricity generation are detailed in Tables S9 and S12, as per the investment analysis parameters presented in Table VII. The NPV for conventional renewable electricity generation represents the utility value of the black liquor, valued at US$73 million (Table S12). This is subtracted from the NPV of the solvent plant (US$115 million) to produce the cumulative NPV presented in Figure 9. For the nominal TEA model inputs, the solvent plant's net cumulative NPV is US$42 million.

Given the conceptual stage of the TEA, a Monte Carlo simulation was undertaken as per the uncertainty framework outlined in **Table VIII**. The produced probability distribution in **Figure 10** avoids making an investment decision based solely on nominal TEA inputs. The cumulative probability curve presents a 70% probability that the solvent plant will achieve a net cumulative NPV between

Fig. 7. Isopropanol price forecast using a radial basis function time series analysis model in free-run mode. The free-run forecast tracks the historical data appreciably, remaining within the confidence limits for the original one step predictor model fit. The free run prediction settles to a long-term average forecast for isopropanol. The moving average is plotted for comparative purposes. The y-axis is obscured given copyright restrictions associated with the Intratec database

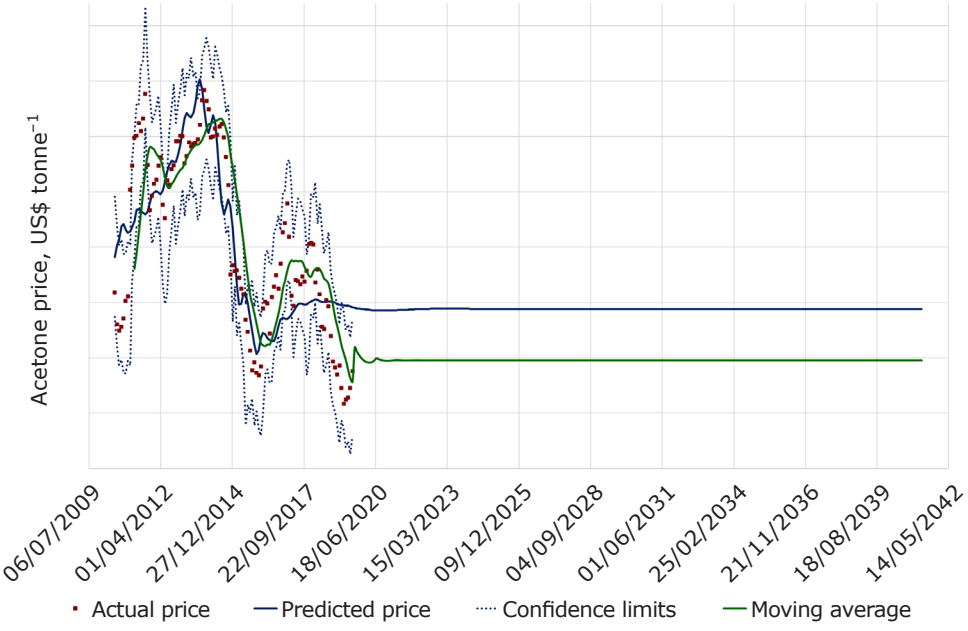

Fig. 8. Acetone price forecast using a radial basis function time series analysis model in free-run mode. The free-run prediction tracks the historical data appreciably, remaining within the confidence limits for the original one step predictor model fit. The free run forecast settles to a long-term average forecast for acetone. The moving average is plotted for comparative purposes. The y-axis is obscured given copyright restrictions associated with the Intratec database

Table IX Solvent Plant Production Summary

Product	Production rates		Product mass purity		Contribution to plant income
	Value	Unit	Value	Unit	%
Isopropanol	13.8	thousand tonnes year^{-1}	99.8	% (w/w)	49
Acetone	2.8	thousand tonnes year^{-1}	99.2	% (w/w)	6
Total renewable electricity	146	GWh year^{-1}	–	–	45

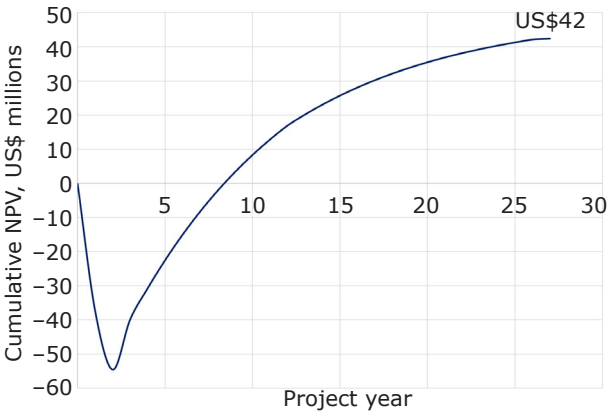

Fig. 9. Investment Analysis for the solvent plant including the utility value for black liquor, taken as the NPV for conventional generation of renewable electricity. For the nominal TEA model inputs, the solvent plant presents a net cumulative NPV of US$42 million

US$35 million and US$85 million, noting that no negative outcomes are predicted.

3.2 Life Cycle Assessment

Figure 11 summarises the outcome of the cradle-to-gate LCA for the solvent plant, compared to the conventional fossil derived processes; using both economic and energy allocation for the isopropanol, acetone and renewable electricity products.

Both solvents achieve negative GHG emissions when produced *via* the solvent plant using economic and energy allocation. The GHG emission for the two allocation methods are comparable, indicating the price per unit energy (US$ MJ^{-1}) is similar for all three products. The negative emissions are an intrinsic outcome of the cradle-to-gate framework, which excludes the end use for the products. As the total GHG emissions of the solvent plant are lower than the overall biogenic carbon sequestered, negative GHG emissions are achieved for the solvent products.

The negative GHG emissions compare favourably to the conventional isopropanol (hydration of propene) and acetone (oxidation of cumene) processes. Additionally, the GHG emissions associated with the excess renewable electricity from the solvent plant also compare favourably to the electricity mix in China (2018). Furthermore, as the end use for the solvents remains the same regardless of the production method, the relative GHG emissions are valid beyond the cradle-to-gate framework.

3.3 Comparison with Anaerobic Fermentation

As highlighted in the Introduction, the commercial implementation of gas fermentation is largely dominated by anaerobic fermentation. Therefore, it is important to compare the results to a best-in-class technology. In addition to successfully commercialising ethanol production *via* gas fermentation, LanzaTech have also investigated gas fermentation to produce acetone, a precursor to isopropanol (64). As such, LanzaTech's investigation undertaken for the US Department of Energy (US DOE), in collaboration with Oak Ridge National Laboratory, USA, is used as a benchmark anaerobic process (65).

As highlighted previously, the primary differences between anaerobic and aerobic fermentation technologies are inherent to the C1 fixation metabolic pathways. Strictly respiratory (aerobic) cell factories require air to be continuously fed into the bioreactor to facilitate carbon fixation. In addition, owed to the intrinsic thermodynamic inefficiency of the Calvin-Benson-Bassham cycle employed by aerobic bacteria, an excess of low temperature heat is produced. As such, a conventional process flowsheet for aerobic fermentation employs operationally costly compressors and chillers. In contrast, for anaerobic fermentation there is a reduced chiller requirement and the compressor duty is less pronounced. Moreover, owed to the presence of oxygen, aerobic fermentations require the use of more costly stainless steel reactors and more complex process control systems. Whilst the latter is an intrinsic requirement of aerobic fermentations, in this work we have reconciled the increased utility demand of aerobic fermentation through process integration (28). This integration employs a heat pump to utilise the low temperature heat generated by aerobic fermentation to heat the SCWG reactor feed, removing the cooling water burden required by the bioreactors. Additionally, the compressor duty is fully supplied through the electricity generated upon letting down the SCWG reactor's high-pressure gas product. As a result, the economic and LCA outcomes for the solvent plant should be comparable to anaerobic fermentation technology.

LanzaTech's anaerobic study achieved a combined selectivity of 94.7% for ethanol and acetone, of which 57.3% was acetone (65). LanzaTech disclosed that by selling acetone at market prices they are able to sell coproduced ethanol at or below the US DOE's 2022 target of US$3 GGE^{-1} (GGE

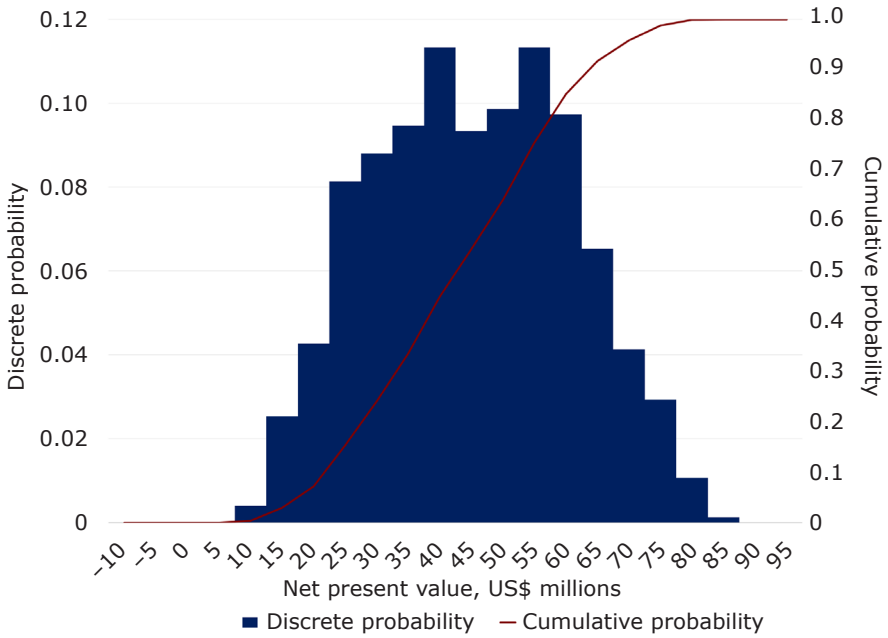

Fig. 10. Monte Carlo simulation for the opportunity cost associated with the solvent plant. The cumulative probability curve indicates that the solvent plant has a 70% probability of achieving US$35 million < net cumulative NPV < US$85 million

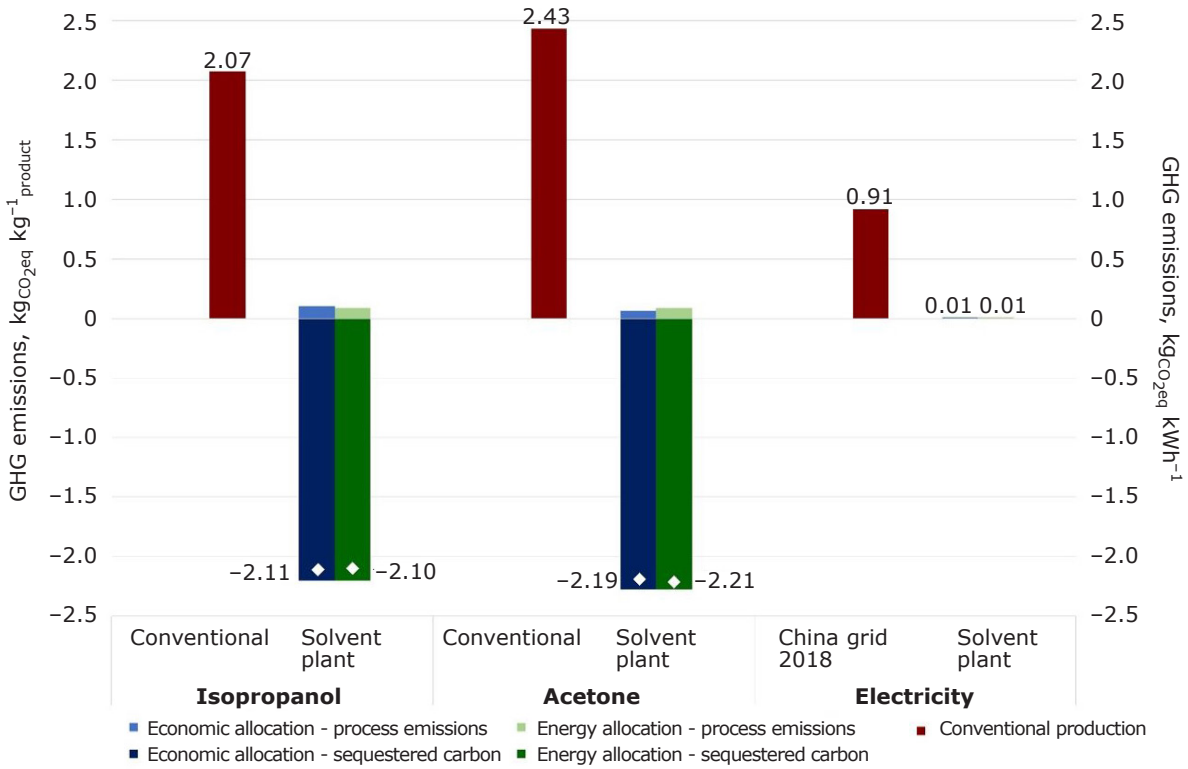

Fig. 11. GHG emissions for the solvent plant compared to the conventional fossil derived processes within a cradle-to-gate LCA framework. The GHG for the 2018 electricity mix in China is also shown, contrasting against near zero net GHG emissions for renewable electricity generation from black liquor

= gallon of gasoline equivalent) (66). Therefore, in this study, the price per GGE was calculated for the solvent products as a biofuel mix, with renewable electricity sold at the current market price. A value of US$2.87 GGE^{-1} (**Figure 12**) was obtained, below the US DOE's target, highlighting the competitiveness of the heat integrated aerobic solvent plant. Notably, neither isopropanol nor acetone are typically used for their fuel value, highlighted by their higher market prices. As such, the solvent plant is profitable as either a biofuel or commodity chemical facility.

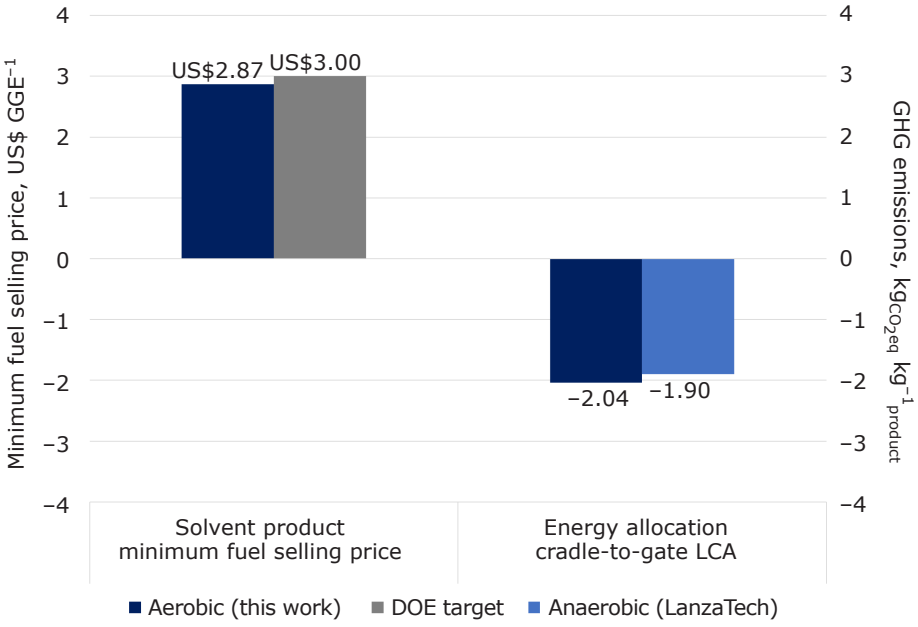

Fig. 12. Minimum selling price for the solvent product mix on a US$ GGE^{-1} basis and comparison between aerobic (this work) and anaerobic (LanzaTech) gas fermentation cradle-to-gate GHG emissions. The solvent product is below the US DOE's 2022 target of US$3 GGE^{-1} and the cradle-to-gate emissions are shown to be comparable to the anaerobic process

For LanzaTech's anaerobic process, the cradle-to-gate LCA using energy allocation produced a calculated GHG emission of −1.9 kg_{CO_2eq} $kg^{-1}_{acetone + ethanol}$ for a heat integrated scenario (see Table S13 for calculation). In **Figure 12**, the LCA for the solvent plant is presented, indicating a net GHG emission of −2.04 kg_{CO_2eq} $kg^{-1}_{isopropanol + acetone}$, which is in line with LanzaTech's study (**Figure 12**). Resultantly, from both the TEA and LCA results, the greater thermodynamic efficiency of the anaerobic Wood-Ljungdahl C1 fixation pathway over the aerobic Calvin-Benson-Bassham Cycle is not evident for the heat integrated solvent plant.

4. Conclusions

In exploiting the available excess black liquor, the solvent plant TEA presents a net cumulative NPV of US$42 million. The solvent plant demonstrates that the sustainable production of commodity chemicals priced near ~US$1000 per tonne is within reach of heat integrated aerobic gas fermentation, whilst achieving an appreciable reduction in GHG emissions compared to conventional production. Moreover, despite having a higher market value, a biofuel mix of the solvent product is able to meet the US DOE's 2022 target of US$3 GGE^{-1}. The heat integration between aerobic gas fermentation and SCWG produces an LCA comparable to a anaerobic gas fermentation technology. The TEA and LCA studies suggest that the intrinsic thermodynamic efficiency of anaerobic fermentation can be attained by aerobic fermentation through process engineering, albeit at a capital expense. Given aerobic cell factories can target a wider product spectrum, the heat integrated aerobic gas fermentation has promise as a best-in-class technology for renewable commodity chemical production.

Author Contributions

Conceptualisation: Alex Conradie and Rajesh Reddy Bommareddy; Methodology: Sarah Rodgers, Alex Conradie, Rebekah King, Fanran Meng, Jon McKechnie; Software: Sarah Rodgers, Alex Conradie, Rebekah King, Fanran Meng, Jon McKechnie; Formal Analysis: Sarah Rodgers, Alex Conradie, Rebekah King, Fanran Meng, Jon McKechnie; Investigation: Sarah Rodgers, Alex Conradie, Rebekah King, Fanran Meng, Jon McKechnie; Writing – Original Draft: Sarah Rodgers and Alex Conradie; Writing – Review & Editing: Sarah Rodgers, Alex Conradie, Rebekah King, Stephen Poulston, Martin Hayes, Rajesh Reddy Bommareddy, Fanran Meng, Jon McKechnie; Visualisation: Sarah Rodgers, Alex Conradie, Fanran Meng; Supervision: Alex Conradie and Jon McKechnie; Funding Acquisition: Alex Conradie and Jon McKechnie

Glossary

Abbreviation	Name
FCI	fixed capital investment
GGE	gallon of gasoline equivalent
GHG	greenhouse gas
GWP	global warming potential
ISBL	inside battery limit
LCA	life cycle assessment
NPV	net present value
NREL	National Renewable Energy Laboratory
OSBL	outside battery limit
RBFNN	radial basis function neural network
SCWG	supercritical water gasification
TCI	total capital investment
TEA	technoeconomic assessment
TS	Towler and Sinnott
US DOE	US Department of Energy

Acknowledgments

This work was supported by an Engineering and Physical Sciences Research Council (EPSRC) Doctoral Training Partnership (DTP) Cooperative Awards in Science and Technology (CASE) studentship with Johnson Matthey and by Industrial Biotechnology (IB) Catalyst project ConBioChem funded by Innovate UK, Biotechnology and Biological Sciences Research Council (BBSRC) and EPSRC (grant BB/N023773/1). Furthermore, this work was supported by the Future Biomanufacturing Research Hub (grant EP/S01778X/1), funded by the EPSRC and BBSRC as part of UK Research and Innovation. Finally, the authors gratefully acknowledge support received from the University of Nottingham Research Beacon of Excellence: Green Chemicals.

References

1. S. N. Naik, V. V. Goud, P. K. Rout and A. K. Dalai, *Renew. Sustain. Energy Rev*., 2010, **14**, (2), 578
2. R. Liguori and V. Faraco, *Bioresour. Technol*., 2016, **215**, 13
3. Y. Sun and J. Cheng, *Bioresour. Technol*., 2002, **83**, (1), 1
4. M. Naqvi, J. Yan and E. Dahlquist, *Bioresour. Technol*., 2010, **101**, (21), 8001
5. M. Suhr, G. Klein, I. Kourti, M. R. Gonzalo, G. G. Santonja, S. Roudier and L. D. Sancho, "Best Available Techniques (BAT) Reference Document for the Production of Pulp, Paper and Board", JRC Science and Policy Reports, European Union, Luxembourg, 2015, 906 pp
6. M. Keshtkar, R. Ammara, M. Perrier and J. Paris, *J. Sci. Technol. Forest Prod. Proc*., 2015, **5**, (1), 24
7. E. Ahmetović, Z. Kravanja, N. Ibrić and I. E. Grossmann, 'A Review of Recent Developments of Water and Energy Optimisation Methods Applied to Kraft Pulp and Paper Mills', 4th South East European Conference on Sustainable Development of Energy, Water and Environment Systems, 28th June–2nd July, 2020, Sarajevo, Bosnia and Herzegovina, Sustainable Development of Energy, Water and Environment Systems (SDEWES), Zagreb, Croatia, 2020
8. T. Berntsson, P. Axegård, B. Backlund, Å. Samuelsson, N. Berglin and K. Lindgren, "Swedish Pulp Mill Biorefineries: A Vision of Future Possibilities", The Swedish Energy Agency, Stockholm, Sweden, 2008, 84 pp
9. Y. Yoshida, K. Dowaki, Y. Matsumura, R. Matsuhashi, D. Li, H. Ishitani and H. Komiyama, *Biomass Bioenergy*, 2003, **25**, (3), 257
10. M. Kumar, A. O. Oyedun and A. Kumar, *Renew. Sustain. Energy Rev*., 2018, **81**, (2), 1742
11. A. Kruse, *J. Supercrit. Fluids*, 2009, **47**, (3), 391
12. 'BP and Johnson Matthey License Innovative Waste-to-Fuels Technology to Biofuels Producer Fulcrum BioEnergy', bp Plc, London, UK, 25th September, 2018, 4 pp
13. M. Mohammadi, G. D. Najafpour, H. Younesi, P. Lahijani, M. H. Uzir and A. R. Mohamed, *Renew. Sustain. Energy Rev*., 2011, **15**, (9), 4255
14. J. Daniell, M. Köpke and S. D. Simpson, *Energies*, 2012, **5**, (12), 5372
15. 'World's First Commercial Waste Gas to Ethanol Plant Starts Up', LanzaTech Inc, Skokie, USA, 8th June, 2018
16. A. G. Fast and E. T. Papoutsakis, *Curr. Opin. Chem. Eng*., 2012, **1**, (4), 380
17. B. Molitor, E. Marcellin and L. T. Angenent, *Curr. Opin. Chem. Biol*., 2017, **41**, 84
18. C. M. Humphreys and N. P. Minton, *Curr. Opin. Biotechnol*., 2018, **50**, 174
19. R. Takors, M. Kopf, J. Mampel, W. Bluemke, B. Blombach, B. Eikmanns, F. R. Bengelsdorf, D. Weuster-Botz and P. Dürre, *Microb. Biotechnol*., 2018, **11**, (4), 606
20. A. Bar-Even, A. Flamholz, E. Noor and R. Milo, *Biochim. Biophys. Acta – Bioenerg*., 2012, **1817**, (9), 1646
21. D. Humbird, R. Davis and J. D. McMillan, *Biochem. Eng. J*., 2017, **127**, 161
22. J. Van Brunt, *Nat. Biotechnol.*, 1986, **4**, 395

23. J. D. McMillan and G. T. Beckham, *Microb. Biotechnol.*, 2017, **10**, (1), 40
24. E. Dheskali, A. A. Koutinas and I. K. Kookos, *Biochem. Eng. J.*, 2020, **154**, 107462
25. S. Gunukula, T. Runge and R. Anex, *ACS Sustain. Chem. Eng.*, 2017, **5**, (9), 8119
26. R. Davis, L. Tao, E. C. D. Tan, M. J. Biddy, G. T. Beckham, C. Scarlata, J. Jacobson, K. Cafferty, J. Ross, J. Lukas, D. Knorr and P. Schoen, "Process Design and Economics for the Conversion of Lignocellulosic Biomass to Hydrocarbons: Dilute-Acid and Enzymatic Deconstruction of Biomass to Sugars and Biological Conversion of Sugars to Hydrocarbons", Technical Report NREL/TP-5100-60223, National Renewable Energy Laboratory, Golden, USA, October, 2013, 147 pp
27. D. Humbird, R. Davis, L. Tao, C. Kinchin, D. Hsu, A. Aden, P. Schoen, J. Lukas, B. Olthof, M. Worley, D. Sexton and D. Dudgeon, "Process Design and Economics for Biochemical Conversion of Lignocellulosic Biomass to Ethanol: Dilute-Acid Pretreatment and Enzymatic Hydrolysis of Corn Stover", Technical Report, NREL/TP-5100-47764, National Renewable Energy Laboratory, Golden, USA, May, 2011, 147 pp
28. R. R. Bommareddy, Y. Wang, N. Pearcy, M. Hayes, E. Lester, N. P. Minton and A. V. Conradie, *iScience*, 2020, **23**, (6), 101218
29. P. Dürre and B. J. Eikmanns, *Curr. Opin. Biotechnol.*, 2015, **35**, 63
30. M. Cardoso, É. Domingos de Oliveira and M. L. Passos, *Fuel*, 2009, **88**, (4), 756
31. M. Schubert, J. W. Regler and F. Vogel, *J. Supercrit. Fluids*, 2010, **52**, (1), 99
32. C. Cao, L. Guo, H. Jin, S. Guo, Y. Lu and X. Zhang, *Int. J. Hydrogen Energy*, 2013, **38**, (30), 13293
33. M. Magdeldin and M. Järvinen, *Appl. Energy*, 2020, **262**, 114558
34. S. O. Odu, A. G. J. van der Ham, S. Metz and S. R. A. Kersten, *Ind. Eng. Chem. Res.,* 2015, **54**, (20), 5527
35. S. van Wyk, A. G. J. van der Ham and S. R. A. Kersten, *Desalination*, 2020, **474**, 114189
36. Y. Hu, M. Gong, X. Xing, H. Wang, Y. Zeng and C. C. Xu, *Renew. Sustain. Energy Rev.*, 2020, **118**, 109529
37. J. A. Okolie, R. Rana, S. Nanda, A. K. Dalai and J. A. Kozinski, *Sustain. Energy Fuels*, 2019, **3**, (3), 578
38. J. Gmehling, J. Menke, J. Krafczyk, K. Fischer, J.-C. Fontaine and H. V. Kehiaian, 'Azeotropic Data For Binary Mixtures', in "CRC Handbook of Chemistry and Physics", ed. J. R. Rumble, 101st Edn., CRC Press, Boca Raton, USA, 2020, 1572 pp.
39. C. Pienaar, C. E. Schwarz, J. H. Knoetze and A. J. Burger, *J. Chem. Eng. Data*, 2013, **58,** (3), 537
40. W. L. Luyben and I.-L. Chien, 'Isopropanol–Water (Cyclohexane as the Entrainer)', in "Design and Control of Distillation Systems for Separating Azeotropes", Part 3, Ch. 8, John Wiley & Sons Inc, Hoboken, USA, 2010, pp. 219–244
41. Y. Cui, X. Shi, C. Guang, Z. Zhang, C. Wang and C. Wang, *Process Saf. Environ. Prot.*, 2019, **122**, 1
42. L. A. H. Petersen, J. Villadsen, S. B. Jørgensen and K. V. Gernaey, *Biotechnol. Bioeng.*, 2017, **114**, (2), 344
43. E. D. Larson, S. Consonni, R. E. Katofsky, K. Iisa and W. J. Frederick, "A Cost-Benefit Assessment of Gasification-Based Biorefining in the Kraft Pulp and Paper Industry", Vol. 1, US Department of Energy, Washington, DC, USA, American Forest and Paper Association, Washington, DC, USA, 21st December, 2006, 164 pp
44. I. A. Zlochower and G. M. Green, *J. Loss Prev. Process Ind.*, 2009, **22**, (4), 499
45. W. D. Seider, D. R. Lewin, J. D. Seader, S. Widago, R. Gani and K. M. Ng, 'Cost Accounting and Capital Cost Estimation', in "Product and Process Design Principles: Synthesis, Analysis and Evaluation", Ch. 16, 4th Edn., John Wiley & Sons Inc, Hoboken, USA, 2017, pp 426–497
46. G. P. Rangaiah, "Multi-Objective Optimization: Techniques and Applications in Chemical Engineering", Advances in Process Systems Engineering Series, Vol. 1, World Scientific Publishing Co Pte Ltd, Singapore, 2009, 376 pp
47. G. Towler and R. K. Sinnott, "Chemical Engineering Design: Principles, Practice and Economics of Plant and Process Design", 2nd Edn., Elsevier Ltd, Oxford, UK, 2013, 1303 pp
48. M. M. El-Halwagi, "Sustainable Design Through Process Integration: Fundamentals and Applications to Industrial Pollution Prevention, Resource Conservation, and Profitability Enhancement", 2nd Edn., Elsevier Inc, Amsterdam, The Netherlands, 2017, 604 pp
49. S. Jenkins, '2019 Chemical Engineering Plant Cost Index Annual Average', Chemical Engineering, New York, USA, 20th March, 2020
50. R. K. Sinnott, "Chemical Engineering Design", Coulson & Richardson's Chemical Engineering Series, 4th Edn., Vol. 6, Butterworth-Heinemann, Oxford, UK, 2005, 1056 pp
51. 'Ammonia Prices, Markets & Analysis', Independent Commodity Intelligence Services (ICIS), London, UK: https://www.icis.com/explore/commodities/chemicals/ammonia/ (Accessed on 1st June 2020)
52. D. C. Y. Foo, N. Chemmangattuvalappil, D. K. S. Ng, R. Elyas, C.-L. Chen, R. D. Elms, H.-Y. Lee, I.-L. Chien, S. Chong and C. H. Chong, "Chemical Engineering Process Simulation", Elsevier Inc, Amsterdam, The Netherlands, 2017, 444 pp

53. F. Takens, 'Detecting Strange Attractors in Turbulence', Dynamical Systems and Turbulence Symposium, University of Warwick, UK, 1980, Lecture Notes in Mathematics, eds. A Dold and B. Eckmann, Springer-Verlag, Berlin, Germany, 1981, pp. 366–381
54. 'Commodity Price Database', Intratec Solutions LLC, San Antonio, USA: https://www.intratec.us/products/commodities-prices/petrochemicals-prices (Accessed on 1st June 2020)
55. J. A. Leonard, M. A. Kramer and L. H. Ungar, *Comput. Chem. Eng.*, 1992, **16**, (9), 819
56. Z. Ming, L. Ximei, L. Na and X. Song, *Renew. Sustain. Energy Rev.*, 2013, **25**, 260
57. C. Kinchin, 'BETO Biofuels TEA Database', National Renewable Energy Laboratory, Washington, DC, USA, 2020
58. 'China to Cut Subsidies for Renewable Power by 30 per Cent to US$807 Million in 2020', South China Morning Post Ltd, Hong Kong, 20th November, 2019
59. 'Environmental Management – Life Cycle Assessment – Principles and Framework', ISO 14040:2006, International Organization for Standardization, Geneva, Switzerland, July, 2006, 20 pp
60. 'Environmental Management – Life Cycle Assessment – Requirements and Guidelines', ISO 14044:2006, International Organization for Standardization, Geneva, Switzerland, July, 2006, 46 pp
61. "IPCC, 2013: Climate Change 2013: The Physical Science Basis. Contribution of Working Group I to the Fifth Assessment Report of the Intergovernmental Panel on Climate Change", eds. T. F. Stocker, D. Qin, G.-K. Plattner, M. Tignor, S. K. Allen, J. Boschung, A. Nauels, Y. Xia, V. Bex and P. M. Midgley, Cambridge University Press, Cambridge, UK, New York, NY, USA, 1535 pp
62. G. Wernet, C. Bauer, B. Steubing, J. Reinhard, E. Moreno-Ruiz and B. Weidema, *Int. J. Life Cycle Assess.*, 2016, **21**, (9), 1218
63. X. Sun, F. Meng, J. Liu, J. McKechnie and J. Yang, *J. Clean. Prod.*, 2019, **220**, 1
64. 'Bioenergy Technologies Incubator 2: Development of a Sustainable Green Chemistry Platform for Production of Acetone and Downstream Drop-in Fuel and Commodity Products Directly from Biomass Syngas via a Novel Energy Conserving Route in Engineered Acetogenic Bacteria', LanzaTech Inc, Skokie, USA, 9th March, 2017
65. S. D. Simpson, T. Abdalla, S. D. Brown, C. Canter, R. Conrado, J. Daniell, A. Dassanayke, A. Gao, R. O. Jensen, M. Köpke, C. Leang, F. Liew, S. Nagaraju, R. Nogle, R. C. Tappel, L. Tran, P. Charania, N. Engle, R. Giannone, R. Hettich, D. Klingeman, S. Poudel, T. Tschaplinski and Z. Yang, "Development of a Sustainable Green Chemistry Platform for Production of Acetone and Downstream Drop-in Fuel and Commodity Products Directly from Biomass Syngas via a Novel Energy Conserving Route in Engineered Acetogenic Bacteria", Final Technical Report, Contract DE-EE0007566, Department of Energy, Washington, DC, USA, 2019, 31 pp
66. "Multi-Year Program Plan", Bioenergy Technologies Office, US Department of Energy, Washington, DC, USA, March, 2016, 258 pp

The Authors

Sarah Rodgers has an MEng in Chemical Engineering with Industrial Experience from the University of Nottingham, UK (2019). Her year in industry was spent in the Process Technology Team with AkzoNobel, Slough, UK (2017). She is currently undertaking an Industrial CASE funded PhD with Johnson Matthey, UK, and the University of Nottingham. Her project is investigating the technical and financial viability of using C1 gases for chemical production.

Alex Conradie was appointed as Chair of Sustainable Chemical Processing at the University of Nottingham in 2016, having worked in the biotechnology industry for two decades as a technology integrator between science and engineering encompassing metabolic engineering, fermentation and downstream processing. He has held engineering science leadership positions in both the industrial biotechnology and biopharmaceutical industries, leading multidisciplinary teams in process development, scale-up and technology transfer.

Rebekah King is studying her MEng in Chemical Engineering at the University of Nottingham. Her previous research experience includes investigating the feasibility of a sustainable microorganism feed for livestock and establishing the feasibility of a novel exoelectrogenic bioreactor design. As a placement student at Fujifilm Diosynth Biotechnologies, Billingham, UK, she led an investigation into the economic viability of transitioning to high throughput automated technologies.

Stephen Poulston is a research chemist at Johnson Matthey, Sonning Common, UK. He has experience of catalytic processes for a range of thermochemical conversions involving syngas to chemicals using both fossil fuel and bio feedstocks.

Martin Hayes is the Biotechnology Lead at Johnson Matthey. He has more than 20 years' experience in the development and operation of catalysts and catalytic technologies in the chemical industry. A chemist by training, he is now particularly interested in the role of biotechnology to enable the chemical industry to achieve its net zero ambitions. Biotechnology can support the transition from linear to circular processes so that waste is minimised or upgraded to valuable products.

Rajesh Reddy Bommareddy is a Vice Chancellor's Fellow at Northumbria University in Newcastle, UK. He is a part of the 'Building Metabolism' research theme within the Hub for Biotechnology in the Built Environment (HBBE) funded by Research England. His research focuses on industrial biotechnology with expertise in metabolic engineering and fermentation technology.

Fanran Meng is a Research Associate at the Department of Engineering at the University of Cambridge, UK. Previously, he was a research fellow in Sustainable Material and Technologies at the University of Nottingham. His research focuses on resource efficiency and life cycle sustainability which integrates engineering and science-based disciplines with insights from economic sciences to develop system optimisation and policy relevant strategies.

Jon McKechnie is Associate Professor in Mechanical Engineering at the University of Nottingham. His research focuses on the development and application of LCA and TEA methodologies. Application areas include industrial biotechnology, renewable and low carbon fuels, transportation systems and emerging materials.

5 Comparative techno-economic analysis of the integrated process for hybrid processing

5.1 Preface

This chapter contributes to the overall thesis aim of developing and applying Techno-Economic Analysis (TEA) methods to evaluate the proposed aerobic gas fermentation and Supercritical Water Gasification (SCWG) process by upgrading the heat integration in the platform's process simulation, undertaking an economic and environmental assessment for the production of 1,3-butadiene, and comparing the results to conventional 1,3-butadiene production and alternative renewable production routes. It therefore contributes to the following thesis objectives:

1. Develop process simulations for the aerobic gas fermentation and supercritical water gasification process, incorporating heat integration and downstream processing.
2. Determine an appropriate techno-economic framework and perform a comprehensive techno-economic analysis of the simulated process.
3. Quantify the greenhouse gas emissions associated with chemical and fuel production from the process and compare them with conventional production methods.
4. Compare the economic and environmental competitiveness of the process with alternative renewable production methods.

Chapter 4 concluded that the proposed heat integrated platform was economically feasible for commodity chemical production under the considered scenario. However, the chemicals produced were direct products from fermentation (isopropanol and acetone). Fermentation products are typically more oxygenated than fossil-based commodity chemicals. The reduction of these chemicals into fossil-based commodity chemicals leads to an intrinsic mass loss, reducing the product yield and negatively impacting the process economics. To assess the platforms capability beyond the niche range of fermentation products, a TEA for the production of an opportunistic platform chemical, 1,3-butadiene, was undertaken. 1,3-Butadiene is seen as an opportunistic platform chemical as there is a projected shortfall in conventional production owing to both the shift to lighter feedstocks in steam crackers and the commercialisation of Methanol-to-Olefin technology in China (Pomalaza et al., 2020).

This work uses the capital and operating expenditure, and price projection methodologies determined during Chapter 4. Similarly, to produce a thorough technology evaluation both an uncertainty analysis and Life Cycle Assessment (LCA) were undertaken.

As suggested in Chapter 4, the rigorous evaluation of technologies necessitates comparison to alternative technologies. As such, in this work the platform was compared against two alternative purely chemo-catalytic renewable production methods. Process models of all three routes were produced using Aspen HYSYS and evaluated using the same techno-economic assumptions. The same biorefinery scenario, a China located paper and pulp mill, was considered as in Chapter 4. All three routes originate from gasification, producing renewable syngas. The benefit of starting from biomass gasification is maximising the recovery of biomass' entire reducing power as syngas for chemical synthesis.

The three comparative routes principally exploit aerobic gas fermentation, mixed alcohol synthesis to ethanol, and the Methanol-to-Propene technology. The mixed alcohol synthesis to ethanol route was conducted as a viable alternative to the bio-derived intermediate from aerobic gas fermentation. The route exploiting the Methanol-to-Propene technology was included as olefin based technologies have been previously investigated for the production of

renewable 1,3-butadiene. So as not to disadvantage any of the technologies each processing route was matched to the most suitable feedstocks within the context of a paper and pulp mill. As SCWG is suited to the use of wet feedstocks, black liquor was used for the gas fermentation route (as in Chapter 4). However, the two chemo-catalytic routes exploit conventional gasification and are therefore suited to dry feedstocks. These two routes therefore utilise woody biomass residues available within the pulp mills collection area as a feedstock. Whilst the feedstocks between these routes differ, they both represent waste streams from a pulp mill that could be valorised for chemical production and are scaled based on resource availability within the reference pulp mills supply chain.

For the gas fermentation platform in Chapter 4, 32% of the gasifier effluent was diverted towards combustion to support platforms energy self-sufficiency. Between Chapter 4 and 5 the platform's heat integration was manually optimised. This improved heat integration enabled 100% of the gasification product to be diverted to the fermenter, whilst still maintaining the platform's energy self-sufficiency. This process improvement increased the chemical production and enabled the export of a greater portion of renewable electricity for sale to the grid.

As an advancement to the techno-economic methodology used in Chapter 4 the evaluated process' Minimum Selling Price (MSP) was also computed alongside the Net Present Value (NPV). This facilitated the comparison of the three routes. In addition, as well as a global uncertainty analysis (Monte Carlo simulation) a single point sensitivity analysis on each process's MSP was undertaken. This demonstrated the individual impact of the variables on the final economic outcome.

The novelty of this work is the rigorous assessment of combining gas fermentation with catalytic upgrading (hybrid processing) for chemical production. Previous hybrid processing using gas fermentation has been undertaken by Haro et al. (2013) for ethylene production and Tan et al. (2016) for distillate range fuels. In the study by Haro et al. (2013), only the catalytic upgrading was modelled, and cost estimates for different ethanol sources were taken from literature. This meant results were reliant on the quality of ethanol price estimates which were taken from various sources. In the study by Tan et al. (2016), four different routes were modelled, two routes were via syngas fermentation and catalytic upgrading, and the other two were purely catalytic technologies. Their study employed anaerobic gas fermentation and targeted distillate range fuels. This is in contrast to the aerobic gas fermentation and opportunistic chemical targeted in this work. Additional novelty exists in the comparison of different routes to 1,3-butadiene. Existing TEA studies for renewable 1,3-butadiene production have investigated either bio-catalytic routes, upgrading fermentation derived ethanol (e.g. Moncada et al, 2018) or purely catalytic production via a renewable olefin intermediate (e.g. Hanaoka et al., 2021). Whereas in this work, a hybrid bio- and chemo-catalytic process is compared with two purely catalytic routes.

This study concluded that the hybrid bio/chemo-catalytic route was the only route profitable using the nominal techno-economic inputs, producing an NPV of $2.8 million and MSP of $1,367 tn^{-1}. In contrast, the two chemo-catalytic routes produced MSPs of $1,954 tn^{-1} (via catalytic ethanol) and $2,196 tn^{-1} (via a propene intermediate). The co-generation and sale of renewable electricity contributed to the aerobic gas fermentation's success. However, using the new heat integration configuration which diverts all the syngas to the fermenter, the electricity generation does not come at the detriment of chemical production. Furthermore, the aerobic gas fermentation and SCWG platform still outperformed the alternative routes when using grid parity prices electricity (MSP using electricity grid parity: $1695/tn) instead of subsidised renewable electricity prices. Sensitivity analyses highlighted the equipment capital

as the main contributor to the MSP for all three processing routes. The aerobic gas fermentation route presented a 19% probability of achieving a positive NPV. Owed to the low process emissions and sequestration of biogenic carbon, all routes produced net negative emissions within a cradle-to-gate framework. The aerobic gas fermentation platform achieved -3.23 $kgCO_{2eq}/kg$, compared to -2.90 $kgCO_{2eq}/kg$, and -2.80 $kgCO_{2eq}/kg$ for the alternative routes, and 1.2 $kgCO_{2eq}/kg$ for conventional production. This demonstrates that renewable 1,3-butadiene production has potential as a net carbon sink for pulp mill residues conventionally destined for energy recovery.

Similarly to Chapter 4, the limitations of this study are the use of guiacol to represent the lignin content of the black liquor in the SCWG (updated in Chapter 7), and the arbitrary percentage used to incorporate future commodity price variability in the sensitivity and uncertainty analysis (upgraded in Chapter 6). In addition, the inclusion of policy implications such as carbon prices was not addressed. This has been addressed in other TEA studies i.e., Michailos et al. (2019) demonstrated that a carbon price of £98-142/tCO_2 was required for their methane production process to break even (Michailos et al., 2019). Klein et al. (2019) illustrated that at a price of \$142/tCO_2 their integrated sugarcane microalgae biorefinery was economically feasible (Klein et al., 2019). Huang et al. (2021) demonstrated credits of \$735/tCO_2, \$470/tCO_2, and \$190/tCO_2 were required for methane, ethanol, and acetic acid production to meet market parity, with no credits required for polyhydroxybutyrate (Huang et al., 2021). Whilst these prices don't represent future carbon pricing initiatives, their inclusion provides further context to both the TEA and LCA results and could have been included to demonstrate the incentives required to achieve a more promising economic outcome.

This work was published in the *Journal of Cleaner Production* on 7th June 2022. The published paper is titled "Renewable butadiene: A case for hybrid processing via bio- and chemo-catalysis" and is presented as Chapter 5. The corresponding supplementary information as published alongside the manuscript is reprinted in Appendix A.2.

Article Title: Renewable butadiene: A case for hybrid processing via bio- and chemo-catalysis

Journal: Journal of Cleaner Production

Date: September 2022

DOI: 10.1016/j.jclepro.2022.132614

Authors: Sarah Rodgers, Fanran Meng, Stephen Poulston, Alex Conradie, Jon McKechnie

Author Contributions: Sarah Rodgers: Conceptualization, Data curation, Formal analysis, Investigation, Software, Visualization, Writing – original draft, Writing – review & editing. Fanran Meng: Conceptualization, Methodology, Writing – review & editing. Alex Conradie: Conceptualization, Formal analysis, Funding acquisition, Resources, Project administration, Software, Supervision, Writing – review & editing. Jon McKechnie: Conceptualization, Funding acquisition, Project administration, Resources, Supervision, Writing – review & editing.

5.2 References

Hanaoka, T., Fujimoto, S., Kihara, H., 2021. Evaluation of n-butene synthesis from dimethyl ether in the production of 1,3-butadiene from lignin: a techno-economic analysis Renew. Energy, 163, pp. 964-973

Haro, P., Ollero, P. & Trippe, F., 2013. Technoeconomic assessment of potential processes for bio-ethylene production. Fuel Processing Technology, Volume 114, pp. 35-48.

Huang, Z., Grim, R. G., Schaidle, J. A. & Tao, L., 2021. The economic outlook for converting CO2 and electrons to molecules. Energy & Environmental Science, Issue 7.

Klein, B.c., Chagas, M.F., Wantabe, M.D.B., Bonomi, A., Filho, R.M., 2019. Low carbon biofuels and the New Brazilian National Biofuel Policy (RenovaBio): A case study for sugarcane mills and integrated sugarcane-microalgae biorefineries. Renewable and Sustainable Energy Reviews, Volume 115.

Michailos, S., Emeike, O., Ingham., D Hughes, K.J., Pourkashanian, M., 2019. Methane production via syngas fermentation within the bio-CCS concept: A techno-economic assessment. Biochemical Engineering Journal, 150(15), pp. 107-290.

Moncada, J., Gursel, I.V., Worrell, E., Ramírez A., 2018. Production of 1,3-butadiene and ε-caprolactam from C6 sugars: Techno-economic analysis. Biofuels Bioprod. Biorefining, 12 (4)

Pomalaza, G., Capron, M., Ordomsky, V., Dumeignil, F., 2016. Recent breakthroughs in the conversion of ethanol to butadiene. Catalysts 6. https://doi.org/10.3390/catal6120203

Tan, E.C.D, Snowden-Swan, L.J., Talmadge, M., Dutta, A., Jones, S., Ramasamy, K.K., Gray, M., Dagle, R., Padmaperuma, A., Gerber, M., Sahir, A.H., Tao, L., Zhang, Y., 2016. Comparative techno-economic analysis and process design for indirect liquefaction pathways to distillate-range fuels via biomass-derived oxygenated intermediates upgrading. Biofuels, Bioproducts & Biorefining.

This page has been left intentionally blank

Journal of Cleaner Production 364 (2022) 132614

Contents lists available at ScienceDirect

Journal of Cleaner Production

journal homepage: www.elsevier.com/locate/jclepro

Renewable butadiene: A case for hybrid processing via bio- and chemo-catalysis

Sarah Rodgers [a], Fanran Meng [b], Stephen Poulston [c], Alex Conradie [a], Jon McKechnie [a,*]

[a] Faculty of Engineering, University Park, University of Nottingham, Nottingham, NG7 2RD, UK
[b] Department of Engineering, University of Cambridge, Trumpington Street, Cambridge, CB2 1PZ, UK
[c] Johnson Matthey Technology Centre, Blounts Ct Rd, Sonning Common, Reading, RG4 9NH, UK

ARTICLE INFO

Handling Editor: Kathleen Aviso

Keywords:
1,3-Butadiene
Techno-economic analysis
Life cycle assessment
Renewable chemicals
Biorefinery

ABSTRACT

1,3-butadiene (butadiene) is a by-product produced during naphtha steam cracking, predominantly used in tyre manufacturing. Recently, steam crackers have converted to using more cost effective, lighter feedstocks such as shale gas, yielding less butadiene. The potential shortfall, coupled with concerns around increasing greenhouse gas emissions, provides a unique opportunity for renewable production. This study investigated the techno-economics and greenhouse gas emissions associated with renewable butadiene production routes within the context of a China located pulp mill. A hybrid bio-catalytic route, utilising black liquor, was compared against two chemo-catalytic routes using forestry residues and pulpwood. The hybrid bio-catalytic route uses a novel aerobic gas fermentation platform, employing heat integrated supercritical water gasification and aerobic gas fermentation to produce acetaldehyde, followed by chemo-catalytic upgrading (Acet-BD). The two chemo-catalytic routes catalytically upgrade biomass derived syngas; where one route (Eth-BD) passes through an ethanol intermediate, and the other (Syn-BD) utilises a series of commercialised catalytic technologies with propene as an intermediate. The hybrid bio/chemo-catalytic route, Acet-BD, was the only route profitable using the nominal techno-economic inputs, producing a Net Present Value of $2.8 million and Minimum Selling Price of $1367 tn^{-1}. In contrast, the two chemo-catalytic routes produced Minimum Selling Prices of $1954 tn^{-1} (Eth-BD) and $2196 tn^{-1} (Syn-BD), demonstrating the competitiveness of this novel platform. Sensitivity analyses highlighted the equipment capital as the main contributor to increased Minimum Selling Price for all cases, and the Acet-BD route presented a 19% probability of achieving a positive net present value. Moreover, owed to the low process emissions and sequestration of biogenic carbon, all routes produced net negative emissions within a cradle-to-gate framework. As such, renewable butadiene production has potential as a net carbon sink for pulp mill residues conventionally destined for energy recovery.

1. Introduction

Currently, the chemical industry is responsible for 7% of anthropogenic greenhouse gas (GHG) emissions and 30% of final industrial energy use (IEA, 2018). However, the carbon content of most chemicals inherently ties the industry to the use of carbon-based feedstocks, making decarbonisation challenging. One approach to reduce emissions is through the replacement of conventional fossil fuel feedstocks with renewable carbon sources. Such resources enable biogenic carbon to be utilised for chemical synthesis, with the potential of achieving negative GHG emissions. Despite the environmental benefit, these sustainable technologies need to be cost competitive with conventional fossil fuel-based processes. Successful implementation of sustainable technologies depends on the identification of opportunistic chemicals based on market trends and technological developments.

Butadiene is an important platform chemical used in synthetic rubber manufacturing, with a global production of 1.5 million tonnes in 2013 (Levi and Cullen, 2018). Currently, 95% of butadiene is produced as a by-product from steam cracking of naphtha to produce ethene (Ren et al., 2006). However, in North America recent technological advances have made shale gas an economically favourable feedstock (Angelici et al., 2013). Consequently, steam crackers have converted operations to cracking this lighter feedstock, yielding less butadiene. Simultaneously, the Methanol To Olefin (MTO) technology is being commercialised in China, which synthesises ethene and propene from coal derived

* Corresponding author.
E-mail address: jon.mckechnie@nottingham.ac.uk (J. McKechnie).

https://doi.org/10.1016/j.jclepro.2022.132614
Received 27 January 2022; Received in revised form 23 May 2022; Accepted 4 June 2022
Available online 7 June 2022

Abbreviations

FCI	Fixed Capital Investment
GHG	Greenhouse Gas
ISBL	Inside Battery Limits
LCA	Life Cycle Assessment
MSP	Minimum Selling Price
MTO	Methanol to Olefins
MTP	Methanol to Propene
NPV	Net Present Value
OSBL	Outside Battery Limits
RBFNN	Radial Basis Function Neural Network
SCWG	Supercritical Water Gasification
TCI	Total Capital Investment
TEA	Techno-economic Analysis

methanol, yielding no butadiene (Tian et al., 2015). These synchronous transitions are projected to reduce global butadiene production (Pomalaza et al., 2020). As such, an on-purpose, selective production method would allow for stable market supply and demand.

In addition to chemical selection, the development of a renewable chemical industry requires renewable resources to be readily available in large quantities. Paper and pulp mills represent an established biomass supply chain. In recent years, interest has grown in developing these facilities into bio-refineries. This increased interest is attributed to decreasing trends in pulp and paper prices and increased competition from low cost paper and pulp suppliers, coupled to the incentives surrounding renewable energy prices and renewable chemical production (Berntsson et al., 2008). Development of existing mills expands the product range of a pulp mill and promotes the full utilisation of woody biomass, making use of residues that are unsuitable for pulp production (Huang et al., 2010). With the existing supply chain infrastructure for biomass delivery, the development of pulp mill bio-refineries can occur using either internal or external (imported) biomass. China is the world's second largest virgin pulp manufacturer (Food and Agricultural Organization of the United Nations (FAO), 2021; Kong et al., 2013), as well as holding the greatest share of the butadiene market (Mordor Intelligence, 2020). Therefore, China's pulp mills hold a distinct market opportunity for renewable, on-purpose butadiene production.

There has been increased global interest in renewable butadiene production in recent years. The most notable being production from ethanol. A recent, in depth, review of insights into the reaction pathway and the varying catalysts that have been considered for the reaction can be found in (Pomalaza et al., 2020). There are two different routes from ethanol, the one-step (Lebedev (1933) or two-step (Ostromisslensky) process (Toussaint et al., 1947). Both routes were used during WWII until the 1960s when the processes became economically uncompetitive with naphtha steam cracking (Shylesh et al., 2016). It is important to highlight a major challenge in producing butadiene from ethanol is the intrinsic mass loss owed to the removal of water and hydrogen molecules. This was emphasised in a recent review by Grim et al. (2019) where they demonstrate the theoretical mass yield of butadiene from ethanol is only 60% in comparison to 80% when producing butanol. This unavoidable mass loss significantly reduces the profit margin between ethanol and butadiene.

The primary focus of recent research into this route has been in catalyst development, but more recently, there have been several Techno-economic Analysis (TEA) and Life Cycle Assessment (LCA) studies. Despite this, no existing TEAs have investigated China as a potential location. Notably, in the first LCA of an ethanol route, undertaken by Cespi et al. (2016), the location was dismissed owed to the high ethanol prices. The first LCA was undertaken by Cespi et al. (2016), comparing results of the two production methods for three different locations, the US, Brazil and Europe. Shylesh et al. (2016) later conducted a cradle-to-grave LCA on the one step method using USA Midwest-grown corn grain, USA Midwest-grown corn stover, and Brazilian sugarcane. Farzad et al. (2017) undertook the first TEA, they performed an integrated TEA and LCA on the Two Step process using bagasse derived ethanol. IEA, 2018, the first TEA to evaluate the One Step production method was undertaken by Moncada et al. (2018), who looked at the production of butadiene and ε-caprolactam from C6 sugars. Very recently, the techno economics of the One Step production of butadiene using experimental data under industrial conditions was undertaken (Cabrera Cabrera Camacho et al., 2020). Finally, the most recent integrated TEA and LCA was undertaken by Dimian et al. (2021). The study evaluated the Two Step process using market ethanol as the feedstock for an undisclosed plant location. Notably, the LCA outcomes have proven to be highly dependent on the feedstock, with some first generation crops yielding poorer outcomes than conventional naphtha cracking (Cespi et al., 2016), highlighting the benefit of integrated studies. Despite the potential of on-purpose routes, and level of interest, no existing studies have demonstrated butadiene's cost-effective production at current market prices. It is thought that the exploitation of China's large pulp industry, substantial share in butadiene market, and lower capital and operating costs may provide a lucrative opportunity to renewable butadiene production.

Butadiene can also be produced through the catalytic dehydrogenation of butane or the oxidative dehydrogenation of butene, both of which are mature industrial technologies (Grub and Löser, 2011). However, these technologies rely on a petroleum derived C4 feedstock. Resultantly, some authors have looked at the renewable production of butene for butadiene production. Hanaoka et al. (2017, 2019, 2021) and Tripathi et al. (2019) evaluated the production of butadiene from lignin via an olefin intermediate. They evaluated three different olefin technologies; the direct production of light olefins, dimethyl ether to light olefins, and methanol to light olefins, all originating from gasification (Hanaoka et al., 2017, 2019, 2021; Tripathi et al., 2019). At present, these olefin technologies are optimised for the production of ethene and propene, meaning butene yields are typically low (Bender, 2014). As a result, these studies have all demonstrated comparatively low butadiene yields.

In this study, three renewable butadiene production routes are compared using renewable resources available within the context of a Kraft paper and pulp mill located in China. The aim of this study is to determine the most promising process through matching an opportune renewable feedstock within the mill's supply chain to a synergetic technology. The study innovatively integrates methods of rigorous process simulation, techno-economic analysis, life cycle assessment, sensitivity, and uncertainty analysis to comprehensively compare impacts of three alternative routes on resources, society and the environment, each exploiting renewable syngas produced via gasification. The principal benefit of gasification is the ability to maximise the recovery of reducing power from the biogenic biomass as syngas for chemical synthesis (Griffin and Schultz, 2012). Furthermore, gasification enables the valorisation of recalcitrant, low value carbon sources. However, to date, the only studies to consider syngas as a feedstock employed chemo-catalytic olefin-based technologies for butadiene production. A hybrid bio/chemo-catalysis route; Acetaldehyde to Butadiene (Acet-BD), is compared against two alternative chemo-catalytic technologies Ethanol to Butadiene (Eth-BD) and Syngas to Butadiene (Syn-BD). The Acet-BD and Eth-BD routes both explore ethanol production methods hitherto investigated for butadiene production, namely heat integrated aerobic gas fermentation (Rodgers et al., 2021), and mixed alcohol synthesis (Dutta et al., 2011). Similarly, the Syn-BD route employs an alternative olefin technology, exploiting the high yield propene fraction obtained from the established Methanol-to-Propene (MTP) technology, as opposed to the low yield butene obtained from the Methanol-to-Olefins (MTO) process. The Syn-BD route therefore represents commercialised technologies that could be integrated to

produce renewable butadiene. Overall, our study considers new processing routes with the feedstocks, technologies, and bio-refinery scenario differing from previous studies.

2. Materials and methods

This study explores three processing routes to butadiene from the renewable resources available within a Kraft paper and pulp mill. The three routes principally exploit aerobic gas fermentation (Acet-BD), mixed alcohol synthesis (Eth-BD) and the Methanol-to-Propene technology (Syn-BD). The hybrid bio-/chemo-catalytic route, Acet-BD, investigates the exploitation of a portion of the pulp mill's black liquor co-product; whilst the two chemo-catalytic routes, Eth-BD and Syn-BD, utilise imported biomass consisting of 80% forestry residues and 20% pulpwood, to limit ash content (Hartley et al., 2020). A block flow diagram of the three conceptual processes is presented in Fig. 1. These three routes are rigorously modelled in Aspen HYSYS V11 using the best publicly available data and industrial insights. The conceptual processes are described in detail in the Supplementary Information: Section S1, Detailed Conceptual Process Design. The process models inform the TEA and LCA used to evaluate the economic performance and environmental impact of each route. Single point sensitivity analyses and a Monte Carlo simulation are also undertaken.

The Acet-BD process utilises gasified black liquor as feedstock, followed by gas fermentation to the 2-oxoacid pyruvate, which is decarboxylated to acetaldehyde in a subsequent enzyme plug flow reactor. Acetaldehyde was chosen as the platform intermediate given its high volatility (Eckert et al., 2006), allowing for its low energy intensity recovery from the aqueous media compared to ethanol. The black liquor feedstock is gasified using supercritical water gasification (SCWG), which is heat integrated with the aerobic gas fermentation process using a heat pump, as described by Bommareddy et al. (2020). The novel coupling of technologies provides a synergistic solution which benefits both the endothermic SCWG and exothermic aerobic gas fermentation process, further detail on this technology pairing can be found in Section S1.1, Acet-BD Process Description. This unique pairing also produces renewable electricity for sale to the grid, supplementing the routes income. The acetaldehyde intermediate is hydrogenated to ethanol prior to catalytic upgrading to butadiene. As previously mentioned, two processes exist for butadiene production from ethanol, the one-step Lebedev and the two-step Ostromisslensky process. Currently, there is no consensus which process holds sway. However, it has been previously reported that the Ostromisslensky process has a higher conversion and yield (Corson et al., 1950), where the Lebedev process has been shown to outperform the Ostromisslensky process from an economic and environmental perspective, as only one reactor and catalyst is required (Cespi et al., 2016). In this study, the Lebedev process was investigated due to the presumed economic benefit and the high productivity reported in an experimental study by Dai et al. (2017) using a zeolite-confined bimetallic catalyst.

In the Eth-BD route ethanol is produced via mixed alcohol synthesis of biomass derived syngas, as per the 2011 NREL report (Dutta et al., 2011). The ethanol product is catalytically upgraded to butadiene using the same catalyst as detailed for the Acet-BD route. A detailed description of the process and data used to model the route is outlined in Section S1.2, Eth-BD Process Description.

The Syn-BD route exploits the Methanol-to-Propene process and uses the commercial oxidative dehydrogenation of n-butene to produce

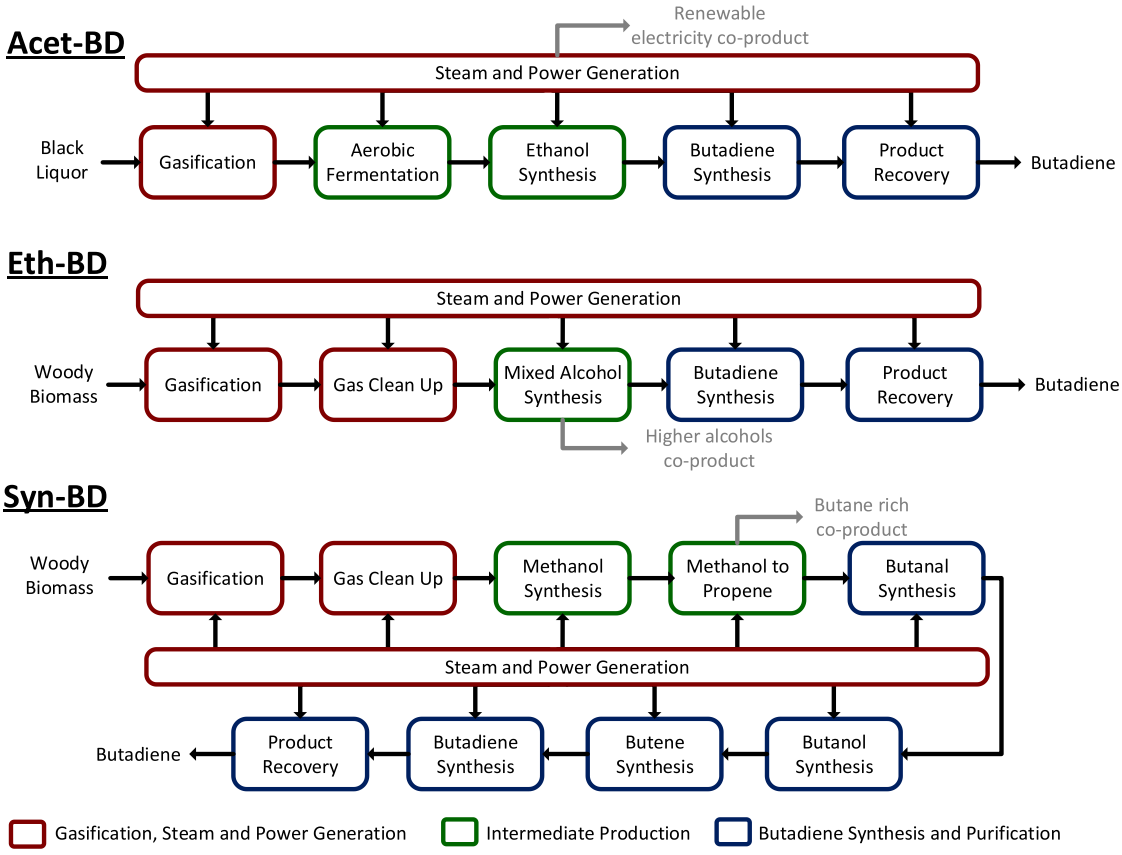

Fig. 1. Conceptual Block Flow Diagram of the three green butadiene production routes using renewable resources from a paper and pulp mill as feedstock. The hybrid gas fermentation route through an Acetaldehyde intermediate (Acet-BD) is compared against two chemo-catalysis technologies, Ethanol to Butadiene (Eth-BD) and Syngas to Butadiene (Syn-BD).

butadiene (White, 2007). Though, rather than using a fossil-derived C4 feedstock, this is synthesised from indirect gasification of woody biomass. The produced syngas is upgraded using various industrialised catalytic steps, i.e. (1) syngas to methanol, (2) methanol to propene, (3) propene to butanol via the oxo-alcohols process, (4) dehydration of butanol to butene and (5) oxidative dehydrogenation to butadiene. The MTP process was selected over the MTO process given its enhanced propene selectivity, >70% (Rothaemel and Holtmann, 2002). A detailed description of the process and data used to model the route is outlined in Section S1.3, Syn-BD Process Description.

2.1. Plant Capacity

The reference pulp mill's capacity, used as the basis for this study, is detailed in Table 1. The Acet-BD route exploits the use of 25% of the mill's black liquor for chemical production (Rodgers et al., 2021). In contrast, the Eth-BD and Syn-BD routes utilise the forestry residues available within the pulp mills collection area, along with a modest collection increase required for the pulpwood fraction. The exploitation of the mill's black liquor co-product or forestry residues within the mills collection area allows mills to generate additional revenue from biochemical production without expanding collection capacity. The capacity of the routes is outlined in Table 1.

2.2. Feedstock costs

Black liquor is a by-product from pulp production, conventionally exploited for its energy value (Naqvi et al., 2010; Suhr et al., 2015). New heat integration opportunities have highlighted the potential to reduce mill energy consumption (Ahmetovi and Grossmann, 2020; Keshtkar et al., 2015), freeing up some of this by-product for alternate uses. As black liquor currently has no market value, it is costed at its utility value.

Table 1
Reference pulp mill capacity and capacity of proposed routes.

Parameter	Value	Unit	Comment	Reference
Pulp mill capacity	130	Air dried $tn.h^{-1}$	Capacity of a large pulp and paper mill in China	Cossalter (2006)
Black Liquor Feedstock				
Total weak black liquor production	1300	$tn.h^{-1}$	10 times pulp production	Naqvi et al. (2010)
Black liquor solids content	17.5	% (w/w)		
Lignin content in black liquor	7.3	% (w/w)	41.5% lignin content in solids modelled as guaiacol	Cardoso et al. (2009)
Woody Biomass Feedstock				
Pulpwood removal rate	12	m3. $ha^{-1}yr^{-1}$	80% of productivity	Barr and Cossalter (2004)
Pulp mill collection area	377,650	ha	Based on 4.15 m^3. (Air dried tn^{-1})	
Pulpwood mass loss during debark and delimb	10	%		Jacobson et al. (2014)
Additional collection area required for chemical production	10,154	ha		
Forestry residue removal rate	1.89	m3. $ha^{-1}yr^{-1}$	0.157 of pulpwood removal rate	Cossalter and Barr (2005)
Residue mass loss during clean-up	40	%		Jacobson et al. (2014)
Total wood chip production	336,388	$tn.yr^{-1}$	1.63 m^3.dry tn^{-1} of chips	Cossalter and Barr (2005)

As per our previous work, Rodgers et al. (2021), this was calculated as the foregone Net Present Value (NPV) associated with its conventional use for renewable electricity generation. For conventional electricity generation, the weak black liquor with solids concentration 17.5% w/w is used. This is concentrated to 75% w/w in multi-effect evaporators prior to being combusted in the Tomlinson boiler to generate steam. This steam is then used to generate renewable electricity for sale to the grid. The NPV associated with this conventional renewable electricity generation translates to a cost of \$4.19 tn^{-1} of black liquor.

Pulpwood costs were estimated using data from the report prepared for the Guangxi Forestry Bureau on the development of industrial wood demand in the district (Cossalter and Barr, 2005). The mill gate prices presented for labour intensive hill areas were used, as these represent the majority of southern China plantations (Cossalter and Barr, 2006). The average of the three competitive production profiles and locations was taken and updated to a 2020 basis using the Lumber and Wood Products Producer Price Index (U.S. Bureau of Labor Statistics, 2021a) resulting in a cost estimate of \$102.62 tn^{-1}, similar to US pulpwood chip costs, \$109.64 tn^{-1}, as analysed by Idaho National Laboratory (Jacobson et al., 2014). All costs are reported on a dry basis. Whilst there is limited data availability for forestry residue costs in China, detailed cost estimates have been undertaken by the Idaho National Laboratory for delivered forestry residues in the US. Owed to the closeness of the China and US values for pulpwood chips the ratio between these estimates was used to approximate the cost of forestry residues in China, resulting in a cost of \$69.67 tn^{-1}. This price is in line with the range reported by Anttila et al. (2015), who undertook a study on availability of forestry residues for energy production in northern China, and to the prices reported in Gosens (2015) database for Chinese biomass power projects. Anttila et al. (2015) estimated costs of €30-42 tn^{-1} (wet basis), translating to \$51-72 tn^{-1}, whilst the average for facilities using wood residues as part of their feedstock in the Gosens (2015) database was RMB 297 tn^{-1} (wet basis), equivalent to \$65.09 tn^{-1}. Both prices were updated to a dry 2020 basis and assumed a 30% moisture content for delivered chips. Accordingly, using a blend of 20% pulpwood and 80% forestry residues the delivered biomass cost is \$76.26 tn^{-1}.

2.3. Costing models

Each of the three butadiene process simulations comprise a rigorous mass and energy balance and associated equipment sizing, used to calculate the capital and operating costs. Free on board equipment costs were calculated from cost correlations in Seider et al. (2017) and updated to 2020 prices using the Chemical Engineering Plant Cost Index of 596.2 (Jenkins, 2021).

The Fixed Capital Investment (FCI) was calculated using the Hand method, outlined in Sustainable Design Through Process Integration (El-Halwagi, 2017), where commissioning costs and working capital were calculated as per Table 2.

The fixed operating costs were calculated using the methodology

Table 2
Fixed capital cost model.

Economic Parameters	
Free on board equipment purchase cost	Seider et al. (2017)
Installed capital cost	Hand method
Chemical Engineering Plant Cost Index in 2020	596.2 (Jenkins, 2021)
Production Year	8,400[a] or 8,110[b] hours
Installed Cost – Inside Battery Limit (ISBL) Factor	Tables S4–S6
Outside Battery Limit (OSBL)	25% of ISBL
Commissioning Cost	5% of ISBL
Fixed Capital Investment (FCI)	ISBL + OSBL + Commissioning
Working Capital	10% of ISBL + OSBL
Total Capital Investment (TCI)	FCI + Working Capital

[a] Used for Eth-BD and Syn-BD route.
[b] Used for Acet-BD route. Based on bioreactor cycle time.

proposed by Sinnott and Towler (2009) and Ulrich and Vasudevan (2004) and are outlined in Table 3. The number of plant operators is based on both the methods proposed by Wessel (1952) accounting for the number of processing steps, production capacity, and process complexity, and by Ulrich and Vasudevan (2004) accounting for process equipment. The Acet-BD and Eth-BD routes both have 4 operators. Owing to the greater number of unit operations in the Syn-BD process, 5 operators are required.

Variable operating costs were estimated using the respective mass and energy balance and the raw material costs detailed in Table S2. The costs for utilities were taken from Seider et al. (2017). Specialist chemical costs are taken as spot prices and catalyst costs were taken from data available in existing TEA studies or, in the absence of cost data, based on the material composition. Chemical and catalyst costs were updated from their base year using the Chemicals and Allied Products Producer Price Index (U.S. Bureau of Labor Statistics, 2021b). Variable operating costs were subjected to an annual inflation of 2% throughout the life of the project.

2.4. Product prices

Time series analysis was used to obtain a long-term average price prediction for butadiene based on Takens Theorem (Takens, 1981). An embedding dimension of ten was used to represent approximations for the underlying state variable trajectory, and a Radial Basis Function Neural Network (RBFNN) containing eight neurons was employed to reconstruct an unbiased, one step ahead predictor of the future butadiene price. The historic pricing data for the embedding were obtained from the Intratec database (Intratec, 2020). The confidence limits for the nonlinear RBFNN model were calculated to validate the free-run model prediction (Leonard et al., 1992). Given this predicted long-term price average, the butadiene price lies within an uncertainty framework spanning the project life of 25 years and is therefore subject to sensitivity analysis.

In addition to butadiene, each route produces a co-product, namely; renewable electricity, higher alcohols and a butane rich co-product for the Acet-BD, Eth-BD and Syn-BD routes respectively. The prices used for these products are detailed in Table S3. For the Acet-BD route, China's renewable electricity price for biomass, 0.109 $.kWh^{-1} (Ming et al., 2013), was used to value black liquor and the additional electricity sales. For the Eth-BD route, the higher alcohols co-product produced during mixed alcohol synthesis was valued at 90% of its energy value relative to gasoline, using the Energy Information Administration's prediction for wholesale gasoline (EIA, 2021a) as per Dutta et al. (2011). For the Syn-BD route, the butane rich co-product was valued based on its energy content relative to butane. The long-term average price for butane was forecast using the RBFNN methodology, as outlined for butadiene, with historic pricing data taken from EIA (2021b).

2.5. Investment analysis

The aforementioned cost models informed the investment analysis. The NPV and Minimum Selling Price (MSP) was calculated for each project. The investment analysis parameters are detailed in Table 4.

2.6. Sensitivity and uncertainty analysis

A sensitivity analysis was conducted using a tornado chart to determine the relative importance of different variables. A Monte Carlo simulation was utilised to determine the probability of achieving a positive NPV. Both analyses were based on the parameters presented in Table 5. The Monte Carlo simulation was run 2000 times, generating a parameter set for each scenario stochastically using a uniform distribution within the defined lower and upper limits for the parameters.

The lower and upper limit distributions were taken from Sinnott and Towler (2009), with the exception of the renewable electricity price. This was capped at the current biomass subsidy owed to the decreasing trend in renewable electricity subsidies (Reuters, 2019). The lower limit was set to 0.48, translating to an electricity price of 0.052 $.kWh^{-1}. This allows for scenarios where grid parity is met, based on coal electricity prices for 2018 (Lee, 2019).

2.7. Life cycle assessment

A cradle-to-gate LCA model was developed following ISO Standards 14040 (International Organization for Standardization, 2006a) and 14044 (International Organization for Standardization, 2006b). Greenhouse gas (GHG) emissions were calculated based on the most recent Integrated Pollution Prevention and Control 100-year Global Warming Potential factors, thereby quantifying GHG emissions in terms of CO_2 equivalents (CO_2eq) (Stocker et al., 2014).

The functional units were defined as 1 kg for butadiene and 1 kg/kWh for the respective co-products. Life cycle environmental impacts were allocated between butadiene and the respective co-products using energy allocation. The co-products are; renewable electricity, higher alcohols, and a butane rich co-product for the Acet-BD, Eth-BD, and Syn-BD routes respectively.

The black liquor feedstock used in the hybrid Acet-BD route is a waste stream from pulp production, moreover it is utilised prior to the conventional multi-effect evaporator process, as such no emissions were assigned to it. Conversely, the two chemo-catalytic routes utilising forestry residues and pulpwood feedstocks have associated emissions. As a by-product from pulpwood harvest, forestry residues constitute 80% of the feedstock and the emissions associated with collection, chipping and loading were taken from McKechnie et al. (2011). The estimated emissions for pulpwood production, excluding land use change, were taken from Bernstad Saraiva et al. (2017) for the pulpwood fraction. For both the residues and pulpwood the transport emissions were updated to

Table 3
Fixed operating cost model.

Parameters	Acet-BD	Eth-BD	Syn-BD
Operating Labour	Salary estimates in China obtained from salaryexpert.com ($13,373 per year) employing 4 shift teams		
	4 Operators per shift	4 Operators per shift	5 Operators per shift
Supervisory Labour	25% of Operating Labour		
Direct Salary Overhead	50% of Operating and Supervisory Labour		
Maintenance	3% of ISBL		
Property Taxes and Insurance	1% of ISBL		
Rent of Land	1% of FCI		
General Plant Overhead	65% of Total Labour and Maintenance		
Allocated Environmental Charges	1% of FCI		

Table 4
Investment analysis parameters.

Parameters	Value	Comments
Corporation Tax	25%	Corporation tax in China
Annual Inflation	2%	Long-term average product prices forecast as above. All other costs are subject to annual inflation.
Plant Life (Operational)	25 years	
Discounted rate of return	10%	
Depreciation	10 year	Straight line
Plant Salvage Value	No value	
Construction Period	2 years	

Table 5
Monte Carlo simulation parameters.

Monte Carlo Input Parameter	Lower Limit	Upper Limit
Feedstock and Product Pricing		
Butadiene Price	0.8	1.2
Gasoline Price	0.8	1.2
Butane Price	0.8	1.2
Renewable Electricity Price	0.48	1
Woody Biomass Cost	0.7	1.3
Costing uncertainty Factor		
ISBL Capital Cost	0.8	1.5
OSBL Capital Cost	0.8	1.5
Labour Costs	0.8	1.5

correspond to the latest ecoinvent data for EURO 6 freight lorries and a 131 km transport distance, based on the average distance of the Chinese production profiles used for the wood chip cost estimation (Cossalter and Barr, 2005).

The GHG emissions for the utilities used by each butadiene route were calculated using the ecoinvent 3.7 inventory database using the allocation at the point of substitution system model (Wernet et al., 2016). The GHG emissions for grid electricity were taken as the 2018 China electricity mix (Sun et al., 2019). The full life cycle inventory can be found in Table S9.

Renewable butadiene is credited with negative GHG emissions owed to its sequestered biogenic carbon. As the downstream use of butadiene is independent of the production method, the calculated GHG emissions relative to conventional production are valid beyond the employed cradle-to-gate framework.

3. Results and discussion

The three routes, Acet-BD, utilising black liquor as a feedstock, and the Eth-BD, and Syn-BD routes, using forestry residues and pulpwood, each produce a co-product in addition to butadiene, detailed in Table 6. The energetic conversion efficiency (using lower heating value as the basis) for each route is also displayed. The energetic efficiency is lower for the Acet-BD route than the other two routes, attributed to the enthalpy lost in the supercritical water gasification effluent. The vast quantity of water in the gasification process and feedstock results in a loss in overall efficiency if any residual heat is left unexploited. Further heat integration opportunities could be found to improve the energy efficiency and increase the platforms renewable electricity generation. The carbon yield for butadiene is also lowest for the hybrid Acet-BD route, 6.3% compared to 19% for and 16% for the Eth-BD and Syn-BD routes, respectively. Whilst fermentation displays higher product selectivity with fewer by-products in comparison to catalytic transformation, conversion efficiencies for gas fermentation are typically lower given mass transfer limitations with limited opportunity to cost-effectively recycle feed gases.

The different production capacity between the Acet-BD and the Eth-BD and Syn-BD routes, presented in Table 6, is attributed to the availability of the feedstock as detailed in Section 2.1 Plant Capacity. The production capacity of the Syn-BD and Eth-BD routes are comparable, despite the greater number of catalytic steps involved in the Syn-BD route. This is attributable to the mass loss associated with the upgrading of ethanol and the greater efficiency of the commercial technologies utilised by the Syn-BD route.

3.1. Total capital investment

The capital cost estimations for each route are detailed in Tables S4–S6. A breakdown of these costs for the three plant sections; Gasification, Steam and Power Generation, Intermediate Production and Butadiene Production and Recovery are presented in Fig. 2. The intermediates for each route are; acetaldehyde, ethanol and propene for the Acet-BD, Eth-BD, and Syn-BD routes respectively. Owed to the heat pump used in the Acet-BD route the capital associated with steam and power generation is grouped with the gasification section for all three routes.

The normalised capital cost breakdown on the basis of tonnes of butadiene produced in Fig. 2 highlights the greater capital intensity of the Acet-BD route. The major capital contribution is associated with the Gasification, Steam and Power Generation section, incorporating the SCWG reactor and heat pump cycle. This section contributes 51% of total capital, in contrast to the 35–40% contribution for the Eth-BD and Syn-BD routes, highlighting the capital expense required to heat integrate the bioreactor and SCWG reactor. Conversely, the difference in capital between the routes Intermediate Production and Butadiene Synthesis and Purification plant sections is attributable to the greater economies of scale for the Eth-BD and Syn-BD routes.

3.2. Operating costs

A summary of the fixed and variable operating costs for all three butadiene production routes is presented in Tables S7 and S8. Fig. 3 plots the free-run long-term average price for butadiene. For comparative purposes the moving average for the previous 10 time steps is also plotted. The free-run forecast is shown to track the historic prices before settling on the long-term predicted price of \$1421 tn^{-1}, which is used as the nominal value in the investment analysis. The free-run long-term

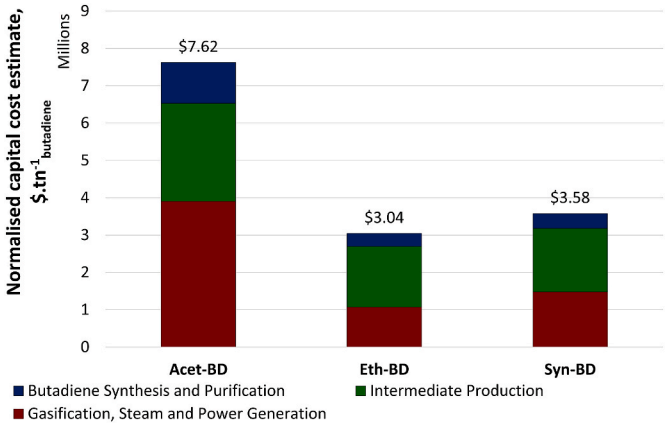

Fig. 2. Normalised capital cost estimate for the three butadiene production routes. The intermediate for the three routes are; acetaldehyde, ethanol and propene for the Acet-BD, Eth-BD, and Syn-BD routes respectively.

Table 6
Production summary for the three butadiene production routes, Acet-BD, Eth-BD and Syn-BD routes.

Route		Conversion	Butadiene		Co-Product		
	Feedstock	Energy efficiency %	Production kt.yr^{-1}	Income contribution %	Co-product	Production	Income contribution %
Acet-BD	Black liquor	20	9.2	39	Renewable electricity	192 Gwh.yr^{-1}	61
Eth-BD	Forestry residues and pulpwood	31	36	88	Higher alcohols	12 kt yr^{-1}	12
Syn-BD		30	31	92	Butane-rich product	11 kt yr^{-1}	7.9

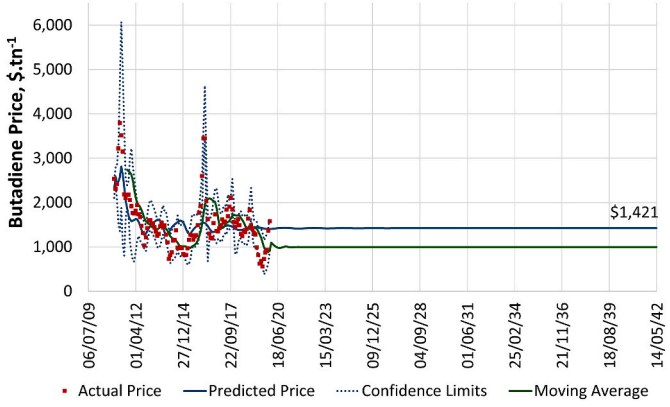

Fig. 3. Butadiene long term average price forecast. The free-run radial basis function neural network prediction tracks the historical prices within the confidence limits, before the unbiased, long-term price prediction emerges beyond the historical data.

average price forecast for n-butane predicts a nominal price of \$376 tn^{-1} and is presented in Fig. S4.

3.3. Minimum selling price

The MSP and the contributing cost breakdown of each butadiene production route is presented in Fig. 4. A case considering the catalytic upgrading of market ethanol is also included. The long-term price prediction for ethanol was obtained using the aforementioned RBFNN methodology, yielding a price of \$542 tn^{-1} (Fig. S5). Despite China being the 4th largest producer of fuel bioethanol, it is still heavily subsidised (USDA Foreign Agricultural Service, 2019), meaning ethanol priced at \$542 tn^{-1} would likely be imported from either the US or Brazil.

In all cases the largest MSP contributor is the feedstock cost. The Eth-BD, Syn-BD and market ethanol routes produce MSPs, 1.38, 1.55 and 1.20 times the nominal forecast price respectively. Markedly, despite having a greater capital intensity, the hybrid Acet-BD route is the only route able to produce butadiene below its predicted price, producing a cumulative NPV of \$2.8 million, see Fig. S6. This demonstrates how the high capital investment of the Acet-BD route preserves the profit margin by making the plant largely self-sufficient in its utility consumption.

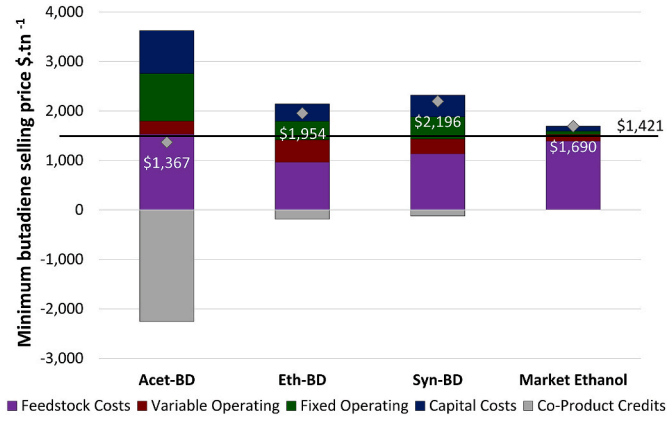

Fig. 4. Minimum butadiene selling price breakdown. The hybrid (Acet-BD) route is the only route capable of producing butadiene below the long-term average forecast price. The co-products for each route are; renewable electricity, higher alcohols (sold as gasoline) and a butane rich co-product for the Acet-BD, Eth-BD, and Syn-BD routes respectively. Market Ethanol represents a scenario considering the catalytic upgrading of ethanol purchased at market value using the Eth-BD route.

An additional case was considered for the two chemo-catalytic routes (Eth-BD and Syn-BD), whereby the capacity of the facilities was increased to 2000 tn. day^{-1} as assumed in NREL's U.S based studies (Dutta et al., 2011; Tan et al., 2015). The CAPEX was updated to reflect this capacity increase using a scaling factor of 0.6 (Sinnott and Towler, 2009). A 60,555 ha increase in the reference mill's collection area would be required to support the 2000 tn. day^{-1} capacity. All of the pulpwood from the additional collection area would be directed towards chemical production, resulting in a new feedstock composition of 67% pulpwood and 33% residues, and commanding a higher feedstock cost of \$91.73 tn^{-1}. This increase in feedstock cost partially offsets the benefit achieved through economies of scale, emphasising the advantage of exploiting waste, low cost, resources. Using the scaled CAPEX, OPEX, and new feedstock costs the consequent MSP's are \$1907 for the Eth-BD route, and \$2135 for the Syn-BD route. The increased capacity yields a lower MSP for both routes however, the Acet-BD route still produces the lowest nominal MSP. Moreover, the greater capacity necessitates expansion of the mills collection area and the use of a large portion of virgin wood.

The success of the Acet-BD route is largely attributed to the income generated from the renewable electricity. However, as this renewable electricity is inherent to the heat integrated technology platform its generation facilitates butadiene's cost-effective production.

Additionally, mills may receive an additional benefit from utilising black liquor for chemical synthesis. By diverting this co-product away from the recovery boiler, pulp mills have the potential to expand pulp production by up to 25% (Berntsson et al., 2008).

3.4. Sensitivity analysis

Tornado plots for the MSP of the three butadiene production routes, using the uncertainty framework outlined in Table 5 are presented in Fig. 5. In all three cases, ISBL capital costs led to the greatest increase in MSP. Importantly, using the grid parity price for electricity sales, 0.052 $\$.kWh^{-1}$, the Acet-BD route produces an MSP of \$1695 tn^{-1}, lower than the nominal MSP for the Eth-BD and Syn-BD routes, \$1954 tn^{-1}, and \$2196 tn^{-1} respectively. Resultantly, even using a pessimistic electricity price, the Acet-BD route is the most promising renewable production route evaluated. However, the exclusion of renewable electricity subsidies increases the MSP by \$328 tn^{-1}. This price is no longer below butadiene's long term forecast price, highlighting the importance of renewable electricity subsidies in facilitating the success of this technology platform.

Monte Carlo simulations of all three routes were undertaken using all of the uncertainty parameters in Table 5. As the only route presenting a positive NPV using the nominal inputs, the outcome for the hybrid Acet-BD route is presented in Fig. 6, with the results from the Eth-BD, and Syn-BD routes presented in Figs. S7 and S8. The Acet-BD route demonstrated a 19% likelihood of producing a positive NPV, presenting a higher probability of producing a negative NPV than positive. There is therefore a greater likelihood of this process losing money over its projected lifetime, making it unlikely to attract investment. However, this was the only route to demonstrate any probability of producing a positive NPV outcome, making it the most promising of the technologies evaluated. Furthermore, these results are based on a long-term forecast price for conventionally produced butadiene. There is potential to attract a higher market price, and thus a more favourable economic outcome, for renewably produced, low carbon butadiene.

3.5. Life cycle analysis

All three butadiene production routes produce net negative GHG emissions within a cradle to gate framework (Fig. 7). Outcomes are also presented for the use of market ethanol, imported from either the US or Brazil, with US ethanol being corn-based, and Brazil being sugar cane-based. Details of the emissions associated with both ethanol sources are presented in Table S10.

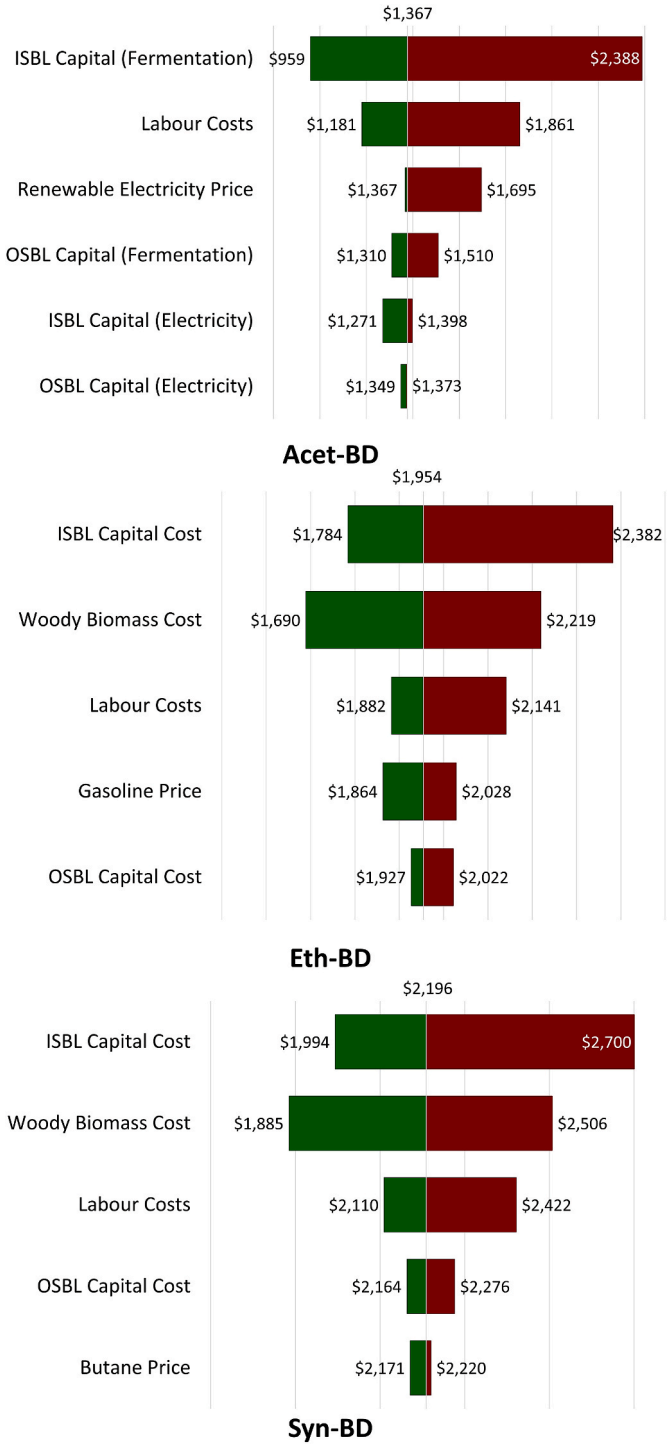

Fig. 5. Tornado plots for the MSP of the three butadiene production routes. a) Acet-BD route b) Eth-BD route c) Syn-BD Route.

The slightly greater emissions for the Syn-BD route compared to the Eth-BD route are attributed to the energy self-sufficiency and the greater butadiene yield of the Eth-BD route. The Syn-BD route relies on the import of 4.3 GWh.yr^{-1} of electricity, contributing 0.13 $kgCO_{2eq}$ $kg^{-1}_{butadiene}$. The greatest emission contributor for both chemo-catalytic routes is from the feedstock as demonstrated in Fig. 7. Despite this, the feedstock emissions are only marginal, 0.33–0.31 $kgCO_{2eq}$ $kg^{-1}_{butadiene}$. The Acet-BD route achieves the lowest emissions, owing to no emissions being attributed to the black liquor feedstock. In comparison to its conventional use, the platform produces a greater amount of renewable

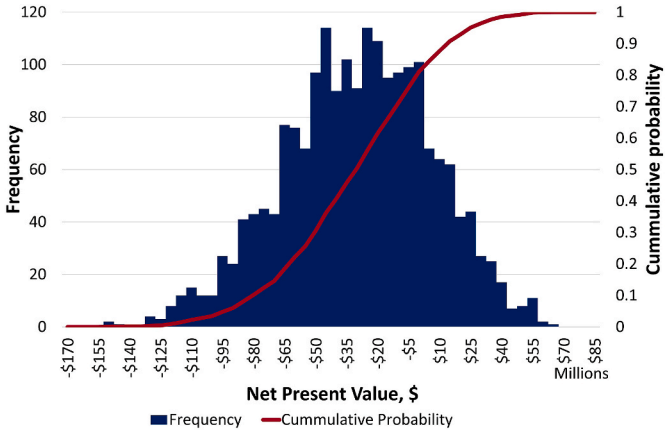

Fig. 6. Monte Carlo simulation of the Acet-BD presenting a 19% likelihood of achieving a positive NPV.

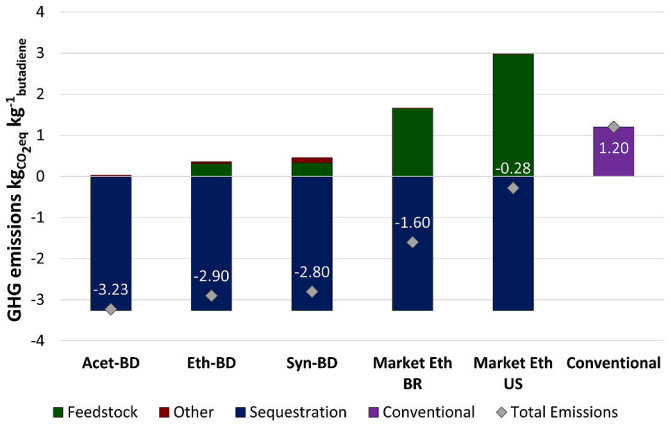

Fig. 7. Greenhouse gas emissions attributed to butadiene based on the three butadiene production routes and the Eth-BD route fed with market ethanol. Conventional represents butadiene production from naphtha as in the ecoinvent database.

electricity to export to the grid, meaning no emissions are associated with the diversion of this feedstock. Furthermore, the energy self-sufficiency of the Acet-BD and Eth-BD routes highlights their efficient biomass utilisation.

Conventionally, black liquor is burned for electricity generation (Naqvi et al., 2010), and forestry residues are seen as an promising feedstock for bio-energy production (Fu et al., 2020), technologies which both ultimately release CO_2 into the atmosphere. The net negative emissions achieved through butadiene production demonstrate the carbon sequestration achievable by directing these resources to chemical synthesis. The emission reduction potential of sinking biogenic carbon into ethene was previously highlighted by Zhao et al. (2018) in the context of China's chemical industry. The net negative emissions achieved by all three routes in this study reinforce this claim. However, for this carbon sink to be effective, it needs to be retained over long timescales. Further work is required considering the use of butadiene and the end-of-life management of these products. Nevertheless, the technologies highlight the contribution that Chinese paper and pulp mills can make in reaching China's goal of net neutrality by 2060.

3.6. Comparison to existing work

Studies investigating butadiene production from ethanol and an olefin intermediate have been previously undertaken, but no study has compared these production routes in terms of technical, environmental

and financial performances. In this study, the LCA and TEA results of the Acet-BD and Eth-BD routes are compared to existing ethanol studies, and the Syn-BD route is compared to studies evaluating routes via an olefin intermediate.

3.6.1. Ethanol to butadiene

The MSPs for previous TEA studies investigating butadiene production from ethanol are presented in Table 7. Where necessary prices were converted to US $ using the € to $ exchange rate of 1.14 for 2020 (Macrotrends, 2021). The lowest butadiene selling price, achieving a return on investment of 13.25%, was previously reported as $1523 tn^{-1}, using an ethanol price of $500 tn^{-1} (Dimian et al., 2021). All previous studies produce MSPs greater than that achieved by the Acet-BD route in this work, including the much greater facility size considered by Cabrera Camacho et al. (2020). The favourable China location factor, reducing capital costs, likely plays a significant role in this outcome, highlighting the competitive position Chinese paper and pulp mills hold in the potential for market penetration of renewable butadiene.

All existing LCA outcomes are also detailed in Table 7. Notably, in the LCA undertaken by Cespi et al. (2016), emissions were reduced by over a quarter by swapping the wheat portion of the European feed for residual wood chip, thereby highlighting the environmental advantage of utilising lignocellulosic feedstocks. In the cradle-to-grave study by Shylesh et al. (2016), both sugar cane and corn stover achieved net negative emissions, whilst the GHG emissions from corn grain ethanol were too high to be offset by the achieved carbon sequestration. The study by Cabrera Camacho et al. (2020), investigating first generation feedstocks, i. e corn grain and a Europe-centric mix of sugar beet, rye, corn and wheat; also found production emissions were too high to be offset by carbon sequestration. Farzad et al. (2017) found the bio-based production of butadiene from bagasse-derived ethanol to be environmentally advantaged compared to conventional production, further supporting the environmental benefit of utilising lignocellulosic feedstocks. Whilst GHG emissions between studies are not directly comparable, the undivided conclusion of existing studies is the large impact that the ethanol source has on the overall process emissions. This is reinforced by the results of this study, whereby the use of first-generation market ethanol performed worse than the three modelled routes. The favourable emissions for renewable butadiene found in this study can therefore be attributed to the use of second-generation lignocellulosic feedstocks.

3.6.2. Methanol to olefins

A number of modelling studies have been undertaken producing butadiene via a renewable olefin intermediate (Hanaoka et al., 2017, 2019, 2021; Tripathi et al., 2019). These studies investigated upgrading the minor C4 fraction, resulting in relatively low butadiene yields. Tripathi et al. (2019) rationalised this low butadiene yield by stating that the production of butadiene through these olefin technologies necessitates the co-production of lower value propene and ethene. Conversely, Hanaoka et al. (2021) recently undertook a study focused on improving the olefin reaction conditions to favour butene production. The produced results represent the highest butadiene yield, 7.0%, higher than the previously reported 3.9% by both (Hanaoka et al., 2017; Tripathi et al., 2019). These studies all use different model compounds for lignin. As such, to ensure the yields are comparable, they are reported based on carbon conversion.

Despite this, the yield is lower than the 16% realised through a propene intermediate in this study, highlighting the inefficiency of C4 production through current olefin technologies. However, even with this

Table 7
Published LCA and TEA studies producing butadiene investigating the route to butadiene via ethanol.

Study	Route	Carbon Source	Plant Location	Butadiene Produced (kt. yr^{-1})	MSP ($. tn^{-1})	GHG emissions (kg CO_2eq.kg^{-1} butadiene)	Comments
Cespi et al. (2016)	One Step	Sugar Cane	Brazil	–	–	1.04	Cradle to gate LCA
		Corn, Wheat, Rye, Sugar-beet	Europe			2.04	
		Corn, Residual Wood Chips, Rye, Sugar-beet	Europe			1.49	
		Corn	US			2.30	
	Two Step	Sugar Cane	Brazil	–	–	2.18	
		Corn, Sugarcane, Rye, Sugar-beet	Europe			3.62	
		Corn	US			4.00	
Shylesh et al. (2016)	One Step	Corn Grain	US	–	–	1.81	Cradle to grave LCA
		Sugar Cane				−0.65	
		Corn Stover				−0.52	
Farzad et al. (2017)	Two Step	Bagasse	South Africa	37	2645	0.08	BD-b (Energy self-sufficient)
					2385	0.06	BD-c (Coal burning)
Moncada et al. (2018)	One Step	C6 Sugars	Netherlands	24	4981	–	Case I (base case)
					3883		Case II (process with possible improvement)
Cabrera Camacho et al. (2020)	One Step	Sugar Cane	Brazil	200	2197	−0.07	Median Values
		Sugar Beet, Rye, Corn and Wheat	Europe			3.19	Scenario B1 Cradle to grave LCA
		Corn	US			3.98	
		Sugar Cane	Brazil		1962	−0.05	Median Values Scenario B2
		Sugar Beet, Rye, Corn and Wheat	Europe			2.64	Cradle to grave LCA
		Corn	US			3.31	
Dimian et al. (2021)	Two Step	–	–	91	1523	1.6	MSP achieves a return on investment of 13.25% using ethanol prices at $500 tn^{-1} GHG emissions are specific CO_2 emissions
This Work	One Step	Black Liquor	China	9	1367	−3.23	Cradle to gate LCA
		Woody Biomass		36	1954	−2.80	
		Sugarcane (BR)			1690	−1.60	
		Corn (US)				−0.28	

greater yield obtained through a propene intermediate, the MSP is still 1.36 times the projected market price. In addition, the route relies on the integration of a vast number of technologies, making for complex commercial implementation. Therefore, our findings are aligned with previous studies and confirm that currently available olefin technologies are inefficient pathways for butadiene production.

3.7. Challenges in developing the renewable chemical industry

The production of drop-in, or direct replacement, chemicals presents the fewest barriers to introducing biomass-derived chemicals to market (Christensen et al., 2008; Straathof and Bampouli, 2017). Nevertheless, it is important to recognise the challenge in producing these chemicals. Naphtha, used to produce traditional commodity chemicals, has a very low oxygen content in comparison to biogenic feedstocks (Haveren et al., 2008). This higher oxygen content necessitates the use of catalytic technologies to efficiently remove the undesired oxygen. Common catalytic technologies employed to remove oxygen include decarbonylation, dehydration, and hydrodeoxygenation. This oxygen removal inherently lowers the overall mass yield, with butadiene as a leading example. Consequently, the ability to produce these chemicals at market prices is highly dependent on feedstock costs and availability, and technology efficiency. Fundamentally, feedstocks need to be priced at fuel value or below, e.g. utility value such as in the case of black liquor.

Whilst butadiene holds a unique market position, it represents a challenging target chemical owed to its conjugated diene structure and lack of oxygen. Of the technologies evaluated, the hybrid biochemical Acet-BD route was the only economically viable route to butadiene using the nominal TEA inputs. Moreover, this route demonstrates the lowest GHG emissions, reinforcing the platforms efficient biomass utilisation. This builds on our previous work (Rodgers et al., 2021), by demonstrating the novel platform's economic advantage over traditional chemo-catalytic technologies within the context of a pulp mill biorefinery. Moreover, the unique coupling of SCWG with aerobic gas fermentation overcomes the energetic inefficiency of SCWG, one of the major barriers to commercialisation (Lee et al., 2021). This integration of technologies also generates a vast amount of renewable electricity, the income of which facilitates the platforms favourable economics. Whilst SCWG is yet to reach commercial scale, this study highlights heat integrated SCWG and aerobic gas fermentation as an efficient platform to valorise wet, recalcitrant feedstocks for biochemical production.

Importantly, whilst this work investigated the use black liquor as a feedstock, SCWG can be used for a variety of wet feedstocks which are uneconomical for traditional gasification technologies (Kumar et al., 2018). Potential feedstocks include; stillage, produced at a rate of 8–20 L per litre of fuel ethanol (Gebreeyessus et al., 2019), and wastewater residuals, animal and food waste, with an estimated combined availability of 77 million dry tons in the US alone (Bioenergy Technologies Office, 2017). The heat integrated SCWG and aerobic gas fermentation platform's ability to valorise these waste resources demonstrates the technology's importance in the transition to a renewable chemical industry towards carbon neutrality.

4. Conclusion

The hybrid gas fermentation route (Acet-BD) demonstrates marginal techno-economic feasibility of renewable, on-purpose butadiene in the context of Chinese paper and pulp mills. The technology produces a minimum selling price of \$1367 tn^{-1}, outcompeting the \$1954 tn^{-1} and \$2196 tn^{-1} achieved by chemo-catalytic ethanol production (Eth-BD), and via an olefin intermediate (Syn-BD), respectively. Notably, the Acet-BD is the only route capable of producing butadiene below the forecast price, producing a cumulative NPV of \$2.8 million using the nominal TEA inputs. Whilst the co-generation of renewable electricity contributes to the technology's success, its generation does not come at the detriment of butadiene production. The results of the Monte Carlo simulation demonstrate a 19% probability of the Acet-BD route achieving a positive NPV, with a 70% probability of producing an NPV between -\$50 million and \$60 million. Whilst 19% probability is low, the cost-effective production of renewable butadiene has hitherto been demonstrated. Moreover, the analysis is based on a price for conventionally produced butadiene. Renewable, low carbon chemical production has the potential to attract a higher market price, realising a more favourable economic outcome. All three routes evaluated produce net negative GHG emissions within a cradle-to-gate framework, with the Acet-BD producing the lowest emissions overall ($-3.23\ kgCO_{2eq}\ kg^{-1}_{butadiene}$ versus $1.2\ kgCO_{2eq}\ kg^{-1}_{butadiene}$ for conventional production). Resultantly, the heat integrated SCWG and aerobic gas fermentation platform can facilitate the decarbonisation of the chemical sector by exploiting wet, previously uneconomical, waste feedstocks in support of developing circular economies.

CRediT authorship contribution statement

Sarah Rodgers: Conceptualization, Data curation, Formal analysis, Investigation, Software, Visualization, Writing – original draft, Writing – review & editing. **Fanran Meng:** Conceptualization, Methodology, Writing – review & editing. **Alex Conradie:** Conceptualization, Formal analysis, Funding acquisition, Resources, Project administration, Software, Supervision, Writing – review & editing. **Jon McKechnie:** Conceptualization, Funding acquisition, Project administration, Resources, Supervision, Writing – review & editing.

Declaration of competing interest

The authors declare that they have no known competing financial interests or personal relationships that could have appeared to influence the work reported in this paper.

Acknowledgments

This work was supported by an EPSRC DTP CASE studentship with Johnson Matthey and by Industrial Biotechnology (IB) Catalyst project ConBioChem funded by Innovate UK, Biotechnology and Biological Sciences Research Council (BBSRC) and Engineering and Physical Sciences Research Council (EPSRC) (grant BB/N023773/1). Furthermore, this work was supported by the Future Biomanufacturing Research Hub (grant EP/S01778X/1), funded by the EPSRC and BBSRC as part of UK Research and Innovation. Finally, the authors gratefully acknowledge support received from the University of Nottingham Research Beacon of Excellence: Green Chemicals.

Appendix A. Supplementary data

Supplementary data to this article can be found online at https://doi.org/10.1016/j.jclepro.2022.132614.

References

Ahmetovi, E., Grossmann, I.E., 2020. A review of recent developments of water and energy optimisation methods applied to Kraft pulp and paper mills. In: The 4th South East European Conference on Sustainable Development of Energy, Water and Environment Systems, pp. 1–12, 4th SEE SDEWES).

Angelici, C., Weckhuysen, B.M., Bruijnincx, P.C.A., 2013. Chemocatalytic conversion of ethanol into butadiene and other bulk chemicals. ChemSusChem 6, 1595–1614. https://doi.org/10.1002/cssc.201300214.

Anttila, P., Vaario, L.M., Pulkkinen, P., Asikainen, A., Duan, J., 2015. Availability, supply technology and costs of residual forest biomass for energy - a case study in northern China. Biomass Bioenergy 83, 224–232. https://doi.org/10.1016/j.biombioe.2015.09.012.

Barr, C., Cossalter, C., 2004. China's development of a plantation-based wood pulp industry: government policies, financial incentives, and investment trends. Int. For. Rev. 6, 267–281. https://doi.org/10.1505/ifor.6.3.267.59977.

Bender, M., 2014. An overview of industrial processes for the production of olefins - C4 hydrocarbons. ChemBioEng Rev 1, 136–147. https://doi.org/10.1002/cben.201400016.

Bernstad Saraiva, A., Valle, R.A.B., Bosquê, A.E.S., Berglin, N., v Schenck, A., 2017. Provision of pulpwood and short rotation eucalyptus in Bahia, Brazil – environmental impacts based on lifecycle assessment methodology. Biomass Bioenergy 105, 41–50. https://doi.org/10.1016/j.biombioe.2017.06.004.
Berntsson, T., Axegard, P., Backlund, B., Samuelsson, A., Berglin, N., Lindgren, K., 2008. Swedish Pulp Mill Biorefineries.
Bioenergy Technologies Office, 2017. Biofuels and Bioproducts from Wet and Gaseous Waste Streams: Challenges and Opportunities. United States.
Bommareddy, R.R., Wang, Y., Pearcy, N., Hayes, M., Lester, E., Minton, N.P., Conradie, A.V., 2020. A sustainable chemicals manufacturing paradigm using CO2 and renewable H2. iScience 23. https://doi.org/10.1016/j.isci.2020.101218.
Cabrera Camacho, C.E., Alonso-Fariñas, B., Villanueva Perales, A.L., Vidal-Barrero, F., Ollero, P., 2020. Techno-economic and life-cycle assessment of one-step production of 1,3-butadiene from bioethanol using reaction data under industrial operating conditions. ACS Sustain. Chem. Eng. 8, 10201–10211. https://doi.org/10.1021/acssuschemeng.0c02678.
Cardoso, M., de Oliveira, É.D., Passos, M.L., 2009. Chemical composition and physical properties of black liquors and their effects on liquor recovery operation in Brazilian pulp mills. Fuel 88, 756–763. https://doi.org/10.1016/j.fuel.2008.10.016.
Cespi, D., Passarini, F., Vassura, I., Cavani, F., 2016. Butadiene from biomass, a life cycle perspective to address sustainability in the chemical industry. Green Chem. 18, 1625–1638. https://doi.org/10.1039/c5gc02148k.
Christensen, C.H., Rass-Hansen, J., Marsden, C.C., Taarning, E., Egeblad, K., 2008. The renewable chemicals industry. ChemSusChem 1, 283–289. https://doi.org/10.1002/cssc.200700168.
Corson, B.B., Jones, H.E., Welling, C.E., Hinckley, J.A., Stahly, E.E., 1950. Butadiene from ethyl alcohol. Catalysis in the one-and two-stop processes. Ind. Eng. Chem. 42, 359–373. https://doi.org/10.1021/ie50482a039.
Cossalter, C., 2006. Hardwood Fiber for Pulp in Southern China Scenarios of Supply – Demand Balance to 2010. The Forests Dialogue. https://theforestsdialogue.org/sites/default/files/cossalter_supply-demand_tfd_impf_china_406.pdf.
Cossalter, C., Barr, C., 2005. Fast growing plantation development and industrial wood demand in China's Guangxi Zhuang autonomous region. Center for International Forestry Research. https://www.cifor.org/publications/pdf_files/research/governance/foresttrade/Attachment8-WBReport-InsideCover_Content_Acknowledgement.pdf.
Cossalter, C., Barr, C., 2006. Fast-Growing Plantation Development and Fiber Supply in South China. Center for International Forestry Research. https://landmatrix.org/media/uploads/cifororgpublicationspdf_filesresearchgovernanceforesttradeattachment19-cossalter-risi-0406pdf.pdf.
Dai, W., Zhang, S., Yu, Z., Yan, T., Wu, G., Guan, N., Li, L., 2017. Zeolite structural confinement effects enhance one-pot catalytic conversion of ethanol to butadiene. ACS Catal. 7, 3703–3706. https://doi.org/10.1021/acscatal.7b00433.
Dimian, A.C., Bezedea, N.I., Bildea, C.S., 2021. Novel. Two-stage process for manufacturing butadiene from ethanol. Ind. Eng. Chem. Res. 60, 8475–8492. https://doi.org/10.1021/acs.iecr.1c00958.
Dutta, A., Talmadge, M., Hensley, J., Worley, M., Dudgeon, D., Barton, D., Groenendijk, P., Ferrari, D., Stears, B., Searcy, E.M., Wright, C.T., Hess, J., 2011. Process Design and Economics for Conversion of Lignocellulosic Biomass to Ethanol Thermochemical Pathway by Indirect Gasification and Mixed Alcohol Synthesis. NREL technical report NREL/TP-5100-51400.
Eckert, M., Fleischmann, G., Jira, R., Bolt, H.M., Golka, K., 2006. Acetaldehyde. In: Ullmann's Encyclopedia of Industrial Chemistry. Wiley-VCH Verlag GmbH & Co. KGaA, pp. 191–208. https://doi.org/10.1002/14356007.a01_031.pub2.
EIA, 2021a. ANNUAL ENERGY OUTLOOK 2021 [WWW Document]. URL. https://www.eia.gov/analysis/projection-data.php#annualproj. accessed 4.20.2021.
EIA, 2021b. Hydrocarbon Gas Liquids Explained Prices for Hydrocarbon Gas Liquids [WWW Document]. URL. https://www.eia.gov/energyexplained/hydrocarbon-gas-liquids/prices-for-hydrocarbon-gas-liquids.php.
El-Halwagi, M.M., 2017. Sustainable Design through Process Integration: Fundamentals and Applications to Industrial Pollution Prevention, Resource Conservation, and Profitability Enhancement, second ed. Elsevier.
Farzad, S., Mandegari, M.A., Görgens, J.F., 2017. Integrated techno-economic and environmental analysis of butadiene production from biomass. Bioresour. Technol. 239, 37–48. https://doi.org/10.1016/j.biortech.2017.04.130.
Food and Agricultural Organization of the United Nations (FAO), 2021. FAOSTAT - Forestry Production and Trade [WWW Document]. URL. http://www.fao.org/faostat/en/#data/FO.
Fu, T., Ke, J.H., Zhou, S., Xie, G.H., 2020. Estimation of the quantity and availability of forestry residue for bioenergy production in China. Resour. Conserv. Recycl. 162 https://doi.org/10.1016/j.resconrec.2020.104993.
Gebreeyessus, G.D., Mekonen, A., Alemayehu, E., 2019. A review on progresses and performances in distillery stillage management. J. Clean. Prod. 232, 295–307. https://doi.org/10.1016/j.jclepro.2019.05.383.
Gosens, J., 2015. Biopower from direct firing of crop and forestry residues in China: a review of developments and investment outlook. Biomass Bioenergy 73, 110–123. https://doi.org/10.1016/j.biombioe.2014.12.014.
Griffin, D.W., Schultz, M.A., 2012. Fuel and chemical products from biomass syngas: a comparison of gas fermentation to thermochemical conversion routes. AIChE J. 31, 219–224. https://doi.org/10.1002/ep.11613.
Grim, R.G., To, A.T., Farberow, C.A., Hensley, J.E., Ruddy, D.A., Schaidle, J.A., 2019. Growing the bioeconomy through catalysis: a review of recent advancements in the production of fuels and chemicals from syngas-derived oxygenates. ACS Catal. 9, 4145–4172. https://doi.org/10.1021/acscatal.8b03945.
Grub, J., Löser, E., 2011. Butadiene. In: Ullmann's Encyclopedia of Industrial Chemistry. Wiley-VCH Verlag GmbH & Co. KGaA, pp. 381–396. https://doi.org/10.1002/14356007.a04_431.pub2.
Hanaoka, T., Fujimoto, S., Yoshida, M., 2017. Efficiency estimation and improvement of the 1,3-butadiene production process from lignin via syngas through process simulation. Energy Fuel. 31, 12965–12976. https://doi.org/10.1021/acs.energyfuels.7b02237.
Hanaoka, T., Fujimoto, S., Kihara, H., 2019. Improvement of the 1,3-butadiene production process from lignin – a comparison with the gasification power generation process. Renew. Energy 135, 1303–1313. https://doi.org/10.1016/j.renene.2018.09.050.
Hanaoka, T., Fujimoto, S., Kihara, H., 2021. Evaluation of n-butene synthesis from dimethyl ether in the production of 1,3-butadiene from lignin: a techno-economic analysis. Renew. Energy 163, 964–973. https://doi.org/10.1016/j.renene.2020.08.158.
Hartley, D.S., Thompson, D.N., Cai, H., 2020. Woody Feedstocks 2019 State of Technology Report. https://doi.org/10.2172/1607741. United States.
Haveren, J. van, Scott, E.L., Sanders, J., 2008. Bulk chemicals from biomass. Biofuels, Bioprod. Biorefining 2, 41–57. https://doi.org/10.1002/bbb.43.
Huang, H.J., Ramaswamy, S., Al-Dajani, W.W., Tschirner, U., 2010. Process modeling and analysis of pulp mill-based integrated biorefinery with hemicellulose pre-extraction for ethanol production: a comparative study. Bioresour. Technol. 101, 624–631. https://doi.org/10.1016/j.biortech.2009.07.092.
IEA, 2018. The Future of Petrochemicals – Analysis. International Energy Agency, Paris.
International Organization for Standardization, 2006a. ISO 14040:2006: Environmental Management - Life Cycle Assessment - Principles and Framework. London.
International Organization for Standardization, 2006b. ISO 14044:2006 Environmental Management — Life Cycle Assessment — Requirements and Guidelines. London.
Intratec, 2020. Petrochemical Prices [WWW Document]. URL. https://www.intratec.us/products/commodities-prices/petrochemicals-prices.
Jacobson, J.J., Roni, M.S., Cafferty, K.G., Kenney, K., Searcy, E., Hansen, J., 2014. Biomass Feedstock and Conversion Supply System Design and Analysis. https://doi.org/10.2172/1173107. United States.
Jenkins, S., 2021. 2020 ANNUAL CEPCI AVERAGE VALUE [WWW Document]. Chem. Eng. Online. URL. https://www.chemengonline.com/2020-annual-cepci-average-value/.
Keshtkar, M., Ammara, R., Perrier, M., Paris, J., 2015. Thermal energy efficiency analysis and enhancement of three Canadian Kraft mills. J. Sci. Technol. For. Prod. Process. 5, 24–60.
Kong, L., Hasanbeigi, A., Price, L., Liu, H., 2013. Analysis of Energy-Efficiency Opportunities for the Pulp and Paper Industry in China.
Kumar, M., Olajire Oyedun, A., Kumar, A., 2018. A review on the current status of various hydrothermal technologies on biomass feedstock. Renew. Sustain. Energy Rev. 81, 1742–1770. https://doi.org/10.1016/j.rser.2017.05.270.
Lebedev, S.V., 1933. Preparation of bivinyl directly from alcohol .I. Zhurnal Obs. Khimii 3, 698–717.
Lee, H.M., 2019. China's Electricity Price from Gas Drops, but Still over 30% Higher than Coal. NEA [WWW Document]. S&P Glob. Coal. URL. https://www.spglobal.com/platts/en/market-insights/latest-news/coal/110619-chinas-electricity-price-from-gas-drops-but-still-over-30-higher-than-coal-nea#:~:text=The energy watchdog said the.
Lee, C.S., Conradie, A.V., Lester, E., 2021. Review of supercritical water gasification with lignocellulosic real biomass as the feedstocks: process parameters, biomass composition, catalyst development, reactor design and its challenges. Chem. Eng. J. 415, 128837 https://doi.org/10.1016/j.cej.2021.128837.
Leonard, J.A., Kramer, M.A., Ungar, L.H., 1992. A neural network architecture that computes its OWN reliability. Comput. Chem. Eng. 16, 819–835. https://doi.org/10.1016/0098-1354(92)80035-8.
Levi, P.G., Cullen, J.M., 2018. Mapping global flows of chemicals: from fossil fuel feedstocks to chemical products. Environ. Sci. Technol. 52, 1725–1734. https://doi.org/10.1021/acs.est.7b04573.
Macrotrends, 2021. Euro dollar exchange rate (EUR USD) - historical chart [WWW Document]. URL. https://www.macrotrends.net/2548/euro-dollar-exchange-rate-historical-chart.
McKechnie, J., Colombo, S., Chen, J., Mabee, W., MacLean, H.L., 2011. Forest bioenergy or forest carbon? Assessing trade-offs in greenhouse gas mitigation with wood-based fuels. Environ. Sci. Technol. 45, 789–795. https://doi.org/10.1021/es1024004.
Ming, Z., Ximei, L., Na, L., Song, X., 2013. Overall review of renewable energy tariff policy in China: evolution, implementation, problems and countermeasures. Renew. Sustain. Energy Rev. 25, 260–271. https://doi.org/10.1016/j.rser.2013.04.026.
Moncada, J., Gursel, I.V., Worrell, E., Ramírez, A., 2018. Biofuels Bioprod. Biorefining 12 (4). https://doi.org/10.1002/bbb.1876.
Mordor Intelligence, 2020. BUTADIENE MARKET - GROWTH. TRENDS, AND FORECAST, 2021 - 2026.
Naqvi, M., Yan, J., Dahlquist, E., 2010. Black liquor gasification integrated in pulp and paper mills: a critical review. Bioresour. Technol. 101, 8001–8015. https://doi.org/10.1016/j.biortech.2010.05.013.
Pomalaza, G., Arango Ponton, P., Capron, M., Dumeignil, F., 2020. Ethanol-to-butadiene: the reaction and its catalysts. Catal. Sci. Technol. 10, 4860–4911. https://doi.org/10.1039/d0cy00784f.
Ren, T., Patel, M., Blok, K., 2006. Olefins from conventional and heavy feedstocks: energy use in steam cracking and alternative processes. Energy 31, 425–451. https://doi.org/10.1016/j.energy.2005.04.001.
Reuters, 2019. China to Cut Subsidies for Renewable Power by 30 Per Cent to US$807 Million in 2020. South China Morning Post.

Rodgers, S., Conradie, A., King, R., Poulston, S., Hayes, M., Bommareddy, R.R., Meng, F., McKechnie, J., 2021. Reconciling the sustainable manufacturing of commodity chemicals with feasible technoeconomic outcomes. Johnson Matthey Technol. Rev. 375–394. https://doi.org/10.1595/205651321x16137377305390.

Rothaemel, M., Holtmann, H.-D., 2002. Methanol to propylene MTP - lurgi's way. Erdol ErdGas Kohle 118, 234–237.

Seider, W.D., Lewin, D.R., Seader, J.D., Widago, S., Gani, R., Ming Ng, K., 2017. Cost accounting and capital cost estimation. In: Product and Process Design Principles: Synthesis, Analysis and Evaluation. John Wiley & Sons Inc., New York, pp. 427–499, 2017.

Shylesh, S., Gokhale, A.A., Scown, C.D., Kim, D., Ho, C.R., Bell, A.T., 2016. From sugars to wheels: the conversion of ethanol to 1,3-butadiene over metal-promoted magnesia-silicate catalysts. ChemSusChem 9, 1462–1472. https://doi.org/10.1002/cssc.201600195.

Sinnott, R., Towler, G., 2009. Costing and project evaluation. In: Towler, G., Sinnott, R.B. (Eds.), Chemical Engineering Design. Butterworth-Heinemann, Oxford, pp. 291–388.

Stocker, T.F., Qin, D., Plattner, G.-K., Tignor, M., Allen, S.K., Boschung, J., Nauels, A., Xia, Y., Bex, V., Midgley, P.M., IPCC Working Group I, 2014. Climate Change 2013 – The Physical Science Basis: Working Group I Contribution to the Fifth Assessment Report of the Intergovernmental Panel on Climate Change. Intergovernmental Panel on Climate Change. Cambridge University Press.

Straathof, A.J.J., Bampouli, A., 2017. Potential of commodity chemicals to become bio-based according to maximum yields and petrochemical prices. Biofuels, Bioprod. Biorefining 11, 798–810. https://doi.org/10.1002/bbb.1786.

Suhr, M., Klein, G., Kourti, I., Rodrigo Gonzalo, M., Giner Santonja, G., Roudier, S., Delgado Sancho, L., 2015. Best Available Techniques (BAT) Reference Document for the Production of Pulp. https://doi.org/10.2791/370629. Paper and Board. Luxembourg.

Sun, X., Meng, F., Liu, J., McKechnie, J., Yang, J., 2019. Life cycle energy use and greenhouse gas emission of lightweight vehicle – a body-in-white design. J. Clean. Prod. 220, 1–8. https://doi.org/10.1016/j.jclepro.2019.01.225.

Takens, F., 1981. Detecting strange attractors in turbulence. Lect. Notes Math. 898 https://doi.org/10.1007/bfb0091924.

Tan, E.C., Talmadge, M., Dutta, A., Hensley, J., Schaidle, J., Biddy, M., Humbird, D., Snowden-Swan, L.J., Ross, J., Sexton, D., Yap, R., Lukas, J., 2015. Process Design and Economics for the Conversion of Lignocellulosic Biomass to Hydrocarbons via Indirect Liquefaction.

Tian, P., Wei, Y., Ye, M., Liu, Z., 2015. Methanol to olefins (MTO): from fundamentals to commercialization. ACS Catal. 5, 1922–1938. https://doi.org/10.1021/acscatal.5b00007.

Toussaint, W.J., Dunn, J.T., Jackson, D., 1947. Production of butadiene from alcohol. Ind. Eng. Chem. 39, 120–125. https://doi.org/10.1021/ie50446a010.

Tripathi, N., Palanki, S., Xu, Q., Nigam, K.D.P., 2019. Production of 1,3-butadiene and associated coproducts ethylene and propylene from lignin. Ind. Eng. Chem. Res. 58, 16182–16189. https://doi.org/10.1021/acs.iecr.9b00664.

Ulrich, G.D., Vasudevan, P.T., 2004. Manufacturing cost estimation. In: Chemical Engineering: Process Design and Economics A Practical Guide. Process Publishing, Durham, New Hampshire, pp. 409–438.

U.S. Bureau of Labor Statistics, 2021a. Producer Price Index by Commodity: Lumber and Wood Products: Logs, Bolts, Timber, Pulpwood and Wood Chips. Reserv. Bank, St. Louis [WPU085] [WWW Document]. FRED, Fed.

U.S. Bureau of Labor Statistics, 2021b. Producer Price Index by Commodity: Chemicals and Allied Products. Reserv. Bank, St. Louis [WPU06] [WWW Document]. FRED, Fed.

USDA Foreign Agricultural Service, 2019. China - Peoples Republic of Biofuels Annual China Will Miss E10 by 2020 Goal by Wide Margin, GAIN Report.

Wernet, G., Bauer, C., Steubing, B., Reinhard, J., Moreno-Ruiz, E., Weidema, B., 2016. The ecoinvent database version 3 (part I): overview and methodology. Int. J. Life Cycle Assess. 21, 1218–1230. https://doi.org/10.1007/s11367-016-1087-8.

Wessel, H., 1952. New graph correlates operating labor data for chemical processes. Chem. Eng. 59, 209–210.

White, W.C., 2007. Butadiene production process overview. Chem. Biol. Interact. 166, 10–14. https://doi.org/10.1016/j.cbi.2007.01.009.

Zhao, Z., Chong, K., Jiang, J., Wilson, K., Zhang, X., Wang, F., 2018. Low-carbon roadmap of chemical production: a case study of ethylene in China. Renew. Sustain. Energy Rev. 97, 580–591. https://doi.org/10.1016/j.rser.2018.08.008.

6 Creation of an unbiased price selection procedure for techno-economic analyses

6.1 Preface

This chapter contributes to the overall thesis aim of developing and applying Techno-Economic Analysis (TEA) methods to evaluate the proposed aerobic gas fermentation and Supercritical Water Gasification (SCWG) process by developing a machine learning (ML) methodology to produce 20-25 year probabilistic commodity price projections for techno-economic, sensitivity, and uncertainty analyses. The proposed method was demonstrated by recalculating the techno-economic outcome for the case studies investigated in Chapters 4 (isopropanol and acetone) and 5 (1,3-butadiene). It therefore contributes to the following thesis objective:

5. Develop a methodology to project future prices, considering future price variability, for use in techno-economic, sensitivity, and uncertainty analyses.

The selection of commodity chemical prices has a significant impact on the process economics, however, as outlined in Chapter 2 it is often an overlooked area in TEAs. In Chapters 4 and 5 a Radial Basis Function Neural Network (RBFNN) was used to select the long-term average price of the product for use in the investment analysis and stochastic uncertainty was accounted for using a uniform distribution of ±30/20% from the nominal projected price (Rodgers et al., 2021 & 2022). This method introduced an unbiased price projection method for TEAs but had various limitations. For example, the choice of an RBFNN with eight neurons and ten historic time-steps was arbitrary and may not be optimal; training the model on the entire historic time series may have led to overfitting; model initiation relied on ten real historic prices, excluding recent data; and price variability for sensitivity and uncertainty analyses were determined subjectively.

Machine Learning (ML) methods offer benefits over traditional statistical price projection methods such as Autoregressive Integrated Moving Average models and Generalised Autoregressive Conditional Heteroscedasticity models, as they are able to exploit complex, non-stationary, and non-linear trends (Lago et al., 2018). This chapter develops the previously proposed ML approach (Chapters 4 and 5), but instead employing Long-Short Term Memory (LSTM) neural networks. LSTMs are able to learn long-term dependencies in time series data, making them well-suited and adopted in traditional price forecasting fields. The commodity's historic pricing data (2009-2021) and the Energy Information Administration's (EIA's) reference case projection of future Brent crude oil prices were as model inputs. The historic commodity price allows for the exploitation of deterministic trends and/or stochastic variability specific to the commodity whilst the EIA's projection acts as a proxy for future global energy market trends. An ensemble of 100 models was used to generate a probabilistic projection of the commodity's future price. The ensemble of models, each trained to reproduce the entire historic time series, facilitates the exploitation of different underlying deterministic trends and/or stochastic variability within the historic time series producing a distribution of potential futures. From the probabilistic projection from the 100 LSTMs the 5th, 25th, 50th, 75th, and 95th price percentiles were calculated and used as the nominal price (50th), price range (5th and 95th), and price distribution (5th, 25th, 50th, 75th, and 95th) in the corresponding economic, sensitivity, and uncertainty analyses. As such the methodology makes the need for using heuristic uncertainty bounds obsolete.

During model training the datasets were split into training and validation sets based on the ratio between the historic data (12 years, 30%) and projection horizon (26 years, 70%) required for the TEA. This ensured that the selection of optimal hyperparameters was carried out on a task representative of the final model projections. The projection horizon was 26 years, thereby allowing direct comparison to the TEAs in Chapters 4 and 5. A test set was not employed due to the limitations in dataset size. Given the projection horizon of the final model, the use of a test set would necessitate a split of 30% for the training and validation set, and 70% for the test set. The training set would then constitute 30% of the training and validation set, resulting in only 9% of the data being used for training, 21% for validation, and 70% for the test set. As no test set was used, the ability of the model to generalise was assessed based on the performance against the validation set. In addition, when using the methodology in a TEA, a test set would not be used, and the hyperparameters would be selected based on validation set accuracy. The learning rate, number of epochs, and maximum number of hidden units in the LSTM layer were optimised during the grid search procedure.

This work presents and implements the method by projecting five commodity chemical prices 26 years into the future. Furthermore, the nominal Net Present Value (NPV) and NPV range from the uncertainty analysis obtained from the previous two TEAs in Chapters 4 and 5 were compared to the new outcomes obtained from the developed price projection method. This was undertaken to highlight the importance in price selection procedures and their impact on economic outcomes.

The novelty of this work is, to the best of the authors knowledge, the first application of machine learning to produce probabilistic commodity prices for TEAs. Previous price projection methods employed in TEAs are stochastic modelling (e.g. Manca et al., 2011), correlating prices to an existing projection for a different commodity (e.g. Brown & Wright, 2015), or employed traditional econometric tools (e.g. Nguyen and Tyner, 2021). In addition, the probabilistic price projection provides the ranges for the sensitivity and uncertainty analyses, rather than relying on heuristics. Previous approaches to account for price variability have relied on historic variability (e.g. Diniz et al., 2018), or applied an arbitrary percentage (e.g. Moncada et al., 2018).

This study found the projected commodity price distributions demonstrated appreciable price variability. These results suggest that pricing uncertainty considerations in TEAs should be tailored to each commodity rather than dictated through heuristics. These results were put into the two previous TEAs. Comparing the previous RBFNN price projections to the developed LSTM method, the 70% probability window for the NPV distributions were changed from $35 - $95 million to $45 - $80 million for Chapter 4, producing isopropanol and acetone, and from -$45 - $65 million to -$35 - $80 million for Chapter 5 for the 1,3-butadiene process. A two-tailed t-test verified a statistically significant difference between the NPV distributions.

A limitation of this study was the number of hyperparameters considered during the validation procedure. In addition to the number of LSTM units, epochs, and learning rate the number of layers, number of neurons in the fully connected layer, use of a fully connected layer, number of time-steps being predicted etc. could have also been considered. However, as the increased number of hyperparameters being optimised vastly increases the computational expense there is a trade-off between these two factors. Cross-validation was also omitted from this analysis, relying only on a single validation set to select the hyperparameters. Additionally, the inclusion of the EIA's projection was not effectively input into the model. An improved approach would have involved staggering inputs, using future crude oil price projections from the EIA for corresponding commodity predictions, thereby enabling the model to learn the relationship between future crude oil prices and commodity prices for improved predictions. A

further limitation was that no comparison between price projection methods was undertaken to compare accuracy. In traditional forecasting fields new methods are commonly compared against traditional econometric methods and various simpler ML methods e.g. Wu et al. (2019) and Lago et al. (2018). However, the specific requirements of the projection problem defined in this work, namely, a probabilistic projection, inclusion of the EIAs crude oil price projection, and applicability to any time series, meant econometric methods were unsuitable for the studied problem. Alternative ML methods could have been compared to assess the most appropriate model. This was omitted to keep the focus of the work on the application of the price projections within TEAs, rather than on comparing algorithms based on their accuracy. Furthermore, algorithm accuracy cannot be compared on the final predictions, as price projections are produced 20-25 years into the future, where real prices are unavailable. Despite this, future work has been suggested to explore decomposition-based methods such as variational mode decomposition and other wavelet decomposition methods along with the proposed ensemble approach. These methods aim to reduce the burden on the ML algorithm by first extracting features from the data. However, such methods were deemed excessive for the presented problem, adding unnecessary computational expense.

This work comprises a published paper entitled “Probabilistic commodity price projections for unbiased techno-economic analyses” and was published in *Engineering Applications of Artificial Intelligence* in June 2023. The published paper is presented in this thesis as Chapter 6. The corresponding supplementary information as published alongside the manuscript is reprinted in Appendix A.3.

Article Title: Probabilistic commodity price projections for unbiased techno-economic analyses

Journal: Engineering Applications of Artificial Intelligence

Date: June 2023

DOI: 10.1016/j.engappai.2023.106065

Authors: Sarah Rodgers, Alexander Bowler, Fanran Meng, Stephen Poulston, Jon McKechnie, Alex Conradie

Author Contributions: Sarah Rodgers: Conceptualization, Data curation, Formal analysis, Investigation, Methodology, Software, Visualization, Writing – original draft, Writing – review & editing. Alexander Bowler: Conceptualization, Data curation, Formal analysis, Methodology, Software, Writing – review & editing. Fanran Meng: Conceptualization, Methodology, Supervision, Writing – review & editing. Stephen Poulston: Supervision, Writing – review & editing. Jon McKechnie: Conceptualization, Funding acquisition, Methodology, Project administration, Resources, Supervision, Writing – review & editing. Alex Conradie: Conceptualization, Formal analysis, Funding acquisition, Methodology, Project administration, Resources, Software, Supervision, Writing – review & editing.

6.2 References

Brown T.R., & Wright M.M., 2015. A framework for defining the economic feasibility of cellulosic biofuel pathways. *Biofuels*, 579-590

Diniz A.P.M.M., Sargeant R., Millar G.J., 2018. Stochastic techno-economic analysis of the production of aviation biofuel from oilseeds. *Biotechnology and Biofuels*, 11, 1-15

Lago, J., De Ridder, F., De Schutter, B., 2018. Forecasting spot electricity prices: Deep learning approaches and empirical comparison of traditional algorithms. *Applied Energy*, 221, 386-405.

Manca D., Fini A., Oliosi M., 2011. Dynamic conceptual design under market uncertainty and price volatility. *Computer Aided Chemical Engineering.*

Moncada, J., Gursel, I.V., Worrell, E., Ramírez A., 2018. Production of 1,3-butadiene and ε-caprolactam from C6 sugars: Techno-economic analysis. *Biofuels Bioproducts and Biorefining*, 12 (4)

Nguyen N. & Tyner W.E., 2021. Assessment of the feasibility of the production of alternative jet fuel and diesel using catalytic hydrothermolysis technology: a stochastic techno-economic analysis. *Biofuels Bioproducts and Biorefining*,16 (1), pp. 91-104

Rodgers, S., Conradie, A., King, R., Poulston, S., Hayes, M., Bommareddy, R.R., Meng, F., McKechnie, J., 2021. Reconciling the Sustainable Manufacturing of Commodity Chemicals with Feasible Technoeconomic Outcomes. *Johnson Matthey Technology Review*, 375–394.

Rodgers, S., Meng, F., Poulston, S., Conradie, A., McKechnie, J., 2022. Renewable butadiene: A case for hybrid processing via bio- and chemo-catalysis. *Journal of Cleaner Production,* 364, 132614.

Wu, Y.X., Wu, Q.B., Zhu, J.Q., 2019. Improved EEMD-based crude oil price forecasting using LSTM networks. *Physica A: Statistical Mechanics and its Applications*. 516, 114–124.

This page has been left intentionally blank

Engineering Applications of Artificial Intelligence 122 (2023) 106065

Contents lists available at ScienceDirect

Engineering Applications of Artificial Intelligence

journal homepage: www.elsevier.com/locate/engappai

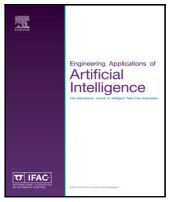

Probabilistic commodity price projections for unbiased techno-economic analyses

Sarah Rodgers [a], Alexander Bowler [b], Fanran Meng [c], Stephen Poulston [d], Jon McKechnie [a], Alex Conradie [a,*,1]

[a] Sustainable Process Technologies Research Group, Faculty of Engineering, University of Nottingham, Nottingham, NG7 2RD, UK
[b] Food, Water, Waste Research Group, Faculty of Engineering, University of Nottingham, Nottingham, NG7 2RD, UK
[c] Department of Engineering, University of Cambridge, Trumpington Street, Cambridge CB2 1PZ, UK
[d] Johnson Matthey, Blounts Court Road, Sonning Common, Reading, RG4 9NH, UK

ARTICLE INFO

Keywords:
Techno-economic analysis
Monte Carlo simulation
Price uncertainty
Price projection
Long Short-Term Memory
Machine learning

ABSTRACT

Techno-economic analysis is a core methodology for assessing the feasibility of new technologies and processes. The outcome of an analysis is largely dictated by the product's price, as selected by the practitioner. Representative future price distributions are required as inputs to investment, sensitivity, and uncertainty analyses across the 20 to 25 year plant life. However, current price selection procedures are open to subjective judgment, not adequately considered, or neglected by calculating a minimum selling price. This work presents a machine learning methodology to produce unbiased projections of future price distributions for use in a techno-economic analysis. The method uses an ensemble of 100 neural network models with Long Short-Term Memory layers. The models are trained on the Energy Information Administration's (EIA) long-term crude oil projections and a commodity's historic price data. The proposed method is demonstrated by projecting the price of five commodity chemicals 26 years into the future using 12 years of historic data. Alongside the economic outlook extracted from the EIA projections, the five commodity price distributions capture stochastic and deterministic elements specific to each commodity. A statistically significant difference was observed when using the price projections to revise the Net Present Value distributions for two previous techno-economic analyses. This suggests that relying on heuristics when selecting price ranges and distributions is unrepresentative of a commodity's price uncertainty. The novelty of this work is the presentation of an unbiased machine learning approach to project long-term probabilistic prices for techno-economic analyses, emphasising the pitfalls of less rigorous approaches.

1. Introduction

The development of a sustainable chemical industry requires novel processes that are cost-competitive against current fossil-derived production. A Techno-Economic Analysis (TEA) evaluates the economic feasibility of full-scale processes, allowing for the prioritisation of early-stage research and development (Scown et al., 2021). Depending on the technology maturity and intended audience, TEA outcomes can be used for a variety of purposes; e.g. determining cost drivers, ranking prospective technologies, producing targeted policy initiatives, and assessing optimal resource valorisation. Effectively interpreting TEA outcomes requires analyses to be objective, comparable, and transparent (Langhorst et al., 2022). Product prices significantly affect these outcomes, usually considered over a 20 to 25 year project life to obtain the comulative Net Present Value (NPV). However, long-term prices are selected by the practitioner and subjective heuristics are typically relied upon to select the corresponding range and distribution for use in sensitivity and uncertainty analyses. The robust, unbiased projection of representative, long-term prices are thus essential as inputs to investment analyses, thereby assessing the economic feasibility of new technologies and processes.

At present, it is commonplace for TEAs to use spot prices either from literature, market values and price indices, or to bypass selection by calculating the Minimum Selling Price (MSP). Unfortunately, references to representative prices can be difficult to come by, and uncertainty often exists concerning the reliability of the source, the geographic location, and the time frame for which the price is representative (Hubbard, 2018). Furthermore, objective future price projections are required to ultimately contextualise calculated MSPs. As part of a TEA, sensitivity and uncertainty analyses provide for greater robustness

* Corresponding author.
E-mail address: a.conradie@ucl.ac.uk (A. Conradie).
[1] Present address: The Manufacturing Futures Laboratory, Department of Biochemical Engineering, University College London, Gower Street, London, WC1E 6BT, UK.

https://doi.org/10.1016/j.engappai.2023.106065
Received 21 November 2022; Received in revised form 2 February 2023; Accepted 24 February 2023
Available online 10 March 2023

Abbreviations

CNN	Convolution Neural Network
CRPS	Continuous Ranked Probability Score
EIA	Energy Information Administration
EMD	Empirical Mode Decomposition
LSTM	Long Short-Term Memory
MIMO	Multi Input Multi Output
ML	Machine Learning
MMBTU	Million British Thermal Units
MSP	Minimum Selling Price
NPV	Net Present Value
RBFNN	Radial Basis Function Neural Network
RNN	Recurrent Neural Network
TEA	Techno-Economic Analysis
VMD	Variational Mode Decomposition

given the underlying assumptions. These analyses frame the economic outcome within a band of uncertainty based on the initial assumptions. Sensitivity analyses necessitate both a nominal price and range, whilst uncertainty analyses require a nominal future price and the corresponding distribution. However, lower and upper bounds are often selected as an arbitrary percentage. Towler and Sinnott (2013) recommend varying prices by ±20% as a rule of thumb, though bounds employed in literature vary considerably. For example, Moncada et al. (2018) varied their product prices by ±50% with the nominal price selected from Alibaba averages. Similarly, Zhang et al. (2021) used a bio-methanol price from literature with an arbitrary ±$200 tn^{-1} range (~18%) in their sensitivity analysis. Distribution data is often taken from historic prices. However, there is no guarantee historic variability will be representative of the future, and the use of historic data necessitates the selection of a historic time period, introducing subjectivity as historic time periods used in practice vary. Campbell et al. (2018) used a triangular distribution for biofuel selling prices with the minimum, maximum, and mean prices taken from historic gasoline, diesel, and heating oil prices from 2005 to 2017. Cheali et al. (2014) analysed historic gasoline, diesel, and ethanol prices for 2012 and selected a distribution to appropriately describe the historical data. Diniz et al. (2018) used Pert distributions with the range based on observed fluctuations in crude oil prices over the five preceding years. The probabilistic projection of future prices would bypass the use of heuristics for range and distribution selection, the assumption that historic price variability is representative into the future, and the subjective selection of historic time periods.

Several existing TEAs have considered the projection of future prices as a solution to the volatile and uncertain nature of commodity prices across a plant's lifetime. The principal approaches adopted are, (1) modelling the time series as a stochastic process where the data follows a random walk (Manca et al., 2011; McGarvey and Tyner, 2018), (2) correlating prices to an existing projection for a different commodity (Brown and Wright, 2015; Zhang et al., 2013), and (3) the use of traditional econometric tools (Amigun et al., 2011; Ioannou et al., 2018; Nguyen and Tyner, 2021; Puig-Gamero et al., 2021; Yao et al., 2017). All three previously employed approaches have their limitations. Modelling the time series as a purely stochastic process prevents the exploitation of any deterministic trends within the historic price data. Existing projections are often only single point, providing no probabilistic uncertainty bound. Finally, whilst traditional econometric tools exploit determinism within the historic data, the models are not universally applicable and require practitioners to undertake statistical tests to prepare and analyse the data. Moreover, these methods require the time series to be near linear and are unable to extract complex features (Lago et al., 2018).

Despite not being common practice in TEAs, price forecasting is a well-developed field. Current research is primarily focused on machine learning (ML) methods owing to their ability to accommodate non-linear, non-stationary, and complex sequences compared to statistical methods. Commonly adopted ML methods in forecasting include artificial neural networks, support vector machines, and random forests (Herrera et al., 2019). LSTMs are of particular prominence owing to their ability to learn long-term dependencies within time series data (Wu et al., 2019). They are being increasingly applied to price forecasting problems such as crude oil (Wu et al., 2019), electricity (Lago et al., 2018), gold (Livieris et al., 2020), and the stock market (Li and Bastos, 2020). However, traditional forecasting procedures differ from the requirements for a TEA, which necessitate a probabilistic price projection 20 to 25 years into the future to provide representative prices for the investment, sensitivity and uncertainty analyses. This 20 to 25 year horizon is often longer than the historic pricing data available for model training. Traditional forecasting problems typically consider much shorter horizons and focus on pricing fluctuations relative to previous prices, aiming to minimise short-term investment losses and risk. For example, time horizons of, days (Liang et al., 2020) or months (Bukhari et al., 2020) are often considered for stock price forecasting, a three month forecast horizon was utilised in a supply chain procurement optimisation problem (Liu et al., 2022), and three years is considered long-term for electricity price forecasting (Ziel and Steinert, 2018). Furthermore, TEAs are undertaken based on a plant being built at the outset of a long-term investment proposition. The projected price distributions directly impact the TEA outcome and could be decisive in whether a capital investment is sanctioned. As the true future prices are unavailable, the long-term projection accuracy cannot be evaluated. Therefore, the purpose of price projections is to provide an unbiased nominal price and distribution to evaluate a technology without subjective judgement from either the TEA practitioner or the intended audience. Importantly, an investment opportunity is often weighed against a portfolio of other opportunities, making a consistent approach to price projection paramount to fair comparisons. This contrasts with traditional price forecasting problems, where model performance is evaluated through the comparison of the forecast to actual prices.

Leveraging LSTMs ability to learn long-term dependencies in time series data, an ensemble of 100 ML models, containing a fully connected layer and LSTM layer, is implemented to produce a probabilistic projection of the commodity's future price for use in TEAs. LSTMs allow for the exploitation of features from the entire historic dataset. This means the model is not limited by the feature horizon, which is key to uncovering long-running historic trends. For this reason, no feature extraction is used before the LSTM layers, enabling the models to learn feature time-lengths relevant to the task and use interdependencies between features of different frequencies. Resultantly, the number of LSTM units is selected during model training to optimise the network size for feature extraction and trajectory learning capabilities. The projected distribution is used to calculate the 5th, 25th, 50th, 75th and 95th price percentiles, removing bias from the nominal price, range, and distribution selection procedures. The EIA's reference case projection of future Brent crude oil prices is used as an additional model input. The EIA's projection is based on assumptions that include economic factors, resource availability, global energy markets, and technological developments (EIA, 2019); which are unavailable to TEA practitioners. As such, the use of this projection acts as a proxy for future global energy market trends, whilst the historic commodity price allows for the exploitation of deterministic trends and stochastic variability specific to the commodity. This work aims to present and implement a method to produce unbiased price distribution projections for TEAs. The method is demonstrated by projecting five commodity chemical prices 26 years into the future and using the pricing projections in two existing TEAs. The novelty of this work lies in:

1. The use of machine learning to produce 20 to 25 year probabilistic commodity price projections for techno-economic, sensitivity, and uncertainty analyses.
2. The use of an ensemble of LSTMs to exploit the underlying determinism and/or stochastic variability within the commodity's historic price time series.
3. Using the price projections to draw attention to the inadequacy of currently employed price, range, and distribution procedures in TEAs.
4. Applying the produced projections to existing TEAs, thereby evidencing the importance of price selection procedures to techno-economic outcomes.

The remainder of the article is organised as follows. Section 2 provides a literature review of forecasting methods previously undertaken within TEAs and briefly covers the use of LSTMs within price forecasting fields. Section 3 describes the methods used and developed in this work. Section 4 presents the price projections and discusses their impact by utilising them in two existing TEAs. Lastly, Section 5 summarises the key findings and proposes recommendations for future work.

2. Relevant literature

Price projections are seldom undertaken for price selection procedures in TEAs. Those studies that have considered it, are discussed below. Recent applications of LSTMs in traditional price forecasting fields are also discussed, reflecting upon their relevance to TEA price projections.

2.1. Techno-economic analyses

Manca et al. (2011), is a rare example highlighting the challenge posed by commodity price variability across a chemical plant's lifetime. In their work, a forecast for a reference component is produced using a stochastic Markovian process and Monte Carlo methods were used to produce a distribution of prices (Manca, 2012). Other commodities were correlated to this reference component using an Autoregressive Distributed Lag model (Manca et al., 2011). The proposed method led to the creation of a systematic method, named Predicted Conceptual Design, used to produce optimal plant designs under market uncertainty. The authors have utilised their framework in several case studies, i.e. styrene monomer manufacturing (Barzaghi et al., 2016), the cumene process (Sepiacci et al., 2017), and a CO_2 separation process (Gutierrez et al., 2019). Whilst this method is applicable to any commodity's time series, a major drawback of stochastic modelling is the inability to exploit any underlying deterministic trends within the historic time series.

Several econometric approaches have been considered within economic assessments. In a TEA for bioethanol production in South Africa, prices were modelled stochastically using a multi-variate empirical distribution methodology based on historical fluctuations between 1999 and 2008 (Amigun et al., 2011). Yao et al. (2017) undertook statistical tests on the historic price data of each commodity in their stochastic TEA of alcohol to jet fuel. Different models were then selected to represent each commodity (Yao et al., 2017). In the price growth scenario in the study by McGarvey and Tyner (2018), jet fuel price growth was represented by geometric Brownian motion using a 1% growth rate and a stochastic component with a PERT distribution, where the first year commenced using a mean of historic prices (McGarvey and Tyner, 2018). Ioannou et al. (2018) compared Geometric Brownian motion, Autoregressive Integrated Moving average, and a model combining Mean-Reversion and Jump–Diffusion models to forecast electricity prices in an economic assessment of offshore wind energy production, finding the Autoregressive Integrated Moving average model performed best over the validation set (Ioannou et al., 2018). Nguyen and Tyner (2021) forecast jet fuel and carinata oil by analysing the data using @Risk software (Nguyen and Tyner, 2021). The price distributions were produced to ensure the observed probability distribution function and trend between commodities were maintained. More recently, Puig-Gamero et al. (2021) considered three econometric models, damped trend, local linear trend, and local linear trend with cycle in their economic analysis of methanol produced from olive waste (Puig-Gamero et al., 2021). A gaussian distribution of forecast errors based on the historic data was produced and used in the Monte Carlo simulation. Whilst these econometric models utilise information within the historic dataset to make a projection, they all use different approaches. As highlighted by Yao et al. (2017), the underlying price movements are different for each commodity, meaning no econometric method is applicable to all commodities. This requires the TEA practitioner to undertake statistical tests to prepare and analyse the data. In addition, these methods require the time series to be near-linear and are unable to extract complex long-running features.

Some analyses have made use of the EIA's price projections to predict future prices. Zhang et al. (2013) considered future prices by using the EIA's long-term price prediction for petroleum and correlating other commodity prices to this for their TEA (Zhang et al., 2013). The disadvantage of this approach is the EIA's projections are point forecasts, neglecting probabilistic uncertainty, required for use in sensitivity and uncertainty analyses (Kaack et al., 2017). Incorporating uncertainty and the EIAs projections, Brown and Wright (2015) simulated future commodity prices using a random walk with drift. The random changes were based on the probability density function of historic prices, whilst the drift ensured the mean of monthly price distributions matched the EIAs 2013–2032 projections (Brown and Wright, 2015).

To the best of the authors' knowledge, the only previous application of ML for price selection procedures within TEAs was by Rodgers et al. (2021, 2022). A Radial Basis Function Neural Network (RBFNN) was used to produce long term average commodity price projections and stochastic uncertainty was accounted for using a uniform distribution of ±20% from the nominal projected price (Rodgers et al., 2021, 2022). Whilst this method is applicable to any time series, the heuristic used to account for stochastic uncertainty has no bearing on the observed time series and was therefore unrepresentative of the commodity's price setting mechanism.

The only methods applicable to any time series are purely stochastic processes and ML methods. A disadvantage of modelling as stochastic process is the inability to exploit any underlying trends within the commodity's price data. Whilst ML methods overcome this challenge, the previous application of ML relied on an arbitrary heuristic to account for price uncertainty (Rodgers et al., 2021, 2022). Ideally, a probabilistic price projection should be produced, providing a projection of the nominal price, range, and distribution for use in the investment, sensitivity, and uncertainty analysis during a technology evaluation.

2.2. Price forecasting

Both statistical and ML methodologies have been applied to price forecasting fields. ML's ability to accommodate complex, non-linear, and non-stationary time series has led to its widespread application to numerous forecasting problems with reported improved performance. For example, Herrera et al. (2019) found superior performance of ANNs and Random Forests compared to statistical methods for long-term energy commodities (Herrera et al., 2019).

Among machine learning methods, LSTMs are of increasing importance owing to their ability to learn long-term dependencies within time series data. LSTMs are a type of Recurrent Neural Network (RNN), which are an artificial neural network containing at least one feedback connection, allowing learning of temporal patterns. As an advancement on standard RNNs, LSTMs use gate units to update their internal network state (Hochreiter and Schmidhuber, 1997). These gate units enable LSTM cells to regulate the inward and outward flow of information, reducing the likelihood of exploding and vanishing gradients that

hinder long-term time series analyses. Ultimately, these gates prevent the network from only remembering information from recent time steps. This makes them particularly suited to time series predictions and has led to their increased implementation in price forecasting fields. Notably, Li and Bastos (2020) found them to be the most commonly applied deep learning algorithm to stock market forecasting (Li and Bastos, 2020).

In this work, LSTMs ability to learn features from the entire dataset was exploited. This allows for long-running trends spanning the entire time series to be utilised in the price projections. Recent applications of LSTMs in price forecasting fields have been focused on enhancing model accuracy using feature extraction methodologies, such as combining them with Convolution Neural Networks (CNNs), or the use of decomposition methods. These feature extraction methods aim to reduce the burden on the LSTM units to both extract features and learn the feature trajectories.

In gold price forecasting, Livieris et al. (2020) incorporated CNN layers prior to LSTM layers, to aid the LSTMs' performance (Livieris et al., 2020). The CNN was used to identify spatial information in the time series and was found to enhance forecasting performance compared with LSTMs in isolation. However, within the context of TEA price projections, a disadvantage of this approach is that the models are then limited to extracting features at the size of the kernel window used by the CNN, which may not be as relevant for long-term forecasting problems. The selection of the kernel window size incorporates user bias and may prevent the exploitation of long-running trends within the historic time series that are relevant across the required 20 to 25 year horizon for TEA price projections.

Decomposition-based models aim to reduce the burden on the LSTM layers to learn features, by first extracting different frequency components as independent inputs to the learning algorithm. These predictions are then recombined to produce the forecast. Decomposition methods include, empirical mode decomposition (EMD), Fourier decomposition, wavelet transforms, and variable mode decomposition (VMD) (Liu et al., 2020). Improved accuracy has been observed through these methods, for example, Wu et al. (2019) utilised an ensemble EMD approach to decompose the time series of crude oil, with improved performance over benchmark ML model's and other decomposition and ML algorithm pairings. More recently, improvements have been observed using VMD. In the study by Niu et al. (2022), VMD was used to decompose the carbon price series and extreme learning machine models were used to forecast the prices, with results showing improved performance over both statistical and other ML approaches. Similarly, in metal price forecasting, Liu et al. (2020) found improved performance by combining VMD with an LSTM network. A limitation of these methods as a means of producing price projections for TEAs, is that all frequencies are treated separately. This prevents the ML algorithm from learning frequency interdependencies that could be attributed to global market trends, which are of greater importance within the context of a 20 to 25 year price projection.

3. Methodology

The proposed methodology was implemented in MATLAB R2019a. The code used to produce the price projections can be found in the Supplemental Information, Section S2. A simplified block flow diagram of the method is presented in Fig. 1. Each dataset was standardised by subtracting the dataset's mean and dividing by its standard deviation during pre-processing. This procedure re-scales each time series to have a mean of 0 and a standard deviation of 1, bringing the datasets to a common scale. The time series was then split into training and validation sets. The training sets were used to train LSTM neural network models using both the historic commodity price data and historic Brent crude oil prices as inputs. An ensemble of 100 LSTM neural network models were trained using a random number of hidden units below a selected maximum, creating a distribution of price projections for assessment against the validation set. Annual 5th, 25th, 50th, 75th and 95th price percentiles were calculated from the projected ensemble across each year and used to select the optimal hyper-parameters for each commodity. The optimised hyper-parameters were then used to project prices across the 26-year horizon. Finally, the price projections were processed for use in the techno-economic, sensitivity, and uncertainty analyses.

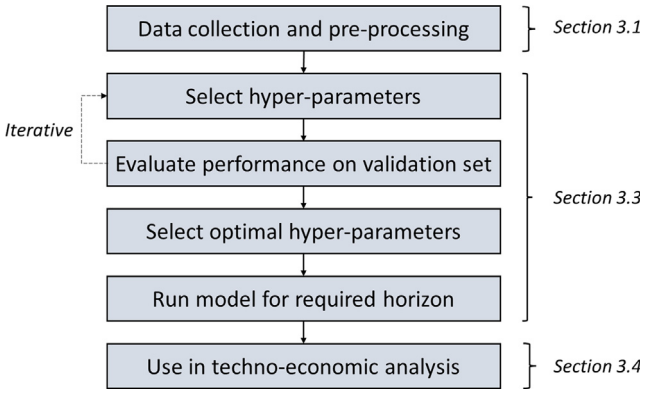

Fig. 1. Simplified block flow diagram of the proposed method. The selection and evaluation of hyper-parameters is an iterative process, whereby the process is repeated using different hyper-parameter combinations until no appreciable improvement in model performance is attained. The section numbers correspond to the methodology sections where more detail is provided.

Table 1
Data sources for the commodity prices used to demonstrate the price projection method.

Commodity	Country	Unit	Range used	Source
Brent crude oil	Europe	$/MMBTU	Jan09 - Dec46	EIA (2021, 2022)
Isopropanol	China	$/tonne	Jan09 - Dec20	Intratec (2020)
Acetone	China	$/tonne	Jan09 - Dec20	Intratec (2020)
Butadiene	China	$/tonne	Jan09 - Dec20	Intratec (2020)
Ethanol	US	$/gal	Jan09 - Dec20	Markets Insider (2021)
Butane	US	$/MMBTU	Jan09 - Dec20	EIA (2021)

3.1. Data collection

The time series price datasets and sources used are presented in Table 1. Historic Brent crude oil prices and commodity prices were used as model inputs from 2009 to 2021, including the EIA's Brent crude oil price projections from 2021 to 2046. Long-term price projections were generated for isopropanol, acetone, butadiene, ethanol, and butane; all considered within previous TEA studies (Rodgers et al., 2021, 2022). Pricing data for ethanol was sourced from a publicly available database (Markets Insider, 2021). Butadiene, isopropanol, and acetone were taken from the Intratec database (Intratec, 2020).

Fig. 2 presents the standardised historic price data for crude oil and the commodities being projected. The EIA's long-term crude oil price projection from the most recent Annual Energy Outlook is also presented (EIA, 2021, 2022), to illustrate the crude oil prices used in the 20 to 25 year projections. The historic price data for all commodities demonstrate the same underlying trend, indicating that crude oil has aligned deterministic trends. Validating this, the Pearson correlation coefficient between crude oil and each commodity was calculated and is presented in Table 2. The Pearson correlation coefficient is a measure of the strength of the association between two continuous variables, a value of −1 or 1 shows a perfect negative or positive correlation. In this case, all five commodity prices demonstrated a strong to moderate positive Pearson correlation.

The EIA's crude oil projection acts as a proxy for future trends in world energy markets and thereby commodity prices. Its inclusion adds information to the price projections regarding economic factors,

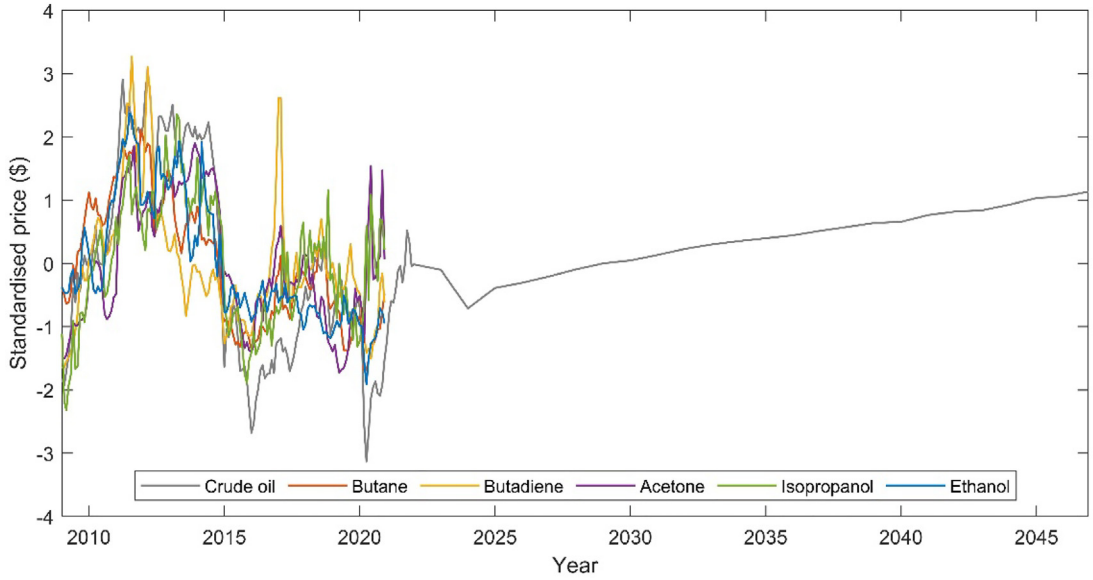

Fig. 2. Standardised historic price data for crude oil and commodity prices subject to projection. The historic commodity price data is for Jan09 - Dec20. The EIA's crude oil price projection is included for Jan21 - Dec46.

Table 2
Pearson correlation coefficients between crude oil and the commodity prices for the time period Jan09 - Dec20. All commodities display a strong to moderate positive Pearson correlation.

Commodity	Pearson correlation coefficient (Jan09 - Dec20)
Isopropanol	0.74
Acetone	0.71
Butadiene	0.61
Ethanol	0.86
Butane	0.88

resource availability, global energy markets, and technological developments (EIA, 2019), which are not present in the historic commodity prices. However, in some instances, e.g. hydrogen pricing, it may be more appropriate to utilise the EIA's long-term projection for natural gas. The Pearson correlation coefficient can be calculated for both crude oil and natural gas and the most appropriate reference component selected. The inclusion of one of these projections is necessary to account for expected global energy market trends in the resulting price projection.

3.2. Forecasting approach

The prices were projected monthly as most commodity price data is available at this frequency and greater granularity was not required for the long-term distributions. Where historic data were more frequent, the average across the month was used. To remove user selection of the projection time step, different time steps could be trialled during the validation procedure i.e. quarterly or annually.

Different strategies can be employed to project long-term prices. These can be split broadly into three categories: the direct, recursive, and joint strategies (Taieb and Atiya, 2016). The direct approach trains independent models for each forecast horizon, whereas the recursive strategy operates iteratively as a one-step-ahead predictor using previously forecast values as inputs. The joint strategy produces one multi-output model for the specified forecast horizon. All three approaches have their shortcomings. The direct strategy assumes no statistical interdependencies between future predictions, whilst recursive models are prone to error propagation (Taieb et al., 2012). In turn, joint strategies constrain all horizons for use within one global model (Taieb et al., 2009). A hybrid direct, recursive, and joint forecasting strategy was implemented owing to better-reported performance than single output methods (Taieb et al., 2012, 2010; Taieb and Atiya, 2016). The adopted approach trains on the entire historic dataset to reconstruct the historic data and predict 12 time steps into the future (joint). After model training, a new model is trained (direct) using the historic data plus the previously predicted 12 time steps (recursive), and so forth. The historic data therefore increases by 12 time steps after each model training. The approach is illustrated in Fig. 3. The use of 12 time steps was selected as a compromise between accuracy and compounding errors. Longer horizons reduce accuracy, as each model must project further into the future. Conversely, a shorter horizon requires the training of more models to predict the required projection horizon which exacerbates error propagation, given the greater number of predicted data points used in each subsequent model training. In addition, 12 time steps represents annual projections, the required frequency appropriate as input to a TEA. If desired, the optimal number of time steps could be investigated as part of the validation procedure.

3.3. Machine learning

The datasets were split into training and validation sets based on the ratio between the historic data (12 years, 30%) and projection horizon (26 years, 70%) required for the TEA. This ensured that the performance of the model prediction during validation was representative of the performance during the final projections. The projection horizon for this work was 26 years, thereby allowing direct comparison to previous TEAs studies (Rodgers et al., 2021, 2022). Henceforth, prediction is used to mean the model output over the validation period (2012 to 2021) and projection is used to mean the model output for the projection horizon (2021 to 2046). As only 12 years of historic data were available for each commodity, translating to 30% of the final projection horizon, a training and validation split of 30% and 70% was necessary to obtain representative hyper-parameters. A test set was not employed due to the limitations in dataset size. As no test set was used, the ability of the model to generalise was assessed based on the performance against the validation set. The accuracy of the final price projections (2021 to 2046) cannot be assessed given true prices are not available.

The network architecture is presented in Fig. 4 and consists of a fully connected layer and a LSTM layer. The fully connected layer contains

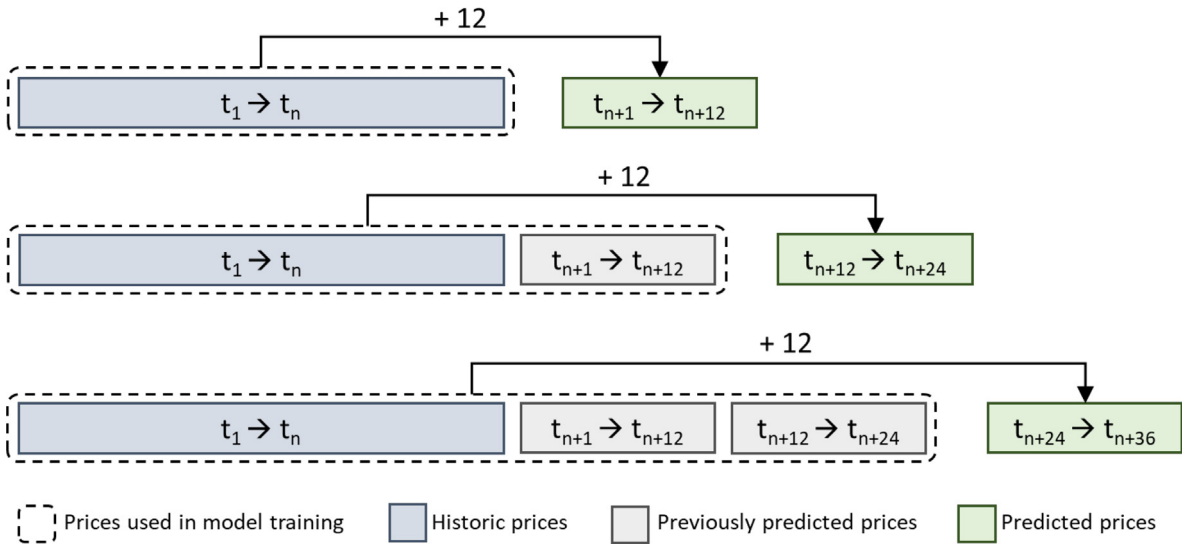

Fig. 3. The model forecasting approach. Each model is trained to reconstruct the historic time series and predict 12 time steps into the future. The predicted time steps are added to the historic dataset and used as inputs to train the subsequent model. The dataset increases by 12 time steps after each model training. Note that actual crude oil prices and the EIA's projections are used as model inputs at each time step, i.e. it is only the commodity price being projected that uses predictions as model inputs.

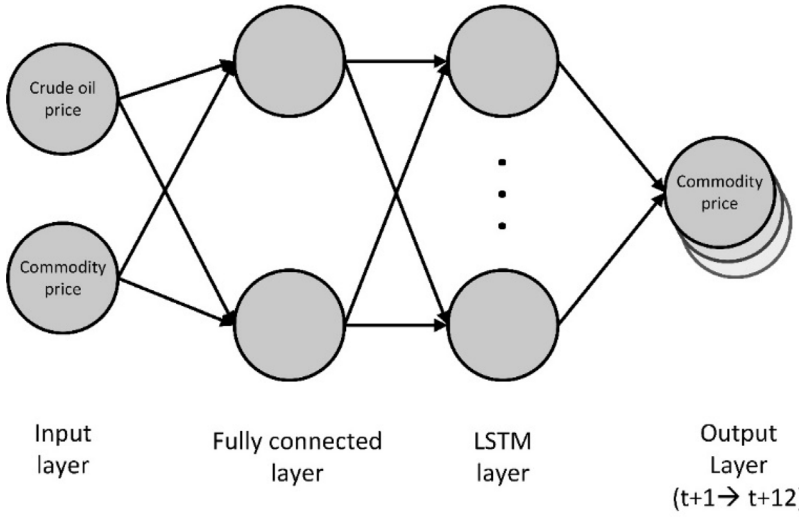

Fig. 4. Model structure for commodity price projections. The input layer consisted of the historic and projected Brent crude oil prices from the EIA and the historic dataset for the commodity being projected. The prices are fed into a fully connected layer containing two neurons, followed by an LSTM layer. The number of LSTM hidden units is optimised as part of the validation procedure. The output layer consists of the future price predictions for 12 time steps into the future.

two neurons, creating new feature combinations to feed into the LSTM layer. If desired, the optimal number of neurons in the fully connected layer could be determined during the validation procedure. This layer facilitates the use of any interdependencies present between the crude oil and commodity price being projected by the network. The size of the LSTM layer was determined through the validation procedure for each commodity.

During each model training, the networks were trained using the entire historic dataset allowing the learning of patterns across the whole time series. Preventing concerns with exploding and vanishing gradients, the models were trained to produce an output at each time step and a gradient threshold of 1 was implemented (Brownlee, 2017). An ensemble of 100 ML models was trained using a randomly assigned number of hidden units below a maximum selected during the grid search. This ensemble of models, each trained to reproduce the entire historic time series, facilitates the exploitation of different underlying trends embedded within the historic time series, producing a distribution of potential futures.

Each model was trained to reduce the mean squared error between the training data and the model predictions using the Adam optimisation algorithm (Mathworks, 2018). As depicted in Fig. 3, the models were trained recursively whereby, after each model was trained, the newly projected prices were used as inputs to train the next model. Therefore, the historic price dataset increased by 12 time steps after each iteration of the model training.

A grid search of optimal hyper-parameter combinations was undertaken to evaluate the probabilistic forecast performance over the validation set. The Continuous Rank Probability Score (CRPS) (Eq. (1)) was used to evaluate the performance where; F is the forecast, y is the prediction, and x is the actual value (observation).

$$CRPS(F,x) = \int_{-\infty}^{\infty} (F(y) - 1(y-x))^2 \, dy \tag{1}$$

CRPS is a generalisation of the mean absolute error for application in probabilistic forecasting. It is a proper scoring rule that encompasses both sharpness and calibration (Gneiting and Katzfuss, 2014). Sharpness refers to the variance of the forecast, i.e. the sharper the forecast

Table 3
Method to implement the projected price distribution in a techno-economic analysis.

TEA parameter	Percentiles required	Methodology
Nominal NPV	50th	Use as price to calculate nominal NPV.
Sensitivity analysis	5th and 95th	Use to represent lower and upper bounds for prices.
Uncertainty analysis	5th, 25th, 50th, 75th and 95th	Run 25% of simulations between each percentile, uniformly distributing data within each percentile.
Primary product MSP	5th, 25th, 50th, 75th and 95th	Use to contextualise the MSP calculated for the process.

the narrower the projected distribution. Calibration is the accuracy of the estimates, it reflects the consistency between the predictions and observations.

The learning rate, number of epochs, and maximum number of hidden units in the LSTM layer were optimised during the grid search. The unique nature of each time series required different hyper-parameter combinations for each commodity. Once the optimised hyper-parameters were selected, the final models were trained on the combined training and validation sets to project the prices for the 26-year horizon.

3.4. Techno-economic analysis implementation

The annual 5th, 25th, 50th, 75th and 95th percentiles were calculated from the 100 monthly ensemble projections (12 × 100). Table 3 outlines how the calculated percentiles should be implemented into techno-economic, sensitivity, and uncertainty analyses, noting that more percentiles could be calculated from the projected distribution if desired. NPV is selected as the profitability indicator to illustrate this method. However, in cases where the discounted rate of return is unknown, Internal Rate of Return could be calculated using the same price projections. The only difference to the methodology presented in Table 3 would be that the objective function is the Internal Rate of Return rather than NPV.

When computing the process' MSP, the price projection is used to contextualise the economic outcome rather than being implemented into the investment analysis. TEAs are read by a broad range of audiences including funding agencies, policy makers, and research and development experts. These audiences will likely have varying knowledge and awareness of future product prices. Without some way of contextualising the MSP the result is less meaningful, allowing for easy misinterpretation of future market competitiveness.

Importantly, price projection procedures should be applied to all commodity chemicals consumed in a process (Manca, 2012). This is of particular importance when a process is upgrading a commodity chemical, where the variability in the feedstock price (i.e. the commodity chemical being upgraded) will have as much impact as the product selling price. Contrastingly, whilst other costs are also subject to variability over a plant's lifetime, e.g. operating labour, maintenance, rent of land etc., their impact is less pronounced, and these variables are subjected to annual inflation within a TEA. Countries have their own inflation targets, therefore the use of this uniformly applied inflation rate is more appropriate than projecting how this might change over a plant's life.

4. Results and discussion

Table 4 presents the optimised hyper-parameters used for each commodity price projection. These values can be used to inform other practitioners of typical ranges to evaluate for similar commodity price projections.

Table 4
Optimised hyper-parameters obtained during the grid search. Hyper-parameters were selected to reduce the CRPS on the validation set during model training.

Commodity	Optimised hyper-parameters		
	LSTM units	Epochs	Learning rate
Isopropanol	1	500	0.1
Acetone	3	200	0.01
Butadiene	2	100	0.01
Ethanol	15	500	0.0001
Butane	3	100	0.00001

4.1. Model validation

As the true prices for the projection horizon (2021 to 2046) are unknown, the accuracy of the model was confirmed through the performance of the optimised model on the validation set. During the validation procedure the models were trained on the commodity's historic data from 2009 to 2012 (30%) to produce predictions from 2012 to 2021 (70%). Historic crude oil prices were used as model inputs for the entire time series. Fig. 5 presents the model predictions overlaid onto the actual prices for the validation set. The percentiles are annualised, representing the 12 × 100 ensemble predictions required to produce the distribution as inputs to a TEA. The CRPS for each commodity was calculated using the non-standardised data. This was standardised by dividing the CRPS by the standard deviation of the commodity dataset to bring the errors to a relative scale. The standardised CRPS is presented in the corresponding figure captions.

The predictions were able to effectively capture the observed trend in market prices for all commodities, illustrating the method's applicability to any commodity's price time series. The underlying price trend was comparable for all commodities (Fig. 2), suggesting that the model's ability to track the observed trend during the validation procedure was attributable to the inclusion of crude oil prices as a model input.

The validation set for butadiene had the poorest performance, producing the highest CRPS. This is unsurprising as butadiene produced the lowest Pearson correlation coefficient with crude oil (Table 2). Neither the decrease in prices observed after 2012 nor the spike around 2017 was captured by the prediction over the validation set. This suggests that these events and the volatility within butadiene's historic pricing were due to external factors, outside of those captured either historically or observed by crude oil. Butadiene has historically been produced via steam cracking of naphtha, a derivative of crude oil. Recent technological advances in shale gas extraction have shifted crackers to the use of this lighter feedstock, leading to volatility in butadiene supply and demand (Angelici et al., 2013). The volatility observed here is likely an artefact of these changing market dynamics.

4.2. Commodity price projections

Fig. 6 presents the probabilistic price projections for the five commodities. The plotted annual percentiles are representative of the 12 × 100 projections from the 100 ML models. The upward trajectory presented in all commodity projections is owed to the EIA's price projection for crude oil. The probability band is a product of the different model projections trained on the observed time series. Notably, the price distributions vary appreciably between commodities. This suggests that the commonly adopted heuristic of accounting for price variability across the plant life using a uniformly applied percentage is unsatisfactory. Currently adopted approaches are clearly unrepresentative of a commodity's actual price uncertainty, emphasising the need for price projection methods that can exploit the underlying determinism and stochastic variability to produce unbiased projections.

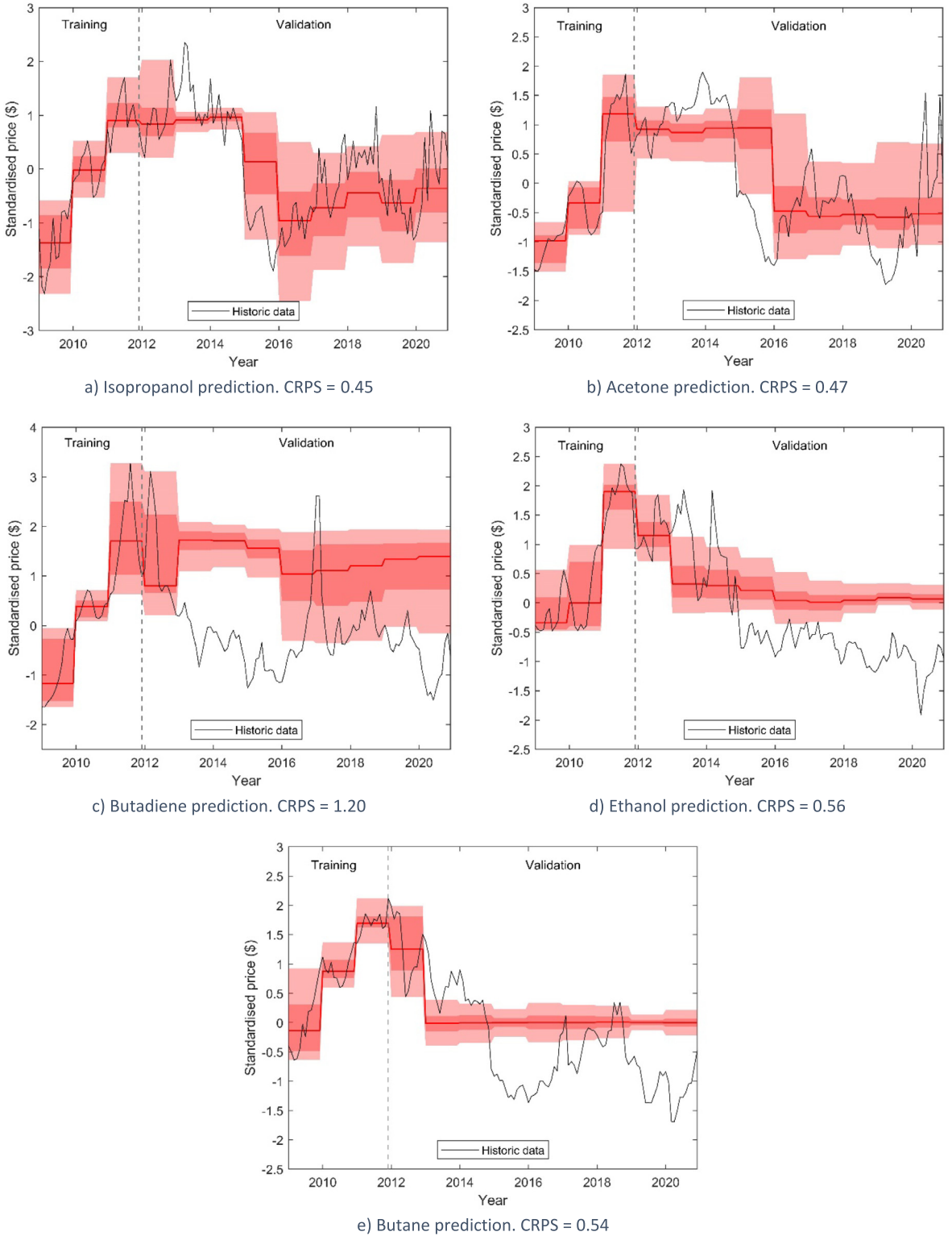

Fig. 5. a–e: Probabilistic predictions over the validation period for the five commodity prices. The historic commodity and crude oil prices were used as model inputs. The models were trained on the commodity's historic data from 2009 to 2012 (30%) to produce predictions from 2012 to 2021 (70%). Historic crude oil prices were used as model inputs over the entire training and validation set. Black lines represent the historic data for each commodity from the sources listed in Table 1. The red line represents the annualised median projection percentile (50th percentile). The darker shaded region bounds the annualised 25th and 75th percentile as determined from the 100 ML models. The lighter shaded region bounds the annualised 5th and 95th percentile as determined from the 100 ML models. Vertical dashed lines represent the end of the training dataset and the start of the validation set. The y-axis shows the standardised price data.

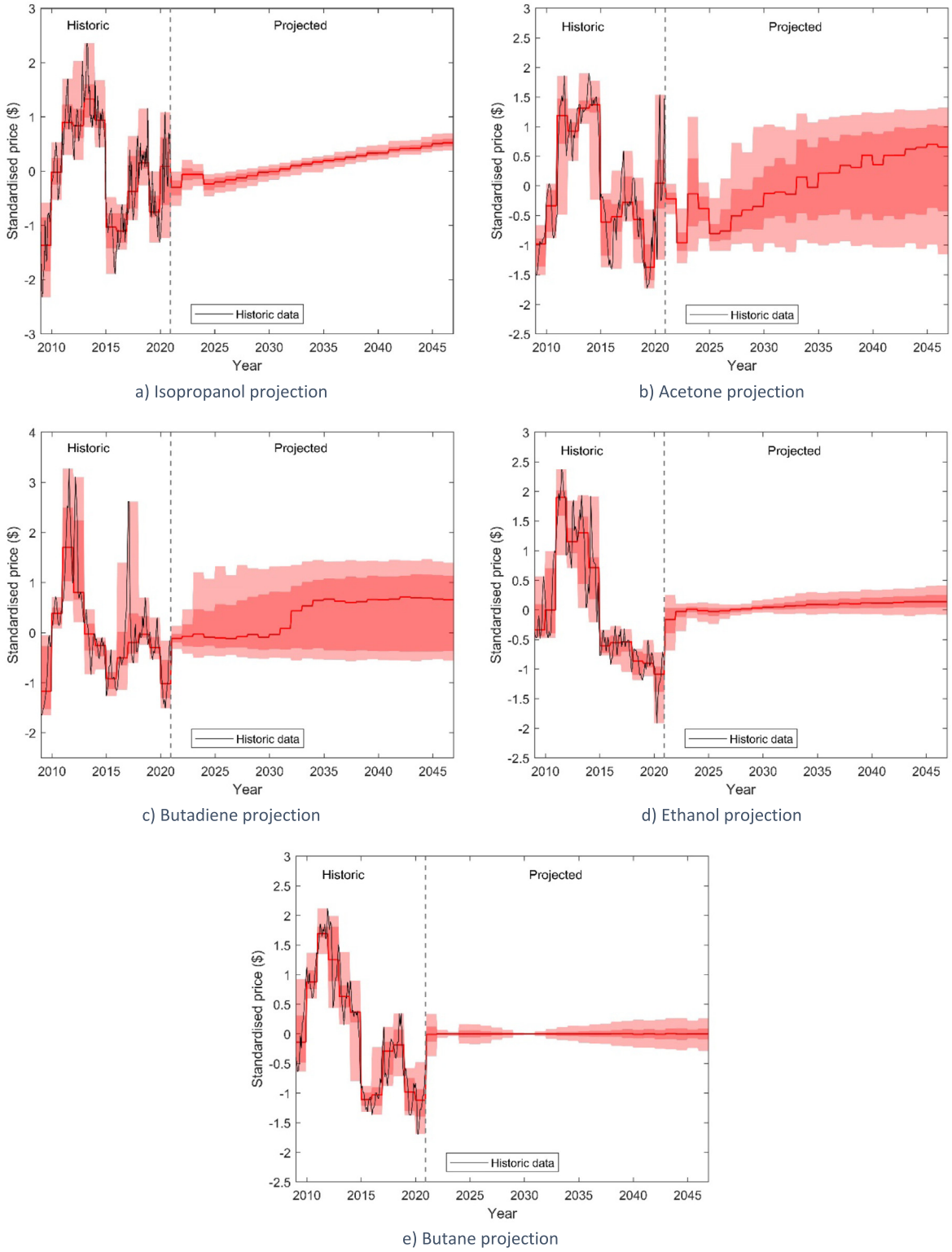

Fig. 6. a–e: Probabilistic projections using the EIA's crude oil projection and historic prices as model inputs. Black lines represent the historic data for each commodity from the sources listed in Table 1. The red line represents the annualised median projection percentile (50th percentile). The darker shaded region bounds the annualised 25th and 75th percentiles and the lighter shaded region bounds the annualised 5th and 95th percentiles calculated from the 100 ML models. Vertical dashed lines represent the end of historic dataset and the start of the projection time window. The y-axis shows the standardised price data.

4.3. Impact of EIA projections for crude oil

The ability of the models to track the observed trend during the validation procedure and the upward trajectory predicted for the long-term projections is attributable to the inclusion of crude oil. Validating this, isopropanol prices were projected based solely on historic prices. This model had no fully connected layer as the network contained only one model input. The new network architecture and model inputs necessitated a different optimal hyper-parameter set. A grid search was undertaken as outlined previously. The optimal hyper-parameters were,

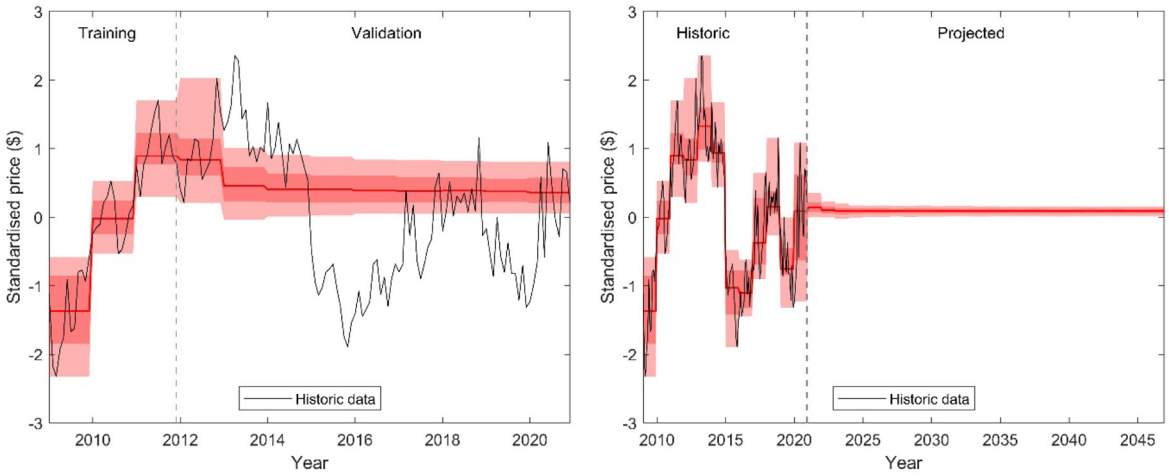

a) Isopropanol prediction, excluding crude oil. CRPS = 0.72 b) Isopropanol projection, excluding crude oil

Fig. 7. a–b: Probabilistic prediction and projection for isopropanol using only historic prices as a model input, excluding crude oil. (a) the validation set prediction and (b) the long-term projection. Black lines represent the historic data, the red line represents the annualised median price (50th percentile). The darker shaded region bounds the annualised 25th and 75th percentiles and the lighter shaded region bounds the annualised 5th and 95th percentiles calculated from the 100 ML models. Vertical dashed lines represent the end of the validation set in (a) and historic data in (b). The *y*-axis shows the standardised price data.

5 LSTM units, 200 epochs, and a learning rate of 0.001. The resulting model prediction for the validation set and projection for the long-term projection horizon are presented in Fig. 7. Excluding crude oil, the validation prediction and long-term price projection clearly illustrate different results from those including crude oil (Figs. 5a and 6a).

Without crude oil as a model input, the validation prediction produced a higher CRPS (0.45 including crude oil vs 0.72 excluding crude oil) and was unable to track the observed trend, suggesting that the drivers behind this trend are external to isopropanol's historic time series (Fig. 7a). The long-term projection shows no upward trajectory, indicating that this was also due to use of the EIA's crude oil projection (Fig. 7b). These disparate results reveal that using crude oil as a model input provides additional information not embedded in the historic commodity price data. Over the validation set, the EIA's projection provides real trends that were observed by crude oil during the historic time period and for the long-term projection, it provides crude oil pricing projections. Whilst the EIA's long-term projection may not be accurate into the future, it acts as a proxy for predicted trends in global energy markets, important when considering emerging process technologies and otherwise unavailable to TEA practitioners.

4.4. Projection comparisons and impact on economics

The proposed method produces different price distributions for each year of the projection horizon. The different yearly predictions mean the projections are not directly comparable to the author's previous RBFNN projections which produced only a long term average price for the entire projection horizon. Nevertheless, the nominal price predicted using the ensemble projections (50th percentile) was, on average, higher than the RBFNN projections (Supplementary Information Tables S.1–5). This is attributable to the inclusion of the crude oil projection which gradually increases over the projection horizon. The ensemble projections illustrate different percentage variability for the lower and upper bounds between commodities. This suggests that the uniformly applied ±20% heuristic in the RBFNN method, or arbitrary percentages commonly applied in other TEAs, are unsatisfactory for representing a commodity's actual price variability. Furthermore, the ±20% heuristic applied in the RBFNN method has a uniform distribution, whereas the ensemble projections implicitly produce a dynamic distribution informed by the input data.

The purpose of the produced projections is for use within TEAs to assess a technology's economic feasibility. To illustrate this, the results of two previously undertaken TEAs are recalculated using the new price projections. Previously, the two TEAs used pricing projections obtained from an RBFNN's nominal prediction with a uniformly applied uncertainty distribution of ±20%. The two processes evaluated were an aerobic gas fermentation process producing isopropanol and acetone from gasified black liquor (Rodgers et al., 2021), and a hybrid bio/chemo catalytic process catalytically upgrading an acetaldehyde gas fermentation product to butadiene (Rodgers et al., 2022). The newly projected median price (50th percentile) for each plant year from the ensemble projection was used to calculate the nominal NPV. In addition, the uncertainty analyses were re-run using 2000 simulations for both the previous RBFNN and new ensemble price projections. The results between the previously calculated and new techno-economic outcomes are compared in Table 5, with the Monte Carlo simulation uncertainty analyses illustrated in Fig. 8.

Table 5
Comparative NPV results for the RBFNN (Rodgers et al., 2021, 2022) and the ensemble projections. The RBFNN projection uses the previously projected price using RBFNNs and a ±20% uniform distribution in the Monte Carlo simulation. The ensemble projection uses the 50th percentile for each year as the nominal price and the 5th and 95th percentiles as the lower and upper bounds, while distributing 25% of the simulations uniformly between the 25th, 50th, and 75th ranges.

Study	Nominal NPV (millions)		NPV 70% probability window (millions)	
	RBFNN	Ensemble	RBFNN	Ensemble
Aerobic gas fermentation producing isopropanol and acetone	$42	$54	$35–$95	$45–$80
Renewable butadiene production via aerobic fermentation and catalytic upgrading	$2.8	$19	−$45–$65	−$35–$80

Owing to the higher nominal price and upward trajectory of the ensemble projections (Tables S.1–5), higher nominal NPVs were produced for both TEAs. Notably, the 70% probability window for the NPV for each process also changed (Table 5). For both processes, a two-tailed t-test assuming equal variance was conducted for the NPV Monte Carlo populations. A statistically significant difference (p value $\ll 0.05$) was found between the two populations for the isopropanol and acetone process using the RBFNN projections (mean = $43 million, standard deviation = $18 million) and ensemble projections (mean=

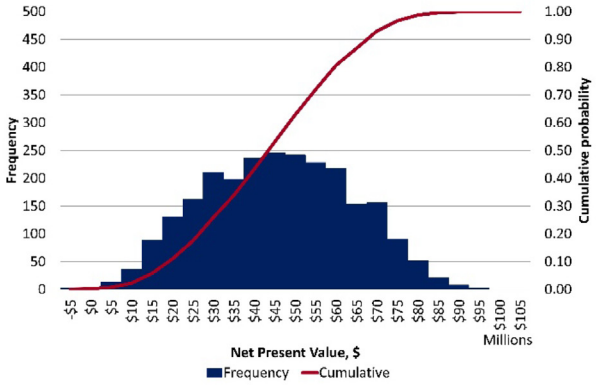

ai) RBFNN projection for aerobic gas fermentation producing isopropanol and acetone

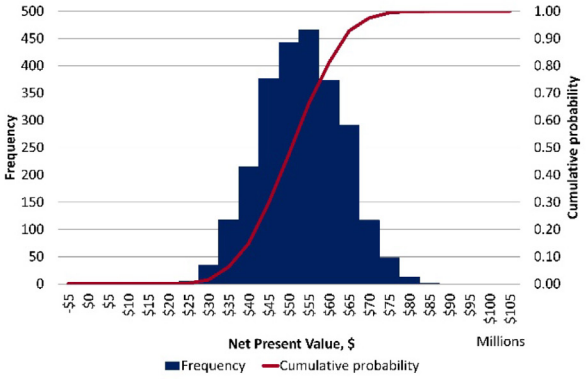

aii) Ensemble projection for aerobic gas fermentation producing isopropanol and acetone

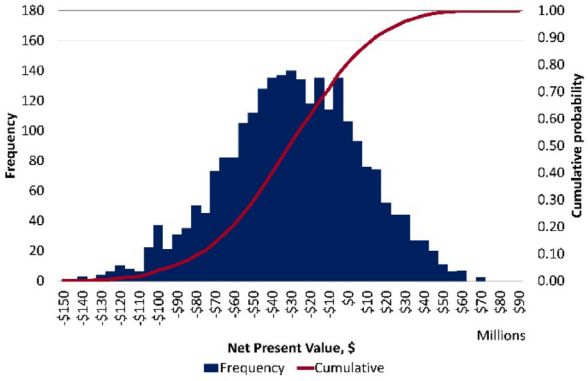

bi) RBFNN projection for renewable butadiene production via aerobic fermentation and catalytic upgrading

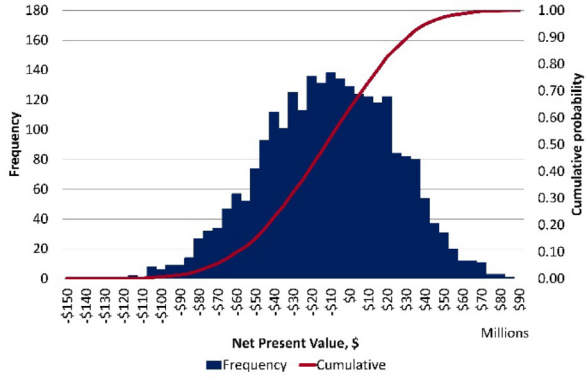

bii) Ensemble projection for renewable butadiene production via aerobic fermentation and catalytic upgrading

Fig. 8. a–b: Comparative Monte Carlo simulations. The left graphs were simulated using the RBFNN projection for the long-term average price and a ±20% uniform price distribution. The right graphs correspond to distributing 25% of the simulations uniformly between the 5th, 25th, 50th, 75th and 95th percentiles from the ensemble projection.

$51 million, standard deviation = $10 million). Equally, the difference in the two populations for the renewable butadiene process using the previous RBFNN projections (mean = −$31 million, standard deviation = $36 million) and ensemble projections (mean = −$13 million, standard deviation = $35 million) was also statistically significant (p value $\ll 0.05$). Avoiding erroneous investment decision-making during technology evaluations, these results highlight the significant impact that price and distribution selection have on the outcome of early-stage TEAs, reinforcing the requirement for unbiased probabilistic price projection procedures.

4.5. Challenges with long-term projections

Non-linear long-term forecasts are able to use extracted deterministic trends and stochastic variability from historical data and predict how the price may change into the future. However, models cannot account for unexpected, abrupt changes to the status quo that introduce novel determinism and stochastic variability as drivers of a commodity's future price. This is highlighted in the EIA's projections, whose Annual Energy Outlook is renewed annually (EIA, 2022). A retrospective analysis is produced every two years, where the EIA's projections are compared to recent history. A study based on these projections and retrospectives by Sherwin et al. (2018) demonstrated that both the unpredictability and volatility of the US energy system have increased markedly in the past decade compared to the two preceding decades. This was partially attributed to the large increase in domestic oil and gas production since 2007, the financial crisis of 2008 and resulting recession, de-industrialisation, and increased energy demand. Sherwin et al. (2018) highlight that the actual cause is most likely several interlinked, unanticipated developments. More recent examples of unexpected external factors are the impact of the Covid-19 pandemic (Bourghelle et al., 2021), and sanctions on Russian oil imports (Khan and Kelly, 2022). It is improbable to foresee these unexpected external disturbances or to predict sudden technological advances such as emerging renewable technologies. This remains a major challenge with producing long-term projections in many areas. Within the context of TEAs, a way to ensure a technology assessment's longevity and relevance in the context of future prices is to concurrently compute the process' MSP. Importantly, this result needs presenting alongside today's expectations of future market prices, thereby providing a contextualised result to funding agencies, policy makers, and research and development experts.

5. Conclusions and future work

This work presents a methodology for producing long-term price distribution projections for use in TEAs and their subsequent sensitivity and uncertainty analyses. TEAs require probabilistic 20 to 25 year price projections into the future, where true prices are unavailable. This contrasts with traditional price forecasting problems where forecast horizons are much shorter. Furthermore, the price projections for TEAs are used in investment analyses to evaluate a technology based on a capital investment sanctioned at the outset of the long-term projection. The selected price and price distributions could therefore be the difference between the deployment or redirection of capital. Unbiased price projection procedures are therefore pertinent to assess the economic feasibility of new technologies and processes.

The presented method negates the need for heuristics during price selection procedures in TEAs. The approach uses an ensemble of 100 neural networks with LSTM layers to produce a probability distribution of potential future prices. Both the commodity's historic dataset (i.e., isopropanol, acetone, butadiene, ethanol, and butane) and the EIA's long-term crude oil price projection are used as model inputs. This simultaneously accounts for insights into future energy markets as well as deterministic trends, or stochastic variability, within an individual commodity's price data. The method was demonstrated by projecting 26 years into the future using 12 years of historic data, necessitating a training and validation split of 30% and 70% to obtain representative hyper-parameters. The approach objectively sets the nominal long-term price (50th percentile), determines the lower and upper bounds (5th and 95th percentiles), and the distribution to be applied between the lower and upper bounds (25th and 75th percentiles). As such the methodology makes the need for using heuristic uncertainty bounds obsolete.

The importance of price selection procedures in TEAs is evidenced through both the commodity price projections, and their use in reproducing two previous TEAs. The projected commodity price distributions demonstrated appreciable price variability, suggesting that pricing uncertainty considerations in TEAs should be tailored to each commodity rather than dictated through heuristics. Regarding techno-economic outcomes, the 70% probability window for the NPV distributions were changed from $35 – $95 million to $45 – $80 million for an isopropanol and acetone process, and from −$45 – $65 million to −$35 – $80 million for a hybrid bio/chemo catalytic butadiene process. A two-tailed, equal variance t-test verified a statistically significant difference between the NPV distributions.

Future work should explore the use of emerging methods in traditional forecasting fields such as, VMD and EMD decomposition methods along with the proposed ensemble LSTM approach. These methods aim to reduce the burden on the LSTM by first extracting features from the data. Model accuracy would need to be compared over the validation set, as data for the 20 to 25 year horizon is unavailable. Therefore, the method achieving the lowest CRPS across the validation set should be employed for the TEA price projections. The inclusion of historic errors from the EIA's previous long-term projections, where actual prices are now available, also represents an interesting area for further investigation. A study investigating the use of these errors to produce energy density forecasts was undertaken by Kaack et al. (2017), where the produced distributions were found to be more accurate than the EIA's scenario projections (Kaack et al., 2017). Incorporating these historic errors would add additional projection uncertainty associated with the long-term projection of world energy markets, rather than the price distribution being solely due to variability in the historic time series of the commodity being projected. It is worth noting that the absolute average percentage difference between projected and observed crude oil prices between 1994 and 2021 is 45.6%. Incorporating these errors may therefore lead to excessively large distributions, meaning investigations into their inclusion should be assessed to ensure a sufficiently sharp projection is maintained. This should be evaluated using the CRPS as the performance metric across the validation set. In addition, the TEAs explored in this work only applied product price projections, as other commodity chemicals were not used in the evaluated process. Future TEA studies should also incorporate price projections for the consumed commodity chemicals as well as product prices (Manca, 2012).

CRediT authorship contribution statement

Sarah Rodgers: Conceptualization, Data curation, Formal analysis, Investigation, Methodology, Software, Visualization, Writing – original draft, Writing – review & editing. **Alexander Bowler:** Conceptualization, Data curation, Formal analysis, Methodology, Software, Writing – review & editing. **Fanran Meng:** Conceptualization, Methodology, Supervision, Writing – review & editing. **Stephen Poulston:** Supervision, Writing – review & editing. **Jon McKechnie:** Conceptualization, Funding acquisition, Methodology, Project administration, Resources, Supervision, Writing – review & editing. **Alex Conradie:** Conceptualization, Formal analysis, Funding acquisition, Methodology, Project administration, Resources, Software, Supervision, Writing – review & editing.

Declaration of competing interest

The authors declare that they have no known competing financial interests or personal relationships that could have appeared to influence the work reported in this paper.

Data availability

The data that has been used is confidential.

Acknowledgements

This work was supported by an EPSRC DTP CASE studentship with Johnson Matthey and by Industrial Biotechnology (IB) Catalyst project ConBioChem funded by Innovate UK, BBSRC and EPSRC (grant BB/N023773/1). Furthermore, this work was supported by the Future Biomanufacturing Research Hub (grant EP/S01778X/1), funded by the Engineering and Physical Sciences Research Council (EPSRC), United Kingdom and Biotechnology and Biological Sciences Research Council (BBSRC), United Kingdom as part of UK Research and Innovation. Fanran Meng would also like to acknowledge the Alan Turing Institute Post-Doctoral Enrichment Awards (grant G117736). Finally, the authors gratefully acknowledge support received from the University of Nottingham Research Beacon of Excellence: Green Chemicals.

Appendix A. Supplementary data

Supplementary material related to this article can be found online at https://doi.org/10.1016/j.engappai.2023.106065.

References

Amigun, B., Petrie, D., Görgens, J., 2011. Economic risk assessment of advanced process technologies for bioethanol production in South Africa: Monte Carlo analysis. Renew. Energy 36 (11).

Angelici, C., Weckhuysen, B.M., Bruijnincx, P.C.A., 2013. Chemocatalytic conversion of ethanol into butadiene and other bulk chemicals. ChemSusChem 6, 1595–1614.

Barzaghi, R., Conte, A., Sepiacci, P., Manca, D., 2016. Optimal design of a styrene monomer plant under market volatility. Comput. Aided Chem. Eng. 38, 1653–1658.

Bourghelle, D., Jawadi, F., Rozin, P., 2021. Oil price volatility in the context of Covid-19. Int. Econ 167, 39–49.

Brown, T.R., Wright, M.M., 2015. A framework for defining the economic feasibility of cellulosic biofuel pathways. Biofuels 579–590.

Brownlee, J., 2017. Techniques to Handle Very Long Sequences with LSTMs [WWW Document]. URL https://machinelearningmastery.com/handle-long-sequences-long-short-term-memory-recurrent-neural-networks/. (accessed 1.14.22).

Bukhari, A.H., et al., 2020. Fractional neuro-sequential ARFIMA-LSTM for financial market forecasting. IEEE Access 8, 71326–71338.

Campbell, R.M., Anderson, N.M., Daugaard, D.E., Naughton, H.T., 2018. Financial viability of biofuel and biochar production from forest biomass in the face of market price volatility and uncertainty. Appl. Energy 230, 330–343.

Cheali, P., Gernaey, K.V., Sin, G., 2014. Toward a computer-aided synthesis and design of biorefinery networks: Data collection and management using a generic modeling approach. ACS Sustain. Chem. Eng. 2, 19–29. http://dx.doi.org/10.1021/sc400179f.

Diniz, A.P.M.M., Sargeant, R., Millar, G.J., 2018. Stochastic techno-economic analysis of the production of aviation biofuel from oilseeds. Biotechnol. Biofuels 11, 1–15.

EIA, 2019. The National Energy Modeling System: An Overview 2018. Washington DC.

EIA, ., 2021. Hydrocarbon gas liquids explained prices for hydrocarbon gas liquids [www document]. URL https://www.eia.gov/energyexplained/hydrocarbon-gas-liquids/prices-for-hydrocarbon-gas-liquids.php (accessed 6.10.21).

EIA, ., 2022. Annual Energy Outlook 2022 with Projections to 2050: Narrative. Washington DC.

Gneiting, T., Katzfuss, M., 2014. Probabilistic forecasting. Annu. Rev. Stat. Appl. 1, 125–151.

Gutierrez, J.P., Erdmann, E., Davide, M., 2019. Optimal design of a carbon dioxide separation process with market uncertainty and waste reduction. Processes 7 (6).

Herrera, G.P., et al., 2019. Long-term forecast of energy commodities price using machine learning. Energy 179, 214–221.
Hochreiter, S., Schmidhuber, J., 1997. Long short-term memory. Neural Comput. 9, 1735–1780.
Hubbard, D.E., 2018. Chemical pricing information for student design projects and cost engineering: Challenges and opportunities. In: ASEE Annual Conference and Exposition. Salt Lake City, Utah.
Intratec, 2020. Petrochemical prices [www document]. URL https://www.intratec.us/products/commodities-prices/petrochemicals-prices (accessed 6.1.20).
Ioannou, A., Angus, A., Brennan, F., 2018. Effect of electricity market price uncertainty modelling on the profitability assessment of offshore wind energy through an integrated lifecycle techno-economic model. J. Phys. Conf. Ser..
Kaack, L.H., Apt, J., Morgan, M.G., McSharry, P., 2017. Empirical prediction intervals improve energy forecasting. Proc. Natl. Acad. Sci. 144 (33), 8752–8757.
Khan, S., Kelly, S., 2022. Oil prices hit 14-year highs on Russia oil ban talks, Iran deal delay [www document]. Reuters URL https://www.reuters.com/business/energy/oil-spikes-2008-highs-us-europe-mull-russian-oil-import-ban-iran-delay-2022-03-07/ (accessed 3.15.22).
Lago, J., De Ridder, F., De Schutter, B., 2018. Forecasting spot electricity prices: Deep learning approaches and empirical comparison of traditional algorithms. Appl. Energy 221, 386–405.
Langhorst, T., McCord, S., Zimmermann, A., Müller, L., Cremonese, L., Strunge, T., Wang, Y., Zaragoza, A.V., Wunderlich, J., Marxen, A., Armstrong, K., Buchner, G., Kätelhön, A., Bachmann, M., Sternberg, A., Michailos, S., Naims, H., Winter, B., Roskosch, D., Faber, G., Mangin, C., Olfe-Kräutlein, B., Styring, P., Schomäcker, R., Bardow, A., Sick, V., 2022. Techno-economic assessment & life cycle assessment guidelines for CO2 utilization (version 2.0).
Li, A.W., Bastos, G.S., 2020. Stock market forecasting using deep learning and technical analysis: A systematic review. IEEE Access 8.
Liang, C., Wei, Y., Zhang, Y., 2020. Is implied volatility more informative for forecasting realized volatility: An international perspective. J. Forecast..
Liu, Y., Yang, C., Huang, K., Gui, W., 2020. Non-ferrous metals price forecasting based on variational mode decomposition and LSTM network. Knowl.-Based Syst. 188.
Liu, Y., et al., 2022. A systematic procurement supply chain optimization technique based on industrial internet of thing and application. IEEE Internet Things J..
Livieris, I.E., Pintelas, E., Pintelas, P., 2020. A CNN–LSTM model for gold price time-series forecasting. Neural Comput. Appl. 32, 17351–17360.
Manca, D., 2012. A methodology to forecast the price of commodities. Comput. Aided Chem. Eng. 1306–1310.
Manca, D., Fini, A., Oliosi, M., 2011. Dynamic conceptual design under market uncertainty and price volatility. Comput. Aided Chem. Eng. 336–340.
Markets Insider, 2021. Ethanol commodity [www document]. URL https://markets.businessinsider.com/commodities/ethanol-price (accessed 11.1.21).
Mathworks, 2018. TrainingOptionsADAM [www document]. URL https://uk.mathworks.com/help/deeplearning/ref/nnet.cnn.trainingoptionsadam.html (accessed 10.10.21).
McGarvey, E., Tyner, W.E., 2018. A stochastic techno-economic analysis of the catalytic hydrothermolysis aviation biofuel technology. Biofuels, Bioprod. Biorefin. 12 (3), 474–484.
Moncada, J., Gursel, I.V., Worrell, E., Ramírez, A., 2018. Production of 1, 3-butadiene and ε-caprolactam from C6 sugars: Techno-economic analysis. Biofuels Bioprod. Biorefining 12, 600–623.
Nguyen, N., Tyner, W.E., 2021. Assessment of the feasibility of the production of alternative jet fuel and diesel using catalytic hydrothermolysis technology: a stochastic techno-economic analysis. Biofuels, Bioprod. Biorefin. 16 (1), 91–104.
Niu, X., Wang, J., Zhang, L., 2022. Carbon price forecasting system based on error correction and divide-conquer strategies. Appl. Soft Comput. 118.
Puig-Gamero, M., et al., 2021. Impact of the forecast price on economic results for methanol production from olive waste. Fuel 295.
Rodgers, S., Conradie, A., King, R., Poulston, S., Hayes, M., Bommareddy, R.R., Meng, F., McKechnie, J., 2021. Reconciling the sustainable manufacturing of commodity chemicals with feasible technoeconomic outcomes. Johnson Matthey Technol. Rev. 37, 5–394.
Rodgers, S., Meng, F., Poulston, S., Conradie, A., McKechnie, J., 2022. Renewable butadiene: A case for hybrid processing via bio- and chemo-catalysis. J. Clean. Prod. 364, 132614.
Scown, C.D., Baral, N.R., Yang, M., Vora, N., Huntington, T., 2021. Technoeconomic analysis for biofuels and bioproducts. Curr. Opin. Biotechnol. 67, 58–64.
Sepiacci, P., Depetri, V., Manca, D., 2017. A systematic approach to the optimal design of chemical plants with waste reduction and market uncertainty. Comput. Chem. Eng. 102, 96–109.
Sherwin, E.D., Henrion, M., Azevedo, I.M.L., 2018. Estimation of the year-on-year volatility and the unpredictability of the United States energy system. Nat. Energy 3, 341–346.
Taieb, S.B., Atiya, A.F., 2016. A bias and variance analysis for multistep-ahead time series forecasting. IEEE Trans. Neural Netw. Learn. Syst. 27, 62–76.
Taieb, S.B., Bontempi, G., Atiya, A.F., Sorjamaa, A., 2012. A review and comparison of strategies for multi-step ahead time series forecasting based on the NN5 forecasting competition. Expert Syst. Appl. 39, 7067–7083.
Taieb, S.B., Bontempi, G., Sorjamaa, A., Lendasse, A., 2009. Long-term prediction of time series by combining direct and MIMO strategies. Proc. Int. Jt. Conf. Neural Networks 3054–3061.
Taieb, S.B., Sorjamaa, A., Bontempi, G., 2010. Multiple-output modeling for multi-step-ahead time series forecasting. Neurocomputing 73, 1950–1957.
Towler, G., Sinnott, R.K., 2013. Chemical Engineering Design - Principles, Practice and Economics of Plant and Process Design, second ed. Elsevier.
Wu, Y.X., Wu, Q.B., Zhu, J.Q., 2019. Improved EEMD-based crude oil price forecasting using LSTM networks. Physica A 516, 114–124.
Yao, G., Staples, M.D., Malina, R., Tyner, W.E., 2017. Stochastic techno-economic analysis of alcohol-to-jet fuel production. Biotechnol. Biofuels Bioprod. 10.
Zhang, Y., Brown, T.R., Hu, G., Brown, R.C., 2013. Techno-economic analysis of two bio-oil upgrading pathways. Chem. Eng. J. 895–904.
Zhang, Z., Delcroix, B., Rezazgui, O., Mangin, P., 2021. Simulation and techno-economic assessment of bio-methanol production from pine biomass, biochar and pyrolysis oil. Sustain. Energy Technol. Assess. 44, 101002.
Ziel, F., Steinert, R., 2018. Probabilistic mid- and long-term electricity price forecasting. Renew. Sustain. Energy Rev. 94, 251–266.

7 Creation of a surrogate model for the economic evaluation of feedstocks

7.1 Preface

This chapter contributes to the overall thesis aim of developing and applying Techno-Economic Analysis (TEA) methods to evaluate the proposed aerobic gas fermentation and Supercritical Water Gasification (SCWG) process by providing an early-stage feedstock screening tool for SCWG. This enables the identification of promising feedstock scenarios for valorisation to maximise the economic potential of the technology. Furthermore, the simulation of SCWG is upgraded to allow for biomass feedstocks to be modelled based on their ultimate analysis. The new simulation is used to undertake an economic and environmental assessment for hydrogen production and a surrogate model of the techno-economic analysis is created. It therefore contributes to the following thesis objectives:

1. Develop process simulations for the aerobic gas fermentation and supercritical water gasification process, incorporating heat integration and downstream processing.
2. Determine an appropriate techno-economic framework and perform a comprehensive techno-economic analysis of the simulated process.
3. Quantify the greenhouse gas emissions associated with chemical and fuel production from the process and compare them with conventional production methods.
6. Create a machine learning surrogate model of a techno-economic analysis to rapidly evaluate the economic potential of feedstock-capacity-location combinations for supercritical water gasification.

Detailed TEAs (such as those presented in Chapter 4 and 5) are time consuming and require engineering knowledge to produce realistic process designs (Scown et al., 2021). As evidenced in Chapter 2, there are increasing trends towards lightweight TEA tools. However, the usability of these methods comes at the expense of some accuracy (Scown et al., 2021). With emerging tools such as Machine Learning (ML) more complex processes can be represented by reduced order models, creating more accurate tools for user-friendly process and biorefinery scenario evaluation. This Chapter presents a ML surrogate model of a TEA for feedstock evaluation for hydrogen production via SCWG. This represents the upstream portion of the heat integrated aerobic gas fermentation platform, removing the bioreactor and downstream separation sections.

A dataset consisting of the ultimate analysis of 40 biomass feedstocks was collected from experimental literature investigating low-temperature SCWG (380 - 500°C). A process simulation of the low-temperature SCWG and separation and purification to produce renewable hydrogen was created for each of the biomass compositions in Aspen HYSYS. The simulations were based on a fixed SCWG temperature at 430°C. This was selected owing to the economic benefit of low-temperature SCWG which reduces the energetic burden required to preheat the feedstock (Lee et al., 2021). A feedstock concentration corresponding to a Chemical Oxygen Demand (COD) of 75 g/L_{COD} was also selected. This concentration was selected as low solids concentrations lead to increased hydrogen production through enhancing Steam Methane Reforming (SMR) and water gas shift reactions (Lee et al., 2021). The TEA was undertaken considering five different processing scales (10 to 200 m^3/hr) and three geographic locations (China, Brazil, and the UK), giving rise to 600 TEAs. The selected processing capacities allow for comparison to other low-carbon hydrogen technologies and represent realistic point source waste stream availability. The geographic locations were

selected as case studies with abundant wet wastes suitable for SCWG, i.e., black liquor in China, vinasse in Brazil, and distillery wastewater in the UK and provide global coverage.

In Chapters 4 and 5 the SCWG reactor model was represented using a plug flow reactor with kinetics based on low temperature gasification of guiacol. However, in this Chapter a Gibbs reactor was used to model the gasifier, this enables the ultimate analysis of the biomass feedstocks to be directly input into the simulations. In contrast to the kinetic model, the predicted gas composition from the Gibbs reactor had a higher methane concentration. At lower temperatures a higher methane fraction is anticipated from a thermodynamic perspective as lower temperatures favour exothermic methanation reactions. However, to shift the SCWG effluent to a CO_2 and H_2 rich product a series of reactors namely; steam methane reformer, high temperature shift, and low temperature shift were employed.

The TEA methodology was adopted from Chapters 4 and 5. However, owing to the range of feedstocks evaluated, a universal method of computing the feedstocks utility value was created based on the feedstocks higher heating value (HHV) relative to natural gas. An efficiency factor of 70% was applied to the HHV based on anaerobic digestion as a next best alternative waste utilisation method. Anaerobic digestion can only exploit the Biological Oxygen Demand of a feedstock, whereas SCWG exploits the entire COD. The 70% efficiency factor reflects a high Biological Oxygen Demand to COD ratio (Kumar et al. 2010). The feedstock's price was then computed based on the adjusted HHV relative to the HHV of natural gas using the Energy Information Administration's natural gas prices (EIA, 2022).

Considering the ML surrogate model, the biomass' ultimate analysis, processing capacity, and geographic location were the model inputs, and the model outputs were the nominal Levelised Cost of hydrogen (LCOH) and corresponding 70% probability band. The 70% probability band represents the upper 70% of economic outcomes obtained from the Monte Carlo simulation probability distribution, i.e., 100 % - 30 %. This therefore represents an optimistic range of potential economic outcomes. In retrospect, presenting the 95% probability around the mean, representing two standard deviations, would have provided a statistically robust range for comparison to alternative technologies.

Three ML algorithms were compared for the surrogate model, Random Forests (RF), Support Vector Regression (SVR), and Artificial Neural Networks (ANNs), as they have been previously considered for predicting hydrogen production via SCWG (Li et al., 2021; Zhao et al., 2022). An ensemble of 10 ANNs was used for the ANN model owing to proposed improved performance from ensemble-based methods. The 600 TEA combinations were split into a training set of 360, a validation set of 120, and a test set of 120 parameter combinations. As the hydrogen yield varied between biomass feedstocks, the 40 biomass feedstocks were distributed among the sets to facilitate the generalisation across feedstock compositions. This resulted in 24 biomass feedstocks in the training set, 8 in the validation set, and 8 in the test set. The best-performing hyperparameters were selected based on cross-validation performance. A 4-fold cross-validation procedure was undertaken on the combined training and validation sets using a grid search to determine the optimal hyperparameters for each ML algorithm. SHapley Additive exPlanation Values were used to highlight the relative importance of the input features on the model's output.

The surrogate model's utility was demonstrated by comparing the economic outcome of the 40 different feedstocks at the different processing scales and locations. The LCOH computed was compared to other low carbon hydrogen production methods namely; electrolysis using renewable electricity and SMR with carbon capture and storage. Levelized costs for these comparisons were obtained from the International Energy Agency (IEA) for China (IEA, 2021a;

IEA, 2022) and Brazil (IEA, 2021b), and the UK Department for Business, Energy and Industrial Strategy (BEIS) for the UK (BEIS, 2021).

The novelty of this work is the development of a published surrogate model representing a TEA of SCWG. This enables the quick economic evaluation of different feedstock-capacity-location combinations. To the best of the authors' knowledge, the only other study to produce a surrogate model for a full TEA was Huntington et al. (2023), who used hydrolysis-based ethanol production as a case study. Another novel contribution was the creation of the reliability measure to determine the confidence in the model's predictions for unseen biomass samples input by the user. The validity of predictions made by the surrogate model on unseen data was not discussed in the work by Huntington et al. (2023). The reliability measure developed in this Chapter takes principles from anomaly detection using autoencoders where an anomaly threshold is set by the reconstruction error (Ndubuaku et al., 2019). However, in this application the threshold is based on the error between the predictions by the ensemble of ANNs using a 5-fold validation procedure on the entire dataset.

In terms of techno-economic outcomes, this study found that at a SCWG capacity of 50 m^3/hr, the LCOH (2.76 - 4.21 $/kg$_{H2}$ for China, 3.41 - 5.07 $/kg$_{H2}$ for Brazil, 4.31 - 6.62 $/kg$_{H2}$ for the UK) was cost competitive with hydrogen production via MW-scale electrolysis using renewable electricity (3.10 - 6.70 $/kg$_{H2}$ for China, 3.70 - 5.90 $/kg$_{H2}$ for Brazil, and 4.81 - 6.31 $/kg$_{H2}$ for the UK). With regards to the surrogate model, the ensemble of ANNs performed the best, achieving a test set accuracy of, Mean Absolute Percentage Error: <4.6%, Route Mean Squared Error: <0.39, and R^2: >0.99. Processing capacity was found to be the most important feature followed by geographic location. However, appreciable LCOH differences were also observed between different biomass compositions. This highlights the need for early-stage screening tools to maximise the economic potential of a technology and inform targeted research and development into promising feedstock valorisation opportunities.

The limitations of this study are the limited scenarios considered, i.e., constant dilution rate (75g/L_{COD}), 430°C gasification temperature, and limited geographic locations. Future work to incorporate variability in technical parameters would facilitate the use of the surrogate model for process optimisation in addition to feedstock evaluation. In addition, the SCWG was represented via a Gibbs reactor in Aspen HYSYS. This simplifies the gasification process by assuming complete conversion to gaseous products and attainment of thermodynamic equilibrium. Studies creating surrogate models of SCWG reactors based on experimental undertaken at various temperatures, pressures, and the inclusion of different catalysts have been previously undertaken (Gopirajan et al., 2021; Li et al., 2021; Zhao et al., 2022; Shenbagaraj et al., 2021; Khan et al., 2023; Fózer et al., 2021). The creation of a low temperature SCWG surrogate model using experimental data to input into the TEA model would represent the true state of technology, opposed to the economic potential. However, at present there is limited experimental data for complete, or almost complete, conversion of biomass feedstocks using low temperature SCWG. Furthermore, the use of experimental data has the potential to bias feedstocks that are obtained under varying conditions or different levels of experimental rigour. Finally, the study considered SCWG for hydrogen production rather than the integrated aerobic gas fermentation and SCWG technology. Whilst the results from this study will be indicative of the integrated technology, future work to create an ML surrogate of the entire platform to enable the economic evaluation of further biorefinery scenarios is proposed.

The work presented in this chapter contributed to a paper entitled "A surrogate model for the economic evaluation of renewable hydrogen production from biomass feedstocks via supercritical water gasification" and was published in *International Journal of Hydrogen Energy, currently in press*. The published paper is presented in this thesis as Chapter 7. The

corresponding supplementary information as published alongside the manuscript is reprinted in Appendix A.4.

Article Title: A surrogate model for the economic evaluation of renewable hydrogen production from biomass feedstocks via supercritical water gasification

Journal: International Journal of Hydrogen Energy

Date: Currently In Press

DOI: https://doi.org/10.1016/j.ijhydene.2023.08.016

Authors: Sarah Rodgers, Alexander Bowler, Jon McKechnie, Edward Lester, Chai Siah Lee, Fanran Meng, Laura Wells, Martin Hayes, Stephen Poulston, Alex Conradie

Author Contributions: Sarah Rodgers: Conceptualization, Data curation, Formal analysis, Investigation, Methodology, Software, Visualization, Writing – original draft, Writing – review & editing. Alexander Bowler: Data curation, Formal analysis, Methodology, Software, Writing – review & editing. Jon McKechnie: Funding acquisition, Methodology, Project administration, Resources, Supervision, Writing – review & editing. Ed Lester: Supervision, Writing – review & editing. Chai Siah Lee: Conceptualization, Methodology, Writing - review & editing. Fanran Meng: Methodology, Supervision, Writing – review & editing. Laura Wells: Methodology, Investigation, Writing – review & editing. Martin Hayes: Supervision, Writing – review & editing. Stephen Poulston: Supervision, Writing – review & editing. Alex Conradie: Conceptualization, Formal analysis, Funding acquisition, Methodology, Project administration, Resources, Supervision, Writing – review & editing.

7.2 References

BEIS, 2021. Hydrogen production costs 2021, s.l.: Gov.uk.

EIA, 2022. ANNUAL ENERGY OUTLOOK 2022, Washington DC: s.n.

Fózer, D., Tóth, A. J., Varbanov, P. S., Klemeš, J. J., & Mizsey, P., 2021. Sustainability assessment of biomethanol production via hydrothermal gasification supported by artificial neural network. *Journal of Cleaner Production*, 318, 128606.

Gopirajan, P. V., Gopinath, K. P., Sivaranjani, G. & Arun, J., 2021. Optimization of hydrothermal gasification process through machine learning approach: Experimental conditions, product yield and pollution. *Journal of Cleaner Production,* 306, 127302.

Huntington, T., Baral, N. R., Yang, M., Sundstrom, E., Scown, C. D., 2023. Machine learning for surrogate process models of bioproduction pathways. *Bioresource Technology*, 370, 128528.

IEA, 2021a. An energy sector roadmap to carbon neutrality in China. [Online] Available at: https://www.iea.org/reports/an-energy-sector-roadmap-to-carbon-neutrality-in-china [Accessed 08 February 2023].

IEA, 2021b. Hydrogen in Latin America. [Online] Available at: https://www.iea.org/reports/hydrogen-in-latin-america [Accessed 08 February 2023].

IEA, 2022. Opportunities for Hydrogen Production with CCUS in China. [Online] Available at: https://www.iea.org/reports/opportunities-for-hydrogen-production-with-ccus-in-china [Accessed 08 February 2023].

Khan, M. N. A., Haq, Z. U., Ullah, H., Naqvi, S. R., Ahmed, U., Zaman, M., Amin, N. A. S., 2023. Prediction of hydrogen yield from supercritical gasification process of sewage sludge using machine learning and particle swarm hybrid strategy. *International Journal of Hydrogen Energy.*

Kumar, A., Dhall, P., Kumar, R., 2010. Redefining BOD:COD ratio of pulp mill industrial wastewaters in BOD analysis by formulating a specific microbial seed. *International Biodeterioration & Biodegradation*, 64, 197-202.

Lee, C. S., Conradie, A. V. & Lester, E., 2021. Review of supercritical water gasification with lignocellulosic real biomass as the feedstocks: Process parameters, biomass composition, catalyst development, reactor design and its challenges. *Chemical Engineering Journal*, 145, 128837.

Li, J., Pan, L., Survarna, M. & Wang, X., 2021. Machine learning aided supercritical water gasification for H2-rich syngas production with process optimization and catalyst screening. *Chemical Engineering Journal*, 426, 131285.

Ndubuaku, M. U., Anjum, A., Liotta., A., 2019. Unsupervised Anomaly Thresholding from Reconstruction Errors, in: Montella, R., Ciaramella, A., Fortino, G., Guerrieri, A., Liotta, A. (Eds.), *Internet and Distributed Computing Systems*. IDCS 2019. *Lecture Notes in Computer Science*. Springer, Cham. 123–129.

Scown, C.D., Baral, N.R., Yang, M., Vora, N., Huntington, T., 2021. Technoeconomic analysis for biofuels and bioproducts. *Current Opinion in Biotechnology*, 67, 58-64.

Shenbagaraj, S., Sharma, Pankaj K., Sharma, A. K., Raghav, G., Kota K. B., Ashokkumar V., 2021. Gasification of food waste in supercritical water: An innovative synthesis gas composition prediction model based on Artificial Neural Networks. *International Journal of Hydrogen Energy,* 46 (24), 12739-12757

Zhao, S., Jian, L., Chen, C., Yan, B., Tao, J., & Chen, G., 2022 Interpretable machine learning for predicting and evaluating hydrogen production via supercritical water gasification of biomass. *Journal of Cleaner Production,* 316, 128244.

This page has been left intentionally blank

Available online at www.sciencedirect.com

ScienceDirect

journal homepage: www.elsevier.com/locate/he

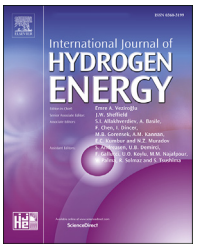

A surrogate model for the economic evaluation of renewable hydrogen production from biomass feedstocks via supercritical water gasification

Sarah Rodgers [a], *Alexander Bowler* [b], *Laura Wells* [c], *Chai Siah Lee* [d], *Martin Hayes* [e], *Stephen Poulston* [f], *Edward Lester* [d], *Fanran Meng* [g], *Jon McKechnie* [a], *Alex Conradie* [h,*]

[a] *Sustainable Process Technologies Research Group, Faculty of Engineering, University of Nottingham, Nottingham, NG7 2RD, UK*
[b] *School of Food Science and Nutrition, University of Leeds, Woodhouse Ln., Leeds, LS2 9JT, UK*
[c] *Johnson Matthey, 5 Farringdon St, London, EC4A 4AB, UK*
[d] *Advanced Materials Research Group, Faculty of Engineering, University of Nottingham, NG7 2RD, UK*
[e] *Johnson Matthey, 28 Cambridge Science Park, Milton Road, Cambridge, CB4 0FP, UK*
[f] *Johnson Matthey, Blounts Court Road, Sonning Common, Reading, RG4 9NH, UK*
[g] *Chemical & Biological Engineering, University of Sheffield, Mappin Street, Sheffield, S1 3JD, UK*
[h] *The Manufacturing Futures Laboratory, Department of Biochemical Engineering, University College London, Gower Street, London, WC1E 6BT, UK*

HIGHLIGHTS

- A techno-economic surrogate model for supercritical water gasification is created.
- Model predicts the LCOH for different biomass compositions, scales, and locations.
- RF, SVR, and ANN algorithms were compared for the surrogate model.
- ANNs achieved the highest prediction accuracy during cross-validation.
- Final model is published to facilitate early-stage feedstock evaluation.

GRAPHICAL ABSTRACT

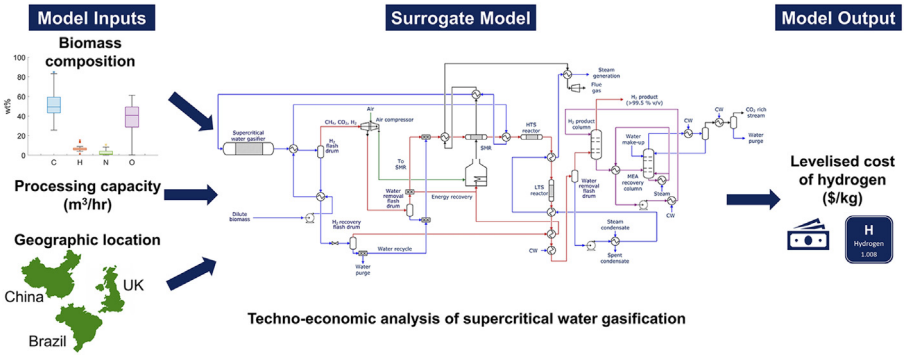

ARTICLE INFO

Article history:
Received 23 May 2023
Received in revised form
12 July 2023

ABSTRACT

Supercritical water gasification is a promising technology for renewable hydrogen production from high moisture content biomass. This work produces a machine learning surrogate model to predict the Levelised Cost of Hydrogen over a range of biomass compositions, processing capacities, and geographic locations. The model is published to

* *Corresponding author.*
E-mail address: a.conradie@ucl.ac.uk (A. Conradie).
https://doi.org/10.1016/j.ijhydene.2023.08.016

Accepted 1 August 2023
Available online 18 August 2023

Keywords:
Supercritical water gasification
Surrogate model
Renewable hydrogen
Techno-economic analysis
Machine learning

facilitate early-stage economic analysis (doi.org/10.6084/m9.figshare.22811066). A process simulation using the Gibbs reactor provided the training data using 40 biomass compositions, five processing capacities (10–200 m^3/h), and three geographic locations (China, Brazil, UK). The levelised costs ranged between 3.81 and 18.72 $/kg$_{H2}$ across the considered parameter combinations. Heat and electricity integration resulted in low process emissions averaging 0.46 kgCO_2eq/GJ$_{H2}$ (China and Brazil), and 0.37 kgCO_2eq/GJ$_{H2}$ (UK). Artificial neural networks were most accurate when compared to random forests and support vector regression for the surrogate model during cross-validation, achieving an accuracy of MAPE: <4.6%, RMSE: <0.39, and R^2: >0.99 on the test set.

Abbreviations

AD	Anaerobic Digestion
ANN	Artificial Neural Network
CCS	Carbon Capture and Storage
COD	Chemical Oxygen Demand
EIA	Energy Information Administration
GHG	Greenhouse Gas
HHV	Higher Heating Value
HTS	High Temperature Shift
LCA	Life Cycle Assessment
LCOH	Levelised Cost of Hydrogen
LTS	Low Temperature Shift
MAPE	Mean Absolute Percentage Error
MEA	Monoethanolamine
ML	Machine Learning
MSP	Minimum Selling Price
RF	Random Forests
RMO	Ratio of Moles of Oxygen
RMSE	Route Mean Squared Error
SCWG	Supercritical Water Gasification
SHAP	SHapley Additive exPlanation
SMR	Steam Methane Reforming
SVR	Support Vector Regression
TEA	Techno-Economic Analysis

1. Introduction

Supercritical Water Gasification (SCWG) combines thermal decomposition and reforming by using supercritical water as the solvation and reaction medium, thereby converting various biomass feedstocks to syngas (H_2, CH_4, CO_2 and CO) whilst minimising char formation. SCWG provides advantages for processing wet feedstocks over other bioenergy generation approaches (e.g. direct combustion and conventional gasification) such as energy savings by avoiding the need to pre-dry the feedstock, lower operating temperatures, shorter reaction times and tuneable gas compositions [1].

The past decade has seen an increased focus on experimental investigations of hydrogen production via SCWG using various types of plant-based biomass feedstocks, such as sugarcane bagasse, stillage, and black liquor [2]. To understand the economic potential of a feedstock it is necessary to conduct a Techno-Economic Analysis (TEA). Several TEAs have been undertaken using SCWG for renewable hydrogen production from specific feedstocks including the valorisation of digested sewage sludge [3], black liquor [4], and soybean straw [5]. However, detailed TEAs are time consuming and require engineering knowledge and economic modelling expertise [6]. This hinders the creation of TEA models by non-experts i.e. experimentalists and industrialists. Moreover, TEA models are most often specific to a particular process, scale, feedstock, and cost base, limiting the ability to generalise effectively from existing models. Without understanding how operating conditions, feedstock sources, and cost considerations impact on the overall investment case, targeted experimental research is impeded, which is detrimental to subsequent commercialisation. Therefore, it is desirable for TEA practitioners to create flexible TEA models that generalise effectively to a wide range of opportunities and for these models to be independent of specialised software tools.

Surrogate models map inputs to outputs of more complex processes. Machine learning (ML) is often used to create these correlations and is increasingly being used for modelling, optimising, and monitoring thermal conversion processes [7]. However, surrogate modelling for SCWG has focused on predicting process outputs such as hydrogen or syngas yields [8–10]. Several studies have used these to suggest optimal processing parameters [8], screen catalysts [9], or create interpretable models to better understand the relationship between process parameters and biomass characteristics on gas yields [10]. Feedstock-specific surrogate models have also been developed to predict hydrogen yields for SCWG. For example, Shengagaraj et al. (2021) used an Artificial Neural Network (ANN) to predict the syngas yields from food waste biomass [11]. Similarly, Khan et al. (2023) created a model for the SCWG of sewage sludge, where they created a graphical user interface of their ML model. The model predicts the H_2 yield based on the proximate and ultimate analysis of the sample, as well as the input of gasification conditions [12]. In addition, Fózer et al. (2021) created an ANN surrogate model of

a microalgae SCWG reactor and used it within their economic and environmental analysis for methanol production [13].

In the broader context of hydrogen production and generation, ML has been widely applied to determine and develop efficient processes [14]. For example, Yahya et al. (2021) used an ANN coupled with a genetic algorithm and response surface methodology to optimise the production of hydrogen via steam reforming of toluene, finding the ANN to be a more robust predictor than response surface methodology [15]. Kargbo et al. (2023) utilised a bootstrapped aggregated neural network to represent waste wood gasification in their hydrogen production optimisation study [16]. Regarding predicting hydrogen production rates, Sultana et al. (2023) developed a Bayesian algorithm and Support Vector Regression (SVR) model to predict the hydrogen and methane yield via dark fermentation [17]. Model inputs included the pretreatment duration, feedstock concentration, and pH. Sezer et al. (2021) created an ANN model of an Aspen Plus simulation, representing a bubbling fluidised bed gasifier for hydrogen production [18]. The ANN was trained to predict the exergy value of the produced syngas based on the biomass' elemental composition, gasifier temperature, steam flowrate and fuel flowrate.

Outside of hydrogen production, ML surrogate models have been applied to a limited number of studies within TEA and Life Cycle Assessments (LCAs). Liao et al. (2020) developed a combined ML and kinetic-based process simulation to assess the Greenhouse Gas (GHG) emissions, energy, and product consumption of producing activated carbon from 73 different woody biomasses under different operating conditions [19]. Olafasakin et al. (2021) investigated replacing first principles modelling of pyrolysis kinetics with a Kriging-based reduced order model for predicting the pyrolysis yields of 314 feedstocks, where the model outputs were used within a biorefinery process model to predict the corresponding Minimum Selling Price (MSP) and GHG emissions [20]. Whilst Liao et al. (2020) and Olafasakin et al. (2021) both used ML to create surrogate process models for use within TEAs and LCAs, additional detailed process modelling was still required to use the surrogate model predictions. Therefore, the use of these models still requires user expertise, making such models ineffective for decision-making by most experimentalists and industrialists. In contrast, Huntington et al. (2023) presented an auto-ML approach for generating a process model surrogate of a fixed lignocellulosic bioethanol process flowsheet for use within a TEA, where the surrogate model mapped 21 key operating and cost parameters to the MSP [6]. Notably, these operating parameters allowed adjustment of the plant throughput, the feedstock composition, conversion efficiencies, and cost considerations. Their method used the Tree-Based Pipeline Optimisation Tool considering four ensemble regression models, Random Forests (RF), Stacking, Extra Trees, and Gradient Boosting. Their approach provided direct TEA outputs, negating the need for modelling expertise or further incorporation of the surrogate models within a broader modelling framework.

This study uses ML to create a surrogate model for the TEA of renewable hydrogen production from low-temperature SCWG (380–500 °C). The Gibbs reactor in Aspen HYSYS is used as the simulation basis. The carbon footprint of the proposed process is verified alongside the TEA results for the range of biomass feedstock compositions and processing capacities in three different geographic locations. The biomass' ultimate analysis, processing capacity, and geographic location for the facility are the surrogate model inputs and the model outputs are the nominal and 70% probability band for the Levelised Cost of hydrogen (LCOH). Three ML algorithms were investigated for the surrogate model: RF, SVR, and ANNs, as these algorithms have been previously investigated for predicting hydrogen production via SCWG [9,10]. Additionally, a reliability measure was developed to evaluate the confidence in the surrogate model's predictions for new biomass feedstocks inputted by a user. The novelty of this work lies in the creation of an ML surrogate model representing the TEA of hydrogen production via SCWG. Whilst surrogate models have been previously developed for SCWG for hydrogen production [8–13], this is the first study to create a surrogate model representing a TEA of the process. The best performing surrogate model has been made publicly available (doi.org/10.6084/m9.figshare.22811066). The purpose of the published model is to provide indicative production costs, enabling researchers and manufacturers to quickly determine the economic potential of feedstocks and facilitate comparisons with other hydrogen production technologies.

2. Methodology

A data-set of 40 biomass feedstocks was collected from experimental literature investigating low-temperature SCWG (380–500 °C). The ultimate analysis (carbon (C), hydrogen (H), oxygen (O) and nitrogen (N)) of each of these feedstocks was collated. A process simulation of the low-temperature SCWG and purification to renewable hydrogen was created for each of the biomass compositions in Aspen HYSYS. The simulation was based on a fixed SCWG temperature at 430 °C. This was selected owing to the economic benefit of low-temperature SCWG which reduces the energetic burden required to preheat the feedstock [1], and the recent experimental study into the SCWG of biomass wastewaters by Lee et al. (2023) which was conducted at this temperature [2]. A conservative residence time of 5 min was assumed, thereby providing sufficient residence time for the equilibrium as predicted by the Gibbs reactor to be attained. This was selected to exceed the residence times used experimentally for continuous low-temperature SCWG, where a 20s residence time achieved a total organic carbon reduction efficiency of 53.9–55.7% [2] and 88.4% at 150s [21]. A feedstock concentration corresponding to a Chemical Oxygen Demand (COD) of 75 g/L_{COD} was also selected.

Two hundred process simulations were created for the range of collected biomass compositions and five processing capacities (10, 20, 50, 100, and 200 m^3/h). These processing capacities were selected to allow for comparison to other low-carbon hydrogen technologies and represent realistic point source waste stream availability. A TEA and LCA was undertaken on each of the resulting simulations in three geographical locations (China, Brazil, and the UK) producing 600 data points. These geographic locations were selected as case studies with abundant wet wastes suitable for SCWG, i.e., Black liquor in China, vinasse in Brazil, and distillery

wastewater in the UK. These waste streams are also later used as case studies to compare the produced LCOH to alternative low carbon hydrogen production technologies. Furthermore, the selected three locations provide global coverage with differing economic inputs.

The TEA results are presented as the nominal LCOH ($/kg$_{H2}$) and the LCA results as the process' GHG emissions (kgCO_2eq/GJ$_{H2}$) for each combination of feedstock, processing capacity, and geographic location. A Monte Carlo simulation for each parameter combination was undertaken to illustrate the relative uncertainty around the nominal LCOH. The economic and environmental impact of transporting wastes to a larger capacity facility was also investigated. Finally, a ML surrogate model was created to predict the nominal, lower (5th), and upper (75th) LCOH computed from the TEA and Monte Carlo simulation using the feedstock's ultimate analysis, capacity, and geographic location as model inputs. Owing to the low utility usage of the SCWG process, the variability in GHG emissions between feedstocks was minimal. As such, the surrogate model was not trained to predict process emissions.

2.1. Data collection and pre-processing

The ultimate analysis consisting of the weight percent of C, H, O, and N was collected for each of the 40 biomass feedstocks and converted onto a 100% C, H, O, N basis. The compositions collected from literature are presented in the Supplementary Information, Table S1. Descriptive statistics of the data-set are presented in Table 1. The biomass feedstocks were selected to obtain a range of compositions to produce a generalisable surrogate model that can predict the LCOH for unseen, user inputted, biomass feedstocks.

The biomass' Ratio of Moles of Oxygen (RMO) to moles of oxidisable compounds (mol/mol) was calculated to determine the weight percent required for each feedstock to yield a COD of 75 g/L$_{COD}$. The RMO is the required amount of oxygen to fully oxidise a compound to CO_2, H_2O and NH_3 as expressed in Eq. 1. Eq. 2 defines the theoretical COD, where W (g/L) represents the solids concentration of oxidisable compound and Mr (g/mol) is the molecular mass of oxidisable compound.

$$C_nH_aO_bN_c + \left(n + \frac{a}{4} - \frac{b}{2} - \frac{3}{4}c\right)O_2 \rightarrow nCO_2 + \left(\frac{a}{2} - \frac{3}{2}c\right)H_2O + cNH_3 \quad (1)$$

$$COD = \frac{W}{Mr} * \left(n + \frac{a}{4} - \frac{b}{2} - \frac{3}{4}c\right) * 32 \quad (2)$$

The COD was used as the model basis as it is a required measurement of effluent streams and represents the stream's reduction potential, i.e. reducing power. Effluent streams with the same COD possess the same theoretical potential to produce H_2 regardless of composition, where more reduced compounds require a lower solids concentration than more oxidised compounds to attain the same COD. In contrast, the solids concentration also includes inorganic matter which does not contribute to the production of H_2. By using the COD as the model basis, the economic potential of the organic biomass content is easily interpreted.

Table 1 – Descriptive statistics of the biomass compositions collected from experimental literature for the SCWG of real biomass compounds.

Descriptive Statistic	Ultimate analysis (wt%)			
	C	H	N	O
Mean	47.82	6.11	1.98	32.39
Standard Deviation	17.69	3.06	1.77	17.05
Minimum Value	18.94	0.75	0.00	0.20
25th Percentile	38.01	4.43	0.70	16.97
50th Percentile	43.52	5.98	1.26	36.51
75th Percentile	57.39	6.65	3.19	46.83
Maximum Value	84.74	14.90	6.27	55.80

2.2. Process simulation

A temperature of 430 °C was used for the SCWG, owing to the economic benefit of low-temperature SCWG [1]. The COD for each biomass feedstock was fixed at 75 g/L$_{COD}$. For the considered biomass feedstocks, this translates to 5 wt% solids on average, though the actual content varies depending on the reduction potential of the biomass. This concentration was selected as low solids concentrations lead to increased hydrogen production through enhancing steam methane reforming and water gas shift reactions [1]. However, from an economic standpoint the solids concentration directly affects the energy balance, with more dilute feedstocks requiring greater energy to heat to supercritical conditions. The concentration was selected as a trade-off between these two factors. This consideration may require evaporation or dilution of the actual feedstock being evaluated but is not factored into the TEA or LCA as different dilution and evaporation requirements would vastly increase the model complexity. Costs and emissions associated with evaporation or dilution to the 75 g/L$_{COD}$ necessitates external quantification by the user.

A TEA was undertaken on the process simulation using five different processing capacities (10, 20, 50, 100, and 200 m^3/h). This led to 200 process simulations, considered over three geographical locations (China, Brazil, and the UK), resulting in 600 economic analyses. The TEA results were presented as the nominal LCOH.

The 50 and 100 m^3/h capacities yield between 7.5-10 and 15–20 MW of hydrogen, respectively. These results are directly comparable to green electrolysis LCOH prices produced by BEIS (10 MW) [22]. Furthermore, the range of capacities investigated represent realistic effluent production rates for the considered countries. For example, Brazil's Sebigas plant processing vinasse has a capacity of 500 tn$_{COD}$/day, corresponding to 277 m^3/h of wastewater at 75 g O_2/L COD concentration [23]. In addition, a 200 m^3/h throughput scale corresponds to a modest-sized pulp mill with a processing capacity of approximately 12,000 ADt/yr of pulp, based on 10 t $_{\text{black liquor}}$/t$_{\text{ADt pulp}}$ [24]. By comparison, China's largest pulp mill produces 1.2 million ADt/yr [25]. With regards to distillery wastewater, pot ale and wet draff are produced at rates of 7.9 L/L$_{alcohol}$ and 2.55 kg/L$_{alcohol}$ [26]. Using both these waste streams, the processing capacities explored in this study correspond to a distillery capacity between 5 and 104 million

litres/yr, noting that the largest operational Scottish Distillery is 100 million litres [27]. Considering anaerobic digestate as a feedstock, the 10 m^3/h throughput scale corresponds to approximately 500 kg/h of dry solids based on a 5 wt% solids concentration and digestate production at 0.87 $kg/kg_{feedstock}$ [28]. This is equivalent to an anaerobic digestion (AD) facility capacity of 100 kt/yr, where currently 20 facilities in the UK operate at a capacity >96 $kt/yr_{digestate}$.

2.2.1. Gasification

The SCWG reaction was modelled in Aspen HYSYS using a conversion reactor to decompose the unconventional biomass compound into its base compounds (H_2, O_2, N_2 and C). As such, only the ultimate analysis was required to represent each considered biomass compound. The stochiometric coefficients for the decomposition reaction in the conversion reactor were modified for each biomass sample using a MATLAB script. This was followed by a Gibbs reactor to predict the gasifier effluent assuming full conversion to gaseous products and the attainment of equilibrium at the specified temperature and pressure. This is a common approach in techno-economic studies of SCWG [29]. For example, this method has been used previously for the valorisation of black liquor [4], digested sewage sludge [3], and soybean straw [5]. The simulation considers the achievement of thermodynamic equilibrium and complete biomass conversion to gaseous products. It is recognised that equilibrium may not be reached in industrial conditions and achieved gas yields may differ from those predicted by the Gibbs reactor. Also, formation of solid by-products, such as tar and char, may not be negligible. However, in the absence of extensive complete conversion data for low-temperature SCWG, the approach enables the evaluation of different feedstocks on an equivalent basis. As such, the results represent the economic potential for a biomass feedstock. Moreover, the continuous SCWG reactor is sized based on a relatively conservative residence time of 5 min, translating to an additional capital expense. This residence time was selected to exceed the reported experimental results for continuous low-temperature SCWG where a 20s residence time achieved a total organic carbon reduction efficiency of 53.9–55.7% [2] and 88.4% at 150s [21].

An additional reactor was used to convert 100% of the fuel bound nitrogen to NH_3, similarly to Ref. [3]. Most of the NH_3 is removed with the high-pressure water flash after the SCWG reactor and it is assumed no further separation is required. The formation of sulphur compounds and ash were not considered. In practicality sulphur would form H_2S during gasification which would be removed along with CO_2 during H_2 purification. The formation of ash would be removed with any char formed during gasification and be subsequently combusted.

To satisfy the simulation's energy balance, the heats of formation for the hypothetical biomass compounds were estimated by subtracting the heat of combustion of the free elements (carbon (−393.15 kJ/mol) and hydrogen (285.83 kJ/mol)) from the biomass' Higher Heating Value (HHV) [30]. A correlation was used to estimate the HHV for each biomass based on its elemental composition. The correlation created by Huang & Lo (2020) was used to estimate the feedstock's HHV given the correlation was established using a large number and range of biomass feedstocks [31].

2.2.2. Syngas upgrading

The Gibbs reactor model predicts a higher methane fraction in the product gas at temperatures around 400 °C compared to temperatures above 500 °C, as shown in Table S2 in the Supplementary Information. At lower temperatures, the formation of hydrogen through endothermic gasification reactions is inhibited, while the exothermic reactions that form methane are favoured [32,33]. The observed trend in increased methane fractions at lower temperatures therefore aligns with thermodynamic principles. Whilst the focus of this study is hydrogen production, higher reaction temperatures are heavily disadvantaged from an economic perspective owing to the higher energy burden required to heat the gasifier feed [1]. By shifting this methane fraction to hydrogen post-gasification using mature chemo-catalytic technology, the economic benefit of low-temperature SCWG can be exploited whilst still maximising hydrogen production.

To shift the reactor effluent towards hydrogen, the mature Steam Methane Reforming (SMR), High-Temperature Shift (HTS) and Low-Temperature Shift (LTS) technologies were employed. A fraction of the SCWG effluent was directed towards combustion to support the endothermic SMR reaction, ensuring the process remained energetically self-sufficient. The operating conditions and kinetics used to model the SMR, HTS and LTS reactors are presented in Table 2. The hydrogen produced was then recovered using a primary amine stripper employing monoethanolamine (MEA) as a mass separating agent to absorb the CO_2.

A process flow diagram of the evaluated hydrogen production process is presented in Fig. 1. After reducing the temperature of the SCWG effluent to sub-critical conditions and flash drum separation, a turbo-expander recovers the energy from the vapour as electricity. In addition, electricity is generated upon letting down the spent flue gas after it has been used for steam generation. Most of the generated electricity is utilised within the process. However, the unused fraction is exported for sale to the grid as renewable electricity.

2.2.3. Automation

The ActiveX function in MATLAB was used to automate the input of the different biomass compounds. The biomass properties were transferred from MS Excel to Aspen HYSYS via a MATLAB script. To ensure each feedstock was evaluated on the same basis, a set of constraints was defined to be adhered to by all simulations. Owing to the different feedstock compositions, each simulation required manual adjustments to achieve these same constraints.

- Split between combustion and SMR adjusted to maintain energetic self-sufficiency
- Steam to carbon ratio maintained at 5.5 mol/mol by adjusting water flowrate to SMR
- MEA flowrate adjusted to achieve hydrogen purity >99.5% v/v
- Temperatures adjusted to prevent temperature crosses in heat exchangers

2.2.4. Techno-economic analysis

The LCOH was computed for each biomass composition, processing capacity, and location combination. This was

Table 2 – Operating conditions and modelling parameters used in the process simulation.

Parameter	Value	Comments
SMR temperature (°C)	1000	Kinetics based on a commercial Ni/α-Al_2O_3 catalyst [34].
SMR pressure (kPa)	1000	
Steam/carbon ratio (mol/mol)	5.5	To avoid carbon formation on the catalyst.
HTS temperature (°C)	420	Power law kinetics) for a commercial iron-based catalyst [35].
LTS temperature (°C)	200	Power law kinetics for a commercial Sud-Chemie Cu/ZnO/Al_2O_3 catalyst [36].

calculated from the discounted cash flow analysis across the considered 25-year plant life. The costing models and investment analysis parameters as used in the authors' previous work were used for the TEA, summarised in Tables S3–4 in the Supplementary Information [24,37]. An 8% discount rate was used in line with Europe's hurdle rates for electricity generation costs from biomass sources, e.g. 8.3% for AD and 7.9% for dedicated biomass (5–100 MW) and energy from waste (combined heat and power) [38]. The economic models were created for three geographic locations (China, Brazil, and the UK). As such, different location factors, operator salaries, and renewable electricity prices were used between the techno-economic models. These are summarised in Table 3.

2.2.5. *Feedstock cost*

A universal method for computing the utility value of the feedstock was developed based on the HHV of the biomass relative to natural gas. Methane production from AD is an alternative treatment method for dilute biomass feedstocks. However, AD can only exploit the Biological Oxygen Demand of a feedstock, whereas SCWG exploits the COD. An efficiency factor of 70% was thus applied to the calculated HHV, reflecting a high Biological Oxygen Demand to COD ratio [44]. The feedstock's price was then computed based on the adjusted HHV relative to the HHV of natural gas and using the EIA's price projections [45].

2.2.6. *Uncertainty analysis*

An uncertainty analysis was undertaken on the LCOH for each biomass composition, processing capacity, and location considered. A Monte Carlo analysis was conducted comprising 2,000 simulations where the fixed capital (80%–150%), variable operating (80%–200%), feedstock cost (90%–130%), and renewable electricity prices (80%–200%) were stochastically varied using a uniform distribution of the outlined ranges. This produced a probability distribution of the LCOH for each parameter combination. The calculated 5th and 75th percentiles from the Monte Carlo simulations were predicted along with the nominal LCOH by the surrogate model. This provided the 70% probability band of the LCOH for the investigated feedstock, capacity, and geographic location.

2.3. *Life cycle assessment model*

A cradle-to-gate LCA was undertaken for each biomass feedstock for the two products, hydrogen and renewable electricity. The considered functional units were 1 GJ of hydrogen (GJ_{H2}) and 1 MWh of renewable electricity. The emissions were allocated between these two products using energy allocation.

As the model was created for waste biomass feedstocks, no feedstock emissions were allocated. Furthermore, the CO_2 emitted is of biogenic origin and so does not contribute to the overall GHG emissions. Carbon capture units were not considered owing to the uncertainty around storage arrangements for small production streams, such as those generated in this study. The products were compared to other hydrogen production methods and each country's respective electricity grid emissions. The GHG emissions for MEA and water were obtained from the ecoinvent 3.7 inventory [46]. Emissions for transportation were considered using EURO 6 freight lorries of

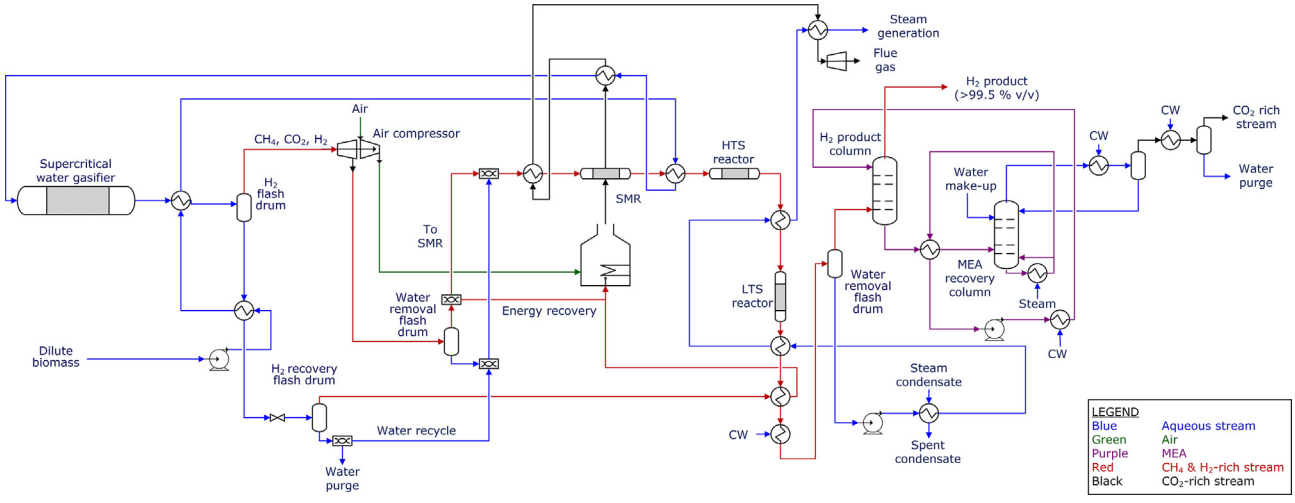

Fig. 1 – Process flow diagram of the low-temperature SCWG of biomass feedstocks for renewable hydrogen production.

Table 3 – Location factors, operator salaries, and renewable electricity selling price for the different global locations considered for the TEA. For comparison, the values are converted to 2022 US$ and presented in brackets.

Geographic Location	Location Factor	Average Operator Salary (yr) [39]	Renewable electricity price (kWh)	Currency conversion [43]
China	0.66	¥ 172,172 ($ 24,104)	¥ 0.75 ($ 0.105) [40]	0.14
Brazil	1.06	R$ 81,840 ($ 15,550)	R$ 0.315 ($ 0.059) [41]	0.19
UK	1.04	£ 33,776 ($ 41,207)	£ 0.126 ($ 0.154) [42]	1.22

16–32 tn capacity. A full life cycle inventory can be found in Table S5 in the Supplementary Information. Whilst cooling and process water were assigned emissions, the emissions associated with dilution or evaporation of feedstocks to the 75 g/L_{COD} were not considered.

2.4. *Transportation*

In the TEA and LCA, each feedstock was assessed at its point of origin, meaning no transportation costs or emissions were included. However, as the impact of capacity on processing costs is assessed, an investigation into of the impact of transporting localised waste streams to larger facilities is warranted. This analysis was undertaken on distillery wastewater in the context of the UK. The cost of transporting the feedstocks was taken as £ 0.25 t/km based on costs for digestate transportation [47] and updated using the ratio of UK diesel prices in 2022 to 2016. The waste transportation capacity was selected based on the evaluated facility sizes (10, 20, 50, 100 and 200 m^3/h). Thereby, a 100 m^3/h facility could be located at a facility producing a waste stream of either 100, 50, 20, or 10 m^3/h, necessitating the additional waste to achieve the 100 m^3/h capacity to be transported to it. A nominal 30 km transport distance was selected.

2.5. *Surrogate model*

For each feedstock, six input variables were provided to each model, including the weight percentage of C, H, O, and N (descriptive statistics of the biomass compositions are presented in Table 1), processing capacity (10, 20, 50, 100 or 200 m^3/h), and geographic location (China, Brazil, or the UK). The geographic location was defined as 1 (China), 2 (Brazil), or 3 (the UK) to input into the model. The outputs of the model were the nominal LCOH and corresponding 5th and 75th percentiles, representing the 70% probability band. Due to minimal variability in the process emissions across different feedstocks and capacities, the surrogate model was not trained to predict the process emissions. Three ML algorithms, RF, SVR, and ANNs, were investigated for the surrogate model, as they have been previously considered for predicting hydrogen production via SCWG [9,10].

2.5.1. *Model optimisation and evaluation*

The 600 TEA combinations were split into training, validation, and test sets. As the hydrogen yield varied between biomass feedstocks, the feedstocks were distributed among these sets. Thereby, if a biomass feedstock was placed in the test set, the entire set of parameter combinations for that feedstock, i.e. processing capacities and geographic location, was also included in the test set. This approach ensured that the model was trained to generalise across feedstock compositions rather than capacity and location and supports the goal of developing a generalisable model to evaluate the economic potential of hydrogen production from different biomass feedstocks. The data-set was split into a training set of 360, a validation set of 120, and a test set of 120 parameter combinations. Distributing the biomass feedstocks among the sets resulted in 24 biomass feedstocks in the training set, 8 in the validation set, and 8 in the test set. The best-performing hyperparameters were selected based on cross-validation performance, ensuring that the test set's performance indicated the model's generalisation potential for user input feedstocks. To optimise each ML algorithm a 4-fold cross-validation procedure was undertaken on the combined training and validation sets using an exhaustive grid search. The hyperparameters that were optimised for each algorithm are presented in Table 4. GridSearchCV from scikit-learn was used to determine optimal hyperparameters for each ML algorithm [48]. During the cross-validation process, the Root Mean Squared Error (RMSE) was used as the performance metric for each algorithm and as the loss function in the ANN.

An ensemble of predictions is produced by the RF algorithm, with the final output being the average of each decision tree's prediction. Ensemble methods typically have higher prediction accuracy because they reduce dispersion error and bias by averaging model predictions. They have previously shown improved prediction performance for hydrogen production via SCWG [10]. Consequently, an ensemble approach was also applied to ANNs, which randomly initialise starting weights and biases. This diversity allows each model to capture different aspects of the data. The average prediction from ten ANN models using the optimised hyperparameters was used to evaluate the algorithm's performance. Unlike ANNs, SVR does not contain random elements during model training, so an ensemble of SVR using optimised hyperparameters was not implemented.

After determining the optimal hyperparameters for each algorithm, it was evaluated on the test set to provide an indicative performance measure of the model's generalisability to unseen feedstocks. Three performance metrics were used to assess the model's prediction accuracy: RMSE, Mean Absolute Percentage Error (MAPE), and the determination coefficient (R^2). Each metric has different advantages: RMSE measures the standard deviation of the prediction errors, penalising large errors and making it more sensitive to outliers; MAPE measures the absolute error between the true and predicted values and presents them as a percentage, being less sensitive to larger errors than RMSE; and R^2 represents the fitness of the model to the true values and provides an intuitive result, with a value of 1 representing a perfect fit.

Table 4 – Hyperparameters and ranges considered for each algorithm during the cross-validation grid search procedure.

Random forests	Support vector regression	Artificial neural network
Number of trees (10–500)	L2 Regularisation penalty (1.1–1000)	Number of layers (1–3)
Maximum number of features for split (1–6)	Kernel type (linear, polynomial, radial basis function, sigmoidal)	Neurons in each layer (2–256)
Maximum depth of the tree (10–500)	Kernel coefficient (0.01–100)	L2 Regularisation penalty (0.00001–0.1)
Minimum number of samples before split (1–10)	Degree (for polynomial kernel function only) (1–3)	Learning rate (0.00001–0.1)
Minimum data in a leaf (1–10)	Epsilon (0.001–10)	Epochs (1000–10,000)
Bootstrap sampling (with or without replacement)		Batch size (2–256)

Eqs (3)–(5) present these metrics, where N is the number of datums, y_j is the true value, $\hat{y}_t$ is the predicted value, and y_M is the mean value. The published surrogate model was trained on the entire data-set using the algorithm and hyper-parameter set that produced the most accurate predictions during the cross-validation procedure.

$$RMSE = \sqrt{\frac{1}{N}\sum_{t=1}^{N}\left(y_j - \hat{y}_t\right)^2} \tag{3}$$

$$MAPE = \frac{1}{N}\sum_{t=1}^{N}\frac{y_j - \hat{y}_t}{y_j} \tag{4}$$

$$R^2 = \frac{\sum_{t=1}^{N}\left(y_j - y_M\right)^2}{\sum_{t=1}^{N}\left(\hat{y}_t - y_M\right)^2} \tag{5}$$

2.5.2. *Feature importance*

ML models are often referred to as "black box" models due to the complexity of their internal workings, which are not easily interpretable. To address this interpretability challenge, feature importance methods are employed. One such method is SHapley Additive exPlanation (SHAP) values. These values assign a contribution score to each feature, indicating its importance in the model's output. By utilising SHAP values, users can gain a better understanding of the relationships between input features and model outputs [49]. In previous studies, SHAP values have been applied to identify redundant input data, thereby reducing the computational cost of ML models [9]. However, in this work, SHAP values are used to highlight the relative importance of the input features. The SHAP values were obtained for the best-performing ML model using the SHAP library in Python.

3. Results and discussion

The TEA and LCA results are presented for the 600 parameter combinations (biomass composition, capacity, and geographic location). The impact of feedstock transportation is also presented and discussed. The production costs and process emissions are compared to both MW-scale electrolysis using renewable electricity and SMR with CCS (Carbon Capture and Storage). The performance of the three ML algorithms is also presented and compared.

3.1. *Techno-economic analysis*

The LCOH for the 600 techno-economic parameter combinations were computed, achieving levelised costs of 1.66–11.89 $/kg$_{H2}$ (China), 2.61–16.82 $/kg$_{H2}$ (Brazil), and 2.46–18.73 $/kg$_{H2}$ (UK). Different feedstock compositions and capacities led to significant variations in the economic outcome.

3.1.1. *Location*

Fig. 2 presents the LCOH for the 600 techno-economic parameter combinations. Fig. 2a presents the results for China, 2b for Brazil, and 2c for the UK. The geographic location produces a considerable difference in the LCOH. The UK produced the highest prices, followed by Brazil and then China. The higher prices for both the UK and Brazil are attributed to higher capital and operating costs (Table 3).

3.1.2. *Processing capacity*

The capacity of the SCWG facility is shown to have a substantial impact on the LCOH (Fig. 2a–c). As the scale increases, the LCOH decreases following an inverse power law relationship. The observed power law relationship is likely because most equipment cost correlations follow power law relationships. Furthermore, in capital cost estimation the 'six-tenths rule' can be applied to update the capital cost of a plant or processing equipment based on the cost of the same item at a different capacity by using a 0.6 exponent (average for the chemical industry) [50]. Applying a power law to the average LCOH for each geographic location gives rise to three different correlations, each with an $R^2 > 0.93$ and exponents ranging between −0.48 and −0.58. However, these correlations represent the average LCOH and the correlation for each biomass composition and corresponding location would be different (Fig. 2a–c). This prevents the use of a simple correlation to predict the LCOH for different feedstocks and illustrates the utility of a TEA surrogate model applicable to a wide range of inputs.

3.1.3. *Uncertainty analysis*

A Monte Carlo simulation comprising 2,000 simulations was undertaken on each of the 600 techno-economic scenarios by varying the fixed capital, variable operating, feedstock, and renewable electricity costs within the uncertainty ranges summarised in Section 2.2.6 Uncertainty Analysis. All parameters were varied stochastically using a uniform distribution between the defined ranges. The LCOH for each stochastic parameter combination was computed and the 5th,

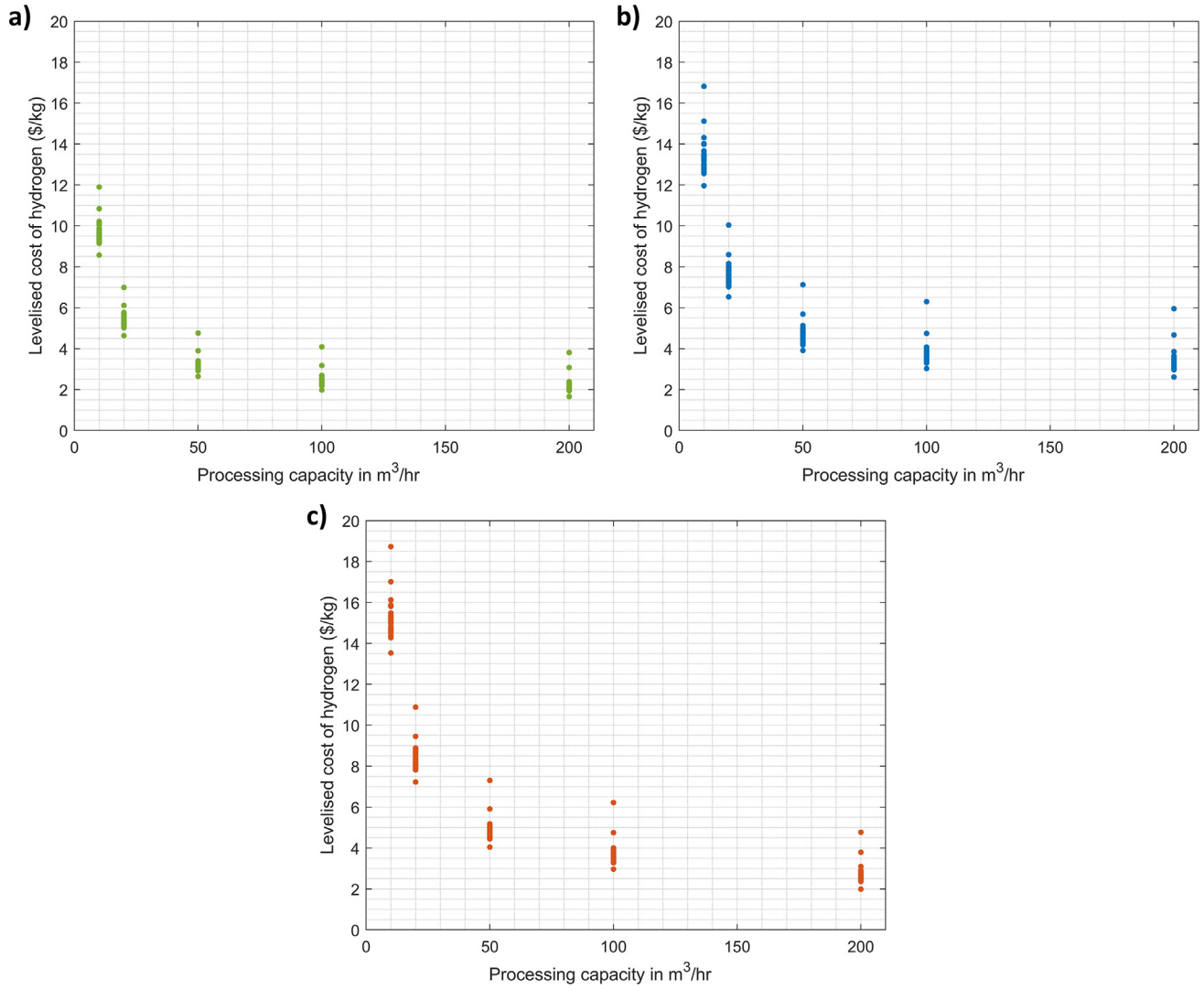

Fig. 2 – a–c: LCOH ($/kg$_{H2}$) for different processing capacities (m^3/hr). a) Presents the results for China, b) presents the results for Brazil, and c) presents the results for the UK. Each location has 40 data points representing the biomass feedstocks and is presented using the same y-axis.

25th 50th, 75th, and 95th percentiles were calculated. The 5th and 75th percentiles represent the 70% probability band for the LCOH. On average, this probability band displayed a −13% and +28% deviation from the nominal value for all parameter combinations. The deviations were similar for all cases, ranging from −22% to +32%. The greater positive variability observed is attributed to the larger upward deviations assigned to the uncertainty parameters.

3.1.4. *Gate fee*

Some feedstocks could command a gate fee to handle their disposal, forming an additional source of revenue. For example, the median gate fees in the UK for AD and energy from waste disposal options are £30/t and £95/t, respectively [51]. Food waste is a typical AD feedstock [47] and is used here to illustrate the impact of including a gate fee for SCWG in the UK. Gate fees of £10/t, £20/t, and £30/t ($12/t, $24/t, and $37/t), up to and equalling that of AD, were selected (Fig. 3). Notably, the inclusion of a gate fee significantly reduces the LCOH, creating economically viable solutions at smaller capacities. At a capacity of 10 m^3/h, a gate fee of $37/t (equalling that of AD) leads to an LCOH of $4.82/kg, comparable to MW-scale electrolysis using renewable electricity, which ranges from $4.81/kg to $6.31/kg [22]. However, at a capacity of 20 m^3/h, a gate fee of only $12/t is required to achieve a comparable LCOH, and a gate fee of $37/t results in a negative LCOH. At capacities >50 m^3/h, the addition of a gate fee results in a low or even negative LCOH (Fig. 3), demonstrating the technology's potential to outperform AD as a waste treatment option and the economic potential of valorising waste streams at these capacities.

3.2. *Life cycle assessment*

The range in cradle-to-gate GHG emissions of the evaluated feedstocks in Brazil and China was 0.32–0.65 kgCO_2eq/GJ$_{H2}$ (0.038–0.078 kgCO_2eq/kg$_{H2}$) with an average of 0.46 kgCO_2eq/GJ$_{H2}$ (0.055 kgCO_2eq/kg$_{H2}$). In the UK, the GHG emissions ranged between 0.25 and 0.52 kgCO_2eq/GJ$_{H2}$ (0.031 and 0.063

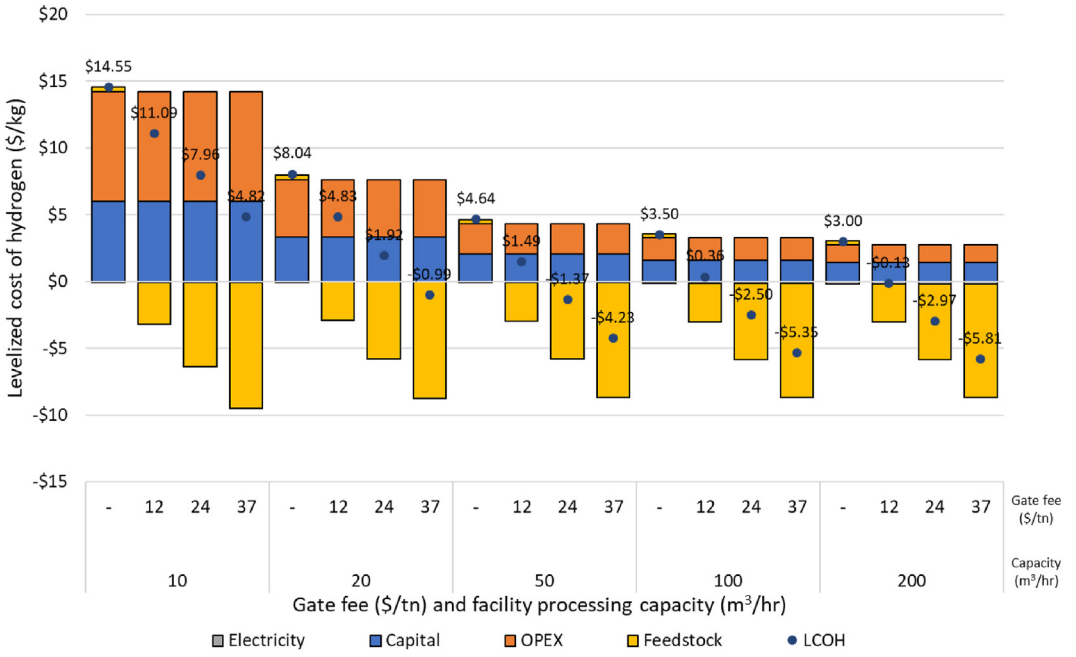

Fig. 3 – Impact of the inclusion of a $12/t, $24/t and $37/t gate fee on the LCOH for food waste biomass.

$kgCO_2eq/kg_{H2}$) with an average of 0.37 $kgCO_2eq/GJ_{H2}$ (0.044 $kgCO_2eq/kg_{H2}$). The difference between countries is due to the use of global emission factors for both Brazil and China and European emission factors for the UK. The low overall emissions are attributed to its energetic self-sufficiency of the SCWG process, negating the need for external energy sources. The only utilities used throughout the process are MEA make-up to account for losses during CO_2 removal and deionised water for both cooling and water make-up in the stripper. The GHG emission ranges for all feedstocks considered comfortably meet the European Union CertifHy scheme for low carbon hydrogen ($\leq$36.4 $kgCO_2eq/GJ_{H2}$) based on a 60% reduction in emissions from SMR [52]. In contrast, SMR with CCS produces 8 $kgCO_2eq/GJ_{H2}$, at 90% capture efficiency [53]. However, including emissions associated with natural gas leakage increases this estimate to 21 $kgCO_2eq/GJ_{H2}$ [53], over an order of magnitude higher than estimates for SCWG.

The emissions attributed to the exported renewable electricity were also minimal, with an average of 0.04 $kgCO_2eq/MWh$ for Brazil and China and 0.03 $kgCO_2eq/MWh$ for the UK. This is in comparison to the grid intensity of China, Brazil, and the UK being 850 $kgCO_2eq/MWh$ [54], 292 $kgCO_2eq/MWh$ [54], and 194 $kgCO_2eq/MWh$ [55], respectively.

3.3. *Transportation impact*

The impact of transporting wastes to a larger facility was investigated for both the economics and process emissions and is presented in Fig. 4a and b for distillery wastewater in the UK. Due to the dilute nature of pot ale, only draff (solids content 21.6 wt% [26]) was considered for transportation in this analysis.

Transporting draff to a different distillery for processing demonstrates a decrease in the LCOH compared to solely processing point source distillery waste (Fig. 4a). For example, a distillery producing 10 m^3/h of wastewater at 75g/L_{COD} yields a LCOH of $15.37/kg by processing only point source waste. However, transporting enough draff to operate a SCWG facility of 50 m^3/h (located at the same distillery producing 10 m^3/h) leads to a decrease in the LCOH to $8.26/kg. This decreasing trend in LCOH is demonstrated for all point source feedstock processing capacities between 10 and 50 m^3/h. The observed decrease is due to the capital and operating cost intensity decreasing more appreciably than the added cost of transportation. Conversely, at a point source of 100 m^3/h of wastewater, the transportation of draff to support a 200 m^3/h SCWG plant increases the LCOH from $3.51/kg to $3.78/kg.

Regarding process emissions (Fig. 4b), any transportation of waste proves detrimental to the GHG emissions. In all cases considering draff transportation the transport emissions dominate the overall process emissions. However, the emissions are still well below SMR with CCS, which are 8 $kgCO_2eq/GJ_{H2}$ (excluding emissions associated with natural gas leakage) [53].

It is important to note that the transportation of biomass is logistically challenging. Studies considering large capacity plants often explore decentralised supplies that enable satellite pre-processing or combine multiple modes of transportation, depending on the transportation distance [56]. The assumptions made for this analysis do not consider these complexities, and further investigation should be undertaken for specific feedstocks, alongside the actual transport distances required. In addition, biomass compositions may be more or less dilute than considered here. This would change the associated transport costs, as evaporation would occur at the point of origin, and dilution would occur at the point of processing.

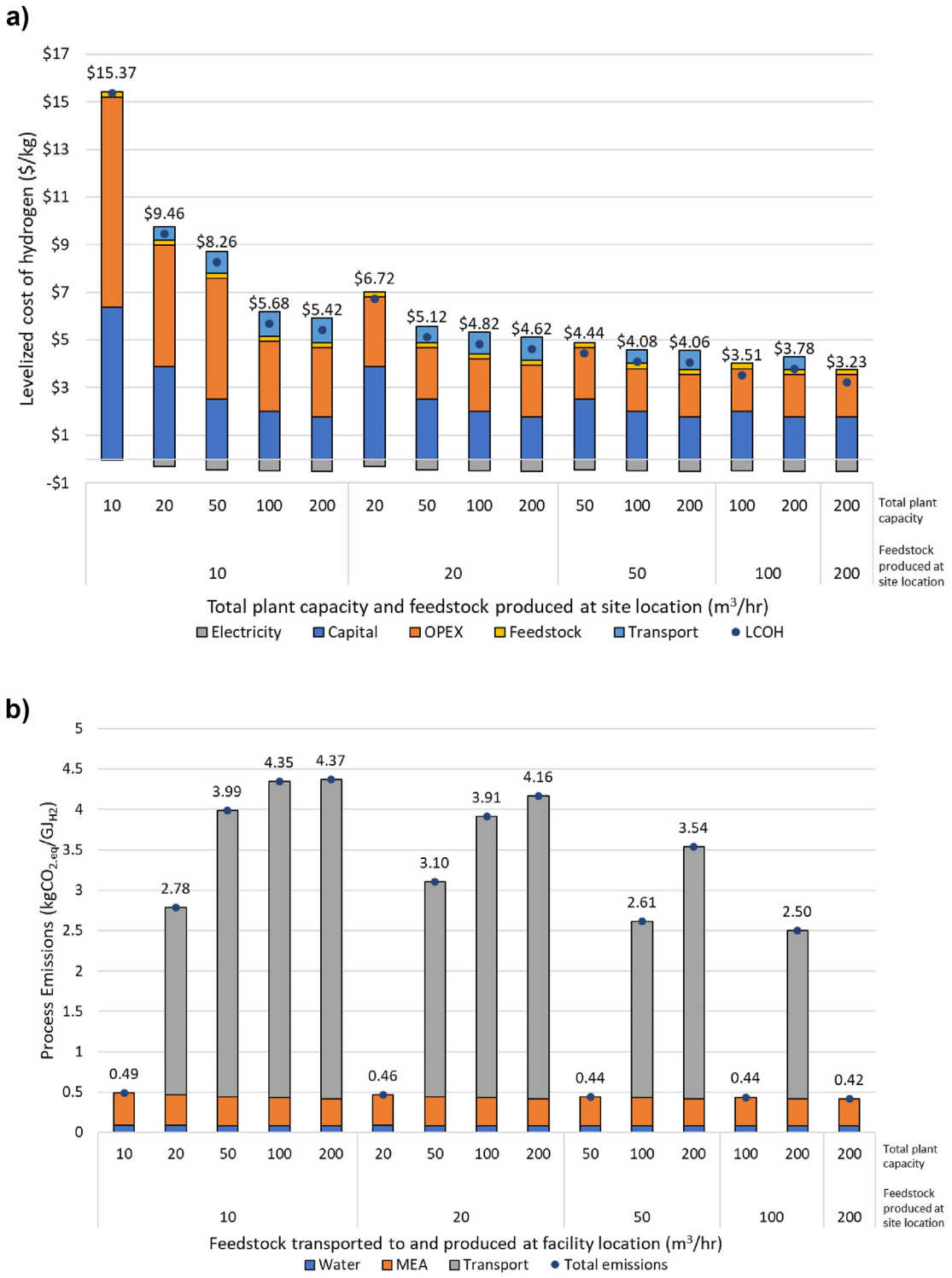

Fig. 4 – a–b: Impact of transporting distributed waste streams to larger processing facilities on the LCOH ($/kg$_{H2}$) (4a) and process emissions (kgCO2eq/GJ$_{H2}$). (4b). Analysis results are for distillery wastewater in the UK.

3.4. *Comparison to alternative low carbon hydrogen production*

Hydrogen production costs are significantly impacted by capital costs, technology efficiency, capacity factors, energy costs, and the plant location [57]. Fig. 5 presents the 70% probability band of the LCOH at the considered SCWG capacities for black liquor in China, vinasse in Brazil, and distillery wastewater in the UK. These biomass feedstocks were selected as they represent feedstocks readily available in

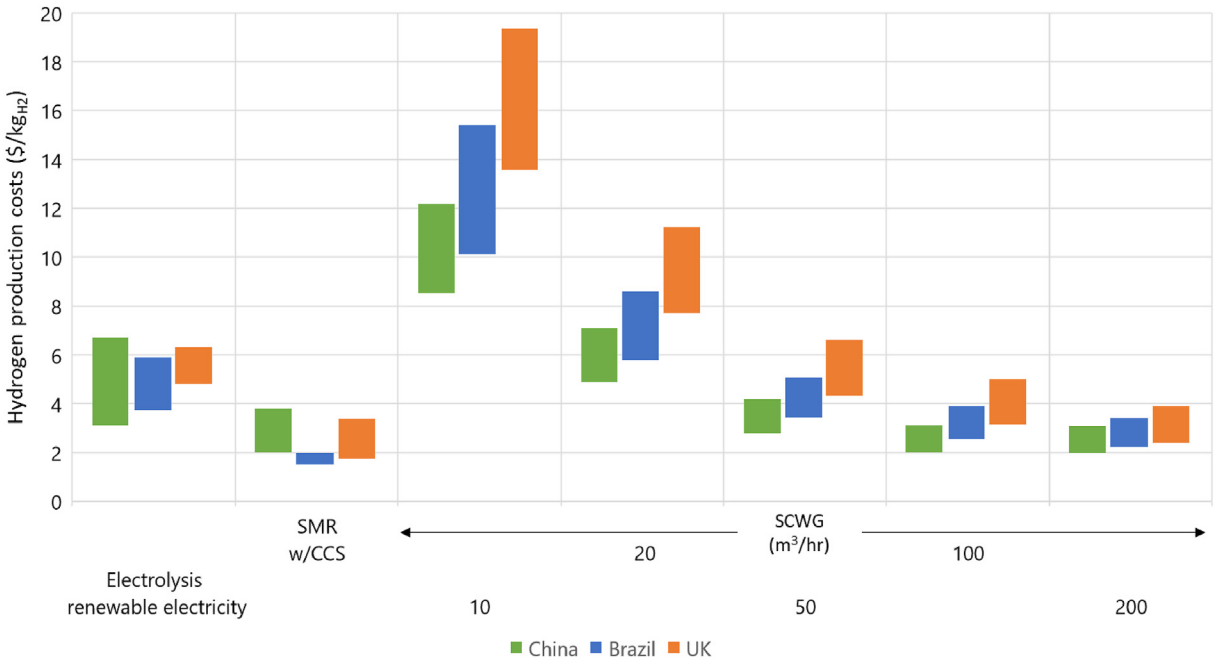

Fig. 5 – Comparative LCOH for MW-scale electrolysis using renewable electricity, SMR with CCS, and SCWG for black liquor in China, vinasse in Brazil, and distillery wastewater in the UK. The displayed results exclude transportation or gate fee considerations.

these countries. The resulting LCOH's are compared to each country's cost estimates for alternative low carbon hydrogen production methods, namely, hydrogen production via MW-scale electrolysis using renewable electricity and SMR with CCS. Estimates are obtained from the IEA for China [58,59] and Brazil [60], and BEIS for the UK [22].

In all countries, at a SCWG capacity of 50 m^3/h, the LCOH (2.76–4.21 $/kg_{H2}$ for China, 3.41–5.07 $/kg_{H2}$ for Brazil, 4.31–6.62 $/kg_{H2}$ for the UK) is cost competitive with hydrogen production via MW-scale electrolysis using renewable electricity (3.10–6.70 $/kg_{H2}$ for China, 3.70–5.90 $/kg_{H2}$ for Brazil, and 4.81–6.31 $/kg_{H2}$ for the UK). This demonstrates the potential for isolated feedstock valorisation using low-temperature SCWG at capacities >50 m^3/h. Additionally, in China SCWG capacities >50 m^3/h are comparable to SMR with CCS (2.00–3.80 $/kg_{H2}$) and in the UK, the 200 m^3/h SCWG capacity achieves a similar LCOH (2.36–3.92 $/kg_{H2}$) to SMR with CCS (1.74–3.40 $/kg_{H2}$). However, SMR with CCS is notably cheaper than even the largest SCWG facility size in Brazil. As SMR is the dominant commercial hydrogen production technology globally, the lower production costs for SMR with CCS are unsurprising.

Importantly, SCWG is ideally suited to wet feedstocks that are uneconomical for use via conventional energy recovery methods. Therefore, valorising these feedstocks via SCWG has limited resource competition and represents a renewable hydrogen source from otherwise under-utilised resources. In contrast, MW-scale electrolysis and SMR utilise renewable electricity and natural gas, both of which have numerous alternate uses and competition. As such, electrolysis and SMR are subject to price fluctuations in world energy markets. This means that changes in global energy markets directly affect the predicted prices in Fig. 5. A timely example is natural gas prices, which averaged $6.45/MMBTU in 2022, up from $2.03/MMBTU in 2020 [61].

3.5. *Surrogate model*

The optimal hyperparameters obtained during the 4-fold cross validation procedure are presented in Table 5. Table 6 illustrates the performance metrics for the ML models using the optimal hyperparameters for the nominal LCOH on both the validation and training sets. Overall, ANN's achieved the highest model performance for both the validation and test sets, achieving accuracy values of MAPE: <4.6%, RMSE: <0.39, and R2: >0.99 on the test set. This is likely due to their ability to combine inputs into new features and thus utilise the relationship between inputs. A parity plot of the ANN's performance on the test set is presented in Fig. S1 in the Supplementary Information. Owing to the comparison of models, optimisation of hyperparameters, exhaustive grid search, and 4-fold cross validation procedure the outcome reflects the final accuracy of the ML task. Since the hyperparameters have been selected based on the validation set and the training, validation, and test sets were segregated based on biomass composition, the models' performance on the test set is a robust indicator of generalisation to new, unseen, biomass feedstocks. This is important as it represents the model's accuracy when utilised by researchers assessing their feedstock compositions.

The relative feature importance for the ensemble of ten ANN models is presented using SHAP values in Fig. 6. Fig. 6a presents the absolute significance of each feature, larger values indicate a greater impact on the model output (LCOH). Regarding the relative importance, the processing capacity was the dominant feature for the ML models. This is

Table 5 – Optimal hyperparameters determined during the 4-fold cross-validation grid search.

Random forests	Support vector regression	Artificial neural network
Number of trees: 100	L2 Regularisation penalty: 100	Number of layers: 1
Maximum number of features for the split: 2	Kernel type: radial basis function+	Neurons in each layer: 64
Maximum depth of the tree: 100	Kernel coefficient: 4	L2 Regularisation penalty: 0.001
Minimum number of samples before split: 2	Degree (for polynomial kernel function only): N/A	Learning rate: 0.001
Minimum data in a leaf:1	Epsilon: 0.5	Epochs: 5000
Bootstrap sampling: without replacement		Batch size: 16

unsurprising considering the substantial variability in LCOH observed across different capacities, as shown in Fig. 2. Geographic location was the second most important feature, attributed to the different economic inputs (Table 3) producing different LCOH's for the same biomass composition and processing capacity combinations. Among the biomass composition features, the hydrogen content demonstrated the greatest impact. Fig. 6b displays the impact of each feature using a bee swarm plot, where negative values indicate a negative impact on the model output (LCOH). The feature value scale from pink (high) to blue (low) indicates the feature input value. For example, a high processing capacity (coloured in pink), has a negative impact on the model output, thereby reducing the LCOH. It is also evident that higher H wt% leads to a reduction in the LCOH. This is to be expected as biomass with a higher hydrogen content yields more hydrogen, thereby lowering the LCOH. Increases in the other composition features all had a positive impact on the model output, indicating that higher C, N, and O wt% leads to an increase in the LCOH. This can be attributed to a greater wt % of these elements reducing the H wt%, subsequently decreasing the hydrogen yield obtained from the biomass.

The published model uses an ensemble of ten ANNs trained using the entire data-set of 600 TEAs using the optimal hyperparameters determined during the cross-validation procedure. The model inputs are the biomass' ultimate analysis, the processing capacity, and the geographic location. The nominal, lower (5th), and upper (75th) LCOH are the model outputs. The surrogate model was trained using data from five specific processing capacities (10, 20, 50, 100, and 200 m^3/h). However, the model is intended to predict the LCOH for the range of capacities 10–200 m^3/h. To demonstrate the model's ability to interpolate between the capacities used for training, Table S6 in the Supplementary Information presents a comparison between the model predictions with simulated results for an unseen biomass sample in Brazil. Processing capacities of 10, 15, 20, 35, 50, 75, 100, 150 and 200 m^3/h were considered for the comparison. All the model predictions achieved a percentage error less than the MAPE of 4.42% obtained over the test set when compared to the simulated results. This low percentage difference highlights the model's capability to accurately predict beyond the specific training capacities used during its development, thus demonstrating its predictive ability. Extrapolation beyond the scales considered during model development (10–200 m^3/h) is not permitted by the model and is therefore not demonstrated.

3.5.1. *Model uncertainty*

The accuracy of a ML model's prediction on new, unseen inputs depends on this data's similarity to the model's training data. A method to estimate model uncertainty can be used to determine when this new data deviates significantly from the training set. This can be used to estimate when the models produce unreliable predictions. This is important for predictions made using new biomass samples inputted by the

Table 6 – Performance metrics for the ML algorithms. Metrics are displayed for both the validation and testing sets. The best performing model for each metric is presented in bold.

Prediction	Data-set	Evaluation metric	RF	SVR	ANN
Nominal	Validation	RMSE	0.414	1.321	**0.197**
		MAPE	3.39%	19.7%	**1.56%**
		R^2	0.989	0.885	**0.998**
	Testing	RMSE	0.303	1.898	**0.291**
		MAPE	**4.00%**	39.3%	4.42%
		R^2	0.994	0.761	**0.994**
5th percentile	Validation	RMSE	0.332	1.170	**0.166**
		MAPE	3.16%	20.5%	**1.47%**
		R^2	0.990	0.881	**0.998**
	Testing	RMSE	**0.264**	1.758	0.279
		MAPE	**0.041**	0.425	4.58%
		R^2	**0.994**	0.731	0.993
75th percentile	Validation	RMSE	0.532	1.664	**0.236**
		MAPE	3.45%	17.6%	**1.63%**
		R^2	0.988	0.885	**0.998**
	Testing	RMSE	0.394	2.313	**0.389**
		MAPE	**4.07%**	35.4%	4.43%
		R^2	0.994	0.777	**0.994**

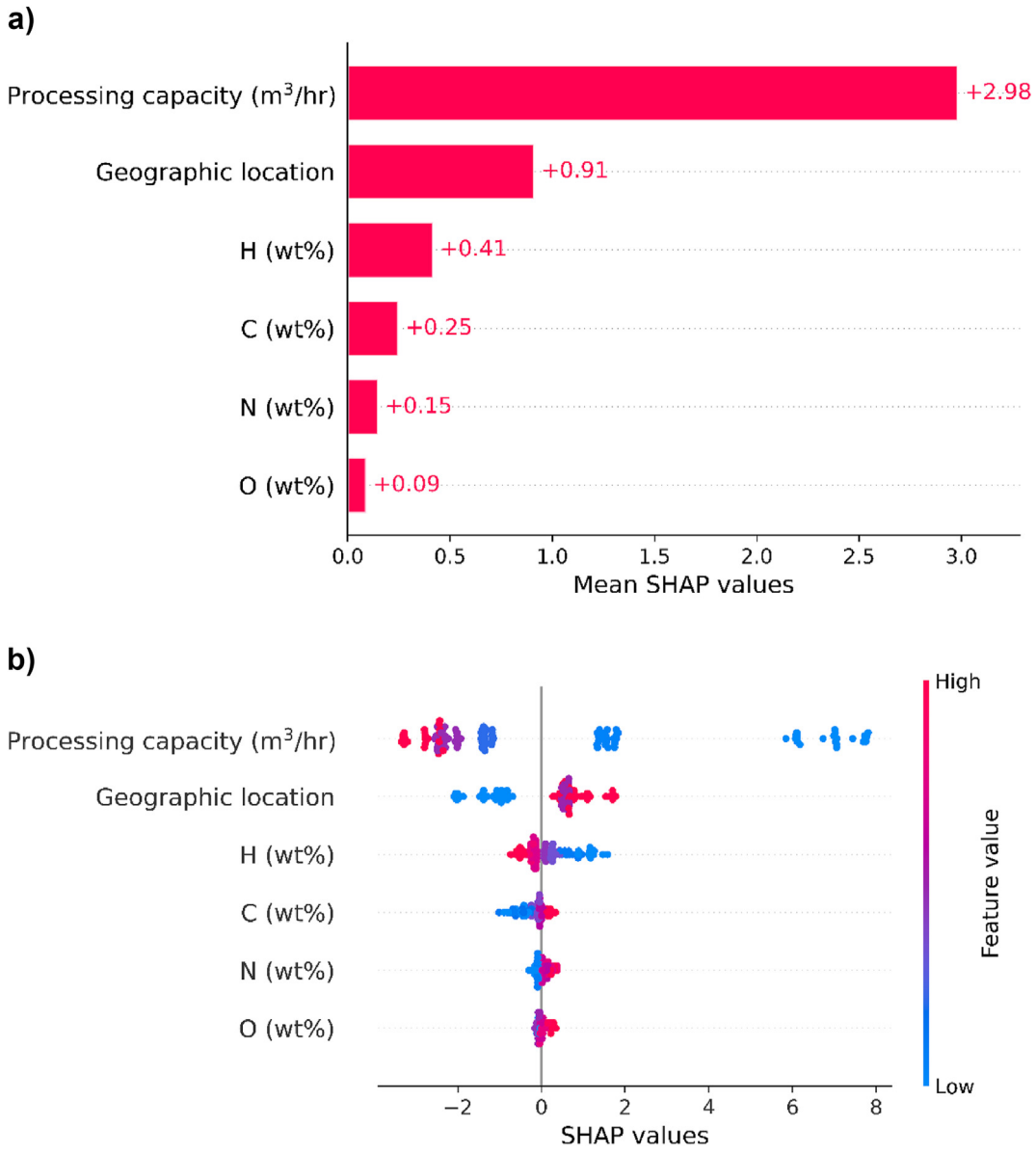

Fig. 6 – a–b: Feature importance of the model inputs on the LCOH Predictions using SHAP values. a) Absolute importance of input features on model output. b) Impact of input features on the model output. High feature values (inputs) are displayed in pink and low feature values are displayed in blue.

end user. In the ensemble approach, each ANN has different weights and biases owing to random initialisation. The diversity between each model will be greater in regions that were less well represented in the training data. Therefore, greater variance between the model predictions is observed in these regions. As such, the variance between the ensemble of predictions gives an indication of the model's uncertainty, with larger variations between predictions suggesting greater model uncertainty [62]. By setting a threshold for the allowable variance between predictions, unreliable predictions can be identified. This approach is similar to anomaly detection using autoencoders where an anomaly threshold is set by a reconstruction error [63].

For the published model, the permissible uncertainty threshold was set as the maximum variance observed for the nominal predictions during a 5-fold validation procedure on the entire data-set (600 parameter combinations). I.e. the ensemble models were trained on 80% of the data and 20% of the data was held back from training (the validation set). This was repeated five times for different folds in the data. The maximum variance observed on the validation sets was used as the uncertainty threshold. As an additional indication of uncertainty, it is known that the lower, nominal, and upper LCOH should be predicted in ascending order. In instances where this is not upheld, the model inputs represent an area poorly represented during model development.

To illustrate this principle, Table 7 presents the model predictions for three fictitious biomass compositions at different capacities and locations. The predictions are classified as anomalous if the prediction variance exceeds the

Table 7 – Surrogate model predictions for fictitious biomass compositions at different processing scales and geographic locations. The predictions are classified as anomalous if the prediction variance exceeds the variance threshold, and implausible if the predicted lower, nominal, and upper LCOH are not in ascending order.

Fictitious biomass composition				Scale (m^3/hr)	Location	LCOH ($/$kg_{H2}$)			Anomalous prediction	Implausible prediction
C	H	N	O			Lower	Nominal	Upper		
35	15	15	35	15	China	6.85	8.19	9.12	✓	✗
				35		3.57	4.16	3.18	✓	✓
				150		2.46	2.54	2.02	✓	✓
40	15	5	40	5	Brazil	12.71	14.3	18.14	✗	✗
				150		2.33	2.37	3.52	✗	✗
				250		2.43	2.17	3.1	✗	✓
40	21	0	39	20	UK	6.06	6.23	8.35	✗	✗
				80		2.24	2.09	2.67	✓	✓
				110		1.81	1.63	2.62	✓	✓

uncertainty threshold, and implausible if the lower, nominal, and upper LCOH are not predicted in ascending order. All predictions for the first composition trialled were deemed anomalous. This is attributed to the unrealistic biomass composition, as the high nitrogen and hydrogen content is unlike the compositions used for training. Despite this, in two out of three instances the model produced plausible predictions, i.e. the lower, nominal, and upper predictions were in ascending order. Contrastingly, for the second biomass composition, all predictions were below the uncertainty threshold and not deemed anomalous. This composition was representative of a realistic biomass composition, and therefore likely represented by the training set. However, at a scale of 250 m^3/h the model prediction was implausible but was not detected as an anomaly. This capacity exceeded the range used during model training (10–200 m^3/h). Therefore, the implausible prediction is attributed to model extrapolation beyond the region used during training. The final biomass composition trialled also represents a realistic biomass compound. However, the prediction was deemed anomalous and implausible for two out of three predictions. This result demonstrates the utility of the uncertainty threshold as despite the input representing a reasonable biomass composition, the model demonstrates high variability which should be brought to the user's attention when using the prediction.

Based on the results in Table 7, the published model contains user warnings and restrictions to prevent its misuse. Firstly, the range of capacities are limited to those used during model training (10–200 m^3/h), preventing model extrapolation. Secondly, the user is warned if the prediction contains high variability i.e. the variance threshold is exceeded. Thirdly, if the variance is not exceeded, but the biomass composition is outside of the range of compositions used during training the user is warned. In both these instances the prediction is provided alongside the warning. Finally, no prediction is provided, and the user is warned if an implausible prediction is produced.

4. Study limitations

The Gibbs model is a valuable tool for simulating gasification, as it eliminates the need for defining complex equations. The model ensures that the mass and energy balance of the system is maintained, making it useful for initial process evaluations [29]. In TEA studies, the Gibbs model is widely employed to model SCWG [3–5]. One significant advantage of using the Gibbs model in an economic analysis is its ability to evaluate different feedstocks on an equivalent basis, avoiding biases that may arise from using experimental data obtained under varying conditions or levels of experimental rigour. However, it is important to note that the Gibbs reactor assumes the full conversion to gaseous products the attainment of thermodynamic equilibrium, which may not always hold true in an industrial setting. As a result, the gas composition may deviate from the predictions of the Gibbs model.

The Gibbs reactor's ability to model thermodynamic equilibrium in SCWG has been validated using high temperatures (600–900 °C) [64–67]. At elevated temperatures, reactions occur at faster rates, increasing the likelihood of attaining thermodynamic equilibrium at low residence times. A comparison between experimentally reported gas compositions and predictions from the Gibbs reactor for low-temperature SCWG (380–500 °C) are presented in Fig. S2 in the Supplementary Information. The experimental results of Louw et al. (2016), Osada et al. (2012), Yamaguchi et al. (2019), and Gökkaya Selvi et al. (2020) align reasonably well with the predictions of the Gibbs reactor [68–71]. However, the most notable deviation is observed between methane and hydrogen concentrations. This is most prominent in the results experimental by Lu et al. (2019), where significantly higher concentrations of methane and lower concentrations of hydrogen are predicted by the Gibbs model [72]. The discrepancy between hydrogen and methane concentrations has been reported previously at lower SCWG temperatures [65,66]. Higher methane formation is thermodynamically anticipated at lower temperatures owing to methanation entailing exothermic formation reactions [32,33]. As such, the differences between the Gibbs and experimental results suggest that the experimentally obtained SCWG gas compositions were not at equilibrium. To account for the assumption that thermodynamic equilibrium is obtained in this TEA study, a conservative 5-min residence time was considered for the continuous SCWG. This residence time is greater than previously investigated for continuous SCWG [2,21], and translates to an additional capital burden by oversizing the gasifier.

Table 8 – Sensitivity of the LCOH to the residence time assumed for SCWG. Biomass sample: chicken manure [73].

Processing capacity (m3/hr)	Levelised cost of hydrogen ($/kg)			
	5 min	10 min	15 min	20 min
10	14.60 (+0%)	15.64 (+7%)	16.57 (+13%)	17.43 (+19%)
20	8.21 (+0%)	9.04 (+6%)	9.80 (+11%)	10.51 (+16%)
50	4.67 (+0%)	5.33 (+5%)	5.94 (+9%)	6.52 (+13%)
100	3.55 (+0%)	4.11 (+4%)	4.65 (+8%)	5.16 (+11%)
200	3.05 (+0%)	3.55 (+3%)	4.03 (+7%)	4.50 (+10%)

As full conversion and the attainment of thermodynamic equilibrium using the assumed residence time is yet to be confirmed, a sensitivity analysis around this parameter has been conducted considering the impact of a 10, 15, and 20-min residence time on the LCOH for chicken manure [73] in the UK. The results of this analysis are presented in Table 8. A fourfold increase in residence time (20 min) led to a 10%–19% increase in the LCOH, with the greatest impact observed at the smallest processing capacity. This represents a relatively minor impact on the overall process economics and falls within the 70% probability band obtained from the Monte Carlo uncertainty analysis (+28%, on average). As such, the potential increased capital requirement to attain full conversion and thermodynamic equilibrium is comfortably captured within the considered probability band predicted by the ML surrogate model.

It is important to emphasise that the surrogate model predictions represent the economic potential of a feedstock considering full conversion to gaseous products and the attainment of thermodynamic equilibrium using continuous SCWG at 430 °C followed by SMR, HTS, and LTS. The predicted costs should therefore serve as a guide for identifying promising feedstocks based on their composition, location, and processing capacity. This allows for prioritisation of future research and development. Notably, the identification of a promising feedstock would still necessitate the optimisation of experimental conditions, i.e. residence time, catalyst type, and catalyst concentration as is undertaken in experimental studies such as [2].

5. Conclusion

A machine learning surrogate model has been created to predict the LCOH from low-temperature SCWG using different feedstock compositions, processing capacities, and geographic locations. This type of early-stage economic analysis tool helps to inform targeted research directions and investment decisions. A data-set of 600 process simulations using the Gibbs reactor provided the data to train the surrogate model. Three algorithms were investigated: RF, SVR, and ANNs. The highest prediction accuracy during cross-validation was by ANNs, achieving a test set accuracy of <4.6% (MAPE), RMSE: <0.39, and R^2: >0.99. The published surrogate model is trained on the entire dataset: doi.org/10.6084/m9.figshare.22811066.

Credit authorship contribution statement

Sarah Rodgers: Conceptualization, Data curation, Formal analysis, Investigation, Methodology, Software, Visualization, Writing – original draft, Writing – review & editing. **Alexander Bowler:** Data curation, Formal analysis, Methodology, Software, Writing – review & editing. **Jon McKechnie:** Funding acquisition, Methodology, Project administration, Resources, Supervision, Writing – review & editing. **Ed Lester:** Supervision, Writing – review & editing. **Chai Siah Lee:** Conceptualization, Methodology, Writing - review & editing. **Fanran Meng:** Methodology, Supervision, Writing – review & editing. **Laura Wells:** Methodology, Investigation, Writing – review & editing. **Martin Hayes:** Supervision, Writing – review & editing. **Stephen Poulston:** Supervision, Writing – review & editing. **Alex Conradie:** Conceptualization, Formal analysis, Funding acquisition, Methodology, Project administration, Resources, Supervision, Writing – review & editing.

Declaration of competing interest

The authors declare that they have no known competing financial interests or personal relationships that could have appeared to influence the work reported in this paper.

Acknowledgements

This work was supported by an EPSRC DTP CASE studentship with Johnson Matthey and by Industrial Biotechnology Catalyst project ConBioChem funded by Innovate UK, BBSRC and EPSRC (grant BB/N023773/1). Furthermore, this work was supported by the Future Biomanufacturing Research Hub (grant EP/S01778X/1), funded by the EPSRC and BBSRC, as part of UKRI. Finally, the authors gratefully acknowledge support received from the University of Nottingham Research Beacon of Excellence: Green Chemicals.

Appendix A. Supplementary data

Supplementary data to this article can be found online at https://doi.org/10.1016/j.ijhydene.2023.08.016.

REFERENCES

[1] Lee CS, Conradie AV, Lester E. Review of supercritical water gasification with lignocellulosic real biomass as the feedstocks: process parameters, biomass composition, catalyst development, reactor design and its challenges. Chem Eng J 2021;145:128837.

[2] Lee CS, Conradie AV, Lester E. The integration of low temperature supercritical water gasification with continuous in situ nano-catalyst synthesis for hydrogen generation from biomass wastewater. Chem Eng J 2023;445:140845.
[3] Sanaye S, Alizadeh P, Yazdani M. Thermo-economic analysis of syngas production from wet digested sewage sludge by gasification process. Renew Energy 2022;190:524–39.
[4] Liang J, Lie Y, Chen J, J E, Leng E, Zhang F, Liao G. Performance comparison of black liquor gasification and oxidation in supercritical water from thermodynamic, environmental, and techno-economic perspectives. Fuel 2023;334:126787.
[5] Okolie JA, Nanda S, Dalai AK, Kozinski JA. Techno-economic evaluation and sensitivity analysis of a conceptual design for supercritical water gasification of soybean straw to produce hydrogen. Bioresour Technol 2021;331:125005.
[6] Huntington T, Baral NR, Yang M, Sundstrom E, Scown CD. Machine learning for surrogate process models of bioproduction pathways. Bioresour Technol 2023;370:128528.
[7] Khan M, Raza Naqvi S, Ullah Z, Ali Ammar Taqvi S, Nouman Aslam Khan M, Farooq W, Taqi Mehran M, Juchelková D, Štěpanec L. Applications of machine learning in thermochemical conversion of biomass-A review. Fuel 2023;332:126055.
[8] Gopirajan PV, Gopinath KP, Sivaranjani G, Arun J. Optimization of hydrothermal gasification process through machine learning approach: experimental conditions, product yield and pollution. J Clean Prod 2021;306:127302.
[9] Li J, Pan L, Survarna M, Wang X. Machine learning aided supercritical water gasification for H2-rich syngas production with process optimization and catalyst screening. Chem Eng J 2021;426:131285.
[10] Zhao S, Jian L, Chen C, Yan B, Tao J, Chen G. Interpretable machine learning for predicting and evaluating hydrogen production via supercritical water gasification of biomass. J Clean Prod 2022;316:128244.
[11] Shenbagaraj S, Sharma Pankaj K, Sharma AK, Raghav G, Kota KB, Ashokkumar V. Gasification of food waste in supercritical water: an innovative synthesis gas composition prediction model based on Artificial Neural Networks. Int J Hydrogen Energy 2021;46(24):12739–57.
[12] Khan MNA, Haq ZU, Ullah H, Naqvi SR, Ahmed U, Zaman M, et al. Prediction of hydrogen yield from supercritical gasification process of sewage sludge using machine learning and particle swarm hybrid strategy. Int J Hydrogen Energy 2023 [in press].
[13] Fózer D, Tóth AJ, Varbanov PS, Klemeš JJ, Mizsey P. Sustainability assessment of biomethanol production via hydrothermal gasification supported by artificial neural network. J Clean Prod 2021;318:128606.
[14] Bilgiç G, Bendes E, Öztürk B, Atasever S. Recent advances in artificial neural network research for modeling hydrogen production processes. Int J Hydrogen Energy 2023;48(50):18947–77.
[15] Yahya HSM, Abbas T, Amin NAS. Optimization of hydrogen production via toluene steam reforming over Ni–Co supported modified-activated carbon using ANN coupled GA and RSM. Int J Hydrogen Energy 2021;46(48):24632–51.
[16] Kargbo HO, Zhang J, Phan AN. Robust modelling development for optimisation of hydrogen production from biomass gasification process using bootstrap aggregated neural network. Int J Hydrogen Energy 2023;48(29):10812–28.
[17] Sultana N, Hossain SMZ, Aljameel SS, Omran ME, Razzak SA, Haq B, Hossain MM. Biohydrogen from food waste: modeling and estimation by machine learning based super learner approach. Int J Hydrogen Energy 2023;48(49):18586–600.
[18] Sezer S, Özveren U. Investigation of syngas exergy value and hydrogen concentration in syngas from biomass gasification in a bubbling fluidized bed gasifier by using machine learning. Int J Hydrogen Energy 2021;46(39):20377–96.
[19] Liao M, Kelley S, Yao Y. Generating energy and Greenhouse gas inventory data of activated carbon production using machine learning and kinetic based process simulation. ACS Sustainable Chem Eng 2020;8(2):1252–61.
[20] Olafasakin O, Chang Y, Passalacqua A, Subramaniam S, Brown RC, Wright MM. Machine learning reduced order model for cost and emission assessment of a pyrolysis system. Energy Fuels 2021;35(12):9950–60.
[21] Kıpçak E, Akgün M. Biofuel production from olive mill wastewater through its Ni/Al2O3 and Ru/Al2O3 catalyzed supercritical water gasification. Renew Energy 2018;124:155–64.
[22] BEIS. Hydrogen production costs 2021, s.l. Gov.uk; 2021.
[23] Messenger, B.. Sebigas to develop 17.5 MW biogas plant to process Brazilian sugar cane waste. 2018 [Online] Available at: https://waste-management-world.com/artikel/sebigas-to-develop-175-mw-biogas-plant-to-process-brazilian-sugar-cane-waste/. [Accessed 16 December 2022].
[24] Rodgers S, Conradie A, King R, Poulston S, Hayes M, Bommareddy RR, Meng F, McKechnie J. Reconciling the sustainable manufacturing of commodity chemicals with feasible technoeconomic outcomes. Johnson Matthey Technol. Rev 2021:375–94.
[25] Pulp & Paper Canada. Hainan PM2 raises the bar for speed, water conservation. 2011 [Online] Available at: https://www.pulpandpapercanada.com/hainan-pm2-raises-the-bar-for-speed-water-conservation-1000734203/. [Accessed 7 July 2023].
[26] Kang X, Lin R, O'Shea R, Deng C, Li L, Sun Y, Murphy JD. A perspective on decarbonizing whiskey using renewable gaseous biofuel in a circular bioeconomy process. J Clean Prod 2020;255:120211.
[27] Whiskeymate. The distillery list. 2016 [Online] Available at: https://whiskymate.net/the-distillery-list/. [Accessed 22 December 2022].
[28] NNFCC. Assessment of digestate drying as an eligible heat use in the Renewable Heat Incentive. York: s.n 2016.
[29] Okolie JA, Epelle EI, Nanda S, Castello D, Dalai AK, Kozinski JA. Modeling and process optimization of hydrothermal gasification for hydrogen production: a comprehensive review. J Supercrit Fluids 2021;173:105199.
[30] Chase MW. NIST-JANAF thermochemical tables. 4th ed. New York: American Chemical Society, and the American Institute of Physics for the National Institute of Standards and Technology; 1998.
[31] Huang Y, Lo S-L. Predicting heating value of lignocellulosic biomass based on elemental analysis. Energy 2020;191:116501.
[32] Tavasoli A, Aslan A, Salimi A, Balou A, Pirbazari SM, Hashemi H, Kohansal K. Influence of the blend nickel/porous hydrothermal carbon and cattle manure hydrochar catalyst on the hydrothermal gasification of cattle manure for H2 production. Energy Convers Manag 2018;173:15–28.
[33] Hantoko D, Antoni, Kanchanatip E, Yan M, Yan, Weng Z, Gao Z, Zhong Y. Assessment of sewage sludge gasification in supercritical water for H2-rich syngas production. Process Saf Environ Protect 2019;131:63–72.
[34] Hou K, Hughes R. The kinetics of methane steam reforming over a Ni/α-Al2O catalyst. Chem Eng J 2001;82:311–28.
[35] Hla S, Park D, Duffy G, Edwards J, Roberts D, Ilyushechkin A, Morpeth L, Nguyen T. Kinetics of high-temperature water-gas shift reaction over two iron-based commercial catalysts using simulated coal-derived syngases. Chem Eng J 2009;146(1):148–54.
[36] Choi Y, Stenger H. Water gas shift reaction kinetics and reactor modeling for fuel cell garade hydrogen. J Power Sources 2003;124(2):432–9.

[37] Rodgers S, Meng F, Poulston S, Conradie A, McKechnie J. Renewable butadiene: a case for hybrid processing via bio- and chemo-catalysis. J Clean Prod 2022;364:132614.
[38] BEIS. BEIS electricity generation costs (2020). 2020 [Online] Available at: https://www.gov.uk/government/publications/beis-electricity-generation-costs-2020. [Accessed 1 February 2023].
[39] Salary Expert. Salary expert. 2022 [Online] Available at: https://www.salaryexpert.com/. [Accessed 1 December 2022].
[40] Guo H, Cui J, Li J. Biomass power generation in China: status, policies and recommendations. Biomass power generation in China: status, policies and recommendations. Energy Rep 2022;8:687–96.
[41] Renewables Now. Brazil sets price cap for May 27 auction. 2022 [Online] Available at: https://renewablesnow.com/news/brazil-sets-price-cap-for-may-27-auction-782505/. [Accessed 1 December 2022].
[42] Low Carbon Contracts Company. CfD register. 2022 [Online] Available at: https://www.lowcarboncontracts.uk/cfd-register/. [Accessed 1 December 2022].
[43] XE. Xe currency converter.. 2022 [Online] Available at: https://www.xe.com/currencyconverter/. [Accessed 12 January 2022].
[44] Kumar A, Dhall P, Kumar R. Redefining BOD:COD ratio of pulp mill industrial wastewaters in BOD analysis by formulating a specific microbial seed. Int Biodeterior Biodegrad 2010;64:197–202.
[45] EIA. Annual energy outlook 2022. Washington DC: s.n 2022.
[46] Wernet G, Bauer C, Steubing B, Reinhard J, Moreno-Ruiz E, Weidema B. The ecoinvent database version 3 (part I): overview and methodology. Int J Life Cycle Assess 2016;21:1218–30.
[47] WRAP. Digestate and compost use in agriculture. Banbury: s.n 2016.
[48] Pedregosa F, et al. Scikit-learn: machine learning in Python. J Mach Learn Res 2011;12:2825–30.
[49] Sison Arnold E, Etchieson Sydney A, Güleç Fatih, Epelle Emmanuel I, Okolie Jude A. Process modelling integrated with interpretable machine learning for predicting hydrogen and char yield during chemical looping gasification. J Clean Prod 2023;414:137579.
[50] Sinnott R, Towler G. Chemical engineering design. 5th ed. Oxford: Elsevier; 2009.
[51] WRAP. Comparing the costs of alternative waste treatment options. Banbury: WRAP; 2022.
[52] Velazquez Abad A, Dodds PE. Green hydrogen characterisation initiatives: definitions, standards, guarantees of origin, and challenges. Energy Pol 2020;138.
[53] Longden T, Beck FJ, Jotzo F, Andrews R, Prasad M. 'Clean' hydrogen? – Comparing the emissions and costs of fossil fuel versus renewable electricity based hydrogen. Appl Energy 2022;306:118145.
[54] IGES. IGES list of grid emission factors. 2022 [Online] Available at: https://www.iges.or.jp/en/pub/list-grid-emission-factor/en?_ga=2.151364921.1686382296.1673188108-667943912.1673188108. [Accessed 12 January 2023].
[55] BEIS. Government conversion factors for company reporting of greenhouse gas emissions. 2022 [Online] Available at: https://www.gov.uk/government/collections/government-conversion-factors-for-company-reporting. [Accessed 17 January 2023].
[56] Ko S, Lautala P, Handler RM. Securing the feedstock procurement for bioenergy products: a literature review on the biomass transportation and logistics. J Clean Prod 2018;200:205–18.
[57] El-Elmam RS, Özcan H. Comprehensive review on the techno-economics of sustainable large-scale clean hydrogen production. J Clean Prod 2019;220:593–609.
[58] IEA. An energy sector roadmap to carbon neutrality in China. 2021 [Online] Available at: https://www.iea.org/reports/an-energy-sector-roadmap-to-carbon-neutrality-in-china. [Accessed 8 February 2023].
[59] IEA. Opportunities for hydrogen production with CCUS in China. 2022 [Online] Available at: https://www.iea.org/reports/opportunities-for-hydrogen-production-with-ccus-in-china. [Accessed 8 February 2023].
[60] IEA. Hydrogen in Latin America. 2021 [Online] Available at: https://www.iea.org/reports/hydrogen-in-latin-america. [Accessed 8 February 2023].
[61] EIA. Natural gas. 2023 [Online] Available at: https://www.eia.gov/dnav/ng/hist/rngwhhdA.htm. [Accessed 18 March 2023].
[62] Jin B, Tan A, Liu X, Yue Y, Chen Y, Sangiovanni Vincentelli A. Using ensemble classifiers to detect incipient anomalies. Preprint 2020. https://doi.org/10.48550/arXiv.2008.08710.
[63] Ndubuaku MU, Anjum A, Liotta A. Unsupervised anomaly thresholding from reconstruction errors. In: Montella R, Ciaramella A, Fortino G, Guerrieri A, Liotta A, editors. Internet and distributed computing systems. IDCS 2019. Lecture notes in computer science. Cham: Springer; 2019. p. 123–9.
[64] Sanaye S, Alizadeh P, Yazdani M. Thermo-economic analysis of syngas production from wet digested sewage sludge by gasification process. Renew Energy 2022;190:524–39.
[65] Liang J, Liu Y, Chen J, E J, Leng E, Zhang F, Liao G. Performance comparison of black liquor gasification and oxidation in supercritical water from thermodynamic, environmental, and techno-economic perspectives. Fuel 2023;334:126787.
[66] Qian L, Wang S, Wang S, Zhao S, Zhang B. Supercritical water gasification and partial oxidation of municipal sewage sludge: an experimental and thermodynamic study. Int J Hydrogen Energy 2021;46(1):89–99.
[67] Louw J, Schwarz CE, Knoetze JH, Burger AJ. Thermodynamic modelling of supercritical water gasification: investigating the effect of biomass composition to aid in the selection of appropriate feedstock material. Bioresour Technol 2014;174:11–23.
[68] Louw J, Schwarz CE, Burger AJ. Catalytic supercritical water gasification of primary paper sludge using a homogeneous and heterogeneous catalyst: experimental vs thermodynamic equilibrium results. Bioresour Technol 2016:111–20.
[69] Osada M, Yamaguchi A, Hiyoshi N, Sato O, Shirai M. Gasification of sugarcane bagasse over supported ruthenium catalysts in supercritical water. ENERG FUEL 2012;26(6):31179–3186.
[70] Yamaguchi A, Watanabe T, Saito K, Kuwano S, Murakami Y, Mimura N, Sato O. Direct conversion of lignocellulosic biomass into aromatic monomers over supported metal catalysts in supercritical water. Mol Catal 2019;477.
[71] Gökkaya Selvi D, et al. Hydrothermal gasification of the isolated hemicellulose and sawdust of the white poplar (Populus alba L.). J Supercrit Fluids 2020;162.
[72] Lu Y, Jin H, Zhang R. Evaluation of stability and catalytic activity of Ni catalysts for hydrogen production by biomass gasification in supercritical water. Carbon Resour. Convers. 2019:95–101.
[73] Babaei K, Bozorg A, Tavasoli A. Hydrogen-rich gas production through supercritical water gasification of chicken manure over activated carbon/ceria-based nickel catalysts. J Anal Appl Pyrolysis 2021;159:105318.

This page has been left intentionally blank

8 Conclusions, Limitations, and Future work

The aim of this thesis was to develop and apply Techno-Economic Analysis (TEA) methods to evaluate the proposed aerobic gas fermentation and Supercritical Water Gasification (SCWG) process. Table 8.1 summarises the individual contributions of each Chapter (published article) included in this thesis. The following section outlines the overall thesis conclusions, limitations addressed within the thesis, and the recommendations for future work based on remaining limitations.

Table 8.1: A summary of the articles in each chapter of this thesis

Chapter	Article Title	Novelty
4: Initial techno-economic analysis of the integrated platform	Reconciling the Sustainable Manufacturing of Commodity Chemicals with Feasible Technoeconomic Outcomes: Assessing the investment case for heat integrated aerobic gas fermentation	First TEA and LCA of the proposed aerobic gas fermentation and SCWG platform. The novel platform consisted of SCWG heat integrated with aerobic gas fermentation. Three different methods of calculating the capital and fixed operating costs are assessed.
5: Comparative techno-economic analysis of the integrated platform	Renewable butadiene: A case for hybrid processing via bio- and chemo-catalysis	Comparative TEA and LCA for the production of 1,3-butadiene. The aerobic gas fermentation and SCWG platform was followed by catalytic upgrading to produce the reduced 1,3-butadiene product. Two alternative purely chemo-catalytic routes to 1,3-butadiene were modelled and compared to the aerobic gas fermentation route.
6: Creating a robust, unbiased, price selection procedure for techno-economic analyses	Probabilistic commodity price projections for unbiased techno-economic analyses	ML was used to produce 20-25 year probabilistic commodity price projections for techno-economic, sensitivity, and uncertainty analyses. An ensemble of 100 LSTMs was used to exploit the underlying determinism and/or stochastic variability within the commodity's historic time series.
7: Creation of a surrogate model for the economic evaluation of feedstocks	A surrogate model for the economic evaluation of renewable hydrogen production from biomass feedstocks via supercritical water gasification	An ML surrogate model of the TEA for hydrogen production via low temperature SCWG was created. The model predicts the LCOH based on user input feedstock-capacity-location combinations and is made publicly available.

8.1 Conclusions

The specific objectives set to achieve the overall thesis aim and conclusions relevant to these objectives are discussed below.

Objective 1: Develop process simulations for the aerobic gas fermentation and SCWG process, incorporating heat integration and downstream processing.

In Chapter 4, an initial process simulation of the heat integrated aerobic gas fermentation and SCWG platform was created in Aspen HYSYS for isopropanol and acetone production. A heat pump using isopentane as the working fluid was incorporated to utilise the abundant low temperature heat from the fermentation to support the SCWG reaction. Furthermore, a turbo-expander was employed to recover energy from the high-pressure SCWG effluent, supplying air to the fermentation process. Owing to the significant energy recovery from the turbo-expander, surplus renewable electricity was fed back into the grid as an additional source of revenue. However, the technology platform necessitated the diversion of 32 % of syngas to combustion to ensure energy self-sufficiency. In Chapter 5, the platform's heat integration was updated, enabling the exploitation of 100% of the produced syngas for chemical production while maintaining energy self-sufficiency. This process improvement also enabled the export of a greater portion of renewable electricity for sale to the grid. Although not implemented on the aerobic gas fermentation platform flowsheet, Chapter 7 undertook an update to the representation of the SCWG reactor. This update allowed for the simulation of the gasification of any biomass compound using its ultimate analysis and replaced the previous SCWG representation that relied on kinetics of guiacol gasification, acting as a model compound for lignin.

These incremental process enhancements and representations were pivotal in evaluating the potential of the proposed technology. Current commodity chemical production contains highly efficient production chains, making the commercialisation of early-stage technologies to compete with these processes challenging (IEA, 2019). As such, a conclusion from this thesis is the need for comprehensive and evolving TEAs to determine and create promising technology alternatives.

Objective 2: Determine an appropriate techno-economic framework and perform a comprehensive techno-economic analysis of the simulated process.

In Chapter 4, three methods for evaluating capital expenditure and operating expenditure were compared. The cost models yielding the median results in both cases was adopted for the formal technology analysis. These cost models were adopted in the TEAs conducted in Chapters 5 and 7, establishing a consistent methodology for the economic analyses in this thesis. In addition, a Monte Carlo uncertainty analysis was conducted to provide an expected probability range for the economic outcome. This approach was also applied in Chapter 5 and 7. However, in Chapter 5 an additional single-point sensitivity analysis was performed to assess the impact of each variable on the technology's Minimum Selling Price (MSP), facilitating a comparison between the modelled routes in this chapter.

In both Chapters 4 and 5 the TEA was conducted in the context of a China-based paper and pulp mill. The studies assumed 25% of the pulp mill's black liquor production could be diverted from conventional energy recovery to chemical production. In Chapter 4, considering isopropanol and acetone production, the aerobic gas fermentation and SCWG technology achieved a cumulative NPV of $42 million using the nominal TEA inputs. The uncertainty analysis demonstrated a 70% NPV probability band ranging from $35 to $85 million, highlighting the technology's potential to produce cost-competitive commodity chemicals. Building upon the successful outcome of this analysis, Chapter 5 performed a second TEA for 1,3-butadiene production, involving catalytic upgrading of the fermentation product, acetaldehyde, into the less oxygenated 1,3-butadiene. The catalytic transformation negatively impacts the economics due to the lower mass yield to produce the reduced 1,3-butadiene product compared with direct products from fermentation. Overall, the process demonstrated an NPV of $2.8 million, a 19% probability of achieving a positive NPV, and an MSP of $1,367 tn^{-1}. Despite being less economically viable than isopropanol and acetone production, the

platform still demonstrated economic potential using commodity prices. Furthermore, this analysis did not include carbon pricing incentives, which would likely improve the economic outlook.

In Chapter 7, SCWG was evaluated for hydrogen production considering 40 biomass compositions, five processing capacities (10–200 m^3/h), and three geographic locations (China, Brazil, and the UK) to produce a feedstock evaluation tool. As a commonly reported metric for low-carbon hydrogen production methods the Levelised Cost of Hydrogen (LCOH) was computed. The levelised costs ranged from 3.81 to 18.72 $/kg$_{H2}$ for the considered feedstock-capacity-location combinations.

The results from these case studies demonstrate the techno-economic potential of the proposed integrated aerobic gas fermentation and SCWG technology. The integrated gas fermentation and SCWG platform demonstrated its capability to achieve market prices for both fermentation products (isopropanol and acetone) and more reduced products (1,3-butadiene), necessitating the integration of bio- and chemo-catalytic technologies. The lower NPV of the 1,3-butadiene route is attributed to the intrinsic mass loss required to produce this more reduced product. As most fossil-fuel based chemicals are less oxygenated that fermentation products this highlights a challenge with strategies to directly replace current commodity chemicals. The LCOH range presented for hydrogen production via SCWG emphasises the impact of feedstock-capacity-location considerations during technology evaluation and highlights the need for realistic biorefinery scenario modelling during technology evaluations.

Objective 3: Quantify the greenhouse gas emissions associated with chemical and fuel production from the process and compare them with conventional production methods.

An integrated TEA and Life Cycle Assessment (LCA) was undertaken in Chapters 4, 5, and 7. As the considered feedstocks were deemed by-product streams or wastes no emissions were attributed. As such, the sequestration of biogenic carbon in both Chapters 4 and 5 resulted in net negative emissions on a cradle-to-gate basis. For isopropanol and acetone production (Chapter 4), the platform's Greenhouse Gas (GHG) emissions were -2.1 kgCO_{2eq}/kg and -2.21 kgCO_{2eq}/kg, contrasting with 2.07 kgCO_{2eq}/kg and 2.43 kgCO_{2eq}/kg via conventional production. In the case of butadiene (Chapter 5) produced through the aerobic platform, GHG emissions were -3.23 kgCO_{2eq}/kg, while conventional production emitted 1.2 kgCO_{2eq}/kg. The negative emissions achieved for all three chemicals are attributed to the sequestration of biogenic carbon exceeding the process emissions. Negative emissions were not achieved for hydrogen production (Chapter 7) as no biogenic carbon was sequestered, however low process emissions were achieved, averaging 0.46 kgCO_{2eq}/GJ_{H2} (China and Brazil), and 0.37 kgCO_{2eq}/GJ_{H2} (UK). These results compare favourably with the 8 kgCO_{2eq}/GJ_{H2} attributed to Steam Methane Reforming (SMR) with carbon capture and storage (excluding emissions for natural gas leakage).

The low process emissions achieved for all case studies demonstrate the environmental benefit of renewable resource utilisation compared with conventional fossil-based production methods. Importantly, since the downstream use of each product remains independent of the production method, the comparative renewable and conventional production are valid beyond the considered cradle-to-gate framework.

Objective 4: Compare the economic and environmental competitiveness of the process with alternative renewable production methods.

As the only company to currently operate a commercial gas fermentation facility, the study by LanzaTech investigating the production of ethanol and acetone via anaerobic gas

fermentation was used as a benchmark to compare to the economic and environmental outcomes of Chapter 4, producing isopropanol and acetone using the aerobic gas fermentation and SCWG platform. LanzaTech's findings revealed that by selling acetone at market prices, they could sell co-produced ethanol at or below the US Department of Energy's 2022 target of $ 3/ Gallon Gasoline Equivalent (GGE). Notably, the aerobic platform achieved the same target by selling isopropanol and acetone as a biofuel mix, resulting in a selling price of $2.87/GGE. In addition, the cradle-to-gate GHG emissions for LanzaTech's combined ethanol and acetone product were -1.9 $kgCO_{2eq}$/kg compared with -2.04 $kgCO_{2eq}$/kg for the aerobic gas fermentation's combined isopropanol and acetone product. The TEA and LCA results suggest that through the outlined process engineering solution aerobic gas fermentation demonstrates promise as a renewable biochemical technology platform.

In Chapter 5, the production of 1,3-butadiene via the aerobic gas fermentation and SCWG platform followed by catalytic upgrading was compared to two chemo-catalytic routes involving catalytically upgrading biomass derived syngas. One route involved passing through an ethanol intermediate, while the other employed a sequence of commercialised catalytic technologies with propene as an intermediate. Among the three routes, the aerobic gas fermentation process was the only one profitable using the nominal techno-economic inputs. The MSPs for the three routes were $1367/tn, $1954/tn, and $2196/tn for the aerobic gas fermentation, ethanol, and propene intermediate routes, respectively. Moreover, sensitivity analysis revealed that although the co-sale of renewable electricity contributed to the success of the aerobic gas fermentation route, the platform still outperformed alternative routes even with grid parity prices for renewable electricity (MSP using electricity grid parity: $1695/tn). Overall, this demonstrates the competitiveness of this novel platform. All three renewable routes produced net negative emissions, comparing favourably to both conventional production and the upgrading of market ethanol in Brazil and the US. Minor differences were observed between the renewable routes, -3.23 $kgCO_{2eq}$/kg, -2.90 $kgCO_{2eq}$/kg, and -2.80 $kgCO_{2eq}$/kg for the aerobic gas fermentation, ethanol, and propene intermediate routes, respectively. The lower emissions for the aerobic gas fermentation route are attributed to absence of emissions associated with the black liquor feedstock.

With regards to hydrogen production via SCWG in Chapter 7, at capacities >50 m3/h, the LCOH (2.76–4.21 $/$kg_{H2}$ for China, 3.41–5.07 $/$kg_{H2}$ for Brazil, 4.31–6.62 $/$kg_{H2}$ for the UK) was cost competitive with hydrogen production via MW-scale electrolysis using renewable electricity (3.10–6.70 $/$kg_{H2}$ for China, 3.70–5.90 $/$kg_{H2}$ for Brazil, and 4.81–6.31 $/$kg_{H2}$ for the UK). Low average emissions were achieved by SCWG 0.46 $kgCO_{2eq}$/GJ_{H2} (China and Brazil), and 0.37 $kgCO_{2eq}$/GJ_{H2} (UK), comfortably meeting the European Union CertifHy scheme for low carbon hydrogen (≤36.4 $kgCO_{2eq}$/GJ_{H2}) based on a 60% reduction in emissions from Steam Methane Reforming (Abad & Dodds, 2020).

The favourable prices and emissions achieved compared to alternative renewable/low carbon production methods are testament to the exploitation of low-value and low-emission feedstocks. This highlights a benefit of the use of SCWG as a gasification technology as it is ideally suited to these feedstocks. Furthermore, the low process emissions achieved by both aerobic gas fermentation routes (Chapters 4 and 5) were due to the technology's energetic self-sufficiency, achieved through heat integration, highlighting the technology's efficient resource utilisation.

Objective 5: Develop a methodology to project future prices, considering future price variability, for use in techno-economic, sensitivity, and uncertainty analyses.

The RBFNN method used to project future commodity chemical prices employed in Chapters 4 and 5 was updated in Chapter 6. The initial methodology had several limitations namely, the

arbitrary selection of, the algorithm, use of eight neurons, and use of ten historic time-steps as the model input; the model was trained on the entire historic time series; model initiation relied only on ten real historic prices; and price variability was accounted for using a subjective percentage. The updated methodology in Chapter 6 used a grid search to determine the optimal hyperparameters, used the entire time series as a model input, included a validation set to assess the methods ability to predict beyond the training set, and produced a probabilistic projection of the commodity's future price. To develop this methodology, an ensemble of 100 LSTM models was employed. The commodity's historic pricing data (2009-2021) and the Energy Information Administration's (EIA's) reference case projection of future Brent crude oil prices were as model inputs. The historic commodity price allows for the exploitation of deterministic trends and/or stochastic variability specific to the commodity whilst the EIA's projection acts as a proxy for future global energy market trends. From the probabilistic projection the 5^{th}, 25^{th}, 50^{th}, 75^{th}, and 95^{th} price percentiles were calculated and used as the nominal price (50^{th}), price range (5^{th} and 95^{th}), and price distribution (5^{th}, 25^{th}, 50^{th}, 75^{th}, and 95^{th}) in the corresponding economic, sensitivity, and uncertainty analyses. Comparing the previous RBFNN price projections to the developed LSTM method, the 70% probability window for the NPV distributions were changed from \$35 - \$95 million to \$45 - \$80 million for the previous isopropanol and acetone TEA, and from -\$45 - \$65 million to -\$35 - \$80 million for the 1,3-butadiene process. A two-tailed t-test verified a statistically significant difference between the NPV distributions. Furthermore, the projected commodity price distributions demonstrated appreciable price variability.

The results from this study highlight the importance of price selection during technology evaluations. The variability observed between commodities suggest that pricing uncertainty considerations in TEAs should be tailored to each commodity rather than dictated through heuristics. Furthermore, ML demonstrates promise as a tool to develop unbiased price projection methods that are applicable to any time series. However, when employing ML careful consideration is required to ensure models are trained to effectively tackle the problem. For example, to project prices 26 years with only 12 years of historic data available a 30% training and 70% validation data split was selected to ensure the selection of optimal hyperparameters was carried out on a task representative of the final model projections. Notably, this deviates from conventional ML practices, which often adopt an 80% training and 20% validation split.

Objective 6: Create a machine learning surrogate model of a techno-economic analysis to rapidly evaluate the economic potential of feedstock-capacity-location combinations for supercritical water gasification.

A ML surrogate model was created of a TEA of hydrogen production via low temperature SCWG to aid experimentalists and industrialists in identifying promising biorefinery scenarios to inform targeted research and investment. The biomass' ultimate analysis, processing capacity, and geographic location were the surrogate model inputs and the nominal and 70% probability band for the LCOH were the model outputs. Three commonly employed ML algorithms were investigated for the surrogate model: Random Forests, Support Vector Regression, and an ensemble of Artificial Neural Networks (ANNs). The ANN ensemble was the most accurate during cross-validation and achieved an accuracy of Mean Absolute Percentage Error: <4.6%, Root Mean Squared Error: <0.39, and R^2: >0.99 on the test set. Feature importance was determined using SHapley Additive exPlanation (SHAP) values to determine the importance of each input feature on the model's output. SHAP values revealed processing capacity as the most prominent feature, followed by the geographic location. However, appreciable LCOH differences were also observed between different biomass compositions. A reliability measure was created to warn the user if the surrogate model's

prediction contained high variability. User warnings were set based on the predetermined variance threshold set based on the maximum variance observed for the nominal predictions during a 5-fold validation procedure on the entire dataset.

The creation of ML surrogate models representing TEA's has the potential to facilitate the conduction of early-stage technology evaluations by non-experts. However, the accuracy of a model's prediction on new, unseen inputs depends on the input data's similarity to the model's training data. Predictions made on inputs poorly represented during model training may lead to unreliable results. As such, reliability measures such as those presented in this work should be developed to prevent model misuse by users.

8.2 Wider implications and impact

There is currently a lack of policy for the renewable chemical sector (Hallett & Sparks, 2023). The recent Biomass Strategy published by the UK Government emphasised the need for further work to understand the role of biomass in the chemical industry (DESNZ, 2023). This work contributes to this need by providing a comprehensive techno-economic and environmental assessment of a technology platform for commodity chemical production from underutilised biomass resources. The process demonstrates economic viability at market prices and the opportunity to deliver negative process emissions. As such, this research adds valuable information regarding the current state, economic, and environmental potential of renewable chemical technologies to the public domain. This research and its findings can therefore help to inform future policy decisions surrounding subsidies, technology investment, and future research directions.

The integration of ML techniques impacts stakeholders across various domains. The ML price projection method offers a data-driven approach which enhances economic evaluations. The developed method provides policymakers with unbiased information around market competitiveness. This aids policymakers in determining future subsidies and incentives for emerging sustainable technologies. The ML-driven surrogate model, designed for accessibility by non-experts, facilitates the early-stage evaluation of technologies. This allows industrialists to assess the feasibility of exploiting their waste streams using SCWG. This offers the potential for underutilised resources to be efficiently exploited. Overall, the use of machine learning in this thesis makes sustainable technology assessments more accessible to a wider range of audiences.

8.3 Addressed limitations

Some of the limitations discussed in the chapters of this thesis were addressed in the subsequent chapters. These limitations and their resolutions are discussed under the objectives they correspond to.

Objective 1: Develop process simulations for the aerobic gas fermentation and SCWG process, incorporating heat integration and downstream processing.

In both Chapters 4 and 5 the SCWG of black liquor was modelled based on kinetics for guiacol gasification, a commonly used model compound to represent lignin. However, this approach prevented modelling a range of biomass feedstocks. This simplification was addressed as part of Chapter 7 where the representation of the SWCG reactor was updated to use a Gibbs reactor, allowing the biomass' ultimate analysis to be used as the simulation basis. However, as the Gibbs reactor predicts the equilibrium composition of the produced syngas at the specified temperature and pressure, this amendment led to a greater quantity of methane being produced in the product gas. To shift this gas composition towards the desired H_2 and CO_2 product a SMR, High Temperature Shift (HTS), and Low Temperature Shift (LTS) reactor were used after the gasifier. As such, the simplified SCWG reactor using guiacol kinetics in

Chapters 4 and 5 was replaced by a SCWG (represented sing a Gibbs reactor) followed by SMR, HTS, and LTS reactors (represented using established reaction kinetics).

Objective 2: Determine an appropriate techno-economic framework and perform a comprehensive techno-economic analysis of the simulated process.

In Chapter 4 an uncertainty analysis was undertaken to represent the range of NPV outcomes. However, as a single point sensitivity analysis was not undertaken the specific impact of each variable on the final economic outcome wasn't quantified. This was rectified in Chapter 5 where both uncertainty and single point sensitivity analyses were undertaken. Whilst Chapter 4 computed the $/GGE for the biofuel mix of isopropanol and acetone to compare the results to LanzaTech's study, the MSP for each product wasn't computed. As highlighted in Chapter 2, the computation of multiple metrics is important to contextualise the techno-economic results. In Chapter 5 both the MSP and NPV were presented.

In Chapter 4 the upper limit used for the sensitivity analysis parameters were uniformly set. However, the ranges recommended in Sinnott and Towler (2013) have higher upper bounds for the inside battery limit capital, outside battery limit capital, and labour cost, likely attributed the more common occurrence and severity of cost overruns compared to cost underruns (Brown, 2015). To rectify this, the higher recommended upper bounds were adopted in Chapters 5 and 7.

Objective 4: Compare the economic and environmental competitiveness of the process with alternative renewable production methods.

The technology comparison between the aerobic platform and existing anaerobic study by LanzaTech in Chapter 4 relied on an existing TEA study rather than modelling both technologies. As such, the studies used different biorefinery scenarios and cost model assumptions. To ensure a fairer comparison, the anaerobic gas fermentation route should be modelled and considered within the same biorefinery scenario as the evaluated aerobic platform. While this limitation remains for Chapter 4, the technology comparisons in Chapter 5 were all modelled using the same biorefinery scenario and techno-economic framework.

Objective 5: Develop a methodology to project future prices, considering future price variability, for use in techno-economic, sensitivity, and uncertainty analyses.

To account for price variability and uncertainty of the projected product prices used in the TEAs an arbitrary ±30% was used in Chapter 4 and ±20% in Chapter 5. This percentage deviation was used as a rule of thumb and didn't reflect the commodity price uncertainty. To rectify this a probabilistic price projection methodology was developed in Chapter 6. This developed method produces a price distribution projection, supplying a sensitivity range, and uncertainty distribution tailored to the commodity for use in the economic, sensitivity, and uncertainty analyses.

8.4 Remaining limitations and future work

Despite the development of analysis methods throughout this thesis, there are remaining limitations which form areas for future work. These are outlined in the following section in relation to each of the thesis objectives.

Objective 1: Develop process simulations for the aerobic gas fermentation and SCWG process, incorporating heat integration and downstream processing.

Incorporating the updated SCWG, SMR, HTS, and LTS representation from Chapter 7 into the aerobic gas fermentation platform constitutes an important progression. Importantly, the updated reactor network configuration incorporates a greater number of heat exchangers,

creating further opportunities for heat integration. As such, to realise the best economic outcome it would be appropriate to optimise the internal heat exchanger network and steam generation system. Aspen Energy Analyser software can be used to propose potential heat integration scenarios. However, the software cannot account for additional constraints such as maintaining energy self-sufficiency and also maximising renewable electricity sales. As such, the initial heat integration scenarios proposed by Aspen Energy Analyser can be used as an initial population for a genetic algorithm to then optimise. An objective function incorporating energy self-sufficiency constraints and using NPV as the objective function can then be used to find the optimal heat integration configuration using the new SCWG representation.

Objective 2: Determine an appropriate techno-economic framework and perform a comprehensive techno-economic analysis of the simulated process.

In Chapter 4, a comparison of capital and fixed operating cost models was conducted, however, no assessment was made on individual equipment cost models, a practice observed in studies by Feng & Rangaiah (2011), Symister (2016), and van Amsterdam (2018). A comprehensive evaluation involving diverse cost correlations and software programs would have offered a more thorough analysis. However, due to the absence of true equipment costs, the accuracy of these methods cannot be validated. Similarly, the comparison of overall cost models in Chapter 4 was instrumental in establishing the techno-economic framework for the future case studies, yet it doesn't represent the most precise cost model. In order to quantify the accuracy of approaches vendor quotes and cost estimates from commissioned commercial scale projects would need to be broadly publicised. In the work by Tsagkari et al. (2020) a process block methodology that utilised data from press releases of commercial biorefineries to cost various blocks was introduced. Following on from this, an interesting avenue of future work would be to leverage data available in press releases and using ML to extract costs for process blocks or specific equipment. Using the extracted data, new exponents and constants for equipment cost equations such as those in Sinnot & Towler (2013) and Seider et al. (2017) could be defined. Alternatively, ML surrogate models could be created from the extracted data to represent equipment costs.

Further investigation is warranted to evaluate the techno-economic performance of the aerobic gas fermentation platform with diverse feedstocks in varying biorefinery scenarios, e.g., vinasse in Brazil and distillery wastewater in the UK. While these feedstocks were considered in the case studies of Chapter 7 for comparison with alternative renewable hydrogen technologies, it would be valuable to also determine their competitiveness for commodity chemical production through the integrated aerobic gas fermentation process.

TEAs are based on a set of assumptions and thereby uncertainty. Whilst the use of a sensitivity and uncertainty analysis can provide a range of outcomes to represent this uncertainty, ultimately the simulations, costs, and designs need revisiting and refining throughout the evolution of a technology or process. The studies undertaken in this thesis represent theoretical designs based on early-stage technologies. The economic outcomes are therefore an indication of whether the technology demonstrates promise. The economic outcome is not a true representation of the technology’s performance once commercialised. Further work through scale-up and improved cost estimates is therefore required to verify and refine the assumptions made and reassess technologies.

Objective 3: Quantify the greenhouse gas emissions associated with chemical and fuel production from the process and compare them with conventional production methods.

In Chapters 4 and 5, while calculating the GHG emissions during the technology assessments, no quantifiable policy incentives were incorporated into either study. Such incentives would have been particularly valuable in Chapter 5, where only a 19% probability of achieving a positive NPV was attained. Reference is made to the fact that a higher market price could be demanded for low-carbon products. As such, quantifying the CO_2 price required to shift the probability of achieving a positive NPV to 100%, in a manner similar to Michailos et al. (2019) and Huang et al. (2021), forms an interesting area for future work. Notably, this would necessitate the LCA framework to be expanded to cradle-to-grave to incorporate end of life considerations for the products. The CO_2 pricing analysis would be useful for policymakers as it provides insights into the necessary incentives required to mitigate risk in commercialising biochemical technology. Furthermore, the required CO_2 price could be contextualised through comparison to current and projected CO_2 pricing.

Objective 4: Compare the economic and environmental competitiveness of the process with alternative renewable production methods.

As emphasised within this thesis, the aerobic and anaerobic comparison in Chapter 4 weren't directly comparable due to them being conducted in separate studies with distinct biorefinery scenarios and different TEA frameworks. Thus, modelling a direct comparison between aerobic and anaerobic gas fermentation utilising the same biorefinery scenario and techno-economic framework would provide greater clarity on the proposed platform's competitiveness in comparison to anaerobic gas fermentation. Moreover, further comparisons between the proposed platform and conventional biomass gasification, or CO_2 utilisation and electrolysed H_2 would make for interesting future assessments.

Objective 5: Develop a methodology to project future prices, considering future price variability, for use in techno-economic, sensitivity, and uncertainty analyses.

Future work should be undertaken considering the impact of including further hyperparameters in the grid search procedure i.e., number of neurons in the fully connected layer, use of a fully connected layer, number of time-steps being predicted. However, their inclusion should be considered alongside their added computational expense. Additionally, the use of a cross-validation procedure to assess the model's performance across different stages of the historic time series should be undertaken. A suitable approach involves leveraging different time series lengths for validation. For instance, using a 4-fold cross-validation procedure applied to a time series comprising 144 data points, the model's performance can be evaluated using varying time-series lengths: 36, 72, 108, and 144 data points, while maintaining a consistent 30% training and 70% validation split. The optimal hyperparameters could then be determined based on the overall performance across all validation sets. Finally, the impact of incorporating the EIA's projection in a staggered manor should be considered, e.g., inputting ethanol prices from January 2009 to December 2020 alongside the EIA's crude oil prices for January 2010 to December 2021. In theory this should provide the model with insights into future price dynamics, rather than solely based on the current time-step data, potentially increasing prediction accuracy.

Only one method was evaluated to produce the price projections in Chapter 6. In traditional forecasting fields new methods are commonly compared against econometric methods and various simpler ML methods, such as seen in the works by Wu et al. (2019) and Lago et al. (2018). However, the specific requirements of the projection problem defined in this work, namely, a probabilistic projection, inclusion of the EIAs crude oil price projection, and applicability to any time series, meant econometric methods were unsuitable for this problem. Nevertheless, alternative ML methods could have been compared to assess the most appropriate model. Future work could be undertaken concerning the use of emerging methods

in traditional forecasting fields such as, variational mode decomposition and other wavelet decomposition methods along with the proposed ensemble approach. Such methods aim to reduce the burden on the ML algorithm by first extracting features from the data.

The inclusion of the historic errors in the EIA's projections into the probabilistic price projections also offers an interesting avenue for potential future work. This would introduce projection uncertainty linked to historical inaccuracies in EIA's scenario projections for world energy markets, rather than solely based on the commodity's historic time series. However, the inclusion of these errors may lead to the production of excessively broad distributions. To ensure that projection sharpness is maintained when incorporating these errors the Continuous Rank Probability Score should be used as the performance metric across the validation set.

Objective 6: Create a machine learning surrogate model of a techno-economic analysis to rapidly evaluate the economic potential of feedstock-capacity-location combinations for SCWG.

The updated SCWG reactor model used in Chapter 7 relies on the Gibbs reactor in Aspen HYSYS. The Gibbs model is a valuable tool for simulating gasification, as it eliminates the need for defining complex equations. The model ensures that the mass and energy balance of the system is maintained, making it useful for initial process evaluations (Okolie et al., 2021a). Although widely used in TEA studies for SCWG (Sanaye et al., 2022; Liang et al., 2023; Okolie et al., 2021b), the Gibbs reactor assumes complete conversion to gaseous products and thermodynamic equilibrium. These assumptions may not universally hold true in industrial settings. As a result, the gas composition may deviate from the predictions of the Gibbs model. Whilst the simulation considered a conservative 5-minute residence time for the continuous SCWG, a more accurate representation would be to model the gasifier as a surrogate model based on experimental data. Surrogate models have been developed for SCWG to suggest optimal processing parameters (Gopirajan et al., 2021), screen catalysts (Li et al., 2021), or create interpretable models to better understand the relationship between process parameters and biomass characteristics on gas yields (Zhao et al., 2022). However, at present there is limited data available for SCWG near full conversion at low temperatures (380-500°C). Subsequently, greater experimental research into achieving near full conversion is imperative for this to be undertaken.

The ML surrogate model developed in Chapter 7 was developed for hydrogen production. To determine the techno-economic performance of various biorefinery scenarios for the aerobic gas fermentation a surrogate model of the heat integrated platform could also be developed.

Additionally, the created surrogate model was limited to a constant dilution rate (75g/L_{COD}), 430°C gasification temperature, assumed total conversion, and limited geographic locations. These parameters could be expanded to include a broader range of processing parameters, yields, and biorefinery scenarios (locations and transportation considerations). By incorporating these parameters, the surrogate model could be used for both flowsheet and supply chain optimisation. In addition, the inclusion of technical parameters would allow for processing parameters to be varied as part of the Monte Carlo uncertainty analysis. The benefit of using a surrogate model in place of a process simulation for both optimisation and uncertainty analyses is the reduced computational burden and bypassing of convergence issues associated with large changes in processing conditions. However, using a surrogate model in this way would require the incorporation of an uncertainty threshold, as developed in Chapter 7, in order to identify areas with high model uncertainty and prevent predictions and solutions being proposed on areas of data poorly represented during model development.

8.5 References

Abad, A. V., Dodds, P. E., 2020. Green hydrogen characterisation initiatives: Definitions, standards, guarantees of origin, and challenges. *Energy Policy,* 111300.

Brown, T. R., 2015. A critical analysis of thermochemical cellulosic biorefinery capital cost estimates. *Biofuels, Bioproducts and Biorefining*.

DESNZ, 2023. Biomass Strategy 2023.

Feng, Y. & Rangaiah, G., 2011. Evaluating Capital Cost Estimation Programs. *Chemical Engineering Journal*, 22-29.

Gopirajan, P. V., Gopinath, K. P., Sivaranjani, G. & Arun, J., 2021. Optimization of hydrothermal gasification process through machine learning approach: Experimental conditions, product yield and pollution. *Journal of Cleaner Production,* 306, 127302.

Hallett, J., Sparks, J., 2023. BIOMASS STRATEGY: BIO-BASED CHEMICALS AND MATERIALS. Supergen Bioenergy Hub. URL: https://www.supergen-bioenergy.net/news/biomass-strategy-bio-based-chemicals-and-materials/ (Accessed: 07/02/2024)

Huang, Z., Grim, R. G., Schaidle, J. A. & Tao, L., 2021. The economic outlook for converting CO2 and electrons to molecules. *Energy & Environmental Science.*

Kaack, L. H., Apt, J., Morgan, M. G. & McSharry, P., 2017. Empirical prediction intervals improve energy forecasting. *Proceedings of the National Academy of Sciences,* 144(33), 8752-8757.

Lago, J., De Ridder, F. & De Schutter, B., 2018. Forecasting spot electricity prices: Deep learning approaches and empirical comparison of traditional algorithms. *Applied Energy*, 221, 386-405.

Liang, J., Lie, Y., Chen, J., E., J., Leng, E., Zhang, F., & Liao, G., 2023. Performance comparison of black liquor gasification and oxidation in supercritical water from thermodynamic, environmental, and techno-economic perspectives. *Fuel,* 334, 126787

Li, J., Pan, L., Survarna, M. & Wang, X., 2021. Machine learning aided supercritical water gasification for H2-rich syngas production with process optimization and catalyst screening. *Chemical Engineering Journal,* 426, 131285.

Michailos, S., Emeike, O., Ingham, D., Hughes, K.J., Pourkashanian, M., 2019. Methane production via syngas fermentation within the bio-CCS concept: A techno-economic assessment. *Biochemical Engineering Journal*, 150(15), 107-290.

Okolie, J. A., Epelle, E. I., Nanda, S., Castello, D., Dalai, A. K., & Kozinski, J. A., 2021a. Modeling and process optimization of hydrothermal gasification for hydrogen production: A comprehensive review. *Journal of Supercritical Fluids,* 173, 105199.

Okolie, J. A., Nanda, S., Dalai, A. K. & Kozinski, J. A., 2021b. Techno-economic evaluation and sensitivity analysis of a conceptual design for supercritical water gasification of soybean straw to produce hydrogen. *Bioresource Technology,* 331, 125005.

Sanaye, S., Alizadeh, P. & Yazdani, M., 2022. Thermo-economic analysis of syngas production from wet digested sewage sludge by gasification process. *Renewable Energy*, 190, 524-539.

Seider, W.D., Lewin, D.R., Seader, J.D., Widago, S., Gani, R., Ming Ng, K., 2017. '*Cost Accounting and Capital Cost Estimation',* in *'Prododuct and Process Design Principles. Synthesis Analysis and Evaluation'*, Fourth Edition, John Wiley & Sons Inc., 2017, New York.

Sinnott, R. & Towler, G., 2013. *Chemical Engineering Design - Principles, Practice and Economics of Plant and Process Design.* 2nd ed. s.l.:Elsevier.

Symister, O., 2016. *An Analysis of Capital Cost Estimation Techniques for Chemical Processing.* Melbourne, Florida: s.n.

Tsagkari, M., Kokossis, A. & Dubois, J.-L., 2020. A method for quick capital cost estimation of biorefineries beyond the state of the art. *Biofuels, Bioproducts and Biorefining,* 14(5), 1061-1088.

van Amsterdam, M., 2018. *Factorial Techniques applied in Chemical Plant Cost Estimation: A Comparative Study based on Literature and Cases.* Delft: s.n.

Wu, Y.X., Wu, Q.B., Zhu, J.Q., 2019. Improved EEMD-based crude oil price forecasting using LSTM networks. *Physica A: Statistical Mechanics and its Applications*, 516, 114–124.

Zhao, S., Jian, L., Chen, C., Yan, B., Tao, J., & Chen, G., 2022 Interpretable machine learning for predicting and evaluating hydrogen production via supercritical water gasification of biomass. *Journal of Cleaner Production*, 316, 128244.

Appendices

The following section presents the reprinted supplementary information from each chapter as published alongside the manuscript:

- Appendix 1: Supplementary information for Chapter 4: Reconciling the Sustainable Manufacturing of Commodity Chemicals with Feasible Technoeconomic Outcomes: Assessing the investment case for heat integrated aerobic gas fermentation
- Appendix 2: Supplementary information for Chapter 5: Renewable butadiene: A case for hybrid processing via bio- and chemo-catalysis
- Appendix 3: Supplementary information for Chapter 6: Probabilistic commodity price projections for unbiased techno-economic analyses
- Appendix 4: Supplementary information for Chapter 7: A surrogate model for the economic evaluation of renewable hydrogen production from biomass feedstocks via supercritical water gasification

A.1 Supplementary information for Chapter 4: Reconciling the Sustainable Manufacturing of Commodity Chemicals with Feasible Technoeconomic Outcomes: Assessing the investment case for heat integrated aerobic gas fermentation

Table S.I: Typical calculation for calculation of required oxygen mass transfer coefficient (k_{LA}) based on Aspen HYSYS mass and energy balance.

Parameter	Value	Unit	Comments
Bioreactor Outlet oxygen concentration, $C_{g,off\text{-}gas}$	3.35	% (mol/mol)	
Design oxygen uptake rate, *OUR*	230	mmol O_2 $l^{-1}h^{-1}$	
Bioreactor headspace back-pressure, P_b	4	bara	
Loop reactor downcomer hydrostatic pressure, P_h	2.02	bar	Assumes a working volume of 80% (v/v) and a gas hold-up of 25% (v/v).
Inlet oxygen concentration, *Cg,air*	21	% (mol/mol)	
Inlet oxygen saturation in aqueous phase, $C_{L,air}$	1.00	mmol O_2 l^{-1}	Estimated using the Lee Kesler Plocker equation of state.
Outlet oxygen concentration, Cg,off-gas	3.35	% (mol/mol)	
Outlet oxygen saturation in aqueous phase, $C_{L,off\text{-}gas}$	0.26	mmol O_2 l^{-1}	Estimated using the Lee Kesler Plocker equation of state.
Broth dissolved oxygen concentration, *DO*	0	mmol O_2 l^{-1}	Micro-aerobic conditions.
Log mean concentration difference, *LMCD*	0.552	mmol O_2 l^{-1}	$\frac{(C_{L,air}-DO)-(C_{L,off-gas}-DO)}{ln\frac{(C_{L,air}-DO)}{(C_{L,off-gas}-DO)}}$
Required oxygen mass transfer coefficient, k_{LA}	415	h^{-1}	$\frac{OUR}{LMCD}$
Total ungassed broth volume, *V*	298	m^3	
Air Volumetric Flow Rate, *Q*	2927	m^3 h^{-1}	Actual temperature and pressure.
Air superficial gas velocity, u_g	0.075	m s^{-1}	
Power input to achieve required, k_{LA} (1)	450	kW	$\left(\frac{V}{1000}\right)\left(\frac{k_{LA}}{103\cdot u_g{}^{0.824}}\right)^{\frac{1}{0.482}}$

8.6

Table S.II: Capital cost estimation for the solvent plant using the NREL method.

Plant section	Major ISBL equipment item	Quantity	Purchase cost US$	ISBL installed Cost Cran factor	Installed cost (2006) US$	CE cost index adjustment to 2019 US$	Location factor	Total installed cost US$	Total plant section US$
Feedstock pre-treatment	**SCWG thermal cycle**								21,548,182
	High pressure pump	1	86,721	2.30	199,459	242,342	0.51	123,369	
	Heat pump condenser	1	618,283	2.20	1,360,223	1,652,671		841,325	
	Heat pump compressor	1	1,566,961	1.60	2,507,138	3,046,173		1,550,715	
	SCWG recovery HE	1	602,795	2.20	1,326,148	1,611,270		820,249	
	SCWG plug flow reactor	1	417,687	1.50	626,531	761,235		387,522	
	Vapour heater	1	235,313	2.20	517,689	628,993		320,201	
	Heat pump recovery HE	1	272,464	2.20	599,420	728,296		370,754	
	Combustion heater	1	33,243	2.20	73,135	88,859		45,235	
	Supercritical heater	1	75,606	2.20	166,334	202,096		102,881	
	Turbo-expander	1	3,717,523	1.80	6,691,541	7,737,174		3,938,764	
	Air compression after cooler	1	7,281	2.20	16,018	19,462		9,908	
	H_2 bioreactor cooler	1	241,164	2.20	530,561	644,631		328,163	
	Combustion								
	H_2 combustion feed heater	1	26,928	2.20	59,242	71,979	0.51	36,643	
	Bioreactor off-gas combustion feed heater	1	22,629	2.20	49,783	60,487		30,792	
	Combustion chamber	1	2,072,893	1.80	3,731,208	4,533,418		2,307,827	
	Combustion turbine	1	9,281,863	1.80	16,707,353	20,299,434		10,333,834	
Fermentation	**Seed fermenters**								6,109,348
	Seed fermenters	1	186,818	2.00	373,637	453,969	0.51	231,102	
	Seed fermenter recirculation pumps	1	24,809	2.30	57,060	69,328		35,293	
	Seed fermenter HE	1	26,767	2.20	58,887	71,548		36,423	
	Production fermenters								
	Production fermenters	4	2,578,892	2.00	5,157,784	6,266,707	0.51	3,190,193	
	Production fermenter recirculation pumps	4	516,321	2.30	1,187,539	1,442,860		734,517	
	Production fermenter HE	4	788,587	2.20	1,734,891	2,107,892		1,073,065	
	Centrifuge	4	817,228	1.60	1,307,565	1,588,692		808,755	
Product recovery from bioreactor aqueous and vapour	**Absorption**								1,853,509
	Acetone stripper tower	1	125,436	2.40	301,047	365,772	0.51	186,204	
	Water stripper tower	1	106,657	2.40	255,977	311,012		158,327	
	Isopropanol pre-flash distillation tower								
	Pre-flash bottoms recovery heater	1	58,797	2.20	129,354	157,166	0.51	80,008	
	Pre-flash condensate recovery heater	1	8,196	2.20	18,031	21,908		11,153	
	Tower	1	206,398	2.40	495,355	601,857		306,387	
	Reboiler	1	12,468	2.20	27,429	33,326		16,965	
	Condenser	1	8,196	2.20	18,031	21,908		11,153	
	Isopropanol and acetone concentration distillation								
	Column feed heater	1	11,033	2.20	24,273	29,492	0.51	15,013	
	Tower	1	700,026	2.40	1,680,062	2,041,275		1,039,152	
	Reboiler	1	9,476	2.20	20,848	25,330		12,895	
	Condenser	1	11,413	2.20	24,866	30,213		15,530	
Solvent recovery	**Acetone product distillation**								685,795
	Tower	1	180,458	2.40	433,099	526,216	0.51	267,881	
	Reboiler	1	9,772	2.20	21,498	26,120		13,297	
	Condenser	1	7,177	2.20	15,790	19,185		9,767	
	Solvent distillation								
	Pre-heater	1	7,180	2.20	15,797	19,193	0.51	9,771	
	Tower	1	245,120	2.40	588,287	714,769		363,868	
	Reboiler	1	7,225	2.20	15,895	19,313		9,832	
	Condenser	1	8,364	2.20	18,400	22,356		11,381	
Isopropanol pressure swing distillation	**Low pressure swing distillation**								1,539,261
	Feed condenser	1	7,901	2.20	17,383	21,120	0.51	10,752	
	Tower	1	539,856	2.40	1,295,655	1,574,221		801,389	
	Reboiler	1	7,179	2.20	15,794	19,190		9,769	
	Condenser	1	11,597	2.20	25,513	30,998		15,780	
	High pressure swing distillation								
	First pre-heater	1	7,917	2.20	17,417	21,162	0.51	10,773	
	Second pre-heater	1	7,400	2.20	16,280	19,780		10,070	
	Tower	1	447,603	2.40	1,074,247	1,305,211		664,444	
	Reboiler	1	11,968	2.20	26,329	31,990		16,285	
	Steam and water management								785,217

Plant section	Major ISBL equipment item	Quantity	Purchase cost US$	ISBL installed Cost Cran factor	Installed cost (2006) US$	CE cost index adjustment to 2019 US$	Location factor	Total installed cost US$	Total plant section US$
Steam and water management	CO_2 flash drum steam heater	1	33,438	2.20	73,564	89,380	0.51	45,501	
	Steam mechanical vapour compressors	1	706,707	1.60	1,130,732	1,373,839		699,380	
	Water recycle to fermentation cooler	1	11,040	2.20	24,287	29,509		15,022	
	Water recycle to SCWG gasification	1	11,227	2.20	24,700	30,011		15,278	
	IPA cooler to absorber	1	7,376	2.20	16,227	19,716		10,037	

Table S.III: Additional capital cost for the solvent plant associated with the NREL method.

Additional costs for determining Total Capital Investment (TCI)				
Item	**Description**	**Unit (basis)**	**Annual cost US$ year^{-1}**	**Comments**
Additional direct costs				
Warehouse	4	% of installed cost of ISBL equipment	1,300,852	On-site storage of equipment and supplies.
Site development	9	% of installed cost of ISBL equipment	2,926,918	Includes fencing, curbing, parking lot, roads, well drainage, rail system, soil borings, and general paving. This factor allows for minimum site development assuming a clear site with no unusual problems such as right-of-way, difficult land clearing, or unusual environmental problems.
Additional piping	5	% of installed cost of ISBL equipment	1,463,459	To connect ISBL equipment to storage and utilities outside the battery limits.
Indirect costs				
Pro-rateable costs	10	% of TDC	3,821,254	This includes fringe benefits, burdens, and insurance of the construction contractor.
Field expenses	10	% of TDC	3,821,254	Consumables, small tool and equipment rental, field services, temporary construction facilities, and field construction supervision.
Home office and construction	20	% of TDC	7,642,508	Engineering plus incidentals, purchasing, and construction.
Project contingency	10	% of TDC	3,821,254	Extra cash on hand for unforeseen issues during construction.
Other costs	10	% of TDC	3,821,254	Start-up and commissioning costs. Land, rights-of-way, permits, surveys, and fees. Piling, soil compaction/dewatering, unusual foundations. Sales, use, and other taxes. Freight, insurance in transit, and import duties on equipment, piping, steel, instrumentation, etc. Overtime pay during construction. Field insurance. Project team. Transportation equipment, bulk shipping containers, plant vehicles, etc.
TOTAL ADDITIONAL COSTS			**28,618,754**	

Table S.IV: Capital cost estimation for the solvent plant using the TS method.

Plant section	Major ISBL equipment item	Quantity	Purchase cost US$	ISBL installed cost lang factor	Installed cost (2006) US$	CE cost index adjustment to 2019 US$	Location factor	Total installed cost US$	Total plant section US$
Feedstock pre-treatment	**SCWG thermal cycle**								38,484,617
	High pressure pump	1	86,721	3.3	286,180	347,709	0.51	177,008	
	Heat pump condenser	1	618,283		2,040,334	2,479,006		1,261,988	
	Heat pump compressor	1	1,566,961		5,170,973	6,282,732		3,198,351	
	SCWG recovery HE	1	602,795		1,989,222	2,416,905		1,230,374	
	SCWG plug flow reactor	1	417,687		1,378,368	1,674,717		852,548	
	Vapour heater	1	235,313		776,534	943,489		480,302	
	Heat pump recovery HE	1	272,464		899,131	1,092,444		556,130	
	Combustion heater	1	33,243		109,703	133,289		67,853	
	Supercritical heater	1	75,606		249,501	303,144		154,321	
	Turbo-expander	1	3,717,523		12,267,826	14,184,819		7,221,067	
	Air compression after cooler	1	7,281		24,027	29,193		14,861	
	H_2 bioreactor cooler	1	241,164		795,841	966,947		492,244	
	Combustion								
	H_2 combustion feed heater	1	26,928	3.3	88,863	107,969	0.51	54,964	
	Bioreactor off-gas combustion feed heater	1	22,629		74,675	90,730		46,188	
	Combustion chamber	1	2,072,893		6,840,548	7,329,158		3,731,055	
	Combustion turbine	1	9,281,863		30,630,148	37,215,629		18,945,362	
Fermentation	**Seed fermenters**								10,081,936
	Seed fermenters	1	186,818	3.3	616,501	749,048	0.51	381,318	
	Seed fermenter recirculation pumps	1	24,809		81,869	99,471		50,638	
	Seed fermenter HE	1	26,767		88,331	107,322		54,635	
	Production fermenters								
	Production fermenters	4	2,578,892	3.3	8,510,344	10,340,067	0.51	5,263,819	
	Production fermenter recirculation pumps	4	516,321		1,703,860	2,070,190		1,053,872	
	Production fermenter HE	4	788,587		2,602,336	3,161,838		1,609,597	
	Centrifuge	4	817,228		2,696,853	3,276,677		1,668,058	
Product recovery from bioreactor aqueous and vapour	**Absorption**								2,568,914
	Acetone stripper tower	1	125,909	3.3	415,498	504,830	0.51	256,994	
	Water stripper tower	1	106,671		352,014	427,697		217,728	
	Isopropanol pre-flash distillation tower								
	Pre-flash bottoms recovery heater	1	58,797	3.3	194,032	235,748	0.51	120,012	
	Pre-flash condensate recovery heater	1	8,196		27,047	32,862		16,729	
	Tower	1	206,398		681,113	827,553		421,282	
	Reboiler	1	12,468		41,144	49,990		25,448	
	Condenser	1	8,196		27,047	32,862		16,729	
	Isopropanol and acetone concentration distillation								
	Column feed heater	1	11,033	3.3	36,409	44,237	0.51	22,520	
	Tower	1	700,026		2,310,085	2,806,753		1,428,834	
	Reboiler	1	9,476		31,272	37,995		19,342	
	Condenser	1	11,413		37,663	45,760		23,295	
Solvent recovery	**Acetone product distillation**								949,723
	Tower	1	180,458	3.3	595,512	723,546	0.51	368,336	
	Reboiler	1	9,772		32,247	39,180		19,945	
	Condenser	1	7,177		23,686	28,778		14,650	
	Solvent distillation								
	Pre-heater	1	7,180	3.3	23,695	28,789	0.51	14,656	
	Tower	1	245,120		808,895	982,807		500,318	
	Reboiler	1	7,225		23,843	28,969		14,747	
	Condenser	1	8,364		27,600	33,534		17,071	
Isopropanol pressure swing distillation	**Low pressure swing distillation**								2,125,662
	Feed condenser	1	7,901	3.3	26,074	31,680	0.51	16,127	
	Tower	1	539,856		1,781,526	2,164,554		1,101,910	
	Reboiler	1	7,179		23,691	28,785		14,654	
	Condenser	1	11,597		38,269	46,497		23,670	
	High pressure swing distillation								
	First pre-heater	1	7,917	3.3	26,126	31,743	0.51	16,159	
	Second pre-heater	1	7,400		24,420	29,671		15,104	
	Tower	1	447,603		1,477,090	1,794,665		913,610	
	Reboiler	1	11,968		39,494	47,985		24,428	
Steam and water management	**Steam and water management**								1,571,228
	CO_2 flash drum steam heater	1	33,438	3.3	110,346	134,070	0.51	68,251	
	Steam mechanical vapour compressors	1	706,707		2,332,134	2,833,543		1,442,472	
	Water recycle to fermentation cooler	1	11,040		36,430	44,263		22,533	
	Water recycle to SCWG gasification	1	11,227		37,051	45,016		22,916	
	IPA cooler to absorber	1	7,376		24,341	29,574		15,055	

Table S.V: Capital cost estimation for the solvent plant using the Hand method.

Plant section	Major ISBL equipment item	Quantity	Purchase cost US$	ISBL installed cost Hand factor	Installed cost (2006) US$	CE cost index adjustment to 2019 US$	Location factor	Total installed cost US$	Total plant section US$
Feedstock pre-treatment	**SCWG thermal cycle**								30,378,659
	High pressure pump	1	86,721	4.00	346,885	421,465	0.51	214,555	
	Heat pump condenser	1	618,283	3.50	2,163,991	2,629,249		1,338,472	
	Heat pump compressor	1	1,566,961	2.50	3,917,404	4,759,645		2,422,993	
	SCWG recovery HE	1	602,795	3.50	2,109,781	2,563,384		1,304,942	
	SCWG plug flow reactor	1	417,687	4.00	1,670,749	2,029,961		1,033,392	
	Vapour heater	1	235,313	3.50	823,597	1,000,670		509,411	
	Heat pump recovery HE	1	272,464	3.50	953,623	1,158,653		589,835	
	Combustion heater	1	33,243	3.50	116,351	141,367		71,966	
	Supercritical heater	1	75,606	3.50	264,622	321,516		163,674	
	Turbo-expander	1	3,717,523	2.50	9,293,807	10,746,075		5,470,505	
	Air compression after cooler	1	7,281	3.50	25,484	30,962		15,762	
	H_2 bioreactor cooler	1	241,164	3.50	844,074	1,025,550		522,077	
	Combustion								
	H_2 combustion feed heater	1	26,928	3.50	94,249	114,513	0.51	58,295	
	Bioreactor off-gas combustion feed heater	1	22,629	3.50	79,201	96,229		48,987	
	Combustion chamber	1	2,072,893	2.00	4,145,786	4,441,914		2,261,245	
	Combustion turbine	1	9,281,863	2.50	23,204,657	28,193,659		14,352,547	
Fermentation	**Seed fermenters**								11,210,164
	Seed fermenters	1	186,818	4.00	747,274	907,937	0.51	462,204	
	Seed fermenter recirculation pumps	1	24,809	4.00	99,236	120,571		61,379	
	Seed fermenter HE	1	26,767	3.50	93,684	113,827		57,946	
	Production fermenters								
	Production fermenters	4	644,723	4.00	10,315,568	12,533,415	0.51	6,380,386	
	Production fermenter recirculation pumps	4	129,080	4.00	2,065,285	2,509,321		1,277,420	
	Production fermenter HE	4	197,147	3.50	2,760,053	3,353,465		1,707,148	
	Centrifuge	4	204,307	2.50	2,043,071	2,482,331		1,263,680	
Product recovery from bioreactor aqueous and vapour	**Absorption**								3,076,854
	Acetone stripper tower	1	125,909	4.00	503,634	611,916	0.51	311,508	
	Water stripper tower	1	106,671	4.00	426,684	518,421		263,913	
	Isopropanol pre-flash distillation tower								
	Pre-flash bottoms recovery heater	1	58,797	3.50	205,791	250,036	0.51	127,286	
	Pre-flash condensate recovery heater	1	8,196	3.50	28,686	34,854		17,743	
	Tower	1	206,398	4.00	825,592	1,003,094		510,645	
	Reboiler	1	12,468	3.50	43,637	53,019		26,991	
	Condenser	1	8,196	3.50	28,686	34,854		17,743	
	Isopropanol and acetone concentration distillation								
	Column feed heater	1	11,033	3.50	38,616	46,918	0.51	23,885	
	Tower	1	700,026	4.00	2,800,103	3,402,125		1,731,920	
	Reboiler	1	9,476	3.50	33,167	40,298		20,514	
	Condenser	1	11,413	3.50	39,946	48,534		24,707	
Solvent recovery	**Acetone product distillation**								1,138,897
	Tower	1	180,458	4.00	721,832	877,026	0.51	446,468	
	Reboiler	1	9,772	3.50	34,201	41,555		21,154	
	Condenser	1	7,177	3.50	25,121	30,522		15,538	
	Solvent distillation								
	Pre-heater	1	7,180	3.50	25,131	30,534	0.51	15,544	
	Tower	1	245,120	4.00	980,479	1,191,282		606,446	
	Reboiler	1	7,225	3.50	25,288	30,725		15,641	
	Condenser	1	8,364	3.50	29,272	35,566		18,106	
Isopropanol pressure swing distillation	**Low pressure swing distillation**								2,559,872
	Feed condenser	1	7,901	3.50	27,655	33,600	0.51	17,105	
	Tower	1	539,856	4.00	2,159,425	2,623,702		1,335,648	
	Reboiler	1	7,179	3.50	25,127	30,530		15,542	
	Condenser	1	11,597	3.50	40,589	49,315		25,105	
	High pressure swing distillation								
	First pre-heater	1	7,917	3.50	27,709	33,666	0.51	17,139	
	Second pre-heater	1	7,400	3.50	25,900	31,469		16,020	
	Tower	1	447,603	4.00	1,790,412	2,175,351		1,107,406	
	Reboiler	1	11,968	3.50	41,887	50,893		25,908	
Steam and water management	**Steam and water management**								1,229,341
	CO_2 flash drum steam heater	1	33,438	3.50	117,033	142,195	0.51	72,387	
	Steam mechanical vapour compressors	1	706,707	2.50	1,766,768	2,146,623		1,092,782	
	Water recycle to fermentation cooler	1	11,040	3.50	38,638	46,946		23,899	
	Water recycle to SCWG gasification	1	11,227	3.50	39,296	47,745		24,305	
	IPA cooler to absorber	1	7,376	3.50	25,816	31,367		15,968	

Table S.VI: Fixed operating cost for the solvent plant using the NREL method.

Labour and supervision	Salary US$ (2020)	Number of personnel	Annual cost US$ year^{-1}
Plant manager	29,591	1	29,591
Plant engineer	29,977	1	29,977
Maintenance supervisor	20,406	1	20,406
Maintenance technician	14,968	3	44,903
Lab manager	21,569	1	21,569
Lab technician	14,619	1	14,619
Shift supervisor	15,267	4	61,067
Shift operators	13,373	12	160,470
Yard employees	6,184	4	24,735
Clerks and secretaries	11,488	3	34,464
		TOTAL SALARIES	441,800
Labour burden	90% of total salaries		397,620
		TOTAL LABOUR COST	**839,421**
Other overhead			**Annual cost US$ year^{-1}**
Maintenance	3% of ISBL		975,639
Property insurance	0.7% of FCI		427,980
		TOTAL FIXED OPERATING COST	**2,243,040**

Table S.VII: Fixed operating cost for the solvent plant using the TS method.

FIXED OPERATING COST			
Fixed operational consideration	**Assessment basis**	**Unit (basis)**	**Annual cost US$ year^{-1}**
Operating labour	Wage and salary cost for shift team members (excl. supervision)	13,373 US$ operator^{-1}, 4 shift teams with 3 operators each	160,470
Supervisory labour	25	% of operating labour	40,118
Direct salary overhead	50	% of operating + supervisory	100,294
Maintenance	3	% of ISBL	1,673,462
Property taxes and insurance	1	% of ISBL	557,821
Rent of land/buildings	1	% of FCI	725,167
General plant overhead	65	% of total labour + maintenance	1,218,132
Allocated environmental charges	1	% of FCI	725,167
Interest charges (capital)	0	% of total capital investment	0
		TOTAL FIXED OPERATING COST	**5,200,631**

Table S.VIII: Fixed operating cost for the solvent plant using the Coulson and Richardson method.

Labour and supervision	Salary US$ (2020)	Number of personnel	Annual cost US$ year^{-1}
Plant manager	29,591	1	29,591
Plant engineer	29,977	1	29,977
Maintenance supervisor	20,406	1	20,406
Maintenance technician	14,968	3	44,903
Lab manager	21,569	1	21,569
Lab technician	14,619	1	14,619
Shift supervisor	15,267	4	61,067
Shift operators	13,373	12	160,470
Yard employees	6,184	4	24,735
Clerks and secretaries	11,488	3	34,464
TOTAL OPERATING AND SUPERVISORY LABOUR COSTS			**441,800**
FIXED COSTS			
Fixed operational consideration	**Assessment basis**	**Unit (basis)**	**Annual cost US$ year^{-1}**
Maintenance	5	% of FCI	3,099,612
Operating labour			274,703
Laboratory costs	20	% operating labour	54,941
Supervisory labour	20	% operating labour	167,097
Plant overhead	50	% operating labour	137,352
Capital charges	10	% of FCI	0
Insurance	1	% of FCI	619,922
Local taxes	1	% of FCI	619,922
Royalties	1	% of FCI	0
FIXED COSTS			**4,973,549**
Sales expense General overheads Research and development	20	% of direct production costs	34,464
TOTAL FIXED OPERATING COSTS			**5,008,013**

Table S.IX: Investment analysis for the solvent plant using the Hand method for capital estimation and the TS method for fixed operating cost estimation.

Year	Project life	Detailed design	Fixed capital investment	Working capital	Fixed OPEX	Variable OPEX	Plant income	Depreciation	Corporation tax	Total cash flow	NPV	Cumulative NPV	Comments
		US$	US$	US$	US$	US$	US$	US$	US$	US$	US$	US$	
2019	0	-250,000	0	0	0	0	0	0	0	-250,000	-250,000	-250,000	
2020	1	0	-44,262,454	0	0	0	0	0	0	-44,262,454	-40,238,595	-40,488,595	Plant construction and commissioning.
2021	2	0	-22,573,852	0	0	0	0	0	0	-22,573,852	-18,656,076	-59,144,670	
2022	3	0	0	6,578,665	-4,904,838	-798,965	35,292,066	-6,683,631	-5,726,158	30,440,770	22,870,601	-36,274,069	Year 0 for plant operation.
2023	4	0	0	0	-5,002,935	-814,945	35,292,066	-6,683,631	-5,697,639	23,776,548	16,239,702	-20,034,367	
2024	5	0	0	0	-5,102,993	-831,243	35,292,066	-6,683,631	-5,668,550	23,689,280	14,709,179	-5,325,188	
2025	6	0	0	0	-5,205,053	-847,868	35,292,066	-6,683,631	-5,638,879	23,600,266	13,321,735	7,996,547	
2026	7	0	0	0	-5,309,154	-864,826	35,292,066	-6,683,631	-5,608,614	23,509,472	12,064,077	20,060,624	
2027	8	0	0	0	-5,415,337	-882,122	35,292,066	-6,683,631	-5,577,744	23,416,863	10,924,139	30,984,763	
2028	9	0	0	0	-5,523,644	-899,765	35,292,066	-6,683,631	-5,546,257	23,322,401	9,890,975	40,875,738	
2029	10	0	0	0	-5,634,117	-917,760	35,292,066	-6,683,631	-5,514,140	23,226,050	8,954,648	49,830,385	
2030	11	0	0	0	-5,746,799	-936,115	35,292,066	-6,683,631	-5,481,380	23,127,771	8,106,143	57,936,528	
2031	12	0	0	0	-5,861,735	-954,837	35,292,066	-6,683,631	-5,447,966	23,027,528	7,337,280	65,273,808	
2032	13	0	0	0	-5,978,970	-973,934	35,292,066	0	-7,084,791	21,254,372	6,156,634	71,430,442	
2033	14	0	0	0	-6,098,549	-993,413	35,292,066	0	-7,050,026	21,150,078	5,569,477	76,999,919	
2034	15	0	0	0	-6,220,520	-1,013,281	35,292,066	0	-7,014,566	21,043,699	5,037,694	82,037,613	
2035	16	0	0	0	-6,344,931	-1,033,547	35,292,066	0	-6,978,397	20,935,192	4,556,108	86,593,721	
2036	17	0	0	0	-6,471,829	-1,054,218	35,292,066	0	-6,941,505	20,824,514	4,120,019	90,713,740	
2037	18	0	0	0	-6,601,266	-1,075,302	35,292,066	0	-6,903,875	20,711,624	3,725,168	94,438,907	
2038	19	0	0	0	-6,733,291	-1,096,808	35,292,066	0	-6,865,492	20,596,475	3,367,688	97,806,596	
2039	20	0	0	0	-6,867,957	-1,118,744	35,292,066	0	-6,826,341	20,479,024	3,044,076	100,850,672	
2040	21	0	0	0	-7,005,316	-1,141,119	35,292,066	0	-6,786,408	20,359,223	2,751,153	103,601,825	
2041	22	0	0	0	-7,145,422	-1,163,942	35,292,066	0	-6,745,676	20,237,027	2,486,037	106,087,863	
2042	23	0	0	0	-7,288,331	-1,187,220	35,292,066	0	-6,704,129	20,112,386	2,246,114	108,333,977	
2043	24	0	0	0	-7,434,097	-1,210,965	35,292,066	0	-6,661,751	19,985,253	2,029,015	110,362,992	
2044	25	0	0	0	-7,582,779	-1,235,184	35,292,066	0	-6,618,526	19,855,577	1,832,590	112,195,582	
2045	26	0	0	0	-7,734,435	-1,259,888	35,292,066	0	-6,574,436	19,723,307	1,654,893	113,850,475	
2046	27	0	0	-6,578,665	-7,889,124	-1,285,086	35,292,066	0	-6,529,464	13,009,727	992,352	114,842,827	

Table S.X: Capital cost estimation for conventional renewable electricity generation using the Hand method.

Plant section	Major ISBL equipment item	Quantity	Purchase cost US$	ISBL Installed cost Hand factor	Installed cost (2006) US$	CE cost index adjustment to 2019 US$	Location factor	Total installed cost US$	Total plant section US$
Electricity generation	Steam turbine	3	2,791,955	2.50	6,979,888	7,478,452	0.51	3,807,056	3,807,056

Table S.XI: Fixed operating cost estimation for conventional renewable electricity generation using the TS method.

FIXED OPERATING COST			
Fixed operational consideration	**Assessment basis**	**Unit (basis)**	**Annual cost US$ year^{-1}**
Operating labour	Wage and salary cost for shift team members (excl. supervision)	13,373 US$ operator^{-1}, 4 shift teams with 3 operators each	13,373
Supervisory labour	25	% of operating labour	3,343
Direct salary overhead	50	% of operating + supervisory	8,358
Maintenance	3	% of ISBL	114,212
Property taxes and insurance	1	% of ISBL	38,071
Rent of land/buildings	1	% of FCI	47,588
General plant overhead	65	% of total labour + maintenance	85,103
Allocated environmental charges	1	% of FCI	47,588
Interest charges (capital)	0	% of total capital investment	0
		TOTAL FIXED OPERATING COST	**357,636**

Table S.XII: Investment analysis for conventional renewable electricity generation using the Hand method for capital estimation and the TS method for fixed operating cost estimation.

Year	Project life	Detailed design	Fixed capital	Working capital	Fixed OPEX	Variable OPEX	Plant income	Depreciation	Corporation tax	Total cash flow	NPV	Cumulative NPV	Comments
		US$	US$	US$	US$	US$	US$	US$	US$	US$	US$	US$	
2019	0	-25,000	0	0	0	0	0	0	0	-25,000	-25,000	-25,000	
2020	1	0	-3,397,797	0	0	0	0	0	0	-3,397,797	-3,088,907	-3,113,907	Plant construction and commissioning.
2021	2	0	-1,732,877	0	0	0	0	0	0	-1,732,877	-1,432,129	-4,546,036	
2022	3	0	0	505,010	-379,526	-864,501	14,972,100	-513,067	-3,303,751	10,929,331	8,211,368	3,665,332	Year 0 for plant operation.
2023	4	0	0	0	-387,117	-881,791	14,972,100	-513,067	-3,297,531	10,405,661	7,107,206	10,772,538	
2024	5	0	0	0	-394,859	-899,427	14,972,100	-513,067	-3,291,187	10,386,627	6,449,278	17,221,817	
2025	6	0	0	0	-402,756	-917,415	14,972,100	-513,067	-3,284,715	10,367,213	5,852,021	23,073,838	
2026	7	0	0	0	-410,812	-935,763	14,972,100	-513,067	-3,278,114	10,347,410	5,309,858	28,383,696	
2027	8	0	0	0	-419,028	-954,479	14,972,100	-513,067	-3,271,381	10,327,212	4,817,720	33,201,416	
2028	9	0	0	0	-427,408	-973,568	14,972,100	-513,067	-3,264,514	10,306,609	4,371,008	37,572,425	
2029	10	0	0	0	-435,956	-993,040	14,972,100	-513,067	-3,257,509	10,285,594	3,965,542	41,537,967	
2030	11	0	0	0	-444,676	-1,012,900	14,972,100	-513,067	-3,250,364	10,264,160	3,597,525	45,135,492	
2031	12	0	0	0	-453,569	-1,033,158	14,972,100	-513,067	-3,243,076	10,242,296	3,263,511	48,399,003	
2032	13	0	0	0	-462,640	-1,053,822	14,972,100	0	-3,363,909	10,091,728	2,923,214	51,322,217	
2033	14	0	0	0	-471,893	-1,074,898	14,972,100	0	-3,356,327	10,068,981	2,651,477	53,973,695	
2034	15	0	0	0	-481,331	-1,096,396	14,972,100	0	-3,348,593	10,045,779	2,404,880	56,378,574	
2035	16	0	0	0	-490,958	-1,118,324	14,972,100	0	-3,340,704	10,022,113	2,181,104	58,559,678	
2036	17	0	0	0	-500,777	-1,140,690	14,972,100	0	-3,332,658	9,997,974	1,978,046	60,537,724	
2037	18	0	0	0	-510,792	-1,163,504	14,972,100	0	-3,324,451	9,973,352	1,793,795	62,331,519	
2038	19	0	0	0	-521,008	-1,186,774	14,972,100	0	-3,316,079	9,948,238	1,626,616	63,958,135	
2039	20	0	0	0	-531,428	-1,210,510	14,972,100	0	-3,307,540	9,922,621	1,474,934	65,433,070	
2040	21	0	0	0	-542,057	-1,234,720	14,972,100	0	-3,298,831	9,896,492	1,337,319	66,770,388	
2041	22	0	0	0	-552,898	-1,259,414	14,972,100	0	-3,289,947	9,869,840	1,212,470	67,982,859	
2042	23	0	0	0	-563,956	-1,284,603	14,972,100	0	-3,280,885	9,842,656	1,099,210	69,082,068	
2043	24	0	0	0	-575,235	-1,310,295	14,972,100	0	-3,271,642	9,814,927	996,466	70,078,535	
2044	25	0	0	0	-586,740	-1,336,501	14,972,100	0	-3,262,215	9,786,644	903,268	70,981,803	
2045	26	0	0	0	-598,475	-1,363,231	14,972,100	0	-3,252,599	9,757,796	818,732	71,800,535	
2046	27	0	0	-505,010	-610,444	-1,390,495	14,972,100	0	-3,242,790	9,223,360	703,537	72,504,072	

Table S.XIII: Calculation of greenhouse gas emissions on cradle-to-gate basis for LanzaTech's anaerobic gas fermentation technology, producing acetone and ethanol.

Parameter	Value	Unit	Comment
Lower heating value for ethanol	26.70	$MJ\ kg^{-1}_{ethanol}$	Lower Heating Value (LHV).
Reported ethanol greenhouse gas (GHG) emissions	8.10	$g_{CO2eq}\ MJ^{-1}_{ethanol}$	Cradle-to-grave emissions.
Cradle-to-grave ethanol GHG emissions	0.22	$kg_{CO2eq}\ kg^{-1}_{ethanol}$	
Cradle-to-gate ethanol GHG emissions	-1.69	$kg_{CO2eq}\ kg^{-1}_{ethanol}$	Stoichiometry of ethanol combustion in excess O_2, forming two moles of CO_2.
Reported acetone GHG emissions	-2.07	$kg_{CO2eq}\ kg^{-1}_{acetone}$	Case A.
Cradle-to-gate GHG emissions for reported solvent mix.	-1.91	$kg_{CO2eq}\ kg^{-1}$ acetone + ethanol	Reported solvent mix, i.e. 57.3% acetone with balance ethanol on a mass basis.

References

1. L. A. H. Petersen, J. Villadsen, S. B. Jørgensen and K. V. Gernaey, *Biotechnol. Bioeng.*, 2017, **114**, (2), 344 LINK https://doi.org/10.1002/bit.26084

A.2 Supplementary information for Chapter 5: Renewable butadiene: A case for hybrid processing via bio- and chemo-catalysis

Abbreviations:

DEPG	Dimethyl Ether of Polyethylene Guiacol
DME	Dimethylether
MTP	Methanol to Propene
NMP	N-Methyl-2-Pyrrolidone
RBFNN	Radial Basis Function Neural Network
SCWG	Supercritical Water Gasification
WGS	Water Gas Shift
WHSV	Weight Hourly Space Velocity

Section S1: Detailed Conceptual Process Design

The process description and literature used to model each route is detailed below.

S1.1 Acet-BD Process Description

The Acet-BD route uses a black liquor as a feedstock, gasifying the black liquor to renewable CO_2 and H_2 using supercritical water gasification (SCWG). The conceptual process flow diagram is detail in Figure S1. To mitigate plugging the weak black liquor is diluted prior to gasification. This also promotes greater hydrogen yields, as the forward water-gas shift reaction favours increased water concentrations (Okolie et al., 2019). Furthermore, the salts are precipitated out of the SCWG solution prior to entering the reactor. This prevents plugging and fouling and ensures efficient recovery of the pulping chemicals. This process is similar to supercritical water desalination (Odu et al., 2015; van Wyk et al., 2020) and has been modelled for SCWG of black liquor in (Magdeldin and Järvinen, 2020). Furthermore, Hastelloy is used as the material of construction for the SCWG reactor, necessitated by the need to prevent excessive corrosion.

The production of acetaldehyde relies on two unit operations, i.e. a gas fermenter and a thermophilic decarboxlation enzyme reactor. The first uses the chemolithoautotrophic bacteria, *Cupriavidus necator* (formerly, *Alcaligenes eutrophus* and *Ralstonia eutropha*) to produce the 2-oxoacid, pyruvic acid. This is then decarboxylated at elevated temperature to acetaldehyde in an enzyme reactor using a thermophilic *decarboxylase*. The SCWG reactor and bioreactor are integrated as outlined in Bommareddy et al. (2020). The heat pump recovers the low temperature heat of reaction from the bioreactor, removing the need for costly to operate chillers and supporting the endothermic SCWG reaction, reducing the external energy demand. The energy in the high-pressure SCWG effluent is recovered using a turbo-expander, which in turn supplies the air to the bioreactor and produces additional renewable electricity for sale to the grid.

A water removal column is used after the enzyme reactor prior to hydrogenation. The dewatered acetaldehyde is then recovered from the permanent gases in a second distillation column using NMP as an extractive solvent. NMP is used owed to its utilisation for the recovery of butadiene from the crude C4 stream.

Acetaldehyde is readily hydrogenated to ethanol and is a commercial process (Eckert et al., 2006). The process is modelled using the same conditions as outlined for butanal hydrogenation, with ethyl acetate as the primary by-product (Bradley et al., 1982; Pai, 1979).

The catalytic upgrading to butadiene is modelled using the high productivity zeolite-confined bimetallic catalyst reported in the experimental study by Dai et al. (2017). The 2%Zn-8%Y/beta

catalyst displays a productivity of 2.33 $g_{BD}.g^{-1}_{cat}h^{-1}$ at 673K and WHSV=7.9 h^{-1}, exceeding the minimum recommended productivity for commercialisation, 0.15 $g_{BD}.g^{-1}_{cat}h^{-1}$ (Makshina et al., 2012). The catalyst displays a 63% selectivity and 52% conversion (Dai et al., 2017). The by-products are outlined in Table S1. In the reported by-product breakdown, 13% (mole) of by-products are unaccounted for. As such, this study assumes that 7% is propene, owed to the 7% propene selectivity observed in the same study at a lower WHSV, and the remaining 6% a mixture of butenes. Butenes are a commonly reported by-product of the ethanol to butadiene process, requiring operationally complex extractive distillation of 1-butene and the energy intensive separation of 2-butenes (Buell and Boatright, 1947). The co-produced impurities have a large impact on the economic acceptability of this process (Dastillung et al., 2018). Therefore, ignoring the potential butene production would have a significant impact on the process economics. The ratio of 1-butene, trans-butene and cis-butene was modelled as 1:1.3:0.8, based on the Zn catalyst used in the study by Hayashi et al. (Hayashi et al., 2016).

Table S1: Reported 2%Zn-8%Y/beta catalyst selectivity *(Dai et al., 2017).*

Product	Selectivity (mol %)
Acetaldehyde	7
Crotonaldehyde	3
Butadiene	63
Ethene	12
Diethyl ether	2
Total	87

After the ethanol reactor the crude C4 product is recovered by the implementation of a heavies and ethanol removal column. The crude ethanol produced by the second column is sent to an ethanol recycle column which recovers unreacted acetaldehyde and ethanol to be recycled to the reactor. The generated recycle stream contains <10% water. The produced crude C4 stream is subject to extractive distillation using NMP as a physical solvent to recover butadiene from the 2-butenes by-product. This butadiene rich stream is finally purified to 99% in the product column.

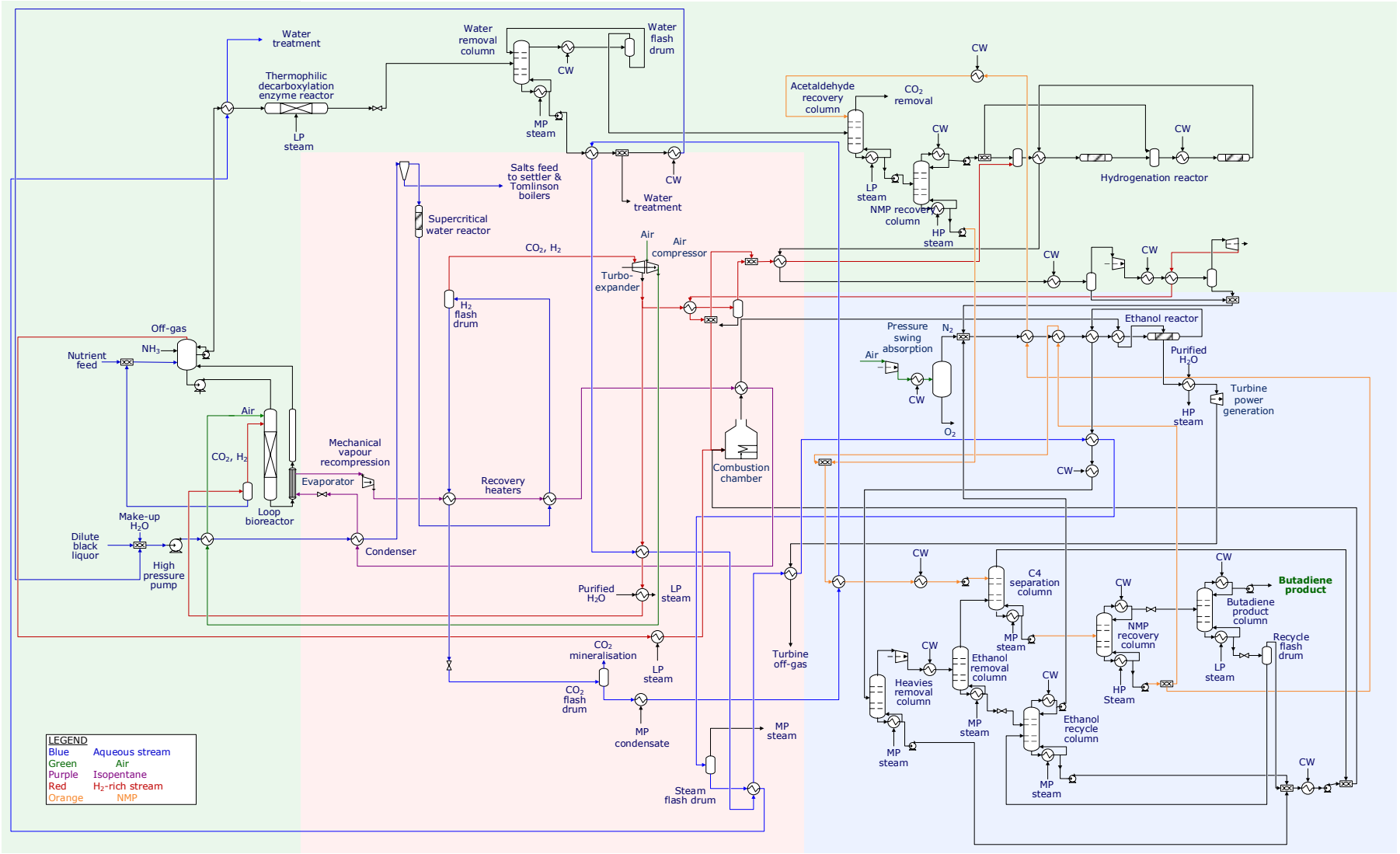

1 **Figure S1: Process flow diagram for the Acet-BD route. The three plant sections are highlighted as outlined in the main text;**
2 **gasification, steam and power generation (red), intermediate production (green) and butadiene synthesis and purification (blue).**

S1.2 Eth-BD Process Description

In the chemo-catalytic Eth-BD route, ethanol is produced as per the 2011 NREL report (Dutta et al., 2011). The chemo-catalytic conversion pathway uses biomass as a feedstock, gasifying the biomass to syngas followed by gas clean-up and tar reforming. The clean syngas is catalytically upgraded to mixed alcohols over a Molybdenum disulphide catalyst. The capital and operating expenditure in the 2011 study were brought to a 2020 basis. The ethanol product is catalytically upgraded to butadiene using the same catalyst and separation sequence as detailed in the Acet-BD route. The conceptual process flow diagram for the downstream processing, butadiene synthesis and purification, is detailed in Figure S2.

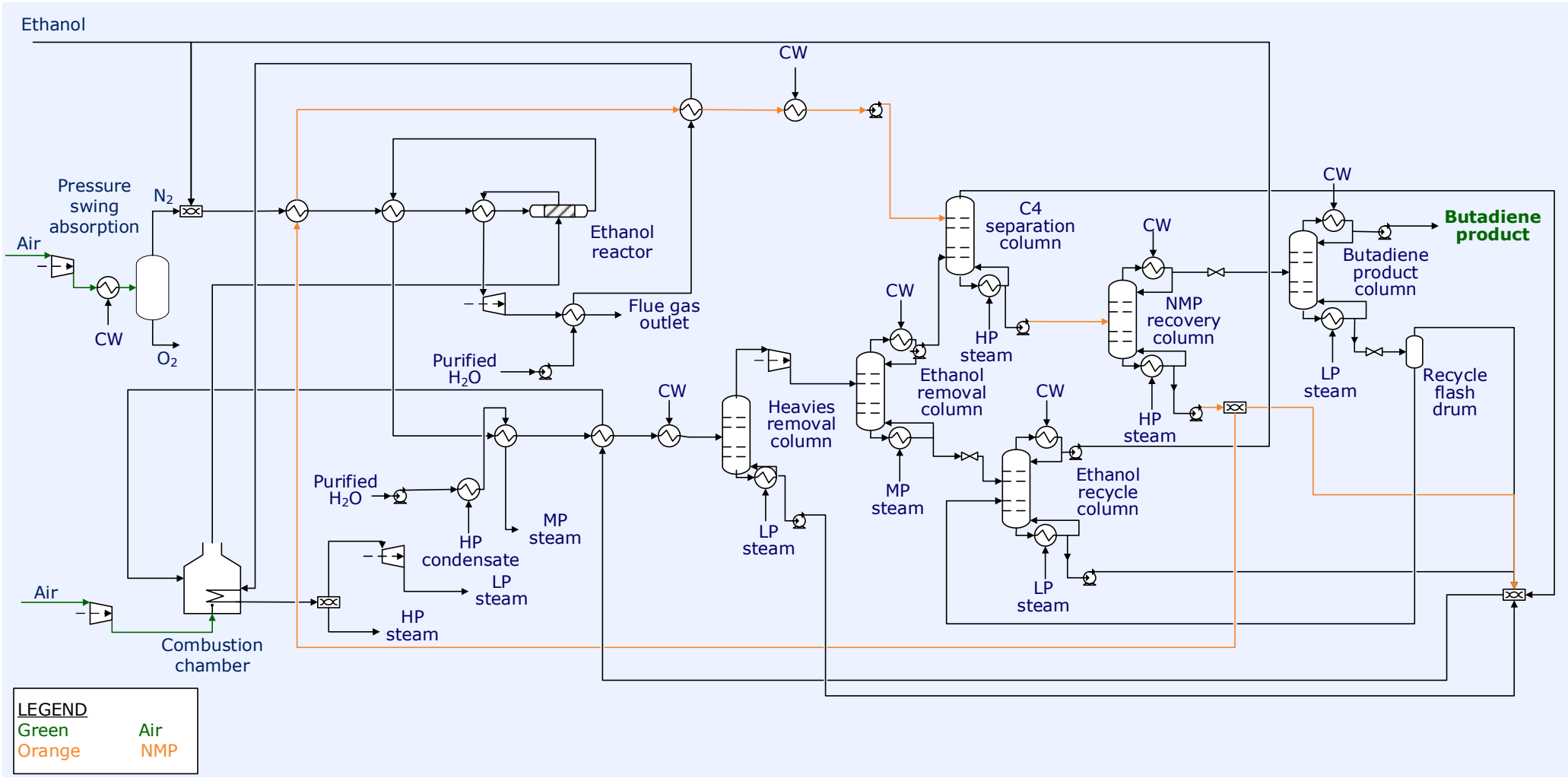

68

69 **Figure S2: Process flow diagram for the Eth-BD route. Only the Butadiene Synthesis and purification step is shown as the upstream**
70 **process is taken from the 2011 NREL report (Dutta et al., 2011) for chemo-catalytic ethanol production.**

S1.3 Syn-BD Process Description

The Syn-BD route involves a series of commercial catalytic processes using gasified woody biomass as a feedstock. The conceptual process flow diagram is detailed in Figure S3. The feed and handling plant section is based on the 2011 NREL report for thermochemical ethanol production as used previously (Dutta et al., 2011). The delivered wood chips are dried to a 10 wt % moisture content in a rotary drier using process flue gases prior to gasification. An indirect gasifier operating at 868°C is implemented with synthetic olivine and magnesium oxide as the heating medium between the combustor and gasifier (Dutta et al., 2011). The syngas composition leaving the gasifier is the same as that used in the 2011 NREL report for thermochemical ethanol production (Dutta et al., 2011).

The tar reformer implemented in both the aforementioned 2011 study and the more recent 2015 NREL study is used with reported yields taken from the 2015 study (Tan et al., 2015). The reformer operates at 2 bara and 870°C inlet and 910°C outlet temperature. The gasifier outlet is fed directly into the tar reformer along with steam at a molar steam to carbon ratio of 4.4:1. The tar reformer is indirectly heated using both the energy created from the catalyst regeneration and supplemental combustion gases. The resulting high temperature syngas is used throughout the process, finally cooled to 60°C before being fed to a direct-contact quench tower.

Despite the tar reformer having significant water shift activity (Tan et al., 2015), a water gas shift (WGS) reactor is implemented to produce the required $(H_2-CO_2)/(CO+CO_2)$ molar ratio of 2, optimal for methanol synthesis (Lange, 2001). The equilibrium constant proposed by Smith, Loganathan and Shantha, (2010) is used to model the WGS activity in both the tar reformer and WGS reactor. A molar steam to CO ratio of 1:1 is used in the shift reactor producing a H_2:CO ratio of 6.36 and a CO_2 mole percentage of 24% (Phillips et al., 2011). The acid gases (H_2S, COS and CO_2) are removed from the shifted syngas using Methyl diethanolamine (MDEA) as a chemical solvent. The process is based on the design parameters reported by Tan et al. (2015). A sulphur guard bed is implemented to ensure the H_2S content is below 0.1ppmv, required by the methanol catalyst (Phillips et al., 2011).

The cleaned syngas is converted to methanol over a commercial $Cu/ZnO/Al_2O_3$ catalyst. The reaction is modelled using the kinetics presented by Vanden Bussche and Froment (Vanden Bussche and Froment, 1996). The reactor operates at 50 bara, with an inlet temperature of 300°C and outlet of 320°C. The reaction heat is used to generate steam utilised throughout the process. The reactor effluent is flashed at 40°C to recover the methanol and water product. Most of the unreacted gases, 95%, are recycled to the reactor inlet. The 5% that is not recycled to the reactor inlet is let down to atmospheric pressure to producing a cold stream, required to recover hydrogen later in the process. A portion of the purge gas is combusted to prevent the build-up of inert gases whilst the remaining gas, 80%, is returned to the tar reformer.

A separate methanol dehydration unit is implemented to produce dimethylether (DME) prior to the MTP reactor. A separate reactor is required owed to the negative effect of increased water generation during methanol dehydration and the cryogenic separation required when separating the DME from the recycled gases (Koempel et al., 2005). The DME reactor is modelled using a γAl_2O_3 catalyst with an inlet temperature of 250°C (Hihman et al., 1998). The kinetics used are taken from Ng, Chadwick and Toseland, (1999), with the equilibrium constant taken from work conducted by Diep and Wainwright, (1987).

The outlet from the DME reactor is co-fed into the MTP reactor with steam (0.5:1 kg of methanol equivalent) (Rothaemel and Holtmann, 2002). The MTP reactor consists of three fixed bed reactors each containing 6 beds of the commercial H-ZSM-5 zeolite catalyst. During

operation two of the three reactors operate in parallel with the other in regeneration mode (Koempel and Liebner, 2007). The reactors operate at 1.5 bara and are modelled using kinetics derived by *Huang et al. (2016),* found to closely approximate the industrial MTP product distribution. The olefin recycle stream, steam, and a portion of the DME reactor outlet are fed into the first reactor at 460°C. The DME reactor outlet is divided between the 6 beds to limit the temperature rise to 50°C, as specified by Hack et al. (Hack et al., 2006).

The MTP product is dewatered using a flash drum prior to compression to 32 bara for the separation sequence. The product then undergoes a series of separation steps to; recover the propylene and butane rich products, recycle the long and short chain olefins to the MTP reactor, and facilitate the removal of paraffins. The separation sequence is detailed in Figure S3.

After separation, the propene rich stream it is fed into a hydroformylation reactor where it is upgraded to butanal. This process follows the principles behind Johnson Matthey's LP Oxo SELECTOR^{SM}10 technology (Johnson Matthey, n.d.). This process uses a homogenous rhodium-triphenylphosphine (TPP) catalyst producing a normal:iso ratio of 10:1 (Tudor and Ashley, 2007a) and operates at <20 bara and 80-120°C (Bahrmann et al., 2013). The rhodium catalyst is supplied as hydridocarbonyltris-(TPP) rhodium at a concentration of 275ppm, as practiced in US patents 4,247,486 and 4,593,127 (Brewster and Pruett, 1981; Bunning and Blessing, 1986). Excess TPP ligand is present in the reactor, at a concentration between 10-12 wt %, critical in determining the normal:iso aldehyde ratio. Two liquid recycle continuous stirred tank reactors are employed in series to ensure a high degree of conversion (Billig and Byrant, 2000). The aldehyde and heavy products are removed from the liquid product at the rate of formation and the catalyst solution is recycled back to the reactor (Tudor and Ashley, 2007a). The separation sequence is modelled after the sequence in US Patent 10,407,372, also based on two continuous stirred tank reactors in series (Simpson and Smith, 2019). Though kinetic studies have been undertaken on the hydroformylation of propene over a Rh/TPP catalyst (Bernas et al., 2008; Murzin et al., 2010), these use operating conditions outside of typical industrial practice (Tuţă and Bozga, 2011). Therefore, in this study conversion data was utilised as detailed for the primary liquid recycle reactor in US patent 4,593,127 (Bunning and Blessing, 1986).

The purified butanal is hydrogenated to butanol according to Johnson Matthey's Hydrogenation Technology whereby, vaporous hydrogen and butanal react over a heterogeneous catalyst (Johnson Matthey, n.d.). Excess hydrogen is fed into the bed as a thermal sink for the heat of reaction. This excess hydrogen is recovered from the gaseous product exiting the hydroformylation reactor. The catalyst consists of a reduced mixture of CuO and ZnO, claimed to produce negligible by-products and have high aldehyde conversion and alcohol yield, >99 mol % (Pai, 1979). The yields are taken from European Patent 0,008,767, operating at 4 bara and inlet temperature of 113°C (Pai, 1979). The reactor design is based on European Patent 0,073,129 (Bradley et al., 1982), utilising the catalyst in the aforementioned patent. The reactor consists of two adiabatic beds each fed with fresh, vaporised, aldehyde.

Whilst butanol dehydration is not currently practiced at industrial scale, it is analogous to ethanol dehydration (Mascal, 2012). Process conditions and conversion data were taken from US Patent 0238788, using a silane-modified γAl_2O_3 catalyst (Wright, 2012). The dehydration reaction occurs at 380°C, 2 bara, and WHSV=0.1h^{-1} and achieves an overall butene yield of 98 mol % with a 1-butene selectivity of 95 mol % (Wang et al., 2016).

Dehydrogenation of C4's to butadiene is a mature technology practiced at industrial scale. Oxidative dehydrogenation is exothermic and occurs at temperatures of 300-550°C, less than non-oxidative dehydrogenation. Similarly, to the methanol reactor, the reaction heat is used to generate steam. Experimental data from Jung et al. (2008) is used to model the reactor, employing a multi-component bismuth molybdate ($Co_9Fe_3Bi_1Mo_{12}O_{51}$) catalyst. The reaction occurs at atmospheric pressure, 420°C and a molar butene:O_2:steam ratio of 1:0.75:15 (Jung et al., 2008).

The butadiene product is then recovered using extractive distillation, employing NMP as a physical solvent, much the same as for the Acet-BD and Syn-BD processes. After extractive distillation butadiene is purified to 99% in the product column.

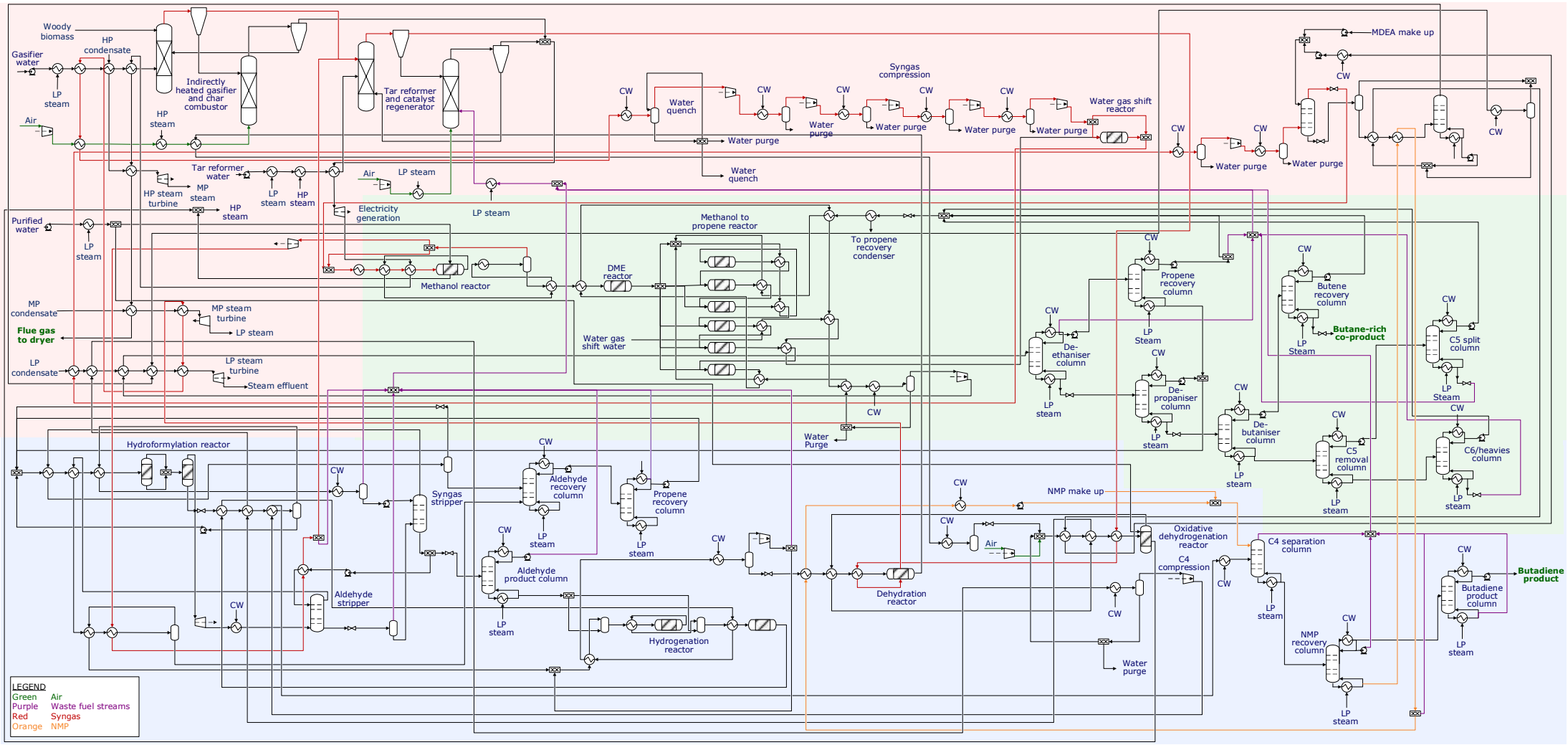

1 **Figure S3: Process flow diagram for the Syn-BD route. The three plant sections are highlighted as outlined in the main text;**
2 **gasification, steam and power generation (red), intermediate production (green) and butadiene synthesis and purification (blue).**

Section S2: Investment Analysis Parameters

Table S2: Raw material costs

Raw Material	Cost	Unit	Reference	Comments
Ammonia	250	$.tn^{-1}	(ICIS, 2020)	Average price for 2019.
Cooling water	0.753	$.m^{-1}	(Foo et al., 2017)	
Electricity	0.08	$.kWh^{-1}	(Zhang, 2019)	
Nutrients	0.75	$.m$^{-3}_{\text{media water}}$	-	Mineral salt media, containing no complex media or vitamins.
Process water	0.53	$.m^{-3}	(Towler and Sinnott, 2013)	
Natural gas	301.77	$.US ton^{-1}	(Dutta et al., 2011)	2007 price.
Diesel fuel	805.89	$.US ton^{-1}	(Dutta et al., 2011)	2009 price.
Wood chips	76.26	$.tn^{-1}		Detailed in section 2.2 Feedstock Costs.
NMP	2000	$.US ton^{-1}	(Future Market Insights, 2021)	
MDEA make-Up	16.94	$.million lb$^{-1}_{\text{acid gas removed}}$	(Tan et al., 2015)	2010 price.
DEPG make-Up	267.02		(Dutta et al., 2011)	2007 price.
LO-Cat chemicals	1,601.5		(Dutta et al., 2011)	2007 price.
WGS catalyst	8	$.lb^{-1}	(Swanson et al., 2010)	2007 price. Replaced every 3 years. GHSV 1,000 h^{-1}.
Methanol catalyst	9.69	$.lb^{-1}	(Tan et al., 2015)	2011 Price. Replace every 4 years.
DME catalyst	10.30	$.lb^{-1}	(Tan et al., 2015)	2011 Price. Replace every 4 years.
MTP catalyst	30.80	$.lb^{-1}	(Tan et al., 2015)	Replace every 1 year.
Hydroformylation catalyst	3.50	$.tn$^{-1}_{\text{butanal produced}}$	(Tudor and Ashley, 2007b)	2007 price.
Hydrogenation catalyst	10.00	$.lb^{-1}	-	Assumed. Replace every 3 years.
Dehydration catalyst	10.30	$.lb^{-1}	(Tan et al., 2017)	2011 price. Replace every 3 years.
Oxidative dehydrogenation catalyst	25	$.lb^{-1}	-	Assumed. Replace every 3 years.
Gasifier bed material: olivine	172.9	$.US ton^{-1}	(Tan et al., 2015)	2004 price. Replace 7.2 wt% per day.
Gasifier bed material: MgO	365	$.US ton^{-1}	(Tan et al., 2015)	2004 price. Replace 7.2 wt% per day.
Tar reformer catalyst	17.64	$.lb^{-1}	(Tan et al., 2015)	2007 price. Replace 0.15 wt% per day. GHSV 2,476 h^{-1}.
Alcohol synthesis catalyst	29.70	$.lb^{-1}	(Dutta et al., 2011)	2007 price. Replace every 2 years.

Butadiene catalyst	275.70	$.kg^{-1}$	-	Assumed. Replace 4 times per year.

Table S3: Co-product prices used in analysis

Route	Co-Product	Price	Comments	Reference
Acet-BD	Electricity	0.109 $.kwh^{-1}	China biomass subsidy.	(Ming et al., 2013)
Eth-BD	Higher alcohols	519-743 $.tn^{-1}	Costed at 90% of its energy value relative to gasoline. EIA yearly forecast up to 2050 used for gasoline price.	(EIA, 2021a)
Syn-BD	Butane rich co-product	348 $.tn^{-1}	Costed at energy value relative to butane. RBFNN forecasting methodology used for butane price.	(EIA, 2021b)

Table S4: Capital cost estimation for the Acet-BD route. The plant subsections are highlighted corresponding to the three major plant sections as outlined in the main text; gasification, steam and power generation (red), intermediate production (green) and butadiene synthesis and purification (blue).

Plant subsection	Equipment	Quantity	Purchase cost ($)	Hand factor	Installed cost (base year) ($)	Installed cost (2020) ($)	Total installed cost ($)	Total plant section ($)
SCWG thermal cycle	High pressure pump	1	83,054	4	332,214	349,323	177,928	17,302,597.70
	Condenser	1	494,774	3.5	1,731,709	1,820,890	927,475	
	Mechanical vapour recompression	1	2,310,581	2.5	5,776,453	6,073,935	3,093,773	
	Supercritical water reactor	1	686,173	4	2,744,691	2,886,040	1,470,011	
	Vapour heater	1	1,041,657	3.5	3,645,798	3,833,553	1,952,629	
	Heat pump recovery heat exchanger	1	20,989	3.5	73,463	77,246	39,346	
	Turbo-expander	1	4,799,936	2.5	11,999,840	12,617,822	6,426,916	
	Air compressor	1	12,769	3.5	44,693	46,994	23,937	
	H_2 Bioreactor Cooler	1	562,265	3.5	1,967,928	2,069,275	1,053,990	
	H_2 Cooler	1	194,688	4	778,751	818,856	417,086	
	Pre condenser recovery heat exchanger	1	71,644	3.5	250,752	263,666	134,299	
	H_2 flash drum	1	614,805	4	2,459,219	2,585,867	1,317,117	
	CO_2 flash drum	1	125,139	4	500,557	526,335	268,090	
Combustion	Bioreactor off-gas combustion feed heater	1	39,647	3.5	138,765	145,912	74,320	17,036,597
	Combustion chamber	1	1,300,373	2	2,600,745	2,734,682	1,392,916	
	Turbine power generation	1	11,627,961	2.5	29,069,903	30,566,977	15,569,360	
Fermentation	Seed fermenters	2	204,443	4	1,635,543	1,719,772	875,970	23,006,996
	Seed fermenter recirculation pumps	2	38,475	4	307,802	323,654	164,854	
	Seed fermenter heat exchangers	2	35,951	3.5	251,655	264,615	134,782	
	Production fermenters	8	731,061	4	23,393,939	24,598,706	12,529,407	
	Production fermenter recirculation pumps	8	402,182	4	12,869,823	13,532,608	6,892,865	
	Evaporator	8	122,057	3.5	3,417,594	3,593,598	1,830,407	
	Bioreactor pre-heater	1	41,541	3.5	145,393	152,881	77,870	
	Thermophilic decarboxylation enzyme reactor	1	233,783	4	935,132	983,291	500,841	
Acetaldehyde recovery	Water Removal Column	1	110,010	4	440,042	462,703	235,679	1,166,222
	Acet Flash Cooler	1	30,486	3.5	106,702	112,197	57,148	
	Acetaldehyde recovery column	1	103,525	4	414,098	435,424	221,784	
	Acetaldehyde pump	1	4,956	4	19,824	20,845	10,618	
	Water flash drum	1	30,362	4	121,447	127,701	65,045	
	NMP recovery column	1	234,784	4	939,135	987,499	502,985	
	NMP cooler	1	38,923	3.5	136,232	143,248	72,964	
Hydrogenation	H_2 int cooler	1	10,527	3.5	36,845	38,742	19,734	1,805,116
	Hydrogen recovery flash 2	1	53,030	4	212,120	223,044	113,608	
	Hydrogenation preheat	1	10,527	3.5	36,845	38,742	19,734	
	Vaporiser 1	1	41,989	4	167,956	176,605	89,954	
	Hydrogenation preheater 1	1	10,527	3.5	36,845	38,742	19,734	
	Hydrogenation reactor 1	1	19,749	4	78,997	83,066	42,310	
	Vaporiser 2	1	41,989	4	167,956	176,605	89,954	
	Hydrogenation preheater 2	1	29,271	3.5	102,449	107,725	54,870	
	Hydrogenation reactor 2	1	19,899	4	79,597	83,697	42,631	
	Ethanol flash cooler	1	29,271	3.5	102,449	107,725	54,870	
	Ethanol recovery flash	1	41,812	4	167,249	175,862	89,576	
	Hydrogen recovery compressor	1	546,778	2.5	1,366,945	1,437,341	732,113	
	Ethanol cooling water heat exchanger	1	29,271	3.5	102,449	107,725	54,870	
	Ethanol refrigeration heat exchanger	1	39,253	3.5	137,387	144,462	73,582	
	Hydrogen recovery flash	1	30,362	4	121,447	127,701	65,045	
	Hydrogen recovery turbine	1	181,134	2.5	452,835	476,156	242,531	

Nitrogen generation	Pressure swing absorption Columns	1	14,531	4	58,122	61,115	31,129	558,150
	Air compressor	1	352,625	2.5	881,562	926,962	472,150	
	Air cooler	1	29,271	3.5	102,449	107,725	54,870	
Reaction	Reactor	2	43,173	4	345,386	363,173	184,983	334,058
	Feed heater 1	1	29,310	3.5	102,586	107,869	54,944	
	Feed heater 2	1	29,310	3.5	102,586	107,869	54,944	
	Feed heater 3	1	10,453	3.5	36,584	38,468	19,594	
	Feed heater 4	1	10,453	3.5	36,584	38,468	19,594	
Reactant recovery	Pre-distillation cooler	1	29,310	3.5	102,586	107,869	54,944	2,747,645
	Heavies removal column	1	97,204	4	388,815	408,839	208,243	
	Ethanol removal column	1	242,972	4	971,888	1,021,939	520,527	
	Ethanol recycle column	1	642,128	4	2,568,511	2,700,787	1,375,652	
	Pre-ethanol column cooler	1	29,271	3.5	102,449	107,725	54,870	
	Flash compressor	1	398,376	2.5	995,940	1,047,230	533,409	
Extractive distillation	NMP recovery column	1	248,518	4	994,072	1,045,266	532,408	1,712,830
	C4 separation column	1	511,414	4	2,045,656	2,151,005	1,095,619	
	NMP recycle heat exchanger	1	38,923	3.5	136,232	143,248	72,964	
	NMP pump	1	5,526	4	22,103	23,241	11,838	
Product Recovery	Butadiene product column	1	1,343,012	4	5,372,046	5,648,702	2,877,179	2,916,019
	Lights flash	1	18,130	4	72,518	76,253	38,840	
Steam and water management	CO2 flash drum steam heater	1	133,301	3.5	466,555	490,582	249,879	1,692,343
	SCWG recovery cooler	1	48,165	3.5	168,579	177,260	90,288	
	Turbo-expander cooler	1	127,894	3.5	447,629	470,682	239,743	
	35 Bar pump	1	5,654	4	22,615	23,780	12,112	
	Fuel cooler	1	38,923	3.5	136,232	143,248	72,964	
	Fuel pump	1	8,018	4	32,072	33,723	17,177	
	SCWG water recycle cooler	1	53,932	3.5	188,764	198,485	101,099	
	SCWG recycle flash	1	49,820	4	199,278	209,541	106,730	
	SCWG recovery flash	1	176,120	4	704,480	740,761	377,308	
	SCWG heat exchanger	1	38,923	3.5	136,232	143,248	72,964	
	35 bar condensate heat exchanger	1	44,790	3.5	156,766	164,840	83,961	
	35 bar steam heat exchanger	1	10,527	3.5	36,845	38,742	19,734	
	Flash outlet cooler	1	90,261	3.5	315,913	332,182	169,198	
	1.9 Bar steam heat exchanger	1	42,243	3.5	147,851	155,465	79,187	

Table S5: Capital cost estimation for the Eth-BD route. The plant subsections are highlighted corresponding to the three major plant sections as outlined in the main text; gasification, steam and power generation (red), intermediate production (green) and butadiene synthesis and purification (blue).

Plant subsection	Equipment	Quantity	Purchase cost ($)	Hand/NREL factor*	Installed cost (base year) ($)	Installed Cost (2020) ($)	Total installed cost ($)	Total plant section ($)
Gasification	Gasifier	1	9,571,110	2.31	22,109,264	23,931,633	12,189,632	12,189,632
Gas clean-up	Steam blowdown/unreacted syngas HE	1	40,470	3.78	152,977	173,591	88,419	8,057,804
	Syngas inlet/make up HE	1	109,314	1.89	206,603	234,444	119,415	
	Syngas quench/Mol sieve HE	1	22,273	3.73	83,078	94,274	48,018	
	Alcohol synth/Combustion air HE	1	20,099	5.19	104,316	118,373	60,293	
	Syngas quench in/Comb air HE	1	26,372	5.55	146,365	166,088	84,597	
	Syngas quench in/Comb air HE	1	51,898	4.07	211,223	239,686	122,085	
	Tar reformer/Comb air HE	1	16,249	4.62	75,069	85,185	43,389	
	Tar Reformer/Comb air HE	1	37,241	3.24	120,659	136,919	69,740	
	Catalyst regen/Tar reformer steam HE	1	223,402	1.83	408,826	463,918	236,298	
	Tar reformer eff/Unreacted syn HE	1	29,602	3.80	112,486	127,644	65,016	
	Comb air blower	1	1,533,860	1.13	1,733,261	1,966,826	1,001,807	
	Quench water recirc pump	1	10,041	4.12	41,369	46,944	23,911	
	Tar reformer	1	4,785,554	2.31	11,054,630	11,965,815	6,094,815	
Alcohol Synthesis	Alcohol syn/Eff HE	1	1,461,470	1.99	2,908,326	3,300,236	1,680,983	51,175,478
	Alcohol syn/Eff HE	1	1,336,837	1.91	2,553,358	2,897,434	1,475,815	
	Comp interstage/Deaerator HE	1	279,924	2.47	691,413	784,584	399,630	
	Comp interstage/Deaerator HE	1	241,028	2.28	549,544	623,598	317,631	
	Comp interstage/Deaerator HE	1	170,371	2.45	417,408	473,656	241,258	
	Comp interstage/Mol Sieve HE	1	82,118	2.13	174,912	198,482	101,097	
	Comp interstage/Mol Sieve HE	1	42,085	2.51	105,633	119,867	61,055	
	Comp interstage/Mol Sieve HE	1	42,706	3.35	143,065	162,343	82,690	
	Alcohol eff/Lo-CAT HE	1	14,015	3.37	47,230	53,594	27,298	
	1st Stage air intercooler	1	157,091	1.20	188,510	204,048	103,932	
	2nd Stage air intercooler	1	50,287	1.20	60,344	65,318	33,270	
	3rd Stage air intercooler	1	63,426	1.23	78,014	84,445	43,012	
	4th Stage air intercooler	1	45,382	1.30	58,997	63,859	32,527	
	5th Stage air intercooler	1	47,428	1.36	64,502	69,818	35,562	
	1st Stage water intercooler	1	64,201	2.21	141,884	161,003	82,007	
	2nd Stage water intercooler	1	33,238	2.78	92,401	104,853	53,407	
	3rd Stage water intercooler	1	30,469	3.18	96,892	109,949	56,003	
	4th Stage water intercooler	1	27,859	3.79	105,585	119,813	61,027	
	5th Stage water intercooler	1	30,996	4.90	151,883	172,349	87,787	
	Syngas air cooler	1	152,010	3.01	457,551	519,209	264,460	
	Syngas cooling water exchange	1	120,299	3.24	389,769	442,292	225,283	
	Alcohol synth effluent/Syngas re HE	1	160,377	2.67	428,206	485,909	247,499	
	Alcohol synth effluent/CO_2 rich HE	1	17,721	3.89	68,936	78,225	39,844	
	Alcohol synth effluent/Mol sieve HE	1	29,912	2.96	88,540	100,471	51,175	
	Alcohol synth effluent/Expander inlet HE	1	49,413	3.64	179,865	204,102	103,960	
	Tar reformer eff/Expander inlet HE	1	20,048	6.99	140,134	159,018	80,996	
	Tar reformer eff/Expander inlet HE	1	54,692	5.15	281,666	319,621	162,800	
	Alcohol synth effluent/Expander inlet HE	1	18,236	5.64	102,852	116,712	59,447	
	Tar reformer eff/Expander inlet HE	1	23,639	4.00	94,557	107,300	54,653	
	Tar Reformer Eff/Expander Inlet HE	1	35,998	3.49	125,635	142,564	72,616	
	Alcohol synth effluent/CO_2 rich HE	1	22,335	6.36	142,052	161,194	82,104	
	Char combustor flue gas/CO_2 rich HE	1	17,626	3.97	69,974	79,403	40,444	
	Tar reformer eff/CO_2 rich HE	1	25,813	4.21	108,673	123,317	62,812	
	Catalyst regen/Alcohol synth HE	1	69,287	5.79	401,173	455,233	231,874	
	Syngas compressor	1	18,175,172	1.80	32,715,310	35,411,888	18,037,126	
	Purge expander stage 1	1	1,269,572	1.80	2,285,230	2,593,175	1,320,839	
	Purge expander stage 2	1	4,272,681	1.80	7,690,825	8,727,199	4,445,219	

	DEPG acid gas removal	1	4,049,473	2.53	10,245,166	11,625,747	5,921,601	
	Ammonia absorption refrig	1	1,953,613	1.15	2,246,655	2,431,836	1,238,661	
	Amine acid gas	1	757,635	2.80	2,121,379	2,407,244	1,226,135	
	Methanol/H_2S	1	285,132	2.00	570,264	647,109	329,607	
	LO-CAT sulphur recovery	1	875,412	1.35	1,181,806	1,350,053	687,653	
	Alcohol synthesis reactor	1	7,918,049	2.47	19,557,582	21,169,627	10,782,798	
	1st interstage KO drum	1	39,366	3.63	142,900	162,157	82,595	
	2nd interstage KO drum	1	27,777	3.21	89,166	101,181	51,537	
	3rd interstage KO drum	1	25,984	2.87	74,574	84,623	43,103	
	4th interstage KO drum	1	45,140	2.45	110,593	125,495	63,921	
	5th interstage KO drum	1	59,045	2.00	118,091	134,004	68,255	
	Pre compressor KO drum	1	78,653	2.65	208,430	236,517	120,470	
Alcohol separation	Crude alcohol distillation	1	1,196,829	1.25	1,496,037	1,697,634	864,694	7,509,130
	Methanol column	1	2,309,979	1.19	2,748,875	3,119,298	1,588,821	
	Ethanol product/mol sieve HE	1	18,795	3.39	63,715	72,301	36,827	
	Higher alcohols product/Mol sieve HE	1	10,362	3.94	40,825	46,327	23,597	
	Syngas quench inlet/water meth HE	1	151,968	1.87	284,179	322,474	164,253	
	Crude alcohol condenser	1	227,092	1.29	292,948	332,424	169,321	
	Crude alcohol reboiler	1	86,769	1.84	159,655	181,169	92,279	
	Methanol col condenser	1	567,521	1.20	681,025	772,796	393,625	
	Methanol col reboiler	1	176,730	1.63	288,071	326,889	166,502	
	Syngas quench inlet /Mol sieve HE	1	65,853	2.14	140,926	159,917	81,454	
	Alcohol syn/Mol sieve HE	1	14,955	6.59	98,554	111,835	56,963	
	Alcohol syn/Mol sieve HE	1	12,968	5.52	71,582	81,228	41,374	
	Cat regen/Water meth HE	1	15,754	3.57	56,241	63,820	32,507	
	Tar reformer edd/Water meth HE	1	15,485	4.35	67,362	76,439	38,934	
	Mol sieve flash cooler	1	-	1.29	-	-	-	
	Methanol condenser	1	186,088	1.29	240,053	272,402	138,748	
	Higher alcohols finishing cooler	1	14,051	3.16	44,403	50,386	25,664	
	Ethanol product cooler	1	10,708	4.32	46,260	52,494	26,738	
	Crude alcohol column pump	1	8,513	5.10	43,419	49,270	25,096	
	Methanol column reflux pump	1	14,806	4.68	69,290	78,627	40,049	
	Condensed methanol pump	1	637,107	1.24	790,012	896,470	456,619	
	Crude alcohol column bottoms pump	1	13,463	4.55	61,255	69,510	35,405	
	Methanol bottoms pump	1	19,361	4.27	82,670	93,810	47,782	
	Mixed alcohol knock out	1	83,539	2.02	168,748	191,488	97,535	
	Mol sieve pre flash	1	37,754	3.84	144,976	164,512	83,795	
	Molecular sieve separator	1	2,486,990	1.80	4,476,582	5,113,888	2,604,771	
	Condensed methanol flash drum	1	12,262	4.89	59,962	68,042	34,657	
	Crude alcohol column overhead	1	18,098	6.16	111,485	126,509	64,437	
	Methanol column overhead	1	26,694	4.97	132,671	150,549	76,682	
Steam and power generation	Steam turbine condenser	1	3,123,607	1.40	4,373,050	4,733,501	2,411,020	13,779,055
	Steam exhaust/Syngas recycle HE	1	19,540	3.45	67,414	76,499	38,965	
	Blowdown cooler	1	12,001	4.32	51,843	58,829	29,965	
	Steam turbine exhaust/Mol sieve HE	1	18,733	3.53	66,128	75,038	38,221	
	Syngas quench inlet/Makeup HE	1	16,808	3.83	64,374	73,048	37,207	
	Syngas quench inlet/BFW HE	1	66,971	2.12	141,979	161,111	82,062	
	Alcohol synthesis/BFW HE	1	102,172	1.95	199,236	226,084	115,156	
	Tar reformer eff/BFW HE	1	451,085	2.53	1,141,244	1,295,032	659,627	
	Catalyst regenerator/BFW HE	1	128,599	3.56	457,812	519,505	264,611	
	Char combustor flue gas/BFW HE	1	212,113	3.23	685,126	777,450	395,996	
	Catalyst regen flue gas steam gen	1	55,686	5.07	282,328	320,373	163,183	
	Char combustor flue gas Superheater	1	321,917	3.00	965,752	1,095,891	558,195	
	Tar reformer eff steam superheater	1	196,214	2.00	392,429	445,310	226,820	
	BFW reverse osmosis	1	1,543,471	1.15	1,774,992	1,921,296	-	
	BFW electrodeionisation	1	-	1.15	-	-	-	
	Hot condensate polishing unit	1	-	1.15	-	-	-	
	Extraction steam turbine stage 1	1	3,129,847	1.80	5,633,725	6,098,088	3,106,075	
	Extraction steam turbine stage 2	1	5,181,066	1.80	9,325,918	10,094,612	5,141,714	
	Start-up boiler	1	183,035	2.47	452,096	681,344	-	
	Brine recovery RO unit	1	-	1.15	-	-	-	
	Make-up pump	1	11,247	4.72	53,088	60,242	30,684	

	Condensate pump	1	19,182	4.61	88,431	100,347	51,112	
	EDI pump	1	19,182	4.61	88,431	100,347	51,112	
	BFW pump	1	483,579	1.35	652,831	740,803	377,330	
	Blowdown flash drum	1	28,626	3.41	97,614	110,768	-	
	Condensate collection tank	1	17,156	6.83	117,172	132,962	-	
	Condensate surge tank	1	16,674	6.51	108,545	123,172	-	
	Deaerator	1	32,321	5.07	163,868	185,950	-	
	Deaerator packed column	1	11,161	5.18	57,814	65,605	-	
	Steam drum	1	63,128	2.28	143,931	163,326	-	
Nitrogen generation	Pressure swing absorption columns	4	111,621	4.00	1,785,938	1,877,912	956,519	2,046,099
	Air compressor	1	799,137	2.50	1,997,844	2,100,731	1,070,012	
	Air cooler	1	10,439	3.50	36,535	38,417	19,568	
Reaction	Reactor	2	45,173	4.00	361,388	379,999	193,553	291,398
	Feed heater 1	1	31,309	3.50	109,580	115,224	58,689	
	Feed heater 2	1	10,444	3.50	36,554	38,436	19,578	
	Feed heater 3	1	10,444	3.50	36,554	38,436	19,578	
Reactant recovery	Flash cooler	1	10,978	3.50	38,424	40,403	20,579	6,146,987
	Heavies removal column	1	151,191	4.00	604,764	635,909	323,902	
	Ethanol removal column	1	355,344	4.00	1,421,375	1,494,574	761,265	
	Ethanol recycle column	1	690,995	4.00	2,763,982	2,906,325	1,480,343	
	Flash compressor	1	2,659,453	2.50	6,648,632	6,991,031	3,560,898	
Extractive distillation	NMP recovery column	1	168,913	4.00	675,651	710,446	361,867	1,918,368
	Extractive distillation column	1	676,024	4.00	2,704,095	2,843,353	1,448,268	
	NMP recycle HE	1	42,397	3.50	148,390	156,032	79,475	
	NMP pump	1	13,423	4.00	53,692	56,457	28,756	
Product recovery	Butadiene product column	1	917,743	4.00	3,670,972	3,860,024	1,966,112	2,018,227
	Recycle flash drum	1	24,326	4.00	97,305	102,316	52,115	
Steam and water management	Combustion chamber	1	516,709	2.00	1,033,417	1,086,637	553,481	4,794,992
	Combustion compressor	1	1,063,781	2.50	2,659,453	2,796,412	1,424,359	
	Steam generation HE	1	10,444	3.50	36,554	38,436	19,578	
	35 bar preheat 2	1	41,941	3.50	146,795	154,354	78,621	
	6 bar preheat	1	39,489	3.50	138,210	145,328	74,023	
	35 bar preheat 1	1	29,261	3.50	102,415	107,689	54,852	
	Fuel preheat HE	1	38,943	3.50	136,302	143,321	73,001	
	35 bar pump	1	11,771	4.00	47,085	49,510	25,218	
	6 bar pump	1	5,521	4.00	22,084	23,222	11,828	
	Steam turbine	1	247,047	3.50	864,664	909,194	463,100	
	Electricity turbine	1	1,075,960	3.50	3,765,860	3,959,798	2,016,932	

*The costs of equipment shaded in light blue are taken directly from the 2011 NREL report (Dutta et al., 2011), along with their corresponding installation factors and updated to a 2020 basis.

Table S6: Capital cost estimation for the Syn-BD route. The plant subsections are highlighted corresponding to the three major plant sections as outlined in the main text; gasification, steam and power generation (red), intermediate production (green) and butadiene synthesis and purification (blue).

Plant subsection	Equipment	Quantity	Purchase cost ($)	Hand/NREL factor*	Installed cost (base year) ($)	Installed Cost (2020) ($)	Total installed cost ($)	Total plant section ($)
Feedstock handling	Biomass cross flow dryer	1	56,462	2	112,925	114,890	58,594	58,594
Gasification	Gasifier steam Pump	1	9,157	4	36,629	38,516	19,618	18,031,447
	Gasifier steam generation HE 4	1	10,438	3.5	36,534	38,415	19,567	
	Gasifier air compressor	1	4,057,733	2.5	10,144,334	10,666758	5,433,138	
	Gasifier air preheat HE 1	1	29,357	3.5	102,749	108,041	55,031	
	Gasifier steam generation HE 1	1	29,347	3.5	102,715	108,004	55,012	
	Gasifier steam generation HE 2	1	36,672	3.5	128,353	134,963	68,744	
	Gasifier steam generation HE 3	1	61,914	3.5	216,700	227,860	116,061	
	Gasifier air preheat HE 2	1	10,469	3.5	36,642	38,529	19,625	
	Gasifier air preheat HE 3	1	29,351	3.5	102,729	108,019	55,020	
	Indirectly heated gasifier and char combustor	1	9,571,110	2.31	2,109,264	3,931,633	12,189,632	
Gas clean-up	Tar reformer and catalyst regenerator	1	4,785,554	2.31	11,04,630	11,965,815	6,094,815	12,858,639
	Tar reformer steam preheat HE 2	1	42,882	3.5	150,087	157,817	80,384	
	Tar reformer steam preheat HE 3	1	10,463	3.5	36,621	38,507	19,614	
	Tar reformer steam pump	1	9,124	4	36,494	38,374	19,546	
	Tar reformer air compressor	1	3,355,790	2.5	8,389,476	8,821,527	4,493,265	
	Tar reformer cooling water HE	1	50,667	3.5	177,334	186,467	94,977	
	Syngas scrubber	1	1,509,795	2.47	3,729,193	4,036,574	2,056,038	
Syngas compression and water gas shift	Water quench	1	42,387	3.5	148,354	155,994	79,456	28,687,806
	Low temperature shift steam pump	1	26,113	4	104,451	109,830	55,942	
	Syngas compressor 1	1	3,122,210	2.5	7,805,526	8,207,504	4,180,511	
	Syngas cooler 1	1	32,922	3.5	115,227	121,161	61,714	
	Syngas flash 1	1	232,948	4	931,793	979,780	499,053	
	Syngas compressor 2	1	2,639,678	2.5	6,599,195	6,939,047	3,534,420	
	Syngas cooler 2	1	29,515	3.5	103,303	108,623	55,327	
	Syngas flash 2	1	331,150	4	1,324,600	1,392,816	709,434	
	Syngas compressor 3	1	3,305,913	2.5	8,264,781	8,690,410	4,426,480	
	Syngas cooler 3	1	29,798	3.5	104,295	109,666	55,858	
	Syngas flash 3	1	280,345	4	1,121,381	1,179,131	600,593	
	Syngas compressor 4	1	2,984,596	2.5	7,461,489	7,845,749	3,996,250	
	Syngas cooler 4	1	29,271	3.5	102,449	107,725	54,870	
	Syngas flash 4	1	439,722	4	1,758,888	1,849,469	942,031	
	Syngas compressor 5	1	3,407,756	2.5	8,519,391	8,958,132	4,562,845	
	Low temperature shift reactor	1	22,965	4	91,861	96,592	49,199	
	Syngas cooler 5	1	32,720	3.5	114,521	120,419	61,336	
	Syngas flash 5	1	157,127	4	628,510	660,878	336,620	
	Syngas compressor 6	1	3,305,453	2.5	8,263,633	8,689,203	4,425,866	
Acid gas removal and methanol synthesis	Syngas cooler 6	1	30,768	3.5	107,689	113,235	57,677	10,250,089
	Syngas flash 6	1	2,112,062	4	8,448,250	8,883,327	4,524,743	
	MDEA stripper	1	146,488	4	585,951	616,127	313,826	
	Water removal flash	1	138,800	4	555,198	583,791	297,355	
	MDEA recovery HE	1	115,639	3.5	404,735	425,579	216,770	
	E-165	1	40,260	3.5	140,909	148,165	75,468	
	MDEA recovery HE	1	203,919	4	815,676	857,682	436,862	
	NMP/MDEA recovery HE	1	38,923	3.5	136,232	143,248	72,964	
	CO2 recovery HE	1	29,271	3.5	102,449	107,725	54,870	
	CO2 removal flash	1	41,812	4	167,249	175,862	89,576	
	MDEA make up pump	1	80,483	4	321,932	338,511	172,421	
	MDEA recycle pump	1	534,315	4	2,137,261	2,247,328	1,144,682	
	LO-CAT sulphur recovery system	1	931,524	1.35	1,257,557	1,436,588	731,730	
	Sulphur guard bed	1	37,810	2.47	93,390	140,604	71,617	
	Methanol preheat 1	1	10,466	3.5	36,630	38,516	19,618	
	35 bar steam preheat 1	1	29,347	3.5	102,715	108,004	19,618	
	Methanol preheat 3	1	10,438	3.5	36,534	38,415	19,567	
	Methanol preheat 2	1	13,027	3.5	45,594	47,942	24,419	
	Methanol synthesis reactor	2	145,884	4	1,167,076	1,227,179	625,067	
	Methanol cooler	1	58,395	3.5	204,383	214,909	109,464	
	Methanol recovery flash	1	158,930	4	635,718	668,457	340,480	
	Methanol purge expander	1	620,852	2.5	1,552,130	1,632,063	831,295	

Methanol to propene	Dimethyl ether preheat 1	1	35,834	3.5	125,419	131,878	67,172	13,280,248
	Dimethyl ether preheat 2	1	10,453	3.5	36,584	38,468	19,594	
	Dimethyl ether reactor	1	99,012	4	396,048	416,444	212,117	
	Methanol to propene reactor	3	340,182	4	4,082,179	4,292,408	2,186,348	
	Refrigeration cooler	1	41,867	3.5	146,536	154,082	78,482	
	Refrigeration compressor	1	2,241,481	2.5	5,603,703	5,892,289	3,001,251	
	Bed 1 cooler	1	10,453	3.5	36,584	38,468	19,594	
	Bed 2 cooler	1	10,453	3.5	36,584	38,468	19,594	
	Bed 3 cooler	1	10,453	3.5	36,584	38,468	19,594	
	Bed 4 cooler	1	29,310	3.5	102,586	107,869	54,944	
	Bed 5 cooler	1	10,453	3.5	36,584	38,468	19,594	
	Bed 6 cooler	1	10,453	3.5	36,584	38,468	19,594	
	Bed 6 cooler 2	1	29,310	3.5	102,586	107,869	54,944	
	Bed 6 cooler 3	1	31,060	3.5	108,710	114,309	58,224	
	Bed 6 cooler 4	1	103,803	3.5	363,309	382,019	194,582	
	Olefin recycle preheat	1	10,453	3.5	36,584	38,468	19,594	
	Water removal flash MTP	1	71,912	4	287,649	302,463	154,060	
	Pre separation compressor	1	2,234,858	2.5	5,587,146	5,874,879	2,992,383	
	Dethaniser column	1	435,971	4	1,743,884	1,833,692	933,995	
	Depropaniser column	1	151,443	4	605,773	636,970	324,442	
	Propene recovery column	1	297,996	4	1,191,984	1,253,370	638,407	
	Debutaniser column	1	113,469	4	453,874	477,248	243,088	
	Butene recovery column	1	214,389	4	857,555	901,718	459,292	
	C5 removal column	1	131,408	4	525,633	552,702	281,520	
	C5 split column	1	250,274	4	1,001,097	1,052,653	536,171	
	C6/heavies column	1	313,522	4	1,254,089	1,318,674	671,669	
Hydroformylation	Hydroformylation reactor 1	1	248,085	4	992,338	1,043,443	531,480	5,153,584
	Hydroformylation reactor 2	1	199,061	4	796,243	837,248	426,454	
	Catalyst recycle pump	1	15,454	4	61,816	64,999	33,107	
	Catalyst recovery flash	1	24,980	4	99,921	105,067	53,516	
	Hydrogen recovery compressor	1	672,942	2.5	1,682,355	1,768,995	901,041	
	Hydrogen recovery HE	1	29,271	3.5	102,449	107,725	54,870	
	Hydrogen recovery stripper	1	44,034	4	176,136	185,207	94,335	
	Hydrogen recovery cooler 1	1	11,074	3.5	38,759	40,755	20,759	
	Stripping aldehyde recovery flash	1	84,632	4	338,527	355,961	181,310	
	Hydrogen recovery cooler 2	1	43,193	3.5	151,176	158,961	80,967	
	Hydrogen recovery cooler 3	1	39,030	3.5	136,604	143,639	73,163	
	Hydrogen recovery flash	1	12,648	4	50,592	53,197	27,096	
	Catalyst recycle HE	1	29,351	3.5	102,729	108,019	55,020	
	Aldehyde byproduct cooler 2	1	38,923	3.5	136,232	143,248	72,964	
	Aldehyde byproduct cooler 1	1	29,607	3.5	103,624	108,960	55,499	
	Hydroformylation product flash	1	30,885	4	123,542	129,904	66,167	
	Aldehyde stripper pump 1	1	21,967	4	87,870	92,395	47,062	
	Aldehyde stripper pump 2	1	23,927	4	95,708	100,637	51,260	
	Aldehyde stripper	1	105,355	4	421,418	443,121	225,705	
	Unreacted syngas cooler	1	11,074	3.5	38,759	40,755	20,759	
	Propene recovery flash	1	27,508	4	110,031	115,698	58,931	
	Syngas stripper	1	168,722	4	674,886	709,642	361,458	
	Propene recovery column	1	235,608	4	942,430	990,965	504,750	
	Aldehyde product column	1	539,557	4	2,158,226	2,269,373	1,155,910	
Hydrogenation	Hydrogen preheat	1	10,527	3.5	36,845	38,742	19,734	1,179,403
	Aldehyde vaporiser 1	1	53,452	4	213,810	224,821	114,513	
	Hydrogenation recovery HE 1	1	10,527	3.5	36,845	38,742	19,734	
	Hydrogenation reactor 1	1	27,688	4	110,751	116,455	59,317	
	Aldehyde vaporiser 2	1	57,632	4	230,526	242,398	123,466	
	Hydrogenation recovery HE 2	1	10,527	3.5	36,845	38,742	19,734	
	Hydrogenation preheat	1	29,519	3.5	103,318	108,639	55,335	
	Hydrogenation reactor 2	1	27,845	4	111,381	117,117	59,654	
	Hydrogenation cooler	1	44,328	3.5	155,147	163,137	83,094	
	Hydrogen recycle compressor	1	392,620	2.5	981,549	1,032,098	525,702	
	Hydrogenation hydrogen recovery flash	1	46,268	4	185,072	194,603	99,122	
Dehydration	Dehydration preheat 1	1	39,030	3.5	136,604	143,639	73,163	492,787
	Dehydration preheat 2	1	29,271	3.5	102,449	107,725	54,870	
	Dehydration preheat 3	1	10,467	3.5	36,635	38,522	19,621	
	Dehydration steam generation preheat	1	29,347	3.5	102,715	108,004	55,012	
	Dehydration reactor	1	71,003	4	284,011	298,638	152,112	
	Butene product cooler	1	38,923	3.5	136,232	143,248	72,964	
	Water removal flash	1	30,362	4	121,447	127,701	65,045	
Dehydrogenation	Oxidative dehydrogenation air compressor	1	118,743	2.5	296,858	312,146	158,992	886,205

	Dehydrogenation preheat 1	1	84,917	3.5	297,209	312,515	159,180	
	Dehydrogenation preheat 2	1	39,622	3.5	138,678	145,820	74,274	
	Dehydrogenation preheat 3	1	38,923	3.5	136,232	143,248	72,964	
	Dehydrogenation preheat 4	1	29,271	3.5	102,449	107,725	54,870	
	Butadiene cooler	1	85,569	3.5	299,492	314,916	160,403	
	Oxidative dehydrogenation reactor	1	95,934	4	383,735	403,497	205,522	
Product purification	Dehydrogenation water removal flash	1	97,589	4	390,355	410,458	209,068	
	C4 compression for separation	1	1,792,988	2.5	4,482,470	4,713,313	2,400,737	
	C4 cooler	1	39,370	3.5	137,794	144,890	73,800	
	C4 cooling Water Cooler	1	38,923	3.5	136,232	143,248	72,964	
	Heavies removal Flash	1	46,268	4	185,072	194,603	99,122	4,429,812
	NMP Pump	1	4,601	4	18,404	19,352	9,857	
	NMP Cooling Water Cooler	1	42,282	3.5	147,985	155,607	79,259	
	C4 separation column	1	257,923	4	1,031,692	1,084,823	552,557	
	NMP recovery column	1	257,900	4	1,031,598	1,084,725	552,507	
	Butadiene product column	1	177,350	4	709,399	745,932	379,942	
Steam and water management	Low pressure steam expander	1	585,525	2.5	1,463,812	1,539,197	783,993	
	Flue gas expander	1	7,824,836	2.5	19,562,090	20,569,521	10,477,133	
	Medium pressure steam expander	1	646,386	4	2,585,543	2,718,696	1,384,774	
	Low temperature shift effluent LP steam HE	1	14,060	3.5	49,210	51,744	26,356	
	Flue gas MP bar steam generation HE	1	32,832	3.5	114,913	120,831	61,546	
	MTP effluent LP steam HE	1	1,361	3.5	4,762	5,007	2,550	
	Tar reformer preheat steam HE	1	29,347	3.5	102,715	108,004	55,012	
	35 bar steam pump	1	36,254	4	145,017	152,485	77,669	14,575,979
	High pressure steam expander	1	586,259	4	2,345,037	2,465,804	1,255,963	
	Dehydrogenation effluent LP steam HE	1	43,586	3.5	152,552	160,408	81,704	
	Fuel streams preheat HE	1	10,466	3.5	36,630	38,516	19,618	
	Tar reformer air Preheat HE	1	10,464	3.5	36,625	38,511	19,616	
	MDEA CO2 LP steam HE	1	96,378	3.5	337,323	354,695	180,665	
	Flue gas HP steam generation HE	1	31,353	3.5	109,734	115,385	58,772	
	Tar reformer LP steam HE	1	37,148	3.5	130,017	136,713	69,635	
	Tar reformer MP steam generation HE	1	11,188	3.5	39,159	41,176	20,973	

*The costs of equipment shaded in light blue are taken directly from the 2011 NREL report (Dutta et al., 2011), along with corresponding installation factors and updated to a 2020 basis.

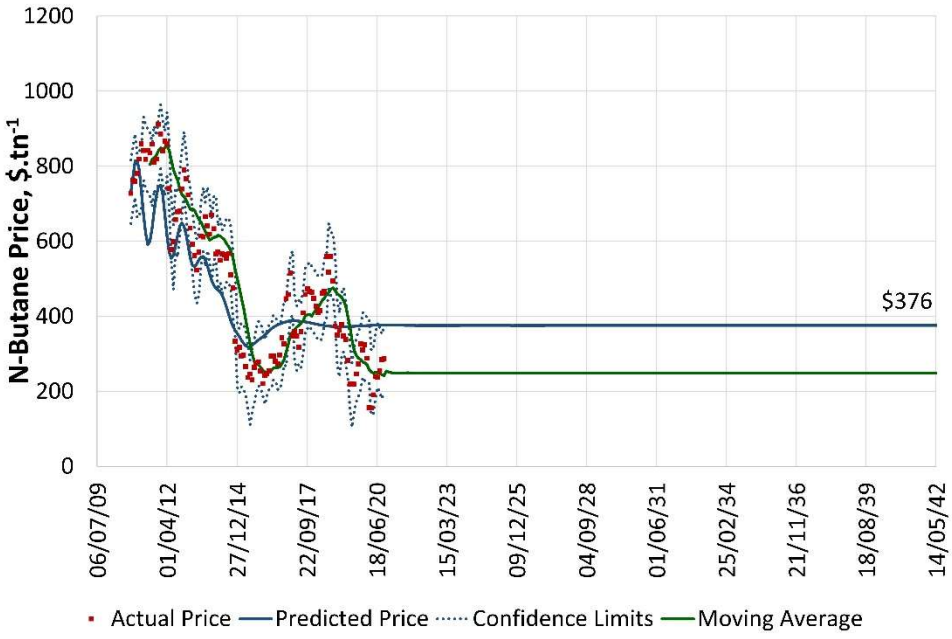

Figure S4: Butane long term average forecast price. The long-term average price is forecast as $376 tn^{-1}.

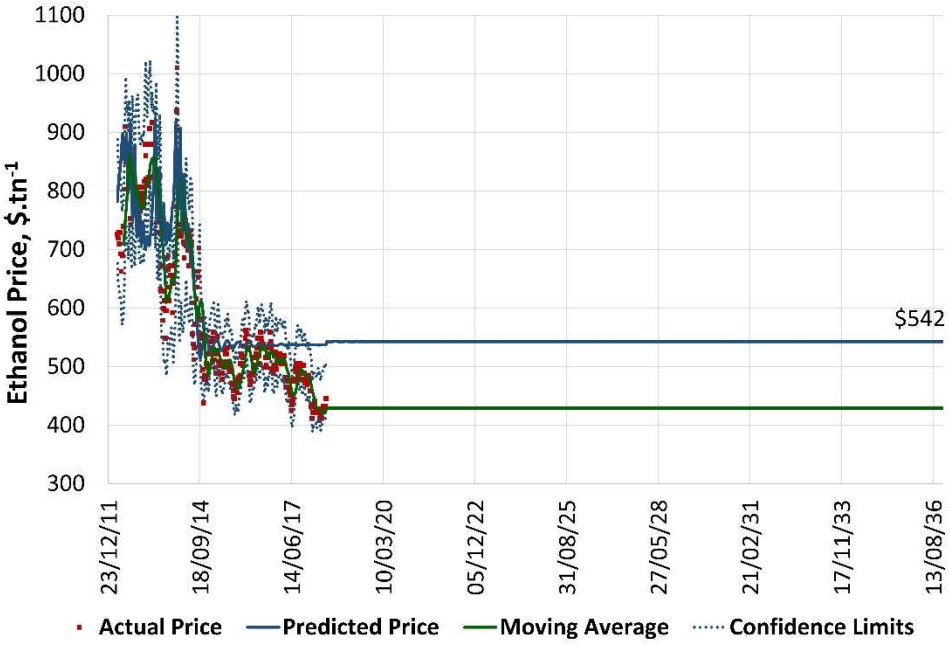

Figure S5: Ethanol long term average forecast price. The long-term average price is forecast as $542tn^{-1}.

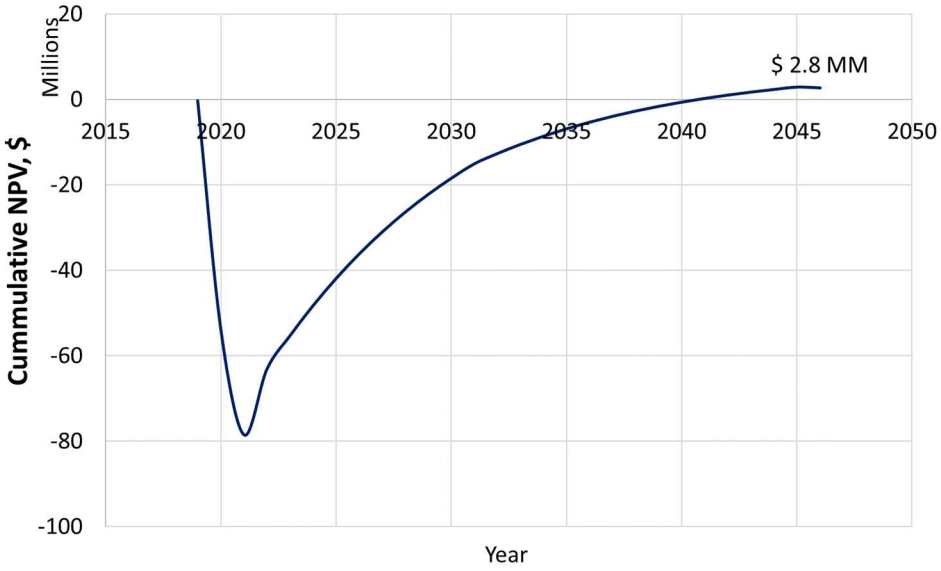

Figure S6: Cumulative Net Present Value (NPV) for Acet-BD route. The cumulative NPV is $2.8 million with a payback period of 22 years.

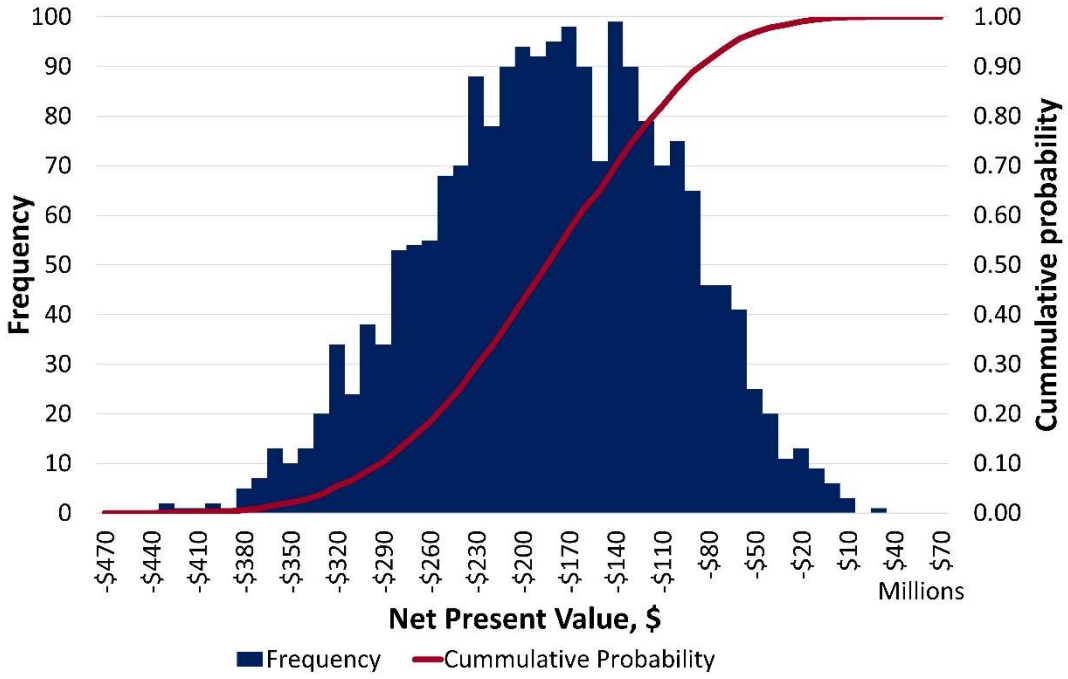

Figure S7: Monte Carlo simulation of the Eth-BD presenting a <1% likelihood of achieving a positive NPV, with a 70% probability of achieving between -$230 million and $30 million.

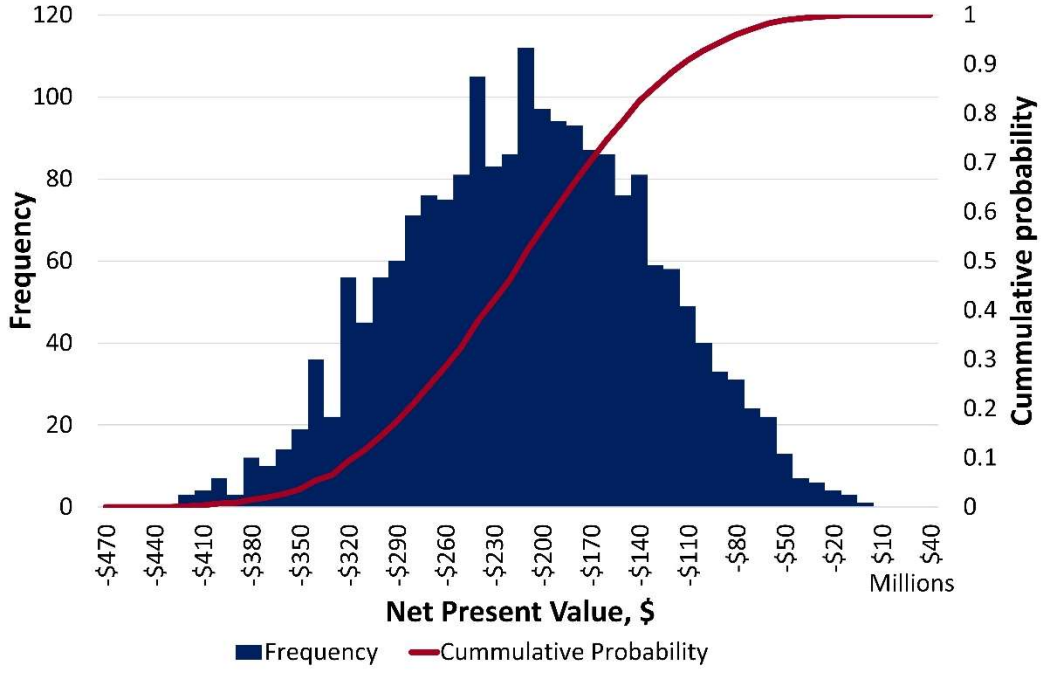

Figure S8: Monte Carlo simulation of the Syn-BD presenting a 0% likelihood of achieving a positive NPV, with a 70% probability of achieving between -$260 million and $0 million.

Table S7: Fixed operating cost summary

Parameter	Assessment basis	Unit	Annual cost ($.yr^{-1})		
			Acet-BD	Eth-BD	Syn-BD
Operating labour	Wage & salary cost for shift team members (excl. supervision)	($.yr-1)	213,960	213,968	267,450
Supervisory labour	25	% of operating labour	53,490	53,492	66,863
Direct salary overhead	50	% of operating + supervisory	133,725	133,730	167,156
Maintenance	3	% of inside battery limit	2,117,977	3,298,813	3,340,494
Property taxes & insurance	1	% of inside battery limit	705,992	1,099,604	1,113,498
Rent of land/buildings	1	% of fixed capital investment	882,490	1,429,486	1,447,547
General plant overhead	65	% of total labour + maintenance	1,550,527	2,318,078	2,388,624
Allocated environmental charges	1	% of fixed capital investment	882,490	1,429,486	1,447,547
Interest charges (capital)	0	% of total capital investment	0	0	0
Total fixed operating cost			6,540,652	9,976,657	10,239,180

Table S8: Variable operating cost summary

Route	Variable operating costs ($.yr^{-1})	Comments
Acet-BD	736,700	Excludes feedstock cost
Eth-BD	29,530,614	Differences between years attributed to frequency of catalyst replacement
	41,070,770	
Syn-BD	30,210,964	
	30,210,964	
	31,367,931	
	30,776,213	

Section S3: Life Cycle Analysis Parameters

Table S9: Life Cycle Analysis inventory data and sources.

Raw material	Emissions ($kg_{CO2eq}.kg^{-1}$)	Comments	Reference
Black liquor	0	Waste stream from pulp production.	
Eucalyptus residue	0.04	Emissions attributed for collection, chipping, loading and transport.	(McKechnie et al., 2011; Wernet et al., 2016)
Eucalyptus chips	0.07		(Bernstad Saraiva et al., 2017; Wernet et al., 2016)
Deionised water	3.73×10^{-4}	RER	(Wernet et al., 2016)
Ammonia	2.34	RER	
Natural gas	0.41	RoW	
Diesel fuel	0.48	Row	
NMP	6.60	GLO	
Butadiene	1.20	RoW	
Electricity	0.91	China grid mix 2018	(Sun et al., 2019)
Olivine	0.41		(Argonne National Laboratory, 2020)
MgO	0.61		
DEPG	2.50		
LO-CAT chemicals	6.78		
Tar reformer catalyst	5.93		
Methanol catalyst	4.01		
DME catalyst	3.76	Gamma Alumina catalyst	
MTP catalyst	6.78	ZSM-5 catalyst	
Dehydration catalyst	3.76	Gamma Alumina catalyst	
Alcohol Synthesis catalyst	4.01		
MDEA	2.91		(Badr, 2016)

Table S10: Market ethanol emissions used in analysis.

Parameter	Brazil	US
Transportation assumptions	Road: 1,000 km (total, to and from port) Shipping: 23,009 km (Santos to Shenzhen)	Road: 1,000 km (total, to and from port) Shipping: 27,915 km (Houston to Shenzhen)
	$kg_{CO2eq}\ kg^{-1}{}_{ethanol}$	
Ethanol production	0.39	0.86
Road transport	0.09	0.09
Shipping transport	0.17	0.21
Total	0.64	1.16

References

Argonne National Laboratory, 2020. GREET®2020 The Greenhouse gases, Regulated Emissions, and Energy use in Technologies Model [WWW Document]. URL https://greet.es.anl.gov/ (accessed 3.9.21).

Badr, S., 2016. Sustainability Assessment of Amine-based Post Combustion CO2 Capture. ETH Zurich. https://doi.org/10.3929/ethz-a-010836627

Bahrmann, H., Bach, H., Fey, G.D., 2013. Oxo Synthesis, in: Ullmann's Encyclopedia of Industrial Chemistry. John Wiley & Sons, Ltd. https://doi.org/10.1002/14356007.a18_321.pub2

Bernas, A., Mäki-Arvela, P., Lehtonen, J., Salmi, T., Murzin, D.Y., 2008. Kinetic modeling of propene hydroformylation with Rh/TPP and Rh/CHDPP catalysts. Ind. Eng. Chem. Res. 47, 4317–4324. https://doi.org/10.1021/ie071401r

Bernstad Saraiva, A., Valle, R.A.B., Bosquê, A.E.S., Berglin, N., v Schenck, A., 2017. Provision of pulpwood and short rotation eucalyptus in Bahia, Brazil – Environmental impacts based on lifecycle assessment methodology. Biomass and Bioenergy 105, 41–50. https://doi.org/10.1016/j.biombioe.2017.06.004

Billig, E., Byrant, D.R., 2000. Oxo process. Kirk-Othmer Encycl. Chem. Technol. 1–17. https://doi.org/10.1002/0471238961.15241502091212.a01

Bommareddy, R.R., Wang, Y., Pearcy, N., Hayes, M., Lester, E., Minton, N.P., Conradie, A. V., 2020. A Sustainable Chemicals Manufacturing Paradigm Using CO2 and Renewable H2. iScience 23. https://doi.org/10.1016/j.isci.2020.101218

Bradley, M.W., Hiles, A.G., Kippax, J.W., 1982. Hydrogenation Process. 0073129.

Brewster, E.A., Pruett, R.L., 1981. CYCLIC HYDROFORMYLATION PROCESS. 4247486.

Buell, C.K., Boatright, R.G., 1947. Furfural Extractive Distillation for Separating and Purification of C4 Hydrocarbons. Ind. Eng. Chem. 39, 695–705. https://doi.org/10.1021/ie50450a003

Bunning, D.L., Blessing, M.A., 1986. HYDROFORMYLATON PROCESS. 4593127.

Dai, W., Zhang, S., Yu, Z., Yan, T., Wu, G., Guan, N., Li, L., 2017. Zeolite Structural Confinement Effects Enhance One-Pot Catalytic Conversion of Ethanol to Butadiene. ACS Catal. 7, 3703–3706. https://doi.org/10.1021/acscatal.7b00433

Dastillung, R., Couderc, S., Thinon, O., 2018. Method for the production of butadiene from ethanol, incorporating extractive distillation. WO2018001982A1.

Diep, B.T., Wainwright, M.S., 1987. Thermodynamic Equilibrium Constants for the Methanol-Dimethyl Ether-Water System. J. Chem. Eng. Data 32, 330–333. https://doi.org/10.1021/je00049a015

Dutta, A., Talmadge, M., Hensley, J., Worley, M., Dudgeon, D., Barton, D., Groenendijk, P., Ferrari, D., Stears, B., Searcy, E.M., Wright, C.T., Hess, J.., 2011. Process Design and Economics for Conversion of Lignocellulosic Biomass to Ethanol Thermochemical Pathway by Indirect Gasification and Mixed Alcohol Synthesis, NREL technical report NREL/TP-5100-51400.

Eckert, M., Fleischmann, G., Jira, R., Bolt, H.M., Golka, K., 2006. Acetaldehyde, in: Ullmann's Encyclopedia of Industrial Chemistry. Wiley-VCH Verlag GmbH & Co. KGaA, pp. 191–208. https://doi.org/10.1002/14356007.a01_031.pub2

EIA, 2021a. ANNUAL ENERGY OUTLOOK 2021 [WWW Document]. URL

https://www.eia.gov/analysis/projection-data.php#annualproj (accessed 4.20.21).

EIA, 2021b. Hydrocarbon gas liquids explained Prices for hydrocarbon gas liquids [WWW Document]. URL https://www.eia.gov/energyexplained/hydrocarbon-gas-liquids/prices-for-hydrocarbon-gas-liquids.php (accessed 6.10.21).

Foo, D.C.Y., Chemmangattuvalappil, N., Ng, D.K.S., Elyas, R., Chen, C.-L., Elms, R.D., Lee, H.-Y., Chien, I.-L., Chong, S., Chong, C.H., 2017. Chemical Engineering Process Simulation. Elsevier.

Future Market Insights, 2021. N-Methyl-2-Pyrrolidone (NMP) Market [WWW Document]. URL https://www.futuremarketinsights.com/reports/global-n-methyl-2-pyrrolidone-market#:~:text=The price of NMP ranges,involving the use of NMP (accessed 4.15.21).

Hack, M., Koss, U., Konig, P., Rothaemel, M., Holtmann, H.-D., 2006. Method for Producing Propylene from Methanol. US 7,015,369 B2.

Hayashi, Y., Akiyama, S., Miyaji, A., Sekiguchi, Y., Sakamoto, Y., Shiga, A., Koyama, T.R., Motokura, K., Baba, T., 2016. Experimental and computational studies of the roles of MgO and Zn in talc for the selective formation of 1,3-butadiene in the conversion of ethanol. Phys. Chem. Chem. Phys. 18, 25191–25209. https://doi.org/10.1039/c6cp04171j

Hihman, C., Konig, P.D., Möller, F.-W.D., Holtmann, H.-D.D., Koss, U., 1998. Process for the preparation of ethylene, propylene and optionally isomers of butene from methanol and/or dimethyl ether. EP0882692B1.

Huang, X., Li, Hu, Li, Hui, Xiao, W.-D., 2016. Modeling and analysis of the Lurgi-type methanol to propylene process: Optimization of olefin recycle. AIChE J. 63, 306–313. https://doi.org/10.1002/aic.15565

ICIS, 2020. Ammonia prices, markets & analysis [WWW Document]. URL https://www.icis.com/explore/commodities/chemicals/ammonia/ (accessed 6.1.20).

Johnson Matthey, n.d. Hydroforylation Technology [WWW Document]. URL https://matthey.com/en/products-and-services/chemical-processes/core-technologies/hydroformylation-technology (accessed 5.11.20a).

Johnson Matthey, n.d. Hydrogenation technology [WWW Document]. URL https://matthey.com/en/products-and-services/chemical-processes/core-technologies/hydrogenation-technology (accessed 4.29.20b).

Jung, J.C., Lee, H., Kim, H., Chung, Y.M., Kim, T.J., Lee, S.J., Oh, S.H., Kim, Y.S., Song, I.K., 2008. Reactivity of n-butene isomers over a multicomponent bismuth molybdate (Co 9 Fe 3 Bi 1 Mo 12 O 51) catalyst in the oxidative dehydrogenation of n-butene. Catal. Commun. 9, 1676–1680. https://doi.org/10.1016/j.catcom.2008.01.026

Koempel, H., Liebner, W., 2007. Lurgi's Methanol To Propylene (MTP) Report on a succesful commercialisation. Stud. Surf. Sci. Catal. 167, 261–268. https://doi.org/10.1016/S0167-2991(07)80142-X

Koempel, H., Liebner, W., Wagner, M., 2005. Lurgi's gas to chemicals (GTC®): Advanced technologies for natural gas monetisation, in: Gastech. Bilbao, pp. 1484–1495.

Lange, J.P., 2001. Methanol synthesis: A short review of technology improvements. Catal. Today 64, 3–8. https://doi.org/10.1016/S0920-5861(00)00503-4

Magdeldin, M., Järvinen, M., 2020. Supercritical water gasification of Kraft black liquor: Process design, analysis, pulp mill integration and economic evaluation. Appl. Energy 262. https://doi.org/10.1016/j.apenergy.2020.114558

Makshina, E. V., Janssens, W., Sels, B.F., Jacobs, P.A., 2012. Catalytic study of the conversion of ethanol into 1,3-butadiene. Catal. Today 198, 338–344. https://doi.org/10.1016/j.cattod.2012.05.031

Mascal, M., 2012. Chemicals from biobutanol: technologies and markets. Biofuels, Bioprod. Biorefining 6, 483–493. https://doi.org/10.1002/bbb.1328

McKechnie, J., Colombo, S., Chen, J., Mabee, W., MacLean, H.L., 2011. Forest bioenergy or forest carbon? Assessing trade-offs in greenhouse gas mitigation with wood-based fuels. Environ. Sci. Technol. 45, 789–795. https://doi.org/10.1021/es1024004

Ming, Z., Ximei, L., Na, L., Song, X., 2013. Overall review of renewable energy tariff policy in China: Evolution, implementation, problems and countermeasures. Renew. Sustain. Energy Rev. 25, 260–271. https://doi.org/10.1016/j.rser.2013.04.026

Murzin, D.Y., Bernas, A., Salmi, T., 2010. Kinetic modelling of regioselectivity in alkenes hydroformylation over rhodium. J. Mol. Catal. A Chem. 315, 148–154. https://doi.org/10.1016/j.molcata.2009.06.023

Ng, K.L., Chadwick, D., Toseland, B.A., 1999. Kinetics and modelling of dimethyl ether synthesis from synthesis gas. Chem. Eng. Sci. 54, 3587–3592. https://doi.org/10.1016/S0009-2509(98)00514-4

Odu, S.O., Van Der Ham, A.G.J., Metz, S., Kersten, S.R.A., 2015. Design of a Process for Supercritical Water Desalination with Zero Liquid Discharge. Ind. Eng. Chem. Res. 54, 5527–5535. https://doi.org/10.1021/acs.iecr.5b00826

Okolie, J.A., Rana, R., Nanda, S., Dalai, A.K., Kozinski, J.A., 2019. Supercritical water gasification of biomass: A state-of-the-art review of process parameters, reaction mechanisms and catalysis. Sustain. Energy Fuels 3, 578–598. https://doi.org/10.1039/c8se00565f

Pai, C.C., 1979. A heterogeneous vapor phase process for the catalytic hydrogenation of aldehydes to alcohols. 0008767A1.

Phillips, S.D., Tarud, J.K., Biddy, M.J., 2011. Gasoline from Wood via Integrated Gasification , Synthesis , and Methanol-to- Gasoline Technologies. Energy. https://doi.org/NREL/TP-5100-47594

Rothaemel, M., Holtmann, H.-D., 2002. Methanol to Propylene MTP - Lurgi's Way. Erdoel Erdgas Kohle 118, 234–237.

Simpson, K., Smith, G.L., 2019. Hydroformylation Process. 10407372.

Smith R J, B., Loganathan, M., Shantha, M.S., 2010. A review of the water gas shift reaction kinetics. Int. J. Chem. React. Eng. 8. https://doi.org/10.2202/1542-6580.2238

Sun, X., Meng, F., Liu, J., McKechnie, J., Yang, J., 2019. Life cycle energy use and greenhouse gas emission of lightweight vehicle – A body-in-white design. J. Clean. Prod. 220, 1–8. https://doi.org/10.1016/j.jclepro.2019.01.225

Swanson, R.M., Platon, A., Satrio, J.A., Brown, R.C., 2010. Techno-economic analysis of biomass-to-liquids production based on gasification. Fuel 89, S11–S19. https://doi.org/10.1016/j.fuel.2010.07.027

Tan, E.C., Talmadge, M., Dutta, A., Hensley, J., Schaidle, J., Biddy, M., Humbird, D., Snowden-Swan, L.J., Ross, J., Sexton, D., Yap, R., Lukas, J., 2015. Process Design and Economics for the Conversion of Lignocellulosic Biomass to Hydrocarbons via Indirect Liquefaction.

Tan, E.C.D., Snowden-Swan, L.J., Talmadge, M., Dutta, A., Jones, S., Ramasamy, K.K., Gray, M., Dagle,

R., Padmaperuma, A., Gerber, M., Sahir, A.H., Tao, L., Zhang, Y., 2017. Comparative techno-economic analysis and process design for indirect liquefaction pathways to distillate-range fuels via biomass- derived oxygenated intermediates upgrading. Biofuels, Bioprod. Biorefining 11, 41–66. https://doi.org/10.1002/bbb.1710

Towler, G., Sinnott, R.K., 2013. Chemical Engineering Design - Principles, Practice and Economics of Plant and Process Design, 2nd ed. Elsevier.

Tudor, R., Ashley, M., 2007a. Enhancement of industrial hydroformylation processes by the adoption of rhodium-based catalyst: Part II. Platin. Met. Rev. 51, 164–171. https://doi.org/10.1595/147106707X238211

Tudor, R., Ashley, M., 2007b. Enhancement of industrial hydroformylation processes by the adoption of rhodium-based catalyst: Part I. Platin. Met. Rev. 51, 116–126. https://doi.org/10.1595/147106707X216855

Tuţă, E.F., Bozga, G., 2011. Performance assessment by simulation of a gas-recycle oxosynthesis plant with propylene recovery. Ind. Eng. Chem. Res. 50, 4545–4552. https://doi.org/10.1021/ie101731f

van Wyk, S., van der Ham, A.G.J., Kersten, S.R.A., 2020. Analysis of the energy consumption of supercritical water desalination (SCWD). Desalination 474. https://doi.org/10.1016/j.desal.2019.114189

Vanden Bussche, K.M., Froment, G.F., 1996. A steady-state kinetic model for methanol synthesis and the water gas shift reaction on a commercial Cu/ZnO/Al2O3 catalyst. J. Catal. 161, 1–10. https://doi.org/10.1006/jcat.1996.0156

Wang, W.-C., Tao, L., Markham, J., Zhang, Y., Tan, E., Batan, L., Warner, E., Biddy, M., 2016. Review of Biojet Fuel Conversion Technologies.

Wernet, G., Bauer, C., Steubing, B., Reinhard, J., Moreno-Ruiz, E., Weidema, B., 2016. The ecoinvent database version 3 (part I): overview and methodology. Int. J. Life Cycle Assess. 21, 1218–1230. https://doi.org/10.1007/s11367-016-1087-8

Wright, M.E., 2012. Process for the Dehydration of Aqueous Bio-Derived Terminal Alcohols to Terminal Alkenes. US 2012 0238788 A1.

Zhang, Z.Y., 2019. China Electricity Prices for Industrial Consumers [WWW Document]. China Breifing. URL https://www.china-briefing.com/news/china-electricity-prices-industrial-consumers/ (accessed 2.7.21).

A.3 Supplementary information for Chapter 6: Probabilistic commodity price projections for unbiased techno-economic analyses

Abbreviations:

CRPS	Continuous Ranked Probability Score
E	Epochs
HU	Hidden Units
LR	Learning Rate
LSTM	Long Short Term Memory
ML	Machine Learning
MSE	Mean Squared Error
RBFNN	Radial Basis Function Neural Network
TEA	Techno-Economic Analysis

Section S1: Comparative price projections

Tables S1-S5 present the comparative price projections between the previously employed RBFNN methodology and LSTM ensemble method for isopropanol, acetone, butadiene, ethanol, and butane. The previous projections use RBFNNs to predict the nominal price and a ±20% for the lower and upper bounds, as per Towler and Sinnott (2013). The ensemble projections use the monthly projections from the ensemble of 100 ML models to calculate the annual 5^{th}, 25^{th}, 50^{th}, 75^{th} and 95^{th} price percentiles. Notably, the RBFNN methodology produces a single long-term average price for the entire projection horizon, whereas the ensemble methodology produces a price for each year.

Table S1: Comparative price projections for the previous RBFNN methodology (Rodgers et al., 2021 & 2022) and the ensemble method for isopropanol. On average, the nominal price is higher and the range between the lower and upper limit is narrower for the new ensemble projections.

	Isopropanol ($/tonne)							
	RBFNN projection			Ensemble projection				
Year	Lower	Nominal	Upper	5th (lower)	25th	50th (nominal)	75th	95th (upper)
2020	1002	1252	1503	1108	1238	1390	1506	1606
2021				1235	1277	1309	1336	1369
2022				1298	1336	1359	1382	1417
2023				1313	1341	1358	1373	1400
2024				1274	1298	1322	1341	1360
2025				1286	1309	1329	1347	1363
2026				1292	1318	1337	1354	1370
2027				1304	1329	1346	1362	1377
2028				1314	1339	1355	1369	1383
2029				1329	1352	1367	1379	1391
2030				1339	1357	1371	1383	1398
2031				1350	1370	1382	1392	1406
2032				1356	1382	1394	1403	1414
2033				1368	1390	1400	1410	1425
2034				1367	1397	1408	1417	1428
2035				1381	1404	1414	1423	1434
2036				1389	1409	1418	1429	1449
2037				1401	1416	1426	1435	1450
2038				1408	1425	1433	1443	1466
2039				1415	1431	1443	1455	1474
2040				1418	1434	1444	1454	1476
2041				1426	1444	1456	1467	1492
2042				1438	1450	1461	1473	1493
2043				1437	1451	1463	1476	1495
2044				1445	1459	1471	1486	1508
2045				1451	1468	1481	1498	1520
2046				1454	1471	1485	1500	1522

Table S2: Comparative price projections for the previous RBFNN methodology (Rodgers et al., 2021 & 2022) and the ensemble method for acetone. On average, the nominal price is higher and the range between the lower and upper limit is wider for the new ensemble projections.

Year	Acetone ($/tonne)							
	RBFNN projection			Ensemble projection				
	Lower	Nominal	Upper	5th (lower)	25th	50th (nominal)	75th	95th (upper)
2020	621	776	932	584	854	988	1111	1454
2021				824	876	906	936	983
2022				565	631	673	727	854
2023				629	760	932	1119	1338
2024				696	789	854	917	991
2025				629	681	722	772	910
2026				631	688	736	850	1012
2027				667	733	816	959	1201
2028				670	747	846	954	1150
2029				627	743	866	1019	1284
2030				672	803	933	1077	1297
2031				650	814	940	1119	1285
2032				624	778	930	1087	1267
2033				690	828	1020	1219	1356
2034				671	792	965	1177	1308
2035				659	819	1040	1228	1324
2036				671	821	1042	1210	1336
2037				682	849	1082	1244	1344
2038				655	795	1072	1238	1348
2039				662	824	1135	1258	1362
2040				649	793	1086	1248	1358
2041				648	815	1134	1260	1361
2042				650	796	1135	1283	1376
2043				670	827	1168	1276	1372
2044				640	820	1177	1280	1373
2045				664	858	1193	1296	1379
2046				612	840	1178	1290	1386

Table S3: Comparative price projections for the previous RBFNN methodology (Rodgers et al., 2021 & 2022) and the ensemble method for butadiene. On average, the nominal price is higher and the range between the lower and upper limit is wider for the new ensemble projections.

	Butadiene ($/tonne)							
	RBFNN projection			Ensemble projection				
Year	Lower	Nominal	Upper	5th (lower)	25th	50th (nominal)	75th	95th (upper)
2020	1137	1421	1705	560	700	904	1234	1506
2021				1389	1480	1537	1597	1711
2022				1326	1426	1566	1731	1941
2023				1263	1417	1597	1944	2463
2024				1291	1433	1554	1921	2370
2025				1284	1401	1544	2016	2549
2026				1307	1409	1534	2003	2419
2027				1272	1407	1560	2072	2561
2028				1260	1390	1592	2121	2520
2029				1251	1376	1553	2151	2505
2030				1264	1390	1592	2189	2542
2031				1260	1381	1680	2187	2548
2032				1229	1400	1921	2271	2562
2033				1257	1384	1993	2327	2614
2034				1242	1399	2070	2355	2636
2035				1240	1371	2088	2373	2610
2036				1240	1370	2056	2370	2615
2037				1215	1364	2037	2401	2632
2038				1232	1374	2050	2387	2618
2039				1248	1363	2082	2415	2623
2040				1233	1357	2079	2401	2615
2041				1231	1358	2088	2402	2637
2042				1227	1353	2115	2412	2628
2043				1218	1353	2108	2434	2623
2044				1237	1355	2103	2429	2647
2045				1246	1355	2089	2422	2615
2046				1223	1361	2079	2411	2598

Table S4: Comparative price projections for the previous RBFNN methodology (Rodgers et al., 2021 & 2022) and the ensemble method for ethanol. On average, the nominal price is higher and the range between the lower and upper limit is narrower for the new ensemble projections.

	Ethanol ($/gal)							
	RBFNN projection			Ensemble projection				
Year	Lower	Nominal	Upper	5th (lower)	25th	50th (nominal)	75th	95th (upper)
2020				0.92	1.16	1.29	1.34	1.45
2021				1.47	1.60	1.70	1.79	1.88
2022				1.61	1.72	1.76	1.79	1.82
2023				1.71	1.76	1.78	1.79	1.82
2024				1.68	1.74	1.77	1.79	1.83
2025				1.67	1.73	1.76	1.78	1.82
2026				1.70	1.74	1.76	1.78	1.81
2027				1.73	1.76	1.77	1.79	1.81
2028				1.74	1.76	1.78	1.79	1.82
2029				1.75	1.77	1.79	1.80	1.84
2030				1.75	1.78	1.79	1.81	1.85
2031				1.74	1.77	1.79	1.82	1.86
2032				1.74	1.78	1.80	1.83	1.88
2033	1.28	1.61	1.93	1.74	1.78	1.80	1.84	1.90
2034				1.73	1.78	1.81	1.85	1.91
2035				1.74	1.78	1.81	1.85	1.90
2036				1.74	1.78	1.81	1.85	1.91
2037				1.74	1.79	1.82	1.86	1.91
2038				1.74	1.78	1.82	1.85	1.91
2039				1.74	1.79	1.82	1.87	1.93
2040				1.74	1.78	1.82	1.86	1.92
2041				1.73	1.79	1.82	1.87	1.93
2042				1.73	1.79	1.83	1.87	1.93
2043				1.72	1.79	1.83	1.87	1.93
2044				1.73	1.79	1.83	1.88	1.94
2045				1.74	1.79	1.83	1.88	1.95
2046				1.73	1.79	1.83	1.89	1.96

Table S5: Comparative price projections for the previous RBFNN methodology (Rodgers et al., 2021 & 2022) and the ensemble method for butane. On average, the nominal price is higher and the range between the lower and upper limit is narrower for the new ensemble projections.

	Butane ($/MMBTU)							
	RBFNN projection			Ensemble projection				
Year	Lower	Nominal	Upper	5th (lower)	25th	50th (nominal)	75th	95th (upper)
2020	6.46	8.07	9.68	3.34	4.59	5.78	6.58	8.51
2021				8.95	9.99	10.52	11.07	12.00
2022				10.28	10.49	10.56	10.62	10.86
2023				10.40	10.51	10.55	10.59	10.70
2024				9.85	10.32	10.56	10.82	11.26
2025				9.81	10.30	10.56	10.82	11.25
2026				9.89	10.35	10.55	10.74	11.15
2027				10.13	10.44	10.56	10.70	11.01
2028				10.28	10.48	10.56	10.64	10.85
2029				10.47	10.54	10.56	10.57	10.63
2030				10.50	10.54	10.56	10.57	10.61
2031				10.39	10.50	10.56	10.62	10.75
2032				10.20	10.44	10.56	10.67	10.91
2033				10.11	10.39	10.55	10.69	11.03
2034				10.07	10.39	10.55	10.70	11.13
2035				9.92	10.38	10.56	10.75	11.12
2036				9.85	10.34	10.56	10.78	11.23
2037				9.84	10.34	10.56	10.77	11.28
2038				9.69	10.33	10.57	10.82	11.45
2039				9.68	10.26	10.57	10.88	11.50
2040				9.58	10.23	10.53	10.85	11.57
2041				9.58	10.25	10.57	10.89	11.52
2042				9.49	10.16	10.53	10.83	11.57
2043				9.45	10.18	10.57	10.96	11.68
2044				9.38	10.12	10.53	10.96	11.69
2045				9.54	10.23	10.55	10.87	11.51

Section S2: Code used for the LSTM ensemble price projections

The code comprises three sections, 1) the grid search for optimal hyper-parameters, 2) the use of the optimal parameters on the validation set, and 3) running the models for the projection horizon. All three sections read data from the same Excel sheet which should be organised as follows:

- Column A contains the date corresponding to the start of the historic dataset to the end of the desired projection horizon (e.g., 01/01/2009 to 01/12/2046).
- Column B contains the standardised price data for the commodity being projected (e.g., 01/01/2009-01/12/2020). The remaining cells, where the data is to be projected are empty.
- Column C contains the standardised historic and EIA's projected crude oil prices for the desired projection horizon.
- Cell F3 contains the mean of the historic data for the commodity price data.
- Cell F3 contains the standard deviation of the original historic data for the commodity price data.

The below script codes for processing the historical data contained within the Excel sheet:

```
% Processing historic data
clc;
clear all;

% Select file containing historic data
filename = 'Butane';
A = readtable('Butane.xlsx');

% Set x = column containing standardised data
x = xlsread(filename,'B:B');

% Set z = column containing dates of historic data and projection horizon
% (i.e 01/01/2008-01/01/2042)
z = table2array(A(:,1));

% Set xplot = column containing standardised data
xplot = table2array(A(:,2));
crude = table2array(A(:,3));

% Set std_com = cell containing the commodity's standard deviation
% Set mean_com = cell containing the commodity's mean
std_com = xlsread(filename,'F3:F3');
mean_com = xlsread(filename,'E3:E3');

X2 = x;
Y2 = [];

for a = 1:size(X2,1)-12
    Y2(a,:) = cat(1,x(a+1),x(a+2),x(a+3),x(a+4),x(a+5),x(a+6),x(a+7),...
        x(a+8),x(a+9),x(a+10),x(a+11),x(a+12));
end

X2 = X2(1:(size(Y2,1)));

% Assign training and validation sets based on horizon length and data
availability
free_run = (size(z,1)-size(X2,1))/size(z,1);
val = round(free_run*size(X2,1))+2;
train = round(size(X2,1)-val);

X2_train = cat(2,X2(1:train),crude(1:train));
```

```
X2_val = cat(2,X2(train+1:val+train),crude(train+1:val+train));

Y2_train = Y2(1:train,:);
Y2_val = Y2(train+1:val+train,:);
```

S2.1: Model training - grid search for optimal hyper-parameters

The below script codes the grid search for optimal hyper-parameters. Three hyper-parameters, i.e. number of hidden units (HU), number of epochs (E), and initial learning rate (LR), are optimised. The models are trained to minimise the mean squared error (MSE) between the projections and training data.

Each combination of hyper-parameters is assessed based on the ensemble's performance against the validation set. The ensemble is evaluated based on the Continuous Rank Probability Score (CRPS) between the predicted and historical prices within the validation set. This is calculated using the 'CRPS' function for ensemble projections from the MATLAB file exchange (Shrestha, 2014).

Three 3x3 matrices of the CRPS are produced per run. This code should be run until no appreciable decrease in CRPS is observed. The combination of hyper-parameters giving rise to the lowest CRPS should be used in the following subsections.

The initial values for HU, E, and LR in the subsequent code are based on the results from executing this script for the five projected commodities. A wider range for these hyper-parameters can be explored as required, noting that the unique nature of a time series may require different parameter combinations.

```
% % Model training - grid search for optimal hyper-parameters

% Grid search: Hidden units (HU), epochs (E) and initial learn rate (LR)
% The initial values are based on results from the previously projected commodities
HU = [1,2,3];                       %1-500
E = [200,300,500];                  %100-1000
LR = [0.1,0.01,0.001];              %0.1-0.0000001

% Setting up network
for i = 1:size(HU,2)
    for j = 1:size(E,2)
        for k = 1:size(LR,2)

            Ypreds = [];
            for p=1:100

                h = randperm(HU(i));
                h = h(1);

                Ypred2 = [];
                Ypred3 = [];

                X2_train_LSTM{1} = [];
                Y2_train_LSTM{1} = [];
                X2_train_LSTM{1} = X2_train';
                Y2_train_LSTM{1} = Y2_train';
                numResponses = 12;
                m = round(val/12);
                c = 1;
                for n = 1:m
                    net = [];
                    layers = [ ...
                        sequenceInputLayer(2)
                        fullyConnectedLayer(2)
```

```
                        lstmLayer((h),'OutputMode','sequence')
                        fullyConnectedLayer(numResponses)
                        regressionLayer];
                    options = trainingOptions('adam', ...
                        'GradientThreshold',1, ...
                        'MaxEpochs',E(j), ...
                        'MiniBatchSize',1, ...
                        'InitialLearnRate',LR(k), ...
                        'Shuffle','every-epoch');
                    net = trainNetwork(X2_train_LSTM,Y2_train_LSTM,layers,options);

% Initialise real values
% Xpred = values to be predicted by the network
% The model operates recursively, i.e. previously projected values become inputs to
the model
                     Xpred{1} = cat(2,X2_train_LSTM{1},...
                                 cat(1,Y2_train_LSTM{1}(:,end)',...
                                 (crude(train+c:train+c+11))'));

% Ypred = network projection based on Xpred
                     Ypred = predict(net,Xpred);
                     X2_train_LSTM{1} = cat(2,X2_train_LSTM{1},...
                           cat(1,Xpred{1}(1,end-11:end),...
                           (crude(train+c:train+c+11))'));
                     Y2_train_LSTM{1} = cat(2,Y2_train_LSTM{1},...
                           Ypred{1}(:,end-11:end));

                     c = c + 12;
                end

% Ypred2 = projections on the validation set
% Ypred3 = projections up to the end of the projection horizon
                Ypred2 = X2_train_LSTM{1}(1,train+1:train+val);
                Ypred3 = X2_train_LSTM{1}(1,:);

                Ypreds = cat(1,Ypreds,Ypred2);
            end

            obs = ((X2_val(:,1)')*std_com)+mean_com;
            fcst = (Ypreds*std_com)+mean_com;
            [meanCRPS] = crps(fcst,obs);

% Calculating yearly percentiles of the ensemble projections for the entire data
series
             y_q =[];
             for q = 1:((size(Ypreds,2))/12)
                 q = q*12;
                 Y = cat(1,Ypreds(:,q-11),Ypreds(:,q-10),Ypreds(:,q-9),...
                           Ypreds(:,q-8),Ypreds(:,q-7),Ypreds(:,q-6),...
                           Ypreds(:,q-5),Ypreds(:,q-4),Ypreds(:,q-3),...
                           Ypreds(:,q-2),Ypreds(:,q-1),Ypreds(:,q));
                 YQ = quantile(Y,[0.05 0.25 0.50 0.75 0.95]);
                 YQ_12=repmat(YQ,12,1);
                 y_q = cat(1,y_q,YQ_12);
             end

% Positions i,j,k reflect the HU,L2,LR parameters used in the grid search,
respectively
            err_c_t = meanCRPS;
            err_val_c(i,j,k) = err_c_t;
        end
    end
end
```

S2.2: Model training – validation set using optimal hyper-parameters

The optimal hyper-parameters, determined during the grid search, inform the HU, E and LR values utilised in the below script. Running the following script will give rise to the CRPS between the real and predicted values based on the unseen validation set, producing a plot representing the predictions overlaid onto the historic data. The 'shade' function from the MATLAB file exchange is used to generate the shaded plots (Tordera, 2018).

```
% Running validation set - use of optimal hyper-parameters

% HU, L2, LR selected from grid search
HU = [1];
EP = [500];
LR = [0.1];

Ypreds = [];
Ypreds3 = [];

% Setting up network
for p=1:100

    h = randperm(HU);
    h = h(1);

    Ypred2 = [];
    Ypred3 = [];

    X2_train_LSTM{1} = [];
    Y2_train_LSTM{1} = [];
    X2_train_LSTM{1} = cat(2,X2_train');
    Y2_train_LSTM{1} = cat(2,Y2_train');
    numResponses = 12;
    m = round(val/12)+1;
    c = 1;
    for n = 1:m
        net = [];
        layers = [ ...
            sequenceInputLayer(2)
            fullyConnectedLayer(2)
            lstmLayer(h,'OutputMode','sequence')
            fullyConnectedLayer(numResponses)
            regressionLayer];
        options = trainingOptions('adam', ...
            'GradientThreshold',1, ...
            'MaxEpochs',EP, ...
            'MiniBatchSize',1, ...
            'InitialLearnRate',LR, ...
            'Shuffle','every-epoch');
        net = trainNetwork(X2_train_LSTM,Y2_train_LSTM,layers,options);

% Initialise real values
% Xpred = values to be predicted by the network
% The model operates recursively, i.e. previously projected values become inputs to
the model
                    Xpred{1} = cat(2,X2_train_LSTM{1},...
                               cat(1,Y2_train_LSTM{1}(:,end)',...
                               (crude(train+c:train+c+11))'));

% Ypred = network projection based on Xpred
                    Ypred = predict(net,Xpred);
                    X2_train_LSTM{1} = cat(2,X2_train_LSTM{1},...
                                       cat(1,Xpred{1}(1,end-11:end),...
                                       (crude(train+c:train+c+11))'));
                    Y2_train_LSTM{1} = cat(2,Y2_train_LSTM{1},...
                                       Ypred{1}(:,end-11:end));

                    c = c + 12;
                end
```

```
% Ypred2 = projections on the validation set
% Ypred3 = projections up to the end of the projection horizon
     Ypred2 = X2_train_LSTM{1}(1,train+1:train+val);
     Ypred3 = X2_train_LSTM{1}(1,:);

     Ypreds = cat(1,Ypreds,Ypred2);
     Ypreds3 = cat(1,Ypreds3,Ypred3);
end

obs = ((X2_val(:,1)')*std_com)+mean_com;
fcst = (Ypreds*std_com)+mean_com;
[meanCRPS] = crps(fcst,obs);

% Calculating yearly percentiles of the ensemble projections for the validation set
             y_q =[];
             for q = 1:((size(Ypreds,2))/12)
                 q = q*12;
                 Y = cat(1,Ypreds(:,q-11),Ypreds(:,q-10),Ypreds(:,q-9),...
                     Ypreds(:,q-8),Ypreds(:,q-7),Ypreds(:,q-6),...
                     Ypreds(:,q-5),Ypreds(:,q-4),Ypreds(:,q-3),...
                     Ypreds(:,q-2),Ypreds(:,q-1),Ypreds(:,q));
                 YQ = quantile(Y,[0.05 0.25 0.50 0.75 0.95]);
                 YQ_12=repmat(YQ,12,1);
                 y_q = cat(1,y_q,YQ_12);
             end

% Calculating yearly percentiles of the ensemble projections for the entire
data series
 t_q =[];
 for q = 1:((size(Ypreds3,2))/12)
     q = q*12;
     T = cat(1,Ypreds3(:,q-11),Ypreds3(:,q-10),Ypreds3(:,q-9),...
         Ypreds3(:,q-8),Ypreds3(:,q-7),Ypreds3(:,q-6),...
         Ypreds3(:,q-5),Ypreds3(:,q-4),Ypreds3(:,q-3),...
         Ypreds3(:,q-2),Ypreds3(:,q-1),Ypreds3(:,q));
     TQ = quantile(T,[0.05 0.25 0.50 0.75 0.95]);
     TQ_12=repmat(TQ,12,1);
     t_q = cat(1,t_q,TQ_12);
 end


% Assign q1, q2, q3, q4, and q5 to predicted percentiles
q1 = double(t_q(:,1));
q2 = double(t_q(:,2));
q3 = double(t_q(:,3));
q4 = double(t_q(:,4));
q5 = double(t_q(:,5));


% Plot historic data
zplot = z(1:size(q1,1));
xplot = xplot(1:size(q1,1));
plot(zplot,xplot,'k');
hold on;

% Plotting projections
shade(zplot,q1,zplot,q3,'linestyle','none','FillType',[2 1;1 2],'FillColor', [1 0
0;1 0 0],'Color',[1 1 1]);
shade(zplot,q5,zplot,q3,'linestyle','none','FillType',[2 1;1 2],'FillColor', [1 0
0;1 0 0],'Color',[1 1 1]);
shade(zplot,q2,zplot,q3,'linestyle','none','FillType',[2 1;1 2],'FillColor', [1 0
0;1 0 0],'Color',[1 0 0]);
shade(zplot,q3,zplot,q4,'linestyle','none','FillType',[2 1;1 2],'FillColor', [1 0
0;1 0 0],'Color',[1 0 0]);
Coloralpha = 0.1;
```

```
plot(zplot,q3,'r','linewidth',1);
plot(zplot,xplot,'k');

% Graph formatting

% Create dashed line to signify end of historic data
TrainX = [z(train),z(train)];
TrainY = [-10,10];
plot(TrainX,TrainY,'--','Color',[0.5 0.5 0.5],'linewidth',1);

% Label historic and projected sections of plot
Train = z(round(train/4));
Val = z(round(val/2)+(train));
txt2 = {'Training','Validation'};
text([Train Val],[2.7 2.7],txt2);

alpha = 0.25;
ylim([-3,3]);
xlabel('Year');
ylabel('Standardised price ($)');
legend({'Historic data'},'Location','south')
```

S2.3: Model training – using the model for the projection horizon

Finally, the model for the desired projection horizon should be executed, again utilising the optimal hyper-parameters determined during the grid search. The below code runs the final model, producing a plot of the projected percentiles, stores the ensemble of projections in the table `'Ensemble'`, and the annual 5th, 25th, 50th, 75th and 95th price percentiles in the table `'Percentiles'`. These percentiles should be saved externally and used in the techno-economic, sensitivity and uncertainty analyses. As before, the 'shade' function from the MATLAB file exchange is used to generate the shaded plots (Tordera, 2018).

```
% Running validation set - use of optimal hyper-parameters

% HU, L2, LR selected from grid search
HU = [1];
EP = [500];
LR = [0.1];

Ypreds = [];
Ypreds3 = [];

% Setting up network
for p=1:100

    h = randperm(HU);
    h = h(1);

    Ypred2 = [];
    Ypred3 = [];

    X2_train_LSTM{1} = [];
    Y2_train_LSTM{1} = [];
    X2_train_LSTM{1} = cat(2,X2_train',X2_val');
    Y2_train_LSTM{1} = cat(2,Y2_train',Y2_val');
    numResponses = 12;
    m = round((size(z,1)-a)/12);
    c = 1;
    for n = 1:m
        net = [];
        layers = [ ...
            sequenceInputLayer(2)
            fullyConnectedLayer(2)
            lstmLayer(h,'OutputMode','sequence')
            fullyConnectedLayer(numResponses)
            regressionLayer];
```

```
        options = trainingOptions('adam', ...
            'GradientThreshold',1, ...
            'MaxEpochs',EP, ...
            'MiniBatchSize',1, ...
            'InitialLearnRate',LR, ...
            'Shuffle','every-epoch');
        net = trainNetwork(X2_train_LSTM,Y2_train_LSTM,layers,options);

% Initialise real values
% Xpred = values to be predicted by the network
% The model operates recursively, i.e previously projected values become inputs to
the model
         Xpred{1} = cat(2,X2_train_LSTM{1},cat(1,Y2_train_LSTM{1}(:,end)',...
                    (crude(train+val+c:train+val+c+11))'));

% Ypred = network projection based on Xpred
         Ypred = predict(net,Xpred);
         X2_train_LSTM{1} = cat(2,X2_train_LSTM{1},...
                            cat(1,Xpred{1}(1,end-11:end),...
                            (crude(train+val+c:train+val+c+11))'));
         Y2_train_LSTM{1} = cat(2,Y2_train_LSTM{1},Ypred{1}(:,end-11:end));

         c = c + 12;
    end

% Ypred2 = projections on the validation set
% Ypred3 = projections up to the end of the projection horizon
     Ypred2 = X2_train_LSTM{1}(1,train+1:train+val);
     Ypred3 = X2_train_LSTM{1}(1,:);

     Ypreds = cat(1,Ypreds,Ypred2);
     Ypreds3 = cat(1,Ypreds3,Ypred3);
end

% Calculating yearly percentiles of the ensemble projections for the entire data
series
 t_q = [];
 for q = 1:((size(Ypreds3,2))/12)
     q = q*12;
     T = cat(1,Ypreds3(:,q-11),Ypreds3(:,q-10),Ypreds3(:,q-9),Ypreds3(:,q-8),...
         Ypreds3(:,q-7),Ypreds3(:,q-6),Ypreds3(:,q-5),Ypreds3(:,q-4),...
        Ypreds3(:,q-3),Ypreds3(:,q-2),Ypreds3(:,q-1),Ypreds3(:,q));
     TQ = quantile(T,[0.05 0.25 0.50 0.75 0.95]);
     TQ_12=repmat(TQ,12,1);
     t_q = cat(1,t_q,TQ_12);
 end

% Assign q1, q2, q3, q4, and q5 to predicted percentiles
q1 = double(t_q(:,1));
q2 = double(t_q(:,2));
q3 = double(t_q(:,3));
q4 = double(t_q(:,4));
q5 = double(t_q(:,5));

Percentiles = array2table(((t_q*std_com)+mean_com),'VariableNames',...
    {'5th','25th','50th','75th','95th'});
Ensemble_Projections = (Ypreds3'*std_com)+mean_com;
Date = z;
Ensemble = table(Date,Ensemble_Projections);

% Plot historic data
z_p = z(1:q);
x_p = xplot(1:q);
plot(z_p,x_p,'k');
hold on;

% Plotting projections
```

```
shade(z_p,q1,z_p,q3,'linestyle','none','FillType',[2 1;1 2],'FillColor', [1 0 0;1 0
0],'Color',[1 1 1]);
shade(z_p,q5,z_p,q3,'linestyle','none','FillType',[2 1;1 2],'FillColor', [1 0 0;1 0
0],'Color',[1 1 1]);
shade(z_p,q2,z_p,q3,'linestyle','none','FillType',[2 1;1 2],'FillColor', [1 0 0;1 0
0],'Color',[1 0 0]);
shade(z_p,q3,z_p,q4,'linestyle','none','FillType',[2 1;1 2],'FillColor', [1 0 0;1 0
0],'Color',[1 0 0]);
Coloralpha = 0.1;
plot(z_p,q3,'r','linewidth',1);
plot(z_p,x_p,'k');

% Graph formatting

% Create dashed line to signify end of historic data
TrainX = [z_p(a+12),z_p(a+12)];
TrainY = [-10,10];
plot(TrainX,TrainY,'--','Color',[0.5 0.5 0.5],'linewidth',1);

% Label historic and projected sections of plot
Hist = z_p(round((train+val)/2)-36);
Proj = z_p(((size(z,1)-(train+val))/2)+(train+val)-36);
txt2 = {'Historic','Projected'};
text([Hist Proj],[2.7 2.7],txt2);

alpha = 0.25;
ylim([-3,3]);
xlabel('Year');
ylabel('Standardised price ($)');
legend({'Historic data'},'Location','south')
```

References:

Rodgers, S., Conradie, A., King, R., Poulston, S., Hayes, M., Bommareddy, R.R., Meng, F., McKechnie, J., 2021. Reconciling the Sustainable Manufacturing of Commodity Chemicals with Feasible Technoeconomic Outcomes. Johnson Matthey Technol. Rev. 375–394. https://doi.org/10.1595/205651321x16137377305390

Rodgers, S., Meng, F., Poulston, S., Conradie, A., McKechnie, J., 2022. Renewable butadiene: A case for hybrid processing via bio- and chemo-catalysis. J. Clean. Prod. 364, 132614. https://doi.org/10.1016/j.jclepro.2022.132614

Shrestha, D.L., 2014. Continuous rank probability score (https://www.mathworks.com/matlabcentral/fileexchange/47807-continuous-rank-probability-score), MATLAB Central File Exchange. Retrieved June 28, 2022.

Tordera, J.M., 2018. Filled area plot (https://www.mathworks.com/matlabcentral/fileexchange/69652-filled-area-plot), MATLAB Central File Exchange. Retrieved February 12, 2022.

Towler, G., Sinnott, R.K., 2013. Chemical Engineering Design - Principles, Practice and Economics of Plant and Process Design, 2nd ed. Elsevier.

A.4 Supplementary information for Chapter 7: A surrogate model for the economic evaluation of renewable hydrogen production from biomass feedstocks via supercritical water gasification

Section S.1: Experimental data collection

Table S1: Ultimate analysis of biomass compounds used in this study. A broad range of different biomass compositions was selected. The purpose was to create a generalisable feedstock evaluation tool for evaluation of future compositions rather than evaluating each of the feedstocks the compositions represent.

Feedstock	C	H	N	O	Reference
	(wt%)				
Paper waste sludge	49.21	5.90	0.08	44.81	(Louw, et al., 2016)
Sewage sludge	51.43	6.00	7.85	34.73	(Hantoko, et al., 2019)
Diesel	84.79	13.67	0.14	1.40	(Kou, et al., 2018)
Distillery wastewater	35.29	4.99	4.89	54.82	(Seif, et al., 2016)
Sugarcane bagasse	58.21	6.46	0.69	34.64	(Rashidi & Tavasoli, 2015)
Fruit pulp	48.24	6.05	0.47	45.24	(Elif & Nezhie, 2016)
Cattle manure	60.08	5.61	2.37	31.95	(Tavasoli, et al., 2018)
Pinewood	48.86	7.35	0.10	43.69	(Nanda, et al., 2016a)
Food waste	49.10	7.16	3.81	39.93	(Yan, et al., 2019)
Spent lees	39.72	6.32	0.70	53.26	(Lee, et al., 2023)
Olive wastewater	37.65	6.43	1.20	54.72	(Lee, et al., 2023)
Stillage	42.05	7.24	3.22	47.48	(Lee, et al., 2023)
Wheat straw	44.13	6.85	0.52	48.49	(Lu, et al., 2019)
Walnut shell	50.53	5.71	0.85	42.92	(Safari, et al., 2016)
Waste cooking oil	76.44	14.13	1.19	8.24	(Sonil, et al., 2019)
Heavy gas oil	84.72	13.20	1.87	0.21	(Rana, et al., 2020)
Light gas oil	81.89	15.33	1.13	1.65	(Rana, et al., 2020)
Soybean straw	44.21	5.32	0.48	49.98	(Okolie, et al., 2020)
Sugarcane bagasse	41.93	5.73	0.20	52.14	(Kumar & Reddy, 2019)
Mosambi peel	38.18	6.26	1.32	54.24	(Kumar & Reddy, 2019)
Timothy grass	49.38	7.08	1.46	42.08	(Nanda, et al., 2016b)
Hongliulin coal	83.25	5.26	1.12	10.38	(Hui, et al., 2017)
Hongliulin bituminous coal	78.66	4.48	1.12	15.74	(Sun, et al., 2021)
Chicken manure	46.51	7.62	5.73	40.14	(Babaei, et al., 2021)
Dairy wastewater (whey)	34.29	5.64	5.33	54.73	(Khorasani, et al., 2021)
Concentrated vinasse	25.60	8.90	4.18	61.32	(Loppinet-Serani, et al., 2013)
Black liquor	38.16	4.51	0.85	56.48	(Karimi, et al., 2022)
Black liquor (wheat straw)	48.25	4.00	0.33	47.42	(Cao, et al., 2011)
Landfill leachate	75.18	1.36	7.47	16.00	(Gong, et al., 2018)
Waste tires	72.39	7.04	2.03	18.55	(Nanda, et al., 2019)
petroleum coke	81.74	4.80	1.78	11.68	(Rana, et al., 2019)
Sewage sludge	58.63	1.54	10.55	29.28	(Yan, et al., 2021)
Sewage sludge	54.92	8.54	8.32	28.23	(He, et al., 2015)
Sewage sludge	54.55	4.86	6.67	33.92	(Chen, et al., 2013)
Dewatered sewage sludge	43.50	8.25	7.09	41.16	(Wang, et al., 2017)
Dewatered sludge	44.45	6.71	3.52	45.32	(Xu, et al., 2012)
Horse manure	51.57	7.19	1.12	40.11	(Nanda, et al., 2016c)
Hemicellulose poplar	43.12	5.62	0.00	51.26	(Gökkaya Selvi, et al., 2020)
Pinecone	52.20	6.47	1.05	40.28	(Nanda, et al., 2017)
Peanut shell	51.93	5.83	1.80	40.43	(Jin, et al., 2014)

Section S.2 Process and cost models

Table S2: Gibbs model gas composition predictions at different temperatures. P = 24 MPa, biomass concentration = 75 g/L COD, biomass composition (wt%) C: 46.51, H: 7.62, N: 5.73, O: 40.14.

T (°C)	Gas composition (wt%)			
	H_2	CH_4	CO_2	CO
400	9.82	46.44	0.03	43.71
500	29.40	30.90	0.16	39.54
600	45.83	17.81	0.46	35.91
700	57.20	8.67	0.96	33.17

Table S3: Economic parameters used in the investment analysis.

Economic Parameters	Values
Fixed capital cost parameters	
Free on board equipment purchase cost	Seider et al. (2017)
Installed capital cost	Hand method
Chemical Engineering Plant Cost Index in 2021	739
Production Year	8,400
Installed Cost – Inside Battery Limit (ISBL) Factor	Hand factors, specific to equipment type.
Outside Battery Limit (OSBL)	25% of ISBL
Commissioning Cost	5% of ISBL
Fixed Capital Investment (FCI)	ISBL + OSBL + Commissioning
Working Capital	10% of ISBL + OSBL
Total Capital Investment (TCI)	FCI + Working Capital
Fixed operating cost model	
Operating labour	Salary estimates obtained from salaryexpert.com (4 shifts with 2 members each)
Supervisory labour	25% of operating labour
Direct salary overhead	50% of operating and supervisory labour

Maintenance	3% of ISBL
Property taxes and insurance	1% of ISBL
Rent of land	1% of FCI
General plant overhead	65% of total labour and maintenance
Allocated environmental charges	1% of FCI
Investment Analysis Parameters	
Discounted rate of return	8% [1]
Annual inflation	2%
Plant life	25 years
Plant salvage value	No value
Construction period	2 years

[1] In line with Europe's hurdle rates for electricity generation costs from biomass sources, e.g. 8.3% for anaerobic digestion and 7.9% for both dedicated biomass (5-100 MW) and energy from waste (combined heat and power) (BEIS, 2020)

Table S4: Variable operating costs.

Material	Cost	Source
Cooling water ($/m3)	0.753	(Towler, 2013)
Process water ($/m3)	0.530	(Foo, et al., 2017)
MEA solvent ($/kg)	1.5	Assumed solvent losses: 1.6 kg/tn CO_2 removed (Raksajati, et al., 2013)
Grid electricity prices ($/kwh)	0.089 China 0.155 Brazil 0.259 UK	(Global Petrol Prices, 2022)
Steam methane reforming catalyst ($/kg)	8	Replaced every 4.5 years
High and low temperature shift catalyst ($/kg)	10	

Table S5: Life cycle inventory

Material	Emission factor	Comment
Water (kg $CO_{2eq.}/m^3$):		

China and Brazil	3.17×10^{-4}	Global allocation at the point of substitution (Wernet, et al., 2016)
UK	2.95×10^{-4}	Europe allocation at the point of substitution (Wernet, et al., 2016)
MEA solvent (kg $CO_{2eq.}$/kg):		
China and Brazil	3.420	Global allocation at the point of substitution (Wernet, et al., 2016)
UK	2.641	Europe allocation at the point of substitution (Wernet, et al., 2016)
Grid electricity (kg $CO_{2eq.}$/kwh):		
China	0.85	Average combined (IGES, 2022)
Brazil	0.292	Average combined (IGES, 2022)
UK	0.136	(BEIS, 2022)
Transport (kg $CO_{2eq.}$/tn.km):	0.163	EURO 6, 16-32 tn capacity (Wernet, et al., 2016)

Section S.3: Machine learning models

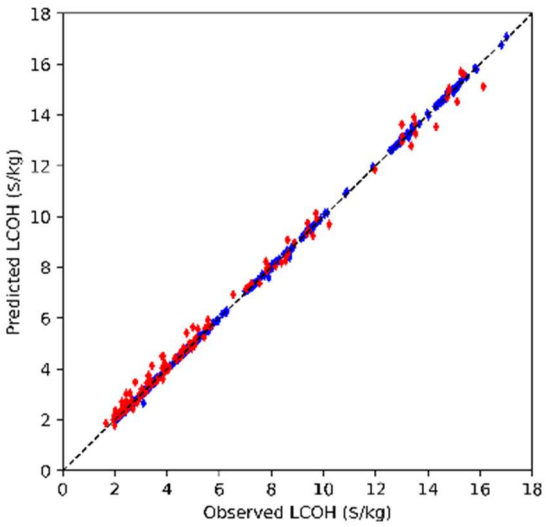

a) Nominal LCOH

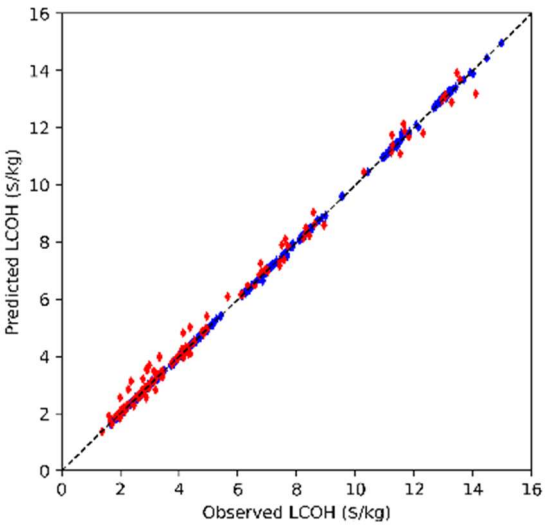

b) Lower bound (5th percentile) LCOH

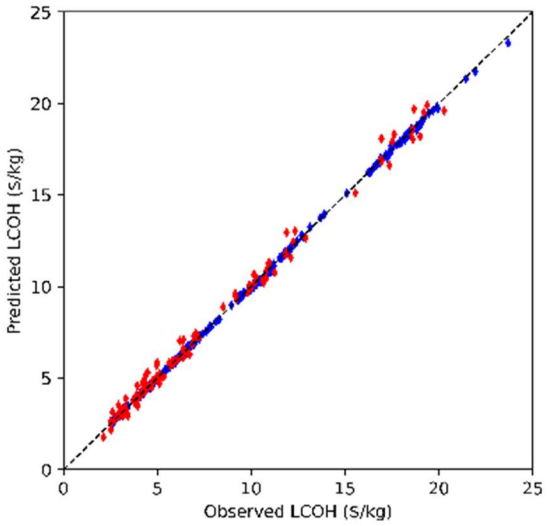

c) Upper bound (75th percentile) LCOH

Figure S1 a-c: Parity plots of observed and predicted LCOH ($/kg$H_2$) using ANNs. Figures a, b, and c represent the model performance on the test set (withheld from training) for the nominal, lower (5th) and upper (75th) bounds. The blue datapoints represent the training data and the red the testing set.

Table S6: Final model performance on an unseen biomass sample at processing capacities used during model training and interpolated results between the considered capacities. Biomass sample, orange peel, composition (wt%) C: 42.34, H: 6.47, N: 0.72, O: 50.46 (Nanda et a., 2016d).

Processing capacity (m^3/hr)	LCOH ($/kg)		Percentage error (%)
	Simulated	Nominal predicted	
10	13.17	13.07	0.76%
15	9.63	9.62	0.09%
20	7.09	7.09	0.02%
35	5.21	5.38	3.12%
50	4.34	4.38	0.88%
75	3.69	3.81	3.08%
100	3.45	3.40	1.51%
150	3.12	3.14	0.59%
200	3.00	3.05	1.73%

Section S.4: Study limitations

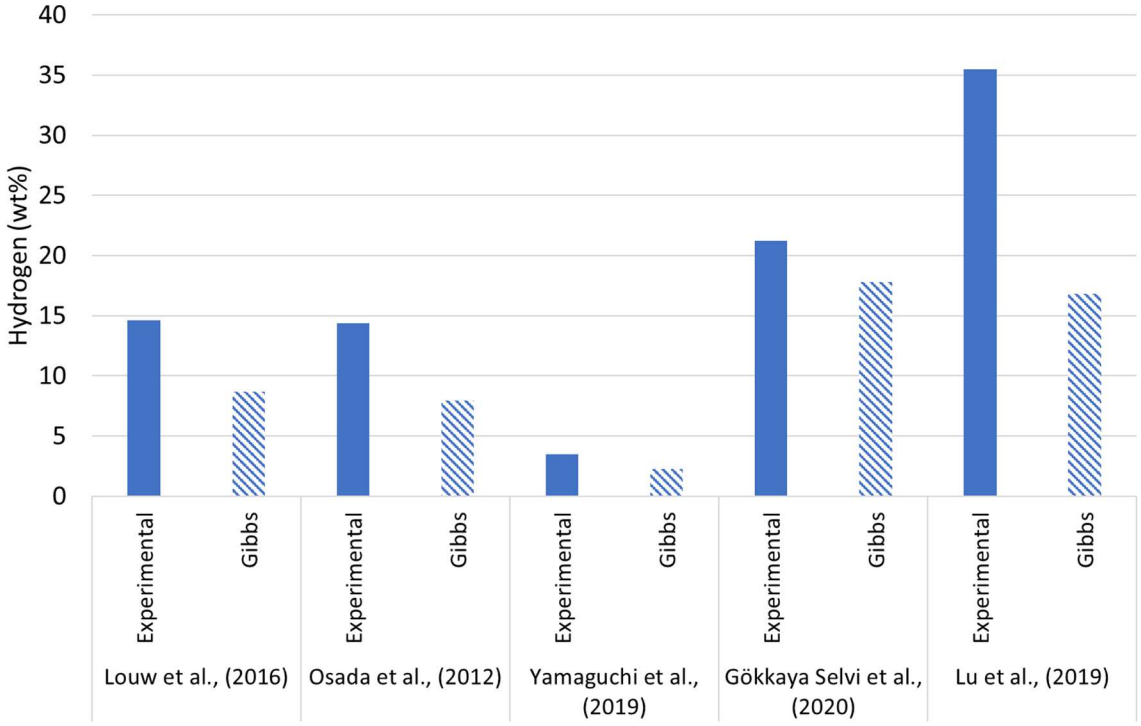

a) Comparison between experimental hydrogen wt% and the Gibbs reactor prediction

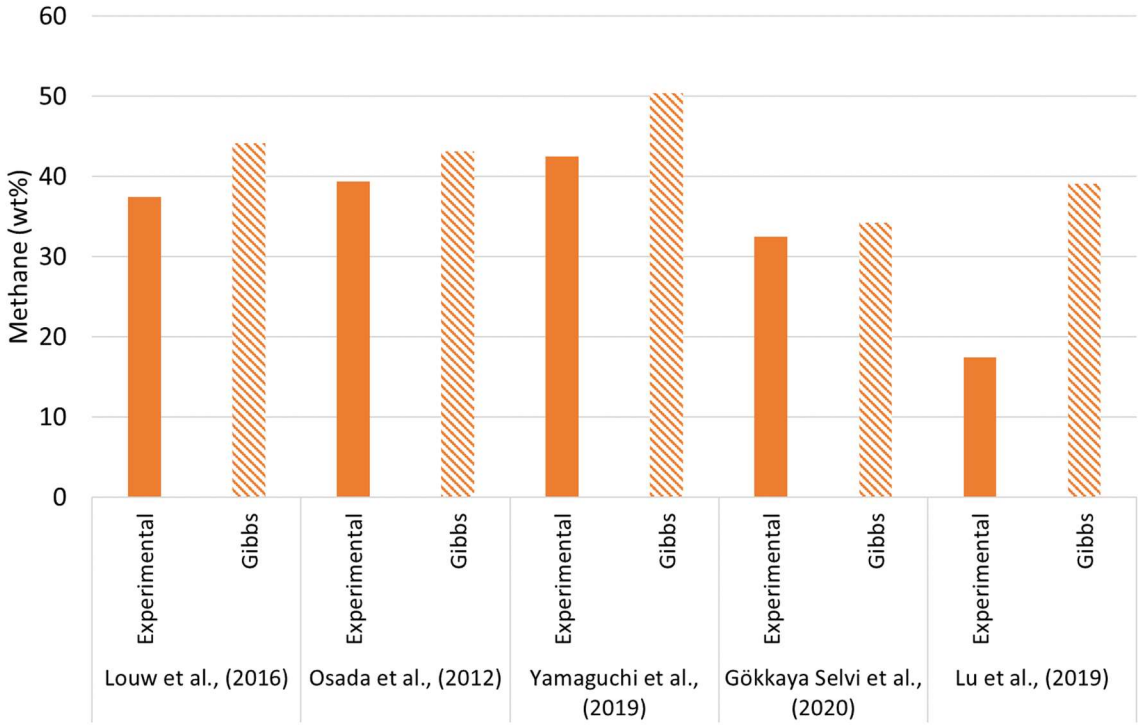

b) Comparison between experimental methane wt% and the Gibbs reactor prediction

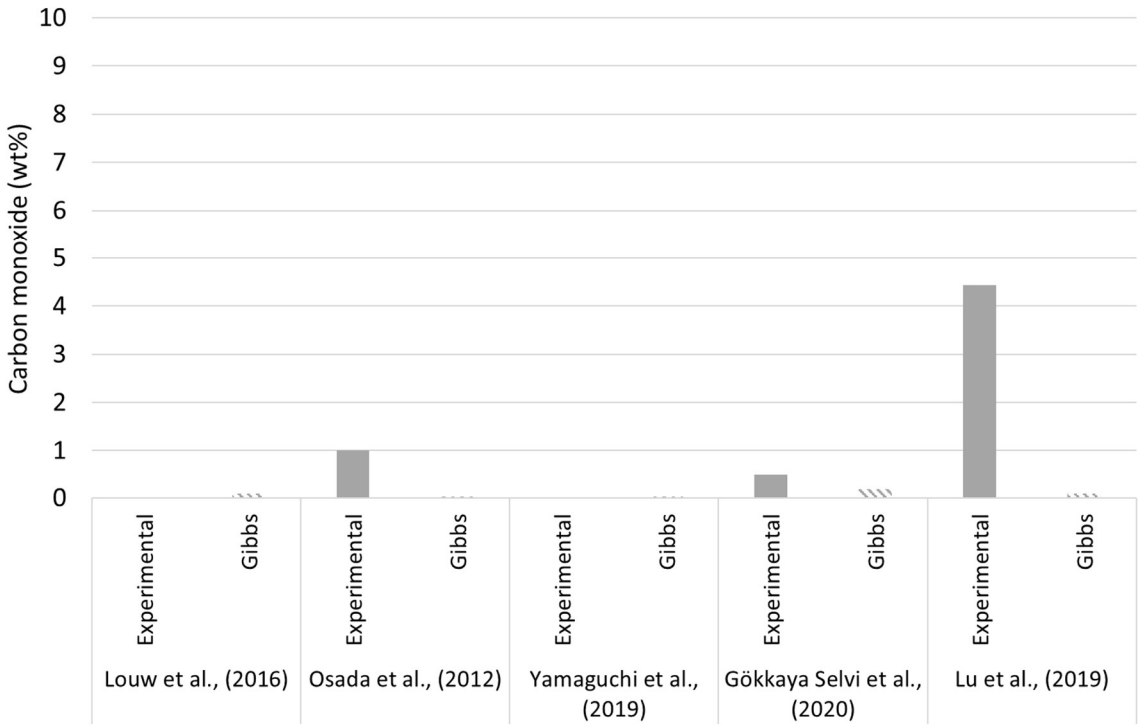

c) Comparison between experimental carbon monoxide wt% and the Gibbs reactor prediction

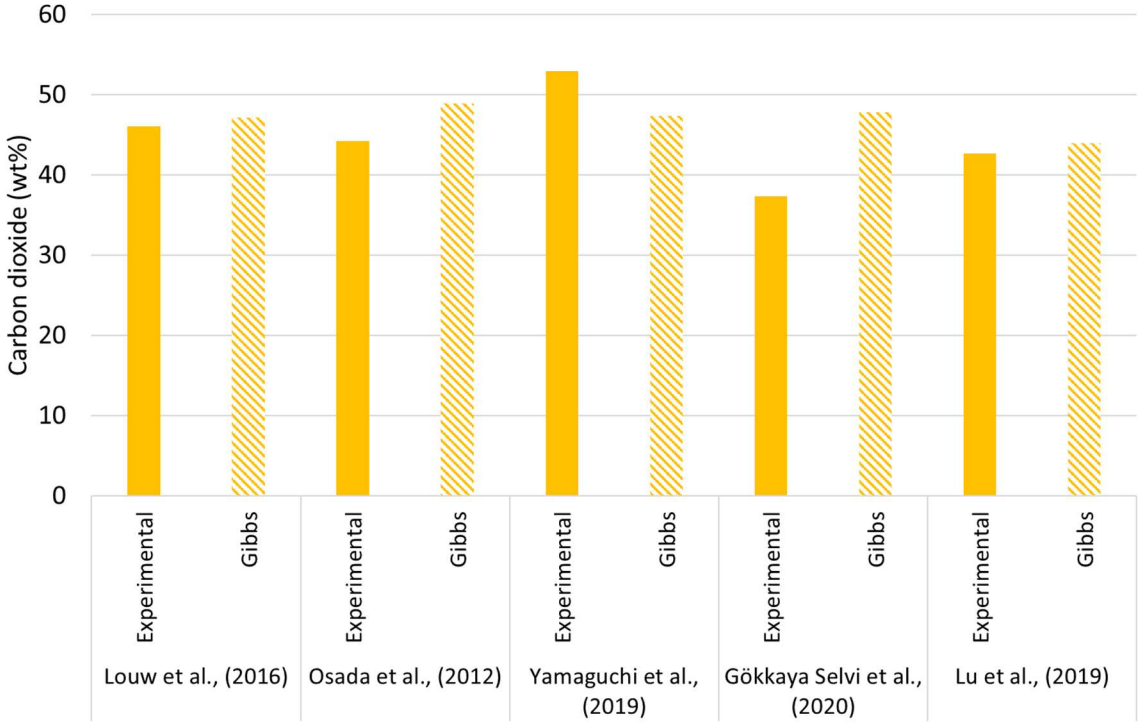

d) Comparison between experimental carbon dioxide wt% and the Gibbs reactor prediction

Figure S2a-d: Comparison between experimentally reported gas compositions and thermodynamic equilibrium predicted by the Gibbs reactor. Louw et al., (2016) is for paper waste sludge at 450 °C, 60 min residence time, Ni Catalyst. Osada et al., (2012) is for sugarcane bagasse at 400 °C, 15 min residence time, Ru/TiO_2 catalyst. Yamaguchi et al., (2019) is for Japanese cedar waste at 400 °C, 60 minute residence time, Ru/C catalyst. Gökkaya Selvi et al., (2020) is for Hemicellulose poplar at 500 °C, 60 minute residence time, K_2CO_3 catalyst. Lu et al., (2019) is for wheat straw at 450°C, 20 min residence time, Ni/MgO catalyst.

References:

1. Babaei, K., Bozorg, A. & Tavasoli, A., 2021. Hydrogen-rich gas production through supercritical water gasification of chicken manure over activated carbon/ceria-based nickel catalysts. Journal of Analytical and Applied Pyrolysis.
2. BEIS, 2020. BEIS Electricity Generation Costs (2020). [Online] Available at: https://www.gov.uk/government/publications/beis-electricity-generation-costs-2020 [Accessed 01 February 01].
3. BEIS, 2022. Government conversion factors for company reporting of greenhouse gas emissions. [Online] Available at: https://www.gov.uk/government/collections/government-conversion-factors-for-company-reporting [Accessed 17 January 2023].
4. Cao, C. et al., 2011. Hydrogen production from supercritical water gasification of alkaline wheat straw pulping black liquor in continuous flow system. International Journal of Hydrogen Energy, pp. 13528-13535.
5. Chen, Y. et al., 2013. Hydrogen production by sewage sludge gasification in supercritical water with a fluidized bed reactor. International Journal of Hydrogen Energy, 38(29), pp. 12991-12999.
6. Elif, D. & Nezhie, A., 2016. Hydrogen production by supercritical water gasification of fruit pulp in the presence of Ru/C. International Journal of Hydrogen Energy, pp. 8073-8083.
7. Foo, D. et al., 2017. Chemical Engineering Process Simulation. s.l.:Elxevier.
8. Global Petrol Prices, 2022. https://www.globalpetrolprices.com/electricity_prices/. [Online] Available at: https://www.globalpetrolprices.com/electricity_prices/ [Accessed 05 December 2022].
9. Gökkaya Selvi, D. et al., 2020. Hydrothermal gasification of the isolated hemicellulose and sawdust of the white poplar (Populus alba L.). The Journal of Supercritical Fluids, Volume 162.
10. Gong, Y. et al., 2018. Gasification of landfill leachate in supercritical water: Effects on hydrogen yield and tar formation. International Journal of Hydrogen Energy, pp. 22827-22837.
11. Hantoko, D. et al., 2019. Assessment of sewage sludge gasification in supercritical water for H2-rich syngas production. Process Safety and Environmental Protection, pp. 63-72.
12. He, C. et al., 2015. Products evolution during hydrothermal conversion of dewatered sewage sludge in sub- and near-critical water: Effects of reaction conditions and calcium oxide additive. International Journal of Hydrogen Energy, 40(17), pp. 5776-5787.
13. Hui, J. et al., 2017. Experimental investigation on methanation reaction based on coal gasification in supercritical water. International Journal of Hydrogen Energy, pp. 4636-4641.
14. IGES, 2022. IGES List of Grid Emission Factors. [Online] Available at: https://www.iges.or.jp/en/pub/list-grid-emission-factor/en?_ga=2.151364921.1686382296.1673188108-667943912.1673188108 [Accessed 12 January 2023].
15. Jin, H. et al., 2014. Hydrogen Production by Supercritical Water Gasification of Biomass with Homogeneous and Heterogeneous Catalyst. Advanced Catalysis and Nanostructure Design for Solar Energy Conversion.
16. Karimi, A., Kazemi, N., Tavakoli, O. & Pirbazari, A. E., 2022. Catalytic supercritical water gasification of black liquor along with lignocellulosic biomass. International Journal of Hydrogen Energy, pp. 16729-16740.

17. Khorasani, R., Khodaparasti, M. S. & Tavakoli, O., 2021. Hydrogen production from dairy wastewater using catalytic supercritical water gasification: Mechanism and reaction pathway. International Journal of Hydrogen Energy, pp. 22368-22384.
18. Kou, J. et al., 2018. Evaluation of modified Ni/ZrO2 catalysts for hydrogen production by supercritical water gasification of oil-containing wastewater. International Journal of Hydrogen Energy, pp. 13896-13903.
19. Kumar, A. & Reddy, S. N., 2019. In Situ Sub- and Supercritical Water Gasification of Nano-Nickel (Ni2+) Impregnated Biomass for H2 Production. Industrial & Engineering Chemistry Research, p. 4780–4793.
20. Lee, C. S., Conradie, A. V. & Lester, E., 2023. The integration of low temperature supercritical water gasification with continuous in situ nano-catalyst synthesis for hydrogen generation from biomass wastewater. Chemical Engineering Journal.
21. Loppinet-Serani, A., Reverte, C., Cansell, F. & Aymonier, C., 2013. Supercritical Water Biomass Gasification Process As a Successful Solution to Valorize Wine Distillery Wastewaters. Sustainable Chemistry and Engineering, pp. 110-117.
22. Louw, J., Schwarz, C. E. & Burger, A. J., 2016. Catalytic supercritical water gasification of primary paper sludge using a homogeneous and heterogeneous catalyst: Experimental vs thermodynamic equilibrium results. Bioresource technology, pp. 111-120.
23. Lu, Y., Jin, H. & Zhang, R., 2019. Evaluation of stability and catalytic activity of Ni catalysts for hydrogen production by biomass gasification in supercritical water. Carbon Resources Conversion, pp. 95-101.
24. Nanda, S., Reddy, S. N., Dalai, A. K. & Kozinski, J. A., 2016a. Subcritical and supercritical water gasification of lignocellulosic biomass impregnated with nickel nanocatalyst for hydrogen production. International Journal of Hydrogen Energy, pp. 4907-4921.
25. Nanda, S., Dalai, A. K. & Kozinski, J. A., 2016b. Supercritical water gasification of timothy grass as an energy crop in the presence of alkali carbonate and hydroxide catalysts. Biomass and Bioenergy, pp. 378-387.
26. Nanda, S., Dalai, A. K., Gökalp, I., Kozinski, 2016c. Valorization of horse manure through catalytic supercritical water gasification. Waste Management, Volume 52, pp. 147-158.
27. Nanda, S., Isen, J., Dalai, A. K., Kozinski, 2016d. Gasification of fruit wastes and agro-food residues in supercritical water, Energy Conversion and Management, Volume 110, pp. 296-306.
28. Nanda, S. et al., 2017. An assessment of pinecone gasification in subcritical, near-critical and supercritical water. Fuel processing Technology, Volume 168, pp. 84-96.
29. Nanda, S. et al., 2019. Catalytic subcritical and supercritical water gasification as a resource recovery approach from waste tires for hydrogen-rich syngas production. The Journal of Supercritical Fluids.
30. Okolie, J. A., Nanda, S., Dalai, A. K. & Kozinski, J. A., 2020. Hydrothermal gasification of soybean straw and flax straw for hydrogen-rich syngas production: Experimental and thermodynamic modeling. Energy Conversion and Management.
31. Osada, M., Yamaguchi, A., Hiyoshi, N., Sato, O., Shirai, M., 2012. Gasification of Sugarcane Bagasse over Supported Ruthenium Catalysts in Supercritical Water. 26 (6), 31179-3186.
32. Raksajati, A., T. Ho, M. & Wiley, D. E., 2013. Reducing the Cost of CO2 Capture from Flue Gases Using Aqueous Chemical Absorption. Industrial & Engineering Chemistry Research, p. 16887–16901.

33. Rana, R. et al., 2019. Comparative evaluation for catalytic gasification of petroleum coke and asphaltene in subcritical and supercritical water. Journal of Energy Chemistry, pp. 107-118.
34. Rana, R. et al., 2020. Catalytic gasification of light and heavy gas oils in supercritical water. Journal of the Energy Institute, pp. 2025-2032.
35. Rashidi, M. & Tavasoli, A., 2015. Hydrogen rich gas production via supercritical water gasification of sugarcane bagasse using unpromoted and copper promoted Ni/CNT nanocatalysts. The Journal of Supercritical Fluids, pp. 111-118.
36. Safari, F., Salimi, M., Tavasoli, A. & Ataei, A., 2016. Non-catalytic conversion of wheat straw, walnut shell and almond shell into hydrogen rich gas in supercritical water media. Chinese Journal of Chemical Engineering, pp. 1097-1103.
37. Seif, S., Fatemi, S., Tavakoli, O. & Bahmanyar, H., 2016. Hydrogen production through hydrothermal gasification of industrial wastewaters using transition metal oxide catalysts. The Journal of Supercritical Fluids, pp. 32-45.
38. Sonil, N. et al., 2019. Hydrothermal catalytic processing of waste cooking oil for hydrogen-rich syngas production. Chemical Engineering Science, pp. 935-945.
39. Sun, J. et al., 2021. Experimental investigation on carbon microstructure for coal gasification in supercritical water. Fuel.
40. Tavasoli, A. et al., 2018. Influence of the blend nickel/porous hydrothermal carbon and cattle manure hydrochar catalyst on the hydrothermal gasification of cattle manure for H2 production. Energy Conversion and Management, pp. 15-28.
41. Towler, G. S. R. K., 2013. Chemical Engineering Design - Principles, Practice and Economics of Plant and Process Design. 2nd ed. s.l.:Elsevier..
42. Wang, C. et al., 2017. Influence of H2O2 and Ni catalysts on hydrogen production and PAHs inhibition from the supercritical water gasification of dewatered sewage sludge. The Journal of Supercritical Fluids, Volume 130, pp. 183-188.
43. Wernet, G. et al., 2016. The ecoinvent database version 3 (part I): overview and methodology. The International Journal of Life Cycle Assessment, Volume 21, pp. 1218-1230.
44. Xu, Z. R., Zhu, W. & Li, M., 2012. Influence of moisture content on the direct gasification of dewatered sludge via supercritical water. International Journal of Hydrogen Energy, 37(8), pp. 6527-6535.
45. Yamaguchi, A., Watanabe, T., Saito, K., Kuwano, S., Murakami, Y., Mimura, N., Sato, O., 2019. Direct conversion of lignocellulosic biomass into aromatic monomers over supported metal catalysts in supercritical water. Molecular Catalysis, 477.
46. Yan, M. et al., 2021. Sulfur conversion and distribution during supercritical water gasification of sewage sludge. Journal of the Energy Institute, Volume 95, pp. 61-68.
47. Yan, M. et al., 2019. Experimental study on the energy conversion of food waste via supercritical water gasification: Improvement of hydrogen production. International Journal of Hydrogen Energy, pp. 4664-4763.